Development & Optimisation of a 3D *In Vitro* Microvascular Model for Non-Penetrating Traumatic Injury Research



Carla Verónica Fuenteslópez

A thesis submitted for the degree of
Doctor of Philosophy

St Hugh's College

Institute of Biomedical Engineering
Department of Engineering Science
University of Oxford

Supervised by
Professor Hua Ye & Professor Mark S. Thompson

Michaelmas Term 2025

A **Ma**, por ser mi inspiración más grande.

A **Chuck**, por siempre impulsarnos a ir más allá y a cumplir nuestros sueños, incluso cuando esto implique irnos lejos.

A **Fer**, por ser la persona más fuerte que conozco y por siempre estar ahí.

A **Papá**, por demostrar todos los días que siempre se sigue adelante. We "*keep moving forward*".

Mum, por acompañarme siempre. No hay nadie que me recargue tanto la pila tanto como tú. Te quiero un chorro y un montón!

A **Vero** y **Gerardo**, por ser siempre el "sí se puede" y por todo el apoyo desde lejos.

A **Pepe**, por ser la primera persona en presentarme la Ingeniería de Tejidos. Quién diría que aquel artículo de Stanford cambiaría mi vida.

y a **Juan**, por siempre sentirte cerca a pesar de la distancia. Tú, más que nadie, has visto de cerca lo que ha implicado este doctorado: desde cuando no había financiamiento ni becas para empezarlo, a venir conmigo al laboratorio los fines de semana, y estar ahí hasta el último segundo. Son gracias infinitas por estos años compartidos, por las aventuras que hemos vivido juntos y por todas las que aún nos faltan!

Tal vez esta tesis y el doctorado tienen mi nombre solamente, pero nunca han sido solo míos. No estaría aquí sin todos y cada uno de ustedes, **siempre**:

Ma & Chuck
Patricia & Juan Carlos
Fer
Verónica, Gerardo, José & Juan Pablo
Pepe, Ale y Jos.

Con muchísimo cariño,
Carla
P.S. Un abrazo de astronauta!

Declaration

I declare that this thesis is entirely my own work and, except where stated, describes my own research. This work has not been submitted to another institution for any other degree or qualification.

Carla Verónica Fuenteslópez

Acknowledgements

It is often said that a doctorate is a solitary adventure, but this could not be further from the truth. Even thousands of kilometres from home and in the midst of a pandemic, I never felt alone. While much of this work was indeed carried out during the dark hours of the night, this thesis is undoubtedly a reflection of the unwavering support and encouragement of many, many people. I am deeply grateful to all those who have been a part of this journey.

First and foremost, I would like to express my sincere gratitude to my supervisors, **Prof Hua (Cathy) Ye** and **Prof Mark Thompson**, whose guidance, patience, and unfaltering support have shaped both this research and my development as a researcher. Your trust, thoughtful advice, and encouragement throughout all my adventures, both in and beyond the lab, have been invaluable. I feel incredibly fortunate to have benefited from your expertise and mentorship throughout my DPhil, and I hope to have made you proud.

I would also like to give special thanks to **Valentín Martínez López** and **Ivett Quiñones Urióstegui** from the *Instituto Nacional de Rehabilitación* (INR) and *Universidad Iberoamericana*. You were the first to believe in me as a scientist. Thank you for opening the doors to the world of Tissue Engineering; it was life-changing. I have come this far thanks to you, and I will never forget it.

I am also very grateful to my friends and colleagues within the *Tissue Engineering Group*, the *Institute of Biomedical Engineering* (IBME), the *Department of Engineering Science*, the *Medical Sciences Division*, and across the University of Oxford. To **Gülşah**, thank you for our Sunday coffee walks, which were often the highlight of my week; to **Sim**, for being such a bright presence in my life; and to **Viorica**, for being my partner in pushing the boundaries of science even further.

I am thankful to all the friends I made in the lab and in the Old Road Campus Research Building (ORCRB) since I first arrived as an MSc student: **Linshan Chu**, **Oscar Dong**, **Tamiris Borges da Silva**, **Jamie Brett**, **Miren Tamayo Elizalde**, **Alex Witt**, **Eliška Kratochvílová**, **Mohammed Alwelyee**, **Alex Wu**, **Guang Yang**, **Xinyi Ouyang**, **Nianlin Li**, **Shuai Ren**, **Li Liu**, **Céline Kayal**, **Bo Zhang**, **Gloria Lam** and **Tong Chen**. Thank you for all the laughter, thoughtful feedback, and the sense of community that made me feel truly happy and at home.

I would also like to thank **Mariella**, **Lucy** and **Jacob** for being wonderful 4YP students, for letting me be a part of your final-year research, and for being such an important part of mine.

I would also like to acknowledge the incredible staff at the ORCRB, whose support was invaluable to both my work and the smooth running of day-to-day life in the lab. In particular, thank you to **Jamie**, **Scott**, **Quinton**, **Alex** & **Alfie** (IBME IT); **Phil**, **Caroline** and **Liza** (IBME Office); **Alwyn** (Autoclave); **Rob** and **Martin** (Goods In); **Dave**, **Dan**, **Jack**, **Mark** and **Chris** (Facilities); **Jelani**, **Jayne** and **Sourima** (Reception); **Mag**, **Nicky** and **Sam** (Café); and **Jim Fisk** (Workshop).

Thank you to **St Hugh's College** for its generous support throughout my DPhil, enabling me to complete my research, present my work around the world, and undertake fieldwork in some incredible and remote places, from Príncipe Island to Greenland. These opportunities have allowed me to explore science beyond bioengineering and have been some of the most memorable experiences of my time at Oxford.

I am also grateful to **Oxford University Innovation (OUI)** for supporting me through my first (of hopefully many!) patent and my first steps into entrepreneurship. I am particularly thankful to **Roger** for his mentorship and for teaching me how to communicate science beyond academia, and to **Alan** for introducing me to scientific entrepreneurship and making the prospect of turning research into a commercial venture feel achievable. Thank you also to the *Biofragment* team for sharing this adventure and showing me how our research could make a difference beyond the lab.

This research would not have been possible without the generous financial support I received throughout my doctoral studies. I gratefully acknowledge funding from the ***Consejo Nacional de Ciencia y Tecnología (CONACYT)***, through the fellowship *Becas CONACYT para estudios de Doctorado en el Extranjero* (2019–2023), and from the **Bank of Mexico** through the *Fondo para el Desarrollo de Recursos Humanos (FIDERH)* (2019–2022). I am also deeply thankful for the support provided by the *COVID-19 Fund* from **St Hugh's Student Support Committee** (2020), **QCRF–QR** funding (2020–2021), the **Oxford Assistance Fund** (2024 & 2025), the *Foundation Grant* (2023–2024) and the *Emergency Grant* (2024–2025) from **Funds for Women Graduates**, and the *DPhil Fund – MPLS Scholarship* from **Oxford Women in Engineering, Science, and Technology (OxWEST)**.

Beyond academia, I am profoundly thankful for the friends I made during this adventure, especially those from the *Oxford Príncipe Expedition 2023*: **Bastiaan**, **Denise**, and **Sophie**; the *Oxford University Exploration Club*; the *Oxford Arctic Centennial Expeditions*, especially my co-founder **Sofya**; the *Magdalen College Boat Club*; and *OxVent*. Your friendship, humour, and understanding sustained me through moments of doubt and exhaustion. Thank you for reminding me, time and again, that there is life beyond my research, and for the wonderful memories and experiences — I could not have asked for more.

Abstract

This thesis investigated the development, optimisation, and application of an *in vitro* three-dimensional (3D) microvascular model for traumatic injury research, focusing on non-penetrating traumatic injuries (NPTIs). Traumatic injuries are a major cause of morbidity and mortality worldwide, yet their immediate and short-term effects on the microvasculature remain poorly understood. Existing experimental approaches often lack physiological relevance, while clinical data are constrained by injury unpredictability, thereby limiting investigation of microvascular damage. To address this gap, this research developed and validated a physiologically relevant 3D microvascular platform capable of modelling NPTIs under controlled conditions.

The initial phase evaluated natural polymers for hydrogel scaffold fabrication to identify compositions that best support endothelial cell (EC) viability, migration, and tube formation. Fibrin was identified as a promising scaffold material, setting the foundation for subsequent work. A systematic review (SR) of fibrin-based tissue engineering (TE) scaffolds clarified how scaffold composition influences angiogenic outcomes, informing scaffold design. Building on this knowledge, a long-lasting 3D *in vitro* microvascular model was developed using microvascular endothelial cells (MVECs) and validated against a well-established and widely used endothelial cell line (human umbilical vein endothelial cells; HUVECs). Scaffold material properties were characterised, and robust microvascular networks were achieved.

As a proof of concept, the model was applied to *in vitro* NPTI research by subjecting cell-embedded and network-embedded hydrogels to contusion, crush, and strain injuries. Injury responses were assessed using EC tracking and quantitative analysis of microvascular network architecture before and after injury. Varying the biomechanical inputs (*e.g.* drop height, crush duration) established relationships between defined mechanical insults and patterns of microvascular disruption.

In conclusion, this thesis presents a novel and physiologically relevant 3D *in vitro* microvascular model for studying soft tissue NPTIs under controlled conditions. Beyond its immediate scope, the model provides a platform for future applications in therapeutics testing, regenerative medicine, and patient-specific trauma research, advancing both TE and trauma mechanobiology.

List of Publications & Patents

The following research outputs were published or filed during the course of this DPhil in Engineering Science. Scientific publications that are currently in preparation but have not yet been submitted to a journal are also included in this list.

Peer-Reviewed Publications as First Author

1. **Fuenteslópez CV**, Borges da Silva T, Taylor L, Ye H and Thompson MS. *In Vitro* and *In Vivo* Models of Non-Penetrating Traumatic Injuries: A Systematic Review. [In Preparation].

2. **Fuenteslópez CV**, Taylor L, Thompson MS and Ye H. Modelling Non-Penetrating Traumatic Injury in Engineered 3D Microvascular Constructs. [In Preparation].

3. **Fuenteslópez CV**, Bahçevancı S, Patrulea V and Ye H. Fibrin Scaffolds for Angiogenesis in Soft Tissue Models: A Systematic Review.
   Bioactive Materials 2026;56:703–25. DOI: 10.1016/j.bioactmat.2025.10.019.

4. **Fuenteslópez CV**, Papapavlou M, Thompson MS and Ye H. Engineering a Long-lasting Microvasculature *In Vitro* Model for Traumatic Injury Research. *Biomaterials Advances* 2025;174:214310. DOI: 10.1016/j.bioadv.2025.214310.

5. **Fuenteslópez CV**, Gray M, Bahçevancı S, Martin A, Smith CAB, Coussios C, Cui Z, Ye H and Patrulea V. Mesenchymal Stem Cell Cryopreservation with Cavitation-mediated Trehalose Treatment. *Communications Engineering* 2024;3(1):129. DOI: 10.1038/s44172-024-00265-6.

6. Mateu-Sanz M*, **Fuenteslópez CV***, Uribe-Gomez J, Haugen HJ, Pandit A, Ginebra M-P, Hakimi O, Krallinger M and Samara A. Redefining Biomaterial Biocompatibility: Challenges for Artificial Intelligence and Text Mining. *Trends in Biotechnology* 2023;42(4):402–17.
   DOI: 10.1016/j.tibtech.2023.09.015. *The two authors contributed equally to this work.

7. **Fuenteslópez CV**, McKitrick A, Corvi JO, Ginebra M-P and Hakimi O. Biomaterials Text Mining: A Hands-on Comparative Study of Methods on Polydioxanone Biocompatibility. *New Biotechnology* 2023;77:161–75. DOI: 10.1016/j.nbt.2023.09.001.

8. **Fuenteslópez CV**, Thompson MS and Ye H. Development and Optimisation of Hydrogel Scaffolds for Microvascular Network Formation. *Bioengineering* 2023;10(8):964. DOI: 10.3390/bioengineering10080964.

9. **Fuenteslópez CV** and Ye H. Electrospun Fibres with Hyaluronic Acid-Chitosan Nanoparticles Produced by a Portable Device. *Nanomaterials* 2020;10(10):2016. DOI: 10.3390/nano10102016.

Additional Peer-Reviewed Publications

1. Flahaut M, Laurent A, **Fuenteslópez CV**, Cui Z, Ye H, Scaletta C, Hirt-Burri N, Applegate LA and Patrulea V. Reassessing Long-term Cryopreservation Strategies for Improved Quality, Safety, and Clinical Use of Allogeneic Dermal Progenitor Cells. *Journal of Investigative Dermatology* 2024;144(10):2125–35. DOI: 10.1016/j.jid.2024.06.1285

2. Corvi JO, McKitrick A, Fernández JM, **Fuenteslópez CV**, Gelpí JL, Ginebra M-P, Capella-Gutierrez S and Hakimi O. DEBBIE: The Open Access Database of Experimental Scaffolds and Biomaterials Built Using an Automated Text Mining Pipeline. *Advanced Healthcare Materials* 2023;2300150. DOI: 10.1002/adhm.202300150

3. Beale R, Beddoe Rosendo J, Bergeles C, Beverly A, Camporota L, Castrejón-Pita AA, Crockett DC, Cronin JN, Denison T, East S, Edwardes C, Farmery AD, Fele F, Fisk J, **Fuenteslópez CV**, Garstka M, Goulart P, Heaysman C, Hussain A, Jha P, Kempf I, Kumar AS, Möslein A, Orr ACJ, Ourselin S, Salisbury D, Seneci C, Staruch R, Steel H, Thompson MS, Tran MC, Vitiello V, Xochicale M, Zhou F, Formenti F and Kirk T. OxVent: Design and Evaluation of a Rapidly-Manufactured COVID-19 Ventilator. *eBioMedicine* 2022;76:103868. DOI: 10.1016/j.ebiom.2022.103868 *Authors are listed in alphabetical order.

4. Corvi JO, **Fuenteslópez CV**, Fernández JM, Gelpí JL, Ginebra M-P, Capella-Gutierrez S and Hakimi O. The Biomaterials Annotator: A System for Ontology-Based Concept Annotation of Biomaterials Text. *Proceedings of the Second Workshop on Scholarly Document Processing*. 2021;36–48. DOI: 10.18653/v1/2021.sdp-1.5

Patents

The titles of the filed patent and patent applications under review listed below have been replaced with keywords for confidentiality purposes.

1. Patrulea V, **Fuenteslópez CV**, Ye H and Cui Z. *Cryoprotectants*. Patent Application [GB2501295.6]. Filed in January 2025.

2. **Fuenteslópez CV**, Patrulea V and Ye H. *Bioink A*. Patent Application under review by Oxford University Innovation [22116–A].

3. **Fuenteslópez CV**, Patrulea V and Ye H. *Bioink B*. Patent Application under review by Oxford University Innovation [22116–B].

Conferences, Symposia & Public Outreach

Conferences & Symposia

1. **Podium Institute Annual Conference on Sports Medicine & Technology** (2025). Oral presentation: "3D *In Vitro* Microvascular Model for Traumatic Injury Research".
2. **IBME Bellhouse BioEngenuity** (2024). Poster presentation: "Towards Improved Microvascular Integrity: Engineering Durable 3D Constructs for Traumatic Injury Research".
3. **Botnar Research Centre Symposium** (2024). Poster presentation: "Engineering a 3D Microvasculature Construct for Trauma Research".
4. **XXI Symposium of Mexican Students and Studies in the United Kingdom** (2024). Oral presentation: "Developing a 3D Microvasculature Construct for Traumatic Injury Research".
5. **The Development of Modern Biology: Achievements and Challenges** (2023). Oral presentation: "Engineering a 3D Microvasculature Construct for Trauma Research".
6. **University of Oxford's Chemical Engineering Symposium** (2023). Poster presentation: "Hydrogel Scaffolds Promoting Microvascular Network Formation for Traumatic Injury Research".
7. **TERMIS – Asia-Pacific Chapter** (2022). Oral presentation: "Development of an *In Vitro* Microvasculature Model for Non-Penetrating Trauma Research".
8. **TERMIS – Asia-Pacific Chapter** (2022). Poster presentation: "Biomaterials Text Mining: A Hands-on Comparative Research on the Biocompatible Polymer Polydioxanone".
9. **TERMIS – Asia-Pacific Chapter** (2022). Joint poster presentation: "Biomimetic 3D-Bioprinted Skin Scaffolds for Wound Healing and Regeneration".
10. **Graduate Joint Consultative Committee (GJCC)** (2022). Oral presentation: "Nanoparticle-embedded Electrospun Scaffolds for Nerve Repair and Regeneration".
11. **18th European Mechanics of Materials Conference** (2022). Oral presentation: "Development of an *In Vitro* Microvasculature Model for Trauma Research".
12. **TERMIS – World Congress** (2021). Poster presentation: "Electrospun Fibres with Hyaluronic Acid-Chitosan Nanoparticles Produced by a Portable Device".
13. **TERMIS – World Congress** (2021). Poster presentation: "Biomaterial Data Mining: A Comparative Study of Methods on Polydioxanone Literature".
14. **European Society for Biomaterials** (2021). Poster presentation: "Data Extraction using Text Mining Methods on Polydioxanone Literature".
15. **European Society for Biomaterials** (2021). Joint oral presentation: "DEBBIE 1.0: Biocompatibility Data Mining from MEDLINE into an Open Access Database".
16. **XXIX International Materials Research Congress** (2021). Oral presentation: "Electrospun Fibres with Hyaluronic Acid-Chitosan Nanoparticles Produced by a Portable Device".
17. **IET Appropriate Healthcare Technologies** (2020). Joint oral presentation: "OxVent: A Low-cost Rapid Manufacture Ventilator for COVID-19".
18. **Polygeia Annual Conference** (2019). Poster presentation: "Cancer in the Humanitarian Sector: Curative and Palliative Care".

Guest Speaker Presentations

1. **Institute of Biomedical Engineering (IBME) Open Day** (2025). Guest speaker/Demonstrator: "From Solution to Solid: The Science of Wet Spinning".
2. **Women in Engineering DPhil Panel** (2024). Guest speaker: "Bioengineering".
3. **50th Anniversary of Biomedical Engineering at Universidad Iberoamericana** (2024). Plenary speaker: "Tissue Engineering: Building the Future of Regenerative Medicine".
4. **International Women in Science Day, Department of Engineering Science, University of Oxford** (2024). Guest speaker: "Engineering a 3D Microvasculature Construct for Trauma Research".
5. **International Women in Science Day, Department of Engineering Science, University of Oxford** (2024). Poster presentation: "Tissue Engineering Strategies for Traumatic Injury Research".
6. **STEM Exploration Day Outreach, Theme: "Empowered Women Empower Women"** (2024). Guest speaker: "Development of a Microvasculature Model for Trauma Research".
7. **Department of Engineering Science's UNCOVER Programme** (2024). Guest speaker: "Engineering a 3D Microvasculature Construct for Trauma Research".
8. **Women in Engineering (WiE) $\times$ Engineers Without Borders Oxford (EWBOx) DPhil Flash Talks** (2024). Guest speaker: "Development of a Microvasculature Model for Trauma Research".
9. **Oxford Suzhou Centre for Advanced Research (OSCAR) Generation Programme** (2024). Invited speaker: "Tissue Engineering".
10. **III Encuentro Estatal de Jóvenes Investigadores, Consejo de Ciencia y Tecnología del Estado de Puebla** (2022). Guest speaker: "Biomaterials Text Mining".
11. **International Women in Engineering, Department of Engineering Science, University of Oxford** (2022). Guest speaker: "OxVent".
12. **International Women in Engineering, Department of Engineering Science, University of Oxford** (2021). Guest speaker: "Development of a Vascularised Bioartificial Muscle Model for Trauma Research".

Table of Contents

Table of Contents xv

List of Figures xviii

List of Tables xxi

Abbreviations xxiii

1 Introduction 1
- 1.1 Background & Motivation 1
- 1.2 Aims & Objectives 4
- 1.3 Scope & Structure of This Thesis 4

2 Literature Review 7
- 2.1 The Microvasculature: Structure, Function and Regulation of Perfusion 7
  - 2.1.1 The Cardiovascular System: Blood Vessel Structure and Architecture 7
  - 2.1.2 Organisation, Structure and Function of the Microvasculature 9
  - 2.1.3 Endothelial Cell (EC) Function in Microvessels 9
  - 2.1.4 Regulation of Blood Flow and Tissue Perfusion 12
- 2.2 Soft Tissue 12
  - 2.2.1 Musculoskeletal System 12
  - 2.2.2 Muscle 13
  - 2.2.3 Vascular Supply and Microcirculation in Skeletal Muscle 17
- 2.3 Traumatic Injuries 21
  - 2.3.1 Clinical Relevance 22
  - 2.3.2 Soft Tissue Injuries 23
  - 2.3.3 Non-Penetrating Traumatic Injuries (NPTIs) 24
  - 2.3.4 Microvascular Traumatic Injuries 30
- 2.4 Current Approaches in Traumatic Injury Research 31
  - 2.4.1 Clinical and Epidemiological Approaches 31
  - 2.4.2 Experimental Approaches 32
- 2.5 Tissue Engineering (TE) 33
  - 2.5.1 TE Components 35
  - 2.5.2 TE Scaffolds and Constructs: Design, Fabrication and Biomaterial Selection 42
  - 2.5.3 Microvascular *In Vitro* Models 52
- 2.6 Research Gaps 58

3 Development and Optimisation of Hydrogel Scaffolds for Microvascular Network Formation 59
- 3.1 Introduction 60
- 3.2 Materials & Methods 62
  - 3.2.1 Cell Culture 62
  - 3.2.2 Fabrication of Hydrogels 62
  - 3.2.3 Cell Proliferation 63
  - 3.2.4 Cell Adhesion 63
  - 3.2.5 Cell Migration 63
  - 3.2.6 Cell Viability 63
  - 3.2.7 Hydrogel Consistency 64
  - 3.2.8 Tube Formation 64
  - 3.2.9 Statistical Analysis and Software 65
- 3.3 Results 65
  - 3.3.1 Cell Proliferation by Seeding Density 65
  - 3.3.2 Cell Adhesion 66

3.3.3 Cell Migration 67
3.3.4 Selection of Hydrogel Compositions Based on Cell Adhesion and Migration Rate 70
3.3.5 Cell Viability 70
3.3.6 Hydrogel Consistency 72
3.3.7 Further Selection of Hydrogels Based on Cell Viability and Hydrogel Shape Retention 73
3.3.8 Tube Formation 73
3.4 Discussion 75
3.5 Conclusion 78

4 Fibrin Scaffolds for Angiogenesis in Soft Tissue Models: A Systematic Review 79
4.1 Introduction 81
4.2 Methodology 83
4.2.1 Eligibility Criteria and Study Design 83
4.2.2 Search Strategy 85
4.2.3 Study Selection Process 85
4.2.4 Methods for Data Extraction 86
4.2.5 Strategy for Data Synthesis 87
4.2.6 Risk of Bias (RoB) Assessment 88
4.2.7 Quality Assessment 88
4.2.8 Software 88
4.3 Results 89
4.3.1 Study Selection 89
4.3.2 Overview of the Corpus 90
4.3.3 Fibrin Scaffold Composition: Influence on Successful Endothelial Formation and Migration Processes (EFMPs) 91
4.3.4 Cell Lines and *In Vivo* Models 95
4.3.5 Manufactured Objects and Features 98
4.3.6 Assays Used to Evaluate Endothelial Formation and Migration Processes (EFMPs) 101
4.3.7 Fibrin Tissue Engineering (TE) Scaffolds for Muscle Research 103
4.3.8 Risk of Bias (RoB) and Quality Assessment 105
4.4 Discussion 106
4.5 Conclusion 110

5 Engineering a Long-lasting Microvasculature *In Vitro* Model for Traumatic Injury Research 112
5.1 Introduction 113
5.2 Materials & Methods 115
5.2.1 Cell Culture 115
5.2.2 Comparing HUVECs and MVECs: Morphology & Cell Migration 116
5.2.3 Hydrogel Fabrication 116
5.2.4 Influence of Hydrogel Composition on Endothelial Network: Architecture & Integrity 117
5.2.5 Material Characterisation 117
5.3 Results & Discussion 120
5.3.1 Comparing HUVECs and MVECs 120
5.3.2 3D Hydrogel Constructs with MVECs Enable Successful Endothelial Network Formation 124
5.3.3 Influence of Hydrogel Composition on Endothelial Network: Architecture & Integrity 125
5.3.4 Material Characterisation 129
5.3.5 Developing a Microvascular Construct for Long-term Network Integrity 135
5.3.6 Impact of Hydrogel Composition on Network Architecture and Material Characteristics: Key Results 138
5.4 Conclusion 139

6 Modelling Non-Penetrating Traumatic Injuries in Engineered 3D Microvascular Constructs 140
6.1 Introduction 142
6.2 Materials and Methods 145
6.2.1 Cell Culture 145

6.2.2 Hydrogel Fabrication 145
6.2.3 3D Hydrogel Construct Optimisation 145
6.2.4 Live Imaging for Network Morphogenesis in Hydrogels 146
6.2.5 Mechanical Characterisation: Compressive Loading of Acellular Hydrogels 147
6.2.6 *In Vitro* Modelling of Non-Penetrating Traumatic Injuries (NPTIs) Using Cell- and Network-Embedded Constructs 147
6.2.7 Biocompatibility Evaluation of 3D-Printed Objects 148
6.2.8 Crush Injury 150
6.2.9 Contusion Injury 150
6.2.10 Strain Injury 150
6.2.11 Conditioned Media 152
6.2.12 Image Analysis 153
6.2.13 Statistical Analysis and Software 154
6.3 Results & Discussion 154
6.3.1 Optimisation of Hydrogel Constructs 154
6.3.2 Live Imaging for Network Morphogenesis in Hydrogels 156
6.3.3 Mechanical Characterisation: Compressive Loading of Acellular Hydrogels 160
6.3.4 Biocompatibility Evaluation of 3D-Printed Objects 162
6.3.5 Crush Injury 164
6.3.6 Contusion Injury 166
6.3.7 Strain Injury 167
6.3.8 Conditioned Media 169
6.4 Conclusion 176

7 Conclusions & Future Directions **177**
7.1 Fulfilment of Thesis Aims and Objectives 178
7.2 Positioning of the Work Within the Field 179
7.3 Novelty and Contributions of the Thesis 180
7.4 Limitations 181
7.5 Further Development & Future Work 182
7.6 Concluding Remarks 182

Bibliography **183**

Appendix A Supplementary Materials for Chapter 3 **211**

Appendix B Supplementary Materials for Chapter 4 **213**

Appendix C Detailed Search Strategies Used per Database, displaying the number of records found on 28 October 2024 in PubMed, Scopus and OVID **229**

Appendix D Minimum Information for Fibrin Scaffold Experiments (MIFSE) Checklist **230**

Appendix E Supplementary Materials for Chapter 5 **231**
E.1 Effect of Crosslinking Ratios on Hydrogel Consistency 244
E.1.1 Materials & Methods 244
E.1.2 Key Results 244

Appendix F Supplementary Materials for Chapter 6 **247**

List of Figures

1.1 Schematic overview of the thesis structure. 6

2.1 Vessels of the circulation, shown in the direction of blood flow. 8
2.2 Architecture of a microvascular bed. 10
2.3 Schematic illustration of capillary cross-sections with continuous and fenestrated walls. 11
2.4 Histological comparison of skeletal, cardiac and smooth muscle. 14
2.5 Hierarchical organisation of skeletal muscle. 16
2.6 Skeletal muscle classification based on its blood supply. 17
2.7 Schematic representation of a microvascular unit (MVU) in skeletal muscle. 18
2.8 Schematic illustration of skeletal muscle vascular architecture. 19
2.9 Longitudinal section of skeletal muscle. 20
2.10 Traumatic injury classification. 22
2.11 Leading 25 Level 3 causes of global disability-adjusted life years (DALYs), 1990–2019. 23
2.12 Types of vascular injury caused by traumatic mechanisms. 30
2.13 Schematic representation of tissue engineering (TE) strategies. 34
2.14 Tissue engineering (TE) triad. 35
2.15 Tissue engineering (TE) construct design strategies. 44
2.16 Hydrogel classification by crosslinking method. 46
2.17 Schematic illustration of the hierarchical organisation of collagen and gelatine. 49
2.18 Schematic representation of fibrinogen structure and fibrin assembly. 51
2.19 Schematic illustration of the fabrication methods and features of 3D *in vitro* microvessel models, by category. 53
2.20 Schematic illustration of microfluidic devices as microvessel models. 55
2.21 Schematic illustration of microvessel fabrication using templating techniques. 56
2.22 Schematic illustration of microvessel models fabricated using 3D printing. 57
2.23 Schematic illustration of microvessel models formed by self-organisation. 58

3.1 Schematic illustration of microvascular segments. 64
3.2 Cell proliferation as fold expansion of the initial cell seeding number, at 24 and 48 h. 65
3.3 Cell adhesion as a fold expansion of the cells-only control, by coating and concentration. 66
3.4 Average migration rate (mm/h) as fold expansion of the control, by hydrogel composition. 67
3.5 Closure of the gap area in a HUVEC monolayer over time. 68
3.6 Gap area (mm^2) in a HUVEC monolayer over time (h) by hydrogel composition. 69
3.7 Overview of the performance of the different hydrogel compositions. 70
3.8 Cell viability (%) by hydrogel composition. 71
3.9 Overview of the performance of the different hydrogel compositions. 72
3.10 Tube formation on fibrin in EBM at 3% *w/v*. 73

4.1 PRISMA flow diagram of the study selection process. 89
4.2 Overview of the corpus of included articles in the systematic review (SR; n = 81). 90
4.3 Impact of scaffold formulation on angiogenic outcomes. 92
4.4 Endothelial and non-endothelial cell lines used. 96
4.5 *In vivo* models used. 98
4.6 Tissue engineering (TE) scaffolds successfully supporting endothelial formation and migration processes (EFMPs), categorised by type of manufactured object. 99
4.7 Assays used to evaluate endothelial formation or migration processes (EFMPs). 102
4.8 Fibrin tissue engineering (TE) scaffolds for muscle research. 103
4.9 Risk of bias (RoB) and quality assessment. 105

5.1 Constitutive elements of the endothelial network. 118

5.2 Comparing human umbilical vein endothelial cells (HUVECs) and human dermal microvascular endothelial cells (MVECs). ... 121
5.3 Endothelial network characterisation of HUVECs or MVECs in MES/NaCl or EBM hydrogels using bovine fibrin hydrogel (4 mg/mL), at 3– and 4–days post-seeding. ... 123
5.4 Characterisation of endothelial networks. ... 125
5.5 Impact of variations in fibrinogen concentration and medium on microvascular endothelial network architecture. ... 126
5.6 Impact of variations in crosslinking ratio on microvascular endothelial network architecture. ... 127
5.7 Impact of variations in medium and crosslinking ratio on microvascular endothelial network architecture. ... 128
5.8 Material characterisation of the 3D hydrogel constructs. ... 130
5.9 Degradation of hydrogel scaffolds by fibrinogen source, concentration and medium during a period of 14 days. ... 134
5.10 Optimisation of a microvascular construct for long-term network integrity. ... 137

6.1 Dog-bone hydrogel fabrication process for strain injury induction. ... 151
6.2 Visual classification of hydrogel consistency with and without foetal bovine serum (FBS). ... 155
6.3 Visual classification of hydrogel consistency two days after casting. ... 155
6.4 Phase 1 live-imaging analysis of total occupied area in MVEC-containing hydrogels over 72 h. ... 157
6.5 Phase 2 live-imaging analysis of total occupied area in MVEC-containing hydrogels over 50 days. 158
6.6 Phase 2 live-imaging analysis of tube-like structure count in MVEC-containing hydrogels over 50 days. ... 159
6.7 Phase 2 live-imaging analysis of average object eccentricity in MVEC-containing hydrogels over 50 days. ... 160
6.8 Mechanical response of fibrin hydrogels under compressive loading. ... 161
6.9 Standard curve relating MVEC number to PrestoBlue absorbance. ... 163
6.10 Resin-conditioned media effects on MVECs over 14 days, with estimated cell number. ... 164
6.11 Incremental strain following crush injury in MVEC-containing hydrogels. ... 165
6.12 Maximum extension to failure following crush injury in MVEC-containing hydrogels. ... 165
6.13 Incremental strain components following strain injury in MVEC-containing hydrogels. ... 167
6.14 Total strain as a function of displacement during strain injury. ... 168
6.15 Change in endothelial network confluence following strain injury. ... 168
6.16 Impact of exposure to conditioned media from crush and contusion injury models on MVEC viability. ... 169
6.17 Effects of trauma-conditioned media on MVEC viability. ... 170
6.18 Representative images of MVECs exposed to contusion injury–conditioned media, captured 2 h after live/dead staining (72 h post-exposure to conditioned media). ... 172
6.19 Representative images of MVECs exposed to conditioned media from crush injury-EBM hydrogels. 173
6.20 Representative images of MVECs exposed to conditioned media from crush injury-EBM + VEGF hydrogels. ... 174
6.21 Representative images of MVECs exposed to control media. ... 175

A.1 Cell adhesion as a fold expansion of the cells-only control, by coating and concentration. ... 211
A.2 Cell viability (%) by hydrogel composition. ... 212

B.1 Visual representation of the number of records found in each database when independently searching for each of the four search query components: ‘Soft Tissue’, ‘Microvascular Structures and/or Network’, ‘Tissue Engineering Scaffolds’, and ‘Fibrin’. ... 213
B.2 Systematic review (SR) screening decisions. ... 213
B.3 Aggregated success rates (%) and number of scaffolds used for success rate calculations (n) of fibrin scaffold design parameters. ... 214
B.4 Materials used in combination with fibrin, coagulants and crosslinkers. ... 215
B.5 Features associated with the manufactured objects used in the corpus. ... 216
B.6 Roadmap for fibrin scaffolds from reproducible scaffold design to clinical application. ... 217

E.1 Schematic illustration of gelation determination. ... 231

E.2 Overview of the process to measure pendant drop tensiometry. 231
E.3 Photograph of gelled sample with tracer solution. 232
E.4 Schematic illustration of the shearing process. 232
E.5 Endothelial network characterisation of HUVECs and MVECs in MES/NaCl hydrogels. 232
E.6 Endothelial network characterisation of HUVECs and MVECs in MES/NaCl or EBM hydrogels. 233
E.7 Endothelial network characterisation of HUVECs and MVECs in EBM hydrogels. 234
E.8 Depth visualisation of MVEC-embedded hydrogels at 24 h post-seeding. 235
E.9 Total network length by fibrinogen concentration, at 2 and 24 h. 235
E.10 Total network length by fibrinogen : thrombin : $CaCl_2$ crosslinking ratio for MVECs, quantified every hour during a 24 h period. 236
E.11 Total HUVEC network length quantified every hour during a 24 h period. 236
E.12 Impact of variations in medium and crosslinking ratio on microvascular endothelial network architecture. 237
E.13 Spectrophotometry absorbance plots showing the normalised change in 340 nm light absorbance for 20 min. 237
E.14 Microrheology characterisation. 238
E.15 Interfacial tension values from pendant drop tensiometry. 239
E.16 Dendrite alignment. 239
E.17 Microscopy images of hydrogel samples. 240
E.18 Characterisation of MVEC networks by medium and fibrinogen concentration, quantified throughout a period of 53 h. 241
E.19 MVEC network characterisation at 4-, 5- and 6-days post-seeding by fibrinogen concentration and medium. 242
E.20 Total network length by medium, fibrinogen concentration and crosslinking ratio (fibrinogen : thrombin : $CaCl_2$) as fold expansion of the control, quantified throughout 13 days. 243
E.21 Representative photographs of hydrogel scaffolds 12 days after casting and 1 h after demoulding. 245
E.22 Classification based on the visual inspection of hydrogel consistency and shape retention 12 days after hydrogel casting. 246

F.1 Experimental setup for compressive testing of fibrin hydrogels. 247
F.2 Compressive loading profile of fibrin hydrogel over a single cycle. 247
F.3 3D-printed container and lid design for resin biocompatibility assessment. 248
F.4 Contusion injury model for three-dimensional (3D) microvascular constructs. 248
F.5 Custom tensile loading device used to apply a strain injury. 249
F.6 Effect of FBS on early endothelial cell morphology in hydrogels. 249
F.7 Representative photographs of fibrin hydrogel constructs. 251
F.8 Representative photographs of fibrin hydrogel constructs cast in 24-well plates. 251
F.9 Representative photographs of fibrin hydrogel constructs cast in 12-well plates. 252
F.10 Representative photographs of fibrin hydrogel constructs cast in 6-well plates. 252
F.11 Impact of cell seeding density on fibrin hydrogel constructs: 2.5×10^3, 7.5×10^3 and 1.25×10^4 seeding densities. 253
F.12 Impact of cell seeding density on fibrin hydrogel constructs: 1.75×10^4, 2.25×10^4 and 2.75×10^4 seeding densities. 254
F.13 Impact of cell seeding density on fibrin hydrogel constructs: 3.25×10^4, 3.75×10^4 and 4.25×10^4 seeding densities. 255
F.14 Impact of cell seeding density on fibrin hydrogel constructs: 4.75×10^4, 5.25×10^4 and 5.75×10^4 seeding densities. 256
F.15 Photographs of plate containing hydrogel constructs embedded with MVECs, taken at 21, 28, 48, 56, 63 and 70 days post-seeding. 257
F.16 Phase 1 live-imaging analysis of endothelial cells and tube-like structures count in MVEC-containing hydrogels over 72 h. 257
F.17 Phase 1 heatmap of average object eccentricity in MVEC-containing hydrogels over 72 h. 258
F.18 3D-printed containers and lids fabricated with three resin materials. 258
F.19 Resin-conditioned media effects on MVECs over 14 days, relative to controls. 259
F.20 Photograph of 3D hydrogel construct undergoing strain injury. 259

List of Tables

2.1 Blood vessel characteristics: veins and venules. 8
2.2 Blood vessel characteristics: arteries, arterioles and capillaries. 9
2.3 Soft tissue types: structural characteristics and effects. 13
2.4 Functional comparison of muscle types: skeletal, cardiac and smooth. 15
2.5 Bioactive Factors and Signals in Tissue Engineering (TE) and their roles in various tissues. 41
2.6 Tissue engineering (TE) scaffold fabrication methods overview. 45
2.7 Properties of synthetic and natural hydrogel-forming polymers. 48
2.8 Examples of selected microvessel models, by category. 54

3.1 Characterisation of networks formed by HUVECs when embedded in fibrin in EBM hydrogels at both 3 and 5% *w/v* concentrations. 74

5.1 Summary of hydrogel composition variations explored. 117
5.2 Summary of the impact on microvascular endothelial cell (MVEC) network architecture and material characteristics of variations in the hydrogel composition. 138

6.1 Well sizes and hydrogel volumes (µL) used for construct preparation. 146
6.2 Cell seeding densities used to generate the standard curve relating fluorescence to cell number. 148
6.3 Washing and curing parameters used for post-processing of 3D printed objects. 149
6.4 Summary of experimental and control media used for resin biocompatibility assessment. 149
6.5 Conditioned media groups. 152

B.1 Articles excluded during the 2nd screening round (full-text screening). 217
B.2 Studies included in the corpus (*n* = 81). 218
B.3 Overview of key study details highlighting the heterogeneity of the corpus. 220
B.4 Overview of the key scaffold formulation details, highlighting the heterogeneity of the corpus. .. 222
B.5 Fibrinogen, coagulant and crosslinker formulations used in the corpus. 224
B.6 Polymers, both natural and synthetic, used in fibrin scaffolds. 226
B.7 Growth factors, peptides, amino acids and enzymes (GF/P/AA/E) used in fibrin scaffolds. 226
B.8 Cell media & solutions used in fibrin scaffolds. 227
B.9 Chemicals used in fibrin scaffolds. 227
B.10 Other materials used in fibrin scaffolds. 227
B.11 Composition of modified cell media used for fibrin scaffolds. 228

F.1 Well size and hydrogel volume (µL) used for construct fabrication, with resulting hydrogel height (mm). 250

Abbreviations

3D Three-dimensional

ANOVA Analysis of Variance

bFGF Basic Fibroblast Growth Factor

CAMARADES Collaborative Approach to Meta-Analysis and Review of Animal Data from Experimental Studies

DALY(s) Disability-adjusted Life Year(s)

DMEM Dulbecco's Modified Eagle Medium

EBM Endothelial Cell Basal Medium

EBM + VEGF Endothelial Cell Basal Medium Supplemented with VEGF

EC(s) Endothelial Cell(s)

ECM Extracellular Matrix

EFMP(s) Endothelial Formation and Migration Process(es)

EGM Endothelial Cell Growth Medium

EPC(s) Endothelial Progenitor Cell(s)

FBS Foetal Bovine Serum

FGF Fibroblast Growth Factor

FTE Functional Tissue Engineering

GF/P/AA/E Growth Factors, Peptides, Amino Acids and Enzymes

GFP Green Fluorescent Protein

HDMEC-1(s) Human Dermal Microvascular Endothelial Cell(s)

HIF Hypoxia-inducible Factor

HSD Honest Significant Difference

HUVEC(s) Human Umbilical Vein Endothelial Cell(s)

IGF Insulin-like Growth Factor

iPSC(s) Induced Pluripotent Stem Cell(s)

LMIC(s) Low- and Middle-income Country (Countries)

LS Linear Segment

LSD Least Significant Difference

MeSH Medical Subject Headings

MIFSE Minimum Information for Fibrin Scaffold Experiments

MSC(s) Mesenchymal Stem Cell(s)

MVEC(s) Microvascular Endothelial Cell(s)

MVU(s) Microvascular Unit(s)

Non-EC(s) Non-Endothelial Cell(s)

NPTI(s) Non-penetrating Traumatic Injury (Injuries)

OSF Open Science Framework

PAOEC(s) Porcine Aortic Endothelial Cell(s)

PBS Phosphate-Buffered Saline

PDGF Platelet Derived Growth Factor

PEG Polyethylene Glycol

PRF Platelet-rich Fibrin

PRISMA Preferred Reporting Items for Systematic Reviews and Meta-Analyses

PROSPERO International Prospective Register of Systematic Reviews

PS Primary Segment

RFP Red Fluorescent Protein

RoB Risk of Bias

SMC(s) Smooth Muscle Cell(s)

SR Systematic Review

SYRCLE Systematic Review Centre for Laboratory Animal Experimentation

TE Tissue Engineering

TGF-α Transforming Growth Factor Alpha

TGF-β Transforming Growth Factor Beta

VEGF Vascular Endothelial Growth Factor

YLDs Years of Healthy Life Lost Due to Disability

YLLs Years of Life Lost Due to Premature Mortality

w/v Weight/Volume

Chapter 1
Introduction

1.1 Background & Motivation

Traumatic injuries are one of the most pressing yet neglected [1] health concerns globally [2]. They are a major cause of mortality and morbidity worldwide, accounting for a significant proportion of not only deaths but also long-term disabilities across all age groups [3]. Such injuries occur throughout life, from childhood and young adulthood to older adulthood, and arise in diverse scenarios such as sports, motor vehicle incidents, other accidents, and falls.

Globally, traumatic injuries account for approximately 8% of deaths each year [4, 5]. In 2024 alone, injuries were responsible for 4.4 million deaths [5]. Falls account for over 684,000 deaths annually, and this number continues to rise [5]. For people aged 5–29 years, three of the five leading causes of death are injury-related [5]. Importantly, the health consequences extend beyond the acute event, with evidence showing a sustained increase in mortality risk years after the initial injury [4, 6].

The burden of traumatic injuries falls disproportionately on low- and middle-income countries (LMICs), where over 90% of deaths and disabilities from injuries occur [5, 7]. In these regions, injury mortality rates are higher than in high-income countries [5], with risk further amplified in settings affected by armed conflicts or natural disasters. In 2020, injuries accounted for 20% of the global disease burden [5], underscoring the significant impact on public health [8].

This inequity is shaped by multiple factors. People in low-resource settings, whether in LMICs or high-income countries, are more likely to live, work, travel, and study in precarious conditions, and access to quality trauma care and rehabilitation services is often limited [5]. No demographic or setting is immune to traumatic injuries. What differs, however, is the capacity to prevent and treat injuries. Preventive policies such as road signage, traffic law enforcement, seatbelt use, and speed restrictions can mitigate risk [1]. Nevertheless, while prevention is crucial, it cannot eliminate traumatic injuries altogether.

Injuries are not only a leading cause of death [9] but also a major cause of functional limitations [10]. Major trauma can also lead to prolonged disability and life-threatening complications such as sepsis [11], multiple-organ dysfunction syndrome [2], and opportunistic infections [2, 9, 11, 12]. Critically, half of trauma-related deaths occurring within the first 48 h of hospital admission result from uncontrolled haemorrhage [13, 14], making this an urgent concern and underscoring the need for early intervention. Despite improvements in in-hospital survival, longitudinal studies reveal that post-discharge mortality increased 2.7% in cumulative deaths despite a 3.1% reduction in hospital fatalities [4].

Injury responses depend on both severity and available resources. While minor injuries may heal on their own or with first aid, more severe trauma often requires intensive medical interventions, including physiotherapy and surgery. In life-threatening situations, the primary goal is preserving life, achieved by prioritising the most severe and critical injuries [15]. Consequently, widespread injuries may be overlooked, particularly those affecting the microvasculature [16]. These apparently minor injuries can worsen over time, potentially leading to systemic complications such as multiple-organ failure [17, 18].

Damage to skeletal muscle and its microvasculature can impair quality of life [10]. Skeletal muscle tissue loss compromises locomotion and support [19], while microvascular injury exacerbates tissue damage and can trigger a dysregulated inflammatory response, progressing to multiple-organ failure [17, 18]. Mechanical

contusion to the microvasculature interrupts blood flow, preventing oxygen and nutrient delivery, and induces systemic physiological effects that worsen injury and impair tissue repair [20].

Beyond the direct health effects, traumatic injuries have substantial economic and social consequences. Injury-related disability also creates financial strain, particularly in contexts with underdeveloped trauma care and rehabilitation systems. This burden is further augmented when there is little or no social welfare infrastructure [8]. As a result, traumatic injuries can perpetuate cycles of poverty: these economic constraints can further limit access to care and negatively impact the likelihood of full recovery, with lasting consequences for individuals, families, and communities [7].

Despite the frequency of non-penetrating traumatic injuries (NPTIs), the biological mechanisms underlying tissue damage remain poorly understood [21]. This knowledge gap limits the development of effective acute interventions and therapeutic strategies. While advances and innovations in medical care and bioengineering have improved both survival and quality of life for trauma patients, further progress requires a deeper mechanistic understanding. In particular, there is an urgent need to understand how NPTIs affect vascularised soft tissues. Skeletal muscle, which represents nearly 40% of human body mass and is highly vascularised [19], is one of the most frequently injured tissues in blunt force and crush trauma.

Trauma research encompasses a range of approaches, from descriptive clinical observations and epidemiological studies to the use of animal models and, more recently, *in vitro* systems based on tissue engineering (TE). This progression reflects an increasing emphasis on mechanistic understanding and controlled experimental approaches. Physical trauma involves complex biological responses that demand reliable models to study both initial damage and subsequent healing and regenerative processes [14].

However, directly studying immediate and short-term consequences in patients remains extremely difficult. Trauma incidents are unpredictable, and many patients delay or do not seek timely medical attention, often due to recognition difficulties or logistical barriers [22]. Even when they do, the critical early window after injury is rarely observed because of the inevitable delay between injury and medical care. This means that the period immediately and shortly after trauma, which is critical for understanding mechanobiological responses, is almost never directly observed in humans [23]. Moreover, ethical constraints prevent controlled trauma studies in humans, making early mechanobiological events, which dictate injury severity and recovery, difficult to study.

Consequently, trauma research requires experimental platforms that go beyond clinical observation to elucidate injury mechanisms at the tissue level. In particular, using these platforms in controlled settings would enable researchers to isolate the impact of specific variations in trauma characteristics and establish patterns of injury.

Current understanding of traumatic injuries largely derives from clinical observations, including patient monitoring, epidemiological studies, and the analysis of clinical biomarkers [14, 24–26]. While essential, these approaches provide limited insights into the immediate tissue-level consequences of trauma. Moreover, they do not involve mechanical or biochemical perturbations in a controlled environment, so understanding the damage these provoke without being confounded by systemic effects is very challenging. Capturing the short-term responses to injuries in human patients is inherently difficult, as trauma occurs unpredictably; patients often present with delays driven by logistical, behavioural, or diagnostic factors; and ethical constraints restrict the types of studies that can be conducted [22, 23, 27], leaving key aspects of early injury mechanisms insufficiently characterised.

These challenges have been partly addressed by using *in vivo* models, including rats, mice [28–30], pigs [25, 31], and non-human primates [32, 33]. *In vivo* studies have examined key injury-related processes such as endothelial cell (EC) dysfunction, apoptosis, vascular leakage, and systemic inflammatory activation [24–26, 34].

For instance, blunt force trauma [35] and haemorrhagic shock [26] have been studied to characterise injury mechanisms and evaluate potential therapeutics.

However, the translation of these insights to humans remains limited by interspecies physiological and pathophysiological differences, ethical concerns, and reproducibility challenges [14,36]. Similarly, *ex vivo* models, such as excised tissues, are limited by restricted viability and do not permit controlled manipulation of injury parameters over extended periods. Thus, while *in vivo* and *ex vivo* models have provided valuable insights, their limitations underscore the need for alternative approaches.

Consequently, there is a growing need for physiologically relevant *in vitro* platforms that enable reproducible, ethically acceptable, and finely controlled investigation of soft tissue trauma, with advantages in cost, throughput, and experimental precision [36]. *In vitro* models represent a promising alternative, offering a controlled environment in which specific injury mechanisms can be studied systematically. However, most current *in vitro* systems fail to replicate the microvascular component of soft tissues, which is critical for injury response, tissue repair, and regeneration.

To improve outcomes for trauma patients, tools and models for exploratory research and preclinical testing of interventions are required. Physiologically relevant *in vitro* models could capture immediate and short-term consequences of trauma in controlled environments, avoiding the ethical and translational limitations of *in vivo* studies.

A central challenge in developing physiologically relevant *in vitro* models is engineering microvascular networks [37] within the constructs. The microvasculature is essential for homeostasis, metabolism, immune responses, and regeneration [17, 38, 39], and its absence in most TE constructs restricts size, limits physiological fidelity, and reduces relevance, particularly in skeletal muscle [37, 40, 41]. Most TE constructs lack microvascular structures or networks, relying instead on diffusion for oxygen and nutrient delivery [37,40].

Embedding microvascular networks within engineered tissues would sustain metabolic demand, enable the development of larger and more physiologically relevant constructs, and improve translational potential. The use of human cell lines further enhances clinical relevance, enabling the investigation of injury mechanisms and therapeutic strategies.

Developing such *in vitro* models would allow researchers to explore immediate and short-term consequences of trauma in a controlled setting without relying on clinical markers and manifestations in patients, and avoiding the ethical and translational constraints of *in vivo* studies. A successful soft tissue microvasculature platform could provide mechanistic insights while laying the foundation for preclinical testing of interventions to mitigate injury and enhance tissue repair and regeneration.

Beyond their immediate clinical relevance, physiologically relevant *in vitro* models have broader implications. Advances in biomaterials, microfabrication, and TE now make it possible to design three-dimensional (3D) constructs that closely mimic the architecture and function of native tissues. These models can serve not only as research tools for mechanistic studies but also as platforms for drug testing, device evaluation, and personalised medicine. Moreover, they advance the field of trauma-relevant TE by providing platforms that integrate vascular and soft tissue components, enabling quantitative and mechanistic studies of injury and repair.

The motivation behind this research lies in bridging the translational gap in NPTI research. There is a lack of microvascular preclinical models developed for studying traumatic injuries. Such models are essential for dissecting the mechanobiological processes that occur during the minutes to hours immediately after trauma, a critical window that determines the extent of tissue damage and influences recovery and outcomes. Ultimately, a successful *in vitro* microvascular model for NPTIs could reduce reliance on animal models, accelerate translational research, and provide novel insights into tissue damage and repair.

From this background emerges a central research question: 'How can physiologically and mechanobiologically relevant *in vitro* models of soft tissue microvasculature be developed and optimised to enable the study of NPTIs and improve understanding of the immediate and short-term consequences of trauma?'

1.2 Aims & Objectives

With this in mind, this thesis aims to develop and optimise a 3D *in vitro* microvascular model based on natural polymer scaffolds incorporating physiologically relevant cells, and to apply this model to investigate the microvascular consequences of NPTIs under controlled mechanical loading conditions during the immediate and short-term post-injury period. The research focuses specifically on contusion, strain, and crush injuries. To this end, a 3D construct incorporating an embedded microvasculature is developed and then used to study the microvascular consequences of soft tissue injury. To achieve this aim, four specific objectives are proposed:

1. Develop and optimise a natural polymer–based scaffold capable of supporting EC adhesion, viability, migration, and the formation of microvascular networks *in vitro*.
2. Systematically review and critically evaluate the existing literature on soft tissue scaffolds used in TE fabricated with the natural polymer identified in Objective 1, with a particular focus on identifying scaffold design parameters that lead to successful endothelial formation and migration processes (EFMPs) (*i.e.* tube formation, network formation, and cell migration).
3. Develop, optimise, and characterise a long-lasting (*i.e.* multi-day) 3D *in vitro* microvascular model incorporating a physiologically relevant cell type, capable of maintaining microvascular network integrity beyond 24 h and of extending observations past the immediate and short-term period following network formation.
4. Demonstrate proof of concept for the application of the developed 3D microvascular model as an *in vitro* platform for NPTIs, enabling systematic investigation of the relationships between defined mechanical inputs and microvascular damage.

Beyond the scope of this thesis, the long-term vision is for the model to serve as a platform for evaluating acute interventions aimed at enhancing tissue repair and regeneration. In the future, patient-specific versions of this model could facilitate preventive therapeutics and precision medicine. Importantly, the model also provides a means to generate quantitative insights into how defined mechanical inputs translate into patterns of tissue damage, representing a novel contribution to the fields of trauma mechanobiology and TE. In the longer term, this work could open entrepreneurial pathways to enable widespread adoption of this model.

1.3 Scope & Structure of This Thesis

This thesis is limited to the development, optimisation, and validation of an *in vitro* 3D model with embedded microvasculature for the study of NPTIs. This research does not attempt to replicate the full complexity of traumatic injuries, which also involve immune responses, systemic circulation, and multiple-organ interactions. Instead, the focus is on capturing the mechanisms of injury to soft tissue microvasculature under controlled injury conditions.

The scope is therefore restricted to hydrogel scaffold development, endothelial network formation, and the induction and characterisation of contusion, strain, and crush injuries *in vitro*. Long-term consequences of trauma as well as therapeutic testing are beyond the remit of this work, though the models developed could provide a foundation for such applications in future research.

While this thesis focuses predominantly on soft tissue, including skeletal muscle, the underlying principles are not limited to this tissue type. Although tissue-specific variations in cellular composition and biomechanical properties exist, the 3D model developed as part of this research could be adapted to other tissues by, for example, incorporating relevant cell types and extracellular matrix (ECM) components. This would extend the applicability of the model to a broader range of soft tissues, with mechanically active organs such as the lung and heart, as well as highly perfused organs like the liver and brain, presenting particularly promising targets for adaptation.

This thesis consists of seven chapters (Figure 1.1), centred on three experimental chapters and a systematic review (SR). Chapter 1 introduces the rationale behind this research, as well as the aims, objectives, scope, and structure of this thesis. Chapter 2 comprises a literature review on microvascular and soft tissue anatomy and physiology; traumatic injuries, specifically contusion, strain, and crush injuries; and TE advances in microvascular *in vitro* models.

Chapter 3 focuses on the development and optimisation of hydrogel scaffolds for microvascular network formation. This chapter aims to identify the hydrogel composition best suited for ECs in terms of cell adhesion, migration rate, cell viability, hydrogel consistency and shape retention, and tube formation. Chapter 4 presents a SR on TE fibrin scaffolds for angiogenesis, with a focus on their application in soft tissues and their capacity to support endothelial network formation. Chapter 5 builds on the optimised hydrogel composition, addressing the development of a long-lasting *in vitro* microvascular model using a microvascular endothelial cell (MVEC) line. This chapter covers 3D construct development, optimisation, and characterisation in terms of material properties and endothelial network architecture. Chapter 6 targets the induction of NPTIs on the 3D microvascular construct, aiming to determine the relationship between physical inputs and resulting damage.

Finally, Chapter 7 presents the key results and conclusions from this work, highlighting the novelty and contributions of this research to the fields of TE and mechanobiology. It also summarises the strengths and limitations of this research, proposes potential applications for the 3D microvascular model beyond NPTI research, and outlines future directions to further advance the field.

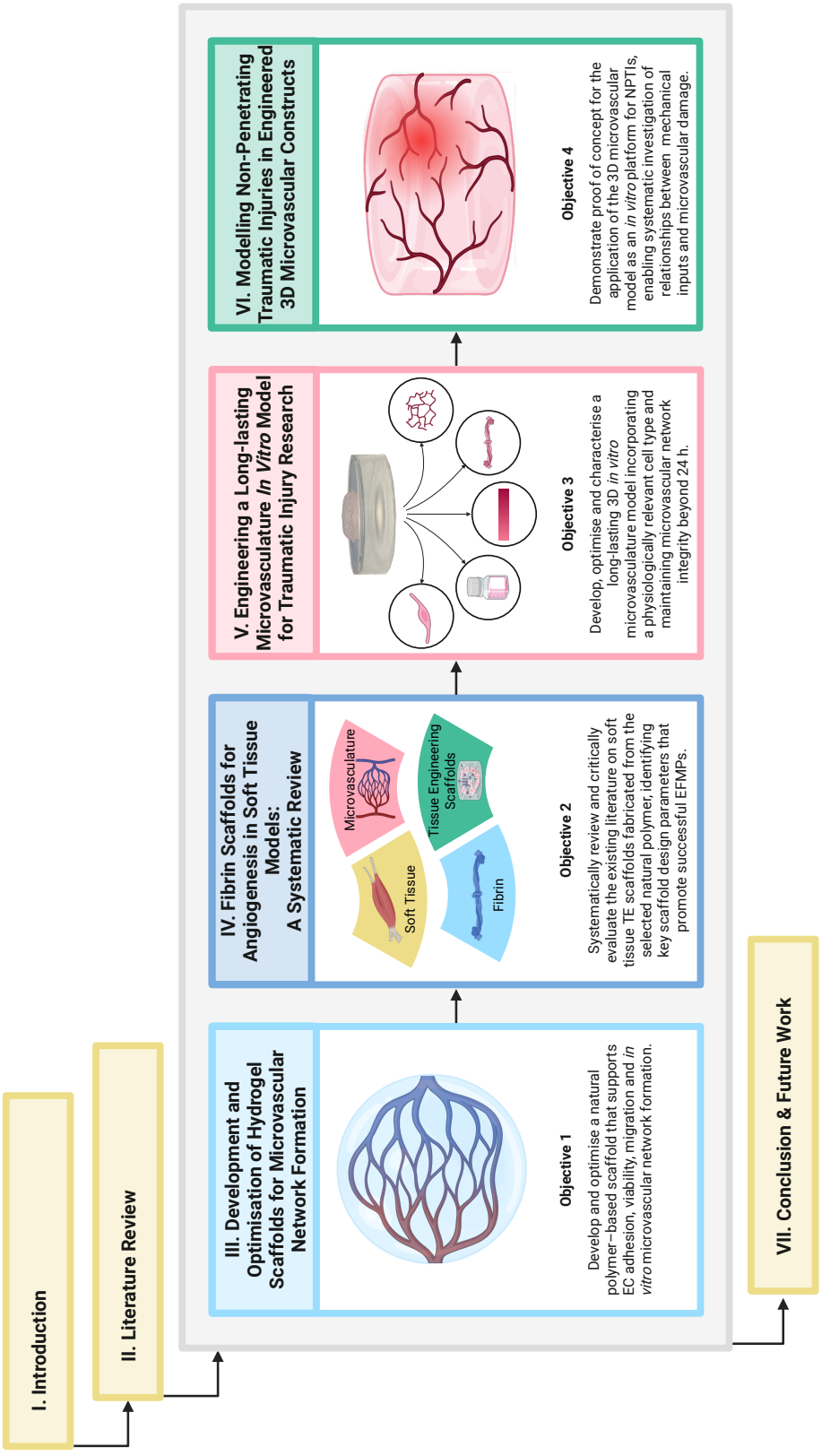


Figure 1.1: **Schematic overview of the thesis structure**, illustrating the seven chapters that constitute this work and the specific objectives addressed by each of the four core thesis chapters. EC: endothelial cell; EFMPs: endothelial formation and migration processes (*i.e.* tube formation, network formation, and cell migration); NPTIs: non-penetrating traumatic injuries; TE: tissue engineering.

Chapter 2
Literature Review

Thesis Integration and Chapter Structure

This chapter establishes the conceptual and scientific foundation upon which the experimental work of the thesis is built. It begins by framing the microvasculature within the broader context of the cardiovascular system, exploring its structural organisation, endothelial cell (EC) function and the regulation of blood flow in tissue perfusion. The focus then shifts to soft tissues, with a particular emphasis on skeletal muscle as a highly vascularised and frequently injured tissue in contusion, crush and strain injuries. The anatomy, physiology and vascular supply of muscle are examined, alongside the processes of injury and repair, to establish the human physiological framework under normal and injured conditions. The chapter then turns to trauma itself, outlining the clinical relevance, types and consequences of non-penetrating traumatic injuries (NPTIs), emphasising microvascular damage. Then, an overview of the models currently used to study NPTIs is provided, highlighting the need for reliable models to study these injuries. Finally, the field of tissue engineering (TE) is presented as a potential means to address this gap, reviewing scaffold design principles, biomaterial selection and current approaches to microvascular *in vitro* models. Particular attention is paid to fibrin as a biomaterial, reflecting its prominence in vascular TE and its direct relevance to the later experimental work of this thesis. In doing so, this chapter establishes both the rationale for model development and the translational need to advance trauma mechanobiology through engineered microvascular constructs.

2.1 The Microvasculature: Structure, Function and Regulation of Perfusion

2.1.1 The Cardiovascular System: Blood Vessel Structure and Architecture

The cardiovascular system delivers oxygen and nutrients to tissues and removes metabolic waste and CO_2 from tissues [42]. This process is conducted at two levels: macrovasculature and microvasculature, which function to maintain circulatory homeostasis. The macrovasculature is made up of large vessels, namely arteries and veins, which transport blood to or from organs [43]. In contrast, the microvasculature comprises small vessels such as arterioles, capillaries and venules that regulate blood perfusion and mediate blood-tissue exchange, and play an essential role in tissue oxygenation, nutrient delivery and immune surveillance [43–45]. As vessels branch and reduce in diameter moving away from the heart, the total cross-sectional area increases while intravascular pressure decreases [46, 47]. Accordingly, vessel structure is adapted to accommodate these changes, with different vessel types optimised for their specific roles [46–48].

Endothelial cells (ECs) line all blood vessels and display phenotypic specialisation depending on the tissue environment. Vessels differ in lumen diameter, wall thickness and composition (*i.e.* relative amounts of elastic tissue, smooth muscle and fibrous tissue) [49], which makes each vessel type uniquely suited to its function (Figure 2.1). Arteries and arterioles have thicker walls than veins and venules, reflecting the need to withstand the higher pressure of blood ejected from the heart [43]. The lumen, or hollow passage through which blood flows, also varies: arteries typically have narrower lumens than veins, which facilitates pressure maintenance but limits volume transport. Veins, in turn, act as low-pressure vessels, returning blood to the heart and serving as reservoirs that can accommodate fluctuations in blood volume [42, 49].

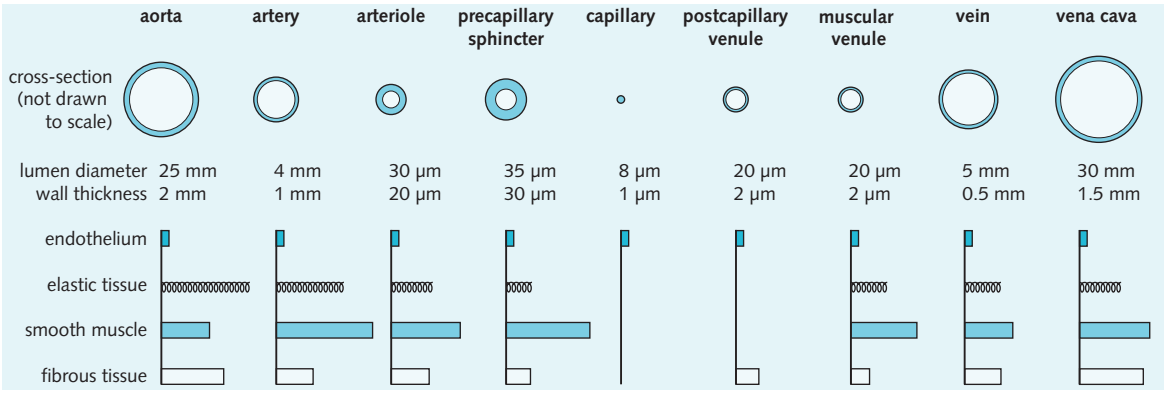


Figure 2.1: **Vessels of the circulation, shown in the direction of blood flow (*left to right*).** For each vessel type, a schematic of a cross-section of the vessel, lumen diameter, wall thickness and composition are shown. Smooth muscle cells (SMCs) predominate in most vessels, except in the aorta, where elastic and fibrous tissue are more abundant, and in capillaries and postcapillary venules, where SMCs are absent. Reproduced from Evans *et al.* (2015) [50].

Structurally, most vessels have three concentric layers: *intima*, *media*, and *adventitia*. In veins (Table 2.1), the *adventitia* is typically the thickest layer, whereas the *media* is relatively thin. In contrast, arteries (Table 2.2) are characterised by a predominant *media* and a comparatively thinner *adventitia* [50]. As vessel size decreases distally from the heart, these layers or *tunicae* thin progressively until the capillaries, which consist of the *intima*. Blood vessels can therefore be classified into large, medium and small arteries and veins; arterioles; muscular and postcapillary venules; and capillaries [21, 47].

Table 2.1: **Blood vessel characteristics: veins and venules.** Vessel diameter and the composition of each vascular layer are summarised for each blood vessel type. Based on Pawlina *et al.* (2024) [47]. *Pericytes are predominantly associated with the microvasculature; however, some authors report that cells with pericyte-like characteristics may also be present in larger vessels [51, 52].

Vessel	Large Vein	Medium Vein	Small Vein	Muscular Venule	Postcapillary Venule
Diameter	>10 mm	1–10 mm	0.1–1 mm	50–100 µm	10–50 µm
***Tunica Intima* (Inner Layer)**	• Endothelium • Connective tissue • Smooth muscle	• Endothelium • Connective tissue • Smooth muscle • Internal elastic membrane in some cases	• Endothelium • Connective tissue • Smooth muscle (2-3 layers)	• Endothelium	• Endothelium • Abundant pericytes*
***Tunica Media* (Middle Layer)**	• Smooth muscle (2-15 layers) • Collagen fibres	• Smooth muscle • Collagen fibres	• Smooth muscle (2-3 cell layers continous with *tunica intima*)	• Smooth muscle (1-2 cell layers)	• None
***Tunica Adventitia* (Outer Layer)**	• Much thicker than the *tunica media* • Connective tissue • Some elastic fibres, longitudinal smooth muscles • Cardiac muscle extensions (myocardial sleeves) into greater veins near the heart	• Thicker than the *tunica media* • Connective tissue • Some elastic fibres	• Thicker than the *tunica media* • Connective tissue • Some elastic fibres	• Thicker than the *tunica media* • Connective tissue • Some elastic fibres	• None

The *intima* consists of a single layer of aligned ECs lying on a basal lamina, often accompanied by pericytes in the microvasculature [47]. The *media* is composed of concentric layers of smooth muscle cells (SMCs) interspersed with elastin and collagen sheets, providing elastic recoil and mechanical stability, respectively [47, 50]. The *adventitia* contains axially aligned collagen fibres that preserve vessel length and calibre while anchoring vessels within surrounding connective tissue. In large vessels, the *vasa vasorum* and *nervi vasorum* are additional structures that provide auxiliary nutrient supply and regulate vasomotor tone, as diffusion alone cannot meet the needs of thicker vessel walls [47]. Owing to their specialised cellular organisation, blood vessels exhibit remarkable plasticity, adapting their structure and contractility in response to physicochemical cues.

Table 2.2: **Blood vessel characteristics: arteries, arterioles and capillaries.** Vessel diameter and the composition of each vascular layer are summarised for each blood vessel type. Based on Pawlina *et al.* (2024) [47]. *Pericytes are predominantly associated with the microvasculature; however, some authors report that cells with pericyte-like characteristics may also be present in larger vessels [51, 52].

Vessel	Large Arteries (Elastic Arteries)	Medium Arteries (Muscular Arteries)	Small Arteries	Arterioles	Capillaries
Diameter	>10 mm	2–10 mm	0.1–2 mm	10–100 µm	4–10 µm
***Tunica Intima* (Inner Layer)**	• Endothelium • Connective tissue • Smooth muscle	• Endothelium • Connective tissue • Smooth muscle • Prominent internal elastic membrane	• Endothelium • Connective tissue • Smooth muscle • Internal elastic membrane	• Endothelium • Connective tissue • Smooth muscle	• Endothelium • Sparse pericytes*
***Tunica Media* (Middle Layer)**	• Smooth muscle • Elastic lamellae	• Smooth muscle • Collagen fibres • Relatively little elastic tissue	• Smooth muscle (8-10 cell layers) • Collagen fibres	• Smooth muscle (1-2 cell layers)	• None
***Tunica Adventitia* (Outer Layer)**	• Thinner than the *tunica media* • Connective tissue • Elastic fibres	• Thinner than the *tunica media* • Connective tissue • Some elastic fibres	• Thinner than the *tunica media* • Connective tissue • Some elastic fibres	• Thin, ill-defined sheath of connective tissue	• None

Within the microvasculature, vessel specialisation becomes more pronounced. Arterioles, surrounded by vascular smooth muscle, are key resistance vessels that control tissue perfusion through vasoconstriction and vasodilatation [42, 43]. These give rise to capillaries, whose walls are reduced to a single layer of ECs to maximise permeability and enable the rapid exchange of gases, nutrients and waste [43, 53]. Capillaries are externally supported by pericytes, which cover roughly 30% of their surface [53]. Pericytes contribute to the regulation of EC proliferation, stabilise vessel structure and can act as precursors of SMCs, thereby facilitating arteriolarisation (*i.e.* transformation of capillaries into arterioles) during microcirculation growth and remodelling [43, 49, 53]. Downstream, postcapillary venules collect blood from capillary beds and function as dynamic reservoirs within the circulation [42]. ECs can be supported by mural cells that provide structural integrity and regulate vessel tone: pericytes in capillaries and SMCs in arterioles and venules [47].

2.1.2 Organisation, Structure and Function of the Microvasculature

The microvascular network is structurally heterogeneous, adapting to the specific requirements of each tissue. Microvascular beds (Figure 2.2) comprise an intricate network of arterioles, capillaries and venules that branch through tissues in the body [54]. In addition to these, metarterioles provide a direct connection between arterioles and venules, allowing blood to bypass capillary networks when precapillary sphincters are closed [45]. Through this organisation, small vessels collectively balance three essential roles: resistance (*e.g.* arterioles) to control blood flow, exchange (*e.g.* capillaries) to allow rapid transfer between blood and tissues, and capacitance (*e.g.* venules) to act as a variable reservoir of blood [42, 49, 50].

2.1.3 Endothelial Cell (EC) Function in Microvessels

The vascular endothelium is a layer of closely connected ECs that lines the inner surface of blood vessels, acting as an interface between the vessel wall and the bloodstream [50]. It functions as a major barrier by limiting the passage of cells, plasma and molecules from the circulation into the organ parenchyma and is crucial in fluid and metabolic homeostasis [45]. During development, vascular networks form through processes such as embryonic vasculogenesis, adult vasculogenesis, angiogenesis, and the splitting of existing vessels [55, 56]. In adults, neovascularisation mainly occurs through angiogenesis, where quiescent ECs transiently differentiate

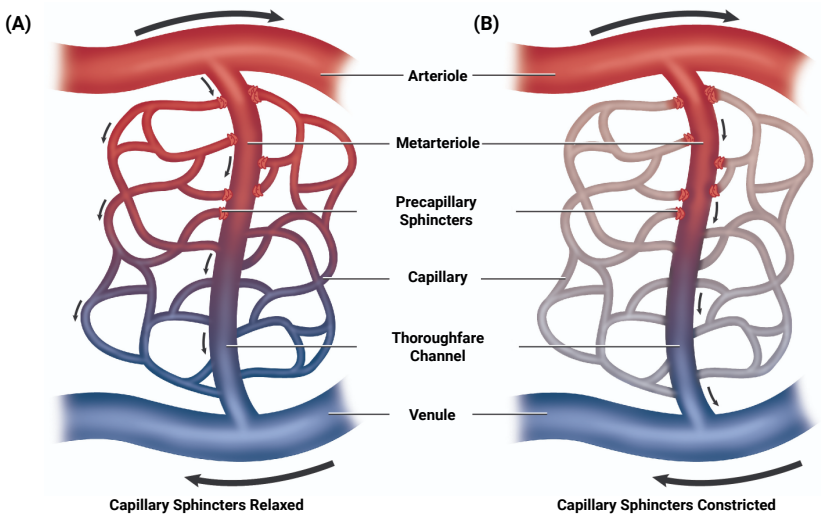


Figure 2.2: **Architecture of a microvascular bed.** Blood flow (indicated by arrows) proceeds from arterioles to capillaries and then to postcapillary venules, while metarterioles provide a direct arteriole–venule route. **(A)** Relaxed sphincter in active tissue: Smooth muscle cells (SMCs) are relaxed, allowing blood to enter capillaries. **(B)** Contracted sphincter: SMCs constrict, diverting blood from arterioles through metarterioles to venules. Modified from Menefee *et al.* (2025) [49].

into tip and stalk phenotypes before returning to a quiescent state. This process is regulated by a number of molecules and growth factors, including angiopoietin (ANG), fibroblast growth factors (FGFs), platelet-derived growth factor (PDGF) and vascular endothelial growth factor (VEGF) [55].

ECs are highly metabolically active and display metabolic adaptations that differ from most other cell types [57]. They rely predominantly on glycolysis to produce adenosine triphosphate (ATP) (∼85%), converting glucose to lactate, which allows rapid energy production while conserving oxygen for surrounding tissues [58]. This reliance on anaerobic glycolysis provides several advantages, such as rapid ATP generation with reduced reactive oxygen species production; oxygen preservation for perivascular cells; metabolic support of vascularisation in hypoxic or glucose-deprived environments; and lactate production that can stimulate angiogenesis [59]. Beyond ATP generation, glycolytic intermediates are channelled into auxiliary pathways, such as the pentose phosphate pathway and the hexosamine biosynthesis pathway, which modulate redox balance, nitric oxide synthesis and nucleotide availability [59–61]. EC metabolism is also mechanically regulated, with shear stress suppressing glycolysis *via* Krüppel-like factor 2 (KLF2) activation [62].

In the microvascular endothelium, this endothelial barrier also regulates blood perfusion by controlling the vasomotor response to vasoactive hormones or metabolites, thereby ensuring that nutrient supply is adequate and fulfils metabolic demand [45, 50]. Appropriate regulation of microvascular fluid hydrodynamics and endothelial barrier function is therefore vital to support normal tissue viability and organ function.

ECs play a critical role in a large number of physiological and pathophysiological processes, including inflammation, wound healing and leukocyte trafficking [63]. The endothelium is also selectively permeable, regulating molecule transport across the vascular wall [54].

Microvascular blood flow is further refined during vessel growth and adaptation. ECs recruit pericytes and SMCs, which are required for vessel maturation and functional stability, through signalling molecules such as PDGF-β, ANG and VEGF [64]. While pericytes promote EC quiescence and stabilise vessels, SMCs support vessel tone and extracellular matrix (ECM) organisation. Quiescent ECs can re-enter the cell cycle during angiogenesis, while tip and stalk cells coordinate sprouting and branching, integrating mechanical and metabolic cues to form functional networks [55].

The continuous tubular structure of the capillary lumen is formed by adjacent microvascular endothelial cells (MVECs) joined together at intercellular (cell–cell) junctions [45]. Moreover, ECs and SMCs are connected by gap and myoendothelial junctions. While the basolateral side of the endothelium is attached to the basal lamina *via* cell–surface integrins, the apical surface, which bears a specialised structure known as the glycocalyx, is exposed to the vessel lumen [38].

The glycocalyx is a complex, multifunctional layer of macromolecules including glycosaminoglycans, proteoglycans, and other glycoproteins, which are attached to the cell membrane [38,65]. It plays an essential role in maintaining vascular permeability and mechanotransduction. Among its components, glycosaminoglycans such as hyaluronan and chondroitin sulphate are tethered to anchoring sites that connect with the underlying cytoskeleton [65, 66].

Functionally, the glycocalyx serves as a barrier between the cell and its external environment, mediates cell–cell interactions, and preserves membrane integrity by protecting the cell surface from direct mechanical forces. It also plays a major role in fluid dynamics, vascular homeostasis, and the regulation of both vascular permeability and tone [38]. Disruption or degradation of the glycocalyx has been closely linked to vascular dysfunction and disease [17, 38, 39]. In ECs, the glycocalyx is thought to act as a mediator of fluid shear stress, transmitting mechanical signals to the actin cytoskeleton [67]. Nonetheless, evidence also suggests that such mechanical cues are propagated to other cellular sites, particularly intercellular junctions, where they may activate alternative signalling pathways [68].

Capillaries can be continuous (less permeable walls) or fenestrated (more permeable walls) depending on whether they have small intercellular gaps or pores [42] (Figure 2.3). The basal lamina or basement membrane is made up of laminin, fibronectin, glycosaminoglycans, and collagen fibrils [45, 50]. This structure is semipermeable to water and non-lipophilic molecules, and serves as a selective pathway for solute transport across the microvascular wall based on size and charge. Importantly, wall permeability is regulated through the interaction of ECs, the basal lamina, the supporting matrix, and the cells in the surrounding tissue [42].

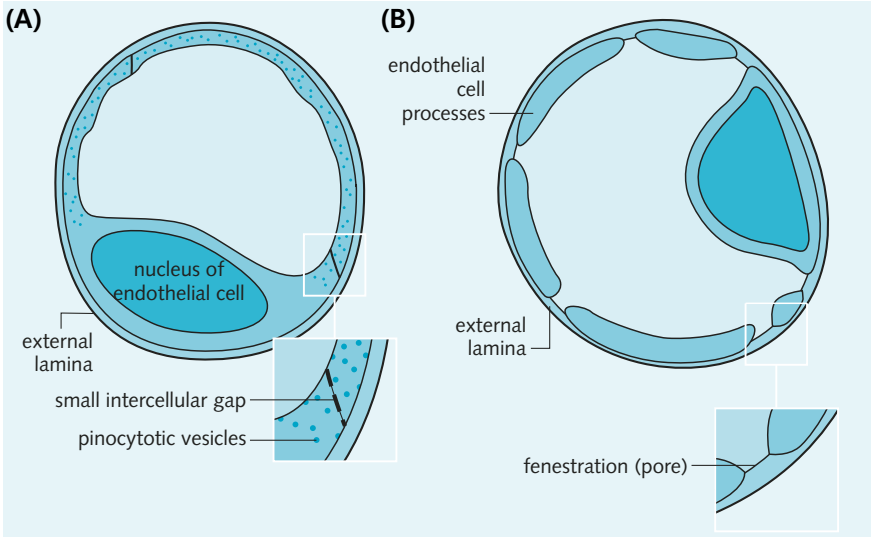


Figure 2.3: **Schematic illustration of capillary cross-sections with continuous and fenestrated walls. (A)** Continuous capillary walls are less permeable, while **(B)** fenestrated capillary walls are more permeable. Reproduced from Evans *et al.* (2015) [50].

ECs sense mechanical forces such as shear stress from blood flow, converting these stimuli into biochemical signals within the cell. This mechanotransduction regulates vascular tone, endothelial quiescence, and vessel remodelling [64, 69, 70]. Several proteins contribute to mediating flow sensing at cell–cell junctions, in-

cluding platelet endothelial cell adhesion molecule-1 (PECAM-1), vascular endothelial cadherin (VE-cadherin), and VEGF receptor-2 (VEGF-R2) [70]. In addition, the glycocalyx serves as an important mechanotransducer, converting shear stress into intracellular signals [71]. Flow dynamics also influence vessel differentiation: high shear stress promotes arterial specification, while low-flow environments favour venous differentiation [55]. Although growth factors are central to EC phenotype specification, they also induce metabolic shifts that drive differentiation and vasculogenesis [56, 60].

2.1.4 Regulation of Blood Flow and Tissue Perfusion

Both systemic and local mechanisms regulate tissue perfusion. Systemically, the autonomic nervous system and circulating hormones adjust vessel tone and cardiac output. Locally, autoregulatory responses ensure adequate oxygen delivery relative to metabolic demand. This is achieved through myogenic, metabolic, and endothelium-dependent mechanisms, including the release of vasodilators. [72]

Blood flow through capillaries is tightly regulated by the contraction or dilation of arterioles and pre-capillary sphincters. Both metabolic cues (*e.g.* nitric oxide, tissue pH) and humoral factors (*e.g.* angiotensin, vasopressin) can trigger vasoconstriction or vasodilatation, adjusting perfusion to meet local demands [45]. By controlling hydrodynamic pressure and blood volume, individual capillary beds ensure that the metabolic and respiratory requirements of tissues are met. MVECs provide a barrier between fluid and proteins in the blood and the surrounding tissue. Following tissue injury or infection, however, the microvascular barrier is often disrupted by MVEC activation and dysfunction [73]. MVEC activation is critical for facilitating the recruitment of inflammatory cells (neutrophils and monocytes) into the injured or infected tissue [50, 73].

2.2 Soft Tissue

Soft tissue comprises the non-skeletal tissues of the human body, which are essential for supporting physiological functions and enabling movement [74–77]. It primarily includes muscle, nervous, connective, adipose and vascular tissue, and skin [47, 74, 78–81]. Soft tissue is organised into distinct layers and structures, such as fascicles in muscle and bundles of collagen fibres in connective tissue, providing mechanical support and directional strength. Soft tissue may be opaque or transparent and is largely composed of water, which acts as its main chromophore, absorbing radiation at specific wavelengths. Other molecules include melanin, lipids, and carbohydrates [82].

The organisation and composition of soft tissue underpin its specialised functions (Table 2.3), such as producing movement in muscle, conducting signals in nerves, storing energy in adipose tissue, and acting as a protective barrier in the skin. Together, these tissues work cooperatively to maintain normal bodily function, with each type fulfilling a unique and indispensable role [74, 93, 94].

Among the soft tissues, skeletal muscle is of particular relevance due to its high vascular density, mechanical loading environment, and susceptibility to injuries. Muscle tissue relies on an extensive microvascular network to meet its substantial metabolic demands, so disruption to its microvasculature can have profound consequences for muscle function, repair, and regeneration following injury. While muscle tissue serves as a representative and clinically relevant soft tissue context within this thesis, the primary focus of the work is on microvasculature rather than muscle tissue.

2.2.1 Musculoskeletal System

The musculoskeletal system provides the structural framework of the body, enabling movement, stability, and the protection of vital organs. It comprises a range of specialised connective tissues of the articulated bony

Table 2.3: **Soft tissue types: structural characteristics and effects.** Here, an overview of muscle, connective, adipose, nervous, and vascular tissue is provided. Based on Ma *et al.* (2025) [46, 47, 74, 81, 83–92].

Tissue Type	Structural Characteristics	Function and Effect
Muscle Tissue	Skeletal muscle is striated and multinucleated; cardiac muscle is branched with intercalated discs; smooth muscle is spindle-shaped and lacks striations.	Produces movement, maintains posture, and generates heat through contraction.
Connective Tissue	Composed of cells embedded in an extracellular matrix containing fibres, a ground substance, and interstitial fluid.	Provides structural support, connects and protects tissues, facilitates nutrient transport, repairs damage, and contributes to immune defence.
Adipose Tissue	Made of fat storing cells with large lipid droplets that displace the nucleus and cytoplasm to the periphery.	Stores energy, insulates the body, cushions organs, and participates in metabolic regulation.
Nervous Tissue	Consists of neurons for signalling and glial cells that support, nourish, and protect them.	Controls body functions *via* electrical signals, enables communication between tissues, and maintains neuronal health.
Vascular Tissue	Comprises layers including the *intima, media,* and *adventitia*, with variations in thickness, cell type, and fibre composition across vessels.	Transports blood, delivers nutrients, removes waste, and regulates blood pressure, temperature, and tissue perfusion.
Skin	Multilayered organ with an outer epidermis, dermis with connective tissue and vessels, and a subcutaneous layer of adipose tissue; contains sensory receptors, glands, and hair follicles.	Protects against mechanical and chemical damage, prevents water loss, regulates temperature, provides sensory input, and contributes to immune defence.

skeleton (*e.g.* bones, cartilage, tendons), as well as skeletal muscles, which work together to support locomotion and maintain posture [83, 95]. Bones provide support and act as levers for movement, while muscles generate the contractile force that drives these actions. Tendons link muscles to bones, transmitting the forces generated by muscle contraction; cartilage cushions and reduces friction at bone-to-bone junctions; and ligaments anchor bones to one another, providing stability to joints [81, 83].

These tissues are continuously subjected to forces such as tension, compression, gravity, friction and impact. Specialised cells embedded within them detect such mechanical loading, and both the presence and absence of force can influence tissue properties, sometimes enhancing mechanical function and at other times contributing to degeneration [96]. Beyond this mechanical role, the musculoskeletal system is also essential for mineral homeostasis, particularly the storage of calcium, phosphorus, and, to a lesser extent, magnesium [97], and for the production of blood cells in the bone marrow [83]. The musculoskeletal system links rigid skeletal elements with contractile tissues, thus enabling coordinated and precise movements while absorbing mechanical stresses that might otherwise damage other organ systems. Its proper function underpins physical activity, resilience, and overall quality of life [81, 83].

2.2.2 Muscle

Muscle tissue is fundamental to the movement of the body, its parts, and the modulation of the size and shape of internal organs. It is composed of elongated, specialised cells arranged in parallel, which are then aggregated [98]. This organisation underpins both voluntary movements, such as locomotion, and involuntary activities, including the rhythmic contractions of the heart and the peristalsis of the gut [81].

The contractile mechanism of muscle is dependent on the interaction of two types of myofilaments: thin filaments (diameter: 6–8 mm; length: 1 µm), built primarily of actin, and thick filaments (diameter: ∼15 mm; length: 1.5 µm), made up of myosin II [81]. These filaments occupy much of the sarcoplasm. Muscle cells have a high density of aligned contractile filaments, which serve exclusively to generate mechanical force [99]. Actin and myosin are also found in many other cell types, albeit in much smaller quantities, where they contribute to processes such as cytokinesis, exocytosis, and cell movement [81].

2.2.2.1 Muscle Tissues: Overview and Classification of Muscle

Muscle is classified into smooth and striated types, based on the appearance of its contractile cells (Figure 2.4). Smooth muscle lacks cross-striations due to a less ordered and highly dynamic arrangement of myosin-containing filaments, and is found primarily in the viscera, blood vessels, *arrector pili* muscles, and intrinsic eye muscles. In contrast, in striated muscle, cross-striations in the cells are visible due to the highly organised arrangement of thin and thick myofilaments [81, 83, 99].

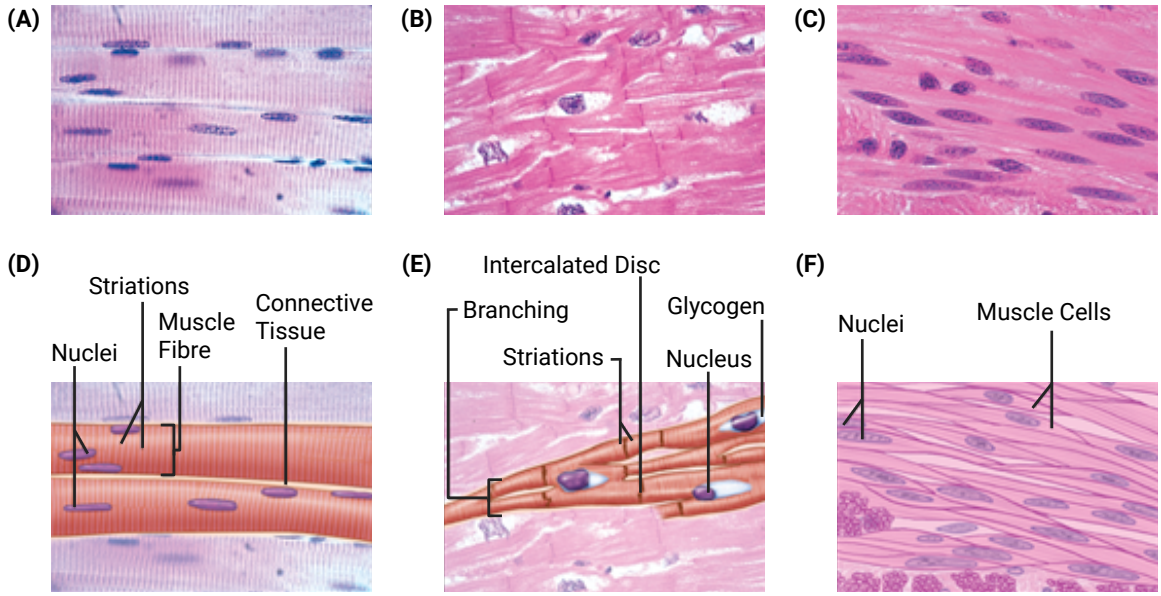


Figure 2.4: **Histological comparison of skeletal, cardiac and smooth muscle. (A–C)** Light micrographs and **(D–F)** schematic illustrations of **(A, D)** skeletal, **(B, E)** cardiac, and **(C, F)** smooth muscle. Skeletal muscle fibres are elongated, multinucleated, and under voluntary control, producing rapid and forceful contractions. Cardiac muscle consists of branched cells connected by intercalated discs that generate vigorous, rhythmic, involuntary contractions. Smooth muscle is composed of fusiform cells arranged in groups that produce slow, weak, involuntary contractions. Modified from Mescher *et al.* (2021) [98].

Striated muscle itself is subdivided into skeletal muscle, visceral striated muscle and cardiac muscle, distinguished by their anatomical location and physiological role [83]. Skeletal muscle is attached to bones and enables body movement, posture, and precise eye motions; visceral striated muscle supports functions like breathing, swallowing, and speech, and is limited to soft tissues such as the tongue, pharynx, diaphragm, and upper oesophagus; and cardiac muscle, found in the heart and the base of large veins, drives heart contractions [81].

There are three major muscle tissue types (Table 2.4), namely: (1) skeletal muscle, attached to bones and responsible for voluntary body movements; (2) cardiac muscle, which forms the myocardium and contracts rhythmically under involuntary control; and (3) smooth muscle, involuntarily regulated by the autonomic nervous system, located in the walls of blood vessels and hollow organs, such as the stomach and intestines [83, 98].

Table 2.4: **Functional comparison of muscle types: skeletal, cardiac and smooth.** Key structural features, functions, and growth and regeneration details for each muscle type are presented here. sER: smooth surfaced endoplasmic reticulum; TnC: troponin C. Based on Pawlina *et al.* (2024) [81].

Muscle Type	Skeletal	Cardiac	Smooth
Muscle Cell	Large, elongated cell. **Diameter:** 10-100 µm. **Length:** up to 100 cm.	Short, narrow cell. **Diameter:** 10-100 µm. **Length:** 80-100 µm.	Short, elongated, fusiform cell. **Diameter:** 0.2-2 µm. **Length:** 20-200 µm.
Location	Muscles of skeleton, visceral striated (*e.g.*, tongue, esophagus, diaphragm).	Heart, superior and inferior venae cavae, pulmonary veins.	Vessels, organs, and viscera.
Structural Features			
Connective Tissue Components	• Epimysium • Perimysium • Endomysium	• Endomysium • Subendocardial • Subpericardial connective tissue	• Endomysium • Sheaths • Bundles
Fibre	Single skeletal muscle cell.	Linear branched arrangement of several cardiac muscle cells.	Single smooth muscle cell.
Sarcomere	✓	✓	✗
Striation	✓	✓	✗
Nucleus	Many peripheral.	Single central, surrounded by juxtanuclear region.	Single central.
T Tubules	Present at A–I junction (triad: with two terminal cisternae), two T tubules/sarcomere.	Present at Z lines (diad: with small terminal *cisternae*), one T tubule/sarcomere; Purkinje fibres have less number of T tubules.	None, well-developed sER, many *caveolae* and cytoplasmic vesicles.
Cell-to-cell Junctions	None.	Intercalated discs containing: (1) Fasciae adherens; (2) Macula adherens (desmosome); and (3) Gap junctions.	Gap junctions (nexus).
Special Features	Well-developed sER and T tubules.	Intercalated discs, Purkinje fibres.	Dense bodies, desmin and vimentin filaments, *caveolae*, and cytoplasmic vesicles.
Functions			
Type of Innervation	Voluntary.	Involuntary.	Involuntary.
Efferent Innervation	Somatic.	Autonomic.	Autonomic.
Type of Contraction	"All or none" (type I and type II fibres).	"All or none" rhythmic (pacemakers, conductive system of the heart).	Slow, partial, rhythmic, spontaneous contractions (pacemakers of stomach).
Regulation of Contraction	By binding of Ca^{2+} to TnC, causes tropomyosin movement and exposes myosin-binding sites on actin filaments.	By binding of Ca^{2+} to TnC, causes tropomyosin movement and exposes myosin-binding sites on actin filaments.	By phosphorylation of myosin light chain by myosin light-chain kinase in the presence of Ca^{2+}–calmodulin complex.
Growth & Regeneration			
Mitosis	None.	None (in normal condition).	Present
Response to Demand	Hypertrophy.	Hypertrophy.	Hypertrophy and hyperplasia.
Regeneration	Limited (satellite cells and myogenic cells from bone marrow).	None (in normal conditions).	Present.

Skeletal Muscle

Skeletal muscle, also referred to as voluntary muscle, is the most abundant type of muscle tissue in the human body [83]. It plays a key role in enabling voluntary movement, as well as providing structural support and protection [99]. The fibres that compose skeletal muscle are long, cylindrical, multinucleated cells, ranging from 10 to 100 µm in diameter and sometimes extending several centimetres in length [81].

Skeletal muscle fibres are organised into bundles known as fascicles, each enclosed within connective tissue sheaths. Individual fibres are surrounded by the endomysium, a network of reticular fibres containing fibroblasts, nerve fibres, and capillaries. Fascicles are encased in the perimysium, while the entire muscle is wrapped by the epimysium, a dense irregular connective tissue (Figure 2.5) [81, 99]. This hierarchical organisation ensures that the forces generated by individual fibres are efficiently transmitted to tendons and skeletal structures [81]. In larger muscles, each muscle fascicle forms a functional unit in which fibres contract together and are supplied by nerves, blood vessels and lymphatics. [99–101].

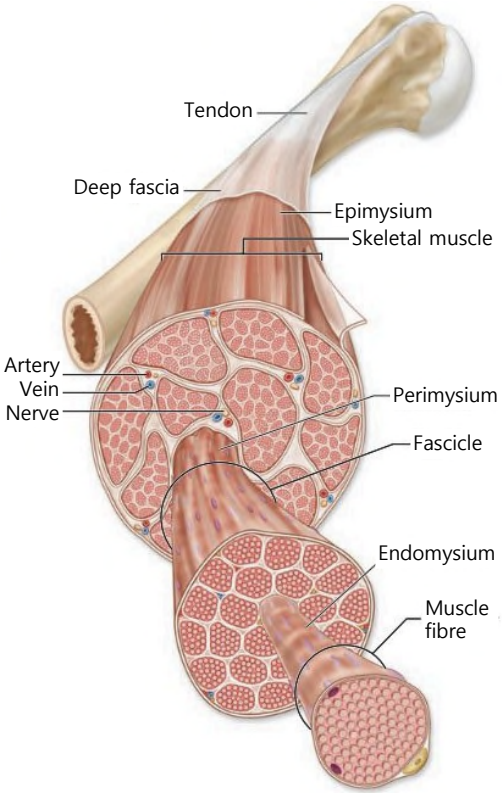


Figure 2.5: **Hierarchical organisation of skeletal muscle.** Schematic representation of skeletal muscle structure, showing individual muscle fibres surrounded by the endomysium, bundled into fascicles enclosed by the perimysium, and the entire muscle being wrapped by the epimysium. The illustration also highlights the associated arteries, veins and nerves, as well as the deep fascia and tendon attaching the muscle to bone. Reproduced from Mescher *et al.* (2021) [98].

Cardiac Muscle

Cardiac muscle shares the same filament organisation as skeletal muscle, with the presence of sarcomeres resulting in striations. It consists of networks of cardiac myocytes (diameter: 15 µm; length: 80 µm), which are short, cylindrical, and typically mononucleated, with a centrally located nucleus (occasionally two) surrounded by a juxtanuclear region rich in mitochondria, Golgi apparatus, glycogen and, in atrial cells, secretory granules containing atrial and brain natriuretic factors that regulate blood volume and vascular tone. [48, 81, 83]

A defining feature of cardiac muscle is the presence of intercalated discs, highly specialised junctions between adjacent cells that contain *fascia adherens*, desmosomes (*maculae adherentes*), and gap junctions. These discs run either linearly or in a staircase-like pattern across the fibres, linking individual cylindrical cells end-to-end and, sometimes, in branched arrangements to form functional cardiac fibres of variable length. Intercalated discs mechanically anchor cells and provide electrical continuity, enabling the myocardium to act as a coordinated syncytium while maintaining the integrity of individual cells. Each cardiac fibre is enveloped by a thin layer of connective tissue, the endomysium, which contains an extensive network of capillaries. This dense capillary supply is essential for sustaining rhythmic contraction and maintaining cardiac function. [81, 98]

Smooth Muscle

Smooth muscle is formed by small, elongated fusiform cells arranged in sheets or bundles, specialised for slow, sustained contractions. Despite lacking sarcomeres, SMCs are interconnected by gap junctions that enable coordinated activity across the tissue. The cytoskeleton includes desmin and vimentin intermediate filaments, while the contractile apparatus consists of thin filaments, thick filaments and regulatory proteins. Thin filaments, composed of actin, tropomyosin (smooth muscle isoform), caldesmon and calponin, are anchored to dense bodies containing α-actinin, which provide structural support. [48, 81]

2.2.3 Vascular Supply and Microcirculation in Skeletal Muscle

Skeletal muscle is highly vascularised, enabling oxygen and nutrient supply to muscle fibres, and metabolic waste removal [46, 47]. Different fibre types are adapted to specific functional demands: slow-twitch fibres rely predominantly on oxidative metabolism for endurance, whereas fast-twitch fibres depend on glycolytic pathways for rapid, powerful contractions. The sarcolemma, a specialised membrane surrounding each fibre, regulates ion fluxes critical for contraction and relaxation [99].

Vascular supply in most muscles is provided by a major source artery, which typically enters at the neurovascular hilum alongside the principal vein and nerve, before branching in the connective tissue. From here, smaller blood vessels extend through the perimysium and the endomysium, largely running parallel with muscle fibres and forming an interconnected capillary mesh. Both capillary density and the gross vascular anatomy of muscle vary between muscles. [83]

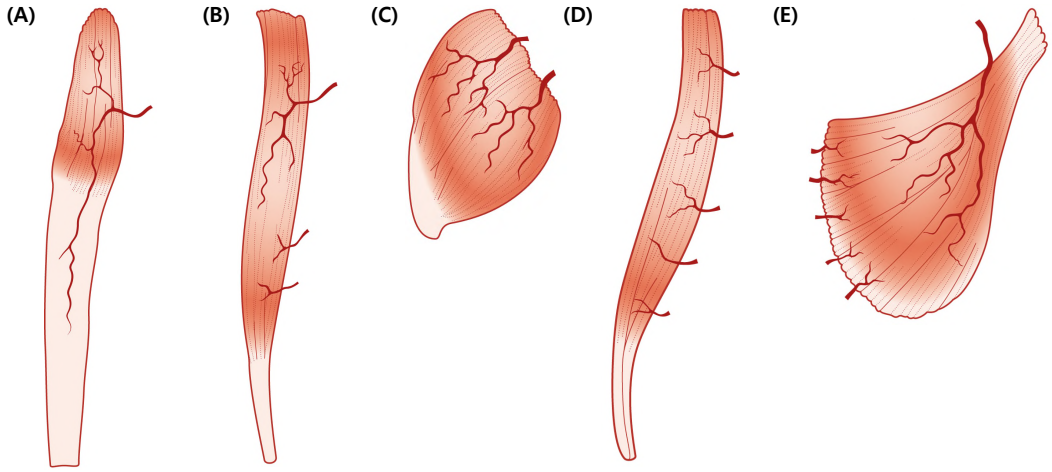


Figure 2.6: **Skeletal muscle classification based on its blood supply.** Based on the number and relative dominance of vascular pedicles, muscles can be classified into five types, listed here with a representative example: **(A)** Type I, *tensor fasciae latae*; **(B)** Type II, *gracilis*; **(C)** Type III, *gluteus maximus*; **(D)** Type IV, *sartorius*; and **(E)** Type V, *latissimus dorsi*. The illustrations are not to scale. Modified from Standring *et al.* (2021) [83, 102].

Muscles can be classified into five types based on the number and relative dominance of vascular pedicles (Figure 2.6). Type I muscles have a single pedicle (*e.g. tensor fasciae latae*, *gastrocnemius*); Type II, one dominant and several minor pedicles (*e.g. gracilis*); Type III, two dominant pedicles, each from a different source artery (*e.g. gluteus maximus*, *rectus abdominis*); Type IV, numerous small pedicles unable to support the muscle alone (*e.g. sartorius*, *tibialis anterior*); and Type V, one dominant pedicle with multiple segmental pedicles (*e.g. latissimus dorsi*, *pectoralis major*) [83, 103].

At the microcirculation level, skeletal muscle has a highly specialised vascular network comprising capillaries, venules, and arterioles that provides oxygen and nutrients while removing metabolic waste, and regulates local perfusion in accordance with metabolic demand [81]. Capillaries are closely aligned with muscle fibres, with each fibre typically surrounded by an extensive capillary bed that runs parallel to its long axis and supports its contractile and metabolic requirements [81]. Capillary density varies with fibre type: oxidative slow-twitch fibres are more densely vascularised than glycolytic fast-twitch fibres, reflecting their reliance on aerobic metabolism and endurance function [104].

In most muscles, the microcirculation branches from a feed (principal) artery into several arterioles, eventually reaching a terminal arteriole. Each terminal arteriole supplies up to 20 capillaries, forming a microvascular unit (MVU; Figure 2.7). Capillary density varies among muscle fibres, with those involved in sustained activity, such as postural maintenance, having a denser capillary network. Muscle fibres have different contractile and metabolic properties and can be classified as glycolytic (fast) and oxidative (fast and slow). Some muscles have predominantly glycolytic or oxidative fibres. In these, capillaries differ in shape and density. [46, 53]

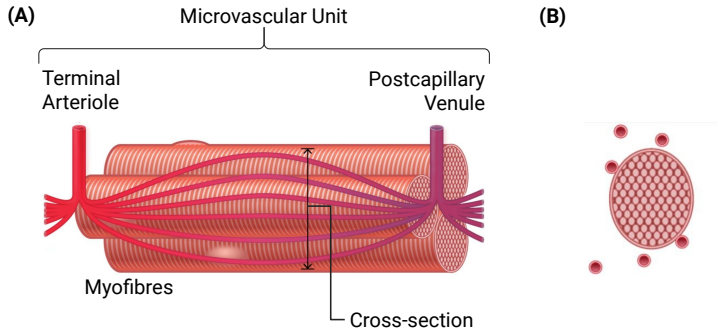


Figure 2.7: **Schematic representation of a microvascular unit (MVU) in skeletal muscle. (A)** Spatial organisation of a human skeletal muscle MVU in relation to a myofibre, showing blood flow from a terminal arteriole through capillaries to postcapillary venules. **(B)** Cross-sectional view of skeletal muscle MVU. Modified from Latroche *et al.* (2015) [105].

Muscles often receive blood *via* multiple arterial routes, creating vascular territories interconnected by reduced-calibre 'choke vessels'. These arterial arcades connect the vascular territories, forming a continuous network. Venous drainage follows a similar arrangement, albeit in reverse, with venous territories mirroring arterial territories. Venous territories are linked by anastomoses that lack valves, allowing for bidirectional flow. Intramuscular veins also contribute to the 'muscle pump', aiding venous return during muscle contraction. Arteriovenous anastomoses provide additional, regulated shunts that bypass the capillary network, while perfusion levels dynamically adapt to functional demand. [53, 83]

Lymphatic drainage begins in the epimysial and perimysial layers and follows the veins to regional lymph nodes. Muscle vessels rarely cross between adjacent muscles, although vascular connections may occur *via* cutaneous or terminal intramuscular branches where the muscle underlies the skin. [83]

Unlike most organs, where capillary flow is regulated by precapillary sphincters, there is no clear morphological evidence for the presence of these structures in skeletal muscle [53]. Instead, microcirculation is

controlled by general mechanisms activated at a whole-body level (*e.g.* hormonal, nervous) and local mechanisms, including myogenic, neurovascular, metabolic, and endothelial influences [53]. Capillary flow is heterogeneous and may be nutritive (to muscle fibres) or non-nutritive (to connective tissues and tendons). In skeletal muscle, microcirculation is adapted to muscle metabolism (Figure 2.8). [53]

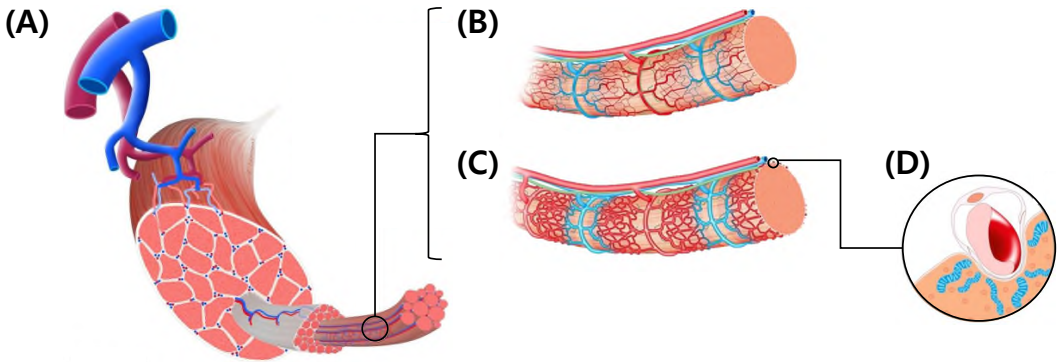


Figure 2.8: **Schematic illustration of skeletal muscle vascular architecture. (A)** Arterioles branch from primary arteries into terminal arterioles, which are oriented perpendicular to muscle fibres. **(B, C)** Two fibres with their microvascular units (MVUs), where terminal arterioles (red) supply multiple capillaries (red to blue), and lymphatic vessels (green) ascend alongside arterioles and venules (blue). **(B)** At rest, perfusion is intermittent and uneven, while **(C)** higher metabolic demand by skeletal muscle during exercise leads to the dilation of terminal arterioles, enhancing blood flow. **(D)** Magnified view of a capillary embedded in a sarcolemma channel, increasing the contact area between myocytes and endothelial cells (ECs). Modified from MediCorporate bv/D & L Graphics, available *via* Kusters *et al.* (2016) [106].

At rest, some terminal arterioles are constricted and prevent perfusion to the capillary bed, so only a fraction of capillaries are perfused. During exercise, vasodilatation and the recruitment of additional capillaries dramatically increase perfusion in skeletal muscle to meet the increased metabolic demand [99]. Even a few contractions can trigger dilation of terminal arterioles and increase capillary perfusion, expanding the diffusion area [42]. ECs are central to this process: they sense shear stress, release vasoactive mediators such as nitric oxide, allow capillary perfusion adjustment, and regulate arteriolar tone [53, 81]. Also, metabolic by-products including adenosine, carbon dioxide and lactate act locally to influence vascular tone. Together, these mechanisms ensure that oxygen delivery closely matches the dynamic energy requirements of contracting muscle while protecting against ischaemia [104].

The microvasculature adapts to long-term changes in activity. Increased muscle activity stimulates angiogenesis through mechanical stimuli (*e.g.* shear stress, wall tension) and growth factors (*e.g.* VEGF), whereas prolonged inactivity leads to regression of the capillary bed [53]. Beyond perfusion, the microvasculature plays a central role in skeletal muscle homeostasis, growth and repair by providing signals that influence satellite cell activation, ECM remodelling and regeneration [99]. Angiogenesis frequently accompanies myogenesis during injury recovery, highlighting the interdependence between vascular and muscular regeneration [99]. Consequently, impairment of skeletal muscle microcirculation, whether due to ageing, metabolic disease or traumatic injury, is associated with limited oxygen supply, reduced regenerative capacity and functional decline [81]. Thus, the integrity of the microvascular network is critical for physiological performance, repair and long-term adaptability [81, 99].

Many of the initial studies on microcirculation in skeletal muscle were performed on thin muscles that could be transilluminated (*e.g.* *spinotrapezius*, *cremaster*), showing microvessels arranged in an arcade pattern (Figure 2.9). Similar arrangements occur in other thin muscles, where muscle fibres and capillaries run parallel (*e.g.* hamster *retractor*, rat *gracilis*) [53].

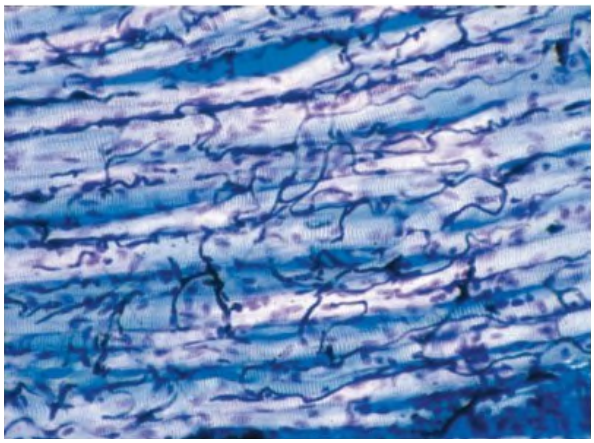


Figure 2.9: **Longitudinal section of skeletal muscle**, showing the capillary network (*dark blue*) in the endomysium surrounding muscle fibres (*light blue*). Blood vessels were filled with dark plastic polymer before longitudinal sectioning and imaging at 200×. Reproduced from Mescher *et al.* (2021) [98].

2.2.3.1 Skeletal Muscle Microvasculature: Healing, Repair and Regeneration

Unlike bone, which heals regeneratively, muscle recovers predominantly through repair and leaves a fibrotic scar instead of returning to its original state [107–109]. There are three repair phases: (1) destruction and inflammation (0–7 days); (2) repair and regeneration (7–21 days); and (3) remodelling (> 21 days) [107]. During the destruction phase, fibres rupture and necrosis occurs alongside haematoma formation. Macrophages remove necrotic material and fibroblasts deposit collagen type III to form a provisional scar. Myosatellite cells (mononuclear progenitors of skeletal muscle cells) are activated, giving rise either to additional satellite cells or to skeletal muscle cells through differentiation in the regenerative zone. By day 5, the scar tissue becomes denser and myotube formation is underway [107].

The repair period involves phagocytosis of necrotic tissue, regeneration of myofibres, deposition of connective scar tissue, and vascular ingrowth to support healing. By day 10, scar breakdown is underway, with progressive reduction by day 14 and, by day 21, regenerated myofibres interlace with minimal residual scar tissue. In the final phase, remodelling, regenerated myofibres mature, the scar tissue retracts and reorganises, and the functional capacity of the muscle is progressively restored [107, 109].

Following necrosis, inflammatory cells infiltrate the injured site, releasing growth factors such as transforming growth factors alpha and beta (TGF-α and TGF-β), VEGF, basic fibroblast growth factor (bFGF), PDGF, and insulin-like growth factor-1 (IGF-1). These factors recruit neutrophils and monocytes to initiate the inflammatory response and activate satellite cells, which proliferate, differentiate, and fuse to form new myotubes in muscle or activate ECs to initiate angiogenesis [110].

Angiogenesis, or neovascularisation, is a process by which new blood vessels form from existing ones that is fundamental to tissue growth, regeneration and repair [111]. Through this process, ECs are stimulated, which leads to their proliferation and migration to form new blood vessels. Vasculogenesis differs in that it involves the *de novo* formation of vessels from precursor cells such as angioblasts, and arteriogenesis results from remodelling and enlargement of existing vessels due to altered blood flow [56, 111, 112].

Angiogenesis follows a coordinated physiological sequence that includes vasodilatation, basement membrane degradation, EC migration and chemotaxis, increased vascular permeability, EC proliferation, new vessel formation and a subsequent reduction in cell death risk [111]. This process is stimulated by microenvironmental cues such as hypoxia, low pH and elevated lactate levels, as well as by soluble mediators including bFGF, TGF-β and VEGF produced by epidermal cells, fibroblasts, ECs and macrophages [110].

Oxygen availability plays a key role in regulating angiogenesis through oxygen-sensing proteins that control the transcription of pro- and anti-angiogenic genes. Under hypoxic conditions, VEGF synthesis by capillary ECs increases through the activation of hypoxia-inducible factor (HIF), which is regulated by oxygen availability. On the other hand, when oxygen levels in the injured tissue increase, oxygen binds to HIF, leading to HIF degradation and a reduction in angiogenic signalling. The process is further modulated by a balance of stimulatory factors, such as VEGF, and inhibitory factors, including angiostatin, endostatin, thrombospondin and pigment epithelium-derived factor (PEDF). Binding of angiogenic factors stimulates ECs adjacent to the damaged site to migrate into the ECM, facilitated by proteolytic enzymes such as matrix metalloproteinases (MMPs), where they proliferate and form sprouts. These sprouts extend and fuse to create new, complete vascular loops and form a capillary network, restoring tissue oxygenation and metabolic balance. [110]

2.3 Traumatic Injuries

Traumatic injuries refer to the damage inflicted on the body by an external force. Severe trauma is classically described using a trimodal model [113]: (1) immediate death, usually occurring within minutes of injury; (2) early death, typically within 24 h and usually due to haemorrhage; and (3) late mortality, occurring days to weeks later [17]. Although mortality often follows this trimodal distribution, nearly half of trauma-related deaths occur within the first 48 h of hospital admission, mainly from uncontrolled haemorrhage [13, 14, 114]. Haemorrhage and haemorrhagic shock result from excessive blood loss, which prevents tissues and organs from receiving sufficient oxygen [114].

Trauma also activates the hypothalamic–pituitary–adrenal axis, along with immune and metabolic pathways, all of which aim to restore homeostasis. While injury mechanisms differ, their causes, outcomes and physiological responses often overlap. A consistent feature is the activation of the autonomic nervous system, although responses vary between individuals and may be modified by underlying chronic conditions. Trauma-induced coagulopathy is another well-recognised complication in trauma patients. [115]

Traumatic injuries may be categorised based on injury features, such as the temporality and mechanism of injury (Figure 2.10). Broadly, these are classified as acute or overuse (chronic) injuries. Acute trauma typically results from a single event and includes penetrating, non-penetrating and polytrauma. Penetrating trauma involves the disruption of the skin barrier with direct injury to underlying tissues. NPTIs refer to closed injuries where energy is transmitted through the body, indirectly damaging underlying structures. Polytrauma involves multiple simultaneous injuries, often sustained in motor vehicle collisions or explosions. In contrast, overuse injuries arise from cumulative stress or repetitive motion. [115–118]

Among NPTIs, the main types are contusion (blunt force), compression (crush) and strain (tensile) injuries. Their impact on the microvasculature remains relatively underexplored, except in the context of traumatic brain injuries. Within these, mechanical injuries are the most common skeletal muscle injuries, encompassing strain, contusion, crush, and laceration injuries [117, 119].

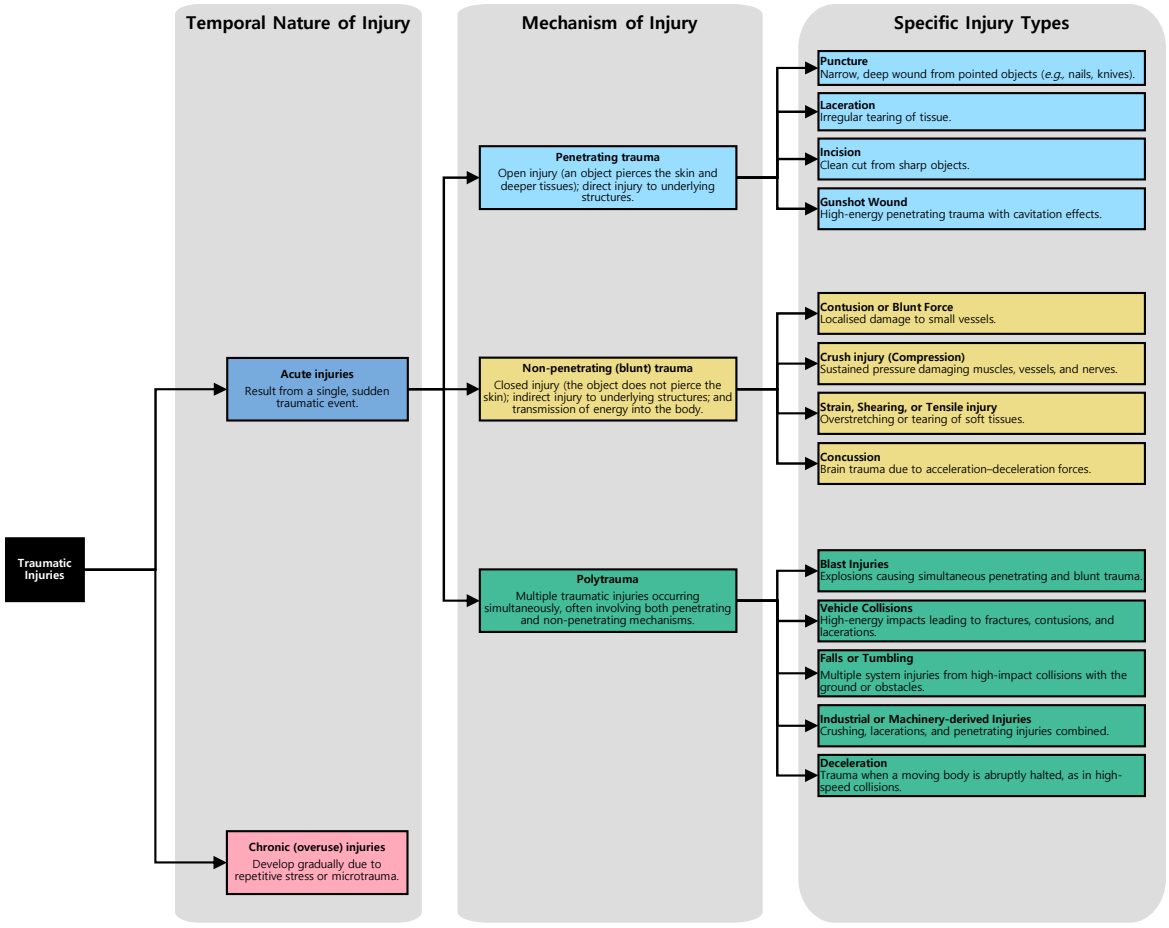


Figure 2.10: **Traumatic injury classification**, showing the temporal nature and mechanism of injury, as well as examples of specific injury types. [115–117].

2.3.1 Clinical Relevance

Traumatic injuries are a leading cause of death worldwide and, among survivors, often result in disability and a reduced quality of life [1]. Each year, nearly one billion people sustain injuries requiring medical care [9, 120]. While mortality is the most immediate concern, non-fatal injuries frequently lead to long-term disability, reducing quality of life, financial stability and overall wellbeing [121].

The combined burden of traumatic injuries can be estimated using disability-adjusted life years (DALYs), which account for both years of life lost and years lived with disability [10]. From 1990 to 2019, injuries remained a major contributor to global DALYs, although the relative ranking of specific causes varied by type and age group (Figure 2.11). Although the order of specific injury types shifted slightly over time, road injuries consistently represented the greatest burden in younger adults, while falls became increasingly prevalent in older populations. Self-harm and interpersonal violence declined modestly in rank, reflecting shifts in injury burden distribution across the lifespan. [3, 12, 122]

Over 90% of global injury-related deaths occur in low- and middle-income countries (LMICs), where the median direct medical costs of trauma are equivalent to 15% of the gross domestic product (GDP) per capita [12, 121]. When indirect and non-medical costs are included, this figure rises to 97%, placing a substantial financial burden on developing nations and perpetuating cycles of poverty [121].

Trauma has often been perceived as a ‘disease of the young’, with adults aged 15–49 years most affected

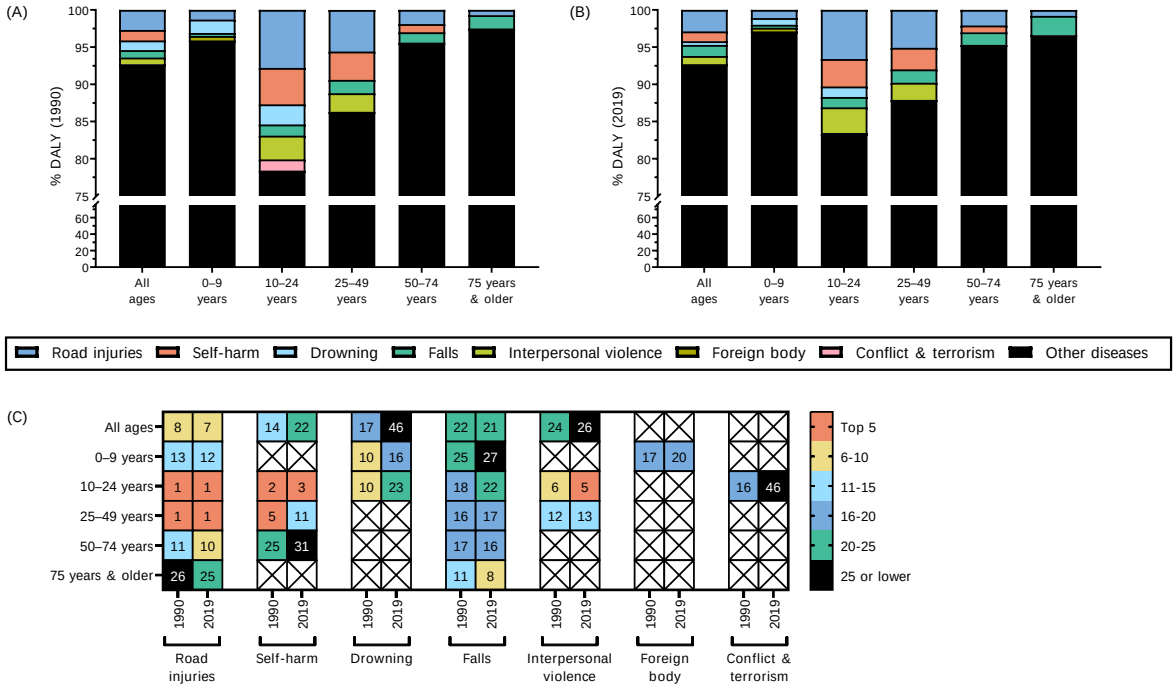


Figure 2.11: **Leading 25 Level 3 causes of global disability-adjusted life years (DALYs), 1990–2019. (A, B)** Percentage (%) of total DALYs in **(A)** 1990 and **(B)** 2019, respectively, for both sexes combined, shown for all ages and by age group (< 10 years, 10–24, 25–49, 50–74 and ≥ 75 years). Other causes (black) include communicable, maternal, neonatal and nutritional diseases, as well as non-communicable diseases and other injuries not listed among the leading causes. **(C)** Rankings of percentage of total DALYs for 1990 and 2019. The ranking of causes listed in the top 25 in either 1990 or 2019 is also shown for the other year, even if they did not appear in the top 25. Crossed-out cells indicate that the ranking was lower than 25 in both 1990 and 2019. The figure was plotted using data from the Global Burden of Disease Report 2019 [122].

by road traffic injuries, self-harm, and interpersonal violence [3, 12, 122]. Although this trend is observed globally, regional variation is significant. For example, rates differ noticeably between high-income Asia-Pacific and western sub-Saharan Africa, and between high-income North America and western Europe [12]. Patterns of injury also vary geographically: road injuries and interpersonal violence are more prevalent in Latin America and sub-Saharan Africa, whereas self-harm is more common in Central Asia and Europe [12]. Although DALY rates have decreased globally for road injuries (–15.7%) and interpersonal violence (–19.1%), these improvements are primarily observed in high-income regions and countries [12].

In the elderly, the prevalence of traumatic injuries is rising, partly due to population ageing [123]. Advances in healthcare have prolonged independence and mobility, but this has increased exposure to falls and age-related frailty [124, 125]. Falls are the leading cause of injury-related DALYs in individuals aged over 80 years [3, 12], and major trauma in geriatric patients increasingly challenges health systems globally [126].

2.3.2 Soft Tissue Injuries

Soft tissue trauma encompasses a wide spectrum of injuries affecting muscles, tendons, ligaments and subcutaneous tissues. These can result from mechanical, thermal or chemical insults, though mechanical trauma is the most prevalent [109]. NPTIs such as contusions, strains and crush injuries are characterised by disruption of muscle fibres, connective tissue, and associated vasculature without breaching the skin. The severity of injury depends on the magnitude, duration, and type of force applied. [127]

Skeletal muscle injuries account for a substantial proportion of sports- and accident-related trauma, and

are often accompanied by microvascular damage, oedema and haemorrhage. The subsequent inflammatory and repair responses determine the extent of functional recovery or the development of fibrosis and chronic dysfunction. [109, 117, 128, 129]

Soft tissue injuries describe pathological changes affecting structures such as muscle, tendon, ligament, fascia, adipose tissue, synovial membrane, nerves and blood vessels [74, 130]. In addition to trauma-derived injuries, soft tissue injuries may be inflammatory, neoplastic or degenerative in origin, each with a distinct aetiology and clinical presentation [74, 131, 132]. Soft tissue injuries pose a significant challenge in clinical practice, as they can markedly impair physical function and quality of life [74, 133].

2.3.2.1 Regeneration, Growth and Adaptation

Skeletal muscle tissue has a moderate capacity for regeneration and remodelling [119]. This process follows three key stages: an immediate destruction or inflammatory phase (minutes to 1–2 weeks), a repair phase with peak myoblast proliferation at approximately 14 days post-injury and a remodelling phase lasting up to four weeks, during which fibroblasts synthesise connective tissue and scar formation may occur [99, 119].

Because skeletal muscle fibres are terminally differentiated and do not normally undergo cell division, growth and repair usually occur *via* hypertrophy of existing fibres or through the activation of satellite cells [81, 83, 100]. These quiescent stem cells (satellite cells) are located beneath the basal lamina and, upon activation by injury, proliferate and fuse with damaged fibres to restore contractile function [99]. Satellite cells are a heterogeneous population characterised by the expression of Pax7 on activation [99, 134, 135] and are regulated by myogenic transcription factors such as MyoD, myogenin, and Pax3 [99, 134, 136]. They are capable of self-renewal and their abundance varies with age and muscle type [99].

However, the regenerative capacity of satellite cells is limited, particularly after major traumatic injuries, where excessive connective tissue deposition, scarring or an exaggerated inflammatory response can impair recovery [119]. The ECM and fibroblasts play essential roles in guiding satellite cell activity during repair, ensuring functional recovery [99]. Importantly, skeletal muscle exhibits remarkable plasticity, adapting its fibre-type composition, metabolic profile and contractile properties in response to exercise, activity or injury [81].

2.3.3 Non-Penetrating Traumatic Injuries (NPTIs)

NPTIs are provoked by mechanical forces applied to the body without disruption of the skin, resulting in a closed and indirect injury to the underlying structures [137]. Such injuries are prevalent in both civilian and military settings and include contusions, crush and strain injuries. In civilian settings, these are commonly caused by motor vehicle collisions where blunt force trauma can lead to internal haemorrhage and inflammation, with or without oedema [138]. Notably, the oedema that accompanies acute inflammation is linked to contraction of, and damage, to the endothelium, resulting in ‘leaky’ microvessels [139].

The consequences of blunt force or non-penetrating trauma depend on the location of the trauma [138], the nature of injury, and the individual characteristics of the patient [123]. These acute physical injuries may require immediate attention depending on their severity. Clinically, NPTIs vary in severity, from minor bruises to extensive muscle necrosis and compartment syndrome. Notably, the absence of an open wound complicates early diagnosis, as internal damage to vasculature and soft tissues may not be immediately evident on clinical examination or medical imaging [140].

The effects of NPTIs on the microvasculature remain relatively underexplored, except in the context of brain injury. Notably, mechanical injuries are the most common type of skeletal muscle trauma, encompassing crush, strain and contusion, including blunt impact [117, 119].

2.3.3.1 Crush or Compression Injury

Crush or compression injuries occur when a body part is subjected to a sustained force (> 4 h), compressing tissues against rigid structures or trapping them between two surfaces [141, 142]. They most commonly affect the limbs and can damage soft tissues (*e.g.* skin, muscle, nerves) as well as underlying bone without necessarily breaching the skin [137, 143]. Injury severity depends primarily on the magnitude and duration of compression (with prolonged force increasing the risk of complications), the contact area, and the mechanical resilience of the affected tissues. [137, 142, 143].

These injuries are a major source of morbidity and mortality, and occur in both civilian and military settings, in the aftermath of natural disasters (*e.g.* earthquakes, landslides), mining incidents, terrorist attacks, armed conflicts and war [141, 144–148]. In civilian settings, crush injuries most often result from motor vehicle collisions, industrial incidents, structural collapse or falling heavy objects [141, 144, 149]. Non-traumatic cases of crush syndrome have also been reported, for example when patients experience prolonged compression under their own body weight, such as after a stroke or intoxication [141, 150].

Prolonged entrapment can result in crush injuries or crush syndrome, which may lead to limb loss or death [147, 148]. Crush injury is the direct physical compression of a muscle [148] and leads to crush syndrome in 40–70% of individuals who sustain crush injuries [148, 151, 152]. Crush syndrome (traumatic rhabdomyolysis) produces severe metabolic disturbances triggered by musculoskeletal trauma, which compromises cellular integrity and leads to the release of intracellular components into the bloodstream [143, 148, 151, 152]. In addition to crush syndrome, two other syndromes derive from compressed muscles: (1) compression syndrome arises from an indirect muscle injury produced by a simple, slow compression of a muscle group, resulting in ischaemic damage that causes muscle breakdown products to enter the bloodstream; and (2) compartment syndrome involves a rapid, localised increase in pressure within a muscle compartment, producing metabolic disturbances comparable to those seen in rhabdomyolysis [143]. This thesis focuses on crush injury itself rather than the systemic features of crush syndrome.

Pathophysiology

The pathology underlying a crush injury involves internal haemorrhage, vascular disruption, and transient or sustained ischaemia–reperfusion injury. The development of complications such as compartment syndrome depends on the characteristics of the initial trauma and contributing factors [28]. In skeletal muscle, crush forces disrupt myofibres, blood vessels and surrounding connective tissue, resulting in fibre rupture, haemorrhage and intramuscular haematoma formation [107, 153]. Prolonged compression exacerbates ischaemic injury, increasing the likelihood of necrosis [107, 153]. Muscle crush injuries share some mechanistic similarities with contusions, particularly regarding fibre damage and haematoma formation. However, crush injuries typically involve sustained force over time, causing more extensive tissue necrosis and secondary complications such as oedema and compartment syndromes. These pathophysiological changes collectively impair tissue oxygenation, and reduced oxygen delivery further increases the risk of cellular dysfunction and death [28, 154].

Crush injuries disrupt cellular integrity and provoke myonecrosis, leading to the release of myoglobin, potassium, magnesium, phosphorus, uric acid and enzymes such as creatine kinase (CK; also known as creatine phosphokinase, CPK), and lactate dehydrogenase (LDH) into the bloodstream [143, 147, 148, 151]. While these substances are essential for normal cellular activity, their presence in the circulation at high concentrations is toxic [143]. Regional ischaemia caused by occlusion of the micro- and macrocirculation leads to fluid shifts, increases muscle swelling and tension, depletes creatine kinase (CK) and ATP, and activates the nitric oxide system, thereby worsening vasodilatation and hypotension [143, 155].

Patient deterioration typically occurs after rescue, when reperfusion of ischaemic muscle disrupts the

sodium–potassium–ATPase mechanism. This sudden release of metabolites and electrolytes into the bloodstream, including lactic acid, uric acid, calcium, potassium, myoglobin degradation products and additional enzymes, can precipitate systemic collapse [143, 156]. Myoglobin filtration can exceed renal capacity, precipitating in the distal tubules and causing obstruction; this obstruction, together with vasoconstriction of the afferent arterioles, contributes to the development of acute kidney injury [143].

Elevated serum creatine phosphokinase is the most reliable marker of muscle damage, while lactic acid levels correlate with ischaemia duration [143, 157]. Notably, oliguria and kidney injury do not always reflect the severity of muscle trauma [143, 158]. Clinically, muscles appear swollen, hard, cold and necrotic [143]. Hyperkalaemia, which arises from the release of potassium into the bloodstream, may induce arrhythmias. Shock may develop, impairing gas exchange through pulmonary oedema and predisposing patients to acute respiratory distress syndrome (ARDS) [143].

Up to 80% of crush injury fatalities result from severe head or chest trauma or asphyxiation [143, 156, 159, 160]. Of the 20% who reach a hospital, approximately half recover uneventfully, whereas the other half develop crush syndrome [141, 143, 156]. Crush injuries of the torso are often fatal, but limb trauma is more survivable, with the legs affected more frequently than the arms [141, 144]. Although less common than other injury types, crush injuries have been associated with chest trauma in up to 10% of cases [143]. Overall, mortality has been reported at around 4.6%, with significantly higher rates in patients requiring amputation, particularly in elderly or other vulnerable populations [148].

Diagnosis, Management and Prevention

Diagnosis requires careful clinical assessment supported by laboratory investigations and, to a lesser extent, imaging. Key indicators include elevated CK and electrolyte disturbances, particularly hyperkalaemia, as well as markers in the bloodstream such as serum myoglobin, creatinine, urea, uric acid and LDH [143, 147, 148, 151, 158]. These markers can be used not only for diagnosis but also for monitoring crush injuries [148]. Imaging (*e.g.* ultrasound, magnetic resonance imaging (MRI), computed tomography (CT)) can be used to assess the extent of muscle, vascular and neural damage, and assist in identifying local complications. Doppler studies and monitoring weight changes can help detect limb ischaemia, while electrocardiograms (ECG), haemograms and blood gas analyses can further aid assessment of crush injuries [143, 155, 156].

Treatment of crush injuries is guided by a range of factors, including extremity perfusion, fracture patterns, the development of compartment syndrome, and haemodynamic status [148]. Management of crush injuries is structured around five phases: rescue, resuscitation, syndrome recognition, treatment, and rehabilitation. Resuscitation should begin at the site of injury, with prompt fluid replacement to protect renal function. Non-nephrotoxic antibiotics may also be necessary to reduce infection risk [143]. Wound infections are common due to impaired perfusion and compromised tissue integrity, affecting nearly one-third of patients and strongly linked with reoperation, especially in those undergoing fasciotomy, debridement or amputation [148, 161, 162]. In high-risk disaster settings, the elevated incidence of soft tissue infections following crush injury underscores the need for extreme caution in early management [148, 162, 163].

Surgical treatment depends on severity, and typically involves wide debridement of necrotic tissue with delayed wound closure. Fasciotomy is indicated if compartment pressures rise, and early interventions within 8–10 h are preferred since delays significantly increase the risk of amputation [143, 146]. Alternative interventions include fracture fixation and tetanus immunisation [141, 146]. Amputation carries higher mortality risk, particularly in elderly patients and those with bilateral lower limb ischaemia [143, 148]. Rehabilitation is essential for addressing late complications such as muscle contractures, although prolonged hospitalisation is required when injury severity is high or the affected populations face logistical challenges [143, 148, 151].

Prevention is key to reducing crush injury incidence, so adherence to occupational safety guidelines and appropriate use of personal protective equipment (PPE) are essential.

2.3.3.2 Blunt Force Trauma and Contusion Injury

Blunt force trauma occurs when a non-sharp object strikes the body, transmitting energy and damaging tissues without penetrating the skin barrier. It is among the leading causes of severe injury, particularly in individuals under 35, and is a major contributor to global mortality [3, 12, 122]. The mechanism usually involves direct contact with a blunt instrument and, depending on the intensity and site of impact, may result in contusions, abrasions, lacerations or fractures. Common causes include falls, motor vehicle collisions and sports-related impacts. Depending on the location and mechanism of injury, blunt trauma may result in haemorrhage. The severity and appearance of the resulting injuries are influenced by factors such as the magnitude of the force, contact area, duration and the resilience of the tissues involved. [117]

A contusion is caused by blunt force that damages soft tissues and organs beneath the intact skin, rupturing capillaries and causing blood to leak into the surrounding tissue. Contusions can display distinctive patterns that link an injury to the object that produced it based on the characteristics of the damage. Their appearance changes over time as haemoglobin degradation progresses and extravasated blood is broken down and reabsorbed, with colour progressing from red and purple to green and yellow. Some bruises, especially deeper or internal ones, may not present immediately [117]. Macroscopic and microscopic wound assessment helps determine injury age so that recent and older lesions can be distinguished. Early lesions typically show acute haemorrhage without organisation, while older contusions are associated with signs of healing such as fibroblast activity, white cell infiltration and haemosiderin deposition. [117]

Muscle contusions are frequent sports injuries (60% of all reported sports injuries in the United States [108]), accounting for approximately 12.1% of all cases [164]. They are more common in males (15.1%) than in females (6.3%) [164, 165], with contact sports such as football, American football and softball showing particularly high rates of muscle trauma [165]. When adjusted for exposure, contusions occur more often during competition than during training [165, 166]. Epidemiological data do not always specify injury sites, although contusions represent 14.2% of thigh injuries in high school sport (15.8% in boys and 11.2% in girls) [164], and 19% of all muscle injuries in professional football [166]. As such, muscle contusions represent a common sports-related injury, and inadequately managed contusions may prolong disability [107]. This thesis focuses on NPTIs affecting soft tissues, particularly contusions.

Pathophysiology

Muscle contusions occur when a blunt force impacts the body and compresses muscle tissue against the underlying bone, rupturing fibres and capillaries [107, 108]. This injury usually provokes bruising and bleeding underneath the skin [137, 143]. The severity depends on the anatomical site, whether the muscle was contracted at the time of impact, and individual factors (*e.g.* age, fatigue) [107]. Haematoma formation is common, occurring in over 90% of sports-related injuries following contusions or strains [108, 109].

Diagnosis, Management and Prevention

Diagnosis usually relies on clinical examination and includes imaging, which enables more detailed assessment of damage severity and distribution. Ultrasound, MRI and spectroscopy can confirm clinical findings, delineate haematomas and track healing progression [107, 167–171]. Injury severity dictates patient management and treatment: some blunt injuries require surgical interventions to control bleeding, although many are managed conservatively with supportive care [117, 172, 173].

Patients should be triaged to trauma centres if they present with major injuries (*e.g.* multiple long bone fractures, pelvic fractures, severely crushed or pulseless limbs, amputations above the wrist or ankle, paralysis, depressed skull fractures) or severe physiological compromise (*e.g.* Glasgow Coma Scale < 13, abnormal respiratory rates, ventilatory dependence) [174, 175]. The mechanism of injury is also a critical factor: those involved in high-risk motor vehicle collisions, significant falls, motorcycle accidents or pedestrian impacts require management in a trauma centre. Moreover, groups with particular needs such as the elderly, pregnant patients, children and those taking anticoagulant medication should be treated in centres equipped to deliver specialised care [117, 174, 175].

Finally, prevention remains vital. Reducing the incidence of and mortality from traumatic injuries relies heavily on effective prevention strategies, such as fall prevention and the use of seat belts and helmets. It is important to remember that outcomes largely depend on age, comorbidities, mechanism, time to treatment and number of involved organs [117]. These factors should be taken into account when managing blunt force trauma to improve recovery and tissue repair.

2.3.3.3 Strain or Stretch Injury

Skeletal muscle strain injuries occur when a muscle experiences excessive tensile force and is stretched beyond its physiological limits, often during rapid or forceful contraction [128, 176]. Strains tend to happen when the muscle is activated but can also occur at rest. In particular, strains happen more frequently during eccentric contractions, when the muscle lengthens while under tension. The tensile force is further amplified by the connective tissue surrounding the muscle, which produces additional resistance as it is stretched [177].

Strain injuries, whether microscopic or macroscopic, typically result from a mechanical initiating event [178], as muscle activation alone is insufficient to cause damage without overstretching beyond resting length [177, 179]. Injury severity depends on the extent of tissue damage, the inflammatory response and loss of function [127]. Strain injuries can affect individual fibres, fascicles, or entire muscle groups and are most common in muscles that cross two joints or are heavily involved in rapid acceleration and deceleration [180]. Severity ranges from mild microscopic fibre tears to full-thickness ruptures with functional impairment, and is influenced by the magnitude of force, the speed of contraction, the length of the muscle under tension and the muscle's previous conditioning [109, 128, 177].

Strains are particularly prevalent in sports [109, 177], but can also occur due to sudden or repeated high loads, physically demanding occupations or activities, and from sudden acceleration or deceleration, repetitive overload or over-stretching [180]. Minor injuries typically allow a full return to physical activity with no long-lasting disability, whereas major strains can result in reduced range of motion and weakness [177]. Although strains most frequently involve the lower limb, particularly the ischiotibial, quadriceps and *gastrocnemius* muscles, they can also occur in the upper limb, trunk and neck [180]. Overuse injuries may develop when tissues are repeatedly strained beyond their tolerance, ultimately leading to structural damage [181]. Risk factors include fatigue, inadequate warm-up, poor flexibility, prior injury, strength imbalance, muscle weakness, dehydration and poor neuromuscular coordination [128, 129, 176].

Pathophysiology

Strain injuries, ranging from minor tearing of individual fibres to complete rupture at the musculotendinous junction, compromise the structural integrity of muscle fibres and their associated connective tissue [177, 182]. Strain injuries are classified into Grade 1 (mild pain or swelling with no noticeable tissue disruption and little to no loss of function), Grade 2 (partial tear with moderate pain and swelling, accompanied by some functional impairment) and Grade 3 (complete tear or disruption of the musculotendinous unit with severe

pain, swelling and complete loss of function) [127, 128]. It is worth noting that the interval between the injury and its presentation varies widely, from several hours to several years [127, 183, 184].

Similar to contusions, local bleeding can lead to haematoma formation, even though strain injuries are predominantly tensile rather than compressive in nature [107, 109]. Variability in sarcomere length produces weaker sarcomeres that stretch faster and more extensively than stronger sarcomeres, provoking distortions along the myofibril, sarcomere disruption, membrane damage and impaired excitation–contraction coupling [178]. Muscle strain also activates stretch-sensitive Ca^{2+} channels, which, coupled with sarcolemmal ruptures, allow an influx of additional Ca^{2+} that elevates intracellular Ca^{2+} concentrations and may trigger proteolytic enzymes such as calpain [178].

Microtears trigger a local inflammatory response, attracting leukocytes (*e.g.* neutrophils, macrophages) and increasing pro-inflammatory cytokines (*e.g.* interleukin-6 (IL-6), interleukin-1β (IL-1β), tumour necrosis factor-α (TNF-α)), which collectively impair muscle function and further degrade muscle tissue [177, 178, 185]. Strains also induce local oedema and haemorrhage [177, 185], while severe strains may even provoke detachment of the muscle from its tendon, resulting in significant functional deficits and requiring prolonged recovery [182, 185].

At the cellular level, disruption of sarcomeres, Z-line streaming and myofibrillar disorganisation may occur, leading to the release of intracellular enzymes (*e.g.* CK, LDH) into the bloodstream [109]. This biochemical profile correlates with the extent of tissue damage and can be used to monitor recovery [178]. Subsequent fibrosis and scar tissue formation may limit contractile function and predispose patients to re-injury if rehabilitation is inadequate [128, 129].

Diagnosis, Management and Prevention

Diagnosis primarily relies on clinical assessment (*e.g.* patient history, palpation of the affected muscle, evaluation of strength and range of motion) [127]. Localised tenderness, swelling and palpable defects may indicate injury severity, but the signs and symptoms of strains vary widely between individuals, complicating diagnosis [127]. Imaging techniques such as MRI or ultrasound can confirm the extent of fibre disruption, detect haematomas and guide management, while X-rays can be used to identify bony avulsion fractures [127–129, 176]. Laboratory tests, including serum CK measurements, may support diagnosis and monitor recovery [178].

Strain injury management is typically staged, beginning with rest, ice, compression and elevation to limit further damage and reduce inflammation [109, 127–129]. Most Grade 1 and Grade 2 injuries are managed conservatively with supportive care, progressive mobilisation, analgesics and non-steroidal anti-inflammatory drugs [127, 129]. However, the outcome of Grade 1 and Grade 2 strain injuries is highly variable and unpredictable [127]. Severe (*i.e.* Grade 3) strains, such as complete tendon ruptures or significant fibre avulsions, as well as cases where conservative management has failed, often require surgical intervention [127, 184]. Following surgery, rehabilitation is essential to restore strength, flexibility and neuromuscular control through progressive reintroduction of load to prevent re-injury [128, 176].

Prevention strategies focus on conditioning, appropriate warm-up, flexibility training and gradual progression of exercise intensity [129]. Fatigue management, adequate rest and sport-specific strength training reduce injury risk [128]. Moreover, early recognition and adherence to rehabilitation protocols are essential to minimise re-injury risk and optimise functional recovery [176].

2.3.4 Microvascular Traumatic Injuries

Microvascular trauma is common but remains relatively understudied [186]. It is most often caused by penetrating (*e.g.* gunshot wounds, stabbing, blast injury) or NPTIs (*e.g.* crush, contusion, strain), but can also arise in cases involving displaced long bone fractures or prolonged immobilisation [187]. Trauma-induced vascular injury (Figure 2.12) primarily occurs at the capillary and arteriolar level [188].

Trauma-induced vascular injury is associated with narrowing of the lumen, endothelial dysfunction, impaired perfusion, altered vascular resistance, macromolecule leakage, increased permeability and compromised EC integrity leading to hypoxia, delayed healing and injury worsening [24, 189, 190]. Microvascular injury further compromises perfusion, promoting a cycle of ischaemia–reperfusion injury, oxidative stress, and EC dysfunction. The loss of endothelial integrity and glycocalyx degradation increase vascular permeability, contributing to interstitial oedema and impaired nutrient exchange between blood and tissues. Thus, permeability is a sensitive indicator of functional vascular injury [191], as it reflects cell barrier dysfunction [192].

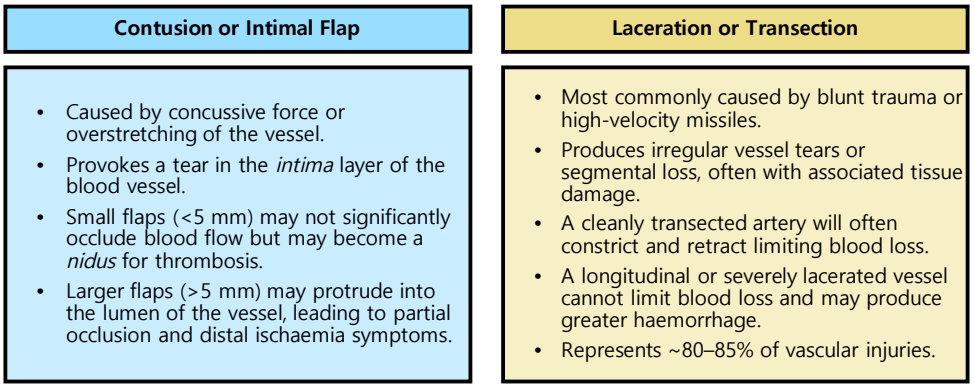


Figure 2.12: **Types of vascular injury caused by traumatic mechanisms**, showing contusion or intimal flap formation and laceration or transection, with their associated pathophysiological consequences. [187].

After trauma, the EC barrier often becomes dysfunctional, presenting as hyperpermeability (*i.e.* the usual selective permeability of the microvasculature is lost, allowing proteins, cells, small molecules and fluids to leak into surrounding tissues). The resulting fluid loss decreases circulating blood volume and reduces tissue perfusion. Hyperpermeability poses a significant risk as it contributes to tissue damage and organ failure. It is often observed as a general response to inflammation such as ischaemia–reperfusion injury, sepsis, ARDS, diabetes, thrombosis and cancer [45, 193].

Disruption of the endothelial glycocalyx is a key contributor to this process, as reduced barrier integrity (manifested as increased permeability) is closely associated with glycocalyx shedding [192]. This has been observed in both acute and chronic conditions (*e.g.* ischaemia, hypoxia, sepsis, inflammation, atherosclerosis) [194]. In trauma, inflammatory signalling, altered haemodynamics (often hypoperfusion), coagulation disturbances and impaired cellular homeostasis can degrade the glycocalyx [39]. Glycocalyx destruction results in higher shedding of glycocalyx components such as syndecans 1–4, hyaluronic acid, heparan sulphate and chondroitin sulphate into the bloodstream [192, 195]. The severity of glycocalyx breakdown appears to correlate with inflammatory state severity and mortality [17, 18]. Leukocyte-derived proteolytic enzymes have also been shown to directly degrade the glycocalyx, a mechanism that occurs during inflammation [196].

Glycocalyx thickness is an inconsistent marker of pathology. It may increase during haemorrhagic hypotension, potentially due to reduced shear stress and structural adaptation [197], but it decreases following haemorrhagic shock [192, 198]. In skeletal muscle, glycocalyx thickness correlates with blood flow, with larger reductions in flow causing more pronounced thinning [17, 198].

Diagnosis of traumatic vascular injury relies on recognising both absolute signs (*e.g.* absent pulses, ischaemia, active bleeding, pulsatile haematomas) and relative signs (*e.g.* unexplained hypotension, injury to adjacent large vessels). As such, these injuries are particularly challenging not only because they can require urgent intervention to prevent loss of life or limbs, but also because severe trauma can present with subtle or delayed signs that may emerge weeks or months later [187]. Such 'late deaths' are typically associated with microcirculatory dysfunction, irreversible microvascular shock and multiple-organ failure, highlighting the critical role of microvascular damage in trauma pathophysiology [17, 187]. Therefore, interventions to protect the microcirculation and maintain oxygen delivery are essential to reduce trauma-associated mortality [17, 187].

2.4 Current Approaches in Traumatic Injury Research

Current understanding of trauma mechanisms is based on a combination of clinical, epidemiological and experimental evidence [2, 14, 24, 26, 28, 199]. Trauma research has shifted from descriptive clinical studies towards mechanistic model-based approaches [14, 24–26]. However, capturing the immediate biological injury response in humans remains challenging due to the unpredictable nature of trauma, presentation delays (often caused by logistical, behavioural or diagnostic barriers), and ethical limitations [22, 23, 27].

2.4.1 Clinical and Epidemiological Approaches

The concept of the 'golden hour' in trauma care underscores the first 60 min after injury as a critical period influencing both survival and tissue preservation [200]. Within this time frame, rapid mechanobiological events occur: cellular and molecular alterations (*e.g.* changes in calcium signalling, phosphorylation patterns, membrane integrity) unfold within minutes, influencing subsequent repair or degeneration [201, 202]. Simultaneously, the immune system is activated, releasing both pro- and anti-inflammatory mediators and initiating leukocyte (including neutrophil) responses that may promote tissue healing or exacerbate damage [34, 203].

For instance, pre-hospital blood analyses indicate that immune and inflammatory responses are triggered almost immediately after trauma (*i.e.* within the first hour), showing evidence of both immune stimulation and suppression alongside early signs of endothelial dysfunction [34]. Biomechanical factors, including the initial mechanical stress and strain experienced by tissues, further dictate the cellular and inflammatory responses observed later [202]. Together, these findings emphasise a brief but critical therapeutic window during which early interventions may reduce secondary injury cascades, highlighting the need for experimental models that replicate the temporal and mechanical context of trauma. The early post-injury period, spanning the first minutes to hours, is therefore pivotal for understanding the mechanobiological processes determining tissue fate, but remains largely inaccessible in direct human studies [21, 23, 27].

Clinical studies employ physiological and biochemical markers such as CK, myoglobin, LDH, and inflammatory mediators including IL-6 and C-reactive protein (CRP) to infer tissue damage, inflammation, and repair processes [2]. These are complemented by imaging modalities such as ultrasound and MRI, which visualise oedema, haematoma and tissue deformation [182, 202]. Epidemiological studies further extend this knowledge by defining the prevalence, mechanisms and outcomes of NPTIs across populations, while identifying risk factors such as age, occupation and activity profile [5]. However, these approaches remain largely retrospective and observational, and therefore offer limited mechanistic insight into the biological processes underlying injury progression and recovery.

2.4.2 Experimental Approaches

To overcome these limitations, experimental approaches, particularly *in vivo* models, have been instrumental in studying NPTIs under controlled conditions. In particular, small animal models have been frequently used for trauma research [14], including rats [24, 28, 35, 199, 204, 205] and mice [28–30], although larger animal models such as pigs [25, 31] and non-human primates [32, 33] have also been employed. *In vivo* models have studied critical processes such as EC dysfunction, apoptosis, vascular leakage, and systemic inflammatory activation [24–26, 34]. Nonetheless, translation to human physiology remains limited by interspecies differences, ethical concerns and reproducibility challenges [14, 36]. Consequently, there is growing demand for physiologically relevant *in vitro* systems that enable precise, reproducible and ethically acceptable investigation of soft tissue trauma, offering lower cost, higher throughput and greater experimental control than *in vivo* approaches [36].

Experimental models aim to replicate the mechanical and biological consequences of NPTIs in a controlled, reproducible and quantifiable manner. These systems are typically categorised by the type of injury they simulate, each offering trade-offs between physiological complexity and experimental control.

Several experimental methods have been used to replicate mechanical injuries on soft tissues, the majority of which use *in vivo* models. Most experimental setups designed to replicate contusion injuries use a blunt non-penetrating impact model, where a metallic weight is dropped through a guide tube. In these setups, parameters such as the object's mass and shape, as well as the height from which it is dropped play a key role in the mechanism of injury [119, 206, 207].

Contusion injuries are frequently modelled using weight-drop, impactor or indenter devices [35, 204, 208]. Weight-drop models, including metallic mass drop systems [204] and miniature impactors [208], rely on dropping a mass or weighted plunger from a defined height. These approaches are applied to skeletal muscle, brain tissue and tissue-engineered constructs [32, 33, 35]. By modifying parameters such as mass, drop height or geometry, researchers can achieve precise control over impact energy and injury severity can be achieved, enabling systematic investigation of vascular disruption, inflammation and tissue regeneration [32, 33].

Impactor systems, which may be electromagnetic [209] or pneumatic [30], use actuators to deliver rapid, controlled displacements or forces to induce reproducible tissue damage, offering fine control over impact velocity, depth and duration across *in vitro*, *in vivo* and *ex vivo* models. Within *in vitro* settings, miniature impactors or indenters such as electromagnetic impactors [209] and mini weight-drop devices [208] have enabled quantitative assessment of impact force, tissue deformation and cellular injury thresholds. These setups have been used with organotypic brain slices, three-dimensional (3D) cultures and engineered tissues (*e.g.* human induced pluripotent stem cells; iPSCs) [30, 208, 209].

Crush or compression injuries are typically replicated *in vivo* and *ex vivo* using forceps (*e.g.* Martin's microsurgical forceps, Dumont forceps) [210, 211], clamps (*e.g.* non-serrated haemostatic forceps, mosquito forceps, Kelly straight clamp) [211, 212], clips (*e.g.* surgical clip, aneurysm clip) [205, 211], and presses or weights [213, 214] to apply controlled pressure for specified durations [14, 26, 211]. Studies using presses or weights typically involve longer crushing durations, often exceeding 6 h [213, 214], whereas those using forceps, clamps or clips are generally applied over timescales of minutes. These models reveal mechanisms such as ischaemia–reperfusion, necrosis and inflammatory progression [36, 211]. However, some approaches, such as surgically exposing and compressing muscle with forceps, are more invasive as they require surgical tissue exposure and introduce an element of penetrating trauma that is not fully representative of clinical crush injuries [119, 207, 215].

Motorised and mechanical compression systems have been developed to overcome these limitations, delivering uniform, reproducible forces that capture microstructural collapse and vascular failure [211, 212]. Examples include custom-made dead-lift devices [211, 212], material testing machines [216], water-hammer

systems [217] and gel-based compression platforms [218], which have been used to apply static or dynamic compressive forces [36] in both *in vivo* and *in vitro* models.

A systematic review (SR) by Kitano *et al.* (2025) [211] reported that clamps were most frequently employed (52.4% of studies), followed by forceps (23.8%) and clips (19.0%), whereas other devices accounted for only 4.8%. Regarding compression duration, 57.1% of studies applied 30 s of pressure [210], 23.8% applied 60 s [219], 14.3% exceeded 60 s [205, 212], and only 4.8% were shorter than 30 s. Some studies induced crush injuries over more prolonged periods (≤ 10 min) to mimic severe ischaemic injury or evaluate reperfusion outcomes [205, 211, 212]. Most experiments involved a single crushing event, although repeated compressions (*e.g.* three cycles lasting either 30 s or 5 s) have been used to investigate cumulative effects.

Strain-based models reproduce deformation caused by stretching or torsion, commonly observed in musculoskeletal trauma and overuse injuries. These approaches employ bioreactors or flexible membranes to impose cyclic or static strain or tension, and include fluid percussion, biaxial stretching (*e.g.* inflation of O-ring-bound flexible membranes), vacuum-driven deformation (*e.g.* Flexcell), captive-bolt and blast injury systems (*e.g.* blast waves) [14, 35, 119, 207, 220–222]. *In vitro*, strain has been applied using cell-injury controllers that deliver calibrated pulses of compressed gas to cultured cells [36], as well as using custom-made devices.

Together, these NPTI models have advanced the understanding of trauma pathophysiology but have been mainly used in *in vivo* models [210, 211, 213, 214, 219]. In contrast, current *in vitro* systems often lack vascularisation, limiting their ability to reproduce the coupled mechanical and biological processes central to soft tissue injury and repair [36].

Since microvessels are essential for oxygen and nutrient delivery, their structural damage, combined with immune responses, can be life-threatening. Thus, a deeper understanding of how the vascular system responds to mechanical trauma is crucial for improving care for this major global health challenge, particularly as LMICs bear the greatest burden. Advances in *in vitro* models, such as organ-on-a-chip technologies, now make it possible to study trauma without relying on animal or human experimentation. [207]

To address these limitations, researchers are increasingly using advanced *in vitro* models, particularly those relying on 3D cell cultures, tissues and organoids, that better mimic the complex architecture and mechanotransductive properties of human tissues [30, 208, 223]. Hydrogels fabricated from biomaterials have emerged as highly promising scaffolds for soft-tissue modelling due to their intrinsic biocompatibility and customisable physicochemical properties (*e.g.* stiffness, porosity, biodegradability), which can be tailored to mirror native tissue mechanics. Their viscoelastic nature allows deformation under load comparable to that of native soft tissues, making them reproducible platforms for studying compressive and impact-induced injuries [223–225]. When engineered to mimic the ECM, hydrogels further enhance physiological relevance by supporting cellular adhesion, signalling and remodelling [225, 226]. Among these, fibrin-based hydrogels are particularly advantageous: as a natural product of the coagulation cascade, fibrin promotes EC adhesion, migration and angiogenesis while enabling matrix remodelling and controlled biodegradation [227].

2.5 Tissue Engineering (TE)

Tissue engineering (TE), which is part of regenerative medicine, is a multidisciplinary field that brings together medicine, materials science and engineering to replace, repair, or regenerate damaged or diseased tissues and organs [228–233]. TE's foundation lies in replicating the structural, mechanical and biochemical characteristics of native tissue environments to guide cell behaviour; for instance, by developing TE constructs. TE constructs consist of scaffolds embedded with cells that, once implanted, provide a means for the body to repair defects that would otherwise not heal due to the limited regenerative capacity of certain tissues. This regenerative

potential is tissue-specific and is also influenced by wound size and host response [234]. TE scaffolds and constructs can be developed using both *in vitro* and *in vivo* approaches [99] (Figure 2.13).

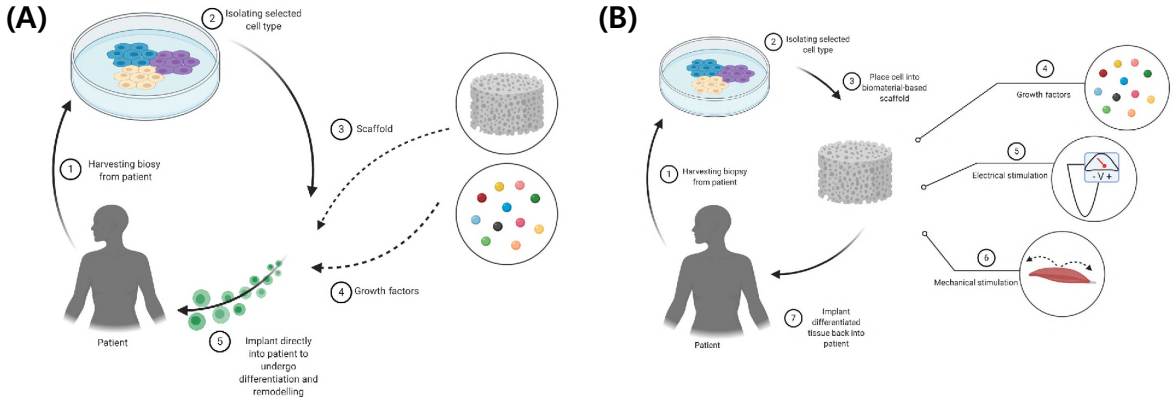


Figure 2.13: **Schematic representation of tissue engineering (TE) strategies: (A)** *in vivo*, where a biopsy is harvested, cells are isolated, expanded and then seeded into a scaffold before direct implantation into the patient, allowing differentiation and remodelling to occur within the host; and **(B)** *in vitro*, where isolated cells are seeded into a biomaterial-based scaffold and exposed to bioactive factors and signals (*e.g.* electrical or mechanical stimulation, growth factors) to generate functional tissue prior to implantation. Here, skeletal muscle is shown as an illustrative example. Modified from Abdalla *et al.* (2022) [99].

The primary objective of TE is threefold: to restore function, repair the damage, and regenerate the disease- or injury-damaged or impaired tissue or organ by delivering elements such as constructs embedded with cells [229]. A further purpose lies in developing *in vitro* tissue and organ models for disease research and modelling, as well as drug and therapeutics testing. While *in vivo* models have traditionally been used for these purposes, they present limitations, including ethical concerns, limited physiological similarity to humans, high costs, and inefficiency. In contrast, *in vitro* bioengineered tissue models offer a promising alternative.

Applications of TE extend across clinical medicine, engineering, and the physical and materials sciences. TE applications have been investigated for nearly all tissue and organ types, including muscle, bone, skin, and liver [235]. However, the stage of development and clinical adoption of TE products varies considerably. While some applications remain in early *in vitro* and *in vivo* research, particularly for more complex tissues, others are readily commercially available [232]. Several TE-based medical products have received approval for clinical use, including for skin (*e.g.* Omnigraft, ReNovaCell, Hyalograft, Dermagraft), bone (*e.g.* Ossron, INFUSE bone graft), cartilage (*e.g.* MACI, Ortho-ACI, Spherox), heart (*e.g.* CardioCel, HeartSheet), and nerve (*e.g.* Avance nerve graft, Neurotube) [236].

Advances in biomaterials and regenerative medicine have enabled researchers to reproduce particular tissue and organ functions and structures in the laboratory [237], enabling the development of models for physiological research [238], drug and therapeutics testing [239], and disease modelling [240]. Moreover, recent advances in TE have introduced novel therapeutic strategies that aim to construct functional replacements for damaged tissues by integrating cells, biomaterials, and bioactive agents [74, 241, 242]. TE applies the combined principles and methods of engineering and life sciences [229].

Although significant progress has been achieved in TE, numerous challenges remain before widespread clinical translation and commercialisation can be achieved [231, 233]. Current limitations include incomplete integration with native tissue, poor quality of regenerated tissues [243], structural and biological complexity of 3D tissues and organs, regulatory restrictions, cell maturation-derived challenges [236], the difficulty of regenerating tissues with predominantly biomechanical functions [231], and high costs [244]. Additional challenges include securing reliable cell sources, minimising the immunogenicity of scaffolds and constructs,

engineering functional vascular and neural networks within bioengineered tissues, and addressing commercial and regulatory barriers [232]. Nevertheless, inadequate vascularisation remains one of the greatest obstacles to clinical translation. Vascular networks are essential for the delivery of nutrients and oxygen and the removal of metabolic waste; consequently, limited or absent vascularisation restricts scaffold size and is a major contributor to the clinical failure of current TE products [223, 232].

2.5.1 TE Components

The cornerstone of TE is a triad (Figure 2.14) of scaffolds, such as hydrogels, which provide a structure for tissue growth; cells, such as human umbilical vein endothelial cells (HUVECs), which enable tissue formation; and bioactive factors and signals, such as growth factors, which promote cell growth and differentiation [225, 228, 230–233, 245].

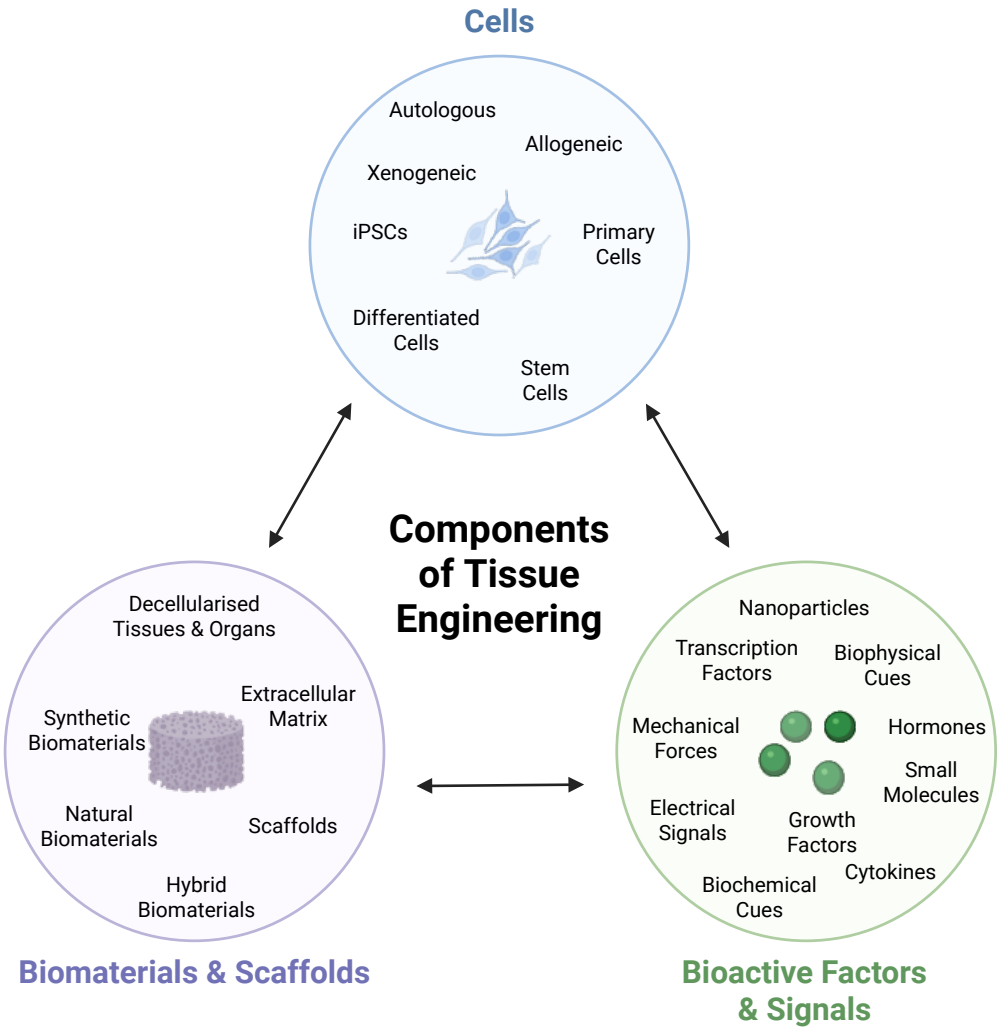


Figure 2.14: **Tissue engineering (TE) triad: biomaterials and scaffolds; cells; and bioactive factors and signals.** Biomaterials may be natural, synthetic, or hybrid, and are used to fabricate scaffolds such as hydrogels and meshes. Scaffolds can also be derived from decellularised tissues, whole organs, or the extracellular matrix (ECM). Cells used in TE are diverse, ranging from autologous to heterologous sources, and may include primary cells, stem cells, differentiated cells, or induced pluripotent stem cells (iPSCs). Bioactive factors and signals encompass a wide spectrum of regulators, including growth factors, biochemical and biophysical cues, mechanical forces, electrical signals, cytokines, small molecules, transcription factors, hormones, and nanoparticles. [230–233]. Created with *BioRender.com*

2.5.1.1 Scaffolds

Scaffolds are 3D matrices that provide temporary structural support to cells, enabling them to attach, proliferate, differentiate, migrate, perform their functions and maintain their native morphology [99, 244, 246–248]. To do so, scaffolds must satisfy several requirements, including suitable biocompatibility, mechanical properties, biodegradability and structural stability, as well as facilitating oxygen and nutrient transport [249].

Scaffolds can be embedded with cells or implanted acellularly to stimulate host cell migration [250] and may also be functionalised (*e.g.* drugs, proteins, nanoparticles) depending on their intended application and target tissue [80, 251]. Since scaffolds are designed to mimic the native ECM, which plays a central role in regeneration, an effective TE scaffold should replicate its structural and biochemical properties to produce more reliable models and implants. Consequently, scaffold design will vary according to the target tissue and the specific aims of the research or clinical application [99, 252].

Biocompatibility with the host tissue, organ and organism is essential to minimise immune rejection [99, 244, 248]. This encompasses properties such as biofunctionality, bioinertia, bioactivity and biostability, as well as minimising or, ideally, avoiding triggering adverse effects like systemic, subacute or subchronic toxicity [253]. Moreover, scaffolds must be biodegradable without producing toxic by-products [254]. Scaffold degradation is particularly important, as embedded cells or those migrating from the host tissue will start producing their own native ECM. Thus, the degradation rate must be carefully controlled: if it is too rapid, the scaffold may collapse before adequate ECM is deposited, but if it is too slow, it may hinder tissue integration and remodelling.

Achieving this relies greatly on the careful selection of an appropriate biomaterial (Section 2.5.2.4), which also plays a key role in the biological, mechanical and structural properties of scaffolds. These can be fine-tuned by altering the materials used, the type of scaffold manufactured (*e.g.* mesh, fibres, hydrogel) and the fabrication methods employed [255]. Mechanical properties are particularly important for replicating the behaviour of native tissues and for enabling processes relevant during research and clinical applications such as handling, preparation and implantation. Scaffolds must also allow for adequate diffusion of nutrients, gases and signalling molecules, while supporting the removal of waste products and neovascularisation, which is critical for cell survival [99, 247, 256]. This can be achieved, for example, by ensuring the scaffold is porous [249].

Scaffolds were once regarded solely as passive structural supports; however, advances in biomaterials, bioengineering, chemistry and physics have enabled the engineering of scaffolds that actively promote regeneration [99, 257] and perform specialised functions such as controlled drug release, for instance, through embedding nanoparticles. They can also direct cell alignment to reproduce the organisation of native tissues; for example, nanofibre matrices aligned in parallel enable unidirectional alignment of myoblasts and neural cells to better replicate muscle fibres or peripheral nerves [99, 252, 257].

Scaffold material properties also play a role in the capacity to withstand forces (*e.g.* unidirectional stress) as well as in biodegradation, which can be tailored to be at a rate similar to the natural tissue. This is particularly important for load-bearing tissues, such as skeletal muscle, where biomechanical performance is essential [99, 258]. 3D matrices with structural, mechanical and chemical properties resembling native environments (*e.g.* fibrous porous scaffolds) have facilitated the development of constructs capable of replacing load-bearing tissues, as well as the maturation of functional tissue engineering (FTE) [231].

Beyond structural and mechanical properties, effective scaffold design also requires consideration of the biochemical and temporal cues provided by the native ECM. Scaffolds play a central role in supporting cells, establishing specific structures, and enabling defined physical and biological functions through biochemical or mechanical signals once implanted [231]. Such models also offer customisation and accurate monitoring of conditions and control parameters including cell types, culture media, substrate properties and applied forces while remaining customisable for each application.

Therefore, scaffolds play a key role in TE by providing structural support, directing cell organisation and enabling specific physical, chemical and biological interactions with cells, for instance through growth factors, once implanted in the body. Scaffolds can be customised not only by varying their formulation and design, but also by embedding different cell types (Section 2.5.1.2) or supplying bioactive factors and signals (Section 2.5.1.4), allowing scaffolds to be tailored for specific research or clinical needs.

Hydrogels

Gels are widely used in TE as scaffolds and may be defined as 3D crosslinked networks swollen by water (hydrogels), a solvent (lyogels) or a gas (aerogels), forming homogeneous biphasic matrices that can be regarded as intermediates between solids and liquids or between solids and gases. As such, they bridge the characteristics of solids and fluids [259]. Hydrogels are a subclass of gels consisting of physically or chemically crosslinked 3D polymer networks [223, 260] capable of absorbing and retaining large amounts of water or biological fluids while maintaining their structural integrity [224, 260]. When exposed to a compatible solvent, liquid becomes entrapped within the pores or interstitial spaces of the network, resulting in swelling and consequent changes in both the dimensions and rheological properties of the hydrogel [224, 260]. They exhibit viscoelastic behaviour, with the storage modulus (G') exceeding the loss modulus (G") [259].

Hydrogels can be fabricated from natural polymers like agarose, alginate, chitosan, collagen, fibrin, gelatine and hyaluronic acid, as well as synthetic polymers such as polyvinyl alcohol (PVA), polyacrylic acid (PAA) and polyacrylamide (PAM) [260–262]. Their intrinsic properties (*e.g.* hydrophilicity, swellability, gelation, porosity, biocompatibility, biodegradability, mechanical strength) make them useful for a wide range of applications across different industries, from water purification to the removal of toxic materials and pollutants and to, relevantly, bioengineering and medicine [224, 260, 262–264]. In particular, their ability to mimic the ECM at structural and biochemical levels [223, 225] has made them very relevant TE scaffolds.

Moreover, hydrogels have been used as an immobilisation matrix suitable for mammalian cells and they have excellent biocompatibility and bioactivity [264], especially when using protein-based polymers (*e.g.* fibrin [225, 227, 265], collagen [225, 266] and gelatine [225]). Hydrogels have also been designed to be cast, injectable, sprayable and implantable, which further expands their range of applications [224].

However, a key challenge associated with hydrogels is finding the optimal balance between biological and mechanical properties. Higher-concentration hydrogels typically exhibit greater mechanical strength but may restrict cell proliferation and migration, whereas lower-concentration hydrogels can better support cell growth and function but possess weaker mechanical properties [28]. As such, integrating both biological assays and material characterisation in the development of hydrogel scaffolds is essential for biomaterial selection, hydrogel formulation and scaffold design [267].

For instance, in the case of ECs, the scaffold materials play a key role in enabling cell infiltration into the scaffold, cell proliferation, and, centrally, the formation of microvasculature stimulated by growth factors [268]. In particular, the mechanical properties of hydrogel substrates can enable or limit cell proliferation or differentiation [269].

Finally, hydrogels have certain features that make them highly valuable in pharmaceutical and biomedical applications. Their composition and mechanical characteristics, often resembling those of the native ECM, enable them to act as effective scaffolds for supporting cells during tissue regeneration and as carriers for therapeutic agents. Their soft, water-absorbing nature enables the formation of hydrated yet structurally stable materials, mimicking the cellular environment within the body. Additionally, the elastic network structure of fully swollen hydrogels helps minimise tissue irritation following implantation. Their inherent hydrophilicity and crosslinked structure also contribute to excellent biocompatibility, while the low interfacial tension between the hydrogel surface and body fluids (once implanted) reduces protein adsorption and cell adhesion,

thus lowering the likelihood of adverse immune responses. In addition, the mucoadhesive and bioadhesive properties of polymers commonly used in hydrogel synthesis, such as polyacrylic acid (PAA), polyethylene glycol (PEG) and polyvinyl alcohol (PVA), enhance drug residence time at biological interfaces (*e.g.* skin, plasma membrane), thereby improving tissue permeability and therapeutic efficacy. [226]

2.5.1.2 Cells

While not all TE scaffolds require cells to be pre-seeded before use in research or clinical settings, when cells are used, the selection of an appropriate and relevant source is critical [270]. The choice of cell type is guided by the intended application, target tissue and experimental or clinical objectives. Cells employed in TE include primary cells, iPSCs and stem cells [271]. Broadly, cells used in TE can be categorised based on their origin as autologous (cells derived from the same individual), allogeneic (cells derived from another individual of the same species), or xenogeneic (cells from an individual of another species) [272]. Each type offers different advantages and limitations concerning biocompatibility, scalability, and ethical and logistical feasibility.

Autologous cells are widely used in regenerative medicine applications due to a generally lower risk of immune rejection since they originate from the patient's own tissue. However, obtaining them in sufficient quantities can be technically and ethically challenging, particularly in elderly or severely ill patients who may have limited regenerative capacity [272, 273]. Moreover, the isolation and expansion of autologous cells are time-intensive processes and the pool of available specialised cells is often limited [255]. Importantly, their use is also restricted to the donor-patient, limiting scalability [274]. Despite these limitations, autologous cells remain a preferred choice for patient-specific therapies and personalised regenerative applications [274].

Allogeneic cells, obtained from healthy donors, offer a more readily available, practical and scalable option. These cells can be expanded, characterised and cryopreserved to generate 'off-the-shelf' TE products and for direct use in research. Therefore, their use enhances reproducibility and standardisation. Nevertheless, challenges persist regarding donor variability, limited donor availability and potential immunogenicity, which may demand immunosuppression or the use of immune-privileged cell types [274]. The generation of specialised, functional cells from allogeneic stem cell sources, such as iPSCs, also remains technically challenging due to the difficulty in precisely directing their differentiation into functional specialised cells. [99, 274].

Xenogeneic cells, commonly sourced from animal tissues, offer advantages in availability and scalability. These cells can be isolated and expanded from well-characterised tissues in which lineage and function are established, facilitating experimental reproducibility [274]. Nonetheless, their translational use is limited by ethical and safety concerns, particularly regarding the risk of viral transmission of zoonotic pathogens (*e.g.* porcine endogenous retroviruses) and immune incompatibility [272, 274, 275]. Despite these challenges, xenogeneic cells remain a viable source for modelling, research and therapeutic applications in human disease [274].

Cell Selection and Potency

To ensure reproducibility and clinical relevance, TE applications benefit from the use of cell populations that are commercially available, capable of appropriate differentiation (when applicable) and suitable for transplantation into human recipients [99]. Cells with high proliferative and differentiation potential (*e.g.* adipose-derived, embryonic or perivascular stem cells, bone marrow-derived or umbilical cord-derived mesenchymal stem cells (MSCs), iPSCs) are particularly advantageous [99, 248]. These cells offer a balance between regenerative potential and scalability, enabling applications across various tissue types.

Among these, pluripotent stem cells are of particular interest because of their ability to generate multiple specialised cell types. For example, myogenic progenitor cells generated *via* Pax7 overexpression have been shown to improve muscle function following transplantation *in vivo* [99, 276, 277]. Similarly, human pluripo-

tent stem cells cultured within 3D systems and transplanted into murine models have successfully formed functional, vascularised skeletal muscle tissue [99, 278, 279].

iPSCs, derived from somatic cells through reprogramming with Yamanaka factors (*e.g.* Oct3/4, Sox2, Klf4, c-Myc), offer a renewable and patient-specific source of cells for TE applications [99, 280]. Their use is particularly promising in skeletal muscle and microvascular engineering, where they can be seeded into scaffolds pre- or post-differentiation into lineage-specific precursors [99, 248]. Such flexibility facilitates the generation of physiologically relevant constructs for both mechanobiological and reparative studies.

Cell–Scaffold Interactions and Functional Tissue Engineering (FTE)

Cells are in constant contact with their surrounding ECM, through which they perceive their mechanical environment. In particular, the mechanical environment plays a key role in determining their responses, which allows blood vessels to adapt [281]. Responses to altered blood flow, clinical treatments and disease processes suggest that blood vessels seek to maintain a homeostatic mechanical state [281]. This has been observed experimentally in isolated microvessels, cell-seeded collagen gels and isolated adherent cells.

Cells are typically incorporated into biomimetic scaffolds designed to emulate the biochemical composition, structural organisation and mechanical properties of the ECM. Synthetic ECMs provide controllable and reproducible environments that can be customised to influence cell adhesion, proliferation and differentiation by providing mechanical and biochemical cues. However, achieving physiologically relevant maturation requires a deeper understanding of the dynamic and temporal nature of native ECM signalling, particularly regarding the timing and interplay of mechanical and biochemical stimuli. [282]

At the mechanobiological level, cell–scaffold interactions greatly influence cell behaviour and function. Mechanical forces such as tension, compression and shear stress modulate cytoskeletal organisation, gene expression and lineage specification, directly affecting tissue formation and functionality. Recognising these interactions has led to the development of the subdiscipline known as FTE, which explicitly integrates biomechanics and mechanobiology into TE design and assessment. FTE is especially relevant to load-bearing tissues like skeletal muscle, where mechanical properties must be considered under both sub-failure and failure conditions to establish benchmarks for evaluating repair strategies and long-term functional outcomes. Importantly, FTE acknowledges that the mechanical properties of constructs must be carefully prioritised and optimised in each case, as fully replicating the complexity of native tissue remains a formidable challenge. [231, 283]

Several factors, such as scaffold material composition, ECM microarchitecture and external stimulation (mechanical, electrical, or biochemical), collectively influence cellular maturation and integration within engineered constructs [99, 231, 283]. Achieving an optimal balance between these parameters remains central to the successful translation of TE strategies from the laboratory to clinical application.

2.5.1.3 Endothelial Cells (ECs)

The choice of EC source is critically influential in microvessel modelling, affecting barrier function, angiogenic responsiveness and stability [45]. ECs show differences in structure, function, and protein and gene expression depending on the location of the body [284]. Primary human ECs (*e.g.* HUVECs) are often used for their well-characterised phenotypes and responsiveness, though donor variability and limited proliferation capacity are drawbacks [285, 286]. Endothelial progenitor cells (EPCs) or iPSC-derived ECs (iPSC-ECs) overcome the limited availability of primary ECs and potentially offer greater plasticity [99, 280]. Nevertheless, stem cell-derived cells may require extensive differentiation protocols and maturation steps to reach a functional phenotype [284]. Ultimately, the selection of ECs should aim to achieve a careful balance of biological fidelity and physiological

relevance with practical considerations in terms of availability, reproducibility and compatibility with the target microvessel model [284, 287].

Both macrovascular and microvascular cell types have been used for microvascular *in vitro* models. Of these, two primary human cell types are particularly promising for TE microvasculature *in vitro* models: HUVECs and MVECs, such as human dermal microvascular endothelial cells (HDMEC-1).

(1) Human Umbilical Vein Endothelial Cells (HUVECs)

HUVECs have been widely used in *in vitro* models, particularly for modelling angiogenesis and vascularisation, due to their availability and demonstrated ability to form neovasculature [270, 285, 286, 288, 289]. These cells are frequently employed in self-organised microvascular models, where they form interconnected networks, facilitating the study of capillary-like structures and angiogenic processes [287, 290, 291]. HUVECs have well-characterised behaviour *in vitro* [285, 286, 288, 289] and are widely regarded as a standard model for cell-based assays investigating angiogenesis [286, 289, 292, 293]. HUVECs have been instrumental in various applications, including pharmaceutical and cancer research, owing to their ability to form tube-like structures on scaffolds [294–296]. However, their utility is limited by the temporary nature of these networks: they typically begin to deteriorate around 18 h after seeding and completely disintegrate within 24 h due to hypoxia and the absence of growth factors, leading to apoptosis [297–299]. Thus, this short lifespan restricts their application in long-term studies.

(2) Human Dermal Microvascular Endothelial Cells (HDMECs)

HDMECs, derived from the microvasculature, possess distinct characteristics that make them highly suitable for modelling microvascular structures in TE. They express proteins associated with tight junctions, which are essential for regulating capillary permeability and maintaining endothelial barrier function [270, 300, 301]. Compared with HUVECs, HDMECs show higher expression of claudin-5 while maintaining equivalent levels of vascular endothelial-cadherin, and they display greater transendothelial electrical resistance (TEER) but lower macromolecular flux [301]. Their phenotype supports the formation of stable, selectively permeable vessels and they are capable of forming microcapillary-like structures *in vitro*, both in the presence and absence of exogenous angiogenic stimuli, for instance when cultured on scaffolds such as polycaprolactone-collagen or when in co-culture with other cell types (*e.g.* fibroblasts, osteoblasts) [270, 302]. Importantly, these cells can differentiate into functional microvessels capable of anastomosing with the host vasculature when implanted *in vivo* [302] and can also be safely harvested from a biopsy and expanded *ex vivo* [270], providing a promising autologous and allogeneic microvascular cell source [270].

2.5.1.4 Bioactive Factors and Signals

The third TE component encompasses bioactive factors and signals, which direct cell behaviour and stimulate tissue formation. These regulatory elements influence key cellular processes, including migration, adhesion, proliferation and differentiation, ultimately guiding tissue development and remodelling within the engineered microenvironment [245, 303]. Bioactive factors and signals encompass a wide range of regulators that play a role in tissues all over the body, many of which can be applied in TE to guide cell behaviour (Table 2.5).

Traditionally, research has often focused on molecules such as mitogens, growth factors and morphogens, which provide biochemical cues that promote tissue-specific cell behaviours [303, 304]. However, cellular responses are rarely dictated by biochemical signals alone. Mechanical, electrical and other biophysical stimuli act together to modulate cellular activity, promote tissue maturation and enhance the overall functionality of engineered constructs [303].

Table 2.5: **Bioactive factors and signals in tissue engineering (TE) and their roles in various tissues**, including growth factors, cytokines, extracellular matrix (ECM) components, small molecules, surface topography, mechanical cues, electrical cues, low-frequency magnetic fields, ultrasonic fields, thermal energy and non-ionising non-thermal light treatment or exposure. Adapted from Bakhshandeh *et al.* (2022) [303].

Type	Factors	Roles in Various Tissues
Growth Factors	Epidermal Growth Factor (EGF)	Wound healing; proliferation and tensile strength of the dermis; epithelium differentiation.
	Fibroblast Growth Factor (FGF)	Morphogenesis; brain patterning; muscle regeneration; RAS-MAPK and PI3K-AKT activation; blood vessel formation; bone formation.
	Transforming Growth Factor-β (TGF-β)	Cell differentiation and proliferation; metabolism of ECM proteins; regulation of the inflammatory responses; stimulation of mesenchymal cells (MSCs); inhibition of ectodermal cells; wound and tissue healing; suppression of autoimmune diseases; matrix synthesis.
	Bone Morphogenic Proteins (BMPs)	Cell proliferation, migration, and differentiation; osteogenesis and cartilage formation; angiogenesis.
	Platelet-derived Growth Factor (PDGF)	Production of autocrine factors, fibronectin, and hyaluronic acid; osteogenesis and cartilage formation; promotion of vascularisation.
	Vascular Endothelial Growth Factor (VEGF)	Vascularisation.
	Neurotrophic Factors (NTF)	Cell growth, survival, migration and proliferation; re-myelination; morphological plasticity; modulating intracellular signalling pathways; axonal regeneration and neural differentiation.
Cytokines		Cell growth and differentiation; immune regulation; regeneration of damaged tissue; bone regeneration; osteochondral regeneration.
ECM components		Cell survival, growth, adhesion, proliferation, and migration; wound repair; cartilage, bone, vascular and skin regeneration.
Small Molecules		Cell differentiation; endogenous stem cell lineage commitment; modulate specific intracellular processes; improve cell–cell and cell–scaffold interactions.
Surface Topography		Cell proliferation and migration; rearrangement of cytoskeletal alignment and intracellular focal adhesion proteins; activation of intracellular signalling and mechanotransduction pathways; chondrogenesis; osteogenesis; nutrient diffusion.
Mechanical Cues		Cell quiescence, division, and differentiation; reorientation and reorganisation of the cell cytoskeleton; tissue-specific ECM components production; gene expression; cell protein profiling; lineage specification and commitment; osteogenesis; organogenesis.
Electrical Cues		Regulating the function of receptors for different ions; neuron synapses; muscle contraction; osteogenesis; cardiogenesis; neurogenesis; wound healing.
Low-frequency Magnetic Fields		Improved cell alignment and proliferation; cytosolic Ca^{2+} and calmodulin activation; effective in musculoskeletal and neurological disorders; fracture healing; chondrogenesis; osteogenesis; neurogenesis.
Ultrasonic Fields		Improved cell alignment and proliferation; cellular metabolism; applying energy to the cellular cytoskeleton; neuron conduction and differentiation; cardiomyocyte beating; cell cycle regulation; activating ERKs/MAPKs pathways; fibroblast proliferation; angiogenesis; osteogenesis.
Thermal Energy		Killing osteosarcoma cells; myogenic and osteogenic differentiation.
Non-ionising, Non-thermal Light Treatment/Exposure		Cell survival; reducing inflammation; promoting tissue healing; osteogenesis; wound healing.

These bioactive factors can be broadly categorised into biochemical, biophysical and material-derived cues. Biochemical regulators include growth factors (*e.g.* EGF, VEGF, FGF, TGF-β), cytokines (*e.g.* interleukins, neurotrophic factors), hormones (*e.g.* IGF-1, IGF-2), transcription factors (*e.g.* MyoD, myogenin, Myf5) and small molecules (*e.g.* cardionogen, cyclosporin A), all of which play key roles in directing specific cellular pathways and differentiation processes. Biophysical stimuli encompass mechanical forces (*e.g.* shear stress, tension, compression) and electrical cues (*e.g.* direct electrical stimulation), which act in concert with biochemical signals to modulate cell activity, promote alignment and enhance tissue functionality. Additional cues, such as ECM components (*e.g.* collagen, fibronectin, hyaluronic acid), nanoparticles (*e.g.* cerium oxide, nanoclays) and surface topographical features (*e.g.* porosity, micropatterning, nanotopography, alignment), provide structural and physicochemical guidance that influences cell adhesion, migration and organisation. [99,242,303,305,306]

These factors enable the precise and controlled modulation of cell behaviour within TE constructs [80, 242, 303, 305, 306]. Importantly, their interplay is crucial for achieving physiologically relevant outcomes, as

these cues rarely act in isolation *in vivo*. In TE systems, the simultaneous application of multiple stimuli (*e.g.* applying electrical stimulation to topographically patterned scaffolds) often yields more robust and functionally mature tissues than single-factor approaches. Mechanical loading, for example, can potentiate the effects of growth factors, while electrical cues promote cell alignment and differentiation, particularly in cardiac and neural tissues. When applied in combination, these cues can act synergistically to accelerate the formation of FTE constructs and enhance their suitability for translational applications. Conversely, certain cues may interact antagonistically; for example, persistent topographical or mechanical signals can, under specific conditions, suppress biochemical induction pathways. Furthermore, the simultaneous application of multiple stimuli increases the complexity of *in vitro* models, potentially complicating reproducibility and hindering the identification of biological responses to individual factors. [99, 303]

These cues may be directly incorporated into scaffolds or delivered in a controlled, spatio-temporal manner, mimicking the dynamic signalling environment of natural tissue processes. Their integration within TE constructs has shown enhanced cell viability, promoted vascularisation and supported the formation of functional, well-organised tissue architectures. Nevertheless, their practical implementation remains challenged by high production costs, limited stability, short half-lives and rapid loss of bioactivity. [303, 305]

2.5.2 TE Scaffolds and Constructs: Design, Fabrication and Biomaterial Selection

2.5.2.1 Design Elements

Scaffold design is a critical determinant of success in TE, as scaffolds provide both the physical framework for tissue formation and the mechanical support required during regeneration. An ideal scaffold should be biocompatible, biodegradable and possess appropriate mechanical strength and porosity to permit cell infiltration, nutrient diffusion and vascular ingrowth [244].

The properties of a scaffold are strongly influenced by the choice of fabrication methods (Section 2.5.2.3) and materials (Section 2.5.2.4), which must be optimised according to the intended application. Key design considerations include biocompatibility, biodegradability, mechanical properties matched to the target tissue and the capacity for remodelling. Three fundamental design elements are mechanical strength, degradation and porosity [255, 255, 307].

Beyond these, case-specific design decisions include: pre-embedding of cells (*e.g.* ECs, pericytes) vs. acellular scaffolds; the delivery of bioactive factors and signals (*e.g.* growth factors, ECM proteins, mechanical stimuli); culture (static vs. dynamic) and microenvironmental conditions (*e.g.* flow, shear, or stretch); and the evaluation strategy of biological and mechanical performance (*e.g.* cell viability, barrier integrity and integration post-implantation). The intended application, ranging from *in vitro* studies to *in vivo* validation or clinical therapeutic delivery, informs these design choices. [255, 307]

(1) Mechanical Strength

The mechanical properties of scaffolds must be tailored to the tissue of interest, with properties such as strength and stiffness closely matching those of the native tissue being replicated [307]. For example, scaffolds designed for bone tissue generally require greater mechanical strength than those designed for soft tissues. Regardless of tissue type, scaffolds must also be sufficiently robust to withstand handling during experimental procedures or clinical implantation [255, 307, 308]. Mechanical strength is determined by both the intrinsic material properties (*e.g.* elastic modulus, failure stress) and the scaffold architecture, including porosity, pore size and geometry, and their spatial distribution, all of which collectively influence load-bearing capacity [308]. Achieving an optimal scaffold is application- and context-specific, requiring careful balancing of these factors to

provide both structural integrity and functional guidance for cellular behaviour [308]. Beyond structural considerations, scaffold mechanical properties can guide cellular orientation and influence directional growth [99].

(2) Degradation

Scaffolds serve as temporary structures until embedded or infiltrating cells from the host tissue synthesise their own ECM, which thereafter provides long-term mechanical support [254]. Therefore, the degradation rate must be carefully balanced with tissue regeneration to ensure that new ECM formation occurs before scaffold resorption and structural collapse while avoiding prolonged persistence of the scaffold *in vivo*, which may provoke inflammatory responses [254, 309]. Although *in vitro* scaffolds are usually required for shorter periods than those implanted *in vivo*, they may demand degradation rates that allow sufficient time for handling and experimentation before scaffold breakdown. Degradation rates and mechanisms largely depend on the material composition: natural polymers generally degrade enzymatically, whereas synthetic polymers predominantly undergo chemical hydrolysis [309]. Additionally, degradation by-products must be biologically inert and sufficiently small to avoid cellular or organ toxicity [99].

(3) Porosity

Porosity is central to scaffold function, affecting cell attachment, migration, angiogenesis, and the delivery of oxygen and nutrients, as well as the removal of metabolic waste [244, 310]. The size, distribution and interconnectivity of pores influence these processes. Thus, careful optimisation is required to balance surface area for cell adhesion with pathways for cell migration and, critically, vascularisation [255, 310]. Since no universally applicable pore size exists, optimal dimensions depend on the cell type, scaffold application and intended tissue [308]. In this context, pores are typically classified as small (< 100 µm), intermediate (100–300 µm), and large (> 300 µm), although the optimal size remains application-dependent. Pore size influences biological performance and overall material functionality: very small pores (< 1 µm) promote protein adsorption; 1–20 µm pores support initial cell attachment; 20–100 µm pores promote cell proliferation and migration; and larger pores enhance vascularisation and tissue ingrowth. Pores of 100–1,000 µm support robust cell growth, while those > 1,000 µm help maintain and direct overall scaffold architecture and functional integrity. Although smaller pores provide greater surface area for cell attachment, an appropriate distribution of pore sizes is required to balance these functions. [308, 311, 312]

(4) Functionalisation and Translational Considerations

Scaffolds may also be functionalised to enhance cellular behaviour and host response [308]. For instance, surface coatings or nanoparticles loaded with therapeutic drugs or antibacterial agents can reduce infection risk while modulating tissue regeneration [313]. In addition to optimising the biological and mechanical properties, successful translation from laboratory research to clinical or commercial applications requires consideration of practical factors, including reproducibility, manufacturability, production time and cost [79, 314].

2.5.2.2 Design Strategies

The main strategies for creating TE constructs are top-down and bottom-up (Figure 2.15). The selection of the most appropriate strategy depends on the requirements of the targeted tissue and application, including morphological heterogeneity, functional demands and cellular complexity [315].

Top-Down Design Strategy

The top-down strategy is, arguably, the earliest and most widely used approach in TE. It is centred on creating a

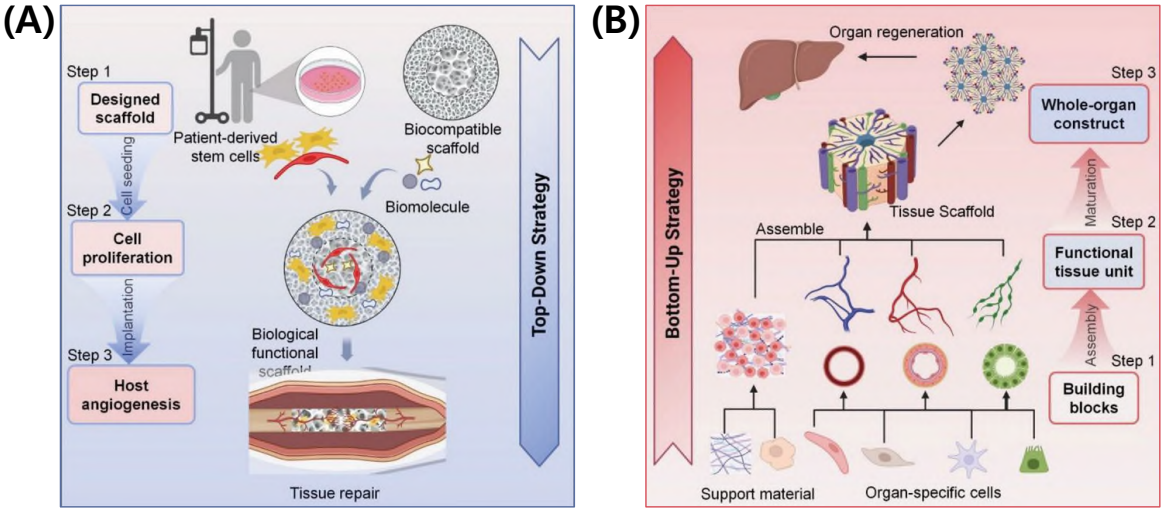


Figure 2.15: **Tissue engineering (TE) construct design strategies: (A)** top-down and **(B)** bottom-up. Reproduced from Chen *et al.* (2024) [315].

scaffold from biocompatible materials that imitates the overall structure of the target tissue or organ [315,316]. Once fabricated, the scaffold can be embedded with cells, usually the primary types found in the native tissue, to encourage tissue development [315,316]. For the construct to support functional regeneration, the scaffold must reproduce the physical and mechanical environment of the tissue, guide structural organisation and offer biochemical cues to guide cellular activity. However, the top-down strategy struggles to recreate the complex microarchitecture and cell–cell interactions present in native tissues, limiting its effectiveness for engineering highly specialised or heterogeneous organs [315–317].

Bottom-Up Design Strategy

Bottom-up or modular TE strategies build tissues from the cellular level into higher-order constructs [315,318] using individual cells or cell aggregates as building blocks, which are strategically assembled [315,318]. These modular building blocks include cell fibres [315, 319], sheets [315, 320], spheroids [315, 321] and organoids [315, 322], which can be organised through self-assembly processes in which cells spontaneously arrange into defined structures or through bioprinting that enables precise spatial positioning [315,323]. Bottom-up design allows finer control over tissue microarchitecture and the overall macroscale, often resulting in constructs with higher levels of structural complexity and heterogeneity [315]. However, scaling up this approach to produce larger constructs or whole organs remains a significant challenge [315, 324].

Hybrid Design Strategy

The decision to adopt a top-down or bottom-up strategy depends largely on the application and the intended properties of the engineered tissue. In many cases, combining both approaches into a hybrid design provides a more effective solution, allowing the precise cellular control of bottom-up techniques to be merged with the ability of top-down methods to generate hierarchical architectures and large constructs. As such, this hybrid design strategy enables the fabrication of constructs that are not only structurally sophisticated but also biologically functional and mimic more closely the native tissues. [315]

2.5.2.3 Fabrication

To study both healthy and diseased tissues, TE has developed a variety of culture platforms [325, 326] that differ in complexity and in their fidelity to native tissue. The most commonly used approach, two-dimensional (2D) culture, involves growing cells as monolayers in flasks, plates, or dishes [327]. However, its physiological relevance has been questioned [325, 326]. To more accurately replicate the cellular microenvironment and create models that are more physiologically relevant, 3D platforms have been increasingly employed [328].

These can be fabricated using a range of techniques (Table 2.6). Conventional techniques include extrusion, gas foaming, casting and *in situ* polymerisation. On the other hand, advanced manufacturing methods include processes such as electrospinning and 3D bioprinting. These techniques enable the production of scaffolds with diverse pore sizes, shapes and architectures, and allow for the fabrication of complex soft tissue architectures. [308, 309, 329]

Table 2.6: **Tissue engineering (TE) scaffold fabrication methods overview.** Based on Bajaj *et al.* (2014) [309].

	Fabrication Method	Principle of Operation	Cell Encapsulation during Fabrication	Advantage(s)	Disadvantage(s)
Traditional Techniques	Solvent casting or particle leaching	Allow leaching of porogen from a polymer matrix to form 3D macroporous scaffolds.	No	Pore size of the scaffold can be controlled by adjusting the parameters of the porogen.	Use of cytotoxic solvents for scaffold fabrication.
	Freeze drying	Creation of thermodynamic instability in a 3D scaffold causing phase separation and pore formation.	No	Pore size can be easily controlled by tuning the freezing regime.	Use of cytotoxic solvents and lengthy timescales for scaffold fabrication.
	Gas foaming	Nucleation and growth of bubbles in a 3D polymer matrix to create macroporous scaffolds.	No	Use of relatively inert foaming agents without employing cytotoxic chemicals; pore size can be controlled by adjusting the operating gas pressure.	Minimal pore interconnectivity at times, which can pose diffusion limitations for the encapsulated cells.
Bioprinting	Drop based	Layer-by-layer drop-based deposition of polymers (with or without cells) onto a substrate controlled by an automated stage.	Yes	Fast deposition of layers over relatively large areas; automated to construct complex architectures.	Spreading and deposition of droplets generally faster than gelation kinetics; possible heating during drop formation, limiting its polymer and cell compatibility.
	Extrusion	Layer-by-layer printing by direct contact of the print head with the substrate, controlled by translation of an automated stage.	Yes	Gentler handling of polymers and cells; automated to allow printing large complex structures.	Slower printing method; only compatible with a few polymer systems.
Photolithography	Mask based	Use of a mask to photopolymerise and cross-link polymers, resulting in a 3D scaffold.	Yes	Uniform cell encapsulation; good spatial and temporal control of reaction kinetics; easy control of pore size by varying the polymer type and concentration.	Requires manual and prefabrication of multiple photomasks for multilayered scaffold constructs.
	Stereo-lithography	Maskless photopolymerisation to crosslink polymers, generating a 3D scaffold.	Yes	Automated and fast processing; easy fabrication of structures with different parameters (pore size, elastic modulus) by changing the polymer parameters.	Feature size that can be polymerised limited to the beam width of the laser.
	Multiphoton	Scanning a femtosecond pulsed laser within 3D hydrogels to localise photochemistries for immobilisation or photodegradation.	Yes	Control local biochemistry or cleave photolabile groups for degradation with high lateral and axial resolution; can be automated to create complex patterns.	Lateral resolution higher than axial (~1 µm versus 5–6 µm); limited depth of patterning (~1 mm).

Hydrogel Fabrication and Crosslinking

Hydrogels can be fabricated into a variety of forms, including films, nanoparticles and semipermeable membranes through several techniques such as casting, particulate leaching, gas foaming, phase separation, melt moulding and freeze-drying [330–337]. Among these, casting is particularly advantageous due to its simplicity and minimal equipment requirements [331]. The process involves dissolving the polymer in an appropriate solvent and then casting it into moulds. This method also control of the porosity, pore size and pore interconnectivity by changing the type and concentration of polymer, the porogen and the ratio between the polymer and the porogen [331]. Nevertheless, the use of cytotoxic solvents in this process can pose biocompatibility concerns [309].

Crosslinking may occur either before casting by incorporating the crosslinking agent directly into the polymer solution or after casting, once the scaffold has been fabricated. Hydrogels fabricated *via* casting and subsequent crosslinking include a wide range of polymers (*e.g.* gelatine) and solvents (*e.g.* phosphate-buffered saline (PBS), Dulbecco's modified Eagle medium (DMEM)) demonstrating the versatility of this technique and its applicability across a large range of biomaterials [332].

A widely employed variation of this technique is solvent casting combined with particulate leaching, which facilitates the production of macroporous scaffolds by removing a porogen from the polymer matrix [338]. The resulting pore size and structure depend on the choice and characteristics of the porogen, which influences pore formation by modulating the mobility and association of polymer clusters during phase separation [338]. Like casting, this method allows control over porosity, pore size and interconnectivity [331] but the use of cytotoxic solvents in this process can pose biocompatibility concerns [309].

Hydrogels can be formed through either physical or chemical crosslinking (Figure 2.16). Physical crosslinking methods do not require chemical crosslinkers or modifications and enable the reversible formation of hydrogel networks; however, they often result in non-uniform internal structures [226, 330, 339].

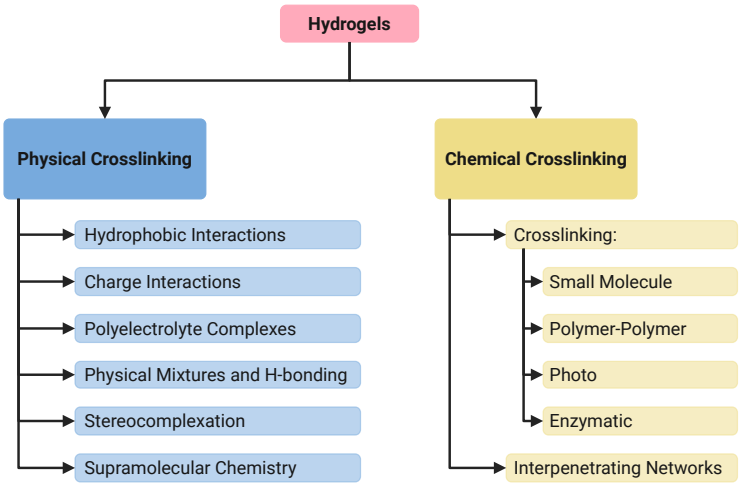


Figure 2.16: **Hydrogel classification by crosslinking method**, including both physical and chemical approaches leading to reversible and permanent hydrogels, respectively. Modified from Parhi, *et al.* (2017) [226].

Physical crosslinking relies on interactions between polymer chains (*e.g.* hydrophobic, electrostatic, hydrogen bonding), which stabilise the network. Since these interactions are reversible, the hydrogel can dissociate under appropriate conditions [226]. Strong physical associations can form structural features (*e.g.* glassy nodules, lamellar microcrystals, double/triple helices), whereas weaker interactions (*e.g.* ionic bonding, hydrogen bonding, self-assembly in block copolymer micelles) produce less stable networks [330, 339].

In contrast, chemical crosslinking uses covalent bonds to link polymer chains, producing stable, permanent hydrogels that retain their structure while allowing for water and bioactive compound absorption without dissolution. This can be achieved using small molecules, polymer-polymer conjugation, photosensitive agents, or enzymes. Importantly, chemical methods offer greater customisation, as parameters such as gelation time, pore size and degradation rate can be adjusted by modifying the crosslinking agent. [226]

2.5.2.4 Biomaterial Selection

Both the mechanical properties and the internal architecture of the materials impact cell behaviour [340]. For example, the stiffness of the ECM can impact fundamental cellular processes, including proliferation, differentiation, migration and signalling, as demonstrated in ECs [223, 340]. Consequently, careful selection of biomaterials is essential for the design of effective TE scaffolds and constructs.

Ceramics, metals and polymers are amongst the materials most used in TE. Ceramic scaffolds from, for instance, hydroxyapatite and tricalcium phosphate, are widely used in bone TE due to their excellent osteoconductivity and their structural resemblance to native bone tissue [244]. Metals and metal alloys, such as gold, platinum, titanium and steel, are also used because of their high mechanical strength, which allows them to support various loads after implantation. However, their limited elasticity and susceptibility to corrosion restrict their use to specific applications [254].

Polymers offer greater versatility in scaffold fabrication and can be derived from natural sources or be synthesised artificially (Table 2.7), or combined to form hybrid materials [99, 248]. Natural polymers include protein-based materials, such as collagen, fibrin and gelatine, as well as polysaccharides (*e.g.* chitosan, alginate, hyaluronan) [99, 248, 341–343]. Natural polymers generally exhibit good biocompatibility and biodegradability (although these properties depend on their source, processing, and degree of modification), support cell adhesion and proliferation, have reduced inflammatory responses and can directly absorb growth factors while adapting to a range of shapes and structures [99, 258, 309]. However, their inherent batch-to-batch variability may hinder reproducibility and could lead to variations in cell responses [99, 257, 258].

Synthetic polymers, such as polyglycolic acid (PGA), polylactic acid (PLA), poly-ε-caprolactone (PCL) and a wide range of copolymers, are well-valued for their mechanical strength, precise chemical control, ease of large-scale production and electrical conductivity [99, 249, 257, 258, 309, 344]. However, depending on their composition and surface properties, synthetic polymers may exhibit limited cell adhesion and slow recellularisation, and their degradation can produce potentially harmful by-products. They may also trigger inflammatory responses, including fibrous capsule formation, and offer limited support for complex tissue remodelling [99, 258].

Beyond mechanical and structural considerations, biomaterial selection can be tailored to introduce additional biological functionalities. For example, protein-based materials such as fibrin and collagen contain intrinsic binding sites for ECs, which enhance the angiogenic potential of scaffolds [232, 345]. Fibrin gels can also stimulate the release of growth factors that promote EC migration and microvascular network formation [345].

Natural polymers are widely used in the fabrication of hydrogels, which can be further engineered to incorporate additional capabilities such as self-healing, enhanced cell adhesion, antimicrobial, or antioxidant properties [332]. Both natural and synthetic polymers have been employed in hydrogel production [346], including fibrin [347–349], hyaluronic acid [347, 350], chitosan [351], collagen [352, 353], alginate [354, 355] and gelatine [356, 357].

Hydrogels have proven particularly effective in engineering vascularised scaffolds due to their ability to replicate the hydrated extracellular environment characteristic of native tissues [260]. Natural polymers such as fibrin, collagen and gelatine are especially advantageous in this context, combining good biocompatibility

with intrinsic bioactivity that supports cell adhesion, proliferation and migration [225]. Furthermore, the mechanical properties of hydrogels can be customised by adjusting factors such as polymer concentration and solvent composition [225, 227, 264–266]. A good biomaterial candidate for vascular TE must not only provide

Table 2.7: **Properties of synthetic and natural hydrogel-forming polymers.** DIFO3, difluorinated cyclooctyne; MMP, matrix metalloproteinases. Adapted from Bajaj *et al.* (2014) [309].

Type	Polymer	Variants	Polymerisation method(s)	Degradable	Supports cell adhesion?	Notes
Synthetic Polymers	Poly(ethylene glycol) (PEG)	PEG-diacrylate (PEGDA)	Photo.	No	No	Can be polymerised via Michael-type addition in the presence of a dithiol.
		PEG-dimethacrylate (PEGDMA)	Photo.	No	No	Can be polymerised via Michael-type addition in the presence of a dithiol.
		PEG peptide	Generally photo.	Yes, if protease-sensitive or photocleavable peptide is used.	No	
	Multiarm PEG (maPEG)	maPEG acrylate	Michael-type addition; photo.	Enzymatic with MMP-sensitive peptide crosslinker.	No	Requires dithiol crosslinker for Michael-type addition.
		maPEG thiol	Michael-type addition.	Enzymatic with MMP-sensitive peptide crosslinker.	No	Requires diacrylate crosslinker.
		maPEG azide	Strain-promoted azide-alkyne cycloaddition.	Enzymatic with MMP-sensitive peptide crosslinker.	No	Requires DIFO3 or similar crosslinker.
		maPEG tetraDIFO3	Strain-promoted azide-alkyne cycloaddition.	Enzymatic with MMP-sensitive peptide crosslinker.	No	Requires diazide crosslinker; not commercially available.
	Poly(acrylamide) (PAm)	N/A	Photo.	No.	No	
	Poly(*N*-isopropyl acrylamide) (PNIPAAm)	N/A	Photo.	No.	No	Thermally responsive.
	Poly(2-hydroxy ethyl methacrylate) (PHEMA)	N/A	Photo.	No.	No	
Natural Polymers	Agarose	N/A	Thermal.	No.	No	
	Alginate	N/A	Ionic, Ca^{2+}.	No.	No	Oligomers of mannuronic acid (M) and guluronic acid (G) and other divalent cations can act as crosslinkers.
	Collagen	N/A	Thermal; Ph.	Enzymatic: MMPs and collagenase.	Yes	Temperature and pH can be altered to adjust fibre size.
	Fibrin	N/A	Enzymatic cleavage of fibrinogen by thrombin.	Enzymatic: plasmin.	Yes	
	Gelatin	N/A	Thermal; pH.	Enzymatic: MMPs and	Yes	Hydrolysed collagen.
		Gelatin methacrylate (GelMA)	Photo.	Enzymatic: MMPs and collagenase.	Yes	
	Hyaluronic acid	N/A	Chemical; requires crosslinker.	Enzymatic: hyaluronidase.	No	A variety of crosslinkers can be used that can react with free hydroxyl or carboxylic acid groups.
		Methacrylate/acrylate hyaluronic acid (MeHA/AHA)	Photo.	Enzymatic: hyaluronidase; can incorporate MMP-sensitive crosslinkers.	No	Methacrylates/acrylates linked via free hydroxyl groups.
	Matrigel	N/A	Thermal.	Enzymatic: primarily MMPs and collagenase.	Yes	Loosely known matrix with batch-to-batch variation.

mechanical support when used to fabricate the scaffold and avoid provoking an immune reaction, but also enable and promote (micro)vessel formation and growth [223, 267].

In light of these requirements, particular attention has been directed towards naturally derived hydrogels whose structural organisation and functional properties closely resemble those of the native ECM [224, 347, 357–359]. Among these, collagen (Figure 2.17A), gelatine (Figure 2.17B) and fibrin (Figure 2.18) stand out as promising candidates due to their bioactivity and their distinct hierarchical structures, which influence cell–matrix interactions and, ultimately, tissue development and organisation [224, 359].

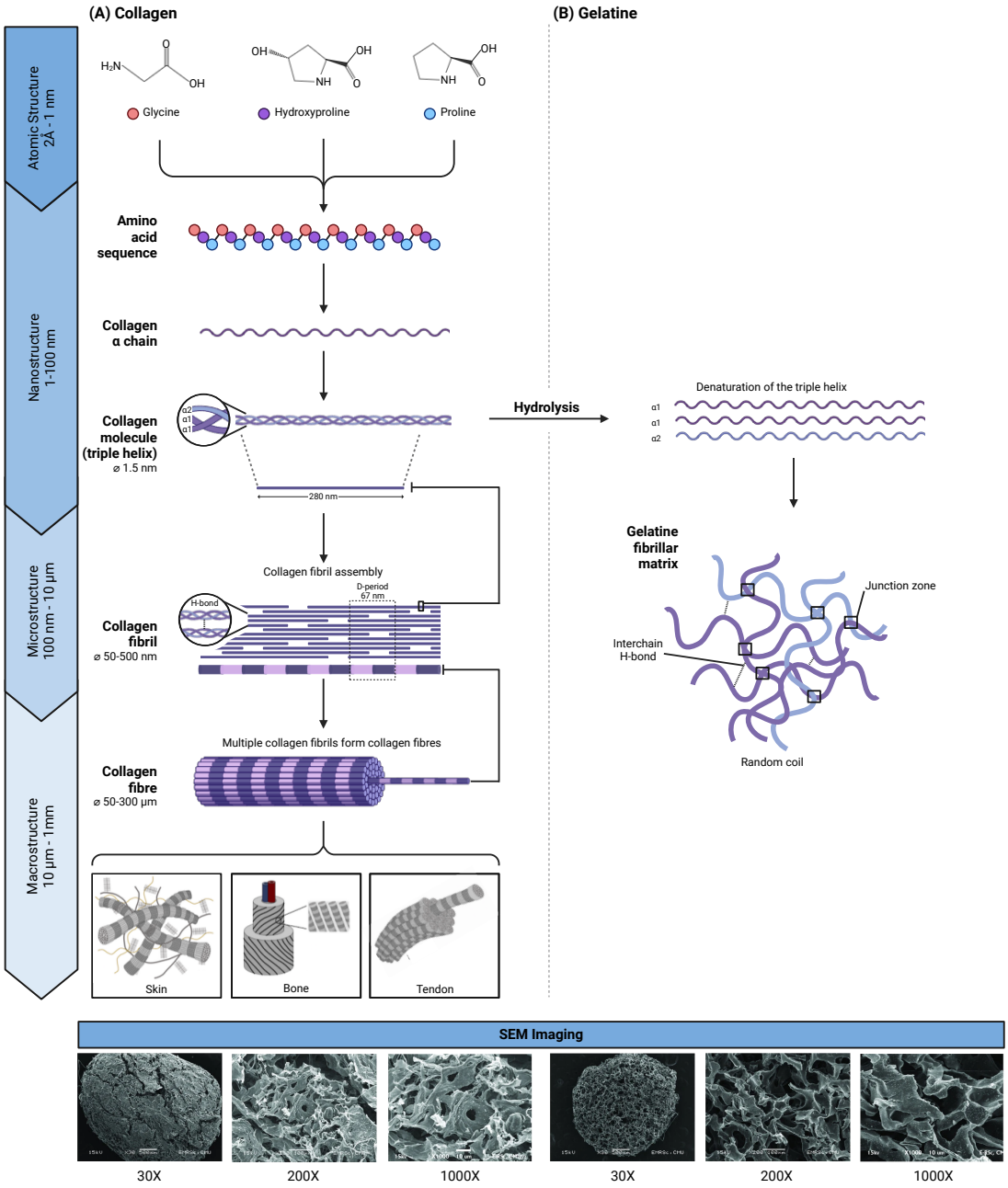


Figure 2.17: **Schematic illustration of the hierarchical organisation of (A) collagen and (B) gelatine**, showing their structural organisation from the atomic to the macroscale. Representative scanning electron microscope (SEM) images of collagen and gelatine scaffold surfaces are shown at magnifications of 30×, 200×, and 1,000×. Created with *BioRender.com* based on Shoulders *et al.* (2009), Broderick *et al.* (2005) and Mikhailov *et al.* (2014), and adapted from Salvatore *et al.* (2021), Roth *et al.* (2009) and Klangjorhor *et al.* (2012) [360–365].

Collagen

Collagen is the most abundant structural protein and the predominant component of the ECM, providing mechanical strength and biological cues across a wide range of tissues [224, 366]. To date, 28 collagen subtypes, comprising at least 46 distinct polypeptide chains, have been identified in vertebrates [360]. Despite their diversity, all collagen types share a common hierarchical structural organisation that underpins their mechanical and biological functions, while creating a dynamic microenvironment that regulates cell behaviour [360, 366, 367].

At the molecular level, collagen consists of three polypeptide chains assembled into a triple helix stabilised by interchain hydrogen bonds (Figure 2.17A) [360, 366, 368]. This structure comprises three parallel, left-handed polyproline II-type helices that intertwine to form a right-handed superhelix [360]. These triple-helical molecules self-assemble into fibrils, which further organise into larger fibres, forming the hierarchical architecture characteristic of collagen-containing tissues [366]. At the microstructural level, this fibrillar and fibrous assembly produces a network that can be either aligned or isotropic at the macrostructural level, depending on tissue type and functional demands. This organisation creates interconnected pores and contact-guidance cues that support cell adhesion, migration and matrix deposition. As a result, scaffold architecture plays a critical role in influencing cell phenotype and tissue organisation. This triple-helical configuration confers high mechanical stability and protects collagen molecules from degradation by most proteolytic enzymes. Consequently, the integrity of this structure is essential for collagen function and stability. Its disruption can alter cell–matrix interactions, tissue remodelling and overall tissue function. [360, 369, 370]

Gelatine

Gelatine is a denatured, collagen-derived biomaterial produced through the hydrolysis of collagen, which disrupts its native tertiary structure while retaining many collagen-derived characteristics, including high water affinity, biological functionality and cell-interactive motifs [357, 361, 371, 372]. It also exhibits improved solubility and lower antigenicity compared with collagen, is biodegradable and contains abundant arginine-glycine-aspartic acid (RGD) sequences that promote integrin-mediated cell attachment, making it widely used in TE applications [357, 361, 372].

Structurally, gelatine is a heterogeneous and polydisperse mixture of partially hydrolysed collagen-derived polypeptide chains, including α, β and γ components, stabilised by the formation of covalent crosslinks, both within the gelatine triple helix and between gelatine helices (Figure 2.17B) [373]. It contains 18 of the 20 naturally occurring amino acids and is particularly rich in glycine, proline and hydroxyproline, which play important roles in its structural organisation [362]. The gelatine molecule is highly elongated and asymmetric, consisting of three parallel α-chains with a diameter of $\sim$14 nm and a length of $\sim$2,850 nm [362]. Although hydrolysis disrupts the highly ordered collagen triple helix, generating predominantly random coils and aggregated chain conformations, some regions may retain collagen-like organisation [360, 362, 366, 368]. Proposed structural models suggest that each α-chain adopts a left-handed helix, with three chains intertwining into a right-handed superhelix stabilised primarily by hydrogen bonding [362, 372].

The molecular organisation of gelatine remains strongly influenced by the collagen-derived Gly-X-Y sequence motif [362, 372]. During cooling, denatured chains can partially reassociate to form ordered junction zones that act as physical crosslinks and serve as the basis of gel formation. These junction zones assemble into a porous, flexible and highly hydrated 3D fibrillar network capable of retaining large quantities of water while permitting the diffusion of small molecules and ions [361, 362, 372]. The resulting architecture supports cell adhesion, migration and matrix remodelling, while network properties such as pore size, connectivity and alignment are determined by gelatine concentration, cooling history, crosslinking conditions and processing methods. However, gelatine is readily degraded by proteolytic enzymes, limiting its long-term stability; con-

sequently, chemical and enzymatic crosslinking strategies are commonly employed to enhance its thermal stability, mechanical performance and resistance to degradation [361].

Fibrinogen and Fibrin

Fibrin is another essential ECM protein formed from fibrinogen, a soluble 340 kDa plasma glycoprotein composed of two identical sets of three polypeptide chains (Aα, Bβ and γ; Figure 2.18) linked by 29 disulphide bonds [349, 374, 375]. The Aα, Bβ and γ chains are encoded by a three-gene cluster located on the long arm of human chromosome 4 [374]. Structurally, fibrinogen is an elongated molecule of ∼45 nm in length, consisting of a central E domain and two terminal D domains linked by α-helical coiled-coil regions [374, 376].

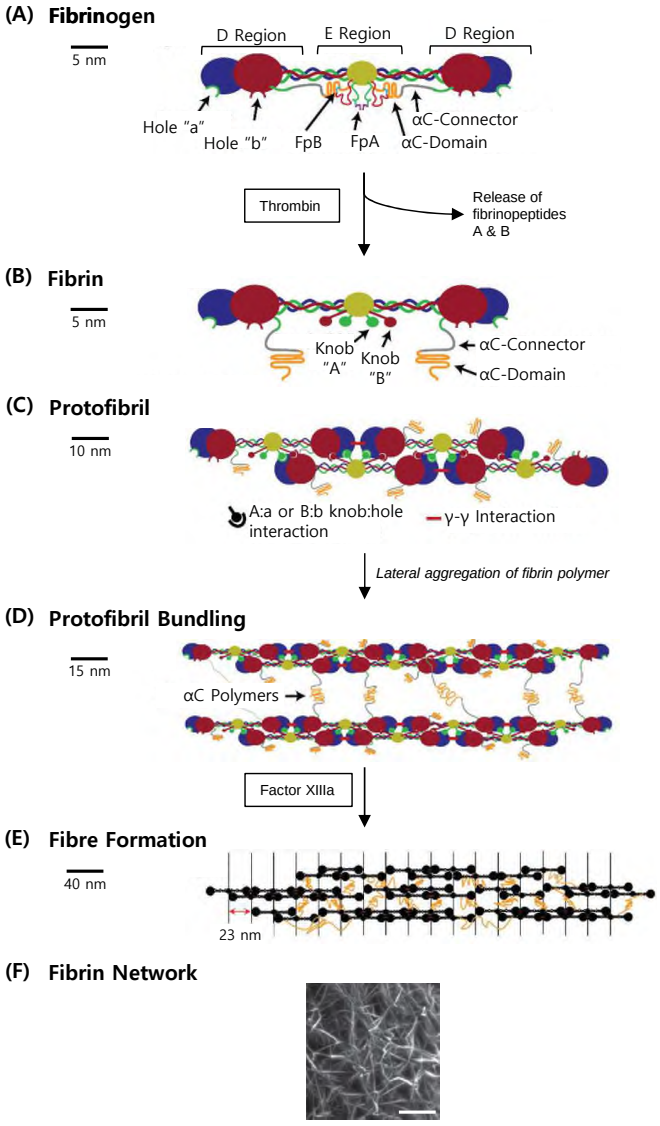


Figure 2.18: **Schematic representation of fibrinogen structure and fibrin assembly. (A)** Structure of the fibrinogen molecule, comprising two sets of three polypeptide chains (α, β and γ), linked through a central E region enriched in disulphide bonds. **(B)** Thrombin-mediated cleavage of fibrinopeptides A and B generates fibrin monomers, exposing complementary knob–hole binding sites. **(C)** Longitudinal assembly of fibrin monomers into half-staggered protofibrils. **(D)** Lateral aggregation of protofibrils mediated by αC-region interactions. **(E)** Formation and stabilisation of mature fibrin fibres through Factor XIIIa-mediated crosslinking. All schematics include a reference scale bar. **(F)** Representative micrograph of fibrin fibres within a fibrin gel (scale bar: 20 µm). Adapted from Belcher *et al.* (2022) [377].

Fibrin formation is initiated during coagulation when thrombin cleaves fibrinopeptides from the central E domain of fibrinogen, exposing binding sites ('knobs') that interact with complementary 'holes' located within the D domains of adjacent molecules [375, 376, 378]. These specific 'knob–hole' interactions convert soluble fibrinogen into an insoluble fibrin polymer by driving the assembly of fibrin monomers into half-staggered oligomers and subsequently into double-stranded protofibrils [375, 376, 378]. The protofibrils exhibit an axial periodicity of ∼22.5 nm and a transverse spacing of ∼13 nm within fibres [375, 378]. At the microscale, these protofibrils undergo lateral aggregation to form fibres, which branch and interconnect into a 3D fibrillar network [375, 376, 378]. The resulting fibrin network provides binding sites for cells, growth factors and other ECM components, supporting cell adhesion, migration and tissue remodelling [374].

Calcium ions (Ca^{2+}) facilitate fibrin polymerisation and network organisation, while factor XIIIa (a transglutaminase activated by thrombin in the presence of Ca^{2+}) covalently crosslinks adjacent fibrin molecules [375, 376]. Together, these processes stabilise the fibrillar network and enhance its mechanical strength, viscoelastic properties and resistance to degradation [375, 376]. The resulting hierarchical and porous architecture underpins fibrin's critical role in haemostasis and contributes to numerous physiological processes, including wound healing, inflammation, angiogenesis, thrombosis, immune defence and tissue repair [349, 374, 375].

2.5.3 Microvascular *In Vitro* Models

The integration of a functional microvascular network remains one of the greatest challenges in TE [223, 232]. A range of techniques have been developed to engineer microvessels. Contemporary approaches largely employ bottom-up strategies, in which one or more cell types are incorporated within a supporting matrix [379, 380]. These models have been widely used to study disease processes, vascular growth and remodelling dynamics, and other physiological processes [379]. Within these strategies, the most promising models are those that provide cells with a 3D microenvironment that emulates key aspects of the ECM. Such models have been extensively applied in blood–brain barrier [381] and tumour research [382], offering valuable insights into how matrix composition and mechanics influence vascularisation [379].

The absence of a microvasculature in TE constructs limits the development of larger and physiologically relevant models [223]. To address this, a wide range of *in vitro* microvascular models have been developed, ranging from organ-on-a-chip models to organogenesis approaches. Organogenesis involves the self-organisation of stem cells or progenitors into tissue structures resembling native organs, a process that is technically demanding and time-consuming, typically requiring 1–2 weeks for endothelial formation. In contrast, organ-on-a-chip devices, created using microfabrication and microfluidics, replicate key aspects of organ structure and function and enable endothelial layer formation within 2–4 days. [207, 284]

Fabrication methods can be broadly classified into four categories: microfluidics, templating, 3D printing and self-organisation (Figure 2.19), each offering unique advantages for replicating the complex architecture and functionality of native microvasculature [284, 287, 291]. These range from moderately complex, high-throughput models, such as organ-on-a-chip platforms, to models that exhibit greater complexity and physiological relevance but lower throughput, including organogenesis-based strategies [284, 383]. These advanced models are indispensable for a wide range of applications, from disease modelling to drug screening, as well as serving as platforms to investigate tissue-specific vascularisation and the critical role of perfusion. [207, 284]

A summary table of selected 3D microvessel models, grouped by category, including their key associated features, advantages and limitations, is presented in Table 2.8.

Microfluidic devices, including membrane-based [384–386] and ECM-containing devices [387, 388], can generate interstitial flow and allow for perfused vascular networks, while also mimicking critical components of the microenvironment like oxygen tension and fluid shear stress control [383, 389]. Templating, exemplified

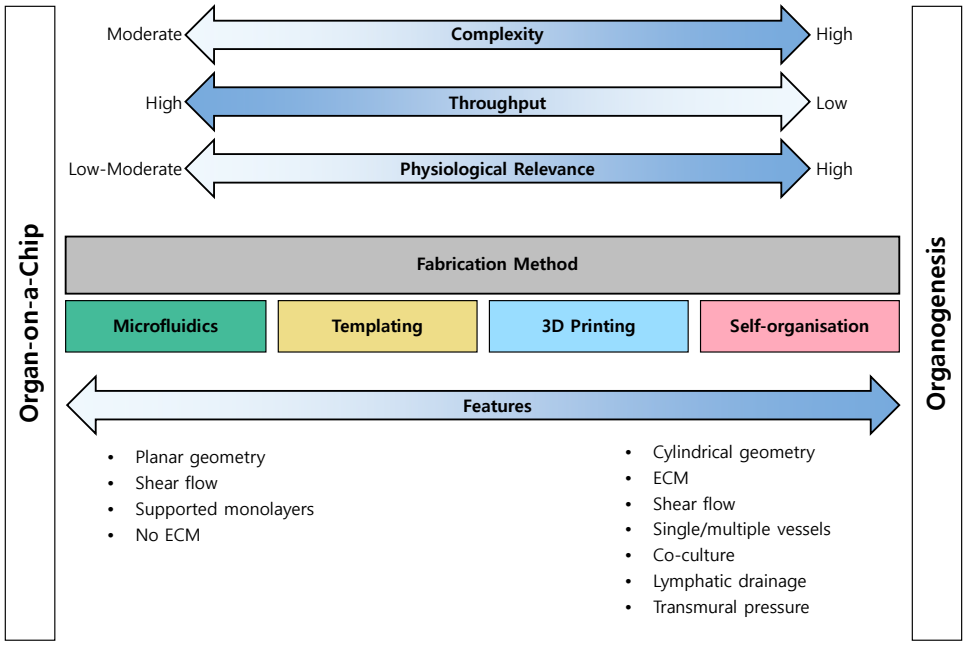


Figure 2.19: **Schematic illustration of the fabrication methods and features of 3D *in vitro* microvessel models, by category.** Models can be broadly classified as organ-on-a-chip platforms, which are moderately complex, high-throughput systems, or organogenesis-based models, which exhibit greater complexity and physiological relevance but lower throughput. Fabrication methods include microfluidics, templating, 3D printing and self-organisation. ECM: Extracellular matrix. [284, 291, 383]

by lithographic patterning [390], permits the generation of a vascular network using a solid substrate within a removable ECM, live cell imaging and solute transport. This is particularly well suited for single microvessels or 2D networks, which display a cylindrical geometry. 3D bioprinting utilises sacrificial inks to form perfusable channels [389], offering the advantage of positioning cells in the desired geometry, which facilitates building up particular structures. However, its resolution forces vessel diameters to be larger, usually at least 500 µm. Finally, self-organised microvascular models have demonstrated that a continuous network of vessels after 4–7 days in culture is formed by mixing endothelial and stromal cells in a hydrogel (*e.g.* fibrin, collagen), which is stable for up to 4 weeks [290, 291]. Relevantly, these have been used to form HUVEC microvessels (diameter: 10–100 µm) and allow for interconnected networks that can be crafted in a parallel array. [207, 284]

Barrier function can be assessed in models from these four categories, mostly through permeability and TEER. Intravasation, extravasation and invasion are possible with microfluidics (except membrane-based models), templating and 3D printing; while mimicking the endothelial structure and function has been achieved with models from all categories except from microfluidics. Importantly, angiogenesis has only been possible in self-organisation *in vitro* models. [207, 284]

It is important to acknowledge that there is a trade-off between biological fidelity and microvascular complexity, on one hand, and throughput and manufacturability, on the other. Microfluidic membrane systems and ECM-containing devices are well suited to reproducible, high-throughput assays but are limited in reproducing capillary-scale 3D architecture. Templating and template-based printing provide robust, perfusable lumina with straightforward endothelialisation, yet struggle to reproduce dense capillary networks. Direct 3D bioprinting approaches enable co-deposition of cells and matrix and permit bespoke architectures but face material- and resolution-driven constraints. Self-organisation and guided angiogenesis deliver the highest degree of biomimicry, producing networks that recapitulate native microvascular morphology, but at the cost of lower throughput, longer culture times and greater experimental variability. [207, 284]

Table 2.8: **Examples of selected microvessel models, by category**, listing key features, advantages, disadvantages and most common applications [284, 291, 383]. ECs: endothelial cells; ECM: extracellular matrix; TEER: transendothelial electrical resistance.

Fabrication Method	Model Type	Key Features	Advantages	Limitations	Application					
					Barrier Function / Permeability	Invasion, Intravasation & Extravasation	Endothelial Structure & Function	Angiogenesis	Inflammation	Drug Delivery
Microfluidics	Membrane-based Models	2D endothelium, easily integrated into live cell chambers, interstitial flow, perfused vascular networks.	· Enable controlled laminar shear flow to study endothelial response and barrier function. · Integrate electrodes for TEER measurement and permeability assays. · Allow co-culture & chemical gradients (e.g., VEGF, cytokines). · High throughput & relatively simple fabrication (2–4 days for endothelium formation).	· Lack cylindrical vessel geometry and continuous lumen. · Membrane-based systems are difficult for live imaging. · ECM-based systems are more complex and limited to quasi-2D geometries (<500 µm thickness).	Yes	No	No	No	No	No
	ECM-containing Models	2D endothelium, ECM, shear stress, co-culture, chemical gradients.			Yes	Yes	No	No	No	No
Templating	Membrane-based and ECM-based Models	Single microvessel or 2D network, cylindrical geometry (diameter ≥ 50 µm), ECM, shear stress, co-culture, interstitial flow, transmural pressure.	· Recapitulate cylindrical geometry and shear stress seen *in vivo*. · Allow measurement of permeability, interstitial flow, transmural pressure. · Compatible with co-culture (*e.g.*, pericytes, cancer cells) and live imaging. · Reproduce physiological BSA permeability (10^{6}–10^{7} cm/s) and barrier function.	· Limited to simple linear vessels or 2D planar networks. · Vessel diameter >50 µm required for seeding ECs. · Template removal may damage soft ECM. · Complex networks require advanced lithography.	Yes	Yes	Yes	No	Yes	Yes
3D Printing	Direct Bioprinting	Single microvessel or networks, cylindrical geometry (diameter ≥ 200 µm), capillary networks by anastomosis (diameter ≥ 10 µm), multiple ECM components, shear stress, co-culture, interstitial flow, transmural pressure.	· Enables fabrication of complex 3D vascular networks and hierarchical architectures. · Incorporates multiple ECMs and cell types in precise geometries. · Allows control of shear stress, interstitial flow & transmural pressure. · Can be combined with self-organization to generate capillary-scale networks (<100 µm).	· Limited resolution (~100 µm): smaller capillaries require secondary angiogenesis. · Time-intensive fabrication (hours per cm-scale vessel). · Vessel diameters typically ≥200 µm (larger than *in vivo* capillaries). · Requires post-printing endothelial maturation (3–5 days).	Yes	Yes	Yes	No	No	Yes
	Template Printing	3D network of microvessels, cylindrical geometry (diameter ≥ 100 µm), multiple ECM components, shear stress, co-culture, interstitial flow, transmural pressure.			Yes	Yes	Yes	No	No	Yes
Self-organisation	Guided Capillary Self-organisation	Interconnected microvessel/capillary networks (quasi-2D), cylindrical geometry (diameter = 10–50 µm), ECM, shear stress, co-culture, interstitial flow, transmural pressure.	· Generate perfusable microvessel networks (10–50 µm) with physiological morphology. · Capture angiogenesis and vasculogenesis processes. · Incorporate chemical & interstitial flow gradients and co-culture (*e.g.*, fibroblasts, tumour, cardiac cells). · High physiological relevance.	· Long formation time (up to 3 weeks for self-organisation). · Often quasi-2D rather than fully 3D. · Complex setup and low throughput. · Network morphology is less predictable.	Yes	No	Yes	Yes	No	No
	Guided Capillary Angiogenesis	Parallel (quasi-2D) capillary array, (diameter = 10–50 µm), ECM, shear stress, co-culture, interstitial flow, transmural pressure.			Yes	No	Yes	Yes	No	No

2.5.3.1 Microfluidics

Microfluidic-based devices can expose EC monolayers to laminar flow and are easily integrated into live imaging platforms, enabling real-time tracking of EC responses to shear stress or other biochemical or mechanical factors. Single or multiple channels (channel height: 100–500 µm) can be used, thus altering the complexity of the model. Microfluidic models can be subdivided based on the substrate on which ECs are cultured: a porous membrane (Figure 2.20A), which separates the upper from the lower channel; or an ECM material (Figure 2.20B) such as collagen or basement membrane extract, which separates two microfluidic channels. ECs are typically cultured either horizontally (membrane) or on a sidewall (ECM material). [284, 318, 334]

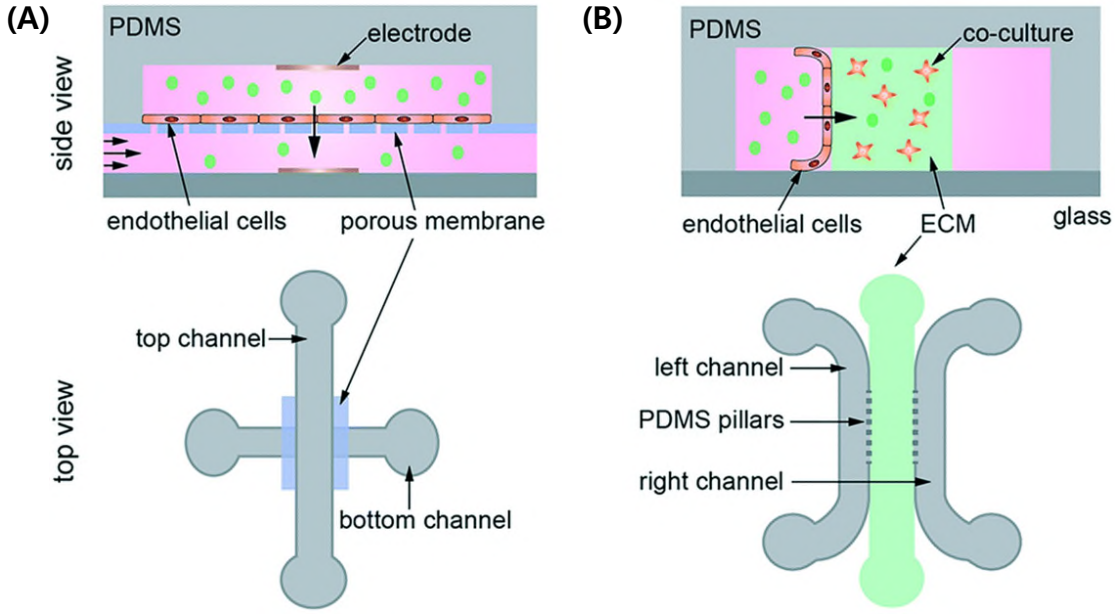


Figure 2.20: **Schematic illustration of microfluidic devices as microvessel models**, depicting examples of **(A)** membrane-based and **(B)** extracellular matrix (ECM)-based models. **(A)** Endothelial cells (ECs) were cultured on a porous membrane and placed between two orthogonal polydimethylsiloxane (PDMS) channels. In this specific device, electrodes were added to enable transendothelial electrical resistance (TEER) measurements. **(B)** An ECM material separated two parallel channels, with ECs seeded onto the vertical sidewall of one of the channels. In this model, other cell types could also be co-cultured alongside the ECs. Reproduced from Bogorad *et al.* (2015) [284].

2.5.3.2 Templating

Templating approaches generate perfusable *lumina* within a surrounding matrix by casting biomaterials around a sacrificial template (*e.g.* rod, needle, wire) that is subsequently removed, leaving a channel which can be lined with ECs (Figure 2.21A). Collagen and fibrin have been widely used in this method. This method allows precise control over lumen diameter and spatial placement of the channel within the surrounding matrix, enabling the fabrication of conduits within hydrogels or polymer scaffolds [391]. Templated channels are particularly useful when mechanical support from the surrounding matrix is required. More complex vascular networks can be created by using lithography to produce removable templates, which can take any form, including interconnected channels to form a network (Figure 2.21B). A popular template design relies on rectangular channels that are interconnected, enabling the creation of junctions [390, 392]. Despite ECs being seeded in a template with rigid corners, semi-cylindrical vessels are formed [390]. Templated models have been used to research diverse applications within TE, from tumour microenvironment to vascular phenomena. [284]

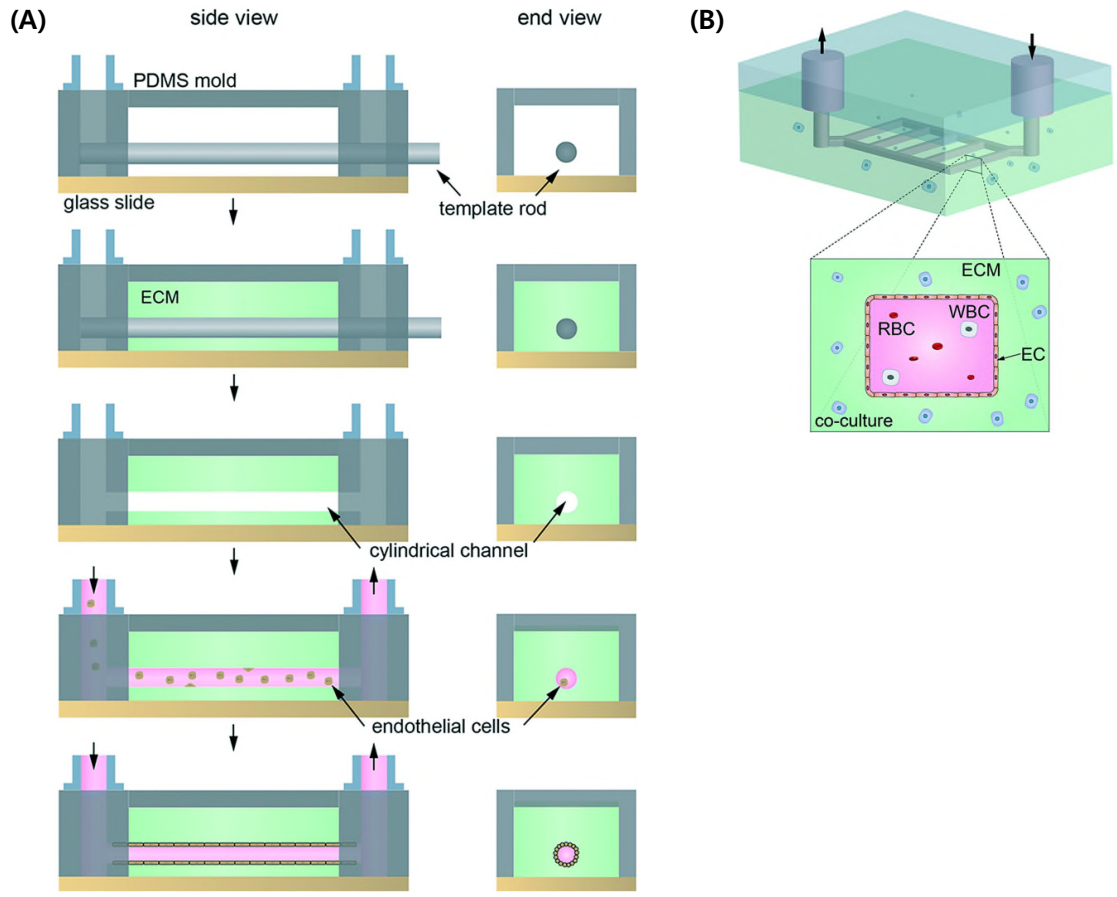


Figure 2.21: **Schematic illustration of microvessel fabrication using templating techniques**, depicting examples of fabrication **(A)** using a cylindrical template and **(B)** by lithographic patterning. **(A)** A template rod was inserted into a polydimethylsiloxane (PDMS) mould, after which, an extracellular matrix (ECM) solution was poured around the template. Once crosslinking or gelation had taken place, the template rod was removed and the endothelial cells (ECs) were seeded into the resulting channel. ECs then adhered to the internal surface of the channel, forming the vessel lumen. **(B)** Lithographic patterning was used to create a 2D array of rectangular channels within a matrix fabricated from an ECM material. ECs were then seeded, as well as additional cell types such as red blood cells (RBCs) and white blood cells (WBCs). Reproduced from Bogorad *et al.* (2015) [284].

2.5.3.3 3D Printing

3D bioprinting utilises elements such as bioinks, liquid droplets containing cells, hydrogels or ECM proteins [284, 315]. These bioinks can be dispensed from a single nozzle, in which case all elements are combined, or from diverse nozzles, enabling complex architectures with different bioinks used at specific locations across the structure [318, 393]. While bioprinting is a very promising strategy for TE scaffold perfusion, particularly for constructs exceeding the critical size, as well as to improve reproducibility, optimising the bioink properties to achieve the desired material characteristics whilst ensuring cells are not negatively affected is not straightforward [322, 393].

3D bioprinting includes direct bioprinting of microvessels in the ECM (Figure 2.22A), where structures are fabricated from ECM blends. This involves extruding cell-laden bioinks composed of ECM components, such as collagen, and ECs to form vessel-like filaments [284, 393]. Other cell types can also be used to create more complex models [393–395]. Direct printing can also be used for suspended vessels, where droplets with cells and an initiator are printed from a single nozzle into a bath of a hydrogel precursor [284, 396]. This

process enables the formation of vessels with diameters in the range of 200–300 µm, while also allowing for the creation of complex, branching architectures with higher fidelity than many direct extrusion methods, because the sacrificial template supports the intended geometry during fabrication [284, 396]. Another 3D printing technique is template printing with post-fabrication cell seeding, which utilises a dissolvable template embedded in a matrix to create channels (Figure 2.22B). ECs are then seeded into these channels, which can take any configuration, thus providing great versatility and enabling more complex architecture [284].

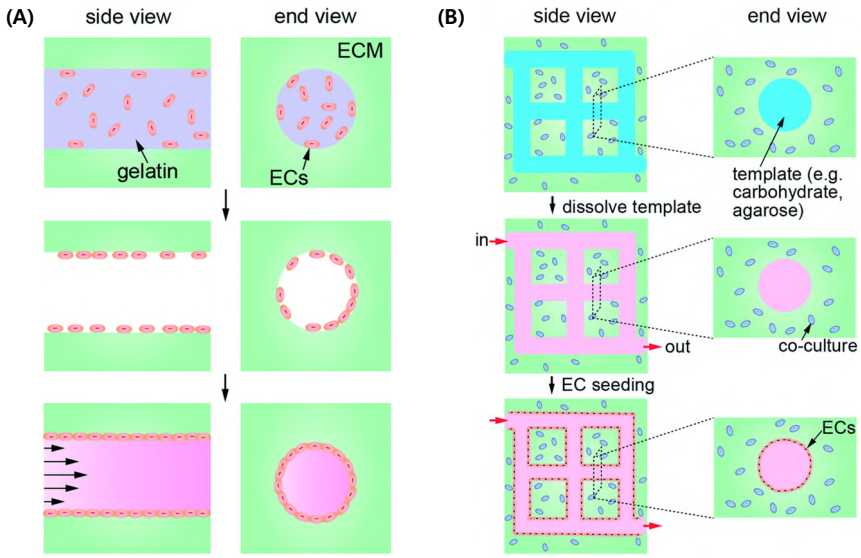


Figure 2.22: **Schematic illustration of microvessel models fabricated using 3D printing**, depicting examples of **(A)** direct bioprinting of microvessels in extracellular matrix (ECM) and endothelial cells (ECs) in a dissolvable matrix, and **(B)** a 3D template-printed model. **(A)** Human umbilical vein endothelial cells (HUVECs) in gelatine were printed as a cylinder and embedded in a collagen ECM. After printing and gelation, the gelatine was dissolved by increasing the temperature to 37 °C while rotating the device to ensure cell adhesion to the internal walls of the channel, leading to the formation of the vessel lumen. This setup was then connected to a flow loop to allow for perfusion. **(B)** A printed 3D network of filaments made with carbohydrate glass was embedded into a hydrogel matrix alongside additional cell types, such as fibroblasts and smooth muscle cells (SMCs). Once the template was dissolved, the resulting perfusable network of cylindrical channels could be seeded with ECs. Reproduced from Bogorad *et al.* (2015) [284].

2.5.3.4 Self-organisation

Self-organisation strategies rely on angiogenesis and tubulogenesis to form perfusable microvessels through guided capillary self-organisation (Figure 2.23A) or guided capillary angiogenesis (Figure 2.23B). While both strategies utilise an ECM to produce the microvessels, capillary self-organisation opts for a microfluidic chamber filled with an ECM to create the microvessel network. To this end, the microfluidic device is designed to allow for a pressure difference between the source and the sink channels to establish an interstitial flow through the ECM, thereby initiating cellular self-organisation. This process leads to the formation of continuous microvessel networks within a 3-week period. A common material used in this setup is fibrinogen, which is crosslinked with thrombin to enable gelation. Guided capillary angiogenesis utilises two or more microfluidic channels, also filled with an ECM material as in the case of guided capillary self-organisation. The parallel microfluidic channels make it possible for media perfusion to happen in the outer channels, thereby providing oxygen and CO_2 exchange, as well as nutrient delivery and waste removal. This also helps establish chemical or pressure gradients, which can be used to stimulate the formation and growth of angiogenic sprouts from the source channel to the sink channel, forming a microvessel network in a week. [265, 284, 290]

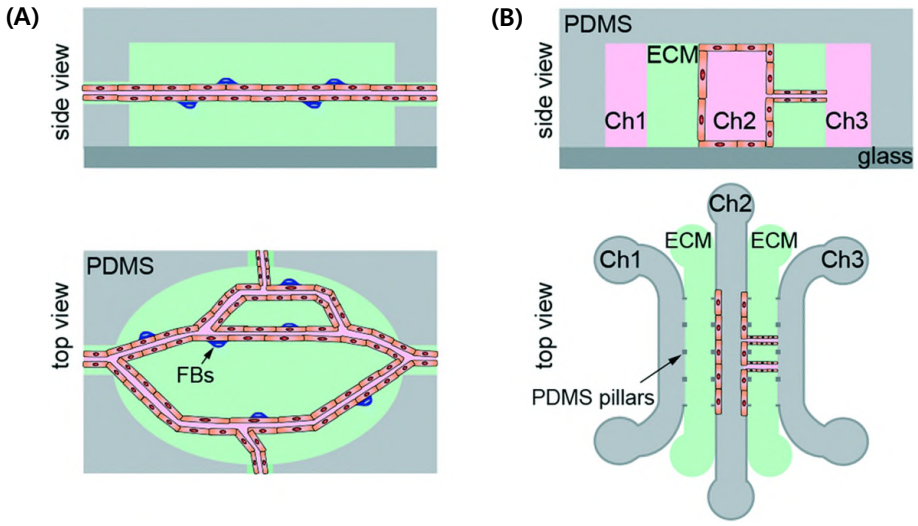


Figure 2.23: **Schematic illustration of microvessel models formed by self-organisation**, showing examples of **(A)** guided capillary self-organisation and **(B)** guided capillary angiogenesis. **(A)** Endothelial cells (ECs) were seeded into an extracellular matrix (ECM) within a polydimethylsiloxane (PDMS) container connected to a system allowing for interstitial flow, which guided self-organisation of cells into a network of perfusable capillaries. **(B)** ECs were seeded into one of the microfluidic channels (Ch2) and formed a monolayer on the sidewall of the ECM. Between the source channel (Ch2) and the sink channel (Ch3), the setup had chemical and/or pressure gradients, which promoted directional formation and growth of angiogenic sprouts. This enabled the formation of a perfused microvessel network between the source and the sink channels. Reproduced from Bogorad *et al.* (2015) [284].

2.6 Research Gaps

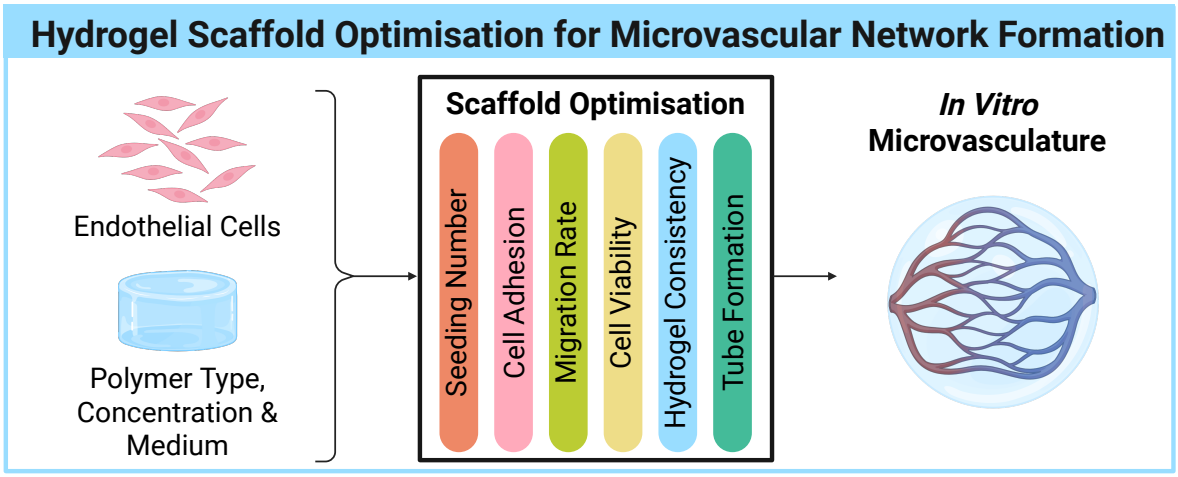
The research on NPTIs highlights significant knowledge gaps, particularly in understanding the immediate and short-term impact on the microvasculature. Despite advances in trauma care and bioengineering, limited progress has been made in developing effective therapies, largely due to the lack of mechanistic insights into how NPTIs affect vascularised soft tissues, such as skeletal muscle. Microvascular traumatic injuries remain underexplored and existing models present ethical challenges, poor physiological relevance and technical difficulties in recapitulating 3D microvascular networks. Furthermore, while acute trauma at the tissue and organ levels has been widely investigated, there is little understanding of how such forces act on microvascular structures or how to quantify their mechanical response under injury. Developing a 3D microvascular model could provide new ways to understand microvascular NPTIs, in particular contusion, crush and strain injuries.

Another critical gap lies in the tools and materials used to study vascularisation in trauma and TE. While fibrin-based scaffolds are widely recognised for their potential in soft tissue regeneration, systematic evaluations of variations in their formulations correlated with their ability to support angiogenesis and stable microvascular network formation are lacking. Existing literature often treats fibrin's mechanical and biological properties in isolation, rarely examining their interconnections. Only a handful of studies have considered the impact of scaffold material properties on endothelial network formation and architecture.

Addressing these issues requires systematic optimisation of hydrogels with defined compositions, supported by material characterisation. In parallel, current EC models, such as HUVECs, are limited by short-lived networks that hinder long-term research, restricting their utility for studying traumatic injury progression and repair. Developing more robust microvascular constructs that incorporate physiologically relevant ECs within 3D fibrin scaffolds would allow sustained monitoring of vascular responses, scaffold optimisation for stability and, ultimately, their use as platforms to study NPTIs and, further down the line, for testing therapeutics.

Chapter 3

Development and Optimisation of Hydrogel Scaffolds for Microvascular Network Formation



Thesis Integration and Chapter Structure

This chapter presents the first experimental step towards addressing Objective 1 of this thesis: to develop and optimise a natural polymer–based scaffold capable of supporting endothelial cell (EC) adhesion, viability, migration, and the formation of microvascular networks *in vitro*. Specifically, it investigates the suitability of different natural polymers for fabricating scaffolds for ECs, evaluates their ability to support tube and network formation, and identifies the most promising hydrogel composition in terms of polymer, concentration, and medium for supporting key endothelial responses such as migration, viability, and proliferation. Building directly on Chapter 2, it systematically compares hydrogel compositions by varying polymer type, ratio, and medium. Scaffold optimisation was guided by a multipronged evaluation of seeding density, adhesion, migration rate, viability, hydrogel consistency, and tube formation capacity. The optimised hydrogels enabled the development of interconnected capillary-like networks, which were further characterised to provide insights into their microarchitecture. By establishing the material and biological parameters that support stable and physiologically relevant endothelial structures, this chapter lays the foundation for the subsequent focus on fibrin scaffolds (Chapter 4) and the development of long-lasting three-dimensional (3D) models (Chapter 5).

This chapter has been published [397] and is available at DOI: 10.3390/bioengineering10080964.

In this section, all the experimental design, experimental work, data analysis, and writing were carried out by Carla V. Fuenteslópez. Prof Hua Ye and Prof Mark Thompson reviewed the manuscript and provided supervision and advice.

Development and Optimisation of Hydrogel Scaffolds for Microvascular Network Formation

Abstract

Traumatic injuries are a major cause of morbidity and mortality worldwide; however, there is limited research on microvascular traumatic injuries. To address this gap, this research aims to develop and optimise an *in vitro* construct for traumatic injury research at the microvascular level. Tissue engineering (TE) constructs were created using a range of polymers (collagen, fibrin, and gelatine), media (phosphate-buffered saline (PBS), serum-free endothelial cell basal medium (EBM), and MES/NaCl buffer), and concentrations (1–5% *w/v*). Constructs created from these hydrogels and seeded with human umbilical vein endothelial cells (HUVECs) were evaluated to identify the optimal composition in terms of cell proliferation, adhesion, migration rate, viability, hydrogel consistency and shape retention, and tube formation. Gelatine hydrogels were associated with lower cell adhesion, whereas fibrin and collagen hydrogels displayed similar or better results than the control. While collagen hydrogels exhibited poor shape retention, fibrin scaffolds, particularly at higher concentrations (3 and 5% *w/v*), displayed good hydrogel consistency, defined here as the ability to retain their shape following removal from the mould. Based on the multipronged evaluation, fibrin hydrogels in EBM at 3 and 5% *w/v* were selected for further experimental work and enabled the formation of interconnected capillary-like networks. The networks formed in both hydrogels displayed a similar architecture in terms of the number of segments (10.3 ± 3.21 vs. 9.7 ± 3.51) and diameter (8.6 ± 3.1 µm vs 7.9 ± 2.4 µm).

Keywords

Microvascular Network • Hydrogel • Tissue Engineering Scaffold • Fibrin • Collagen • Gelatine.

3.1 Introduction

Microvascular traumatic injuries are common but relatively understudied [186]. Although the combined impact of traumatic injuries, both in terms of mortality and morbidity, is largely unknown, an estimate can be calculated using disability-adjusted life years (DALYs) methodology that combines both the years of life lost due to premature mortality (YLLs) and years of healthy life lost due to disability (YLDs) [10]. The 2019 Global Burden of Disease report estimates that injuries account for 7.6% of all deaths and 11.0% of Years of Life Lost [122]. The subsequent Global Burden of Disease report (2021) reaffirms injuries as a major contributor to DALYS. While total DALYs from all diseases and injuries combined increased between 2010 and 2021 due to population growth and ageing, age-standardised DALY rates for injuries decreased from a share of 27.2 to 20.7 in the same period [3].

Major trauma has often been perceived as a 'disease of the young' [12]. However, the prevalence of traumatic injuries has increased in the elderly [123], partly due to the ageing population and an increased exposure to injury risk and age-related frailty [124, 125].

In addition to clinical research, the vast majority of experimental methods used to study traumatic injuries rely on *in vivo* models [14]. Nevertheless, these entail major ethical concerns and display physiological and pathophysiological differences [14], which complicate translational research in trauma. Moreover, utilising

current models in traumatic injury research is associated with a number of challenges, including enabling microvasculature formation within a three-dimensional (3D) structure.

As such, there is an urgent need to develop physiologically relevant *in vitro* models that allow us to gain fundamental understanding of trauma and, at a later stage, test potential therapeutics to enhance tissue repair and regeneration. To address this gap, this research aims to develop and optimise a construct for microvascular network formation.

In an effort to mimic the natural extracellular matrix (ECM), biological substitutes are specially designed to provide a platform that offers specific characteristics for a particular application [282]. These scaffolds play a significant role in providing support, achieving a particular architecture, and allowing for certain physical and biological functions when interacting with cells. The 3D matrices with structural, mechanical, and chemical properties that resemble the natural environment have allowed for the maturation of functional tissue engineering (FTE), where biological constructs mimic load-bearing tissues [231].

Engineering perfusion in *in vitro* models is a major challenge in tissue engineering (TE) [37]. Most *in vitro* constructs do not contain microvascular structures as occurs in the native tissue, so cells in those scaffolds rely to a large extent on simple diffusion for oxygenation and nutrient delivery [37, 40]. The lack of a vascular network is partially responsible for the limited size of *in vitro* engineered tissues, such as skeletal muscle [41].

Broadly, the microvascular *in vitro* models that have been developed to date can be grouped into four general categories: microfluidics, templating, 3D printing, and self-organisation [284]. These have a tendency towards either organogenesis or organ-on-a-chip technology and, as such, are associated with different degrees of complexity, throughput, and physiological relevance.

Self-organised microvascular models, where guided capillary self-organisation and angiogenesis can take place [290], have been developed using human umbilical vein endothelial cells (HUVECs) [291]. Relevantly, these have been used to form microvessels with a diameter ranging from 10 to 100 µm. Furthermore, self-organised microvascular models allow for interconnected networks [287]. The majority of these *in vitro* models have been used in pharmaceutical [295] or cancer [294] research.

The design of microvascular *in vitro* models encompasses not only the architecture of the scaffold itself but also the selection and optimisation of materials. A variety of ECM-mimetic materials have been used to fabricate hydrogels, including natural and synthetic polymers [347]. Polymers in hydrogel format not only partially resemble the physical characteristics of native ECM [224, 358, 359], but they can also be fine-tuned to achieve the desired properties by adjusting their parameters, such as concentration [224, 346].

A range of natural and synthetic polymers have been used to fabricate hydrogels [346], including fibrin [347–349], hyaluronic acid [347, 350], chitosan [351], collagen [352, 353], alginate [354, 355], and gelatine [356, 357]. Hydrogels created from naturally derived materials often exhibit favourable biocompatibility, bioactivity, and biodegradability, depending on composition, processing, and experimental setup [224], thus offering promising alternatives for fabricating TE scaffolds.

In addition, 3D scaffolds have been crafted using Matrigel to provide structural support, as it closely mimics the mechanical and chemical properties of the native ECM [398]. However, its components are poorly defined [398], it is associated with high variability between different batches [399], and its mechanical properties are heterogeneous throughout the samples [400]. In contrast, natural hydrogels such as collagen are associated with higher consistency and reproducibility while maintaining a good biological relevance [399].

The research presented here further investigates three natural polymers to fabricate hydrogel constructs: collagen, fibrin, and gelatine. Collagen is one of the most abundant fibrous proteins in the body, providing biological and mechanical support, and one of the major elements of the ECM [224, 366]. Fibrin is also a major protein in the ECM, and plays a key role in a number of bioactivities including angiogenesis [349]. Gelatine facilitates cell adhesion as it contains specific peptide sequences allowing for integrin cell receptor recognition

[357]. Notably, these polymers have been associated with low cell toxicity and have been used to fabricate hydrogels mimicking the native ECM [224, 357].

3.2 Materials & Methods

3.2.1 Cell Culture

HUVECs (ATCC) were cultured in T-25 and T-75 cell culture flasks (Corning Incorporated-Life Sciences, Oneonta, NY, USA) with endothelial cell growth medium (EGM) supplemented with 1% penicillin/streptomycin (Gibco Life Technologies, Grand Island, NY, USA). EGM was prepared by supplementing endothelial cell basal medium (EBM; Lonza, Walkersville, MD, USA) with SingleQuots[1] (Lonza, Walkersville, MD, USA). Cells were incubated at 37 °C and 5% CO_2. Medium was changed every 48–72 h, as required. Cells were used for experimental work at 80% confluency and up to passage number 7.

3.2.2 Fabrication of Hydrogels

A range of hydrogels was prepared at 1, 1.5, 2, 2.5, 3 or 5% weight/volume (*w/v*) in phosphate-buffered saline (PBS; Gibco Life Technologies, Paisley, UK), EBM or MES sodium salt in NaCl (MES/NaCl) buffer (for fibrin only). After gel casting, plates were incubated at 37 °C for 30 min. Then, they were sterilised under ultraviolet (UV) light for 20 min before cell seeding.

3.2.2.1 Collagen Type I

An adaptation of the protocol described by Lim *et al.* (2018) [401] was used to prepare the collagen gels. Collagen type I from rat tail (Sigma Life Sciences, St Louis, MO, USA) was mixed with EBM or PBS to obtain the desired concentration. pH was measured with a pH meter and adjusted to pH 7.4 using NaOH drops. After casting, collagen hydrogels were crosslinked by irradiating the samples with UV light for 20 min.

3.2.2.2 Gelatine

Gelatine from porcine skin (Sigma Life Sciences, St Louis, MO, USA) was dissolved in warm EBM or PBS, magnetically stirred until fully dissolved, and filtered twice (20 µm filter). Hydrogels were crosslinked by UV irradiation (90 min).

3.2.2.3 Fibrin

Fibrin gels were prepared based on a protocol from Lim *et al.* (2018) [401] and Sharma *et al.* (2015) [402]. Briefly, a fibrinogen (MP Biomedicals, New Zealand) solution at the desired concentration was prepared in MES/NaCl buffer (0.15 M NaCl, 2.5 mM MES in water), PBS or EBM and stored at 37 °C for 30 min or until fully dissolved. pH was adjusted to 7.4 using NaOH drops. To prepare the gel, the fibrin solution was crosslinked with thrombin (Sigma-Aldrich, St Louis, MO, USA) at a 20:1 volume ratio, and a 1 M $CaCl_2$ solution in water was added to the mixture at a volume ratio of 1:100 to thrombin. The solution was pipetted to ensure a homogeneous mixture and quickly poured into the wells as the gelation process begins when the three ingredients come together.

[1] Foetal bovine serum (FBS) 2%; hydrocortisone 0.04%; human fibroblast growth factor-basic (hFGF-b) 0.4%; vascular endothelial growth factor (VEGF) 0.1%; long R3 insulin-like growth factor-1 (R3-IGF-1) 0.1%; ascorbic acid 0.1%; human epidermal growth factor (hEGF) 0.1%; gentamicin sulfate-amphotericin (GA-1000) 0.1%; heparin 0.1%.

3.2.3 Cell Proliferation

HUVECs (P6) were seeded at a density of 0.5, 1, 1.5, or 2×10^4 cells per well (96-well plate) and cultured with EGM for 48 h at 37 °C and 5% CO_2. A total of 22 replicates of each experimental condition and control were used. Medium was replaced every 24 h, and cell proliferation was measured at 24 h and 48 h after seeding. Cells were counted using a microplate reader (SpectraMax i3x, Molecular Devices, LLC., San Jose, CA, USA) and its software (*SoftMax Pro*; version 7.0, Molecular Devices, LLC., San Jose, CA, USA). Cell counts were validated by manually counting five randomly selected wells.

3.2.4 Cell Adhesion

Wells were coated with gelatine, fibrin, or collagen in PBS, EBM, or MES/NaCl (fibrin only) at a concentration of 1, 1.5, 2, 2.5, 3, or 5% *w/v*. The hydrogel suspension was carefully pipetted into the well and plates were incubated at 37 °C for 30 min. Following removal of the excess hydrogel, a thin coat covering the bottom of the well remained. Plates were then sterilised (UV light, 20 min) and washed thrice with PBS. HUVECs (P6) were seeded at a density of 2×10^4 cells/well (96-well plate) and cultured with EGM at 37 °C and 5% CO_2. At 4, 6, 8, and 24 h, the supernatant was discarded, and wells were refilled with fresh EGM. Cells were counted using a microplate reader and randomly chosen wells were validated against manual counting from the images obtained. Four replicates of each coating and of the control with no coating (*i.e.* cells only) were used.

3.2.5 Cell Migration

A cell migration assay, also known as a wound healing or scratch assay, was conducted using HUVECs plated on coated wells to compare cell migration rates across hydrogels based on the protocol by Jonkman *et al.* (2014) [403]. Wells were prepared similarly to those described in the adhesion experiments. HUVECs (P4) were seeded at a density of 1.5×10^4 cells/well and, after reaching confluency, a p20 pipette tip was used to create a 'wound' or a gap (average initial gap area: 2.21 mm^2, standard deviation: 0.42 mm^2) across the monolayer. Then, cell migration was monitored at 0.5, 1, 1.5, 2, 3, 6, 8, 12, and 22 h. Triplicates of each experimental and control conditions were used.

The gap area was measured using *ImageJ* and used to calculate the cell migration rate (Equation (3.1): $v_{\text{migration}}$) and the time taken to fill the gap (Equation (3.2): t). The gap area was plotted against time, and a straight-line fit was used to obtain the trendline. The slope of this trendline was used to calculate the cell migration rate and, together with the initial gap area, to estimate the time required for gap closure.

$$v_{\text{migration}} = \frac{|\text{slope}|}{2 \times \text{length of gap}} \tag{3.1}$$

$$t = \frac{\text{Initial Gap Area}}{2 \times |\text{slope}|} \tag{3.2}$$

3.2.6 Cell Viability

Fibrin and collagen gels were prepared as described in Subsections 3.2.2.1 and 3.2.2.3, and were then carefully pipetted into wells to avoid bubble formation. The fibrin-collagen hydrogels were prepared at a 1:1 ratio. Plates were incubated at 37 °C for 1 h to allow for gelation. Before cell seeding, plates were placed under UV light for 20 min for sterilisation purposes. HUVECs (P6) were seeded on top of the gels (seeding density: 2×10^4 cells/well) and cultured with EGM for up to 96 h at 37 °C and 5% CO_2. Triplicates were prepared, including cells-only controls.

Cell viability was measured every 24 h using a live/dead viability kit (Molecular Probes Invitrogen, Eugene, OR, USA) and a microplate reader, following the manufacturer's instructions. Briefly, 20 µL of a 2 mM EthD-1 solution and 5 µL of a 5 mM calcein AM solution were added to 10 mL of PBS. This solution was added to the cells following media removal and incubated for 30 min at room temperature, protected from light. Calcein AM was used to stain live cells green, whereas dead cells were stained red using EthD-1. A microplate reader (SpectraMax i3x, Molecular Devices, San Jose, CA, USA) was used to measure the fluorescence of calcein AM (485 nm, excited at 530 nm) and EthD-1 (530 nm, excited at 645 nm), separately, for each sample. Background fluorescence, both from the plate and wells with a layer of gel but with no cells, was subtracted from the readings prior to the calculation of the live cell percentage (Equation (3.3)), where *F* denotes the background-corrected fluorescence (F) intensity measured at the specified emission wavelength.

$$\text{Live Cells (\%)} = \frac{\mathrm{F}(530)_{\text{sample}} - \mathrm{F}(530)_{\text{min}}}{\mathrm{F}(530)_{\text{max}} - \mathrm{F}(530)_{\text{min}}} \times 100 \tag{3.3}$$

3.2.7 Hydrogel Consistency

Collagen, fibrin, and fibrin-collagen in PBS, EBM, or MES/NaCl (fibrin only) hydrogels were cast in 96-well plates and incubated at 37 °C for 1 h. Then, each sample was carefully removed from the wells and placed on a Petri dish. After 1 h, the samples were visually inspected and each hydrogel composition was classified as poor, acceptable, or good based on shape retention once removed from the moulds.

3.2.8 Tube Formation

A tube formation assay was carried out to evaluate the impact of the base gel on capillary-like structure formation. Fibrin in EBM (3% and 5% *w/v*) hydrogels were prepared to evaluate tube formation. The term 'tube formation' is used in accordance with standard TE terminology to describe the *in vitro* endothelial network formation assay, in which cells organise into capillary-like structures; it does not demonstrate the formation of functional or lumenised vessels.

Cells were grown using EGM and, once confluent, they were used for experimental work. EBM was used from here on. Separately, fibrin was prepared as previously described and 75 µL was added to each well (96-well plate). Careful attention was paid to ensure that the hydrogel was evenly distributed and that no bubbles were formed. Plates were placed in a humidified incubator (37 °C, 5% CO_2) for 1 h to allow for gelation. Before seeding the cells on top of the gel, plates were placed under UV light (20 min) for sterilisation.

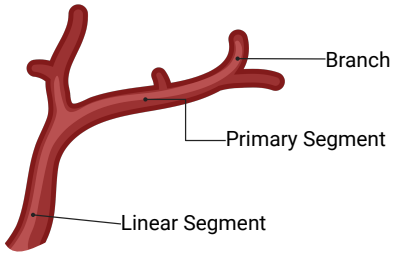


Figure 3.1: **Schematic illustration of microvascular segments**, depicting linear segments (LS), primary segments (PS), and branches.

Cells were carefully pipetted onto the hydrogels, at a density of 2×10^4 cells/well, and were incubated. Tube formation was monitored every hour until a full network of capillary-like structures developed. Length and diameter of each segment were measured and classified (Figure 3.1) as a linear segment (LS; *i.e.* when a

single tube connects two points), a primary segment (PS; *i.e.* segment from which other segments originate), or a branch (*i.e.* a segment that arises from a PS). The branch-to-PS ratio and the angles between these two architectural elements were also quantified. *ImageJ/Fiji* (version 1.54d, National Institutes of Health, Bethesda, MD, USA) [404] was used for image analysis.

3.2.9 Statistical Analysis and Software

Where relevant, data were evaluated using one- or two-way analysis of variance (ANOVA) and post hoc tests using Tukey's honest significant difference (HSD). p values ≤ 0.05 were deemed to be statistically significant. Data analysis was performed using *Microsoft Excel* (version 2208, Microsoft, Redmond, WA, USA). Unless otherwise specified, data are presented as mean values with standard deviation. Figures were created using *GraphPad Prism* (version 10.4.2 (633), Dotmatics, Boston, MA, USA), while the graphical abstract and the microvasculature segments schematic (Figure 3.1) were created using *BioRender.com*.

3.3 Results

3.3.1 Cell Proliferation by Seeding Density

Cell proliferation of HUVECs seeded at different seeding densities was measured at 24 h and 48 h (Figure 3.2), and was graphed as the fold expansion of the initial seeding number for each time point.

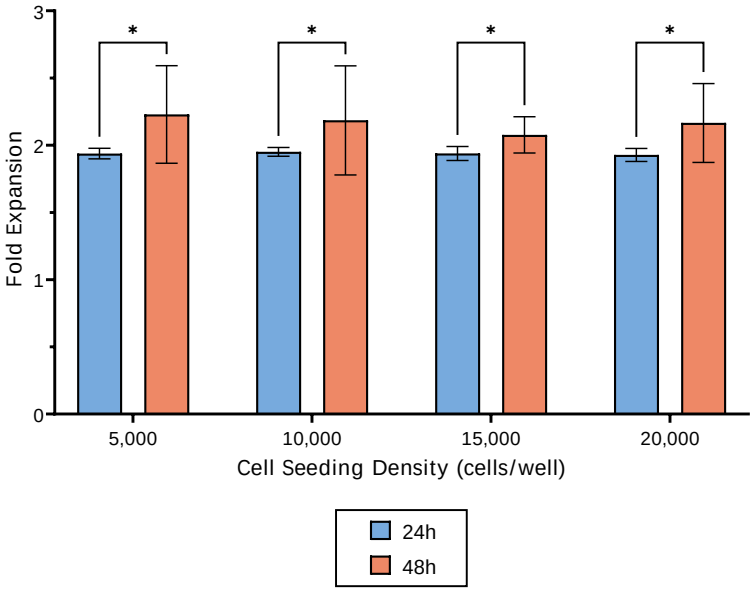


Figure 3.2: **Cell proliferation as fold expansion of the initial cell seeding number, at 24 and 48 h.** Human umbilical vein endothelial cells (HUVECs) were cultured in endothelial cell growth medium (EGM) in 96-well plates. (*) Only statistically significant differences are shown. (ANOVA/Tukey's HSD, $p \leq 0.05$; $n = 22$).

Across all seeding densities, the highest cell proliferation as a fold expansion occurs in the first 24 h after seeding, whereas the variation between 24 h and 48 h is significantly smaller and corresponds to a 1.07– to 1.15–fold increase across seeding densities (p range: 0.000032–0.043). The highest variation is 40.91% (seeding density: 1.5×10^4 cells/well) and the lowest is 33.37% (seeding density: 0.5×10^4 cells/well).

Interestingly, there were no significant differences when comparing seeding densities in the first 24 h. This could suggest that the cell proliferation rate does not vary greatly based on cell seeding density within this

period. However, when comparing the same seeding density at different time points (24 h vs. 48 h), differences are statistically significant in all groups. It is worth highlighting that over a longer period, cell proliferation as a fold expansion of the seeding number might reach a plateau due to the constraints imposed by the limited space and cell culture media available to cells.

Although no statistically significant differences were observed, cell seeding densities of 1.5×10^4 or 2×10^4 cells/well were preferred for further experimental work as these allowed for a higher cell count in a shorter period of time, thereby accelerating experimental work. Careful monitoring of cell proliferation, particularly when confluency is high, is required to avoid cell overcrowding and death.

3.3.2 Cell Adhesion

Cell adhesion in the different hydrogel compositions was compared with the cells-only control and plotted as a fold expansion of the control (Figures 3.3 & A.1). A summary based on this data was created to simplify the comparison of cell adhesion results between hydrogels (Figure 3.7A).

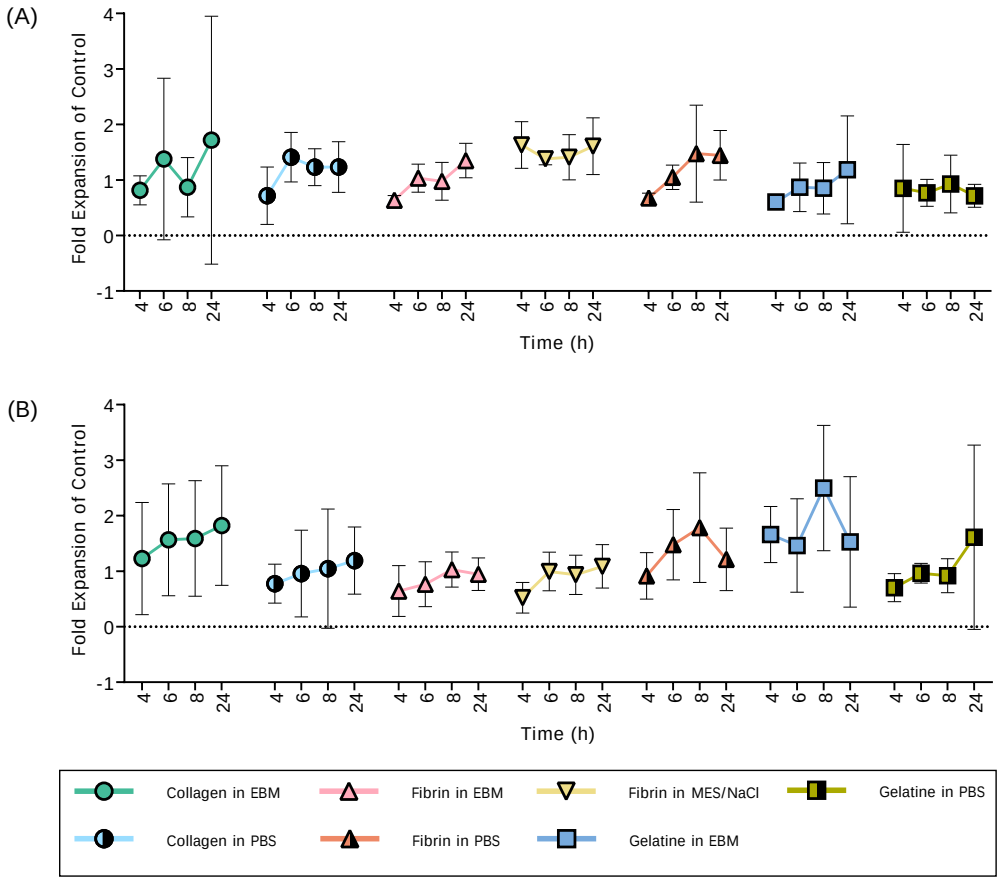


Figure 3.3: **Cell adhesion as a fold expansion of the cells-only control, by coating and concentration.** Coatings of collagen, fibrin, or gelatine in endothelial cell basal medium (EBM), phosphate-buffered saline (PBS), or MES/NaCl (fibrin only) were explored. Here, the concentrations of **(A)** 3% and **(B)** 5% *w/v* are shown. Human umbilical vein endothelial cells (HUVECS) were cultured in endothelial cell growth medium (EGM) and seeded at a density of 2×10^4 cells/well (96-well plate). A total of 14 hydrogel compositions had statistically significant differences compared to the control. A total of 11 compositions exhibited higher cell adhesion (collagen in EBM 1, 1.5, and 2.5%; collagen in PBS 5%; fibrin in EBM 1%; fibrin in MES/NaCl 1.5, 2, 2.5, 3, and 5%; and fibrin in PBS 5%), whereas only three variations had significantly lower values (collagen in PBS 2%; fibrin in PBS 1%; and gelatine in PBS 1%). Data are plotted as average $\pm$ standard deviation. (ANOVA/Tukey's HSD, $p \leq 0.05$; $n = 4$). Please refer to Figure A.1.

The differences in terms of cell adhesion between hydrogel compositions were statistically significant. When looking at the overall performance across time points, 11 hydrogel compositions were associated with a statistically significant higher cell adhesion than the control, whereas only three compositions were lower. The remaining hydrogel compositions were associated with similar cell adhesion to the control. Collagen in EBM (predominantly 1, 1.5 and 2.5%), fibrin in EBM (predominantly 1%), and fibrin in MES/NaCl (predominantly 1.5–5%) exhibited favourable cell adhesion. On the other hand, gelatine in both EBM and PBS shows lower adhesion than the control. This suggests that gelatine may be less well suited for the development of this construct.

3.3.3 Cell Migration

Following the creation of a wound (*i.e.* gap) in the HUVEC monolayer, the gap area was measured immediately after the creation of the gap and at different time points (Figures 3.5 and 3.6). From here, the slope generated by these data points was obtained and used to calculate the average migration rate and the estimated time required to fill the gap (Figure 3.4). A visual summary using these data was prepared to facilitate a comparison of migration rates between gels (Figure 3.7B).

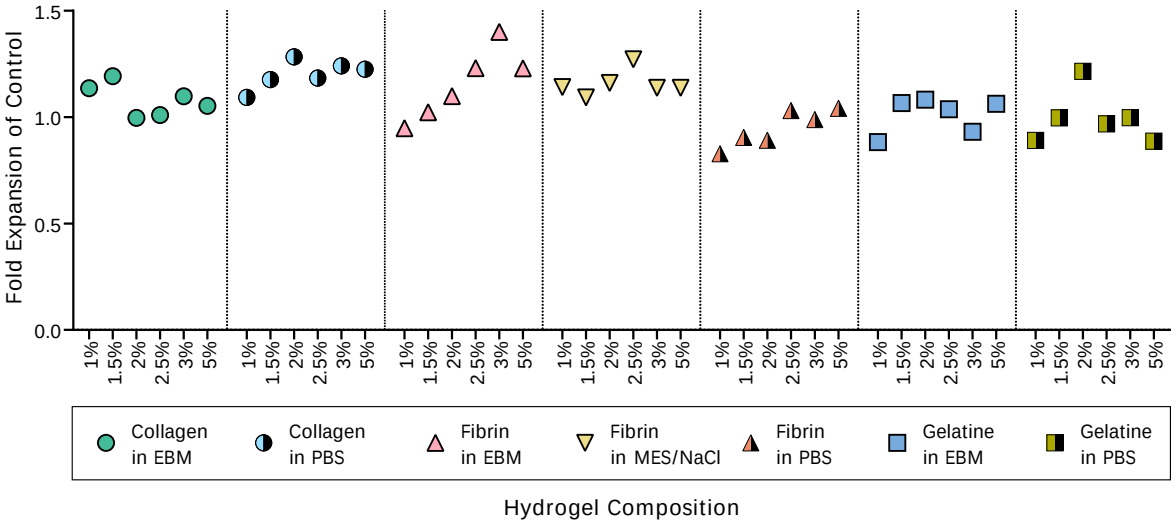


Figure 3.4: **Average migration rate (mm/h) as fold expansion of the control, by hydrogel composition.** The average migration rate was obtained from the gap area measured over a period of 24 h (Figure 3.6). Cells-only controls were used. Cells were cultured with endothelial cell growth medium (EGM) and seeded at a density of 1.5×10^4 cells/well (96-well plate). (ANOVA/Tukey's HSD, $p \leq 0.05$; $n = 3$).

Cells displayed a faster migration rate in the hydrogels containing EBM rather than in hydrogels containing PBS or MES/NaCl. Interestingly, this trend is not mirrored by gelatine hydrogels, where a faster migration rate takes place in PBS hydrogels. No significant differences can be observed within the same hydrogel group (*i.e.* a specific polymer-media combination) when comparing different concentrations (% *w*/*v*).

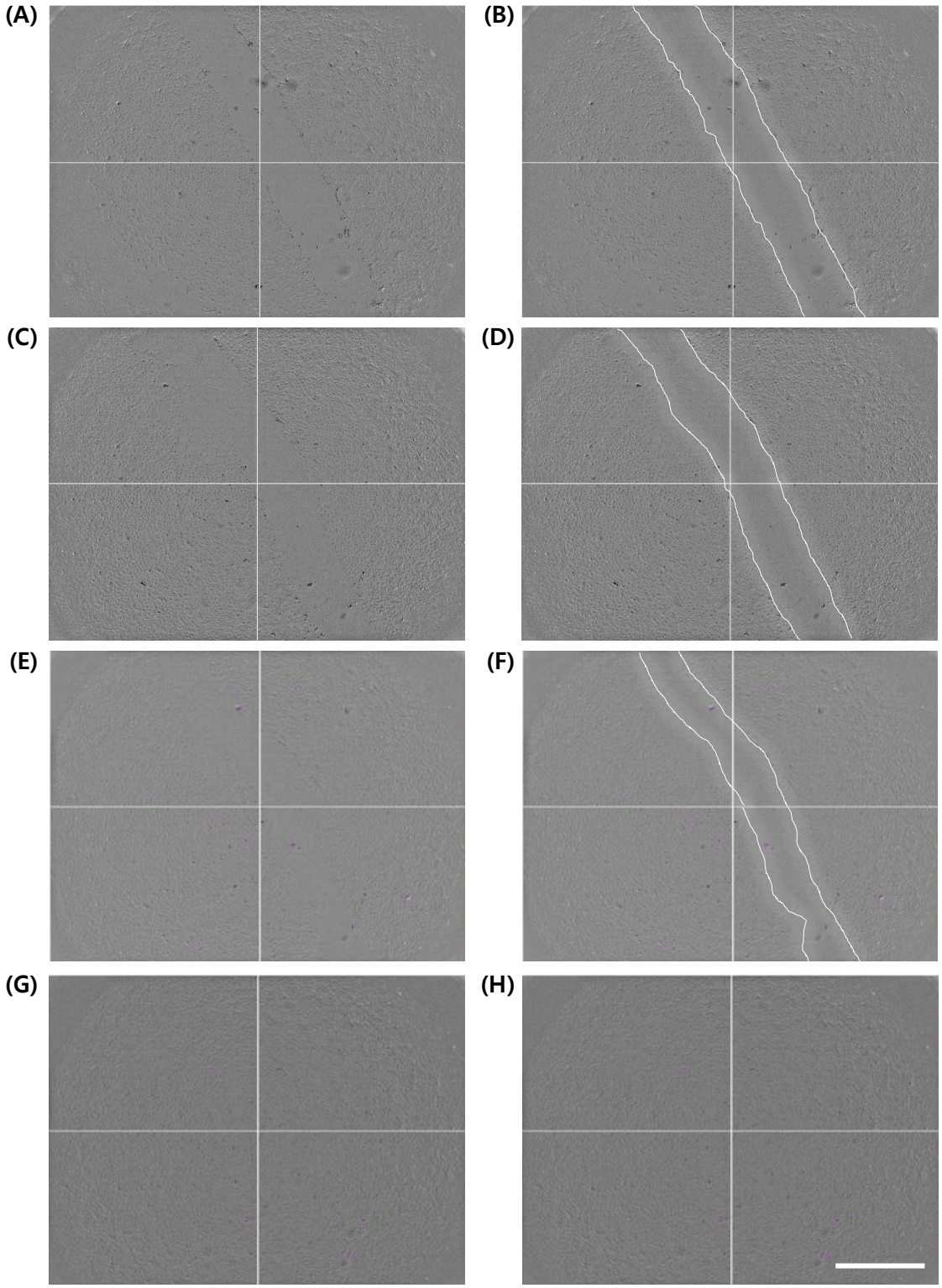


Figure 3.5: **Closure of the gap area in a human umbilical vein endothelial cell (HUVEC) monolayer over time.** The gap area was measured over time and, using this data, Figures 3.6 and 3.4 were plotted. Here, a fibrin in endothelial cell basal medium (EBM) at 2.5% *w/v* sample is shown **(A)** immediately after the gap was created and at **(C)** 1.5, **(E)** 6, and **(G)** 22 h. **(B, D, F, H)** A replicate of each image highlighting the edge between the cell monolayer and the gap is shown next to each original image. **(G, H)** By 22 h, the gap had fully closed. HUVECs were cultured with endothelial cell growth medium (EGM) and seeded at a density of 1.5×10^4 cells/well (96-well plate). Scale bar: 1 mm.

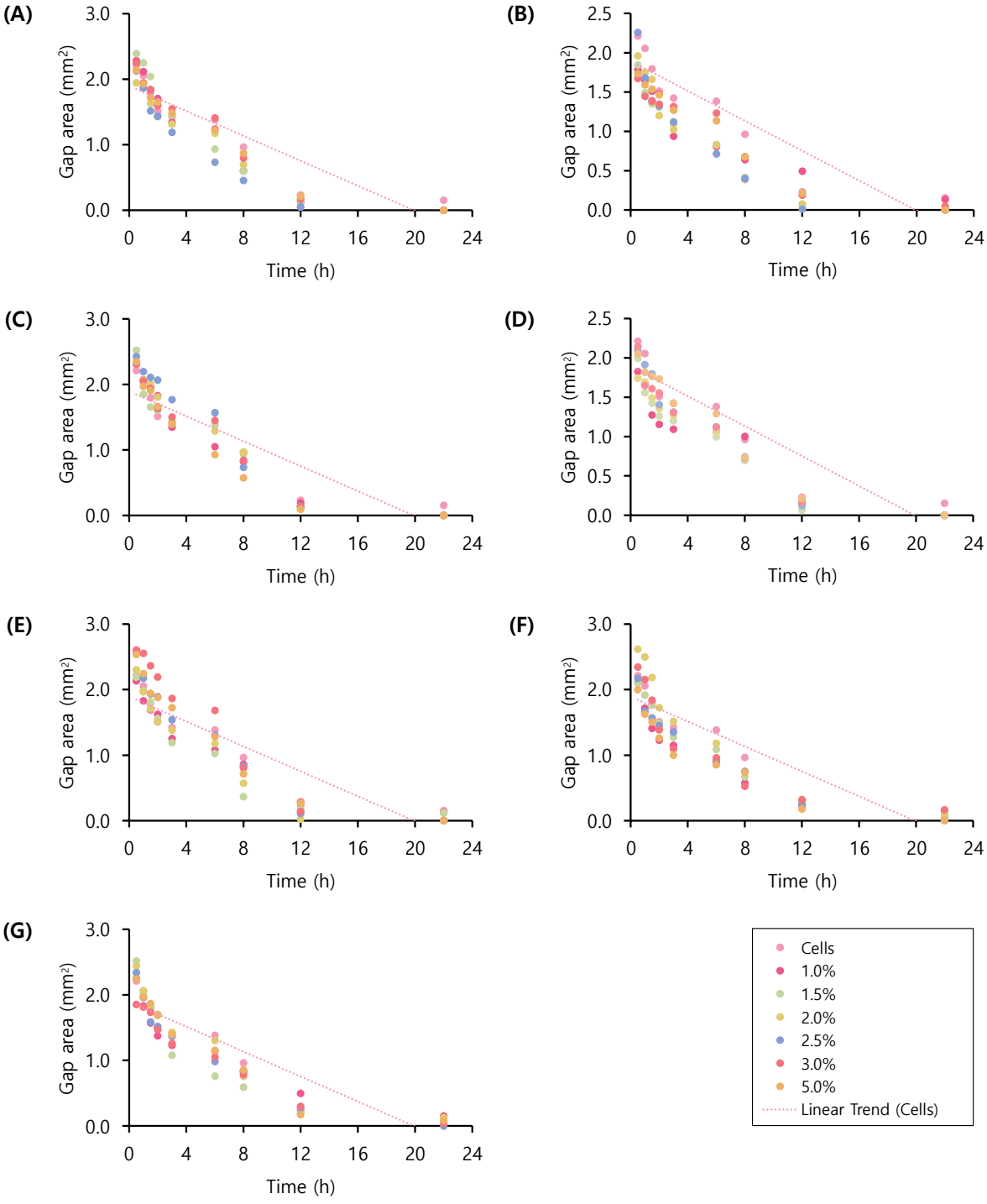


Figure 3.6: **Gap area (mm^2) in a human umbilical vein endothelial cell (HUVEC) monolayer over time (h) by hydrogel composition**, showing the trend line fitted to the cells-only control (replicated in each graph). A range of hydrogels were fabricated using **(A–B)** collagen, **(C–D)** gelatine, or **(E–G)** fibrin in **(A, C, E)** endothelial cell basal medium (EBM), **(B, D, F)** Phosphate-buffered saline (PBS), or **(G)** MES/NaCl at different concentrations. HUVECs were cultured with endothelial cell growth medium (EGM) and seeded at a density of 1.5×10^4 cells/well (96-well plate). (ANOVA/Tukey's HSD, $p \leq 0.05$; $n = 3$).

3.3.4 Selection of Hydrogel Compositions Based on Cell Adhesion and Migration Rate

Based on the results obtained from the cell adhesion and cell migration assays (Figure 3.7), gelatine hydrogels were discarded from further experimental work. Furthermore, considering the promising data produced by fibrin and collagen hydrogels, a combination of these two at a 1:1 ratio was created and included in the following experimental phase.

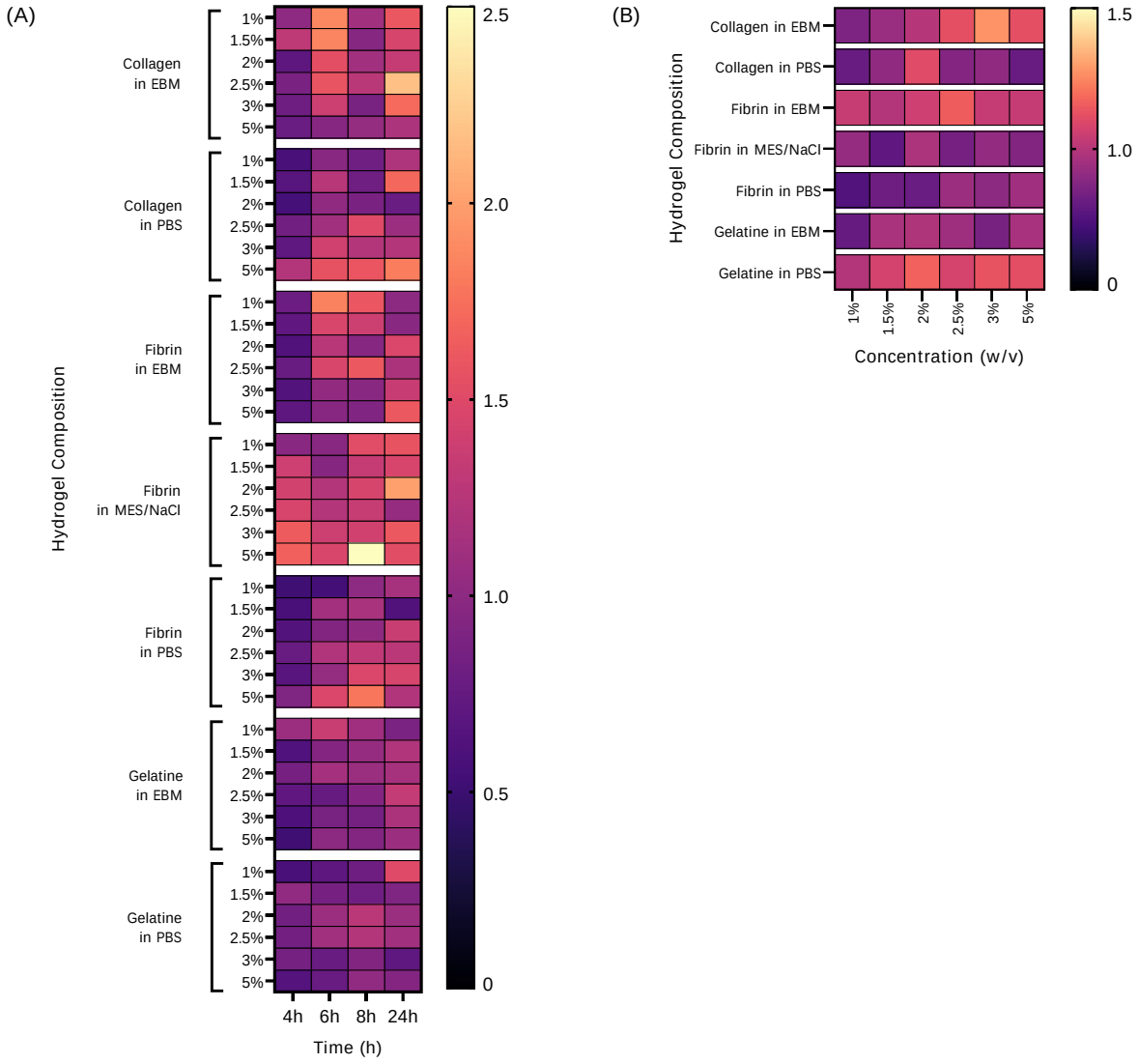


Figure 3.7: **Overview of the performance of the different hydrogel compositions**, as fold expansion of the cells-only control, in terms of **(A)** cell adhesion and **(B)** migration rate. Human umbilical vein endothelial cells (HUVECs) were cultured with endothelial cell growth medium (EGM) and seeded at a density of 2×10^4 or 1.5×10^4 cells/well (96-well plate), respectively.

3.3.5 Cell Viability

Fibrin and collagen gels, including a fibrin-collagen mix (1:1 ratio), were tested to evaluate cell viability at different time points (Figures 3.8 & A.2). A visual summary using this data was drafted to facilitate a comparison of cell viability between hydrogels (Figure 3.9A).

Nearly equal proportions of the tested hydrogels were associated with a similar (45.2%) or lower (47.6%) cell viability in comparison with the cells-only control. Three gels were associated with a statistically significant higher cell viability than the control in at least one time point, with the remaining time points being equivalent to the control: collagen in PBS 3% *w/v*, fibrin in EBM 3% *w/v*, and fibrin in PBS 3% *w/v*.

Collagen shows similar cell viability in both PBS and EBM, except for the 2.5% *w/v* concentration, whereas fibrin in EBM exhibits higher cell viability or equivalent to the control (especially 3% and 5% *w/v*); when using MES/NaCl buffer, these concentrations show the lowest viability. Interestingly, the fibrin-collagen gel at a 1:1 ratio was associated with a lower cell viability, particularly when mixed with PBS at lower *w/v* concentrations. On the other hand, when mixed with EBM, lower cell viability is associated with higher *w/v* concentrations. It is possible that this difference may be associated with hydrogel consistency.

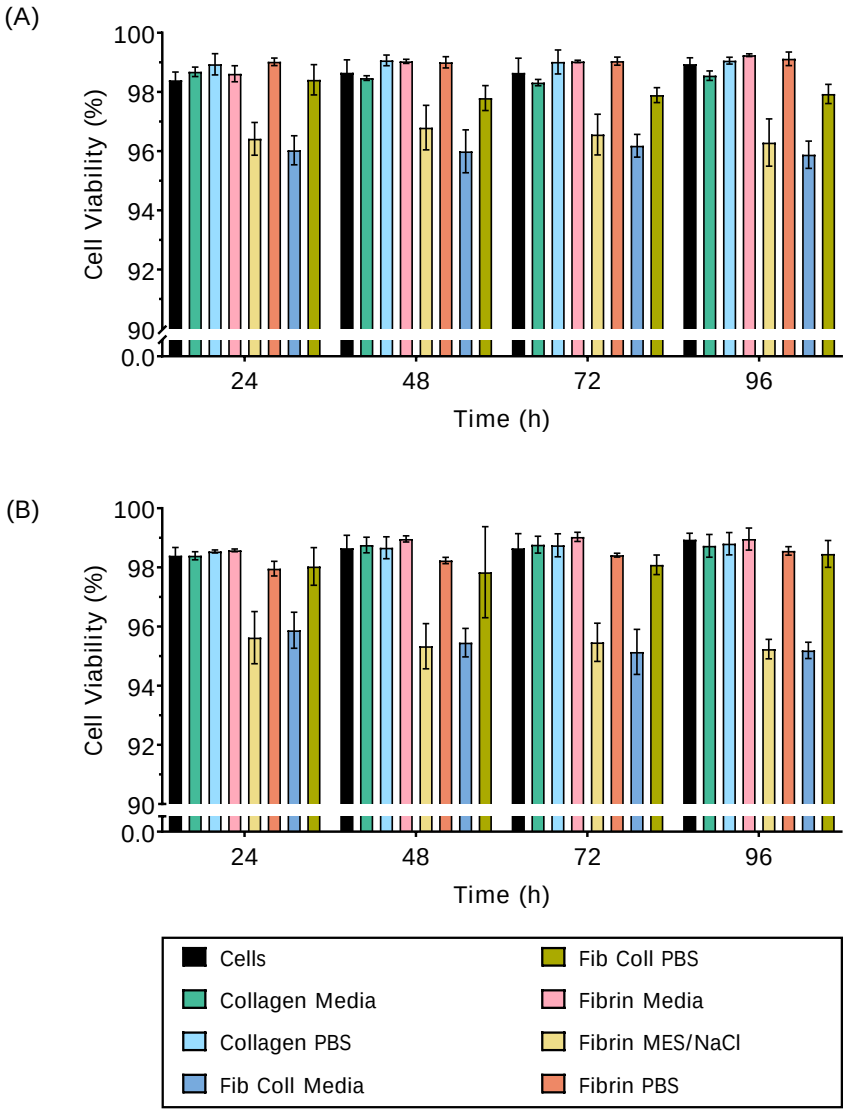


Figure 3.8: **Cell viability (%) by hydrogel composition.** Collagen, fibrin-collagen (1:1 ratio), and fibrin in endothelial cell basal medium (EBM), phosphate-buffered saline (PBS), or MES/NaCl (fibrin only) were prepared at a range of concentrations (1, 1.5, 2, 2.5, 3, or 5% *w/v*). Here, **(A)** 3% *w/v* and **(B)** 5% *w/v* are shown. Human umbilical vein endothelial cells (HUVECs) (seeding density: 2×10^4 cells/well) were cultured with endothelial cell growth medium (EGM) in 96-well plates on top of the hydrogel. Readings were taken at 24, 48, 72, and 96 h. A cells-only control (repeated in every graph for comparison purposes) was used. (ANOVA/Tukey's HSD, $p \leq 0.05$; $n = 3$). Please refer to Figure A.2.

3.3.6 Hydrogel Consistency

The hydrogel consistency was visually inspected and categorised (Figure 3.9B). Upon observation, it was noticeable that PBS and MES/NaCl hydrogels were transparent, while EBM hydrogels were pink. Furthermore, as the % *w/v* increased, hydrogels became more opaque, which was particularly noticeable in the MES/NaCl hydrogels.

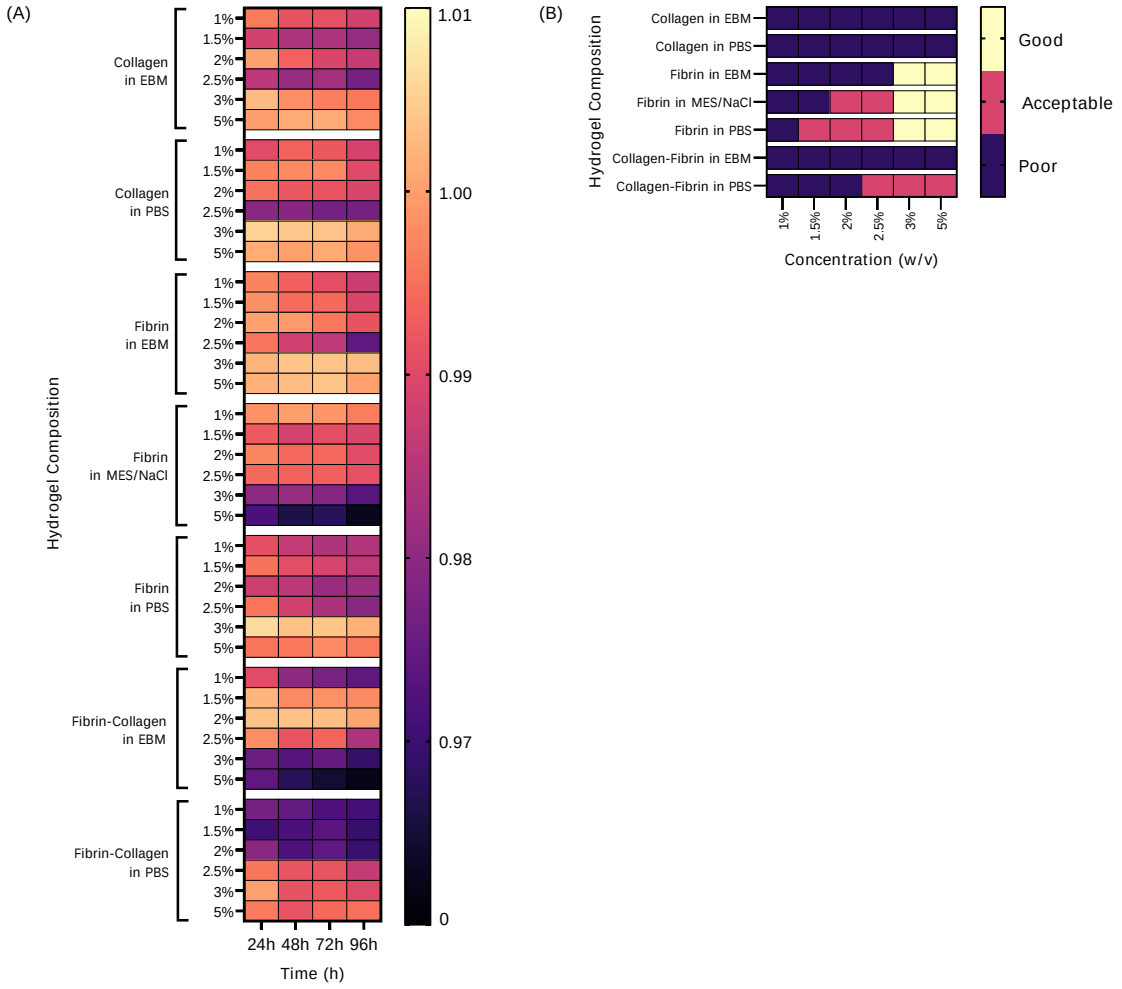


Figure 3.9: **Overview of the performance of the different hydrogel compositions**, as fold expansion of the cells-only control, in terms of **(A)** cell viability and **(B)** hydrogel consistency. Hydrogel consistency was visually evaluated and classified as poor, acceptable, or good based on the desired characteristics for a 3D construct able to retain its shape. Human umbilical vein endothelial cells (HUVECs) were cultured with endothelial cell growth medium (EGM) and seeded at a density of 2×10^4 cells/well (96-well plate).

In terms of hydrogel consistency, higher % *w/v* concentrations delivered more viscous gels and displayed better shape retention after 1 h. Furthermore, collagen hydrogels were less viscous than fibrin or fibrin-collagen ones at the same % *w/v* concentration. Interestingly, none of the collagen hydrogels displayed acceptable or good shape retention. The only hydrogel compositions containing collagen that had an acceptable consistency and shape retention were fibrin-collagen in PBS at 2.5, 3, or 5% *w/v*.

Five fibrin hydrogels (in MES/NaCl: 2 and 2.5%; in PBS: 1.5, 2 and 2.5%) also displayed acceptable shape retention, whereas only high-concentration fibrin hydrogels (3 and 5% *w/v*) had a good consistency. Relevantly, all media used for fibrin hydrogels displayed good shape retention, thus suggesting that both the % *w/v* and the material (fibrin) play a greater role in hydrogel consistency than the medium.

3.3.7 Further Selection of Hydrogels Based on Cell Viability and Hydrogel Shape Retention

The optimal hydrogel composition was further refined based on cell viability and hydrogel consistency and shape retention (Figure 3.9).

Given that around half of the hydrogel compositions were associated with a similar or better cell viability than the control, hydrogel consistency was used to further refine the optimal hydrogel composition for the development of a scaffold for microvascular network formation. The collagen and fibrin-collagen hydrogels were discarded due to their poor shape retention.

From the remaining hydrogel compositions, the 3 and 5% *w/v* ones were selected as they exhibited a good hydrogel consistency and shape retention after removing the scaffold from the casting mould. From these six candidates (fibrin in EBM, MES/NaCl and PBS at 3 and 5% *w/v*), the two most promising hydrogel compositions were also selected considering cell adhesion and migration rate (Figures 3.7 and 3.9). Based on the performance of the different hydrogel compositions, fibrin in EBM at 3 and 5% *w/v* were selected for further study.

3.3.8 Tube Formation

A tube formation assay was used to assess capillary-like network formation on fibrin in EBM (3% and 5% *w/v*) hydrogels. HUVECs developed networks of tube-like structures when seeded on these hydrogels (Figure 3.10). The formation of these structures is essential for the development of microvascular *in vitro* models. Networks formed from 6 h onwards and degraded by 24 h.

Once the networks were formed, characterisation including the number, length, and diameter of segments was carried out (Table 3.1). To gain further understanding of the overarching architecture created with the tube-like structures, segments were classified as LS, PS, or branches (Figure 3.1), and the arrangements between different types of segments (*e.g.* branch-to-PS ratio, the angle formed between PS and branches) were also characterised.

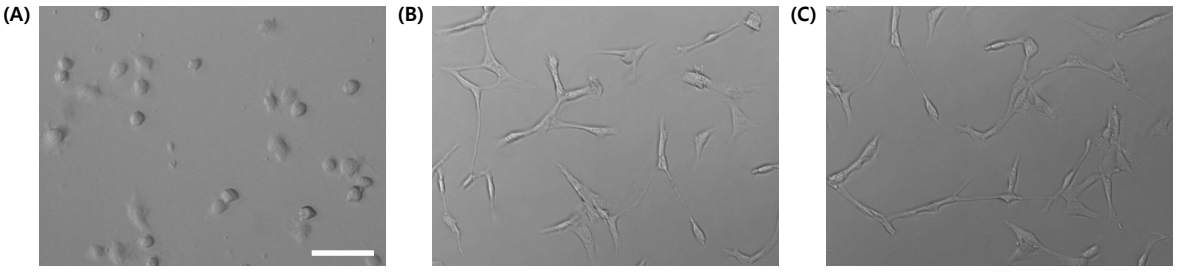


Figure 3.10: **Tube formation on fibrin in endothelial cell basal medium (EBM) at 3% *w/v*, (A)** 0.5 h, **(B)** 8 h, and **(C)** 10 h after seeding (20×). Human umbilical vein endothelial cells (HUVECs) were cultured with endothelial cell growth medium (EGM) and seeded at a density of 2×10^4 cells/well (96-well plate). Scale bar: 100 µm.

Tube-like structures arranged in a network were formed in both both hydrogels (3% and 5% *w/v*). Moreover, the networks formed on both hydrogels were similar in terms of the number, length, and diameter of segments as well as the network architecture. The average diameter of segments was similar between the 3% (8.6 ± 3.1 µm) and 5% (7.9 ± 2.4 µm) *w/v* concentrations.

The 3% and 5% hydrogels had a similar number of average total segments: 10.3 ± 3.2 (3% *w/v*) vs. 9.6 ± 3.5 (5% *w/v*). In the 3% *w/v*, the average number of PS was slightly greater (2.67 vs. 2.33) whereas the branch number average was slightly smaller (3.33 vs. 3). The average number of LS was exactly the same. Regarding the branch to PS ratios, 26.6% of the PS split into two branches whereas the remaining ones continued as a single segment, albeit following a change in the angle.

Table 3.1: **Characterisation of networks formed by Human umbilical vein endothelial cells (HUVECs) when embedded in fibrin in endothelial cell basal medium (EBM) hydrogels at both 3 and 5% *w/v* concentrations.** Network characterisation comprised measurements obtained from the capillary-like networks and by type of architectural elements: linear segments (LS), primary segments (PS), branches, and the relation between PS and branches in angle and ratio. Data is presented as average values ± standard deviation.

Network			
Hydrogel Composition	Segments (n)	Length (µm)	Diameter (µm)
Fibrin in EBM 3%	14	82.5 ± 31.9	8.2 ± 3.6
	9	85.3 ± 47.1	6.0 ± 4.0
	8	107.0 ± 79.0	10.2 ± 2.8
Fibrin in EBM 5%	13	71.8 ± 33.8	7.2 ± 1.6
	10	83.1 ± 44.9	7.2 ± 5.0
	6	254.2 ± 62.0	3.4 ± 3.6
Linear Segments (LS)			
Hydrogel Composition	Segments (n)	Length (µm)	Diameter (µm)
Fibrin in EBM 3%	7	85.5 ± 40.5	6.8 ± 2.2
	2	114.8 ± 78.4	8.7 ± 0.8
	4	86.9 ± 65.0	10.5 ± 2.2
Fibrin in EBM 5%	7	77.5 ± 41.8	7.6 ± 2.0
	2	114.8 ± 78.4	8.5 ± 0.8
	4	265.9 ± 74.5	7.1 ± 0.6
Primary Segments (PS)			
Hydrogel Composition	Segments (n)	Length (µm)	Diameter (µm)
Fibrin in EBM 3%	3	95.1 ± 11.9	8.3 ± 3.9
	3	102.0 ± 26.6	8.9 ± 1.6
	2	150.2 ± 156.1	10.4 ± 3.3
Fibrin in EBM 5%	3	79.8 ± 18.3	7.1 ± 0.5
	3	79.4 ± 52.0	10.9 ± 5.9
	1	209.7	6.4
Branches			
Hydrogel Composition	Segments (n)	Length (µm)	Diameter (µm)
Fibrin in EBM 3%	4	9.4 ± 5.3	10.4 ± 5.1
	4	58.0 ± 39.2	7.0 ± 2.6
	2	104.0 ± 36.3	9.4 ± 5.3
Fibrin in EBM 5%	3	50.7 ± 20.0	6.4 ± 1.0
	5	72.6 ± 31.6	8.7 ± 1.9
	1	251.8	6.7
Relation of Primary Segments (PS) and Branches			
Hydrogel Composition	Angle (°)		Branch:PS Ratio
Fibrin in EBM 3%	49.9 ± 18.4		4:3
	134.0 ± 33.3		4:3
	27.9 ± 34.6		1:1
Fibrin in EBM 5%	23.6 ± 26.4		1:1
	72.4 ± 12.9		5:3
	26.2 ± 15.2		1:1

3.4 Discussion

This chapter presents the development and optimisation of the composition of a hydrogel microvascular scaffold. A range of hydrogels was created from different combinations of materials (collagen, fibrin, gelatine), media (PBS, EBM, MES/NaCl buffer), and concentrations (1–5% *w/v*). The optimisation process comprised a multipronged evaluation combining cell adhesion, migration rate, cell viability, hydrogel consistency and shape retention, and tube formation. A large number of candidates were screened and systematically narrowed down based on the results obtained in the different experimental phases, thereby eliminating those hydrogel compositions that were suboptimal for the development of the construct.

The results obtained in the cell adhesion and migration rate phases clearly suggested that gelatine hydrogels, using either EBM or PBS as the medium, are not well suited for the development of this construct. Low cell adhesion across all *w/v* concentrations and the lack of a significantly higher associated migration rate led to the decision to discard gelatine hydrogels from further experimental work.

Furthermore, hydrogels containing collagen delivered substandard results in terms of cell viability and, particularly, shape retention and hydrogel consistency. Of all the hydrogel compositions containing collagen, 87.5% were associated with significantly lower cell viability values. Moreover, 75% (18 compositions) of the collagen-based hydrogels exhibited such low values in at least three of the four time points. Furthermore, none of the collagen or fibrin-collagen hydrogels exhibited good shape retention or hydrogel consistency. In contrast, six of the fibrin hydrogels had good shape retention (3 and 5% *w/v* fibrin in all media). The experimental results suggest that the hydrogels containing collagen evaluated in this research are not optimal for the development of this construct, so these compositions were not explored further.

Following this multipronged optimisation strategy, the two most promising hydrogel compositions from the initial 42 candidates were selected for the final experimental phase. Shape retention is a crucial characteristic in the development of the construct, as it allows the construct to be removed from the mould and used for further research, such as a stand-alone platform. Therefore, only the hydrogel compositions that exhibited acceptable or good shape retention and hydrogel consistency could be considered promising candidates for the development of the construct. From the hydrogel compositions exhibiting good or acceptable shape retention and hydrogel consistency, the selection was made based on the results obtained in the cell viability, migration rate, and cell adhesion experimental phases.

Fibrin hydrogels in EBM at 3 and 5% *w/v* were the most promising candidates, so their ability to support EC organisation into capillary-like networks was evaluated using a tube formation assay. Although this assay is widely used to assess angiogenic behaviour, it does not demonstrate the formation of functional, lumenised vessels. Both hydrogels enabled the formation of capillary-like networks, which is central to the development of a microvascular construct. The results obtained in this research are further supported by similar findings in the literature. For instance, Teicher *et al.* [296] report successful HUVEC tube formation when seeded on fibrin gels, whereas Narayan *et al.* [297] confirm that all capillary-like vessel sprouting occurs by 24 h, after which no cell spreading takes place.

Relevantly, similar concentrations of fibrin (2.5 and 5% *w/v*) have been found to produce capillary-like networks with the greatest number of junctions and segments when compared with higher or lower concentrations [405]. However, as the networks produced in both hydrogels are similar to each other both in terms of the number of segments and microarchitecture, no clear preference for either hydrogel composition can be declared. Further refinement of the concentration (% *w/v*) should consider long-term applications for these 3D microvascular scaffolds and would benefit from including material characterisation.

As demonstrated in this work and supported by similar studies found in the literature, including Anderson *et al.* [406] and Hasenberg *et al.* [405], fibrin is a suitable scaffold material for the formation of capillary-like

networks. Relevantly, fibrin supports angiogenesis in 2D and 3D environments, and in both single-cell and co-culture models. It is a promising option as the ECM of the engineered construct, promoting desired cell functions.

In the body, fibrin plays an important role as a provisional cellular matrix during wound healing and tissue remodelling [282], and is also involved in cell adhesion and migration, blood clotting, and tissue morphogenesis [270]. Furthermore, its porosity, mechanical properties, and degradation rate can be controlled [270], permitting construct customisation [282]. This makes fibrin, a biodegradable matrix, particularly well suited for TE applications because it can support tissue regeneration.

The optimisation process of the hydrogel composition led to gelatine and collagen hydrogels being discarded from further experimental work. The results produced in this research supporting this decision are further supported by the literature. For instance, collagen hydrogels exhibit poor mechanical properties [224, 353], which, like their structural integrity, can be improved by combining collagen with another biomaterial [407]. On the other hand, gelatine hydrogels at concentrations below 10% *w/v* result in insufficient shape fidelity [407]. These findings further support the conclusion that both collagen and gelatine are suboptimal for the development of a 3D construct, which demands a biomaterial with good shape retention to enable its use in further applications, including as a testing platform for traumatic injury research.

The cell migration assay is a standard *in vitro* technique used to evaluate collective cell migration [403]. This 'cell sheet' migration is exhibited by EC monolayers and was corroborated in the present experimental work. All the hydrogels tested, as well as the cells-only control, closed the gap created by the pipette tip, essentially 'healing' the wound. Interestingly, cells displayed a faster migration rate in hydrogels using EBM compared to those using PBS or MES/NaCl. This highlights the impact of the selection of a medium which, as stated by Rosinska *et al.* [408], has a clear visible influence on the rigidity of the material obtained, impacting cell migration.

Other studies using similar methodologies for wound or gap closure assays produce similar results regarding cell sheet migration. For instance, [406] report that HUVECs seeded on fibrin gels closed the gap almost entirely by the end of the monitoring period (18 h). This is similar to the results obtained in this research for fibrin, collagen, and gelatine hydrogels, where the gap was closed after 20 h in the majority of compositions and after 22 h in all hydrogel variations. The cell migration rate is not only impacted by the hydrogel composition: environmental factors, such as the administration of high glucose [409], can accelerate cell migration.

The cell migration rate was obtained using the slope of the generated linear trendline, as recommended in established protocols in the literature [403]. However, the pattern exhibited by all hydrogel compositions and the cells-only control suggests a larger reduction in gap area in the first hours, which then slows. It would therefore be interesting to explore other trendline fits (*e.g.* exponential, second-order polynomial) to identify alternatives that could fit the data points better. This could provide a more accurate estimation of the area recovered by the cells at a given time point, that accounts for an accelerating or decelerating migration rate over time.

Given that the gap was manually induced, it can be difficult to generate reproducible gaps. For instance, the angle at which the pipette tip is held plays a key role as there needs to be consistent pressure applied to create a consistent gap width. To increase reproducibility, an insert could be placed in the wells before cell seeding, ensuring that no cells can migrate into the space that will later become the gap once the insert is removed. Although this could minimise the variation in gap size across samples, the removal of the insert could tear in the cell monolayer, leaving uneven gap edges.

Regarding cell viability, no clear trend was observed with the choice of PBS, MES/NaCl, or EBM, as most differences in cell viability can be attributed to the choice of fibrin, collagen, or fibrin-collagen. Interestingly,

the fibrin-collagen (1:1) hydrogels, particularly when mixed with PBS at lower % *w/v* concentrations, yielded lower cell viability. Further research is required, particularly into different fibrin-collagen ratios.

It is worth mentioning that the control yielded very high cell viability across all time points, making it more difficult to identify well-performing hydrogels. Nevertheless, the three materials tested at different *w/v* concentrations delivered good cell viability (> 95%). This is expected because these materials have been previously used for cell culture with positive outcomes and have been deemed biocompatible.

When evaluating hydrogel consistency and scaffold shape retention, the fibrin hydrogels outperformed both collagen and fibrin-collagen scaffolds, which performed poorly. Moreover, higher % *w/v* hydrogels produced more viscous gels and displayed better shape retention. Fibrin hydrogels at lower concentrations produced scaffolds with an acceptable consistency, whereas the 3 and 5% *w/v* hydrogels exhibited a good consistency.

Although more viscous gels are associated with better shape retention once demoulded, they may impose greater mechanical resistance to cell migration. On the other hand, hydrogels that are not viscous enough fail to retain their shape after removing them from the wells they were cast in. This limits their application to research that can be conducted on hydrogels contained in their casting moulds and would make it very challenging to produce a 3D construct.

This research aims to develop and optimise 3D scaffolds for microvascular networks. However, a number of the experimental assays conducted as part of the optimisation of the hydrogel composition are carried out in 2D because some of the characteristics that are explored in this research can best be quantified in this way using standard *in vitro* procedures. For instance, the cell migration or wound healing assay is a standard technique for probing collective cell migration widely used in the TE field [409,410]. Nevertheless, the optimisation of the hydrogel composition carried out throughout this research led to the successful formation of capillary-like networks in 3D environments. As addressed by Hasenberg *et al*. [405], the use of fibrin as the material for hydrogel fabrication does not limit the supply of oxygen and nutrients to the cells contained within, therefore allowing for 3D network formation throughout the gel.

HUVECs have been widely used for *in vitro* work because they are easily available and have demonstrated the ability to form new vasculature. Although they are considered the gold standard in EC research, macrovascular cells differ from microvascular endothelial cells (MVECs) in a number of ways, including the prostaglandin secretory profile, types and amounts of cell adhesion molecules, cytoskeletal components, and secreted proteins [56,270,411,412]. In particular, MVECs express specific proteins associated with tight junctions that are required to regulate capillary permeability [300]. As such, it would be interesting to use MVECs such as human dermal microvascular endothelial cells (HDMEC-1) for the development of a microvascular construct so that the construct is more physiologically relevant.

A number of experimental methods are used to carry out traumatic injury research, the majority of which employ *in vivo* models [119]. Nevertheless, modelling trauma in animal models entails major ethical concerns due to, among other reasons, the stress or pain that animals undergo. Moreover, although some *in vivo* models, like pigs, are chosen based on biomechanical and scale similarity, physiological and pathophysiological differences between animal models and humans remain [14]. These differences can make translating trauma research significantly more complex. Given this, there is a need for physiologically relevant *in vitro* models for trauma research that can not only provide a fundamental understanding of the mechanism of injury but also serve as platforms to test potential therapeutics for tissue repair and regeneration.

The research presented here addresses this gap by developing and optimising a hydrogel scaffold tailored for ECs and, in particular, microvascular network formation. This construct not only enables the formation of tube-like structures arranged in a microvascular network, but the optimisation of its design also considers the characteristics required for using this construct as a platform for *in vitro* trauma research.

3.5 Conclusion

There is a need for *in vitro* models for microvasculature trauma research that allow us to gain a fundamental understanding of traumatic injuries and, at a later stage, test therapeutics to enhance tissue repair and regeneration. The selection of polymer type, ratio, and medium impacts the properties of the resulting hydrogel. By optimising these parameters, this research identified the hydrogel composition best suited for the development of microvascular scaffolds. Constructs using a range of collagen, fibrin, or gelatine hydrogels embedded with HUVECs were created and evaluated to identify the most promising construct compositions. These hydrogels were compared based on their performance in terms of cell viability, cell adhesion, cell proliferation, migration rate, hydrogel consistency, and the capacity to form tube-like structures. Based on the results produced in this research, the most promising candidates were fibrin in EBM at 3 and 5% *w/v*.

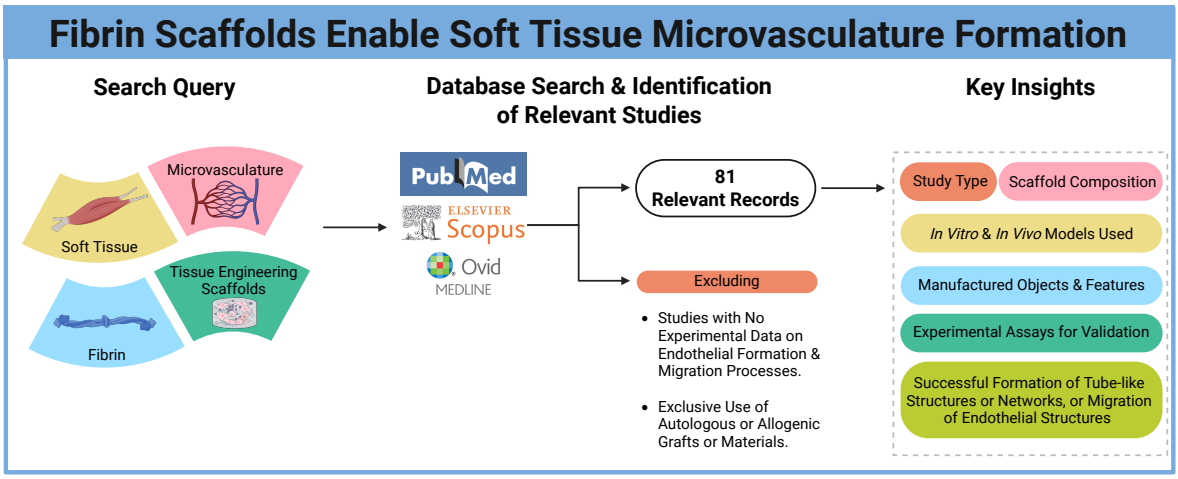
Further work on the optimisation of the construct is required in terms of material characterisation including, for instance, degradation. Moreover, it would be beneficial to incorporate additional cell types into the construct in an effort to mimic the physiological architecture of the natural tissue. Finally, the next step for this microvasculature hydrogel scaffold would be its use for traumatic injury *in vitro* research and validation.

Acknowledgements

HUVECs were a kind gift from Professor Sarah De Val (Department of Physiology, Anatomy and Genetics, University of Oxford). Thanks to Dr Viorica Patrulea (Université de Genève and University of Oxford) for her insightful feedback.

Chapter 4

Fibrin Scaffolds for Angiogenesis in Soft Tissue Models: A Systematic Review



Thesis Integration and Chapter Structure

Having identified fibrin as the most promising scaffold material in Chapter 3, this chapter addresses Objective 2 by systematically reviewing and critically evaluating the existing literature on fibrin-based soft tissue scaffolds used in tissue engineering (TE). The review focuses on identifying scaffold design parameters that enable successful endothelial formation and migration processes (EFMPs), including tube and network formation, and endothelial cell (EC) migration. This chapter critically evaluates reported scaffold compositions and formulations with respect to their ability to support EFMPs, examining how variations in scaffold design, such as fibrinogen source and concentration, coagulant or crosslinker choice, and cell incorporation strategies influence angiogenic outcomes. Through a synthesis of published peer-reviewed studies, key determinants of endothelial behaviour are identified. To connect back to the focus of this thesis, this chapter reviews fibrin-based scaffolds used across soft tissue TE applications, with muscle examined in greater depth as a representative case study. Among these, skeletal muscle is one of the tissues most frequently injured or damaged in non-penetrating traumatic injuries (NPTIs), making the insights derived from these models particularly relevant for trauma research. A major challenge identified through this systematic review (SR) is the absence of standardised reporting on fibrin scaffolds, which hinders reproducibility, cross-study comparison and clinical translation. To address this, a reporting tool was developed to promote consistent inclusion of critical methodological details. Within the broader framework of this thesis, this chapter provides a knowledge-driven rationale for refining fibrin-based constructs, informing the development and optimisation of the three-dimensional (3D) microvascular model presented in Chapter 5.

This chapter has been published [413] and is available at DOI: 10.1016/j.bioactmat.2025.10.019.

In this section, the SR was designed and managed by Carla V. Fuenteslópez, including the search strategy, study design, selection of items for data extraction, and the screening, data extraction and synthesis processes. All figures, schematics, tables and the first manuscript draft were also produced by Carla V. Fuenteslópez. Simge Bahçevancı validated the search strategy and study design, and reviewed and edited the first draft. Carla V. Fuenteslópez, Simge Bahçevancı and Viorica Patrulea independently screened the identified articles and contributed to data extraction. Carla V. Fuenteslópez, Simge Bahçevancı, Viorica Patrulea and Prof Hua Ye reviewed and edited the manuscript. Prof Hua Ye provided supervision and advice.

Fibrin Scaffolds for Angiogenesis in Soft Tissue Models: A Systematic Review

Abstract

Background: Fibrin is a biocompatible, angiogenic biomaterial widely used in soft tissue engineering (TE), with outcomes influenced by scaffold formulation and design.
Aim: This systematic review (SR) evaluates how fibrin scaffold composition and design affect angiogenesis in *in vitro* and *in vivo* soft tissue models.
Methods: PubMed, Scopus and OVID were searched on 28 October 2024. A two-step screening process, conducted by three independent researchers, identified original studies on fibrin scaffolds assessing endothelial formation and/or migration processes (EFMPs). Studies without experimental data or that focused solely on grafts were excluded. Data on scaffold composition, manufactured objects, cell-embedding strategies, and angiogenic outcomes, together with a subset of muscle-specific studies, were narratively synthesised. Risk of bias (RoB) and study quality were assessed using SYRCLE's RoB tool and a modified CAMARADES checklist.
Results and Discussion: The 81 included studies highlight the impact of scaffold composition on angiogenic outcomes, with human-derived fibrinogen and pre-embedding cells consistently supporting successful outcomes. While tube and network formation outcomes typically aligned, endothelial migration exhibited different patterns. Thrombin often contributed positively, but crosslinker effects were less clear. Muscle-focused studies mainly used hydrogels and often included non-endothelial cells (non-ECs).
Conclusions: Fibrin scaffolds are highly relevant for soft tissue TE, with outcomes influenced by formulation, fibrinogen source and cell embedding. However, experimental design variability and a lack of standardised reporting hinder reproducibility and clinical translation. To support future research, a minimum information checklist was created to promote consistent reporting, while aggregated success rates across design parameters could guide scaffold design.
Registration and Funding: PROSPERO [CRD42025612994] and OSF [10.17605/osf.io/nvfdj]. No funding body was directly involved.

Keywords

Fibrin Scaffolds • Soft Tissue Regeneration • Microvascular Network Formation • Endothelial Cell Migration • Angiogenesis • Scaffold Design Optimisation.

4.1 Introduction

Tissue engineering (TE) is a multidisciplinary field focused on replacing, repairing and regenerating damaged tissue, ultimately aiming to reduce or eliminate the need for donor organs [272]. It integrates three main components: scaffolds, cells and biological factors. Scaffolds are three-dimensional (3D) matrices that provide structural support to cells, facilitating essential functions such as cell attachment, migration and proliferation [414]. Scaffolds can take various forms, including pre-made porous structures, decellularised extracellular matrix (ECM), or hydrogels [232, 415]. Importantly, scaffolds can be customised to better replicate the natural tissue, enabling their use for both soft and hard TE applications [232].

Soft tissues comprise the supportive structures of the body other than bone (*e.g.* skin, lymphatic and blood vessels, adipose tissue, connective tissue, peripheral nerves) [416], as well as soft musculoskeletal tissues (*e.g.* cartilage, ligaments, tendons, muscles, other connective tissues) [417]. The specific design criteria for scaffolds (*e.g.* mechanical strength) depend on the target tissue, thus dictating the choice of materials [418].

Both synthetic and natural polymers are widely used to create soft tissue scaffolds. Natural polymers (*e.g.* collagen, fibrin, chitosan, hyaluronic acid) typically offer superior biocompatibility but have limited processability compared to synthetic polymers. To achieve clinical success and enable physiologically relevant models for preclinical research, scaffolds must exhibit specific biological, mechanical and structural properties [241]. This includes being biocompatible and non-toxic, to avoid inducing host immune responses or reactions [419] and having suitable mechanical properties to withstand mechanical stress. Additionally, scaffolds should exhibit degradation profiles comparable to those of the native tissue while maintaining structural integrity [420].

Porosity is another critical factor in scaffold design, supporting cellular functions, especially when pores are interconnected, as they facilitate waste removal, as well as nutrient and oxygen exchange [421]. For larger tissues, vascularisation is essential to ensure adequate nutrient and oxygen delivery and metabolic waste removal [422]. Notably, one of the main challenges in TE is the insufficient vascularisation of the constructs, which limits cell survival, tissue integration [423] and, in turn, restricts the size of functional artificial tissues, as the absence of microvasculature prevents essential nutrient and oxygen delivery throughout the tissue. The increasing prevalence of soft tissue injuries and defects, coupled with the limited effectiveness of current reconstructive techniques, highlights the need for a comprehensive assessment of the capacity of fibrin-based scaffolds to promote angiogenesis, including microvascular formation in soft tissues [233, 424].

Vascular network development can occur through vasculogenesis (*de novo* formation of blood vessels from early endothelial cells; ECs) or angiogenesis (new blood vessels sprouting from pre-existing ones) [422]. For adequate perfusion and cellular viability, TE scaffolds must keep cells within the diffusion limit of 200 µm from a functional capillary [425]. Insufficient vascularisation in these products can lead to ischaemia-induced necrosis and, later, implant failure. Therefore, strategies such as pre-vascularising constructs or incorporating growth factors are being explored to improve construct viability [426].

A strategy for designing pro-angiogenic scaffolds involves the use of proteins such as fibrin because of their cell-binding sites, which facilitate ECs adhesion [426]. Fibrin, a highly angiogenic plasma protein, is formed through the enzymatic conversion of fibrinogen by thrombin [427]. This polymerisation process is further influenced by other biological co-factors such as calcium ions (Ca^{2+}) and factor XIIIa, which stabilise fibrin *via* covalent crosslinking [375]. Due to its crucial role in wound healing, tissue remodelling, haemostasis and angiogenesis, fibrin provides a bioactive matrix that facilitates cell attachment, migration [428] and growth factor binding through specific receptors [344]. Fibrin is, therefore, a promising biomaterial for TE applications due to its excellent biocompatibility, biodegradability and capacity to support endothelial network formation [397, 429]. Recent studies have highlighted the potential of fibrin-based scaffolds in soft tissue TE, including skin [430], cartilage [431] and nerve tissues [432]. Moreover, these scaffolds have been associated with enhanced collagen fibre formation [430], cell differentiation support [431] and rapid tissue healing [430, 432].

Compared with other biopolymers, fibrin stands out for its exceptional properties, especially its pro-angiogenic potential [433]. While collagen type I is the major constituent of the ECM, it does not possess the intrinsic angiogenic properties that make fibrin particularly effective in promoting vascular formation [434]. Studies report that fibrin is more effective in inducing angiogenesis, both *in vitro* and *in vivo*, and that the two may act in synergy [435]. In contrast, gelatine, a denatured derivative of collagen, poses challenges due to its poor thermostability, as it shifts from gel to solid with temperature changes. As such, it requires either physical or chemical crosslinking, which often leads to poor reproducibility and limited translation from *in vitro* studies to therapeutic applications [436].

Fibrin has also been used in emerging technologies such as 3D bioprinting, opening avenues for new applications. Its popularity as a bioink component arises from its biological properties, favourable viscoelastic characteristics and the ability to be readily crosslinked with thrombin before, during, or after printing [395,437]. The mechanical properties of fibrin can be modulated by, for instance, varying the fibrinogen concentration, with studies reporting an almost linear increase in apparent elastic modulus [438]. Fibrin is also uniquely extensible [439], with individual fibres capable of stretching up to 200 times their original length [440]. It has also been used to create organ-on-a-chip models of vascularised tissues, demonstrating its strong potential for developing physiologically relevant and translational systems [441].

Currently, commercial fibrin-based products are limited to fibrin sealants, which are biodegradable materials that form physiologically stable clots for wound healing applications [442]. These sealants have demonstrated clinical success in enhancing wound healing, reducing bleeding, shortening post-operative recovery and pain, and reducing the length of hospitalisation [443]. Despite its remarkable potential, fibrin has yet to be commercialised as a TE scaffold unlike the widely available collagen-based alternatives. This is largely due to the inherent material limitations of fibrin, including its low mechanical strength, rapid enzymatic degradation, dense microstructure in gel form and high shrinkage rate, which pose significant challenges for scaffold development [430,443]. Variations in scaffold design, composition and fabrication techniques can significantly change the mechanical, biological and angiogenic properties of fibrin scaffolds, thereby impacting microvascular network formation [444, 445].

While existing systematic reviews (SRs) have largely focused on broader aspects of TE, none has analysed the evidence on the formulation and use of fibrin-based scaffolds in soft tissue vascularisation. A comprehensive understanding of how scaffold formulation and design influence tube formation, network formation, or EC migration is crucial for creating models that enhance soft tissue regeneration.

This SR aims to address this need by critically examining the current literature on fibrin-based soft tissue scaffolds for TE, with a specific focus on their capacity to support endothelial network formation. The primary objective of this SR is to assess the efficacy of fibrin or fibrinogen-based scaffolds, jointly referred to from here on as 'fibrin scaffolds', in promoting angiogenesis, including microvascular network formation, in soft tissues. This will be achieved by comparing studies that evaluated fibrin scaffolds (intervention) against control groups lacking such scaffolds (comparator), where the primary outcome is the formation of new blood vessels (outcome) in various soft tissue types (population).

We hypothesise that fibrin scaffolds facilitate angiogenesis, including microvascular network formation, and enhance EC migration in soft tissue regeneration, thereby improving angiogenesis in both *in vitro* and *in vivo* studies. Accordingly, this SR seeks to answer the following research question: '*How do variations in fibrin scaffold design and composition affect endothelial formation and migration processes (EFMPs) in soft tissue models, in both in vitro and in vivo settings?*'. By evaluating these factors, this review aims to provide useful insights into the design principles of fibrin-based scaffolds, advancing their application in promoting vascularisation and improving outcomes in soft tissue regeneration.

4.2 Methodology

4.2.1 Eligibility Criteria and Study Design

The eligibility criteria for this SR were carefully defined to ensure the inclusion of relevant studies and the exclusion of those that did not meet the predefined parameters. The study characteristics used to determine eligibility aligned with a modified Population, Intervention, Comparison and Outcome (PICO) framework, as outlined below.

Population: Eligible studies included those employing *in vitro*, *ex vivo* and/or *in vivo* models (male or female animals) of (micro)vasculature in the context of soft tissue regeneration. The inclusion criteria encompassed studies that incorporated clinical, simulation or modelling data in the same article, as long as experimental data from *in vitro*, *ex vivo* or *in vivo* models were generated. Studies were excluded if they were exclusively clinical studies, simulations (*e.g.* computational), or modelling (*e.g.* mathematical) that did not report any experimental data on *in vitro*, *ex vivo* or *in vivo* models of (micro)vascularised soft tissue.

Intervention/Exposure: The primary intervention of interest was the application of fibrin-based soft tissue scaffolds to achieve (a) tube or tube-like structure formation, (b) network or interconnected tube formation and/or (c) EC migration. From here onwards, these three outcomes will collectively be referred to as 'endothelial formation and migration processes' (EFMPs). Specifically, the inclusion criteria were:

- TE scaffolds/constructs containing fibrin (or fibrinogen) in their formulation, either alone or combined with other materials, in any concentration or composition.
- Scaffolds either pre-embedded with cells or acellular.
- Any type of manufactured scaffold (*e.g.* hydrogel, mesh).
- Fibrinogen from any source (*e.g.* commercial) or species (*e.g.* human, bovine).
- Publications reporting data on scaffold design (*e.g.* formulation, manufactured object type).
- Publications reporting outcomes related to at least one of the three EFMPs (*i.e.* tube formation, microvascular network formation, EC migration).
- Single or repeated use of the scaffold.
- Any study type (*e.g.* *in vitro*, *ex vivo*, *in vivo*).

The review excluded studies that only used autologous or allogeneic grafts or materials, including platelet-rich fibrin (PRF), without the development of a TE scaffold.

Comparators/Control: The following control groups were eligible, with no exclusions applied:

- Non-fibrin-based scaffolds or controls using other materials (*e.g.* collagen, synthetic polymers).
- Non-exposed control groups comprising *in vitro* or *in vivo* models where no scaffold was applied.
- Groups subjected to placebo or 'sham' procedures.

Study Design: The review included publications reporting *in vitro*, *ex vivo* and/or *in vivo* studies, either alone or alongside other study types. Excluded studies were those that did not report experimental data (*e.g.* reviews, mathematical or computational simulations without experimental data). This SR was designed following Preferred Reporting Items for Systematic Reviews and Meta-analyses (PRISMA) guidelines and the protocol was registered with the Open Science Framework (OSF[1]) and the International Prospective Register of Systematic Reviews (PROSPERO[2]).

Outcomes: The primary outcome of interest was whether the EFMPs were successful or unsuccessful. Secondary outcomes included data on evaluations of EFMPs, including types of assays and techniques. Studies needed to report quantitative and/or qualitative data on these outcomes. Assessments could include measures such as EC migration distance, microvascular network area coverage, or dichotomous outcomes like successful versus failed network formation. Studies were excluded if they did not measure or report outcomes related to angiogenesis, such as tube and/or microvascular network formation, and/or EC migration within fibrin-based scaffolds in soft tissue models. Additionally, studies lacking quantitative or qualitative data on angiogenesis, endothelial network formation, or EC migration were excluded.

[1] https://osf.io/

[2] https://www.crd.york.ac.uk/prospero/

Exclusion Criteria: All records indexed in the selected databases until 28 October 2024 were considered. Exclusion criteria, in the order in which they were assessed, included:

1. Retracted publications.
2. Non-peer-reviewed publications.
3. Non-original research articles (*e.g.* reviews, editorials).
4. Articles not published in English.
5. Studies that do not include experimental data and/or outcomes of EFMPs.
6. Studies that do not contain fibrin-based scaffolds.
7. Studies that do not focus on soft tissue applications.
8. Studies with exclusive use of autologous or allogeneic grafts or materials.

4.2.2 Search Strategy

A comprehensive and systematic search was conducted across three databases (PubMed[3], OVID MEDLINE[4] and Scopus[5]) on 28 October 2024. The search combined four key elements: soft tissues, TE scaffolds, the use of fibrin or fibrinogen, and EFMPs (Figure 4.1). Each element was incorporated into database-specific search queries tailored to the syntax and indexing conventions of each database. No restrictions were placed on publication date and, when possible, filters were applied to narrow down the search results to original research articles only. The exact search terms and query structures used, as well as the exact number of results obtained on the date of the databases search, are available in Appendix C. Medical Subject Headings (MeSH) terms were used in PubMed to improve recall and precision [446]. The search strategy was designed following PRISMA guidelines and was reviewed by an expert subject librarian (Bodleian Libraries, University of Oxford) to independently validate the search.

4.2.3 Study Selection Process

A two-stage screening process was employed to ensure a thorough and rigorous evaluation of all identified articles, consisting of (a) title and abstract, and (b) full-text screening.

Title and Abstract Screening (1st Screening Round): Three reviewers independently screened titles and abstracts to assess eligibility based on the inclusion criteria. Disagreements were resolved through discussion until consensus was reached. Records marked as 'maybe' by at least one reviewer were also discussed collectively. Records deemed to be relevant by all reviewers proceeded to the second round for full-text assessment.

Full-Text Screening (2nd Screening Round): In the second round, the three reviewers independently assessed the full text of potentially eligible studies. Articles were excluded if they met any of the exclusion criteria, applied in the order listed in Section 4.2.1. As in the first round, disagreements and records marked as 'maybe' were resolved through discussion until full agreement was achieved.

Screening Procedure: Screening was conducted independently and in parallel by three reviewers using *Rayyan* software, with blind mode enabled to minimise bias. The use of blind mode and independent assessment by three reviewers enhanced objectivity. Once all reviewers had made their inclusion or exclusion decisions, blind mode was disabled. Any conflicts or records marked as 'maybe' were resolved through joint discussion. Final decisions were recorded in *Rayyan*.

[3] https://pubmed.ncbi.nlm.nih.gov/

[4] https://www.ovid.com/

[5] https://www.scopus.com/

4.2.4 Methods for Data Extraction

A structured table specifying the planned data entities and their requirements was prepared in advance. All three reviewers participated in detailed discussions to agree on the definitions and requirements for each entity. The included studies were then divided among the reviewers, with each reviewer independently extracting data for their assigned articles and populating the table accordingly.

For each entry, the extracted data were subsequently validated by the other two reviewers. Any discrepancies were resolved through discussion between the reviewers and by reviewing the relevant article or data point to reach a consensus. Upon completion of data extraction, all reviewers collectively reviewed the finalised table to ensure consistency and accuracy.

Data were extracted manually by the research team without contacting original study investigators for clarification. For studies reporting multiple scaffolds, only data from those meeting the inclusion criteria were extracted; data related to excluded scaffold types were omitted accordingly. All reported results relevant to the predefined outcome domains were extracted from each study. Where multiple measurements were provided for the same outcome (*e.g.* several assays for vascularisation), all were recorded as independent data entries. Time frames of outcome measurements (*e.g.* hours, days, or weeks post-intervention) were not extracted, as reporting was inconsistent. Upon completion, the full dataset was reviewed collectively by all three reviewers to confirm completeness and internal consistency. Data were extracted for the following categories:

1. Study Design
    a) Study type(s) reported in the publication (*e.g.* *in vitro*, *ex vivo*).
    b) Source of fibrinogen (*e.g.* commercial vs. extracted as part of the research; manufacturer; species and country of origin).
    c) Soft tissue replicated or studied (*e.g.* skeletal muscle, skin).
2. Model Used
    a) For *in vitro* studies only: Cell line(s), including origin (*e.g.* commercial, isolated) and species (*e.g.* human, rat).
    b) For *in vivo* studies only: *In vivo* model used, including *taxa*, species and sex of specimen.
3. Intervention of Interest
    a) Scaffold formulation (*e.g.* fibrinogen concentration and source; types of coagulant(s) and/or crosslinker(s); and use of additional materials (*e.g.* chemicals, growth factors, polymers).
    b) Type and features of the manufactured object (*e.g.* mesh, gel).
4. Primary Outcome
    a) Overall success or failure of EFMPs.
5. Secondary Outcomes
    a) Quantitative and/or qualitative evaluation of EFMPs:
        i. Continuous measures (*e.g.* average vessel length, area covered by vessels newly formed in, or migrated into, the scaffold).
        ii. Dichotomous assessments (*e.g.* success or failure of EFMPs).
6. Bibliographical data (*e.g.* author, year, PubMed identifier (PMID), digital object identifier (DOI)).

Approach to Masking, Reliability, Reconciliation and Justification: Masking was not employed during the data extraction process. To ensure reliability and objectivity, a multi-reviewer approach was adopted: each reviewer independently extracted data from their assigned studies, after which all three reviewers collectively reviewed the extraction table to ensure consistency and accuracy. Any discrepancies were resolved through group discussion, with each reviewer presenting their rationale until consensus was reached. This process was designed to maximise accuracy and efficiency in data extraction, ensuring that the review is based on reliable, transparent and reproducible methods.

4.2.5 Strategy for Data Synthesis

The synthesis focused on key groupings, including variations in fibrin scaffold composition, manufactured object type used for the scaffolds, cell pre-embedding or acellular scaffolds, and relevant study design characteristics. Studies were considered eligible for qualitative synthesis if they provided sufficient descriptive data on the intervention (*e.g.* fibrin scaffold characteristics, fabrication method) and reported qualitative and/or quantitative data on the outcomes (*e.g.* network formation). A meta-analysis was not conducted because of the considerable heterogeneity in study designs, scaffold formulations and outcomes.

Synthesis Procedure Justification: Given the diversity of methodologies and outcome measures, as well as the heterogeneity of studies, a structured narrative synthesis was employed to ensure a comprehensive and nuanced interpretation of the evidence. Extracted data were organised into summary tables, which were used to create figures to facilitate comparison across studies. The synthesis was structured around the following two core elements: **(1) Intervention:** Characteristics of the intervention vehicles (*e.g.* study type, manufactured object type); and **(2) Outcome:** Evidence of EFMPs. For each included study, an overview of the intervention and its outcomes was provided.

Subgroup Analyses: Data were analysed both individually and as part of one of the two subgroups: **(1) Constructs:** Scaffolds embedded with cells, where the EFMPs were evaluated; and **(2) Scaffolds:** Scaffolds, without pre-embedded cells, usually implanted in *in vivo* models, where endothelial migration and subsequent tube, vessel or network formation were assessed. An additional subgroup was created, separately from the scaffold-construct approach, compiling all muscle-focused studies: cardiac, smooth and skeletal.

Data Presentation and Visualisation: Summary tables and figures were used to present key findings:

1. PRISMA flowchart illustrating the study selection process.
2. Overview of the corpus (*e.g.* number of records per year, soft tissue types, study types, cell lines and *in vivo* models).
3. Fibrin source and scaffold composition paired with a successful or unsuccessful outcome of EFMPs.
4. Types of assays used to evaluate EFMPs.
5. Subgroup analysis focusing on muscle tissue studies.

Synthesis Process and Reliability: The synthesis was conducted collaboratively by three reviewers to ensure comprehensive and balanced conclusions. Any disagreements or uncertainties were resolved through discussion until consensus was achieved. Data were extracted and reported in the original units provided by study authors to preserve fidelity to source data and avoid unverifiable assumptions.

Data Management and Sharing: All synthesis results were presented within the manuscript. Additionally, the database compiling extracted data from included articles was made openly available *via GitHub*.

Additional Considerations:

1. **Missing Data:** Only data reported in the studies were included.
2. **Data Conversion and Validation:** Not applicable.
3. **Criteria for Conclusions:** Not applicable.
4. **Synthesist Blinding:** Not applicable.
5. **Sensitivity Analyses:** None were planned.
6. **Statistical Analyses:** Not applicable.
7. **Publication Bias Analyses:** Risk of bias (RoB) was evaluated using Systematic Review Centre for Laboratory Animal Experimentation's (SYRCLE) RoB tool.
8. **Quality Assessment:** A modified version of the Collaborative Approach to Meta-Analysis and Review of Animal Data from Experimental Studies (CAMARADES) checklist was used.

4.2.6 Risk of Bias (RoB) Assessment

The RoB on studies focused on muscle research was assessed using SYRCLE's RoB tool, which was developed as an adaptation of the Cochrane RoB tool to address sources of bias unique to *in vivo* intervention studies [447–449]. SYRCLE's RoB tool evaluates six types of bias (selection, performance, detection, attrition, reporting and other biases) across ten domains, including sequence generation, allocation concealment, random housing, blinding, incomplete outcome data and selective outcome reporting [447, 450].

Three independent reviewers conducted the RoB assessment in parallel, with blind mode activated to minimise bias during initial evaluation. For each study, reviewers independently answered ten questions[6] with 'Yes', 'No', or 'Unclear', strictly based on the information reported in each article. After completing their independent assessments using the SYRCLE tool, blinding was lifted and all reviewers convened to discuss and resolve any disagreements through group discussion, ensuring consensus for each checklist item. Study investigators were not contacted for additional methodological information and no automation tools were used in the RoB assessment. The results of the RoB assessment informed the interpretation of findings but were not used as a basis for excluding studies from the review.

4.2.7 Quality Assessment

Study quality on articles focused on muscle tissue was evaluated using a modified CAMARADES checklist. The CAMARADES checklist is a reporting quality tool designed for preclinical *in vivo* studies, comprising up to ten items that assess methodological features such as randomisation, blinding, sample size calculation and compliance with animal welfare regulations [451–453]. In this SR, the checklist [454] was adapted by removing two items ('Blinded induction of ischaemia' and 'Statement of control of temperature') as they were not applicable for this SR, resulting in an eight-item assessment[7].

Each article was evaluated across these eight criteria, with three reviewers independently assigning 'Yes', 'No', or 'Unclear' for each item. One point was awarded for each 'Yes' response, resulting in a maximum possible score of eight. No points were awarded to 'No' or 'Unclear' responses. Studies scoring fewer than four points were classified as having 'poor methodological quality', while those with four or more points were considered to have 'good methodological quality'.

The quality assessment process mirrored the RoB procedure: three independent reviewers completed the CAMARADES checklist in parallel and, following independent evaluation, resolved any discrepancies through group discussion to reach consensus on each item. Study investigators were not contacted for clarification and no automation tools were used in the quality assessment.

4.2.8 Software

The following tools were used in this SR: *Rayyan* (online version) [455] for blinded screening and organising studies; *Mendeley* (online version) for managing citations and references; *Microsoft Excel* (version 2503) for manual data extraction and analysis; *GraphPad Prism* (version 10.4.2), *RAWGraphs* (online version) [456] and

[6] **SYRCLE's RoB ten Items:** (1) Was the allocation sequence generated and applied properly? (2) Were the groups similar at baseline or were they adjusted for confounding factors in the analysis? (3) Was the allocation adequately concealed? (4) Were the animals randomly housed during the experiment? (5) Were the carers and/or investigators blinded to the knowledge of which intervention each animal received during the experiment? (6) Were the animals randomly selected for outcome assessment? (7) Was the outcome researcher blinded? (8) Were incomplete outcome data adequately addressed? (9) Are the study reports free of selective reporting of results? (10) Was the study apparently free of other problems that could result in a high RoB?

[7] **Modified CAMARADES checklist's eight items:** (1) Sample size calculation, (2) Random allocation to treatment or control, (3) Blinded assessment of outcome, (4) Use of an appropriate animal model, (5) Use of anaesthetic without significant intrinsic neuroprotective activity, (6) Compliance with animal welfare regulations, (7) Peer-reviewed publication, and (8) Statement of potential conflicts of interest.

BioRender.com [agreement numbers: LU28EG2MJP, BQ28CLLTGW and HO28PQNBZQ] for creating figures and illustrations; *Microsoft Word* (version 2503) and *Overleaf* (online version) for writing up.

4.3 Results

4.3.1 Study Selection

The study selection process was conducted in accordance with PRISMA guidelines (Figure 4.1), encompassing the identification, screening and inclusion stages to ensure a transparent and reproducible review. The process began with the identification of 146 records from PubMed, 39 from Scopus and 28 from OVID (Figure B.1). After removing 30 duplicates, 183 records remained for screening by title and abstract (Figure B.2A). At this stage, 75 records were excluded based on the predefined criteria and the remaining 108 articles were sought for retrieval for full-text assessment (Figure B.2B). Two articles could not be retrieved and, following a detailed evaluation based on the exclusion criteria, 25 articles were excluded (Table B.1). The details of the 81 studies included in the final corpus are available in Table B.2.

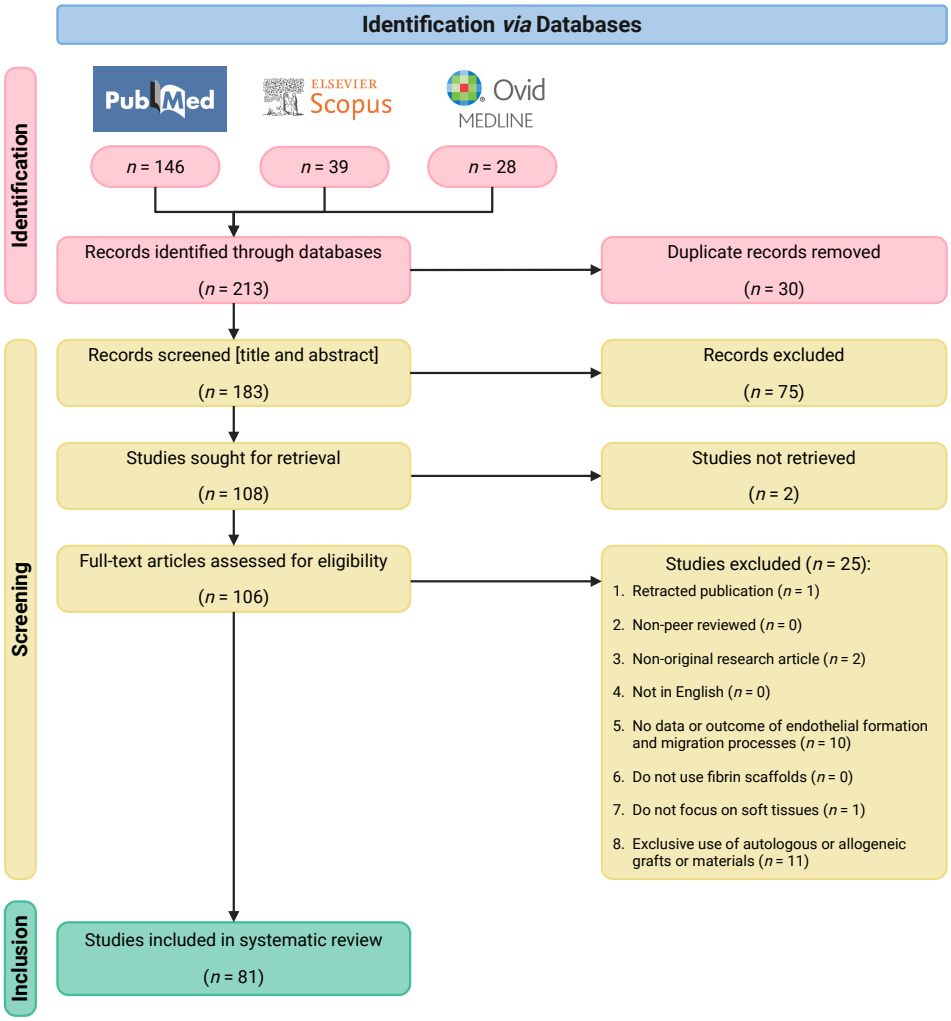


Figure 4.1: **Preferred Reporting Items for Systematic Reviews and Meta-analyses (PRISMA) flow diagram of the study selection process**, summarising the number of records identified, screened, excluded and included at each stage of the systematic review (SR). The diagram provides a detailed account of study progression through the phases of identification, eligibility assessment and final inclusion.

4.3.2 Overview of the Corpus

The 81 articles [41, 297, 405, 434, 457–533] included in the final corpus provide an overview of the current literature on fibrin-based soft tissue scaffolds for TE, with a particular emphasis on their capacity to support EFMPs. By analysing the corpus, we can observe a few trends, such as publication frequency of scientific studies, study aims, soft tissue focus and study types used (Figure 4.2).

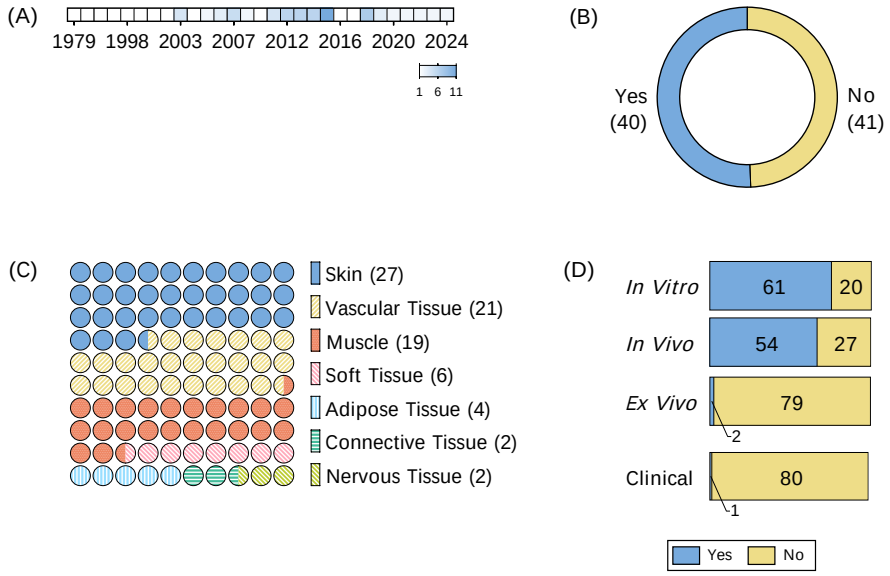


Figure 4.2: **Overview of the corpus of included articles in the systematic review (SR; *n* = 81)**, depicting **(A)** number of publications by year; **(B)** number of articles where the main aim of the study either included (49.38%) or did not include (50.62%) endothelial formation or migration processes (EFMPs); **(C)** distribution of soft tissue types studied; and **(D)** classification of studies by type, including *in vitro*, *in vivo*, *ex vivo* and clinical studies.

The publication dates span from 1979 to 2024 (Figure 4.2A), with the database search conducted on 28 October 2024. Besides the article published in 1979, no articles were published until 1994. From then on, there is a slight increase in the trend, with notable peaks in 2015 (11 articles), as well as in 2018 (n = 7) and consistently between 2012 and 2014 (6 articles per year). Focusing on the study aims (Figure 4.2B), 40 articles identified EFMPs as a central aim, thus providing focused analyses into the role of fibrin scaffolds in promoting vascularisation. The remaining 41 studies reported network formation as a secondary outcome, often within broader investigations of soft tissue repair or regeneration.

The corpus covers a range of soft tissue targets (Figure 4.2C). Skin was the most frequently studied tissue, with 27 articles, followed by vascular tissue, including both microvasculature and macrovasculature, in 21 studies. Muscle tissues, encompassing both cardiac and skeletal muscle, were the focus of 19 articles. Adipose tissue was addressed in four studies, connective tissue (including dental pulp) in two, and nervous tissue (including spinal cord) in another two. Six articles addressed soft tissue regeneration in general, without specifying a particular tissue type. This distribution highlights the broad range of fibrin scaffold applications across various soft TE contexts.

A variety of experimental approaches were employed across the included studies (Figure 4.2D; Table B.3). *In vitro* methods were used in 61 articles, while 54 studies included *in vivo* experiments. *Ex vivo* approaches were reported in two articles, and one study included clinical data. No studies in the corpus used computational modelling. Notably, 35 articles employed more than one study type (dataset available at the *GitHub* repository carla-fuenteslopez/soft-tissue-fibrin-sr), most commonly a combination of *in vitro* and *in vivo* methods. Two articles used three different study types, both of which included *ex vivo* models.

4.3.3 Fibrin Scaffold Composition: Influence on Successful Endothelial Formation and Migration Processes (EFMPs)

The composition and formulation of fibrin scaffolds in the included studies demonstrated a wide variety of approaches (Figure 4.3; Table B.4). The impact of each design parameter on the successful formation or migration of endothelial processes was also evaluated (Figure B.3).

Fibrin scaffolds have emerged as a widely investigated platform for TE, particularly in applications requiring vascularisation. A comprehensive evaluation of the included studies reveals nuanced relationships between fibrin origin, source material, combination with other materials, use of crosslinking agents, coagulants, cell pre-embedding, and the resulting success or failure of tube (Figure 4.3A) or network (Figure 4.3B) formation, or of endothelial migration (Figure 4.3C).

The success of the fibrin scaffolds used in the studies included in this SR in promoting EFMPs was summarised as a variable to facilitate the identification of the key parameters impacting the reported outcomes. This measure was calculated as the success rate by dividing the number of successful cases by the sum of successful cases and unsuccessful cases (Equation 4.1). Scaffolds that were not used for that particular application, or that did not report whether they were successful, were not included in the calculation. Success rate calculations included only those scaffolds that contained fibrin.

$$\text{Success Rate (\%)} = \frac{n_{\text{Successful Scaffolds}}}{n_{\text{Successful Scaffolds}} + n_{\text{Unsuccessful Scaffolds}}} \times 100 \tag{4.1}$$

4.3.3.1 Fibrinogen, Coagulants and Crosslinkers

Considerable variation was observed in the use and reporting of fibrinogen, coagulants and crosslinkers for scaffold fabrication (Figure 4.3 & Table B.5), which may, in turn, influence the expected outcomes related to angiogenesis. For example, fibrinogen concentrations were reported using different units or even volume only (*e.g.* mg/mL, % *w/w*, % *v/v*, µL), or not reported, with some studies specifying stock solution concentrations and others reporting final scaffold concentrations. In 12 cases, the stage at which the concentration applied was unclear and 14 articles did not report fibrinogen concentrations at all. This inconsistency hinders direct comparison and reproducibility.

The majority of studies (72 of 81) reported the use of a coagulant, all of which used thrombin. Nine studies did not explicitly state whether a coagulant was used. Crosslinking agents were used in 32 scaffolds, with four different crosslinkers used across the corpus. $CaCl_2$ was the most common crosslinking agent, used in 27 scaffolds, always in conjunction with thrombin to enhance network stability. Other crosslinkers used were NaCl (n = 3), Ca^{2+} (n = 1) and $MgCl_2$ (n = 1).

Fibrinogen Origin and Source

The majority of studies that specified the origin of fibrinogen (74 scaffolds) employed commercially available fibrinogen (91.89% of scaffolds), while extracted fibrin was markedly less used (8.11%). In 8 scaffolds (9.76%), the origin of the fibrinogen or fibrin was not specified.

Of the studies that reported the fibrinogen source (37 scaffolds; 45.12%), human fibrinogen was the most commonly used (75.68% of scaffolds), followed by bovine (18.92%), porcine and ovine (2.70% each). For the remaining 54.88% of scaffolds, the fibrinogen source was not specified.

When evaluating tube and network formation, scaffolds made with commercial or extracted fibrinogen showed similar success rates. For tube formation, 33 out of 48 scaffolds made with commercial fibrinogen were successful (68.75%), compared to 2 out of 3 scaffolds with extracted fibrinogen (66.67%). Likewise, network formation was successful in 29 of 43 commercial scaffolds (67.44%) and 2 of 3 extracted scaffolds (66.67%).

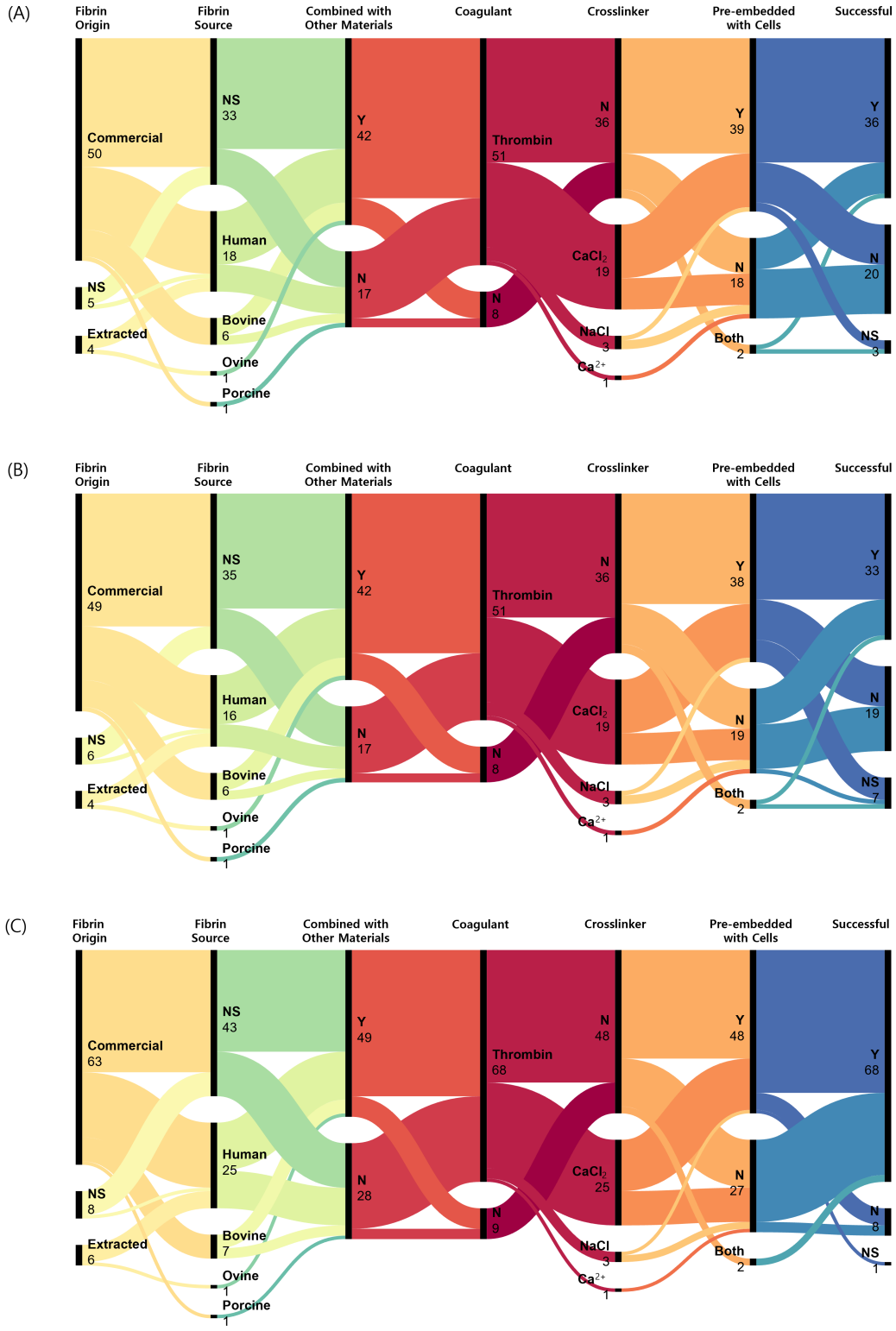


Figure 4.3: **Impact of scaffold formulation on angiogenic outcomes**, illustrating the relationships between scaffold formulation parameters (fibrin origin, source, combination with other materials, crosslinker, coagulant and cell pre-embedding) and the resulting successful endothelial formation and migration processes (EFMPs), by number of scaffolds. Data was aggregated from the included studies, showing the frequency of each parameter and its association with successful angiogenic outcomes: **(A)** tube and **(B)** network formation, and **(C)** endothelial cell (EC) migration. N: no; NS: not specified; Y: yes. Please refer to Appendix B (Tables B.5, B.6, B.7, B.8, B.9, B.10 and Figure B.3) for further details.

However, a different trend emerged when assessing endothelial migration into the scaffolds. Success rates were higher with commercial fibrinogen (33 out of 62 scaffolds; 53.23%) than with extracted fibrinogen (2 out of 6 scaffolds; 33.33%). These results suggest that while both fibrinogen sources support comparable tube and network formation, commercially sourced fibrinogen more reliably promotes endothelial migration than extracted fibrinogen.

As for the choice of fibrinogen origin, opting for human over bovine origin was associated with a higher success rate when evaluating tube (87.50% vs. 66.67%) and network formation (84.62% vs. 66.67%), but the reverse occurred when focusing on endothelial migration (91.67% vs. 100%). This is a small difference in migration success, especially considering that human fibrinogen was used 2–3 times more often than bovine. Due to limited data points, no meaningful conclusions can be drawn regarding ovine (n = 1; unsuccessful) and porcine (n = 1; successful) fibrinogen.

Crosslinkers

A total of 31 scaffolds (37.80%) reported the use of a crosslinker (*i.e.* crosslinker reagents; agents that enable intermolecular or intramolecular interactions of two or more molecules by covalent, ionic, or hydrogen bonding) and specified the one used: $CaCl_2$ (87.10%), NaCl (9.68%) and Ca^{2+} (3.23%). Ca^{2+} is not integrated into the subset of $CaCl_2$ and is analysed separately to distinguish the direct use of the active ionic form, as explicitly reported by the authors [489], from the use of $CaCl_2$, the compound employed by most studies in this corpus.

For tube formation, the absence of a reported crosslinker showed the highest success rate (70.59% success rate of 34 scaffolds), closely followed by the use of $CaCl_2$ as a crosslinker (55.56% of 18). For network formation, a similar trend was observed, with studies not reporting crosslinker use showing the highest success (67.74% of 21), followed by $CaCl_2$ (58.82% of 17). However, in the context of endothelial migration, scaffolds incorporating $CaCl_2$ achieved higher success rate (87.50%, n = 24), closely comparable to those not reporting crosslinker use (89.58%, n = 43). However, these findings are based on small and imbalanced group sizes, so the evidence should be interpreted with caution.

The two other crosslinkers, NaCl (used in 3 scaffolds) and Ca^{2+} (n = 1) were used in considerably fewer scaffolds. Given the limited use of NaCl and Ca^{2+}, the associated success rates (NaCl: 33.33% in tube and network formation and 100% in migration; and Ca^{2+}: 100% in all three processes) should be interpreted with caution, as they may not be representative of broader trends.

Coagulants

Regarding coagulants (*i.e.* agents that cause a liquid to coagulate), 73 scaffolds (89.02%) reported the use of a coagulant. All of them opted for thrombin, though at different concentrations; however, its impact on angiogenic outcomes requires nuanced consideration. For tube formation, thrombin use yielded a 65.31% success rate (49 scaffolds), which was slightly higher than the 57.14% reported for studies not reporting coagulant use (n = 7). Network formation demonstrated a similar trend, with thrombin showing a 64.44% success rate (n = 45) versus 57.14% for studies not reporting coagulant use (n = 7). In contrast, endothelial migration exhibited a lower success rate when using thrombin (88.06% success rate in 67 scaffolds) compared to studies that did not report the use of coagulant (100% success rate in 9 scaffolds).

4.3.3.2 Inclusion of Other Materials in the Formulation

Beyond fibrin, coagulants and crosslinkers, many studies incorporated additional materials into the scaffold formulation (Figure 4.3). These were classified into five categories: polymers (natural and synthetic); growth factors, peptides, amino acids and enzymes (GF/P/AA/E); cell media and solutions; chemicals; and other ma-

terials. GF/P/AA/E were frequently used in combination with other additives, whereas polymers, chemicals and cell media were typically used on their own (Figure B.4A). Based on the frequency of use across the included studies (Figure B.4B), GF/P/AA/E were the most common (34 articles), followed by polymers (n = 32), cell media and solutions (n = 16), other materials (n = 14) and chemicals (n = 4).

A total of 32 articles used at least one type of polymer (Table B.6), with five articles using two and one article using three types. Overall, 19 different polymers were used in the corpus, with the most common being collagen (7 scaffolds), polyethylene oxide (PEO; n = 4) and alginate, fibronectin, heparin, polyethylene glycol (PEG) and succinimidyl glutarate-modified PEG (n = 3 each).

GF/P/AA/E were incorporated in 34 articles, with 26 studies using two or more different types (Table B.7). One scaffold even used 10 different GF/P/AA/E, while two others used five, and a further two used four. A total of 37 different GF/P/AA/E were used, with aprotinin (19 scaffolds), basic fibroblast growth factor (bFGF; n = 11), factor XIII (n = 9, including 3 scaffolds using factor XIIIa) and vascular endothelial growth factor (VEGF; n = 8) being the most frequent.

Cell culture media and solutions were used in 16 scaffolds (Table B.8), with Dulbecco's Modified Eagle Medium (DMEM), foetal bovine serum (FBS), Medium 199 (M199) and NaCl being the most frequent (2 scaffolds each). In total, 12 different cell media and solutions were identified across the included studies.

Four scaffolds used chemicals (Table B.9), specifically ε-aminocaproic acid, tranexamic acid, trisodium citrate and triton X (each in 1 scaffold). Finally, 14 scaffolds incorporated materials classified as 'other' (Table B.10), which included *Cytodex* beads, Fe_3O_4 magnetic nanoparticles and poly(lactic-co-glycolic acid) (PLGA) nanospheres.

The combination of fibrin with other materials is a common strategy to enhance its mechanical properties and bioactivity. Within the studies included in this SR, 52 scaffolds (63.41%) used other materials in the scaffold formulation besides fibrin, coagulants and crosslinkers. Frequently used materials in combination with fibrin were grouped into five overarching categories, including growth factors such as VEGF or bFGF, and polymers like PEG. While the presence of these additional materials may have influenced EFMPs outcomes, the diversity of materials used, along with variability in their concentrations and combinations, precludes definitive conclusions about the effects of individual additives.

The addition of other materials also played a role in determining success, albeit less noticeably than fibrinogen source or origin. Of the scaffolds that reported successful or unsuccessful outcomes, composite scaffolds were associated with lower success rates than the scaffolds not including additional materials besides fibrinogen, coagulants and crosslinkers in their formulations. This occurred in all three scenarios: tube formation (61.54% vs. 70.59%); network formation (58.33% vs. 75.00%); and endothelial migration (85.42% vs. 96.43%). However, it is worth noting that there were also differences in the number of scaffolds used in each case, with composite scaffolds being twice as numerous as the other scaffolds, potentially introducing bias in comparative analyses.

4.3.3.3 Cell Pre-embedded vs. Acellular Scaffolds

Of the scaffolds analysed, 52 (65.82%) were pre-embedded with cells before experimental work, while the remaining 27 (34.18%) were acellular (Figure 4.3). In two cases, the same scaffold formulation was used independently as pre-embedded and acellular, so each configuration was treated as an independent scaffold to ensure that the analysis captured the distinct impact of cell pre-embedding on scaffold performance. Also, one scaffold was used with pre-embedded cells to assess tube formation (not successful), and its acellular form for network formation and migration (successful in both cases).

Pre-embedding cells into fibrin scaffolds demonstrated a generally positive impact on tube and network formation, with higher success rates of 76.32% and 73.53%, respectively, than when not pre-embedded (success rates of 42.11% and 47.37%). In contrast, EC migration showed nearly identical success rates in both conditions, 89.80% for pre-embedded scaffolds and 89.66% for acellular scaffolds. Across the three EFMPs outcomes, the number of scaffolds incorporating pre-embedded cells was consistently 1.7 to 2 times greater than the acellular scaffolds, with group sizes ranging from 19 to 49 scaffolds. These sample sizes support the reliability of conclusions for both pre-embedded and acellular variations.

4.3.3.4 Culture Media Supplementation

Like scaffold formulation, the cell culture environment plays a significant role in the success of TE scaffolds. Most studies (72.84%) used standard cell culture media without supplements; however, 22 publications reported using modified media (Table B.11). Two studies tested two variations in the same study while using the same scaffold formulation. Supplements were typically added to stimulate EC growth and sprouting [509]; enhance cell viability [492]; prevent premature fibrin degradation [41, 405, 498, 520]; stimulate cell adhesion, migration and proliferation [485]; and promote matrix remodelling by mimicking the *in vivo* environment and inducing vascularisation [517] and vessel formation [462, 523, 532].

Among the modified media formulations, the most common supplements were aprotinin (12 studies, concentrations: 0.15–200 U/mL), VEGF (n = 11; concentrations: 25–100 ng/mL or 0.1%) and FGF, including variants such as bFGF and human recombinant-bFGF (n = 7; concentrations: 10–50 ng/mL or 0.4%). Other additives included antibiotics (*e.g.* penicillin, streptomycin), matrix modulators (*e.g.* heparin, heparan) and sera (*e.g.* foetal bovine/calf serum, human serum). As with other parameters, when reported, supplement concentrations varied considerably between studies.

4.3.4 Cell Lines and *In Vivo* Models

4.3.4.1 Cell Lines

Cell line selection for TE scaffolds reflects the specific biological and experimental aims of each study. Here, we categorised the cell lines used in the 81 studies (Figure 4.4) into two main groups: endothelial (Figure 4.4A) and non-endothelial (Figure 4.4B). Of these studies, 40 (49.38%) utilised either EC or non-EC lines, 30 (37.04%) incorporated both groups, and 11 studies (13.58%) did not integrate any cell lines into the scaffolds. EC lines were employed in 39 studies (48.15% of studies; 46 scaffolds), while non-EC lines were used in 61 studies (75.31% of studies; 87 scaffolds).

The evaluation of EFMPs was dependent on the presence or absence of pre-embedded ECs within the scaffold. When ECs were present, either alone or alongside non-ECs, tube and network formation (including post-differentiation) could be evaluated. This outcome may be attributed to the cells interacting with the matrix surrounding them, which not only provides physical support but also promotes cell adhesion and migration, and supports the development of a functional network [288, 534]. Conversely, when ECs were not seeded within the scaffold prior to *in vivo* implantation, only endothelial migration from the surrounding host tissue into the scaffold could occur. Notably, migration from the surrounding host tissue was also reported in some studies where ECs had been pre-embedded into the scaffolds.

Human-derived cell lines dominated both groups, but sourcing strategies differed: endothelial lines were often obtained from commercial sources (20 of 46 scaffolds), whereas non-ECs were mostly isolated from primary tissues as part of the study (57 of 87 scaffolds). Tissue origin also varied: EC lines commonly used

umbilical vein (*n* = 42), while non-ECs were often adipose-derived (*n* = 21), reflecting distinct scaffold design priorities and biological targets across studies.

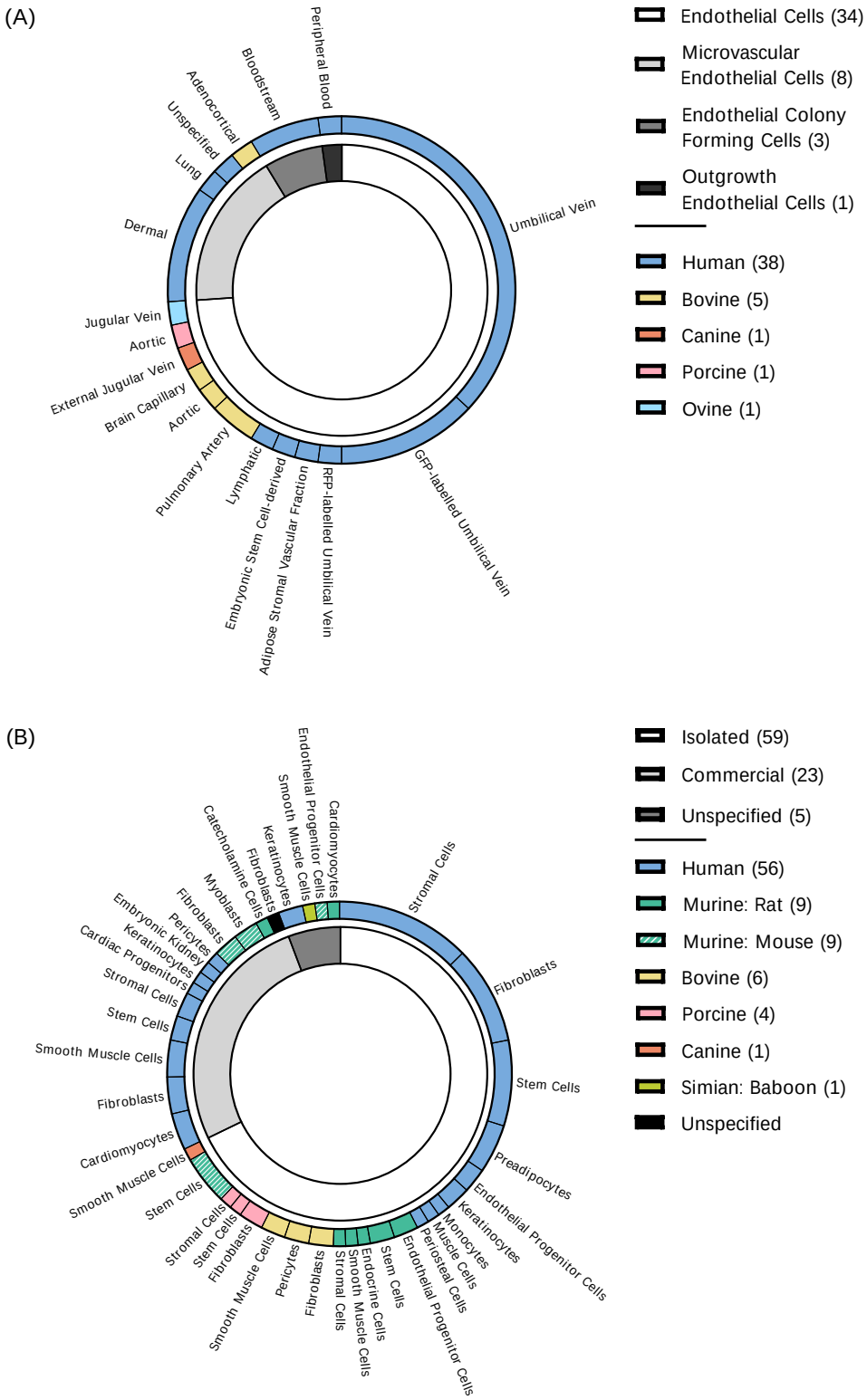


Figure 4.4: **Endothelial cell (EC) and non-endothelial cell (non-EC) lines used**, by number of scaffolds in which they were used. **(A)** ECs by type, species and specific cell line name. **(B)** Non-EC lines used by source, species and specific cell line name.

Endothelial Cell (EC) Lines

A total of 22 different EC lines were used in 46 scaffolds across 40 studies (Figure 4.4A). The EC lines used were classified into four groups: ECs (used in 34 scaffolds), microvascular endothelial cells (MVECs; *n* = 8), endothelial colony-forming cells (*n* = 3) and outgrowth ECs (*n* = 1). Human-derived cell lines were overwhelmingly dominant (*n* = 38), likely due to their greater translational relevance. The other cell lines, derived from bovine (*n* = 5), canine (*n* = 1), porcine (*n* = 1) and ovine (*n* = 1) origins, were used less frequently.

Commercial sources were common (20 scaffolds), potentially chosen for reproducibility, while 18 scaffolds used cells isolated during the study, five were gifts or derived from an existing cell line without specifying their origin (commercial or isolated), and three did not specify the cell source. Fluorescent tagging was rare, mostly used for cell tracking: only six scaffolds used green fluorescent protein (GFP)-expressing human umbilical vein endothelial cells (HUVECs), and one opted for red fluorescent protein (RFP)-expressing HUVECs. Finally, most EC lines were derived from the umbilical vein (24 scaffolds), followed by dermal (*n* = 5), bloodstream (*n* = 3), aortic (*n* = 2) and pulmonary artery (*n* = 2). Other sources (*n* = 9) included brain capillary and external jugular vein tissue, while one scaffold did not specify the origin tissue.

Non-Endothelial Cell (Non-EC) Lines

Non-endothelial lines were more diverse, encompassing 74 cell types and were used across 87 scaffolds (Figure 4.4B), including human (56 scaffolds), murine (mouse, *n* = 9; rat, *n* = 9), bovine (*n* = 6), porcine (*n* = 4), simian (baboon, *n* = 1) and canine (*n* = 1) origins, with one study not specifying the species. Cell types included fibroblasts (*n* = 18), stem cells (*n* = 16) and stromal cells (*n* = 15), followed by keratinocytes (*n* = 5) and preadipocytes (*n* = 4). Twenty-nine other cell types were also used. Adipose tissue was the most frequent source (*n* = 21), followed by skin (*n* = 9) and bone marrow (*n* = 3). Other origins (*n* = 34) included skeletal muscle, alveolar tissue, cornea and pancreas. The origin of 20 cell lines was not specified.

Most non-ECs were isolated from different tissues (59 scaffolds; including 2 transfected cell lines derived from isolated primary cells), with fewer being commercially sourced (*n* = 23; including 6 that were derived or differentiated from commercial sources), potentially suggesting a trend towards tissue-specific customisation. In five scaffolds, the cell source was not specified.

4.3.4.2 *In Vivo* Models

Of the 54 studies employing *in vivo* models (Figure 4.5), most (*n* = 50) utilised a single *in vivo* model. A few studies used multiple models: two studies used two models, one used three, and one used six different models. The most frequent *taxa* were murine models (49 in total), encompassing 31 mouse and 18 rat models. Mouse models included athymic (*n* = 7, including athymic nu/nu and athymic nude), Swiss Albino (*n* = 2), C57BL/6 (*n* = 2) and 20 other mouse strains. As for rat models, Sprague-Dawley (*n* = 6), Lewis (*n* = 3), Wistar (*n* = 2) and a range of other strains (*n* = 7) were used. Other *taxa* included porcine (*n* = 5, Yorkshire pigs), leporine (*n* = 2, New Zealand White rabbits), ovine (*n* = 1, sheep, specific strain unspecified) and cavine (*n* = 1, guinea pig) models. Avian models (*n* = 2) consisted of White Leghorn chicken eggs.

The sex of the *in vivo* models used was reported on a per-study basis: a single sex indicated exclusive use, 'both' meant no sex distinction was made, and 'unspecified' indicated that the sex was not reported. Sex preference varied by species; for example, among the mouse models (*n* = 31), females were used more often (35.48%) than males (19.35%), with 3.23% using both sexes and 41.94% unspecified. In contrast, of the 18 rat models used, males were more common (44.44%) than females (27.78%), with 5.56% using both sexes and 22.22% unspecified.

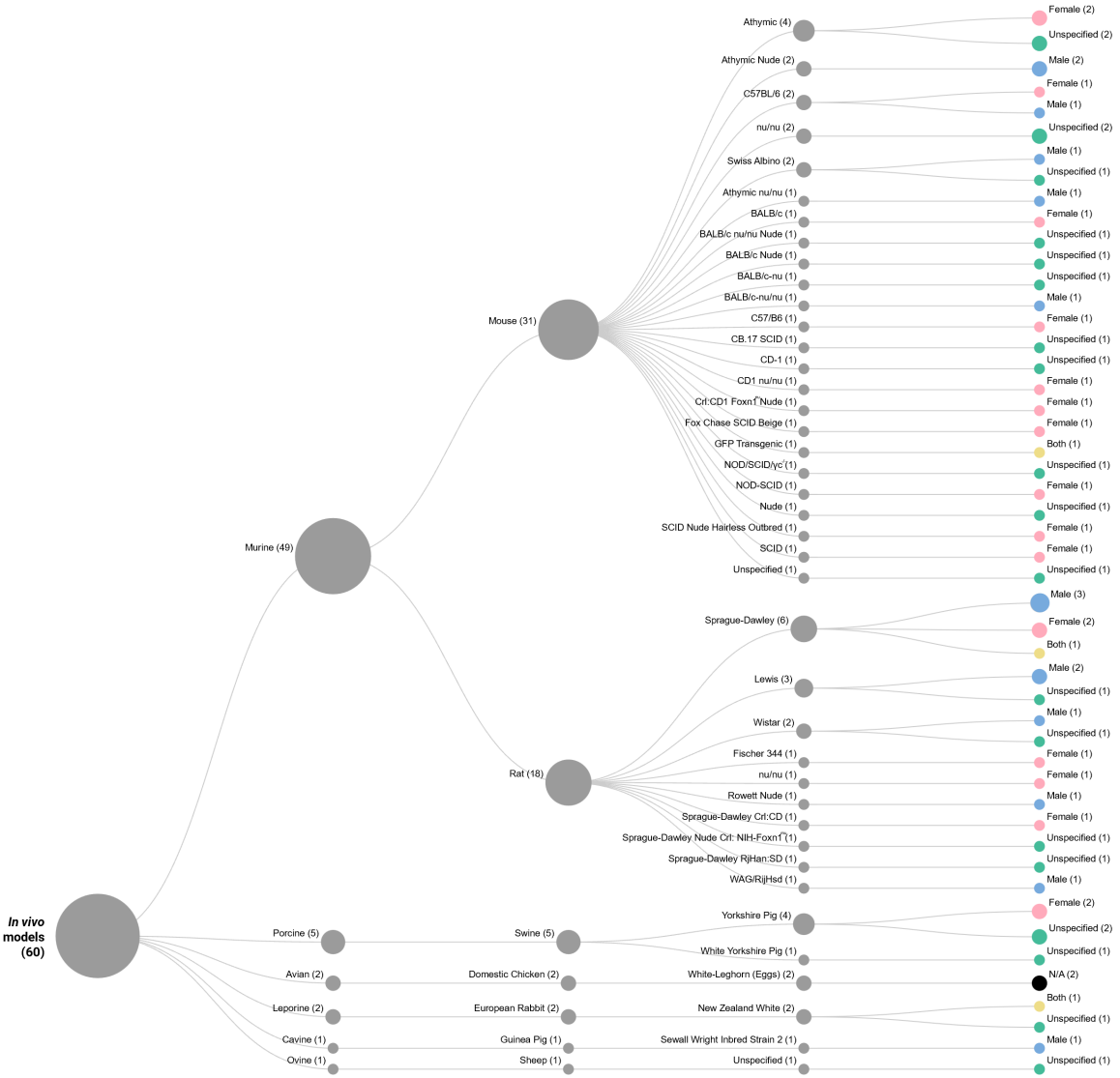


Figure 4.5: ***In vivo* models used**, by *taxa*, species and sex of specimen, showing the number of times a model was used in the corpus.

4.3.5 Manufactured Objects and Features

The selection of TE scaffolds demonstrates varying degrees of success in promoting vascularisation, depending on the scaffold type (*i.e.* manufactured object type), whether cells were pre-embedded, and the type of EFMPs. In the studies analysed, 13 different manufactured object types were identified (Figure 4.6A). In most studies (95.06% of studies), a single type of manufactured object was used, but four studies evaluated two different manufactured objects in each study.

The different types of manufactured objects were identified based on the terminology used by the authors to describe their scaffolds. These terms are treated as separate categories to reflect reported differences in material composition, structural properties and intended function (Figure 4.6B). For example, matrices refer to fibrous or porous structures; gels are soft, semi-solid 3D networks formed from crosslinked polymers; and hydrogels are a subclass of gels characterised by a high water content, with water serving as the primary medium. Composite constructs were also reported, including gel + mesh systems (*i.e.* gels integrated with a structural mesh) and microfibre hydrogels (*i.e.* hydrogels with embedded fibres).

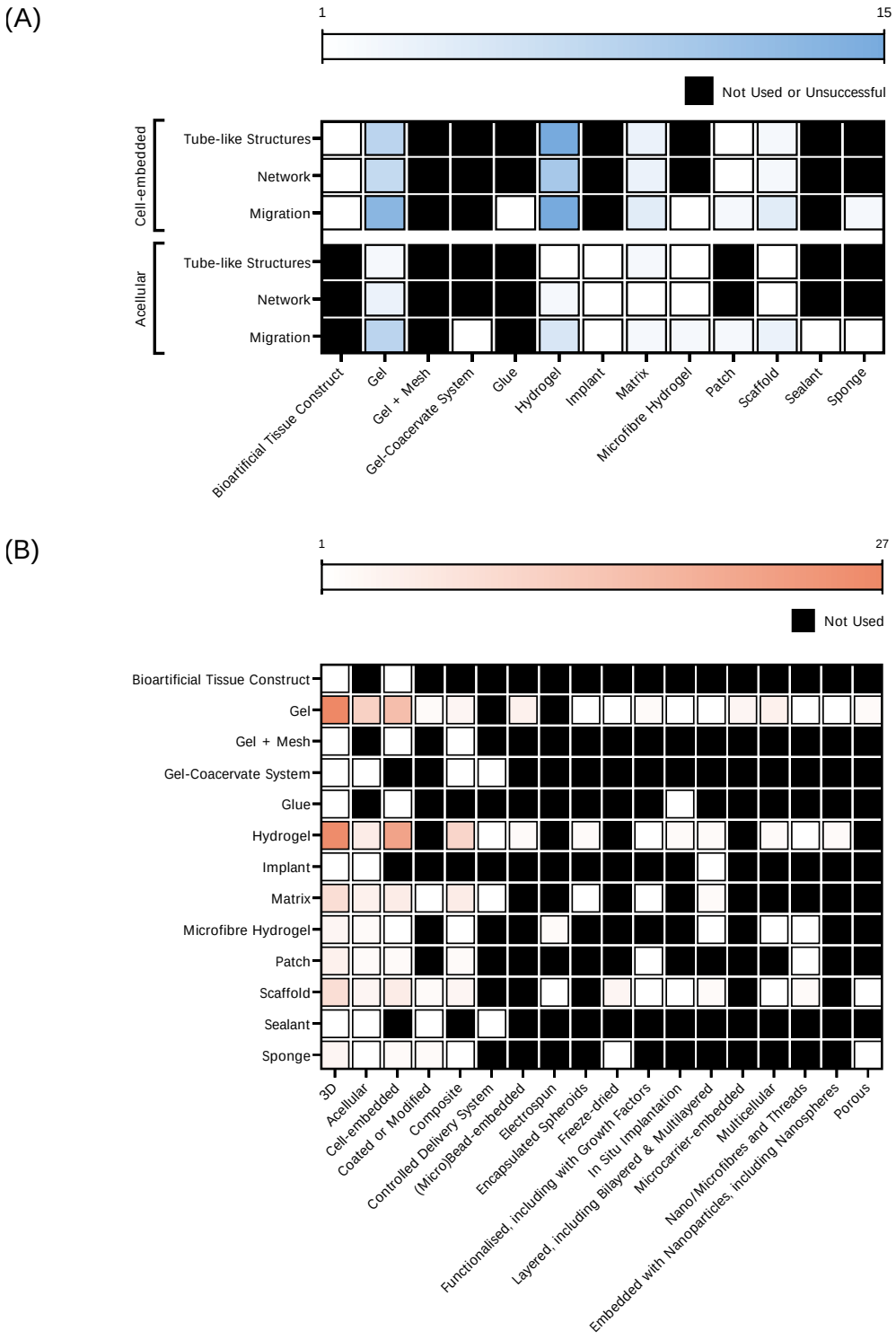


Figure 4.6: **Tissue engineering (TE) scaffolds successfully supporting endothelial formation and migration processes (EFMPs), categorised by type of manufactured object.** Further insights are provided into scaffold or construct design based on **(A)** the successful use of acellular versus cell-embedded models, and **(B)** the associated features of manufactured objects, as reported in the studies. Colours indicate the number of studies in which each manufactured object was reported as successful, with a darker colour indicating higher frequency of use. Only features mentioned in at least three studies are shown here, whereas Figure B.5 presents all features identified in the corpus regardless of the number of studies citing them.

4.3.5.1 Acellular Manufactured Objects

Acellular scaffold performance varied across EFMPs (Figure 4.6A). Gels were the most frequently tested manufactured objects (8–11 scaffolds) but with varying outcomes. Success rates were relatively low in tube (18.18%) and network formation (33.33%), but higher in migration (72.73%). A similar pattern was observed with microfibre hydrogels (n = 2) and scaffolds (n = 3), with tube and network formation success rates being lower (50.00%) than in endothelial migration (100.00%).

However, this pattern was not replicated across all manufactured objects. Matrices showed more consistent success rates (66.67% in both tube formation and migration; and 50.00% in network formation), but only 2–3 scaffolds were used. Hydrogels had greater variations in success rates: 50.00% in tube formation (n = 2), 66.67% in network formation (n = 3) and 100% in cell migration (n = 5). Some manufactured objects were tested only once, limiting confidence in their success rates. For example, whenever tested, patches (n = 2), and implants, sealants and sponges (one scaffold of each type) had 100.00% success rates. On the other hand, gel-coacervate systems failed in both tube and network formation but succeeded in migration. In general, the acellular scaffold category is characterised by overall modest success rates and limited sample numbers, making it difficult to draw strong conclusions regarding the superiority of any specific scaffold type.

4.3.5.2 Cell-Embedded Manufactured Objects

Cell-embedded scaffolds, particularly hydrogels and gels, consistently showed higher success rates across the EFMPs (Figure 4.6A). Hydrogels had a robust performance, with success rates of 92.86% in tube formation (14 scaffolds), 88.89% in network formation (n = 9) and 93.33% in migration (n = 15). Gels also performed well, with 80.00% success rates in tube formation (n = 10), 77.78% in network formation (n = 9) and 92.86% in migration (n = 14). Matrices were also commonly used (n = 5) and yielded moderate success: 60.00% in tube and network formation and 80.00% in migration. Patches (in tube and network formation) and hydrogel matrices (in endothelial migration) showed lower success (50.00%), but were evaluated using only two scaffolds each, limiting interpretability. Other manufactured object types pre-embedded with cells were tested only once and showed either complete success (*e.g.* bioartificial tissue constructs [462], glues [533], microfibre hydrogels [478]) or failure (*e.g.* gel-mesh composites [483]).

Overall, cell pre-embedded hydrogels and matrices consistently outperformed their acellular counterparts, especially where larger sample sizes were available. Notably, some scaffold types (*e.g.* bioartificial tissue constructs) were exclusively tested in cell-embedded configurations, precluding direct comparison with their acellular counterparts. These results highlight the benefits of pre-seeding scaffolds with cells for vascularisation, although acellular scaffolds still have value in broader TE strategies.

4.3.5.3 Manufactured Object Features

Thirteen distinct manufactured object types were identified, collectively described using 39 features (Figure 4.6B & Figure B.5). The most common feature was '3D', mentioned in all 85 scaffolds. Features used to group scaffolds into two primary categories, cell-embedded (63.53%) and acellular (36.47%), were frequently reported. 'Composite' was reported in 27 manufactured objects, while other frequent features included layered structures such as 'bilayered' and 'multilayered' designs (10.58% of manufactured objects); 'surface coating or modification' (9.41%); and 'multicellularity' (9.41%). These terms suggest a move towards more biomimetic and structurally complex designs.

Less common were 'functionalisation', including the incorporation of growth factors; '(micro)bead embedded'; and the integration of 'nano- or microfibres and threads' (each, 7.06%), indicating an interest in

multifunctionality and microarchitectural sophistication.

Advanced fabrication techniques, such as '3D printing' (reported for 1 manufactured object) and 'bioprinting' (n = 2), along with properties like 'magnetic responsiveness' (n = 2), 'slow degradation' (n = 1) and 'structural stabilisation' (n = 1), were rare, suggesting that such features remain specialised approaches. Gels and hydrogels were not only very popular (used in 85 and 86 scaffolds, respectively), they were also associated with the greatest variety of features (n = 22 and n = 21, respectively), highlighting their versatility and prominence. Unique features associated with gels and hydrogels included the encapsulation of spheroids (3 manufactured objects); embedding of microcarriers (n = 3); multicellularity (n = 6); and nanoparticle embedding, including nanospheres (n = 3), emphasising their capacity for complex cellular and material interactions, as well as scaffold functionality.

4.3.6 Assays Used to Evaluate Endothelial Formation and Migration Processes (EFMPs)

Across the 81 studies analysed, methods used to assess EFMPs varied by data type (Figure 4.7A). Five studies relied solely on quantitative data (6.17% of the corpus), 16 on qualitative data only (19.75%) and 60 used both (74.07%), highlighting the value of combining objective metrics with biological context.

Assays were characterised as qualitative when outcomes were reported by visual observation or descriptive assessment of EFMPs (*e.g.* presence or absence of tube-like structures, morphological appearance, or representative microscopy images) without numerical analysis. In contrast, assays were considered quantitative when EFMPs were measured using defined metrics, including those derived from manual or image-based analysis, such as tube length, branch points, vessel density, sprout number, or cell migration distance, enabling statistical comparison between experimental conditions.

A total of 39 distinct assays were identified and grouped into eight categories (Figure 4.7B). Immunological assays were the most frequently employed, featured in 60 studies (74.07%). Of these, the most frequently used were immunostaining and immunofluorescence staining (n = 25), followed closely by immunohistochemistry (n = 24). Other immunological techniques, such as immunochemistry, immunocytochemistry and immunoblotting, were used less frequently, appearing in up to three studies each.

Imaging techniques featured in 47 studies, including fluorescent imaging (n = 5), confocal microscopy (n = 5), and functional assays such as angiogenesis assays (n = 7), tube formation assays (n = 5) and migration assays (n = 3), to visualise morphological changes. Computer-assisted image analysis (n = 31) was often coupled with biological assays (n = 21) and imaging techniques, particularly in the context of standard (n = 7) and 3D (n = 2) angiogenesis assays, as well as migration assays (n = 2). This combination enabled the quantitative assessment of network parameters [41, 297, 471, 485, 492, 513, 523], including total tube or sprout length and the number of branch points.

Histology was used in 27 studies (Figure 4.7B), whereas cytology appeared only once. Molecular (11 studies), biochemical (n = 10) and molecular biology (n = 2) assays were less frequently used across the dataset. Specific techniques within these categories included enzyme-linked immunosorbent assay (ELISA; n = 7), real-time reverse transcription polymerase chain reaction (RT-PCR; n = 4), quantitative RT-PCR (n = 4), Western blot (n = 1) and mRNA expression analysis (n = 1).

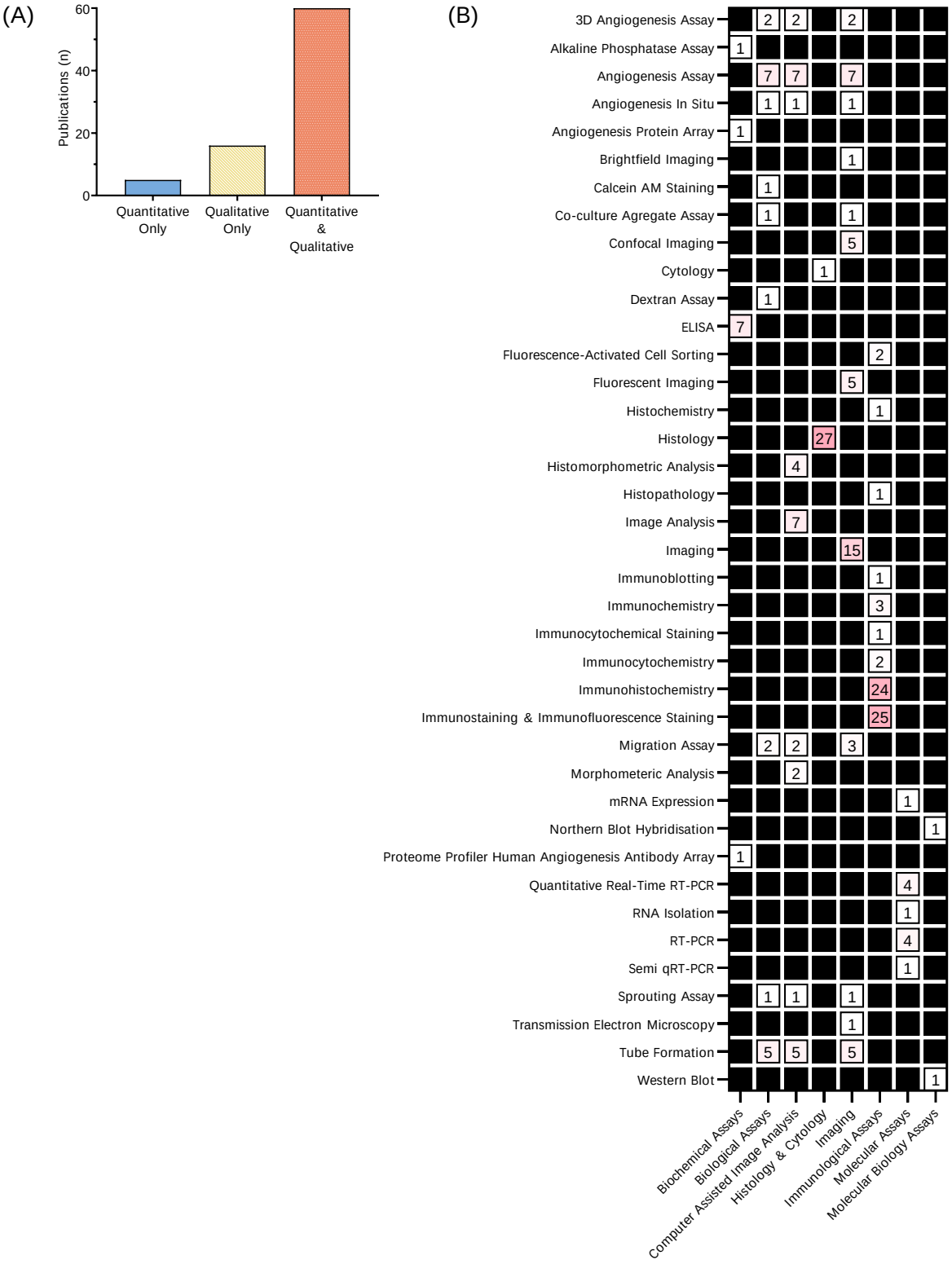


Figure 4.7: **Assays used to evaluate endothelial formation or migration processes (EFMPs). (A)** Type of data used to evaluate EFMPs, shown by number of studies using quantitative, qualitative or combined data types. **(B)** Assays used to evaluate the success of EFMPs, grouped by number of studies in which they were employed. Assays were classified into eight general categories based on the evaluation method.

4.3.7 Fibrin Tissue Engineering (TE) Scaffolds for Muscle Research

To provide a focused overview of fibrin scaffold applications, muscle was selected as the focus of a sub-analysis (Figure 4.8) because it is a widely studied tissue, with sufficient *in vitro* and *in vivo* studies to enable a meaningful synthesis without being overly broad. Its subtypes (cardiac, skeletal and smooth) offer diverse applications and its high metabolic demand makes vascularisation essential, an area where fibrin's pro-angiogenic properties are particularly advantageous for oxygen delivery and function. Moreover, muscle requires strong structural support, making the study of different scaffold designs, including the selection of manufactured objects, especially relevant. This subsection examines the subset of muscle-focused studies in terms of muscle and study types, *in vivo* models, cell lines and manufactured objects employed.

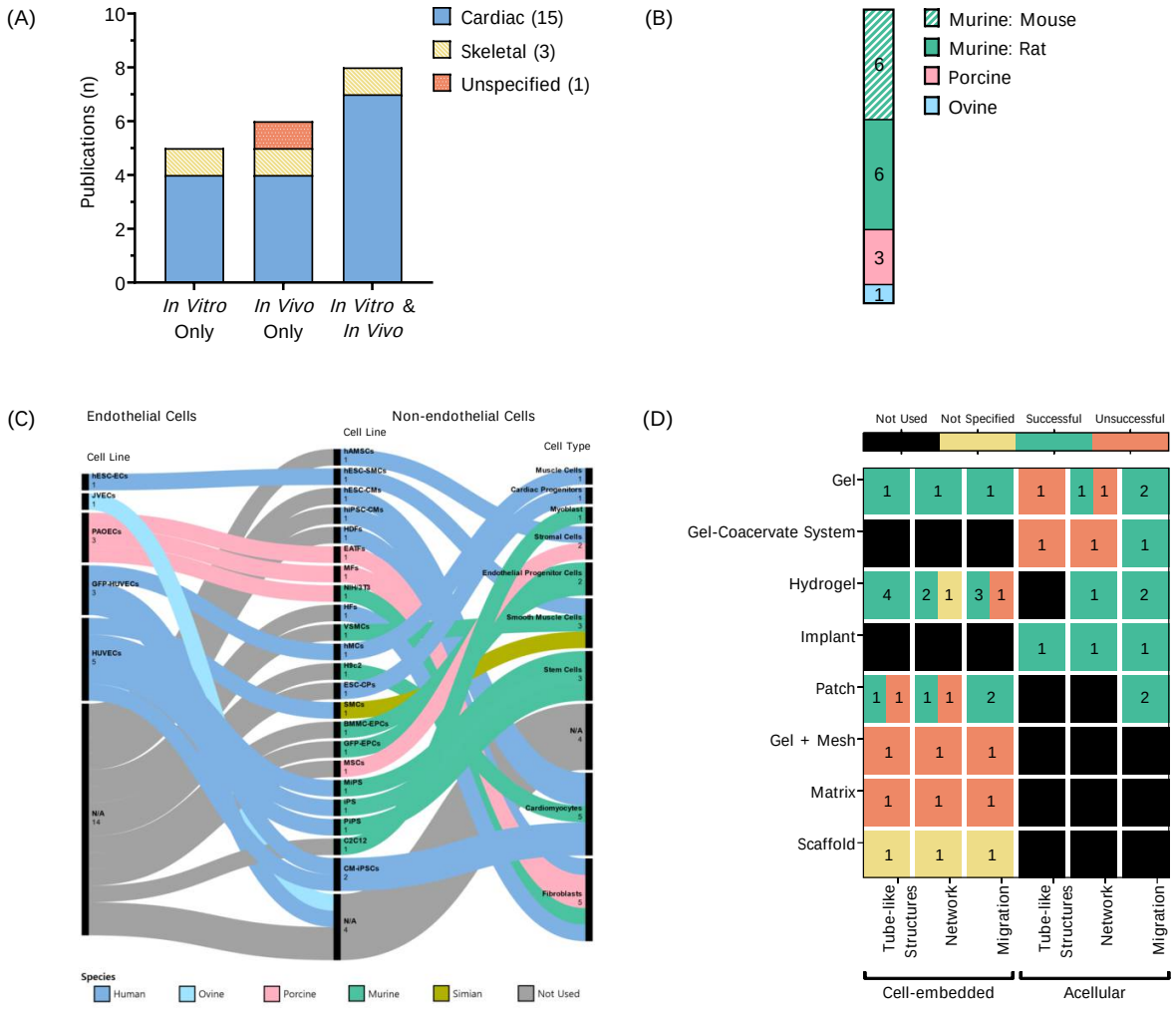


Figure 4.8: **Fibrin tissue engineering (TE) scaffolds for muscle research. (A)** Number of studies categorised by study and muscle type. **(B)** *In vivo* models used. **(C)** Endothelial cell (EC) and non-endothelial cell (non-EC) lines used, classified by species of origin and type. **(D)** Types of manufactured objects tested with or without pre-embedded cells and their reported association with the outcomes of endothelial formation or migration processes (EFMPs). For each manufactured object, the number of successful, unsuccessful and unspecified outcomes is shown.

4.3.7.1 Muscle Types and Study Distribution

Of the 81 studies included in this SR, 19 focused on muscle: 15 on cardiac, three on skeletal and one on muscle tissue in general, but none on smooth muscle (Figure 4.8A). Experimental approaches varied, comprising exclusively *in vivo* (6 studies) or *in vitro* (n = 5) models, or a combination of both (n = 8).

4.3.7.2 *In Vivo* Models

Fourteen studies incorporated *in vivo* work and used a range of models (Figure 4.8B): mice and rats were equally prevalent (used in 6 studies each), followed by swine (n = 3) and sheep (n = 1). While most studies (85.71%) used a single *in vivo* model, two studies used multiple models: (i) immunodeficient NOD/SCID/$\gamma c^{-/-}$ mice and Yorkshire swine; (ii) Sprague-Dawley and nude rats. The most utilised strains were Sprague-Dawley rats and Yorkshire swine (n = 3 each), and C57BL/6 mice (n = 2). Other strains, such as nude rats, Wistar rats, Lewis rats and BALB/c-nu mice, appeared only once.

4.3.7.3 Cell Lines

Cell lines were heterogeneously used across the 17 studies that included *in vitro* research (Figure 4.8C). Many of these studies evaluated different outcomes, with some focusing only on cell migration, others exclusively on tube formation, and a few evaluated both. Of these, nine studies used only non-EC lines, two only EC lines, and six used both. Altogether, 25 distinct cell line combinations were reported. These included fibroblasts and porcine aortic ECs (PAOECs), cardiomyocytes with either GFP-HUVECs or HUVECs, and various stem cell-EC co-cultures. Five studies used multiple cell line combinations within the same study, often pairing different endothelial or non-endothelial types independently.

Eight studies used 5 different endothelial lines and, in some cases, in multiple experimental setups (*i.e.* an EC line used in combination with a non-EC line) per study. These cell lines were predominantly of human origin (6 different studies, in 7 different experimental setups), alongside one porcine and one ovine line (1 study, 1 setup each).

The EC lines used for muscle TE scaffolds were: HUVECs (3 studies, 3 setups), GFP-HUVECs (3 studies, 3 setups), PAOECs (1 study, 3 setups), human embryonic stem cell-derived ECs (1 study, 1 setup) and jugular vein ECs (1 study, 1 setup). Non-EC lines were more diverse, appearing in 15 studies (22 setups) and included human (7 studies, 9 setups), mouse (3 studies, 5 setups), rat (3 studies, 4 setups), porcine (3 studies, 2 setups) and simian (1 study, 1 setup) sources. While most non-EC lines were used only once (*e.g.* mesenchymal stem cells (MSCs), NIH/3T3, C2C12 myoblasts), cardiomyocytes and fibroblasts were the most frequently used (n = 5, each), followed by smooth muscle cells (SMCs; n = 3), stem cells (n = 3), stromal cells (n = 2) and cardiomyocytes derived from induced pluripotent stem cells (CM-iPSCs; n = 2).

4.3.7.4 Impact of Manufactured Objects on Successful Endothelial Formation and Migration Processes (EFMPs)

Each of the 19 studies used a single manufactured object (Figure 4.8D). Hydrogels were the most common (7 studies), followed by patches (n = 4), gels (n = 3), gel-coacervate systems, implants, matrices, gel-mesh composites and scaffolds (n = 1, each). Scaffolds were described as such by the authors, without specifying further details. Of these manufactured objects, 57.89% incorporated embedded cells and the rest were acellular. Testing typically encompassed the three EFMPs (63.16% of studies), but some evaluated only one (26.32%) or two (10.53%) outcomes.

Success rates (Equation 4.1) varied based on manufactured object type and cell embedding (Figure 4.8D). Pre-embedded hydrogels and gels achieved 100.00% success across all processes, except for gels in endothelial migration (75.00%). In contrast, gel-mesh composites and matrices had no successful outcomes. Patches yielded mixed results, with 100% success in endothelial migration but only 50% success in tube and network formation. However, the low number of replicates per scaffold type, often limited to a single study, warrants caution in interpretation. Additionally, three cases did not report the outcome, so these data were excluded from the success rate calculation.

Acellular scaffolds displayed a different trend: all the manufactured objects evaluated (*e.g.* gels, hydrogels, implants, patches) achieved a 100% success rate except for gels in tube (0%) and network formation (50.00%). Gel-coacervate systems failed to support tube and network formation (0% in both cases).

4.3.8 Risk of Bias (RoB) and Quality Assessment

The RoB and quality of the studies were assessed using SYRCLE's RoB and CAMARADES checklists, respectively. The detailed breakdown, per study, of the individual answers for each of the ten items of SYRCLE's RoB and of the eight items in the CAMARADES checklist is available in the online repository (please refer to Data Availability). To provide a visual overview of these assessments, Figure 4.9 presents a graphical summary of the RoB and quality assessment evaluations for the corpus subset of 14 muscle studies comprising *in vivo* work.

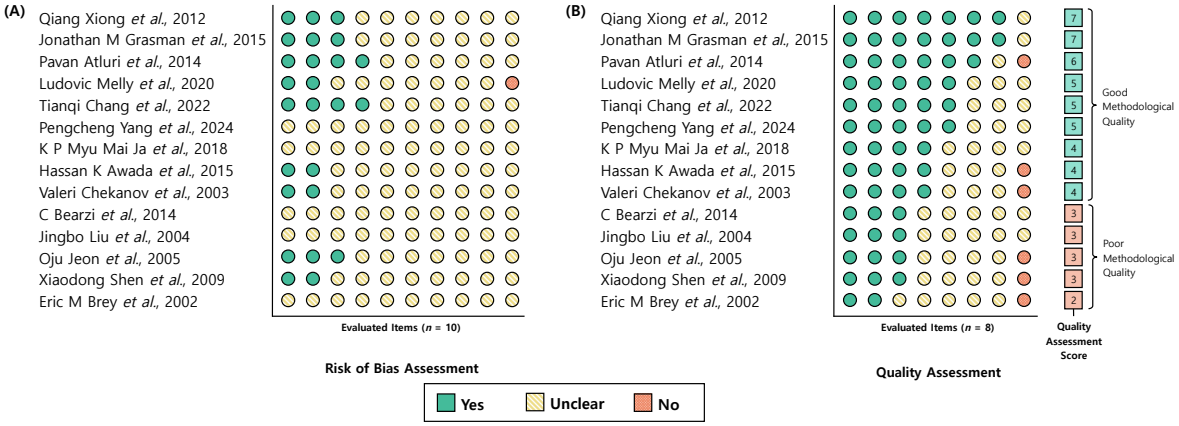


Figure 4.9: **Risk of bias (RoB) and quality assessment.** Studies were assessed using the 10-item Systematic Review Centre for Laboratory Animal Experimentation (SYRCLE) RoB tool and the 8-item Collaborative Approach to Meta-Analysis and Review of Animal Data from Experimental Studies (CAMARADES) tool. Here, the RoB and the quality assessments of *in vivo* muscle models are shown. For each article, items are grouped by assessment outcome: 'Yes', followed by 'Unclear', and then 'No'. Articles are ordered by overall quality assessment score, from highest to lowest. **(A)** RoB was evaluated using all ten items of SYRCLE's RoB tool [447]. **(B)** Methodological quality was assessed using a modified CAMARADES checklist of eight items [454].
SYRCLE's RoB tool (10 items): (1) Was the allocation sequence generated and applied properly? (2) Were the groups similar at baseline or were they adjusted for confounding factors in the analysis? (3) Was the allocation adequately concealed? (4) Were the animals randomly housed during the experiment? (5) Were the carers and/or investigators blinded to the knowledge of which intervention each animal received during the experiment? (6) Were the animals randomly selected for outcome assessment? (7) Was the outcome researcher blinded? (8) Were incomplete outcome data adequately addressed? (9) Are the study reports free of selective reporting of results? (10) Was the study apparently free of other problems that could result in a high RoB?
Modified CAMARADES checklist (8 items): (1) Sample size calculation, (2) Random allocation to treatment or control, (3) Blinded assessment of outcome, (4) Use of an appropriate animal model, (5) Use of anaesthetic without significant intrinsic neuroprotective activity, (6) Compliance with animal welfare regulations, (7) Peer-reviewed publication, and (8) Statement of potential conflicts of interest.

4.3.8.1 Risk of Bias (RoB)

SYRCLE's RoB tool (Figure 4.9A) revealed limited methodological transparency across the studies. For ≥ 60% of the ten items, particularly those related to allocation concealment, random housing, blinding and selective outcome reporting, the RoB was marked as 'unclear' across all studies due to insufficient detail for assessment. Items most often rated as 'low risk' were 'other sources of bias' (57.14% of studies), 'baseline characteristics' (42.86%), 'random outcome assessment' (28.57%), 'sequence generation' (21.43%), and 'blinding' (21.43%). Only one study received a 'high risk' rating for a single item.

4.3.8.2 Quality Assessment

Study quality was evaluated using a modified CAMARADES checklist (Figure 4.9B). Methodological quality varied considerably: of the studies evaluated, 64.29% were rated as having 'good quality' (score ≥ 4), while 35.71% were deemed to be of 'poor quality' (score ≤ 3). The highest score achieved was 7 (14.29% of studies) and the lowest was 2 (7.14%), but no study achieved the maximum score of 8. The median score was 4, which was the minimum required to qualify as 'good methodological quality'.

While all studies 'used an appropriate animal model' and were 'peer-reviewed', 64.29% of them reported data on the 'use of anaesthetics' and 'compliance with animal welfare regulations'. Only 28.57% reported 'random allocation to groups', and 14.29% included 'sample size calculation' and 'blinded outcome assessment'. These items were often marked as 'unclear' due to insufficient information. Notably, 42.86% of studies failed to clearly declare potential conflicts of interest, while 7.14% were 'unclear'.

4.4 Discussion

This SR provides a comprehensive synthesis of current evidence on the use of fibrin-based scaffolds for angiogenesis, including microvasculature formation, in soft tissues, with a particular focus on their capacity to support EFMPs. The findings confirm that fibrin, due to its intrinsic bioactivity and compatibility with (micro)vascular cells, is a promising scaffold material; however, success depends heavily on the scaffold design, particularly the specific formulation and manufactured object type. Scaffold composition played a critical role in determining outcomes, a finding aligned with prior evidence emphasising the importance of the cellular context and scaffold design parameters in enabling EFMPs [340].

A key trend that emerged was that tube and network formation outcomes were generally consistent with one another, but did not necessarily align with those of endothelial migration. This is likely due to the environment in which the scaffold is immersed: successful migration can be achieved with a broader range of scaffold formulations, suggesting that critical parameters for tube and network formation may not be as restrictive for migration processes. Based on these trends, the most promising strategies for supporting successful EFMPs were identified.

For successful tube and network formation, the most effective strategies involve using commercial fibrinogen, particularly of human origin, and avoiding the addition of other materials. Not using a crosslinker, or using $CaCl_2$, generally yielded higher success rates; however, these comparisons are limited by small and unequal group sizes and therefore require cautious interpretation. Crosslinking, typically with $CaCl_2$ or other agents, is commonly employed to enhance the mechanical strength and reduce the biodegradation rate of fibrin scaffolds [433]. In addition, the inclusion of thrombin as a coagulant and pre-embedding cells also contributed positively.

In contrast, preferred strategies for endothelial migration were less distinct. Both human and bovine fibrinogen yielded similarly high success rates, and the inclusion of additional materials had little impact. Out-

comes were comparable regardless of whether $CaCl_2$ was used as a crosslinker or omitted altogether. Avoiding a crosslinker appeared to improve migration, though this finding is based on limited data and should be interpreted with caution. Pre-embedding cells had little influence on migration outcomes, most probably because fibrin serves as a cue directing cell motility [534]. Moreover, like many other cell types, ECs can migrate in different ways (individually, in chains, or as sheets), enabling them to navigate effectively through and populate the scaffolds [535]. This may also suggest that pre-embedding is less critical for migration and that cell motility within the fibrin matrix might be more dependent on other factors (*e.g.* matrix porosity, elasticity, degradability), which may influence cell behaviour and vascularisation [444].

Focusing on the key elements of the scaffold formulation explored here, the fibrinogen origin had no noticeable impact on endothelial tube and network formation success, whereas commercially sourced fibrinogen outperformed extracted fibrin in supporting endothelial migration. This finding may partly reflect inconsistent reporting and differences in extraction methods, and the influence of other scaffold components. However, the use of commercial fibrinogen introduces concerns regarding batch-to-batch variability, which remains a significant challenge in fibrin scaffold production and continues to hinder direct comparison between studies [443].

Among the scaffolds for which the fibrinogen source was reported, human (more frequently used) and bovine (slightly less frequently used) fibrinogen were the most commonly used and were also associated with the highest success rates. Human-derived fibrinogen consistently promoted enhanced tube and network formation; however, when assessing endothelial migration, the difference between human- and bovine-derived fibrinogen was not as large. Beyond some structural differences between human- and bovine-derived fibrinogen, one key distinction is the location of the Arg-Gly-Asp (RGD) sequence, crucial for integrin binding and cell adhesion. Although human fibrinogen contains the analogous Arg-Gly-Gly (RGG) sequence, it still appears able to mediate cell interactions [268, 536]. While bovine fibrinogen promotes cell migration, it may present some limitations, such as increased immunogenicity [537] and faster degradation rates [538] compared to its human counterpart.

Another factor directly impacting the scaffold properties is the concentration of fibrinogen, thrombin and the selected crosslinker used, which, in turn, are associated with variable effects on EFMPs. Although it was not possible to draw conclusions based on specific concentrations used in the studies included in this SR due to inconsistent reporting across papers, it is well established in the literature that variations in fibrinogen and thrombin concentration affect the final fibre thickness, resulting in different mechanical properties, pore sizes and degradation rates which significantly influence cell migration, differentiation and angiogenesis [539].

Fibrinogen and thrombin sources, their addition, and their concentrations directly affect the mechanical properties of the scaffolds [540]. Mechanical properties, such as stiffness, influence cellular processes, as mechanical signals are converted into biochemical signals through cell receptors and integrins [344]. In particular, the mechanical properties of scaffolds influence EC expression of matrix metalloproteinases and growth factors, as well as their differentiation, sprouting and migration [340]. Migration, especially, is highly sensitive to external stimuli and requires degradation of existing ECM and interactions with surrounding cells [541]. The migration process favours a soft matrix, so the negative impact of thrombin addition on migration might be due to an increase in mechanical strength [539, 541, 542].

The literature indicates that higher fibrinogen concentrations result in thicker fibres and smaller, less interconnected pores that can limit cell migration [543]. Conversely, high fibrinogen concentrations may be favourable for cell attachment and other cellular processes such as network formation, due to the increased availability of cell-binding sites within the fibrin matrix [544]. Fibrin interacts with cells through several receptors, particularly with ECs through integrin $\alpha_v\beta_3$, integrin $\alpha_5\beta_1$ [437] and vascular endothelial cadherin [268], which eventually affect cell morphology [545]. This may explain why fibrinogen content has differentially af-

fected tube and network formation compared to cell migration.

On the other hand, the literature shows that increasing thrombin concentration reduces the fibre thickness, resulting in thinner, more tightly packed fibrils [546], which can affect the final pore structure of the scaffold. In this SR, thrombin was the only material chosen as a coagulant and, when used, it positively affected EFMPs. Moreover, thrombin addition induces an angiogenic response in human ECs through the expression of VEGF [547], as well as cell surface receptors such as protease-activated receptors (PAR1 and PAR4) [427]. This may further explain why thrombin addition enhanced tube and network formation. Based on the data, the selection of crosslinking agent is more complex: although calcium-based crosslinkers such as $CaCl_2$ were commonly used to provide structural stability to the scaffold, their contribution to angiogenesis was not always favourable. This may be due to the extracellular concentrations of calcium and chloride interfering with cellular processes and altering osmotic pressure, respectively [542].

Regarding the incorporation of other materials other than fibrin, coagulants, and crosslinkers, the data reveal that composite scaffolds combining fibrin with polymers or growth factors may offer mechanical or biochemical advantages, potentially explaining their inclusion in scaffold formulations [443]. Nevertheless, these composite scaffolds were not universally superior in supporting EFMPs. This suggests that increased complexity of materials does not necessarily translate into improved biological performance. However, composite scaffolds may reflect efforts to tailor scaffold properties to specific soft tissue applications, highlighting the versatility of fibrin as a base material in TE. For example, the inclusion of collagen in skin scaffolds could help mimic the natural tissue more closely and improve cell adhesion [548]. Similarly, incorporating synthetic polymers like PEG can help modify scaffold degradation rates and other properties [549, 550], suggesting that slower scaffold degradation may promote cell infiltration and enhance pro-angiogenic effects [433].

Pre-embedding cells also appeared to be beneficial for scaffold performance, particularly in promoting tube and network formation, although it had a lesser impact on EC migration. This could be attributed to pre-embedded scaffolds regulating vascular formation *in vivo* through cell–cell and cell-matrix interactions, as well as interactions with biochemical cues [393]. Biochemical molecules like growth factors are essential regulators of angiogenesis, interacting through specific receptors. This likely explains why several of them were commonly added to cell culture media [551], as reported in this SR. However, their concentrations must be carefully optimised, as excessively high levels of VEGF can lead to deformity in vascular formations [393]. Overall, EFMPs require a delicate balance between degradation, mechanical strength and biochemical signalling [445].

Beyond the scaffold formulation, other factors such as the cell lines used played a role in the outcomes of EFMPs. Among the non-EC types used in angiogenic models, one of the most common cell sources used in this SR was adipose tissue. This is likely because adipose-derived cells demonstrated angiogenic potential *via* paracrine secretion of growth factors such as VEGF, as well as their ability to differentiate into ECs [552]. Fibroblasts were the most used cells in this SR, likely because most of the included studies focused on connective tissues, where fibroblasts are the main cell type [553]. Moreover, co-culture of fibroblasts with ECs has been shown to promote angiogenesis by supporting EC migration and proliferation [426] through the secretion of angiogenic factors [554]. Among ECs, the most common source was umbilical vein-derived cells. This aligns with the existing literature, which identifies HUVECs as the most frequently used, due to their easy isolation, low immunogenicity and suitability as an *in vitro* endothelial model [286, 426]. More articles reported the use of commercially sourced ECs, which is beneficial as it reduces donor-related variability that could impact experimental outcomes [426].

As demonstrated by the wide range of assays used across the included studies, no single assay emerges as universally ideal for evaluating the various mechanisms involved in angiogenesis, as each offer distinct benefits and limitations. The variety of assays and *in vivo* models used in this SR reflects the complexity of EFMPs [555, 556]. Although several scaffold types were reported, it is not surprising that 3D systems were

the most frequently mentioned, as cell–cell and cell-matrix interactions are closer to the natural physiological environment, regulating cell proliferation, differentiation and signalling [426]. It has also been reported that 3D *in vitro* assays better mimic angiogenesis than 2D assays, with the expression of angiogenic genes being more pronounced in the former [557].

In the studies included in this SR, we identified a wide range of scaffold formulations, with some articles testing multiple combinations per publication, in some cases used as a control. Similarly, the included studies employed a range of experimental approaches, with nearly half of them using more than one study type, primarily a combination of *in vitro* and *in vivo* methods. This methodological diversity highlights both the comprehensive scope of the research and the translational potential of fibrin scaffolds for soft TE. However, it also presents challenges for direct comparison, reflecting the field's exploratory efforts to optimise fibrin scaffolds for EFMPs.

The subset of articles focusing on muscle tissue angiogenesis, including microvasculature formation, revealed a predominance of cardiac over skeletal muscle, with none addressing smooth muscle. Interestingly, these two tissue types were addressed with a wide variety of manufactured scaffold types, suggesting a lack of consensus on optimal design for muscle applications. This is a relevant finding, as existing literature suggests that scaffold type, stiffness and fibrinogen content influence myogenic cell differentiation [558]. The diversity of *in vivo* models and cell lines used, particularly the variety of non-ECs, highlights the complexity of replicating the muscle microenvironment and the multifactorial nature of EFMPs.

While angiogenesis remains a significant clinical challenge in muscle TE, the literature suggests that pre-embedding cells within constructs is a promising strategy to facilitate the formation and interconnectedness of endothelial structures [559]. In this SR, the findings confirmed this, particularly in hydrogel and gel-based scaffolds, which demonstrated the highest success rates across EFMPs. However, the heterogeneity of study designs coupled with the limited number of replicates for each scaffold type limits the generalisation of these findings. Nonetheless, the trends identified reinforce the importance of scaffold-cell interactions and support the use of precellularised constructs to enhance microvascularisation in muscle TE.

This SR revealed several limitations in both the included literature and the review process itself. In terms of the corpus, it is important to note that some studies were reported by the same research groups and overlapping researchers (*e.g.* groups led by Nehls [529, 531, 532], Verseijden [499, 503, 509], Barreto-Ortiz [478, 491] and Borges [513, 517]). This may have led to over-representation of certain experimental procedures and research priorities.

A major limitation of the included studies was the inconsistent and incomplete reporting of parameters such as the source and concentration of fibrinogen, thrombin and $CaCl_2$, coagulant ratios, scaffold fabrication methods, and cell seeding protocols. Such inconsistencies in reporting critical methodological parameters significantly limit reproducibility, making it harder for independent research groups to reliably replicate findings, validate results, or build on existing work. To address this issue, a '*Minimum Information for Fibrin Scaffold Experiments (MIFSE) Checklist*' (Appendix D) was developed to standardise reporting in fibrin scaffold studies. This tool ensures inclusion of critical methodological details and other key parameters, thereby supporting reproducibility and cross-study comparison.

This lack of reporting also affected the SR itself, as it limited the strength and range of conclusions that could be drawn. It restricted conclusions about direct relationships between critical scaffold parameters and final scaffold properties or cell responses, which could have provided valuable insights for scaffold design. These methodological inconsistencies, coupled with considerable heterogeneity in study designs (Table B.3), scaffold formulations (Table B.4) and outcome measures, made it impractical to conduct a meta-analysis, hence making the narrative synthesis the most viable option. Although aggregated success rates were used in this SR, it should be noted that this approach may oversimplify complex parameters and could introduce interpretive

bias. While the data suggest trends, it is important to acknowledge that the definition of 'successful outcomes' used here may vary compared to other studies. An important limitation of this SR is that studies involving different soft tissue types were analysed together, despite variations in their architectures and functions. These differences could influence the effects of fibrin concentration, embedding ECs in the scaffolds, or scaffold formulation on angiogenesis, so pooling these studies may obscure tissue-specific outcomes.

A critical limitation of this review is the exclusion of non-English publications and grey literature, which may have introduced language and publication bias. This could have reduced the comprehensiveness of the review, potentially excluding relevant studies with valuable insights. Furthermore, the database search was deliberately narrow, as we focused exclusively on fibrin-based studies, which could restrict the broader contextual understanding of scaffold-based studies in general. Finally, while efforts were made to minimise bias through multiple independent reviewers and validated tools (*e.g.* SYRCLE, CAMARADES), the presence of subjective interpretation in assessing outcomes, especially when relying on qualitative measures, could not be fully eliminated.

Future research should prioritise the development of factorial experimental designs to systematically evaluate the interactive effects of scaffold materials, crosslinkers, cell types and environmental conditions. Standardising scaffold characterisation and reporting practices is essential for improving reproducibility and allowing meaningful comparisons across studies. This includes uniform reporting of fibrinogen source and concentration, cell incorporation techniques, and angiogenesis evaluation methods and metrics. Moreover, refining cell pre-embedding protocols, such as specifying cell type, density and culture conditions, will be critical to ensure consistent results and advance clinical translation (Figure B.6). Such work will not only support the development of more functional tissue constructs but also inform best practices for scaffold design in *in vitro* and *in vivo* applications.

4.5 Conclusion

This SR highlights that the success of fibrin scaffolds in promoting angiogenesis, including microvascular network formation, in soft tissues highly depends on scaffold formulation, fibrinogen origin, cell pre-embedding, and the selection of coagulant and crosslinker. Human-derived, commercially sourced fibrinogen combined with thrombin and cell pre-embedding are most consistently associated with successful endothelial tube and network formation, while effects on endothelial migration were more variable. These differences reflect the complexity of the endothelial processes, which are highly sensitive to scaffold formulation and design and, in turn, mechanical, biochemical and structural properties. This SR also highlights the importance of selecting cell types, *in vivo* models and assays to evaluate EFMPs. A common finding among the included studies was inconsistent reporting of scaffold parameters, manufacturing methods and characterisation techniques, which limits the ability to draw reliable conclusions. The insights derived from this SR could guide systematic approaches for developing fibrin scaffolds for *in vitro* microvascular models for regenerative medicine applications, disease modelling and preclinical testing by providing reproducible TE platforms.

Within the broader framework of this thesis, this chapter provides an evidence-based, literature-informed foundation for the design and optimisation of the fibrin-based microvascular scaffold developed in this research. The conclusions drawn from the SR inform key experimental decisions in the development of the 3D microvascular construct, while the identified methodological limitations strengthened the rationale for establishing a more reproducible and systematically characterised experimental model. Overall, the insights gained from this SR provide a framework for the development of reproducible fibrin-based *in vitro* microvascular platforms for regenerative medicine, disease modelling and preclinical testing, while directly supporting the wider aim of this thesis to optimise fibrin-based soft tissue TE.

Registration and Protocol

The protocol for this SR was registered with PROSPERO [registration number: CRD42025612994] [560] and with OSF [Registration DOI: 10.17605/osf.io/NVFDJ] [561]. It was also documented as project CTZ8X in OSF [562].

Data Availability

Datasets: Available in a *GitHub* repository (https://github.com/carla-fuenteslopez/soft-tissue-fibrin-sr) and at DOI: 10.5281/zenodo.16921022 [563].
Supplementary Materials: Please see Appendix B. The '*Minimum Information for Fibrin Scaffold Experiments (MIFSE) Checklist*' is also available at DOI: 10.5281/zenodo.16921390 [564].

Acknowledgements

Special thanks to N. Thurley (Bodleian Libraries, University of Oxford) for reviewing the SR's search strategy.

Chapter 5

Engineering a Long-lasting Microvasculature *In Vitro* Model for Traumatic Injury Research

Thesis Integration and Chapter Structure

Building on the scaffold optimisation described in Chapter 3 and the systematic review (SR) presented in Chapter 4, this chapter addresses Objective 3 by developing, optimising and characterising a long-lasting 3D *in vitro* microvascular model. The model is designed to preserve microvascular network integrity beyond 24 h, enabling investigation beyond the immediate and short-term phases of network formation. Here, the physiologically relevant model was validated against a gold-standard cell line; it's key material properties were characterised; the influence of scaffold composition on endothelial network architecture was examined; and construct stability over time were evaluated. To this end, fibrinogen source, origin and concentration, together with crosslinking ratio and medium, were systematically varied across a series of fibrin-based hydrogel formulations. This optimisation yielded durable constructs capable of forming complex microvascular networks and maintaining structural integrity beyond 24 h. The development of this long-lasting 3D microvascular model establishes a versatile platform and represents a critical step towards modelling injury responses in a physiologically meaningful time frame, as explored in Chapter 6.

This chapter has been published [544] and is available at DOI: 10.1016/j.bioadv.2025.214310.

The experimental design was carried out by Carla V. Fuenteslópez, and all experimental work except for gelation time, spectrophotometry, microrheology, crosslink density, pendant drop and SEM imaging, which were performed by Mariella Papapavlou. All data analysis and writing were done by Carla V. Fuenteslópez. Prof Hua Ye and Prof Mark Thompson reviewed the manuscript and provided supervision and advice.

Engineering a Long-lasting Microvasculature *In Vitro* Model for Traumatic Injury Research

Abstract

Microvascular injuries can have systemic physiological effects that exacerbate other injuries and pose a danger to life. Reliable *in vitro* microvascular models are required to enhance understanding of traumatic injuries. This research aims to develop and optimise a three-dimensional (3D) hydrogel construct for the formation and long-term stability of an *in vitro* microvascular model for trauma research. First, we develop a 3D hydrogel scaffold using a physiologically relevant cell type to enable the formation of a durable microvascular endothelial network and validate it against the gold standard: HUVECs. Then, we explore the impact of modifying the hydrogel composition, specifically fibrinogen source and concentration, medium, and crosslinking ratio, on scaffold material properties and on the formation of endothelial networks, their architecture, and long-term integrity. Our results demonstrate that 3D hydrogel scaffolds are crucial for maintaining network stability beyond the initial 24 h. For trauma research applications, the material properties and mechanical behaviour of the hydrogels are critical. Microrheology revealed that fibrinogen concentration significantly influences gelation times, absorbance rate, storage modulus (G'), loss modulus (G") and complex viscosity, while also reducing creep compliance. Our multi-pronged approach to engineering microvascular constructs revealed that variations in hydrogel composition, including fibrinogen concentration and source, crosslinking ratio and choice of medium, strongly affect the hydrogel material characteristics and, in turn, the resulting microvascular networks. Hydrogels made with higher concentrations of human fibrinogen ($\geq$ 6 mg/mL), a 200:10:1 crosslinking ratio, and endothelial cell basal medium (EBM) or EBM supplemented with VEGF (EBM + VEGF) performed best, demonstrating superior long-term network stability. The microvascular construct developed here could be used as a potential platform for studying traumatic injuries, as well as testing interventions aimed at improving recovery and mitigating damage.

Keywords

Microvasculature • *In Vitro* • Fibrinogen • Microvascular Endothelial Cells • 3D Construct • Traumatic Injury.

5.1 Introduction

Traumatic injuries are a leading cause of death worldwide [9], a major contributor to long-term functional limitations [10] and can significantly reduce the quality of life of affected individuals. The severity and extent of soft tissue trauma often determine the outcomes of complex injuries [565]. Current understanding of tissue trauma is primarily derived from clinical findings, including patient monitoring, trauma epidemiology and clinical markers. However, further research is needed to improve understanding of the underlying mechanisms beyond clinical symptoms and patient prognosis.

Deeper insights into the mechanisms and processes underlying traumatic injuries — such as inflammatory response and tissue regeneration — require reliable research models [14]. There are several factors limiting the understanding of soft tissue injuries, in particular of non-penetrating ones, including the lack of tools to evaluate the extent of the damage and the absence of appropriate models that are clinically relevant [565].

Microvascular injuries from trauma can have systemic physiological effects that exacerbate other injuries and may even endanger life. In non-penetrating traumatic injuries (NPTIs) to soft tissue, microvascular perfusion failure and delayed increase in microvascular leakage [565] are major contributors to tissue damage.

The microcirculation is essential for maintaining systemic health, enabling adequate function and long-term tissue survival by delivering oxygen and metabolites to tissues while removing waste products [566]. Microvascular dysfunction has been implicated in numerous diseases, both communicable as COVID-19 [567] and non-communicable as cancer [568]. Despite its importance, research into microvascular traumatic injuries is surprisingly limited [186], especially in tissues other than the brain.

Studying the immediate and short-term effects of trauma is inherently challenging. For instance, microvascular traumatic injuries remain heavily understudied [186], particularly shortly after the trauma has occurred. While *in vivo* models address some of these challenges [24, 25], they are constrained by the ethical concerns associated with the unnecessary pain and stress that the models are subjected to, the physiological differences with humans (*e.g.* varying microvascular trauma responses between species [14]) and logistical limitations. Therefore, there is a need for reliable *in vitro* models to gain further understanding of microvascular traumatic injuries and their underlying mechanisms.

Developing such a model, however, is not straightforward. Vascularisation and microvascularisation remain major challenges in the field of tissue engineering (TE) [37, 569], which also translates into limitations in applications beyond disease modelling, such as decellularisation and recellularisation of tissues and organs for transplantation [570] and the adequate function and long-term survival of implanted tissues [571]. Without a functional vasculature, engineered tissues have repeatedly failed [572] and remain limited in size due to reliance on simple diffusion for oxygenation and nutrient delivery [37, 40].

A number of methods have been used to engineer microvessels. Current strategies often involve bottom-up approaches, where one or more cell lines are incorporated into a matrix [379, 380]. These models can, and have been, used as platforms to study diseases, growth and remodelling dynamics [379], and other physiological processes. Cell culture models have been developed, amongst others, using bioprinting, where sacrificial inks are used to create perfusable channels [389], and microfluidic platforms, where new endothelial segments can be perfused [389]. Within these strategies, the most promising ones provide cells with a 3D environment aiming to partially mimic the extracellular matrix (ECM). Such models have been widely used for brain blood barrier [381] and tumour [382] research, and have been instrumental in advancing knowledge on the effects of matrix properties on vascularisation [379].

In this context, hydrogels have been widely used for the development of vascularised scaffolds as they can closely replicate the hydrated extracellular environment found in native tissues [260]. Hydrogels are 3D, physically or chemically crosslinked polymer networks swollen with water, forming matrices with mechanical properties intermediate between solids and liquids [223, 259]. These crosslinked networks can absorb and retain large amounts of water or biological fluids while maintaining their structural integrity [224, 260], enabling hydrogels to mimic the hydrated ECM [223, 225]. Their properties can be tailored through variations in, for example, polymer concentration, crosslinking and medium selection [224, 225, 227, 260]. These characteristics make hydrogels widely used in TE, where scaffold mechanics influence cell behaviour and tissue organisation.

Hydrogels exhibit viscoelastic behaviour, combining elastic energy storage and viscous energy dissipation, with their mechanical response governed by their molecular architecture and crosslinking. Their viscoelastic properties are commonly characterised by oscillatory rheology, in which a small oscillatory strain is applied within the linear viscoelastic range and the resulting stress response is analysed to determine the storage modulus (G', representing elastic energy storage) and the loss modulus (G", representing viscous dissipation). Hydrogel rheological properties are typically measured using rheometers or dynamic mechanical analysers, although microrheology and scattering techniques can also be used at the microscale. In most hydrogels, G'

exceeds G", indicating predominantly solid-like behaviour, although this depends on the crosslinking mechanism. The viscoelastic response of hydrogels is characterised by a time-dependent relationship between stress and strain and is described by key viscoelastic functions, including (1) the relaxation modulus, G(t), which quantifies stress relaxation following an imposed deformation; (2) creep compliance, which describes the time-dependent deformation under a constant load; and (3) the phase difference between oscillatory stress and strain, from which G' and G" are derived. Together, these rheological parameters describe how hydrogels respond to dynamic loading and are essential for assessing their ability to maintain structural integrity while providing mechanical cues that regulate cell proliferation, migration, differentiation, and tissue organisation. [573]

Human umbilical vein endothelial cells (HUVECs) are extensively used in microvascular research due to their accessibility and well documented ability to form new vasculature [285, 289]. However, they differ from microvascular endothelial cells (MVECs) [270], which are specifically found in the microvasculature. HUVEC models are well characterised [286], widely established and considered to be a standard model for cell-based assays [292] to study angiogenesis [286, 289, 293]. They are particularly prominent in tube formation assays, where they reliably form networks of tube-like structures. However, HUVEC-based networks begin to deteriorate around 18 h after seeding and completely disintegrate within 24 h [298, 299], after which time, hypoxia [574] and the absence of growth factors drive apoptosis [289] and the networks disintegrate [289, 575]. This short lifespan restricts their utility for longer-term research, such as research involving traumatic injury induction and evolution monitoring.

To address this limitation, it is critical to develop an *in vitro* microvascular model that incorporates physiologically relevant microvascular cells, maintains network integrity beyond 24 h, and features a 3D structure to provide spatial cues and mechanical attachment points. Such a model would enable its use for applications in trauma research, such as the induction of traumatic injuries and facilitate monitoring of damage progression and the impact of potential interventions over time.

In this research, we address these gaps by developing and fine-tuning a 3D microvascular construct comprising a hydrogel scaffold embedded with MVECs. The results are structured as follows: First, we validate the suitability of our MVEC-based construct using HUVEC-based models as the benchmark. Then, we investigate how variations in hydrogel composition — specifically fibrinogen concentration and source, medium and crosslinking ratio — affect the material properties of the scaffolds and, consequently, the formation, architecture and longer-term stability of the resulting microvascular endothelial network. Finally, we integrate these findings to optimise the hydrogel composition and develop a long-lasting microvascular construct tailored for traumatic injury research. By focusing on a time frame of up to 14 days post-seeding, we create a platform for traumatic injury research that allows conducting further experimental work, perform additional characterisation, and accounts for the degradation time frame of the hydrogel construct itself.

5.2 Materials & Methods

5.2.1 Cell Culture

HUVECs (ATCC) and immortalised human dermal MVECs (ATCC, CRL–3243) were cultured in T–75 and T–175 cell culture flasks (Corning Incorporated Life Sciences, USA) with endothelial cell growth medium (EGM). EGM was prepared by supplementing endothelial cell basal medium (EBM) with either SingleQuots[1] (Lonza, Walk-

[1]Foetal bovine serum (FBS) 2%; hydrocortisone 0.04%; human fibroblast growth factor-basic (hFGF-b) 0.4%; vascular endothelial growth factor (VEGF) 0.1%; long R3 insulin-like growth factor-1 (R3-IGF-1) 0.1%; ascorbic acid 0.1%; human epidermal growth factor (hEGF) 0.1%; gentamicin sulfate-amphotericin (GA-1000) 0.1%; heparin 0.1%.

ersville, MD, USA or Microvascular SingleQuots[2] (Lonza, Walkersville, MD, USA), respectively, and with 1% penicillin/streptomycin (Gibco Life Technologies, Grand Island, NY, USA). Cells were incubated at 37 °C and 5% CO_2 and the medium was replaced every 48–72 h, as needed. The MVEC cell line was previously immortalised *via* pSVT vector transfection. Cells were used for experimental work at 80% confluency and HUVECs were only used up to passage 7.

5.2.2 Comparing HUVECs and MVECs: Morphology & Cell Migration

To further confirm the morphological similarities between HUVECs and MVECs, cells were cultured in their respective EGM, seeded in glass-bottom dishes (Ibidi, Germany) at a density of 3×10^5 cells/dish, and incubated for 24 h before imaging.

5.2.2.1 Cell Migration

The collective cell migration rates [403] of HUVECs and MVECs on fibrin hydrogels were compared. Hydrogels were prepared as described in Section 5.2.3 using bovine fibrinogen at a concentration of 4 mg/mL and EBM as medium. Cells were seeded on top of a hydrogel coat at a density of 2.5×10^4 cells/well (48–well plate). Once confluent, a p200 pipette tip was used to create a scratch wound across the cell sheet, forming a gap. Cells-only controls for both HUVECs and MVECs were also prepared, with nine replicates used for each experimental or control group. Cell migration was monitored for 24 h, during which the gap area was imaged at various time points and quantified using image analysis [576]. The average cell migration rates were calculated by dividing the change in gap area (final minus initial) by the time elapsed since the gap was created (Equation 5.1).

$$\text{Migration Rate } [\mu m^2/h] = \frac{\text{Gap Area}_{\text{Initial}}\ [\mu m^2]\ - \text{Gap Area}_{\text{Final}}\ [\mu m^2]}{t_{\text{Initial - Final}}\ [h]} \tag{5.1}$$

5.2.3 Hydrogel Fabrication

Hydrogel scaffolds were fabricated and embedded with either HUVECs or MVECs to create TE constructs. Several variations of the hydrogels were explored, arising from different combinations of medium, fibrinogen concentration and source, and crosslinking ratio (Table 5.1). The hydrogels were prepared using fibrinogen from either bovine (MP Biomedicals, New Zealand) or human plasma (Sigma-Life Science; St Louis, MO, USA) at different concentrations (2, 4, 6, 8, 10 mg/mL) and with various media: MES/NaCl buffer (0.15 M NaCl, 2.5 mM MES in distilled water; pH 7.4); EBM; EBM supplemented with Vascular Endothelial Growth Factor (EBM + VEGF; Lonza, Walkersville, MD, USA); EBM supplemented with the full SingleQuot Kit (EGM); or Phosphate Buffered Saline (PBS; pH 7.4; Gibco, United Kingdom).

Each hydrogel was prepared from its corresponding solution. Briefly, fibrinogen at the desired concentration was dissolved in the medium and stored at 37 °C for 30 min or until fully dissolved. The solution was then filtered twice using 0.22 µm filters (Merck Millipore Ltd., Ireland) and irradiated with UV light for 20 min. Next, 100 µL of foetal bovine serum (FBS; Bioclear, United Kingdom) and cells suspended in EBM at the desired concentration were added. The solution was crosslinked with thrombin (Sigma-Aldrich, St Louis, MO, USA), previously diluted to 10 U/mL in MES/NaCl buffer, and a 1 M $CaCl_2$ solution in distilled water. The hydrogel solution was thoroughly mixed to ensure homogeneity before carefully casting it into the well, avoiding bubble formation and ensuring an even distribution. Finally, plates were incubated at 37 °C and 5% CO_2, to complete the gelation process.

[2] FBS 10%; hydrocortisone 0.04%; hFGF-b 0.4%; VEGF 0.1%; R3-IGF-1 0.1%; ascorbic acid 0.1%; hEGF 0.1%; GA-1000 0.1%.

Medium	a) MES/NaCl Buffer b) Endothelial Cell Basal Medium (EBM) c) EBM supplemented with 2% *w/v* Vascular Endothelial Growth Factor (EBM + VEGF) d) EBM supplemented with full SingleQuot Kit* (EGM) e) Phosphate Buffered Saline (PBS)
Fibrinogen Concentration	a) 2 mg/mL b) 4 mg/mL c) 6 mg/mL d) 8 mg/mL e) 10 mg/mL
Fibrinogen Source	a) Bovine b) Human
Crosslinking Ratio (Fibrinogen : Thrombin : $CaCl_2$)	a) 200:10:1 b) 100:10:1

Table 5.1: **Summary of hydrogel composition variations explored.** *SingleQuot Kit: Foetal bovine serum (FBS) 2%; hydrocortisone 0.04%; human fibroblast growth factor-basic (hFGF-b) 0.4%; vascular endothelial growth factor (VEGF) 0.1%; long R3 insulin-like growth factor-1 (R3-IGF-1) 0.1%; ascorbic acid 0.1%; human epidermal growth factor (hEGF) 0.1%; gentamicin sulfate-amphotericin (GA-1000) 0.1%.

5.2.4 Influence of Hydrogel Composition on Endothelial Network: Architecture & Integrity

To assess the impact of varying the hydrogel composition on microvascular network formation, architecture and degradation, multiple tube formation assays were performed and characterised at various time points. The term 'tube formation' is used in accordance with standard TE terminology to describe the *in vitro* assay in which ECs self-organise into capillary-like networks. It does not validate the formation of functional, lumenised vessels. HUVECs and MVECs were cultured in their respective EGM and, once confluent, seeded in a range of hydrogel scaffolds. From here on, EBM was used to culture the cell-embedded constructs. The variations in medium, fibrinogen concentration and source, and crosslinking ratio explored are detailed in Table 5.1.

Tube formation was monitored at different time points and the network architecture was characterised using image analysis. Network characterisation of the endothelial networks included parameters such as the number of junctions (representing bifurcations), segments (elements between two junctions) and branches (elements between a junction and an extremity); the total network length given by the sum of the length of all segments, isolated elements and branches; and the branching interval, which is the mean distance separating two branches (total segments length by number of branches) [577]. A schematic of these architectural elements is presented in Figure 5.1. These parameters are commonly used to characterise microvascular architecture [578], including in clinical contexts [579], as they provide insights into vessel connectivity rather than of individual vessel length and diameter, which are typically analysed through network geometry [580].

5.2.5 Material Characterisation

5.2.5.1 Gelation Time

1 mL of each hydrogel solution was cast per well (12–well plate). The plate was tilted periodically and the time at which the hydrogel retained its shape was manually recorded (Figure E.1). Five replicates were used.

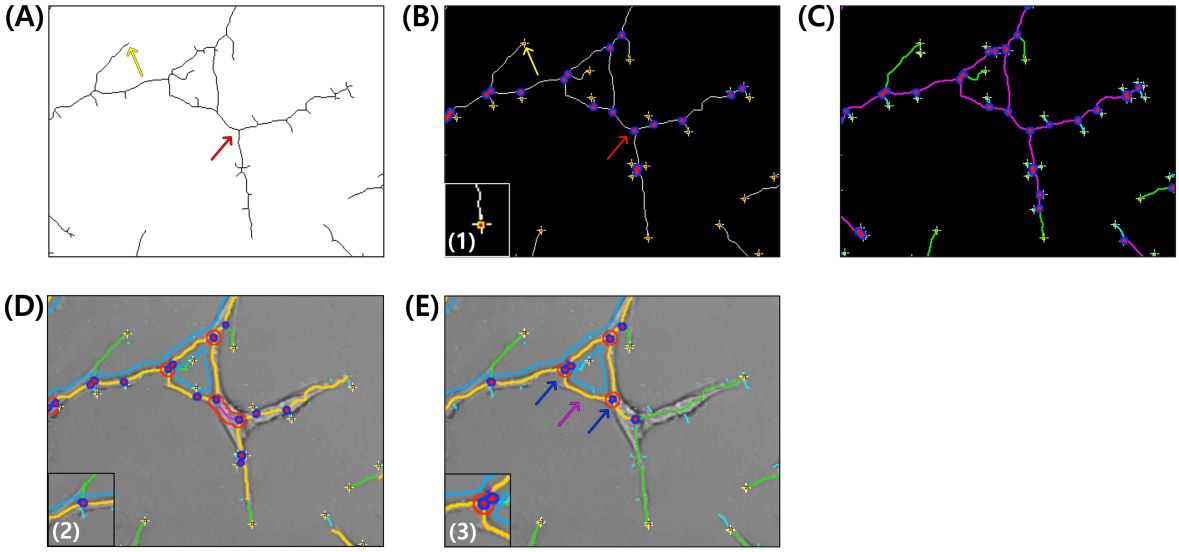


Figure 5.1: **Constitutive elements of the endothelial network. (A, B)** Extremities (*yellow arrow*) are marked by red dots surrounded with a yellow edge (shown in **B1**). **(A, B)** Nodes (*red arrow*) represent bifurcations and are identified as pixels that have at least three neighbours. **(C, D)** Twigs (*cyan*) are branches smaller than a defined threshold; segments (*magenta*) are elements between two junctions (shown in **D2**); and branches (*green*) are elements between a junction and an extremity. **(E)** Some segments and junctions can be further classified as master segments and master junctions, respectively. Master segments (*magenta arrow*) are elements located between by two junctions, neither of which is exclusively associated with a single branch. These junctions, named master junctions (*blue arrows*), occur where at least three master segments meet or (shown in **E3**) where two master junctions merge into a single unique master junction. Master junctions (*blue arrows*) define the boundaries of master segments (*magenta arrow*). Based on Carpentier (2020) [577].

5.2.5.2 Spectrophotometry

To gain further understanding on polymerisation dynamics, turbidity during polymerisation was measured using a spectrophotometer (WPA Lightwave II UV–Vis) at 340 nm absorbance [581–583]. Wavelengths in the 320–360 nm range are well-established for fibrin [581, 584–587], with studies reporting maximal optical density differences between polymerised and non-polymerised states within this region (*e.g.* [584]). Specifically, fibrinogen emission spectra peak within this wavelength range, reaching the maximum at 344 nm [586] and 340 nm [581], which has been explicitly reported for absorbance measurements [581, 583]. 600 µL of hydrogel solution were gently deposited into a quartz cuvette for spectrophotometry readings. The light absorbance of each medium was measured for zero absorbance calibration, then the absorbance of the hydrogels was measured at 1 s intervals for 5 min. Nine replicates were used.

5.2.5.3 Pendant Drop

The surface tension of hydrogel droplets (Figure E.2) was measured by loading the human fibrin hydrogel (10 mg/mL) solution into a 3 mL syringe fitted with a tapered nozzle tip (length: 31.75 mm, diameter: 0.41 mm; Adhesive Dispensing Ltd.) secured to a raised printhead of a 3D bioprinter (BioX Cellink). The bioprinting parameters used were 200 kPa pressure, 5 mm/s printing speed and 6.9 °C temperature.

Droplet evolution was recorded (Nikon D3400 DSLR) and, from this video, still images of the frame prior to droplet detachment from the nozzle were identified and exported. The droplet profiles were extracted from the images and processed using *OpenDrop* [588] to measure pendant drop tensiometry. Drop density was then calculated by measuring the solution's volume and mass. The surface tension of human fibrin hydrogels

was measured pre-gelation and at different time points once gelation begun. Controls of deionised water and EBM were also used. Nine replicates were analysed.

5.2.5.4 Microrheology and Crosslink Density

To investigate energy storage and dissipation at the microscale of the different hydrogel compositions, microrheology studies were conducted using RheoLab (LS Instruments) with a multi-tau duration of 60 s and echo of 30 s. The device was calibrated using distilled water and the manufacturer's polystyrene solution, prior to all readings. 50 µL of a 1% solution of 1 µm polystyrene particle tracer solution (Sigma Aldrich) was added to 450 µL of each hydrogel solution, mixed, and immediately placed into a 2 mm thick glass cuvette. After allowing the mixture to gel for 1 h (Figure E.3), the sample was transferred to the device and equilibrated to 37 °C for 10 min before microrheology readings were performed. The polystyrene particles were stored at 4 °C when not in use. Measurements were repeated 24 h after gelation.

To complement the microrheology data, crosslink density (q; Equation 5.2) was calculated using the molecular weight of the monomer (*Mw*) and the molecular weight between crosslinks (*Mc*; Equation 5.3), with the universal gas constant (*R*), the absolute temperature (*T*) and the polymer density (*d*) [589].

$$q = \frac{M_w}{M_c} \tag{5.2}$$

$$M_c = \frac{RTd}{G'} \tag{5.3}$$

5.2.5.5 Shear

A human fibrinogen in EBM hydrogel solution (10 mg/mL) was prepared and carefully deposited on microscope slides to avoid the formation of bubbles. A second slide was placed on top of the hydrogel and gently sheared until the slides were fully aligned (approximate displacement: 40 mm; Figure E.4). Controls with unsheared samples were also prepared. Samples were then imaged using a widefield microscope or SEM and analysed using the *Directionality* plugin [590] in *ImageJ/Fiji*. Triplicates were used.

5.2.5.6 Hydrogel Degradation

Hydrogel degradation profiles were analysed, focusing on the influence of medium, fibrinogen source and concentration. Hydrogels were fabricated using fibrinogen from bovine and human plasma at different concentrations (2, 4, 6, 8, 10 mg/mL) combined with a range of media (EBM, EBM + VEGF, EGM, or PBS). 100 µL of each hydrogel solution was carefully deposited into each well (96–well plate) to avoid bubble formation. Following hydrogel casting, plates were incubated at 37 °C and 5% CO_2 for 14 days.

The mass of each hydrogel (n = 3) was measured on days 1, 4, 7 and 14 after casting, carefully removing the hydrogel from the well and weighing it, discarding the supernatant. After weighing, the hydrogels were returned to the well and fresh medium was added. The data was normalised to reflect the relative mass changes over time.

5.2.5.7 Evaluating Hydrogel Compositions for Long-term Microvascular Network Integrity

Insights from hydrogel composition analysis and material characterisation informed the selection of optimised hydrogel formulations for further experimental work, with a focus on long-term network durability. Additional hydrogel constructs were prepared as described in Section 5.2.3 and network development was routinely monitored and quantified for up to 13 days.

5.2.5.8 Imaging & Image Analysis

A widefield microscope (Nikon Widefield TiE2000, Japan), equipped with an environmental chamber for temperature and CO_2 levels control, was used for imaging. Each well was imaged in its entirety and all the images that were not disrupted by the edge of the well were analysed using *ImageJ/Fiji* (version 2.14.0, National Institutes of Health, Bethesda, MD, USA) [404]. Endothelial networks were analysed using the *Angiogenesis Analyser* [577] plugin, cell migration data was processed with the *Wound Healing Size Tool* [576], and alignment was quantified using the *Directionality* plugin [590]. Pendant drop tensiometry was measured using *OpenDrop* [588]. Z-stack imaging was performed using a 20× objective lens. Images were captured in 1 µm steps, creating a series of optical sections through the hydrogel. Then, they were processed using *ImageJ/Fiji*'s *Temporal-Color Code* plugin to visualise depth by assigning different colours to each slice, enabling a clearer interpretation of the 3D structure.

5.2.5.9 Statistical Analysis and Software

Data was analysed using one- or two-way analysis of variance (ANOVA), followed by Tukey's honest significant difference (HSD), Fisher's least significant difference (LSD), or Dunnett post hoc tests. p values ≤ 0.05 were considered statistically significant. Data analysis was performed using *Microsoft Excel* 365 MSO (version 2403, Microsoft, Redmond, WA, USA) and *GraphPad Prism* (version 10.2.3 (403), Dotmatics, Boston, MA, USA). Unless otherwise specified, results are presented as mean values with standard deviation. Figures were created using *GraphPad Prism*, while the graphical abstract, the gelation process illustration and the shear process schematic (Figures E.1 & E.4) were created using *BioRender.com* (agreement numbers: PQ284GJ5UK, PJ284GIXSG & QQ28EVUGSX).

5.3 Results & Discussion

The key findings of this research include that MVECs can be used to provide a rich microvascular network that is more durable than HUVECs, the gold standard. Moreover, embedding ECs in a 3D hydrogel construct enables endothelial networks that have a greater total length and are more complex, including a greater number of segments, branches and junctions. Furthermore, varying the hydrogel composition in terms of fibrinogen source and concentration, crosslinking ratio and media has an impact on the material properties of the scaffold, network architecture and long-term network integrity. By enabling longer-term network durability, this opens avenues for further experimental work. For example, it facilitates research into microvascular network damage caused by various traumatic injuries, reducing or eliminating the need for *in vivo* models.

5.3.1 Comparing HUVECs and MVECs

Previously, we demonstrated that fibrin hydrogels not only support the formation of capillary-like networks of HUVECs [397] but were also the most promising polymer of the ones screened for the development of an endothelial network construct. However, macrovascular ECs such as HUVECs differ from microvascular cells in several ways; for instance, types and amounts of cell adhesion molecules, prostaglandin secretory profile and secreted proteins [56,270,411,412]. Moreover, MVECs express specific proteins associated with tight junctions that are required to regulate capillary permeability [300], which is a key feature of the microvasculature.

To develop a microvascular construct that is more physiologically relevant, we explored fibrin hydrogels for the development of a microvascular construct using MVECs. Here, HUVECs were used as the benchmark based on their extensive use in research, particularly as general models for ECs in both diseased and normal

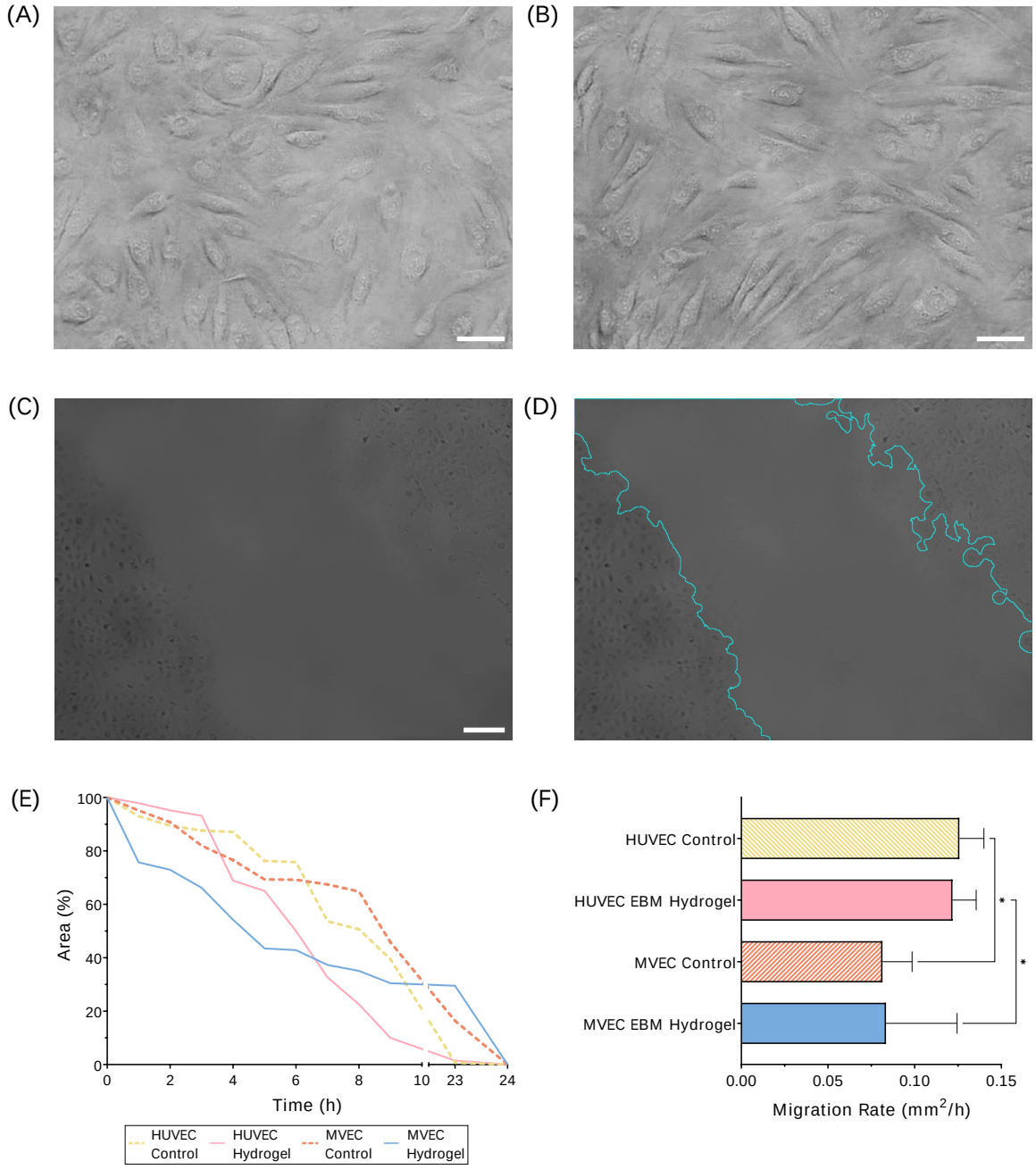


Figure 5.2: **Comparing human umbilical vein endothelial cells (HUVECs) and human dermal microvascular endothelial cells (MVECs).** Both **(A, B)** cell morphology and **(D–F)** cell migration were analysed. 10× microscopy images of **(A)** HUVECs and **(B)** MVECs; scale bar: 150 px. Cells were cultured with their respective EGM, plated in glass-bottom dishes (cell density: 3×10^5 cells/dish) and incubated for 24 h before imaging. **(C–F)** Cell Migration of HUVECs and MVECs in EBM Hydrogels. **(C)** A gap was created using a p200 tip and imaged throughout a 24 h period. Here, the HUVEC control is shown 0.5 h after the creation of the gap. **(D)** Using the *Wound Healing Size Tool* [576] *via ImageJ/Fiji* (version 1.54f, National Institutes of Health, Bethesda, MD, USA) [404], the gap area was measured at each time point. The edge of the gap is automatically identified (*blue*) by the software. **(E)** The gap area was then plotted as the percentage of the initial gap area and, from this data, **(F)** the average migration rate (mm^2/h) was calculated. EBM hydrogels were prepared with 4 mg/mL of fibrinogen of bovine source. HUVECs and MVECs were cultured with their respective EGM and seeded at a density of 2.5×10^4 cells/well (48–well plate). Cells-only controls were used. (One- or Two-way ANOVA/Tukey's HSD; $^*p \leq 0.05$; only statistically significant differences are shown; $n = 12$). Scale bar: 200 µm.

conditions [285]. This comparison aimed to validate the suitability of fibrin hydrogel scaffolds for capillary-like network formation by MVECs.

Prior to the characterisation of endothelial networks created by HUVECs or MVECs, it was of interest to compare cell morphology whilst undergoing standard cell culture, as well as cell migration (Figure 5.2), to validate whether MVECs could be used for the development of a microvascular construct, similarly to the well-established HUVECs, while offering advantages such as longer retention of expected morphology and cellular characteristics over multiple passages.

5.3.1.1 Cell Morphology

As shown in Figure 5.2A & B, and consistent with the literature, both cell lines exhibit an elliptical shape with sharp edges, display clear nuclei in the centre, have an abundant cytoplasm and are arranged in a typical cobblestone arrangement [591].

5.3.1.2 Cell Migration

Collective cell migration of HUVECs and MVECs in EBM fibrin hydrogels and cells-only controls was monitored for 24 h (Figure 5.2C & D). The gap area was measured immediately after its creation and at different time points throughout the 24 h period (Figure 5.2E). Using this data, the average migration rate, representing the area covered per hour, was calculated (Figure 5.2F). For this calculation, the gap area at t = 23 h was used as the final value as the exact time of gap closure is unknown (closure occurred between t = 23 h and t = 24 h).

HUVECs displayed a slightly faster migration rate than MVECs, but this difference was only significant when comparing between controls or hydrogels. This observation may be associated with the faster formation and degradation of HUVEC networks compared to MVECs. Similar methodologies for evaluating cell migration using scratch assays on hydrogel coatings have been reported [592, 593]. These studies often utilise natural biomaterials, as is fibrin, such as collagen [594, 595] and gelatine [596]. Although differences in matrix architecture [597] and hydrogel mechanical properties [598] can influence cell migration speed, the choice of cell line plays a more critical role in determining migration rates than the properties of the scaffold, just as we observed experimentally.

5.3.1.3 Endothelial Network Development & Architecture

To assess the suitability of EBM hydrogels for both cell lines, network formation and architecture were examined over time. Our results suggest that using a 3D hydrogel construct plays a key role in the network architecture, resulting in more extensive and complex endothelial networks in comparison with the controls. The importance of the hydrogel microenvironment becomes even more pronounced as time progresses, particularly from 12 h post-seeding onwards (Figures 5.3, E.5 & E.6).

The results presented in Figure 5.3 highlight significant differences in endothelial network characteristics between HUVECs and MVECs cultured in two hydrogel scaffolds (MES/NaCl and EBM) and their respective controls. These findings underscore the influence of the hydrogel microenvironment on network formation and complexity. While there are significant differences in the network architecture between the cell-embedded hydrogels and the cells-only controls in either cell line, there are no significant differences when comparing both controls or both hydrogels. This suggests that MVECs can be reliably used for the development of a microvascular model as they produce similar networks to HUVECs when embedded in the same hydrogel constructs.

Quantitative analysis revealed that the number of segments and junctions, as well as the total network length, were consistently higher in cell-embedded hydrogels compared to their respective controls at both time

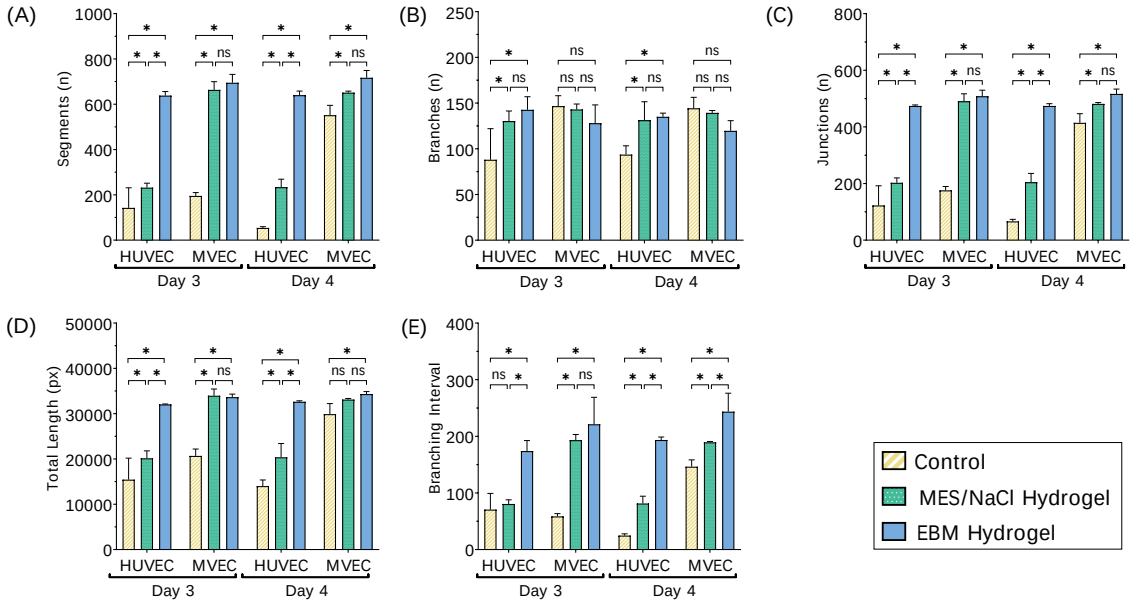


Figure 5.3: **Endothelial network characterisation of HUVECs or MVECs in MES/NaCl or EBM hydrogels using bovine fibrin hydrogel (4 mg/mL), at 3– and 4–days post-seeding.** The **(A)** number of segments; **(B)** number of branches; **(C)** number of junctions; **(D)** total length; and **(E)** branching interval of each sample were obtained. Cell-embedded hydrogels (seeding density: 5×10^4 cells/well) were cultured with EBM in 24–well plates. Cells-only controls were used. (2-way ANOVA/Tukey's HSD; $^*p \leq 0.05$, ns: not statistically significant; $n = 3$).

points. This demonstrates the ability of the hydrogels to support enhanced endothelial network formation. Notably, EBM hydrogels exhibited superior performance compared to MES/NaCl, particularly for HUVECs but also applicable to MVECs. This was reflected in significant increases in the number of segments and junctions, as well as a higher branching interval, indicative of a more complex, interconnected network. These differences became more pronounced over time, suggesting that EBM hydrogels promote sustained network maturation.

Both hydrogels significantly improved total network length and reduced branching intervals for MVECs relative to controls, highlighting their broader applicability for endothelial network formation. These results suggest that EBM hydrogels provide a superior microenvironment for endothelial network development, particularly for HUVECs, and offer sustained support for network maturation. Such findings are critical for advancing the use of fibrin-based hydrogels in TE and regenerative medicine, where robust and interconnected endothelial networks are essential for functional constructs.

MES/NaCl hydrogels (Figure E.5) were used as the starting point for hydrogel development given that fibrin-based biomaterials often utilise this biocompatible medium [402]. This data illustrates the benefit of utilising a 3D hydrogel construct on the network architecture for both cell lines. Variations in the hydrogel medium, for instance MES/NaCl vs. EBM (Figure E.6), reveal that modifying the hydrogel composition impacts endothelial network architecture.

Our results suggest that EBM hydrogels are better suited for endothelial network formation (Figure 5.3), leading to more (HUVECs) or a similar (MVECs) number of segments. However, differences in the number of branches were less pronounced across cell lines and scaffolds. Interestingly, we see larger variations in the branching intervals than in the other parameters. This could potentially be attributed to the addition of new branches or even the disintegration of existing network structures.

To gain deeper insights into endothelial network formation, we monitored the formation of the HUVEC and MVEC networks over 39 h using time-lapse imaging (Figure E.7). This revealed that HUVEC networks form earlier than MVEC ones, with noticeable differences in the number of segments, branches and junctions. While

total network length also increased, the differences were not statistically significant. The hydrogel scaffolds played a key role in ensuring long-term network stability, possibly attributed to the provision of a 3D construct and mechanical support.

The ability of MVECs to form more physiologically relevant networks compared to HUVECs is further supported by studies demonstrating the expression of proteins such as claudins and occludins in MVECs, which are critical for tight junction integrity [301, 599]. These proteins ensure capillary permeability control, a key feature in microvascular constructs designed for trauma research.

Over time, parameters such as the number of segments, branches and junctions increased while branching intervals generally decreased. Interestingly, cells-only controls displayed higher branching larger values at later time points, which microscopy images confirmed to be due to network fragmentation.

The use of immortalised cell lines, such as MVECs, offers significant advantages over primary cells like HUVECs, including sustained proliferative capacity [600], which facilitates reproducibility and reduces batch-to-batch variations. Immortalised cells retain critical biological features that are characteristic of the parent cell [63] rather than pooling cells from multiple donors, as commonly occurs with HUVECs. Therefore, MVECs appear to be more promising for developing reliable and durable microvascular constructs, especially considering for longer term construct integrity and usability.

Collectively, these findings suggest that EBM hydrogels provide the most promising scaffold for endothelial network formation, supporting greater network complexity and more sustained maturation than MES/NaCl hydrogels and control conditions. Together with the reproducibility, phenotypic stability and extended culture capability of MVECs, MVEC-embedded EBM constructs represent a robust platform for the development of physiologically relevant microvascular models.

5.3.2 3D Hydrogel Constructs with MVECs Enable Successful Endothelial Network Formation

The 3D hydrogel constructs developed in this research effectively facilitated the formation of endothelial networks (Figure 5.4A) using both HUVECs and MVECs. Modifications to the hydrogel composition influenced the network's architecture and durability, revealing that specific formulations are more suitable for microvasculature formation. The HUVEC and MVEC networks were characterised by performing image analysis (Figure 5.4B-G). This data was used to evaluate the impact of modifying the hydrogel composition (medium, fibrinogen concentration and source, and crosslinking ratio) on the formation and evolution of the endothelial networks.

To confirm the 3D nature of the construct, z-stack imaging illustrated the spatial arrangement of ECs embedded within the matrix, rather than on the surface of the hydrogel. MVECs are distributed throughout the hydrogel scaffold, highlighting the spatial complexity and physiological relevance of the construct (Figure E.8). These findings underscore the ability of fibrin hydrogels to support the development of intricate, 3D microvascular networks.

The development of a stable 3D microvascular network in the hydrogel scaffold is consistent with findings that emphasise the importance of 3D matrices in recapitulating physiological microenvironments [601, 602]. The interplay between the fibrin hydrogel's mechanical properties and cellular behaviour aligns with prior studies highlighting the role of ECM mimetics in supporting endothelial morphogenesis [542].

From the parameters used to quantify the microvasculature architecture (Figure 5.1), the most important one would be the total network length as is the most critical indicator of an extensive network. While a high number of junctions may suggest a more complex network, this figure should always be evaluated alongside the number of segments and branches. As for the branching interval, this provides insights into how the network splits at every junction; therefore, more complex networks where multiple branches split from every segment could be more easily identified.

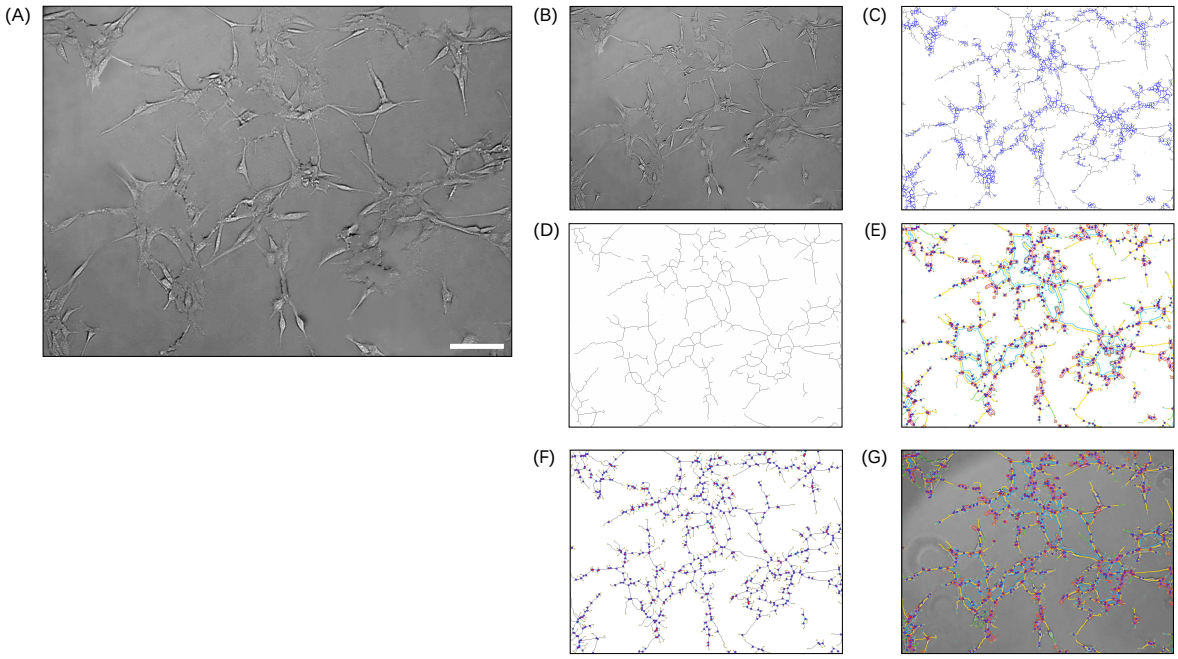


Figure 5.4: **Characterisation of endothelial networks. (A)** Representative image depicting endothelial network formation: an MVEC network in an EBM hydrogel with fibrinogen from human plasma at a concentration of 8 mg/mL and 200:10:1 fibrinogen : thrombin : $CaCl_2$ crosslinking ratio, imaged 7 days post-seeding. Cell seeding density: 2×10^4 cells/well (96–well plate). **(B–G)** Network characterisation was performed *via* image analysis, depicting the various steps involved: **(A)** the original microscopy image with a 100 µm scale bar (applies to all panels); **(B)** the markup of the network tree on the original image; **(C)** the binary tree image indicating the artefactual loops (*blue*) to be removed; **(D)** the resulting master binary tree; **(E)** the analysis of the binary tree depicting the detected vectorised elements: extremities (*red dots with yellow border*), branches (*green*), segments (*magenta*), twigs (*light blue*), junctions (*red dots with blue border*) and segments (*yellow*); **(F)** extremities (*red dots with yellow border*) and junctions (*red dots with blue border*) indicated on the binary tree; and **(G)** the detected vectorised objects on the original image. The scale bar was removed during the image analysis process to prevent its inclusion in the network analysis. Images were analysed using *ImageJ/Fiji* (version 1.54f, National Institutes of Health, Bethesda, MD, USA) [404] and the *Angiogenesis Analyser* [577] plugin.

5.3.3 Influence of Hydrogel Composition on Endothelial Network: Architecture & Integrity

Having validated the use of MVECs for the development of the construct, it was necessary to optimise the hydrogel composition. To this end, the fibrinogen concentration, medium and crosslinking ratio were modified to evaluate their impact on network formation and architecture.

5.3.3.1 Impact of Variations in Fibrinogen Concentration and Medium

The influence of fibrinogen concentration and medium on the development of a microvascular network was explored using a range of fibrinogen concentrations in combination with three medium variations: EBM, EBM + VEGF and EGM (Figures 5.5 & E.9). Higher fibrinogen concentrations (6, 8 and 10 mg/mL) across all media variations resulted in significantly longer networks than the controls (all $p < 0.0001$), corresponding to 6.79– to 7.98–fold (EBM), 7.11– to 8.02–fold (EBM + VEGF) and 7.21– to 8.49–fold (EGM) increases. At lower concentrations, 2 mg/mL EBM hydrogels produced networks comparable to the controls ($p > 0.05$), whereas 4 mg/mL hydrogels generated significantly longer networks at 24 h ($p < 0.0001$).

All but two fibrinogen concentrations and the control have a similar total network length across the three media at 24 h. On the other hand, both 4 and 6 mg/mL display the largest variations between media and time

points. This suggests that the hydrogel scaffolds play a greater role in the later stages of network formation than in the first few hours. Finally, as expected, there are significant increases between 2 h and 24 h across all variations. This further validates the growth of the microvascular network over time, which was also observed in preliminary experimental work.

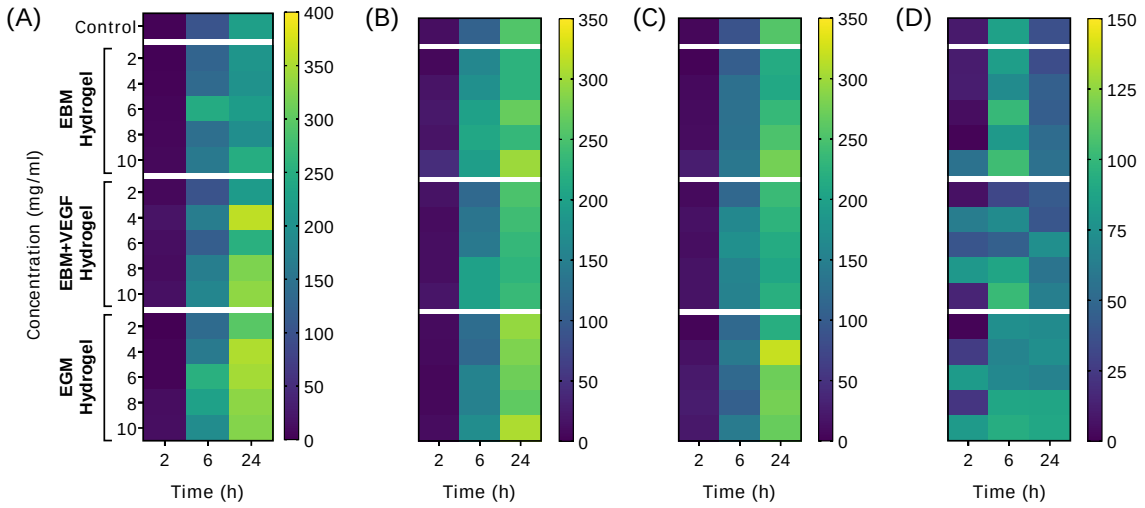


Figure 5.5: **Impact of variations in fibrinogen concentration and medium on microvascular endothelial network architecture**, showing MVEC network characterisation by fibrinogen concentration and medium at 2, 6 and 24 h. The number of **(A)** segments, **(B)** branches, and **(C)** junctions, and the **(D)** branching interval were quantified. Hydrogels were created with bovine fibrinogen. MVECs were cultured with EGM and seeded at a density of 2.5×10^4 cells/well (48–well plate). Cells-only controls were used. (ANOVA/Tukey's HSD; $n = 3$).

Network characterisation (Figure 5.5) revealed an increase in the number of segments, branches and junctions over time, with most hydrogel formulations outperforming controls. This further supports the postulation that fibrin hydrogels are suitable for endothelial network development. At 24 h, EBM hydrogels are associated with more segments, branches and junctions than the control, except for the 2 mg/mL concentration which displays a similar architecture to the networks of the controls. EBM + VEGF hydrogels consistently displayed more segments than controls. On the other hand, the branching interval does not exhibit discernible patterns across time points or hydrogel compositions. This could potentially be attributed to either further development of the network or its fragmentation, making this parameter less reliable for identifying optimal hydrogel compositions.

Combining total network length with architectural metrics suggests that higher fibrinogen concentrations across all three media enable the formation of larger networks. The observed improvements in network formation with higher fibrinogen concentrations may be attributed to enhanced matrix stiffness [603], which impacts EC self-organisation [604], vascular integrity [605] and vessel permeability [606]. Furthermore, increased matrix stiffness has been shown to promote endothelial tubulogenesis and network complexity. This is particularly relevant in trauma research, where matrix properties can influence angiogenic responses during wound healing and regeneration. Considering that the fibrinogen concentration of 4 mg/mL delivers promising results at the later time points, it would be interesting to explore a slightly higher concentration to determine whether 4 mg/mL is the lowest threshold enabling a more complex capillary-like network.

5.3.3.2 Impact of Variations in Crosslinking Ratio

Two crosslinking ratios of fibrin, thrombin and $CaCl_2$ (200:10:1 and 100:10:1) were selected based on the results of the evaluation of hydrogel consistency and shape retention twelve days after casting and 1 h after demoulding (Appendix E: Section E.1), as they exhibited good shape retention and consistency. These ratios were tested to evaluate their impact on the development of capillary-like networks formed by HUVECs and MVECs. The total length of the resulting networks was quantified hourly from 0.5 h after seeding, hourly, for 24 h (Figures 5.6 & E.10). Crosslinking ratios play a key role not only in network development and integrity, but also in hydrogel consistency and scaffold shape retention. Crosslinking ratios have a greater impact on hydrogel consistency than fibrinogen concentration or the selection of medium.

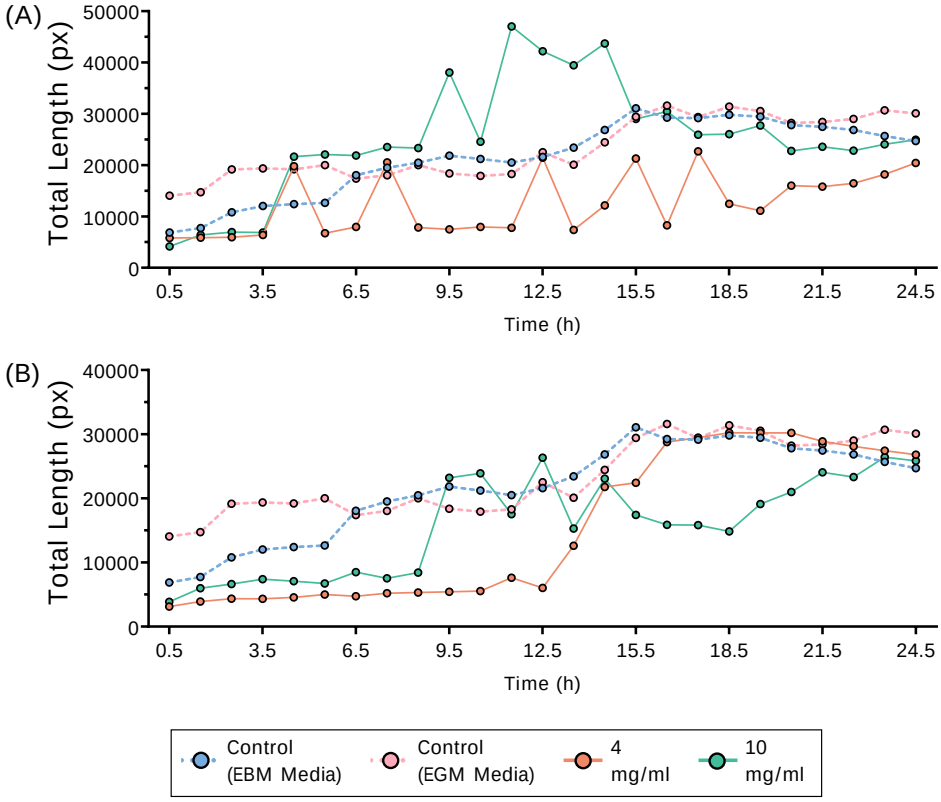


Figure 5.6: **Impact of variations in crosslinking ratio on microvascular endothelial network architecture**, displaying total MVEC network length by fibrinogen : thrombin : $CaCl_2$ crosslinking ratio, quantified from t = 0.5 h every hour during a 24 h period. Two crosslinking ratios were explored: **(A)** 200:10:1 and **(B)** 100:10:1. Hydrogels were created using fibrinogen from human serum at different concentrations, paired with EBM as medium. MVECs were cultured with EGM and seeded at a density of 2×10^4 cells/well (96–well plate). Two cells-only controls, in EBM and EGM, were used. Here, the controls and the 4 and 10 mg/mL concentrations are shown. (ANOVA/Tukey's HSD; $p \leq 0.05$; $n = 6$).

Our results also revealed that using fibrinogen 20× or 10× relative to thrombin improves scaffold shape retention. Networks formed in 200:10:1 hydrogels exhibited steady growth over time (Figure E.11), outperforming the 100:10:1 ratio in supporting longer and more stable networks. This ratio also improved scaffold shape retention and consistency, critical factors for long-term network durability. Interestingly, there seem to be two clusters at the earliest period: (1) the EBM cells only control and the two highest fibrinogen concentrations, and (2) the cells in EGM control with the two lower concentrations. There is also a significant increase in total network length in the 10 mg/mL concentration hydrogels from 5.5 h onwards. We can also observe notable increases in the remaining concentrations within the time frame of 6.5 to 9.5 h.

MVEC networks display a less defined pattern, particularly within the initial 18 h, which represents the primary phase of network growth, as shown in previous experimental work. By the end of this period, all hydrogel compositions with a 200:10:1 ratio, as well as most (except for 8 and 10 mg/mL) hydrogels using a 100:10:1 crosslinking ratio, reach a total network length in the 20,000–40,000 pixels range. Similar results are obtained when quantifying HUVEC networks, further reinforcing the suitability of the MVEC line for endothelial research.

However, it is noteworthy that despite controls being associated with total network lengths in the higher end of the range, they become extremely fragmented by the end of the period, unlike the networks embedded within 3D hydrogel constructs. This highlights the critical role of 3D scaffolds in maintaining long term network integrity. Relying solely on total network length to determine the optimal hydrogel composition has limitations. Additional insights should be derived from other parameters used to characterise the network architecture, which will be addressed in future work. Further work exploring particular pairings of crosslinking ratios and media will enable further refinement of the hydrogel composition.

5.3.3.3 Impact of Variations in Medium

Having refined the fibrinogen concentration (6, 8 & 10 mg/mL), the next step was to investigate the optimal pairings with different crosslinking ratios (100:10:1 or 200:10:1) and medium (EBM, EBM + VEGF, or PBS). Over a 24 h period, the number of segments and total network length (Figures 5.7 & E.12) were quantified.

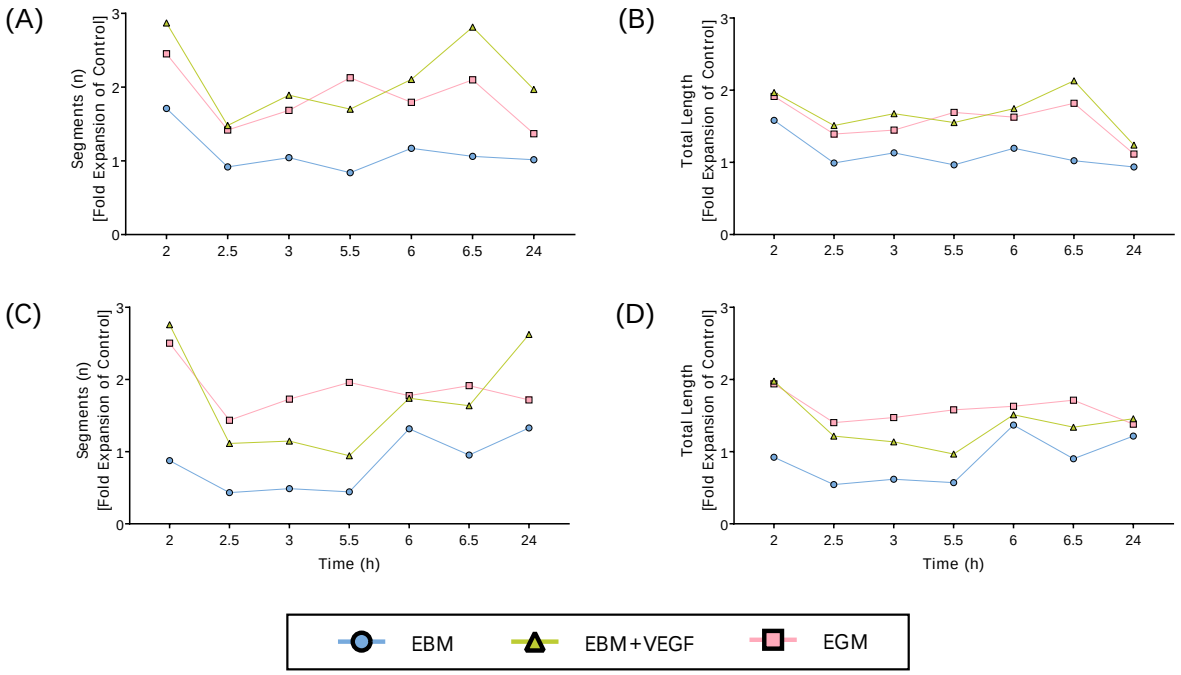


Figure 5.7: **Impact of variations in medium and crosslinking ratio on microvascular endothelial network architecture. (A, C)** Number of segments and **(B, D)** total MVEC network length by medium and crosslinking ratio (fibrinogen : thrombin : $CaCl_2$) during a 24 h period, as a fold expansion of their respective controls. Hydrogels were created using fibrinogen from human serum at a concentration of 10 mg/mL in different media (EBM, EBM + VEGF, or PBS) and a crosslinking ratio of either **(A, B)** 200:10:1 or **(C, D)** 100:10:1. MVECs were cultured with EGM and seeded at a density of 2×10^4 cells/well (96–well plate). Cells-only controls were used. (ANOVA/Tukey's HSD; $p \leq 0.05$; $n = 12$).

EBM hydrogels are associated with a lower number of segments than their EBM + VEGF and PBS counterparts, but this was not statistically significant. This trend was particularly noticeable in higher fibrinogen

concentrations and, even more so, in the 200:10:1 crosslinking ratio. Within the same medium, there are no significant differences between crosslinking ratios, although the data distribution appeared to be slightly higher for the 200:10:1 ratio. The addition of VEGF to the medium did not consistently yield significant improvements in network stability, suggesting that EBM may be preferable for simplicity and reproducibility.

Within the same hydrogel composition, the number of segments remains relatively stable, except at the 24 h time point, where a decrease was observed in all hydrogel formulations. This could potentially be attributed to either the growth of each individual segment or to partial network disintegration.

In terms of total network length, EBM hydrogels displayed less variation across ratios and fibrinogen concentrations compared to EBM + VEGF and PBS hydrogels. The 8 mg/mL concentration in both ratios showed an interesting pattern, forming the largest network in the EBM group at most time points, but with a noticeable decrease at 24 h. A similar pattern was observed in the 10 mg/mL EBM + VEGF hydrogel and four of the PBS hydrogels (8 and 10 mg/mL for both ratios).

Interestingly, lower concentrations of 100:10:1 EBM + VEGF hydrogels exhibited an interesting progression, with total network length decreasing up to 5.5 h, followed by a steady increase until 24 h. The control also exhibits a different pattern, remaining relatively stable throughout the entire period.

5.3.4 Material Characterisation

Material characterisation provided insights into the impact of hydrogel composition on polymerisation dynamics and mechanical properties. This included analysing gelation time, spectrophotometry, microrheology (Figure 5.8) and hydrogel degradation (Figure 5.9). This approach was conducted to better understand how modifications in the hydrogel composition influence microvascular network formation and integrity, as well as to allow the fine tuning of the scaffold to better replicate tissue-specific microenvironments. For example, it could be tailored to simulate soft tissues like skeletal muscle, creating a more relevant and accurate model.

5.3.4.1 Gelation Time

Investigating the role played by gelation time is relevant for TE constructs given its impact on the overall structural and functional properties, mechanical stability [607], cell viability [608] and vascular network formation [609]. Gelation time is also key to ensure optimal cell distribution by balancing sufficient gelation time to allow for uniform cell distribution and avoiding cell aggregation and uneven cell densities.

Higher fibrinogen concentrations significantly reduced gelation times (Figure 5.8A). For example, a five–fold increase in human fibrinogen concentration (EBM hydrogels) decreased gelation time by 1.84–fold (Figure 5.8A). Additionally, gelation times were influenced by the fibrinogen source and medium. For instance, human fibrinogen hydrogels gelled slower than bovine ones at the same concentration; while EBM significantly decreases gelation times compared to PBS but significantly increases it compared to EGM when using the same medium (Figure 5.8B).

The increase in fibrinogen concentration in hydrogels of the same fibrinogen source and medium results in shorter gelation times. As exemplified by EBM hydrogels with human fibrinogen, a fivefold increase in fibrinogen concentration is associated with a 1.84–fold decrease in gelation time.

Maintaining the fibrinogen concentration unchanged (10 mg/mL; Figure 5.8B), we observe that when using human fibrinogen and the same medium (EBM, EGM or PBS), gelation times decrease in comparison with hydrogels made with bovine fibrinogen. The medium also plays a role in gelation times. For instance, within the same fibrinogen concentration (10 mg/mL) and source (bovine), PBS hydrogels have significantly longer gelation times compared to EBM, whereas EBM hydrogels exhibit significantly longer gelation times EGM hydrogels.

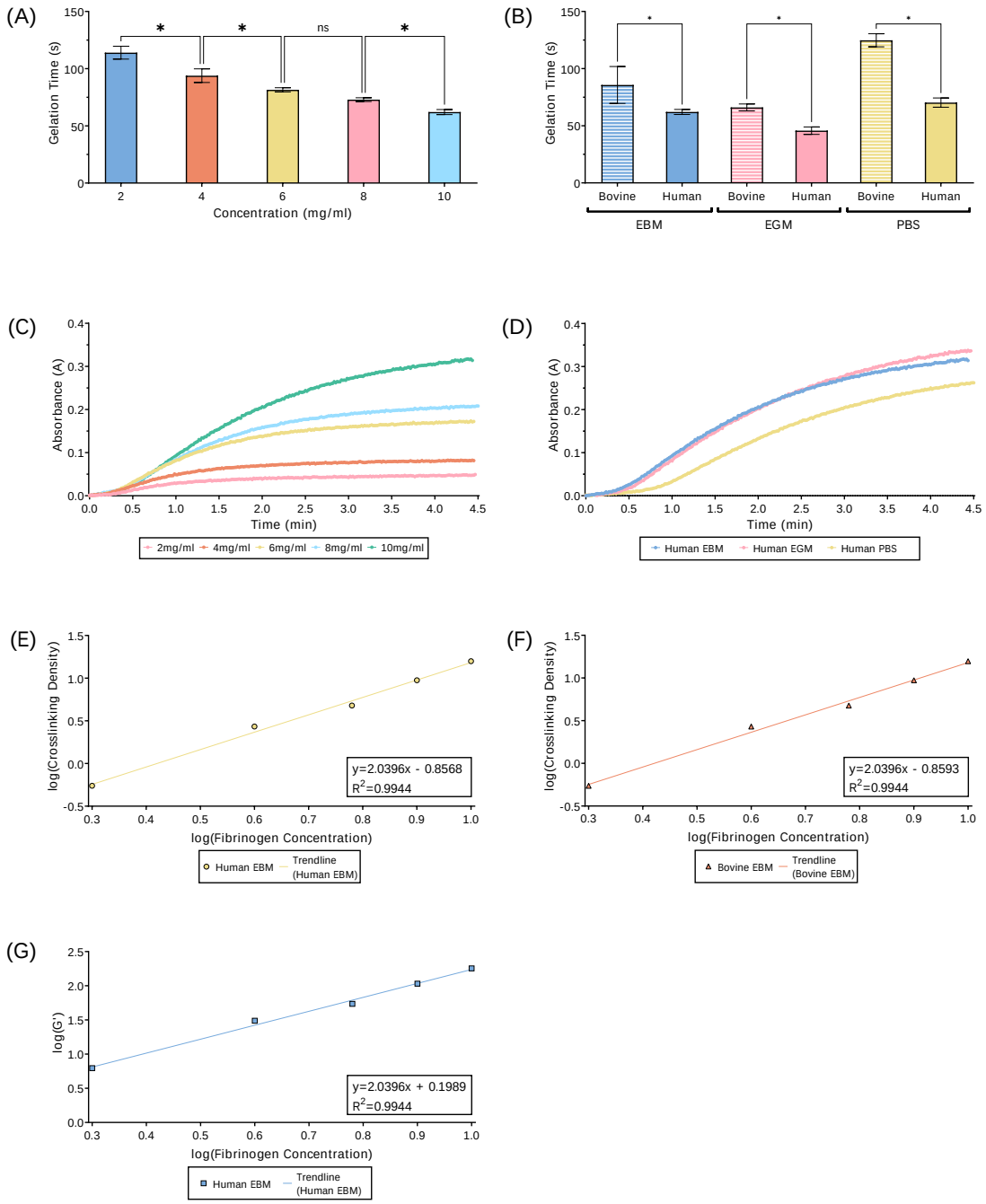


Figure 5.8: **Material characterisation of the 3D hydrogel constructs**, depicting **(A, B)** gelation time, **(C, D)** spectrophotometry, and **(E - G)** microrheology and crosslink density. Average gelation times (s) by hydrogel. **(A)** EBM hydrogels created with different concentrations of human fibrinogen. **(B)** Hydrogels with the same fibrinogen concentration (10 mg/mL) but using different media (EBM, EGM or PBS) or fibrinogen source (bovine or human). Error bars indicate standard deviation. (ANOVA/Tukey's HSD and 2-way ANOVA/Tukey's HSD; $p \leq 0.05$; $n = 5$). Spectrophotometry absorbance plots showing the normalised change in 340 nm light absorbance for 4.5 min. **(C)** EBM hydrogels created with human fibrinogen at different concentrations. **(D)** Human fibrin hydrogels (10 mg/mL) created with EBM, EGM or PBS. ($n = 9$). **(E, F)** Crosslinking density of hydrogel dependence on fibrinogen concentration and **(G)** storage modulus (G') of hydrogels crafted with either **(E, G)** human or **(F)** bovine fibrinogen. From the data points, trend lines were plotted and their equation and goodness of fit (R^2) were obtained. The concentration dependence was found using the method of least squares with upper and lower-bound values.

5.3.4.2 Spectrophotometry

Spectrophotometry provided valuable quantitative information on hydrogel formation and gelation kinetics [610], including concentration profiles [611]. Similarly to gelation times, spectrophotometry data can be used to inform hydrogel formulation to achieve uniform cell density throughout the construct. Here, we measured the normalised change in 340 nm absorbance during 4.5 min (Figure 5.8C & D) and up to 20 min (Figure E.13).

Data from human fibrin EBM hydrogels revealed that increasing fibrinogen concentration led to greater absorbance, especially from 1 min onwards. The differences between hydrogel concentrations became more pronounced over time, with an average absorbance difference of 0.2662 between 2 and 10 mg/mL at 4.5 min (6.58–fold increase). High fibrinogen concentrations also exhibited a greater rate of change in absorbance (dA/dt), whereas lower concentrations showed a noticeably smaller rate of change, particularly after 2 min. The choice of medium also influenced absorbance. PBS consistently had lower absorbance compared with EBM or EGM hydrogels of the same concentration and fibrinogen source. Interestingly, absorbance differences between EBM and EGM hydrogels were minimal until 2.5 min, after which the rate of change increased, particularly after 5 min (Figure E.13).

Turbidity measurements of fibrin gels provided estimates of the mass per unit length of fibrils in the hydrogel [612], allowing for approximation of fibre size and density based on the incident light wavelength measured [613]. Greater turbidity, reflected by higher absorbance, indicates a greater mass per unit length of fibrils and a denser gel structure.

Both gelation times and spectrophotometry provide insights into the polymerisation dynamics of hydrogels, which influence their microstructure and material properties. As reported by Allan [583], increasing fibrinogen concentrations enhances network development, as supported by the shortened gelation times and increased rates of absorbance with time observed here. Thus, hydrogels with higher fibrinogen concentrations were denser at any time point, aligning with Carr's findings that using higher concentrations shortens the time to reach the critical gelation point and, therefore, have a shortened gelation time [612].

Regarding network formation, the increased absorbance rate in higher fibrinogen concentrations may be attributed to an elevated monomer supply rate [583]. Since thrombin volume remained unchanged across all formulations, these results suggest that the reaction rate in these hydrogel formulations is not limited by thrombin availability.

5.3.4.3 Pendant Drop

The interfacial tension of fibrin EBM hydrogel at three time points (pre-gelation; < 5 min into gelation; and < 15 min into gelation) and of two controls (deionised water and EBM) were obtained (Figure E.15).

The calculated interfacial tension values reveal that there are no statistically significant differences between deionised water, EBM and the un-gelled fibrin hydrogel solution (all $p > 0.05$). However, once gelation starts, there are significant differences in interfacial tension, which increases over time. Specifically, the 6–15 min into gelation group exhibited a 1.63–fold increase compared with the 0–5 min into gelation group ($p < 0.0001$) and a 2.16–fold increase compared with the pre-gelation group ($p < 0.0001$). It is also relevant to highlight that as time progresses, the droplet shape evolves from spherical to pear-shaped. Relevantly, relying on the droplet profile demands a trade-off between surface tension and hydrostatic pressure, which favour spherical or pear-shaped profiles, respectively [614, 615].

Here, samples exhibited more spherical profiles, thus indicating an increase in surface tension. However, our results differ from the interfacial tension of fibrinogen at 10 mg/mL reported by Benning [394] to be 63.93 mN/m, which is a 4.67 fold increase compared with the pre-gelation fibrinogen. However, the value obtained for water was 72.8 mN/m [394], a 4.93 fold increase compared to the interfacial tension measured in this

research. When comparing the surface tension of fibrinogen against that of water in each study, the findings are similar: the values for water were 1.08 or 1.13 times greater than those for fibrinogen in this research and Benning's, respectively. Taking this into account, it is likely that the variation in tension values obtained in the two research studies could rather be due to systematic variations and, by taking this into account, should not affect the comparability of the results. it seems that the variation between the tension measured here and the one reported in that study could rather be systematic variations and should not affect the comparability of the results.

5.3.4.4 Microrheology and Crosslink Density

Fibrinogen concentration emerged as the primary factor driving changes in the storage modulus and crosslinking density, displaying a positive relation with their logarithmic values (Figure 5.8E-G). Crosslink density calculations used the following values: polymer density for fibrinogen [616]: 1.395 g/cm^3; molecular weight: 340 kDa (bovine fibrinogen [616]) and 342 kDa (human fibrinogen [617]); and G' at 100 rad/s as an approximation to the plateau value.

Microrheology characterisation revealed similar findings, with fibrinogen concentration having the greatest impact, followed by the fibrinogen source. The storage modulus (G'), loss modulus (G"), complex shear modulus (G*), complex viscosity (η*) and creep compliance 1 h after gelation were obtained for hydrogels with varying fibrinogen concentrations and hydrogels with a 10 mg/mL fibrinogen concentration of bovine or human source (Figure E.14).

Increasing fibrinogen concentration significantly impacted the microrheological properties, leading to higher G', G" and complex viscosity while decreasing creep compliance. For example, at 100 rad/s, an increase in fibrinogen concentration from 2 to 10 mg/mL resulted in a 29–fold rise in G', an 8–fold rise in G", an 18.7–fold rise in complex viscosity and a 27–fold reduction in creep compliance.

Hydrogels created with different media but at the same fibrinogen concentration (10 mg/mL) displayed similar trends across parameters, with some medium-dependent differences. For instance, PBS paired with human fibrinogen exhibited a lower G" minimum than its bovine counterparts. EGM hydrogels displayed a slight increase (≤10%) in G', G" and complex viscosity and a decrease in creep compliance compared to EBM hydrogels. After 24 h, PBS hydrogels were the only medium variation displaying statistically significant differences in the parameters: increase in G', G" and complex viscosity, and decrease in creep compliance.

The fibrinogen source also influenced microrheological properties, with bovine and human fibrinogen exhibiting similar trends in G*, complex viscosity and creep compliance. However, differences were observed at extreme high and low frequencies for G' and G". In EBM hydrogels with the same fibrinogen concentration, bovine fibrinogen produced a slight increase in G' (≤ 10%), a decrease in G", and an increase in complex viscosity and creep compliance compared to human fibrinogen. PBS hydrogels also exhibit some differences when comparing different fibrinogen sources: lower G' and G", higher complex viscosity, but similar creep compliance.

After 24 h, the microrheological properties of the hydrogels exhibited subtle changes. EBM hydrogels with bovine fibrinogen showed higher G', G" and compliance but lower viscosity compared to human fibrinogen hydrogels. Conversely, PBS hydrogels exhibited higher G' and G" with bovine fibrinogen, but unlike EBM hydrogels, displayed increased viscosity and reduced creep compliance relative to human fibrinogen.

5.3.4.5 Shear

Image analysis of sheared and unsheared hydrogels (Figure E.16) revealed that the macroscopic dendrites of sheared samples were formed in the direction of the applied shear. Alignment quantification suggests

that there is an increased intensity between -45 and -80°, with the centre of the Gaussian function at -65.91° (sheared) or -71.587° (unsheared). The dispersion, which reflects the standard deviation of the Gaussian, highlights the smaller variability in sheared samples (24.870°) compared to unsheared ones (47.823°). In contrast with the sheared samples, the dendrites of unsheared hydrogels do not depict an aligned pattern and exhibit a lower range in intensities with direction, distributed evenly. Aligned structures have an increased strength and stiffness along the direction of alignment, which could be useful in the development of constructs where greater strength is desired without the need to further alter the hydrogel composition.

Alignment of macroscopic dendrites was observed under shear, which is consistent with the literature [618]. Dendritic alignment suggests that the application of a shear force leads to a favourable growth direction in crystallographic terms. It is important to highlight that fibrin alignment can direct cell growth [619] and promote direct cell infiltration along an aligned structure [223, 620], which could enable the development of TE constructs for tissues displaying an aligned morphology, such as skeletal muscle, or for tissues requiring the formation of perfusable inlet and outlet sites, as blood vessels.

It's worth mentioning that the *amount* value used in this model underestimates the real proportion of structures that display the preferred orientation. Therefore, the proportion of dendrites that are oriented around a specific value is at least the amount value (*e.g.* in the sheared sample, at least 19% of the dendrites are oriented around -65°).

Visual inspection of the hydrogel dendrites further confirms that these grow alongside the direction of the applied shear whereas those in the control samples depict a random orientation. Interestingly, dendrites were only observed in thin samples, for example those thinner than 1 mm, such as samples mounted on microscope slides. This could potentially be attributed to faster cooling rates, arising from their high surface-area-to-volume ratio. Moreover, in these cases, gelation could be comparable to crystallisation where a nucleation site occurs from the first polymerisation event and then an interface is created. Primary dendrites appear to form with lengths on the centimetre scale, while the dimensions of secondary dendrites range in the millimetre scale (Figure E.17).

5.3.4.6 Hydrogel Degradation

Hydrogel scaffold degradation was monitored over 14 days (Figure 5.9), with 96.67% of samples fully degrading by the end of the period. Only three bovine and one human fibrin hydrogels in EBM did not entirely degrade, but their mass significantly decreased to 1.72–13.81% of their initial values.

Data analysis tested linear, exponential and polynomial trend lines were trialled to describe degradation patterns. The second order polynomial fit provided the highest R^2 value across all samples, significantly outperforming linear fits. This indicates faster degradation in the initial days, followed by slower degradation rates towards the end of the period. Here, the exponential degradation curves suggest hydrolysis as the likely degradation mechanism. Further experimental work conducted at shorter intervals and with an increased number of repeats are required to confirm this.

Lower fibrinogen concentrations generally degraded faster, with some exceptions. For instance, 10 mg/mL human fibrinogen in EBM and in EGM hydrogels degraded faster than 6 and 8 mg/mL. Across the same fibrinogen source, hydrogels with EBM + VEGF or PBS degraded faster than those with EBM or EGM. In most cases, human fibrin hydrogels degraded slower than their bovine counterparts, particularly in EGM and PBS.

These findings align with the literature, showing that mass, including of fibrin samples, decreases by day 7 [394]. The degradation rate is crucial for TE constructs, balancing scaffold breakdown with cell growth. Rapid degradation can lead to the loss of mechanical attachment points for cells and, consequently, impairs cell growth. On the other hand, too slow degradation can lead to cell crowding and death [582].

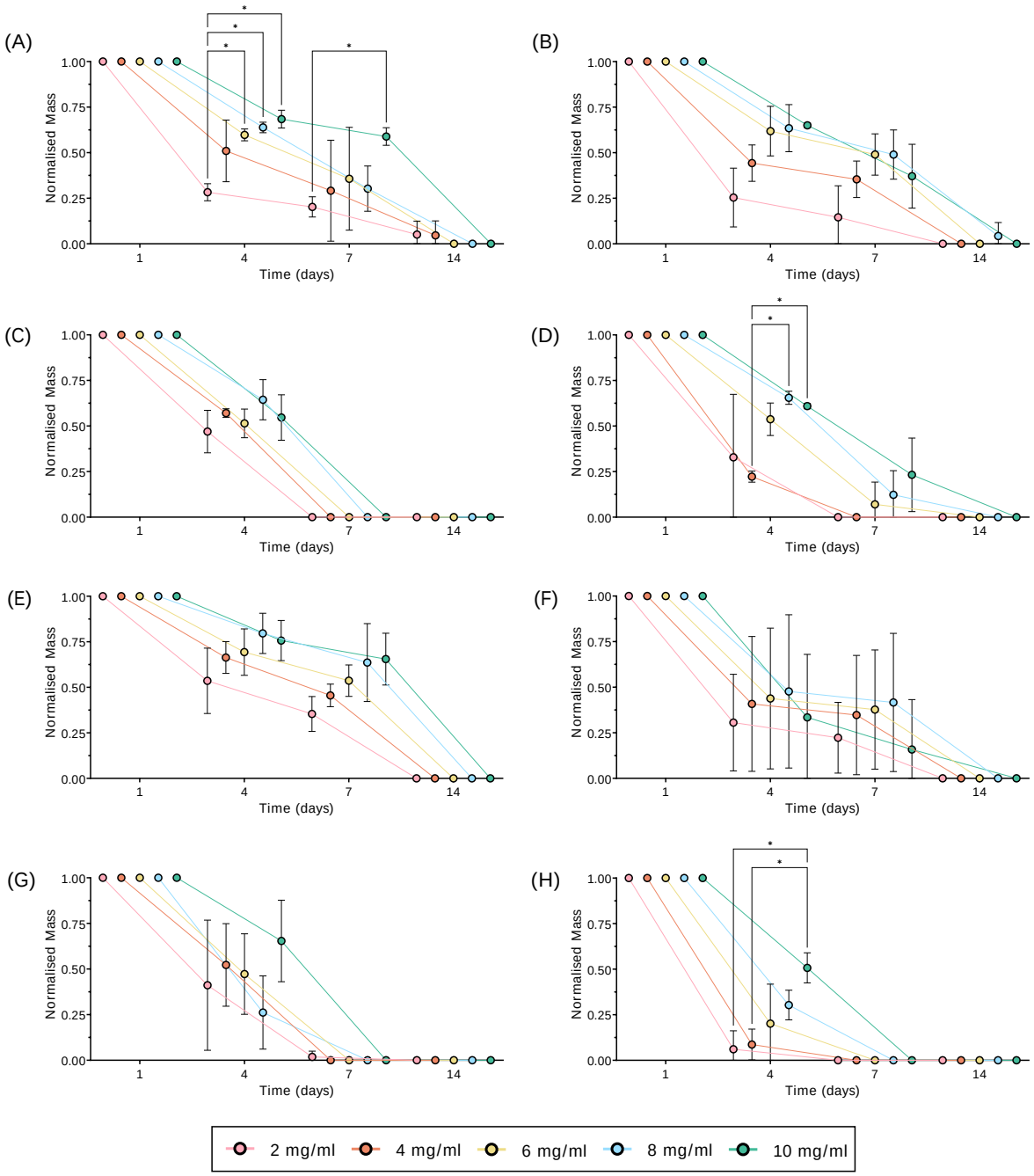


Figure 5.9: **Degradation of hydrogel scaffolds by fibrinogen source, concentration and medium during a period of 14 days.** Hydrogel scaffolds were created using fibrinogen from **(A, C, E, G)** bovine or **(B, D, F, H)** human serum in **(A, B)** EBM, **(C, D)** EBM + VEGF, **(E, F)** EGM, or **(G, H)** PBS. Each hydrogel scaffold was created by casting 100 µL of the hydrogel solution per well (96–well). Data are presented in an interleaved format to improve visual clarity. The horizontal offsets do not represent different sampling times; all datasets were collected at the same four time points. (Two-way ANOVA/Tukey's HSD; $^*p \leq 0.05$; only statistically significant differences are shown; $n = 3$).

Our experimental results indicate that higher fibrinogen concentrations degrade more slowly. Similar findings have been reported and could be attributed to increased crosslinking density and mechanical strength, which have greater resistance to enzymatic degradation [227]. Degradation rates also vary across media, influenced by solubility, structural integrity, β-chain crosslinking and interaction with proteins and organic

molecules [621]. As such, modifying the fibrinogen concentration and, to a lesser extent, changing the media impact the degradation rate.

These factors underscore the importance of fibrinogen's biochemical properties and crosslinking mechanisms in determining scaffold stability and degradation behaviour. Fibrinogen crosslinks with thrombin through thrombin-mediated proteolytic cleavage, forming protofibres and mature fibres that grant both biochemical and mechanical stability [374]. Therefore, the crosslinking mechanism that the fibrin hydrogels undergo enables the scaffolds to display good stability, which is paramount for long term TE applications. Our results suggest that hydrogels with higher fibrinogen concentrations in EBM, EBM + VEGF (human fibrinogen only) and EGM degrade more slowly, making them better candidates for microvascular constructs by maintaining a stable mechanical support structure for embedded cells.

5.3.5 Developing a Microvascular Construct for Long-term Network Integrity

Considering that fibrinogen from both bovine and human plasma source can produce 3D hydrogel scaffolds that enable endothelial network formation, human fibrinogen was selected to preserve species specificity with the cell line. Hydrogels embedded with MVECs were evaluated over 13 days (Figure 5.10) to gain further insights into capillary-like network development and architecture. Embedding MVECs into 3D scaffolds supported long-term network stability and enabled shape retention for at least 13 days post-seeding (Figure 5.10G), demonstrating usability well beyond the 18–24 h period of standard HUVEC-based models [298, 299, 574, 575].

The microvascular networks were imaged and characterised over 53 h (Figures 5.10A & B and E.18), showing that hydrogel constructs sustained a stable network after the first 11 h. Networks in hydrogels showed an increase in the number of segments and total network length unlike the controls, which exhibited network degradation from 24 h onwards. Notably, network formation and disintegration occurred more rapidly in the absence of hydrogels, which could potentially suggest that both of these processes happen at an accelerated pace when there are no 3D structures supporting the endothelial networks, highlighting their role in supporting durable networks.

The trends exhibited in the number of segments and the total network length are remarkably similar, suggesting that the increasing segment count reflects network growth rather than disintegration into independent segments. At the last time point, all hydrogel constructs supported longer microvascular networks and with more segments than the controls, with one exception (2 mg/mL EBM hydrogel). This may result from the natural progression of network formation followed by fragmentation [289], as exhibited by both HUVECs and MVECs. As previously observed and further supported by the literature [289, 298, 299, 575], HUVEC networks disintegrate towards the end of the first 24 h when unsupported by a scaffold. Similarly, MVECs undergo the same process later, leading to network breakage by day 2.

In EBM hydrogels, segment numbers stabilised after 11 h, with higher fibrinogen concentrations associated with longer networks and more segments. A similar trend was observed in EBM + VEGF hydrogels, though more clearly at 53 h. Within this group, the 10 mg/mL concentration produced the longest network and the greatest number of segments, except at 3.5 h. This suggests that this hydrogel composition is particularly well-suited for microvascular network formation and growth. Furthermore, EGM constructs exhibited more consistent behaviour across different fibrinogen concentrations, particularly within the initial 24 h, compared to EBM or EBM + VEGF hydrogels.

VEGF, known to upregulate endothelial nitric oxide synthase production, is crucial for regulating and maintaining healthy vasculature, and can aid in limiting tissue injury [622]. Additionally, VEGF has demonstrated significant protective effects, including improved endothelial preservation, survival time prolongation and in-

creased survival rates [623]. These findings align with the experimental results, suggesting that the use of EBM + VEGF as a medium in hydrogel constructs may enhance the long-term integrity of microvascular networks.

Longer term network characterisation (Figures 5.10C & D and E.19) further highlighted the essential role of 3D scaffolds. Controls exhibited significantly lower segment numbers and shorter network lengths compared to EBM and EBM + VEGF hydrogels. EGM hydrogels, on the other hand, produced poorer results than the hydrogels created with other media. EBM and EBM + VEGF performed comparably, supporting longer networks than EGM scaffolds. For both EBM and EBM + VEGF, higher fibrinogen concentrations generally produced longer networks, though increasing concentrations beyond 6 mg/mL yielded no significant additional benefit in network architecture.

Networks were monitored for up to 13 days to assess stability (Figures 5.10E & F and E.20). The controls, as expected, exhibited a noticeable decrease of network length from day 4 to day 13, likely due to insufficient mechanical support for 3D network development. While hydrogels also showed some reduction in network length, the effect was significantly less pronounced.

PBS hydrogels proved suboptimal for network preservation, as total network length remained relatively stable between days 6 and 13, but was consistently lower than other hydrogel groups. This may be attributed to the absence of specific EBM components necessary for a conducive microvascular environment, beyond the media used to culture the cell-embedded hydrogels.

Both EBM and EBM + VEGF hydrogels supported more stable MVEC networks. Despite a noticeable network length reduction from day 4 to day 6, three fibrinogen concentrations at 200:10:1 ratio of EBM hydrogels remain at similar lengths until the end of the period. Interestingly, the 6 mg/mL concentration in EBM and EBM + VEGF at 100:10:1 hydrogels showed a unique trend: an initial reduction in length followed by an increase between days 6 and 14, which was significant only in the EBM + VEGF hydrogels.

Finally, the 8 and 10 mg/mL concentrations at 100:10:1 ratio of EBM and EBM + VEGF maintained relatively stable networks up to day 7 (EBM) or day 14 (EBM + VEGF). This suggests that higher fibrinogen concentrations combined with a 200:10:1 crosslinking ratio produced the most robust networks and thus provide a more suitable 3D environment for long-term microvascular network stability.

The stability of MVEC-based constructs observed over 13 days correlates with findings that hydrogel scaffolds with optimised stiffness and biochemical cues can support endothelial functionality [624]. This is a key consideration for trauma models, where long-term observations of microvascular injury and repair processes are critical.

Based on the results, five compositions emerged as the best candidates for forming the longest networks and with the best integrity preservation at 4–, 5– and 6–days post-seeding. Interestingly, these were the highest fibrinogen concentrations in EBM (6, 8 and 10 mg/mL) and EBM + VEGF (8 and 10 mg/mL). These hydrogels shared similar architecture between them, making them the most promising candidates for developing microvascular constructs.

It can be argued that, since EBM + VEGF hydrogels did not demonstrate significant advantages in preserving network integrity compared to EBM hydrogels, the latter may be preferable for developing 3D microvascular constructs due to their comparable performance and simpler formulation.

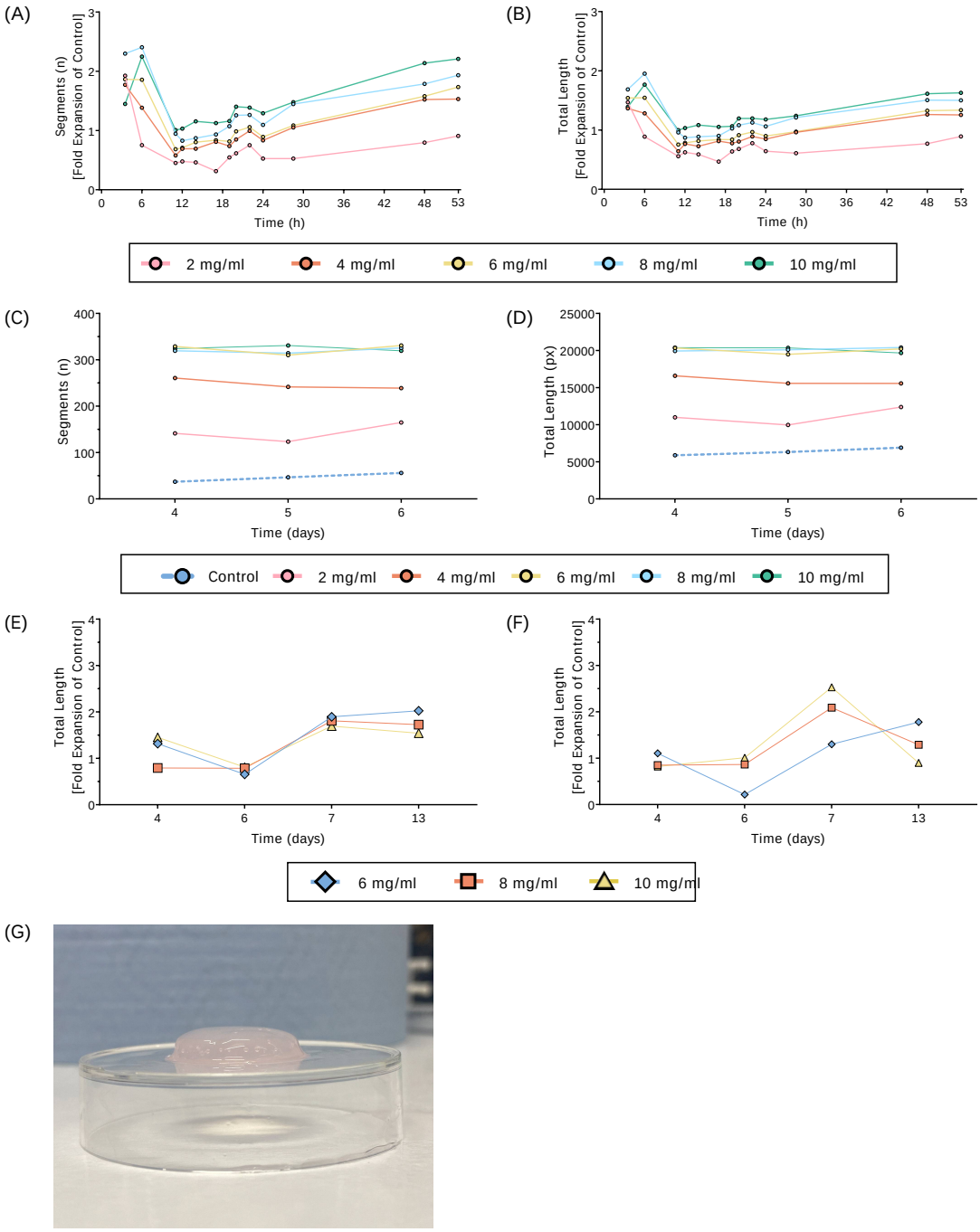


Figure 5.10: **Optimisation of a microvascular construct for long-term network integrity.** Characterisation of MVEC networks embedded in 3D hydrogel scaffolds, quantified throughout **(A, B)** 53 h, **(C, D)** 6 days and **(E, F)** 13 days depicting **(A, C)** number of segments and **(B, D–F)** total network length. Hydrogels were created using fibrinogen from human serum at different fibrinogen concentrations (2–10 mg/mL), EBM and crosslinked at **(A–E)** 200:10:1 or **(F)** 100:10:1 ratio (fibrinogen : thrombin : $CaCl_2$). The data from EBM hydrogels is shown here, while the data related to EBM + VEGF and EGM hydrogels is available in Figures E.18, E.19 & E.20. MVECs were cultured with EGM until hydrogel casting, after which they were cultured with EBM. Cells were seeded at a density of 1.5×10^4 cells/well (48–well plate); **(C, D)** 5.25×10^4 cells/well (24–well plate); or **(E, F)** 2×10^4 cells/well (96–well plate). Cells-only controls were used. **(A, B)** (ANOVA/Tukey's HSD; $p \leq 0.05$; $n = 30$); **(C, D)** (ANOVA/Tukey's HSD; $p \leq 0.05$; seven random images per sample, $n = 15$); **(E, F)** (ANOVA/Dunnett; $p \leq 0.05$; $n = 6$). **(G)** Photograph of 3D construct captured at 13 days after seeding. Here shown is an EBM hydrogel created with human fibrinogen at a concentration of 10 mg/mL and crosslinked at a ratio of 200:10:1 (fibrinogen : thrombin : $CaCl_2$).

5.3.6 Impact of Hydrogel Composition on Network Architecture and Material Characteristics: Key Results

Based on the experimental results obtained in this research, a summary table (Table 5.2) was created to outline the impact of the different elements of the hydrogel composition, such as medium, fibrinogen concentration, source and the fibrinogen : thrombin : $CaCl_2$ crosslinking ratio, on both material properties and network architecture.

Aspect	Impact on Network Architecture	Impact on Material Characteristics
Medium	• EBM vs. MES/NaCl: – Longer networks; – More segments, branches and junctions; – Higher branching interval; – Better network integrity at 3 and 4 days post-seeding. • EBM vs. EGM: – Greater total network length. • EBM vs. EBM + VEGF and PBS: – Less variability in total network length across ratios and fibrinogen concentrations. • EBM & EBM + VEGF vs. EGM: – More segments. – Greater total network length at 4, 5 and 6 days post-seeding. • EBM & EBM + VEGF: – When paired with high fibrinogen concentrations, can preserve network integrity for up to 13 days post-seeding.	• PBS vs. EBM: – Longer gelation times. – Lower absorbance (in human fibrin hydrogels). – Faster degradation. • EBM vs. EGM: – Longer gelation times. – Greater absorbance of human fibrin hydrogels (≤ 3 min). – Hydrogels are slightly softer, more flexible, more easily deformable and have a lower resistance to shear forces. – Lower G', G" and complex viscosity paired with a higher creep compliance, indicating that the hydrogels are slightly softer, more flexible, more easily deformable and have a lower resistance to shear forces • PBS vs. EGM: – Lower absorbance (in human fibrin hydrogels). – Faster degradation. • PBS: – Faster gelation. – Hydrogels are more viscous. • EBM + VEGF: – Faster degradation than EBM or EGM hydrogels.
Fibrinogen Concentration	• Higher fibrinogen concentration: – Greater total network length.	• Higher fibrinogen concentration: – Faster rate of fibrin network development: a 5× increase in concentration leads to 1.84× decrease in gelation time. – Denser hydrogels. – The deformation response is stiffer and more elastic: 5× increase in concentration leads to a 29× increase in G'. – Slower degradation rate.
Fibrinogen Source	• Both bovine and human fibrinogen enable the formation of endothelial networks. • Pairing human fibrinogen with human cells permits species compatibility between the construct components, which can lead to a more physiologically relevant construct with enhanced biocompatibility.	• Bovine vs. Human Fibrinogen: – Longer gelation times. – Faster degradation. – Hydrogels exhibit similar microrheology patterns, except for G' and G" at extreme high and extreme low frequencies. – Paired with PBS, results in less rigid and more viscous hydrogels. – Paired with EBM, has enhanced mechanical stability and greater strength.
Crosslinking Ratio (Fibrinogen : Thrombin : $CaCl_2$)	• 200:10:1 vs. 100:10:1 ratios: – Greater number of segments. – Longer networks.	• 200:10:1 vs. 100:10:1 ratios: – Slower gelation.

Table 5.2: **Summary of the impact on microvascular endothelial cell (MVEC) network architecture and material characteristics of variations in the hydrogel composition.**

5.4 Conclusion

The microvascular construct developed here aims to provide a more physiologically relevant model for trauma research, featuring a 3D structure, microvascular cells and long-term endothelial network integrity. MVECs can create more durable endothelial networks than HUVECs, which are often considered the gold standard. When embedded in a 3D hydrogel construct, MVECs can form extensive and complex networks that are stable for a prolonged period of time, making these constructs a promising model for traumatic injury research.

Modifications to the hydrogel composition — specifically the source and concentration of fibrinogen, the crosslinking ratio and the medium — affect the material properties of the scaffold, the network architecture and its long-term integrity. Through optimisation, it was found that hydrogels using human serum-derived fibrinogen at higher concentrations (≥ 6 mg/mL), crosslinked at a ratio of 200:10:1 (fibrinogen : thrombin : $CaCl_2$) and using EBM as the medium are particularly well suited for maintaining the stability of microvascular endothelial networks. In the long term, these compositions exhibited slower degradation rates, shorter gelation times, enabled longer networks with more segments and branches, and maintained network integrity for at least 13 days post-seeding.

Further work including immunofluorescence staining of the microvascular constructs would be beneficial to further validate the microvascular phenotype, for example with CD36, as well as advanced characterisation of 3D vascular networks using confocal microscopy. It would also be useful to monitor the evolution of material properties during gelation to help gain a further understanding of the mechanical properties of the hydrogel scaffolds as they are formed. Also, material characterisation of cell-embedded hydrogels would be valuable to assess the impact of cell loading and microvascular network formation on scaffold properties.

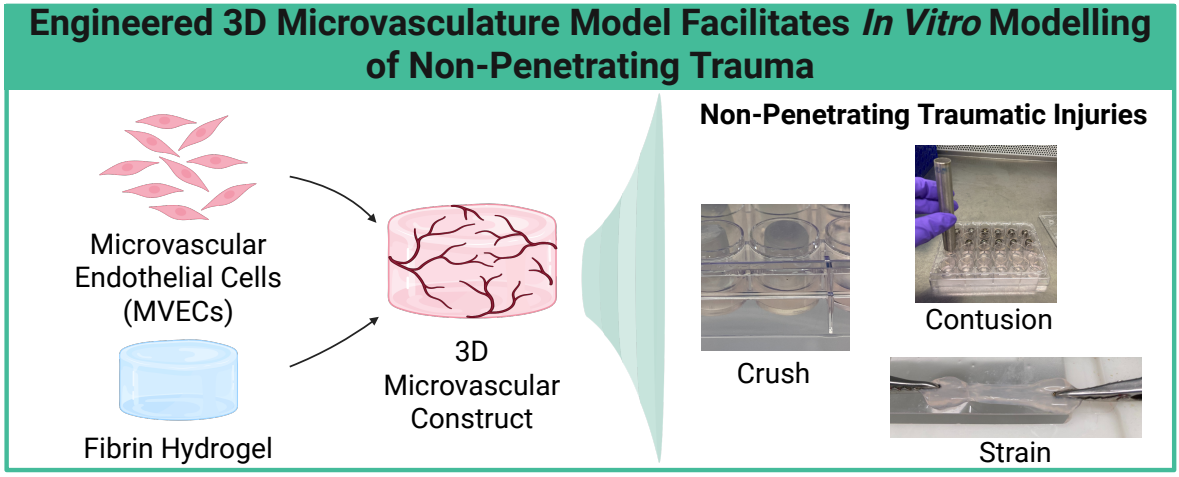
As for the applications of the 3D hydrogel construct embedded with a microvascular endothelial network developed here, future work will use this to study a range of traumatic injuries. In the long term, this microvascular construct could have applications beyond contributing to a further understanding of the mechanisms of trauma; for instance, by serving as a platform for testing potential therapeutics that target not only tissue repair and regeneration, but also help mitigate traumatic injury damage.

Acknowledgements

HUVECs and MVECs were generous gifts, kindly provided by Professor Sarah De Val & Dr Susann Bruche (Department of Physiology, Anatomy and Genetics, University of Oxford), and by Dr Helen Sheldon (Department of Oncology, University of Oxford), respectively.

Chapter 6

Modelling Non-Penetrating Traumatic Injuries in Engineered 3D Microvascular Constructs



Thesis Integration and Chapter Structure

Bringing together the findings of Chapters 3, 4 and 5, which together underpin the development and optimisation of the 3D microvascular model, this chapter addresses Objective 4 by demonstrating proof-of-concept for the application of the optimised model as an *in vitro* platform for non-penetrating traumatic injuries (NPTIs). Here, the optimised microvascular model is subjected to a range of well-defined mechanical inputs representative of NPTIs, enabling systematic investigation of the relationships between defined mechanical inputs and microvascular damage. Specifically, three types of NPTIs are explored here: crush (compression), contusion (blunt force trauma) and strain. These injury types are induced on cell-embedded and network-embedded hydrogel constructs. Injury responses are characterised through quantitative assessment of endothelial cell (EC) displacement and microvascular network architecture before and after injury. By systematically varying biomechanical parameters, such as drop height and loading duration, this chapter establishes clear links between mechanical insult conditions and measurable microvascular damage outcomes. Within the broader thesis framework, this chapter represents the culmination of the model development by applying the engineered 3D microvascular constructs to a trauma research context. In doing so, it validates the model as a reproducible and physiologically relevant platform for investigating microvascular responses to NPTIs and advances understanding of trauma mechanobiology.

A selection of the results presented in this chapter will be submitted as an original article to a peer-reviewed journal for consideration.

All experimental design, data analysis, visualisation and writing were conducted by Carla V. Fuenteslópez. All experimental work was performed by Carla V. Fuenteslópez, except for the strain-injury experiments for single-cell tracking, which were conducted by Lucy Taylor using 3D constructs prepared by Carla V. Fuenteslópez. The tensile loading device and the feature-tracking algorithms were developed by Lucy Taylor (development work not included in this manuscript). These tools were used by Lucy Taylor to perform the strain-injury experiments for single-cell tracking and by Carla V. Fuenteslópez to apply strain injury to 3D network-embedded constructs. The 3D container used in the resin biocompatibility assessment was co-developed by Carla V. Fuenteslópez and Alexander Witt. All other aspects of the biocompatibility assessment were performed exclusively by Carla V. Fuenteslópez. Prof Hua Ye and Prof Mark Thompson provided supervision and advice.

Modelling Non-Penetrating Traumatic Injuries in Engineered 3D Microvascular Constructs

Abstract

Non-penetrating traumatic injuries (NPTIs), such as crush, contusion and strain, are common in soft tissues and are a major contributor to morbidity and mortality, yet the early microvascular responses to these injuries remain poorly understood. This limitation arises in part from the lack of physiologically relevant, controllable and reproducible *in vitro* models that capture both the mechanical and biological components of trauma. Here, we present an engineered three-dimensional (3D) microvascular platform based on fibrin hydrogels embedded with human dermal microvascular endothelial cells (MVECs) to model NPTIs under well-defined mechanical conditions. Optimised 3D constructs supporting stable microvascular network formation were subjected to controlled crush (compression), contusion (drop-weight impact) and strain injuries. The severity of these insults was systematically varied by adjusting parameters such as compression depth, impact height and applied displacement. Injury responses were quantified through cell- and network-level analyses, including strain measurements, microvascular network characterisation and cell tracking. In parallel, conditioned media experiments were used to assess secondary, injury-mediated effects on endothelial cell (EC) behaviour. Together, these results demonstrate the use of the 3D microvascular model developed in this research as an *in vitro* platform for modelling NPTIs, enabling direct investigation of microvascular damage mechanisms while providing a foundation for mechanistic trauma research while reducing reliance on animal models.

Keywords

Non-Penetrating Traumatic Injury • 3D Microvascular Model • Fibrin Hydrogel • Endothelial Mechanobiology • *In Vitro* Trauma Modelling.

6.1 Introduction

Traumatic injuries remain a major global health challenge, substantially contributing to mortality, long-term disability and reduced quality of life across all age groups [3, 5, 9, 10]. Non-penetrating traumatic injuries (NPTIs), including contusions, crush injuries and strains, are particularly prevalent in road accidents, falls, sports and natural disasters [5, 8]. Although often non-fatal, NPTIs can cause extensive soft tissue and microvascular damage, leading to delayed recovery, systemic complications such as multiple-organ failure [2, 17, 18], and opportunistic infections [2, 9, 11, 12]. Moreover, NPTIs represent a disproportionate burden in low-resource settings [5, 7].

The response to trauma depends on injury severity and whether healthcare resources are readily available. While severe cases may require coordinated surgical and rehabilitative care [15], minor injuries often require minimal intervention. Emergency protocols, typically activated for severe trauma cases, prioritise life-saving procedures and often overlook microvascular damage which may initially appear minor [15, 16], but can deteriorate over time, leading to inflammation and systemic complications [17, 18]. Soft tissue trauma can disrupt tissue architecture and microcirculation, yet early mechanobiological events remain poorly understood [21, 23, 27].

Microvascular disruption exacerbates local tissue damage, impairs perfusion (*e.g.* oxygen and nutrient delivery, waste removal) and may trigger maladaptive inflammatory cascades leading to systemic failure [17, 18, 20]. The vasculature also regulates muscle regeneration *via* paracrine signalling and ECM remodelling [81, 99]. Thus, vascular dysfunction resulting from trauma, disease, or ageing compromises repair and function [24, 186]. However, NPTIs affecting soft tissues, such as skeletal muscle, and their microvasculature remain underexplored despite their significant impact on mobility and quality of life [10, 17–20].

Current trauma knowledge derives from a combination of clinical, epidemiological and experimental evidence [2, 14, 24, 26, 28, 199], with increasing use of mechanistic, model-based approaches [14, 24–26]. However, studying immediate biological injury responses in humans is difficult due to delayed presentation (often due to logistical, behavioural or diagnostic barriers), injury unpredictability and ethical limitations [22, 23, 27].

Clinical and epidemiological studies employ physiological and biochemical markers (*e.g.* creatine kinase, myoglobin, lactate dehydrogenase), inflammatory mediators (*e.g.* interleukin-6 (IL-6), C-reactive protein) and imaging (*e.g.* ultrasound, magnetic resonance imaging (MRI), computed tomography (CT)) to infer tissue damage, inflammation and repair processes [2, 182, 202], and to derive NPTI prevalence, mechanisms and outcomes across populations while identifying risk factors including age, occupation and activity [5]. However, these approaches remain largely retrospective and observational, offering limited mechanistic insight into the biological processes underlying injury progression and recovery.

To overcome these limitations, experimental models, especially *in vivo*, have been used to study NPTIs under controlled conditions. In particular, small animal models are frequently used [14] (*e.g.* rats [24, 28, 35, 199, 204, 205] and mice [28–30]), but larger models such as pigs [25, 31] and non-human primates [32, 33] are also employed. *In vivo* models have been used to study critical processes such as endothelial cell (EC) dysfunction, apoptosis, vascular leakage and inflammation [24–26, 34], but translation to humans is limited by interspecies differences, ethical concerns and reproducibility challenges [14, 36]. Consequently, there is a growing demand for physiologically relevant *in vitro* systems that enable precise, reproducible and ethically acceptable investigations of soft tissue trauma, offering lower cost, higher throughput and greater experimental control than *in vivo* approaches [36].

Experimental NPTI models enable controlled, reproducible and quantifiable simulation of mechanical and biological trauma and its consequences. Contusion models use weight-drop systems [204]; miniature, electromagnetic or pneumatic impactors [30, 208, 209]; or indenter devices to control impact energy and assess tissue disruption and response across *in vivo*, *ex vivo* and *in vitro* setups, including skeletal muscle, brain tissue and tissue-engineered constructs [35, 204, 208]. Modifying parameters (*e.g.* mass, drop height, geometry, impact velocity, depth, duration) allows for precise control over impact energy and injury severity, thus enabling quantitative evaluation of impact force, tissue deformation and cellular damage. As such, these models can produce reproducible tissue damage and enable systematic investigation of vascular disruption, inflammation and tissue regeneration [32, 33]. These setups have been used, for instance, with organotypic brain slices and engineered 3D cultures and tissues (*e.g.* human induced pluripotent stem cells; iPSCs) [30, 208, 209].

Crush or compression injuries are typically replicated *in vivo* and *ex vivo* using forceps (*e.g.* Martin's microsurgical forceps, Dumont forceps) [210, 211], clamps (*e.g.* non-serrated haemostatic forceps, mosquito forceps, Kelly straight clamp) [211, 212], clips (*e.g.* surgical clip, aneurysm clip) [205, 211] and presses or weights [213, 214] to apply controlled pressure for set durations [14, 26, 211]. Studies using presses or weights typically employ longer crushing durations, often exceeding 6 h [213, 214], whereas those using forceps, clamps or clips are generally applied over timescales of minutes. These models have revealed mechanisms such as ischaemia–reperfusion, necrosis and inflammatory progression [36, 211]. However, some approaches such as surgically exposing and compressing tissues with forceps introduce an element of penetrating trauma that is not fully representative of clinical crush injuries [119]. Motorised and mechanical compression systems have been de-

veloped to overcome these limitations, delivering uniform, reproducible forces that capture microstructural collapse and vascular failure [211, 212]. Examples include custom-made dead-lift devices [211, 212], material testing machines [216], water-hammer systems [217] and gel-based compression platforms [218], which have been used to apply static or dynamic compressive forces [36] to both *in vivo* and *in vitro* models.

Strain-based models reproduce deformation from stretching or torsion, commonly observed in musculoskeletal trauma and overuse injuries. These approaches employ bioreactors or flexible membranes to impose cyclic or static strain and include techniques such as fluid percussion, biaxial stretch, vacuum-driven deformation (*e.g.* Flexcell), and captive-bolt and blast injury systems [14, 35, 119, 220–222]. *In vitro*, strain has been applied using cell-injury controllers that deliver calibrated pulses of compressed gas to cultured cells, as well as custom-made devices [36].

Together, these NPTI models have advanced the understanding of trauma pathophysiology but have been mainly used in *in vivo* settings [210,211,213,214,219]. However, current *in vitro* systems often lack vascularisation, limiting physiological relevance and their capacity to more accurately reproduce the coupled mechanical and biological processes central to soft tissue injury and repair [36].

To address these limitations, researchers are increasingly utilising advanced *in vitro* models, particularly those relying on 3D cell cultures and tissues as well as organoids, which better mimic the complex architecture and mechanotransductive properties of human tissues [30, 208, 223]. Hydrogels fabricated from biomaterials have emerged as highly promising scaffolds for soft-tissue modelling due to their intrinsic biocompatibility and customisable physicochemical properties (*e.g.* stiffness, porosity, biodegradability), which can be tailored to mirror native tissue mechanics. Their viscoelastic nature allows deformation under load comparable to that of native soft tissues, making them simple and reproducible platforms for studying compressive and impact-induced injuries [223–225]. When engineered to mimic the ECM, hydrogels further enhance physiological relevance by supporting cellular adhesion, signalling and remodelling [225,226]. Among the biomaterials used to date, fibrin-based hydrogels are particularly advantageous: as a natural product of the coagulation cascade, fibrin promotes EC adhesion, migration and angiogenesis while enabling matrix remodelling and controlled biodegradation [227].

Developing *in vitro* trauma models that are both biologically and mechanically representative requires precise control over mechanical loading, scaffold architecture and culture stability. Long-term viability depends on optimising parameters such as cell seeding density, scaffold design and biochemical composition to sustain microvascular networks and preserve structural integrity during prolonged experiments. Such robustness is crucial for examining vascular morphogenesis, injury mechanisms and recovery dynamics over extended imaging and experimental periods.

Moreover, a central feature of physiologically relevant *in vitro* trauma models is the ability to support the formation of microvascular structures and networks. ECs seeded within fibrin matrices can self-assemble into capillary-like structures [397, 544], whose development, remodelling and disruption can be continuously monitored using live-cell imaging. These analyses can provide quantitative insights into how endothelial architecture evolves under varying mechanical and biochemical conditions and how vascular networks respond to controlled mechanical perturbations.

By subjecting 3D vascularised fibrin hydrogels to controlled mechanical perturbations, this research refines fibrin-based hydrogel constructs and establishes them as a platform for systematically investigating the immediate effects of contusion, crush and strain injuries on microvascular integrity. Specifically, it seeks to: (1) optimise 3D hydrogel geometry, seeding density and formulation to support long-term viability and vascular stability; (2) perform extended live-cell imaging and quantitative analyses to monitor endothelial network formation, maturation and disintegration; (3) apply controlled mechanical insults (*e.g.* contusion, crush, strain) to simulate clinically relevant NPTIs; and (4) evaluate injury responses by analysing construct integrity, cellular

morphology, cell tracking or vascular architecture before and after trauma.

6.2 Materials and Methods

6.2.1 Cell Culture

Immortalised human dermal microvascular endothelial cells (MVECs; ATCC; CRL–3243) [63] were cultured in T–75 and T–175 tissue culture flasks (Corning Incorporated-Life Sciences, Oneonta, NY, USA) with endothelial cell growth medium (EGM).

EGM was prepared by supplementing endothelial cell basal medium (EBM; Lonza, Walkersville, MD, USA) with Microvascular SingleQuots[1] (Lonza, Walkersville, MD, USA) and 1% penicillin–streptomycin (Gibco Life Technologies, Grand Island, NY, USA). Cells were cultured in a humidified incubator (37 °C, 5% CO_2; HERACell Vios 160i, Thermo Scientific, Germany) and medium was changed every 48–72 h, as required. Cells were used for experimental work upon reaching 80% confluence.

6.2.2 Hydrogel Fabrication

Hydrogels were prepared using fibrinogen from human plasma (Sigma-Life Science; St Louis, MO, USA) at a concentration of 10 mg/mL in EBM. The solution was stirred overnight using a magnetic stirrer and filtered twice using 0.22 µm filters (Merck Millipore Ltd., Ireland). Next, 100 µL of FBS (Bioclear, United Kingdom) and MVECs suspended in 267 µL of EBM at the required cell seeding density were added.

This mixture was then combined with thrombin (Sigma, St Louis, MO, USA; diluted to 10 U/mL in MES/NaCl buffer) and $CaCl_2$ (Sigma-Aldrich, St Louis, MO, USA; 1 M solution in distilled water) at a crosslinking ratio of 200:10:1 (fibrinogen : thrombin : $CaCl_2$). Finally, the hydrogel solution was thoroughly mixed and carefully cast to avoid bubble formation and ensure an even distribution across the well. Plates were incubated at 37 °C and 5% CO_2 to complete gelation. Once the hydrogels had gelled, EBM was added to each well for cell culture.

6.2.3 3D Hydrogel Construct Optimisation

Building on the findings of Chapter 5, the hydrogel construct was further refined by exploring the effect of foetal bovine serum (FBS) on hydrogel consistency (Section 6.2.3.1) and by optimising well size, hydrogel volume (Section 6.2.3.2) and cell seeding density (Section 6.2.3.3). In these three stages, hydrogels were visually inspected and categorised as ‘good’, ‘acceptable’ or ‘poor’ based on shape retention and overall structural consistency after demoulding.

6.2.3.1 Effect of FBS on MVECs and Hydrogel Consistency

To evaluate the influence of FBS supplementation in the formulation, hydrogels were prepared as described in Section 6.2.2, with and without FBS. In the hydrogels without FBS, the corresponding volume was substituted with EBM. MVECs were embedded into the hydrogels at different cell seeding densities (based on well surface area): 2.5×10^3, 1.75×10^4, 3.25×10^4 and 4.75×10^4 cells/cm^2. Hydrogels were fabricated by casting 500 µL per well (12–well plates). Cells were imaged 3 days after seeding using a light microscope (10× magnification) and microscopy images were used to assess cell morphology.

[1] Foetal bovine serum (FBS) 2%; hydrocortisone 0.04%; human fibroblast growth factor-basic (hFGF-b) 0.4%; vascular endothelial growth factor (VEGF) 0.1%; long R3 insulin-like growth factor-1 (R3-IGF-1) 0.1%; ascorbic acid 0.1%; human epidermal growth factor (hEGF) 0.1%; gentamicin sulfate-amphotericin (GA-1000) 0.1%

6.2.3.2 Hydrogel Size and Volume

To determine the influence of construct size on hydrogel consistency and shape retention after demoulding, varying volumes of the fibrin hydrogel solution, prepared as described in Section 6.2.2, were cast in 24–, 12–, or 6–well plates (Table 6.1). Hydrogels were incubated for two days, after which they were demoulded and photographed.

The estimated hydrogel heights resulting from each hydrogel volume–well size pairing were calculated using the well surface area (cm^2) obtained from the plate manufacturer together with the hydrogel volume added to determine the height of the resulting cylindrical hydrogel constructs.

Table 6.1: **Well sizes and hydrogel volumes (µL) used for construct preparation.** The corresponding surface areas were obtained from the manufacturer (Thermo Fisher Scientific) [625].

Well Size	Well Surface Area (cm^2)	Hydrogel Volume (µL)
24–well	1.9	100, 200, 300, 400, 500, 1,000
12–well	3.5	300, 400, 500, 600, 700, 800, 900, 1,000, 1,500, 2,000, 2,500, 3,000
6–well	9.6	1,000, 2,000, 3,000, 4,000, 5,000, 6,000

6.2.3.3 Cell Seeding Density

Hydrogels were prepared as previously described (Section 6.2.2) and embedded with MVECs at different seeding densities, reported relative to well surface area (2.5×10^3 – 5.75×10^4 cells/cm^2, in 5×10^3 increments). Hydrogels were fabricated by casting 1,000 µL per well (12–well plates). Cells were imaged at five time points: 3, 5, 7, 21 and 28 days after casting.

6.2.4 Live Imaging for Network Morphogenesis in Hydrogels

Hydrogels embedded with MVECs were fabricated and cast in 24–well plates. Two formulations were prepared: (a) an unmodified formulation, as described in Section 6.2.2, termed ‘EBM’; and (b) a modified formulation in which 20 µL of EBM were replaced with VEGF (final concentration: 2%; Lonza, Walkersville, MD, USA), referred to hereafter as ‘EBM + VEGF’.

After casting, constructs were incubated for 30 min to complete gelation. Subsequently, 300 µL of EBM was added to each well, followed by a further 30 min incubation prior to the first imaging round. Network formation was monitored using the *OrganoidQC* module of the Incucyte SX5 Live-Cell Analysis System (Sartorius, Ann Arbor, MI, USA). One image encompassing the entire well (well area imaged: 185.8 mm^2) was acquired per time point at 4× magnification in brightfield and phase contrast modes, and exported for image analysis. Microscopy images at 10× magnification were also captured.

The brightfield images exported from the Incucyte were analysed using *ImageJ/Fiji* and the *Angiogenesis Analyser*, as detailed in Section 6.2.12.1. In parallel, the images were also analysed using *Incucyte* software (Section 6.2.12.1).

The experimental work was conducted in two phases. In **Phase 1**, hydrogels were prepared at two concentrations (8 mg/mL or 10 mg/mL), with 300 µL cast per well. These two fibrinogen concentrations were selected based on previous work [544]. For each concentration, both EBM and EBM + VEGF formulations were tested at six cell-seeding densities: 1.5, 2.5, 3.5, 4.5, 5.5 and 6.5×10^4 cells per construct, resulting in 24 experimental groups. All conditions were prepared in triplicate. Constructs were imaged every 2 h for 3 days.

Based on the optimisation results from *Phase 1*, the fibrinogen concentration that yielded the best results was used for **Phase 2** to fabricate 3D hydrogel constructs. In this phase, the aim was to perform extended live

imaging and quantitative analyses of EC network formation, maturation and disintegration. Constructs were cast at 960 µL per well (24–well plates), embedded with 1×10^4, 5×10^4, or 1×10^5 cells per well and cultured for 50 days. Imaging was performed every 2 h for the first 2.5 days and every 6 h thereafter until day 50. Medium was changed every 3 days. Triplicates were prepared for all conditions.

6.2.5 Mechanical Characterisation: Compressive Loading of Acellular Hydrogels

To supplement the material characterisation of hydrogels presented in Section 5.2.5 [544], particularly the stress–strain properties, and to offer preliminary insights ahead of experimental work involving crush injuries applied to MVEC-embedded hydrogels, the mechanical response of fibrin hydrogels under compressive loading was investigated. This was undertaken to establish how the hydrogel matrix alone responds to compression before analysing the impact of crush injuries in cellularised constructs.

Mechanical testing was carried out using a MicroTester LT (CellScale) apparatus, a micro-scale tension-compression system designed for specimens 80–2,000 µm in size [626]. In this setup, the microbeam and platen are used to deform the sample while measuring the resulting forces.

Hydrogels were prepared as previously described. Briefly, a hydrogel solution was prepared with fibrinogen from human plasma at a concentration of 10 mg/mL in EBM and mixed with 100 µL of FBS prior to crosslinking with thrombin (10 U/mL in MES/NaCl buffer) and $CaCl_2$ (1 M solution in distilled water) at a crosslinking ratio of 200:10:1 (fibrinogen : thrombin : $CaCl_2$). Hydrogels were cast in 96–well plates and incubated at 37 °C and 5% CO_2 to complete gelation.

24 h after hydrogel casting, scaffolds were carefully removed from the mould and mounted on a MicroTester LT (Figure F.1). The testing protocol consisted of four sequential phases: load, hold, recovery and rest (Figure F.2). In the load phase, the sample was compressed to 35% strain over 30 s, followed by a 10 s hold phase in which the deformation was maintained. The recovery phase (30 s) involved the removal of the applied force. The rest phase was set to 0 s, and a single compression cycle was performed per sample. The parameters used were: control axis: Z-Compress; control mode: displacement; control fraction: ramp; and compression magnitude: 35%. Data on force, tip displacement, base displacement, current size and temperature were collected every 0.2 s and plotted as displacement–time, force–time and force–displacement curves.

6.2.6 *In Vitro* Modelling of Non-Penetrating Traumatic Injuries (NPTIs) Using Cell- and Network-Embedded Constructs

To investigate the effects of NPTIs on 3D constructs, three injury models were used: crush (Section 6.2.8), contusion (Section 6.2.9) and strain (Section 6.2.10). Since 3D hydrogel constructs would come into direct contact with 3D-printed objects when inducing crush injuries (Section 6.3.5) and to create the dog-bone-shaped constructs for strain injuries (Section 6.3.7), it was essential to assess the biocompatibility of the materials used. Therefore, the biocompatibility of objects manufactured from commercially available resins using the same fabrication process planned for the crush and strain injury setups was assessed (Section 6.2.7) before NPTI modelling.

The resulting damage was evaluated at two levels: (1) directly on the cells and (2) on the EC networks formed within the construct. For this purpose, two distinct and complementary image analysis methodologies were employed, each comparing images before and after injury. The first approach quantified the localised strain by tracking individual cells as discrete objects. For network analysis, the quantitative metrics described

in Section 6.2.12.1 were assessed. The metrics assessed were object count (number of objects per image), total object area (µm^2 per image) and average eccentricity (a morphology metric used to represent cell roundness).

6.2.7 Biocompatibility Evaluation of 3D-Printed Objects

To support investigations of NPTI effects using crush, contusion and strain injury models, it was first necessary to assess the biocompatibility of the 3D-printed materials that would be in direct contact with the hydrogel constructs during crush injury induction and strain construct fabrication. Since the biocompatibility experiments required reliable quantification of MVEC viability, the initial step was to generate an MVEC number–fluorescence standard curve to serve as a benchmark for the subsequent analysis (Section 6.2.7.1), followed by its application in the biocompatibility assessment of resin-conditioned media.

6.2.7.1 MVEC Number-Fluorescence Standard Curve

To enable accurate quantification of cell viability, a standard curve correlating PrestoBlue fluorescence with cell number was generated. Serial two–fold dilutions of MVECs were seeded in 96–well plates (Table 6.2) and incubated with 100 µL of EGM for 2 h (37 °C, 5% CO_2).

EGM was replaced with 100 µL of a 10% PrestoBlue HS Cell Viability Reagent (Thermo Fisher Scientific, Eugene, OR, USA) in EGM, and fluorescence was measured after incubation for 15 min, 30 min, 1 h and 2 h. Six replicates were included per cell density. Fluorescence was measured using a microplate reader (SpectraMax i3x, Molecular Devices, LLC, San Jose, CA, USA; excitation/emission 560/590 nm) and the corresponding software (*SoftMax Pro*, v7.0; Molecular Devices, LLC, San Jose, CA, USA). Background fluorescence was corrected by subtracting the average fluorescence obtained from wells containing EGM only.

Table 6.2: **Cell seeding densities used to generate the standard curve relating fluorescence to cell number.**

Cells per well ($\times 10^3$)	0, 1, 2, 3, 4, 5, 6, 7, 8, 9, 10, 15, 20, 25, 30, 35, 40, 45, 50

6.2.7.2 Design of 3D-Printed Containers

Three resins (black, clear and BioMed Amber) were selected for their printing properties and compatibility with standard sterilisation and disinfection procedures to minimise contamination risk. To maximise contact between the 3D-printed object and the medium, containers were designed with multiple internal columns, increasing internal surface area and facilitating retention of leached compounds. Containers were designed to hold 20 mL of medium, with a surface area-to-volume ratio greater than 0.75 (Figure F.3).

6.2.7.3 3D Printing and Post-processing

Designs were created in SolidWorks, exported as STL files and prepared for printing using *PreForm* software (v3.34.0, Formlabs, Inc.). Printing was performed using a Form 3B+ SLA desktop printer (Formlabs, Inc., China) with one of the following resins: Black (V4, Formlabs, Inc., Somerville, MA, USA), Clear (V4, Formlabs, Inc., Somerville, MA, USA), or BioMed Amber (V1, Formlabs, Inc., Millbury, OH, USA).

After printing, objects were washed using the Form Wash system and cured using the Form Cure (Formlabs, Inc., China). Rafts and supports were removed prior to curing, and all 3D-printed objects were air-dried. Manufacturer-recommended washing and curing protocols were followed (Table 6.3).

After curing, sterilisation was performed using a four-step protocol: autoclaving, Chemgene wash (5 min), 70% ethanol washes (2 × 5 min) and UV exposure (2 × 20 min). 3D-printed objects were then rinsed thrice with phosphate-buffered saline (PBS; Gibco Life Technologies, Paisley, UK).

Table 6.3: **Washing and curing parameters used for post-processing of 3D printed objects.** Manufacturer-recommended settings were followed for each resin type [627].

Resin	Washing Time (min)	Curing Time (min)	Curing Temperature (°C)
Black (V4: FLGPBK04)	10	30	60
Clear (V4: FLGPCL04)	10	15	60
BioMed Amber (V1: FLBMAM01)	20	30	70

6.2.7.4 Preparation of Conditioned Media

Sterilised containers (Figure F.3) were filled with 20 mL of EBM supplemented with 1% penicillin/streptomycin (P/S; Gibco Life Technologies, Grand Island, NY, USA). Containers were sealed with 3D-printed fitted lids fabricated with the same resin type and Parafilm M (Sigma-Aldrich, USA), then incubated under standard cell culture conditions (37 °C, 5% CO_2) for six weeks, with gentle agitation applied twice weekly. This prolonged exposure period was intended to allow accumulation of any resin-derived leachates in the medium. EBM + 1% P/S served as a control and was incubated under identical conditions in six-well plates for six weeks. After the six-week period, conditioned medium from all experimental and control conditions were collected and stored at 4 °C until use.

6.2.7.5 Biocompatibility Assessment of Conditioned Media

MVECs were seeded at a density of 3,500 cells per well in 96–well plates (Corning Incorporated, Kennebunk, ME, USA) and cultured with 100 µL of fresh EGM. Baseline viability (Day 0) was assessed using the PrestoBlue assay according to the manufacturer's instructions. Briefly, medium was removed and replaced with 100 µL of a 10% PrestoBlue solution in EGM. Plates were incubated for 1 h (37 °C, 5% CO_2). Fluorescence was measured using a microplate reader (excitation/emission 560/590 nm) and background fluorescence was corrected by subtracting fluorescence values from wells containing EGM only (no cells).

After the baseline measurements were obtained, the PrestoBlue solution was removed from all wells and replaced with 100 µL of the corresponding experimental (exposed to one of black, clear or BioMed resins) or control medium formulation (C1: fresh EGM, prepared immediately before being added to the plate; C2: EGM prepared from EBM incubated for six weeks and supplemented immediately before being added to the plate), as summarised in Table 6.4.

Table 6.4: **Summary of experimental and control media used for resin biocompatibility assessment.** Containers 3D-printed with black, clear or BioMed Amber resin were filled with 20 mL of EBM supplemented with 1% penicillin/streptomycin and incubated for six weeks. In parallel, the same EBM formulation was incubated in six-well plates as Control 2 (C2). Fresh EGM prepared on the day of cell seeding (C1: Control 1) was included for comparison. Following incubation, all experimental and control media were supplemented with Microvascular SingleQuots[2] to produce EGM. Abbreviations: EBM, endothelial cell basal medium; P/S, penicillin/streptomycin; EGM, endothelial cell growth medium.

Type	Condition	Exposure to Resin Type	Medium Composition at Incubation Start	Incubation Period	Medium Composition at Cell Seeding
Experimental	Black	Black (V4)	EBM + 1% P/S	6 weeks	EGM + 1% P/S
	Clear	Clear (V4)			
	BioMed	BioMed Amber (V1)			
Control	C1: Fresh EBM	N/A	N/A	N/A	
	C2: Incubated EBM	N/A	EBM + 1% P/S	6 weeks	

Before adding the medium to the wells, all media variations were supplemented with Microvascular SingleQuots[2] (Lonza, Walkersville, MD, USA) to produce EGM. Media supplementation was delayed until this point to prevent degradation of growth factors during the 6–week exposure period while preserving the ability to detect any leached compounds.

Following baseline assessment, viability measurements were performed on days 1, 2, 4, 7 and 14. Prior to each measurement, medium was replaced with 100 µL of a 10% PrestoBlue solution in the respective experimental or control medium. After correcting for background fluorescence, fluorescence values were plotted relative to C1 and C2, and estimated cell numbers were extrapolated using the standard curve (Section 6.2.7.1).

6.2.8 Crush Injury

Two compression experiments were performed on fibrin gels seeded with MVECs and stained with CellLight Plasma Membrane-GFP. The hydrogels were cast in a 12–well culture plate (22 mm diameter, 2–3 mm depth), were compressed using a Perspex cylinder, while remaining in their original wells. Images were acquired at baseline and at 5–min intervals for 1 h per sample. For network-embedded constructs, 3D-printed (Section 6.2.7.3) cylinders (height: 15–18 mm) were used to compress the hydrogels while remaining in their original wells (24–well plate) for 24, 48, 72, 96 and 120 h. Images were acquired before injury and after each time point.

6.2.9 Contusion Injury

Contusion injury was induced in 3D microvascular constructs using a drop-weight impact model. Constructs were formed from fibrin hydrogels prepared with 10 mg/mL fibrinogen dissolved in either EBM or EBM + VEGF. Microvascular networks were allowed to form within the constructs prior to injury.

A metallic mass (diameter: 1 cm; mass: 4.0761 g ± 0.0002 g; commercially available) was released vertically from predefined heights of 5, 10 or 15 cm to generate contusion injuries of graded severity (Figure F.4). The mass was guided to ensure consistent alignment and impact location on the surface of the construct. Following impact, the mass was left in place for 30 min to maintain compressive loading, after which it was carefully removed to avoid inducing any penetrating damage to the hydrogel.

Immediately after mass removal, constructs were either processed for imaging or returned to culture for post-injury analysis, depending on the experimental endpoint. All contusion experiments were performed under identical conditions to minimise variability between samples.

6.2.10 Strain Injury

Fibrin hydrogel constructs were prepared as described in Section 6.2.2 at concentrations of 8 and 10 mg/mL, embedded with MVECs and cast into their respective moulds. For cell-tracking analysis, hydrogels were cast in 12–well plates; 2 h after casting, constructs were carefully released from their moulds and mounted onto the loading device. For network-based analyses, hydrogels were instead cast into 6–well plates fitted with a removable insert that produced dog-bone-shaped constructs (Figure 6.1).

Samples were mounted in a custom tensile loading device [628], secured using crocodile clips, and axially stretched to induce a strain injury (Figure F.5). Samples were stretched in 0.5 mm increments, with images acquired before loading and after each step as increasing block separation elongated the hydrogel. For imaging,

[2]Foetal bovine serum (FBS) 2%; hydrocortisone 0.04%; human fibroblast growth factor-basic (hFGF-b) 0.4%; vascular endothelial growth factor (VEGF) 0.1%; long R3 insulin-like growth factor-1 (R3-IGF-1) 0.1%; ascorbic acid 0.1%; human epidermal growth factor (hEGF) 0.1%; gentamicin sulfate-amphotericin (GA-1000) 0.1%.

samples were observed using a Nikon Zoom SMZ1000 microscope equipped with a Nikon D7100 digital camera, employing a 2× objective with a 5× zoom to enable successive image acquisition throughout the loading protocol.

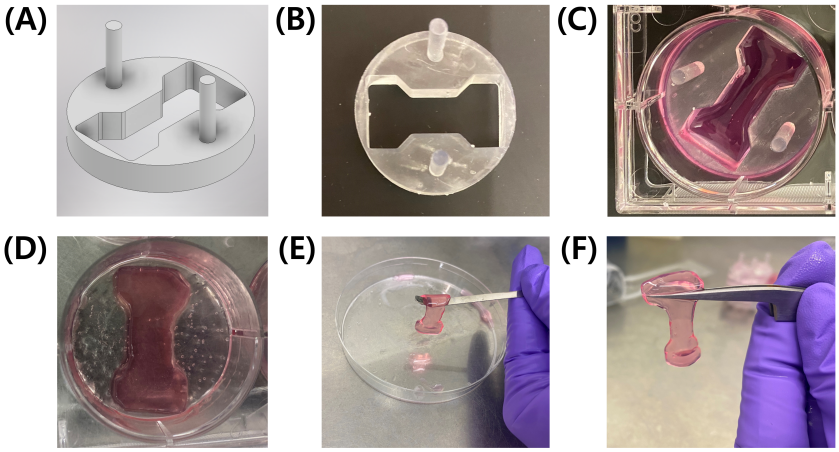


Figure 6.1: **Dog-bone hydrogel fabrication process for strain injury induction.** This figure shows photographs and schematics of the creation of a microvascular endothelial cell (MVEC)-embedded hydrogel cast in the shape of a dog bone to enable controlled strain injury. **(A)** Computer-aided 3D design of the dog-bone mould. **(B)** Photograph of the corresponding 3D-printed insert. **(C)** The 3D-printed insert placed and secured within a 6–well plate. The MVEC-laden hydrogel solution was poured into the mould and allowed to gel for 1 h. **(D)** The hydrogel following gelation and culture, during which endothelial network formation took place. **(E, F)** The dog-bone construct removed from the mould and carefully positioned on the strain device for mechanical injury induction and imaging.

Strain was calculated using *MATLAB* software developed by L. Taylor (2022) [628] (software development not included in this thesis). The feature-tracking tool identifies corresponding markers between successive images and can be used either manually, with user-selected markers, or semi-automatically, where circular cellular features are detected and selected by the user. The same markers were tracked across all images from each experiment, ensuring that measured axial (parallel to stretch) and radial (perpendicular to stretch) changes reflected only sample deformation. Axial and radial marker separations were used to calculate incremental strain between images and total strain relative to baseline, with overall strain magnitude derived from these components.

Network analysis pre- and post-injury was conducted as described in Section 6.2.12.2. Values were plotted as the percent change in confluence relative to pre-injury baseline (Equation 6.1: ΔC) where C_{pre} represents the percent confluence measured immediately prior to injury induction and C_{post} represents the percent confluence measured at the corresponding post-injury time point. Percent change in confluence was used as a normalized metric to quantify injury-induced cell loss and subsequent recovery within the same well, thereby accounting for variability in baseline confluence between wells. Negative values indicate a reduction in confluence following injury, whereas positive values observed at later time points indicate recovery or regrowth relative to the pre-injury baseline. This metric was used for statistical analysis and cross-condition comparisons. Data was plotted as mean values $\pm$ standard deviation.

$$\Delta C = \frac{C_{post} - C_{pre}}{C_{pre}} \times 100 \tag{6.1}$$

6.2.11 Conditioned Media

MVECs were seeded into 96–well plates at densities of either 5×10^3 or 1×10^4 cells per well. Cells were cultured with 100 µL of fresh EGM for 24 h, after which the medium was removed and replaced with conditioned media collected from 3D hydrogel constructs subjected to crush or contusion injury, uninjured hydrogels, fresh EGM, fresh EBM, or ethanol treatment (Table 6.5).

Crush and contusion injuries were conducted as outlined in Sections 6.2.8 and 6.2.9. Conditioned media from crush injuries were harvested 24 h after compression, whereas media from contusion injuries were collected 1 h following impact.

Table 6.5: **Conditioned media groups.** Crush injuries were produced using cylindrical presses of varying heights (15–18 mm), while contusion injuries were generated by dropping a spherical metallic mass from set heights (5–15 cm). Control groups consisted of fresh media (EGM and EBM), an ethanol-induced cell-death control, and media extracted from uninjured EBM and EBM + VEGF hydrogels maintained under identical culture conditions to the injured constructs.

Type	Injury Parameters	Media Source
Conditioned Media: Crush Injury	Cylinder heights: 15, 16, 17 & 18 mm	EBM Hydrogel EBM + VEGF EBM Hydrogel
Conditioned Media: Contusion Injury	Mass drop heights: 5, 10 & 15 cm	EBM Hydrogel EBM + VEGF EBM Hydrogel
Control: Uninjured Hydrogel	N/A	EBM Hydrogel (No Injury) EBM + VEGF Hydrogel (No Injury)
Control: Fresh Media	N/A	Fresh EGM Fresh EBM

After 72 h of exposure, live (calcein AM; green) and dead (EthD-1; red) cells were labelled, using a live/dead Viability/Cytotoxicity Kit (Molecular Probes Invitrogen, Eugene, OR, USA) and following the manufacturer's instructions. Briefly, EGM was removed and cells were washed twice with PBS. Then, a staining solution comprising EthD-1 (20 µL of a 2 mM solution), calcein AM (5 µL of a 5 mM solution) and PBS (10 mL) was added. Cells were incubated for 30 min at room temperature, protected from light, prior to imaging and microplate reading.

Cells were incubated for 2 h before absorbance was measured at 485/530 nm (calcein AM) and 530/645 nm (EthD-1) for excitation/emission using a microplate reader (Varioskan Lux, Thermo Scientific) and its software (*SkanIt Software*, *Research Edition*; version 7.0.2.5, Thermo Fisher Scientific Oy). After background fluorescence correction, values were plotted as relative absorbance against the fresh EBM control of the respective cell seeding number.

Experimental and control samples were imaged using the Incucyte live-cell imaging system. Imaging was performed using an adherent cell-by-cell analysis workflow with a 20× objective (image size: 0.88 × 0.65 mm). Image acquisition was performed using phase contrast and two fluorescence channels to visualise live cells (in green; acquisition time: 300 ms) and dead cells (in red; acquisition time: 400 ms) with the SX5 G/O/NIR optical module. Nine images were captured per well. Data were plotted as the Live–Dead Cell Index (ratio-based; Equation 6.2). Integrated Fluorescence Intensity (IFI) was used as the quantitative fluorescence metric. The index was calculated as the ratio of calcein AM–derived IFI (live cells) to the sum of calcein AM– and EthD-1–derived IFIs (live and dead cells, respectively).

$$\text{Live–Dead Cell Index} = \frac{\text{IFI}_{\text{Calcein AM (Live Cells)}}}{\text{IFI}_{\text{Calcein AM (Live Cells)}} + \text{IFI}_{\text{EthD-1 (Dead Cells)}}} \tag{6.2}$$

6.2.12 Image Analysis

6.2.12.1 Network Analysis: Incucyte

Images were analysed using the *Organoid* analysis of the *Incucyte* software (2024B GUI, version 2024B; Sartorius, Ann Arbor, MI, USA). The image channel used for the analysis was 'Phase + Brightfield'. Image analysis was conducted for each image and each time point.

Four metrics were quantified: (1) Object count (per image) represents the number of detected objects within each well; (2) object total area (µm^2 per image) represents the cumulative area of all brightfield objects within a well and was used to track changes in size and area occupied over time; (3) object average eccentricity is a morphology-based metric describing object roundness, where a value of 0 corresponds to a perfect circle and a value of 1 corresponds to a perfect line. This metric was used as an indicator of morphological changes associated with cells transitioning from a cobblestone-like morphology toward a network-like or tube-forming structure; (4) darkness quantifies the mean brightness intensity of detected objects and was used to monitor changes in organoid brightness over time.

6.2.12.2 Confluence Analysis: Incucyte

For the injury network analysis, the *Basic Analyzer* analysis type was used. Images were acquired as full-well phase contrast images (6–well plates) and image analysis was performed for each image and each time point. Confluence measurements were specifically used to compare cell coverage before and after injury induction within the same well.

Confluence was defined as the percentage of the culture surface area covered by cells, and was determined using classic confluence segmentation applied to phase contrast images. Segmentation parameters were optimised using a segmentation adjustment factor of 1 to ensure accurate detection of cell-covered regions while minimising background inclusion. A minimum object area threshold of 10 µm^2 was used to exclude small artifacts and debris from the analysis. Area-based filtering was used consistently across all conditions.

The primary metric extracted was percent confluence per well, representing the proportion of the total imaged surface occupied by the EC network. Pre-injury confluence values were used as an internal baseline for each well. Post-injury confluence values were compared to this baseline to quantify injury-induced cell loss. All analysis parameters were applied uniformly across experimental groups to enable direct quantitative comparison.

6.2.12.3 Adherent Cell-by-Cell Analysis: Incucyte

For the conditioned media experiments, image acquisition and analysis were performed using the Incucyte system and software (Sartorius) with the Adherent Cell-by-Cell analysis type. Images were acquired at 20× magnification across three channels: brightfield (phase contrast), live-cell fluorescence (green) and dead-cell fluorescence (red). Image analysis was conducted using top-hat segmentation (no mask) with a segmentation radius of 10 µm. Cell boundaries were defined using a segmentation adjustment factor of 1, with hole filling enabled for areas up to 10 µm. Object seeding parameters were set to a cell detection sensitivity of 2, cell contrast of 3 and cell morphology of 3. These parameters were applied consistently across all experimental and control conditions to ensure robust quantitative comparison of cell viability and morphology.

Automatic metrics used were derived from phase-based segmentation of individual cells. The phase count per image was defined as the total number of segmented cells detected within each image. Cell size was quantified as the average cell area (µm^2) of all segmented objects. Fluorescence measurements were calculated for objects defined by the phase mask. Average mean fluorescence intensity (CU) was determined as

the sum of pixel fluorescence intensities within each object divided by the total object area in pixels. Total integrated fluorescence intensity (CU · µm^2 per image) was calculated as the sum of all green or red fluorescence intensity values within the object boundaries, multiplied by the pixel area.

6.2.13 Statistical Analysis and Software

Unless otherwise specified, data was analysed using one- or two-way analysis of variance (ANOVA), followed by Tukey's honest significant difference (HSD) post hoc test. p values ≤ 0.05 were considered statistically significant. For unpaired t-tests, normal distribution was assumed and Welch's t-test was performed; two-tailed p-values and a 99% confidence level were selected. For the biocompatibility evaluation (Section 6.2.7), regression analysis with ANOVA was performed on fluorescence values for each cell seeding number, using a 99% confidence level.

All data analysis was carried out using *GraphPad Prism* (version 10.4.2 (633), Dotmatics, Boston, MA, USA), except for that of the regression analysis with ANOVA which was performed with *Microsoft Excel* (365, version 2508). Unless otherwise specified, results are reported as mean ± standard deviation. Figures were generated using *GraphPad Prism*, while schematics were created with *BioRender.com*.

6.3 Results & Discussion

6.3.1 Optimisation of Hydrogel Constructs

Based on the results obtained in Chapter 5 [544], the hydrogel composition was further refined. It was of interest to explore the impact of FBS on hydrogel consistency (Section 6.3.1.1) and to optimise well size and hydrogel volume (Section 6.3.1.2), as well as cell seeding density (Section 6.3.1.3). The optimisation of the hydrogel constructs provided further insights into how parameters such as FBS supplementation, cell seeding density, and construct size and volume influence both structural integrity and cellular behaviour. Together, these findings further refine practical parameters for fibrin-based hydrogel constructs, providing a foundation for subsequent experimental work on vascularisation and injury modelling.

6.3.1.1 Effect of FBS on MVECs and Hydrogel Consistency

Constructs with and without FBS included in their formulation were assessed based on both cell morphology (Figure F.6) and hydrogel consistency (Figure 6.2) using light microscopy and visual inspection, respectively.

At a seeding density of 2.5×10^3 cells/cm, reported based on well surface area, both FBS and non-FBS constructs contained too few cells to permit meaningful network formation. At higher cell seeding densities (1.75×10^4, 3.25×10^4 and 4.75×10^4 cells/cm; reported based on well surface area), cells in hydrogels without FBS remained predominantly rounded, whereas in FBS-containing hydrogels they formed interconnected networks and show fragments of these networks 3 days post-seeding. These observations suggest that the inclusion of FBS promotes network formation within the hydrogel.

Hydrogel consistency was also assessed by visual inspection. All FBS-containing constructs across the four seeding densities tested were classified as 'acceptable', whilst the corresponding non-FBS hydrogels were rated as 'poor', with the exception of the 2.5×10^3 cells/cm construct which was 'acceptable'.

Adding FBS to the hydrogel formulation had a noticeable effect on both hydrogel consistency and EC morphology. Constructs with formulations supplemented with FBS supported early MVEC network formation. In contrast, the absence of FBS resulted in poor matrix integrity and rounded cell morphology, suggesting lim-

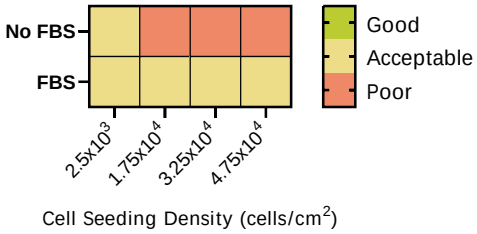


Figure 6.2: **Visual classification of hydrogel consistency with and without foetal bovine serum (FBS)**, by cell seeding density (cells/cm, reported based on well surface area). Hydrogel constructs were assessed three days post-casting for shape retention and overall consistency, and classified as 'good', 'acceptable' or 'poor'. Hydrogels were fabricated using fibrinogen from human plasma (10 mg/mL in EBM) and crosslinked with thrombin (10 U/mL) and $CaCl_2$ (1 M) at a ratio of 200:10:1 (fibrinogen : thrombin : $CaCl_2$). Hydrogels were fabricated with or without FBS and embedded with human dermal microvascular endothelial cells (MVECs) at varying seeding densities. Hydrogels were cast in 12–well plates (500 µL per well).

ited cell–matrix interaction. These findings align with previous reports showing that serum supplementation enhances cell attachment and stabilises fibrin networks during early culture periods.

While these data are insufficient for drawing definitive conclusions, it served a practical role for rapid assessment to narrow down initial design choices for further optimisation. The characterisation of the endothelial network, as well as the evolution of these over time is addressed in Section 6.3.2. Based on the results obtained here, it was decided to include FBS in the hydrogel formulation.

6.3.1.2 Hydrogel Size & Volume

Hydrogels were demoulded two days after casting and photographed (Figures F.7, F.8, F.9 and F.10). Each sample was visually inspected and classified based on shape retention and consistency (Figure 6.3).

Hydrogel consistency varied with both well size and hydrogel volume. For hydrogels cast in 24–well plates (Figure F.8), volumes up to 200 µL were classified as 'poor', 300–400 µL as 'acceptable', and 500 µL or more as 'good'. In 12–well plates (Figure F.9), volumes below 400 µL were 'poor', 500–700 µL were 'acceptable', and 800–3,000 µL were 'good'. Finally, for 6–well plates (Figure F.10), 1,000–2,000 µL were 'poor', 3,000 µL was 'acceptable', and 4,000–6,000 µL were 'good'.

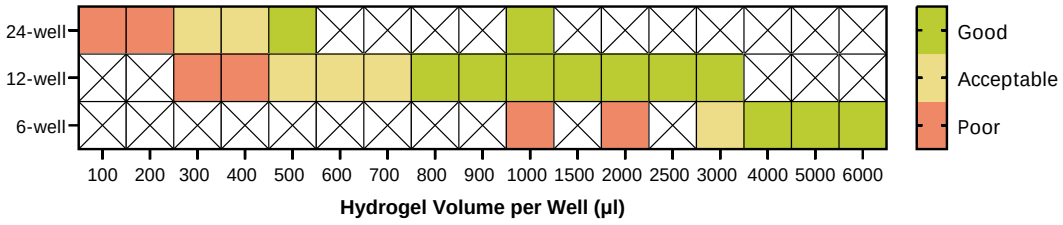


Figure 6.3: **Visual classification of hydrogel consistency two days after casting.** Hydrogel constructs were visually assessed for shape retention and overall consistency, and classified as 'good', 'acceptable' or 'poor'. Hydrogels were fabricated using fibrinogen from human plasma (10 mg/mL in EBM) and crosslinked with thrombin (10 U/mL) and $CaCl_2$ (1 M) at a ratio of 200:10:1 (fibrinogen : thrombin : $CaCl_2$). Crossed-out cells indicate that the corresponding volume in the figure was not used for a given well size.

The resulting hydrogel dimensions for each well size and hydrogel volume combination were also calculated (Table F.1). These heights were estimated based on corresponding cylindrical volumes and were subsequently corroborated by manual measurement, which revealed a small, but negligible, decrease in hydrogel height compared to the theoretical measurement. This reduction may be attributed to the demoulding process itself, as well as slight loss or spreading of the hydrogel structure during removal, resulting in constructs

that were slightly shorter and wider, though the changes were minimal. Whilst no single option was clearly superior, in general, hydrogels of greater height were found to be easier to manage, including removing the constructs from the mould.

Well size and hydrogel volume further influenced construct stability, with larger hydrogel volumes displaying superior shape retention and ease of handling. This effect is most likely a direct result of the geometry of the hydrogel itself, with increased volumes enhancing structural cohesion and reducing surface-to-volume ratio–related dehydration.

6.3.1.3 Cell Seeding Density

To further refine the construct formulation, the effect of EC density upon seeding was explored. Constructs were embedded with a range of cell densities (cells/cm, reported based on well surface area): 2.5×10^3–5.75×10^4 cells/cm. Then, they were monitored for up to 28 days (Figures F.11, F.12, F.13 and F.14).

All hydrogels were of identical composition, prepared in the same well format and used the same hydrogel volumes, therefore enabling a direct comparison of cell seeding density. Constructs maintained long-term stability and preserved overall hydrogel shape across the 28–day culture period.

At seeding densities of 2.5×10^3, 7.5×10^3 and 1.25×10^4 cells/cm^2, too few cells were present for effective network formation. At 1.75×10^4, 2.25×10^4 and 2.75×10^4 cells/cm^2, remnants of networks were visible after 3 days and these conditions were considered 'acceptable'. At 3.25×10^4, 3.75×10^4, 4.25×10^4 and 4.75×10^4 cells/cm^2, networks were present from day 3 and persisted up to 21 days, with remnants still visible at day 28; these seeding densities were therefore classified as 'good'. At 5.25×10^4 and 5.75×10^4 cells/cm^2, networks were visible from day 3 to day 7, with only remnants persisting at days 21 and 28; these were also considered 'good', but to a lesser extent than the preceding group.

Overall, the optimal range for cell seeding density appeared to be above 2.25×10^4 cells/cm^2 and below 5.25×10^4 cells/cm^2, where robust network formation was consistently observed and for longer periods of time.

Furthermore, the constructs were retained in their well plates to assess hydrogel stability over time whilst remaining in the moulds and photographed at 21, 28, 48, 56, 63 and 70 days post-casting (Figure F.15). Hydrogels with higher cell seeding densities exhibited faster degradation. While this was already visible at day 21, it became more pronounced from day 48 onwards. By the end of the 70–day period, all hydrogels had retained their overall shape, albeit appearing thinner. This suggests that the hydrogels maintain structural integrity over extended culture periods, but higher cellular activity accelerates matrix remodelling and leads to a gradual thinning of the constructs.

Finally, optimisation of cell seeding density revealed a distinct range in which endothelial network formation was most consistent. Lower densities led to sparse cell distribution and incomplete network development, whereas excessively high densities appeared to accelerate hydrogel degradation, likely through elevated proteolytic activity. The optimal range (approximately 2.25–5.25×10^4 cells/cm^2) supported stable and interconnected networks that persisted for several weeks. This range represents a compromise between promoting rapid network formation and preserving construct longevity.

6.3.2 Live Imaging for Network Morphogenesis in Hydrogels

During **Phase 1**, live imaging revealed clear time-dependent changes in the total area occupied by endothelial structures, strongly influenced by both cell-seeding density and hydrogel formulation (Figure 6.4). Intermediate seeding densities (2.75–4×10^4 cells/cm^2) consistently showed progressive increases in total occupied over the 72 h period, suggesting spatial expansion or network morphogenesis. In contrast, several low- and

high-density conditions exhibited minimal change or early stagnation (*e.g.* EBM 8 mg/mL hydrogels seeded with 1.5 and 5.25 $\times$ 10^4 cells/cm^2, EBM + VEGF 8 mg/mL hydrogels seeded with 6.5 $\times$ 10^4 cells/cm^2), suggesting insufficient cell numbers to support sustained growth or declining trends consistent with early saturation and partial network disintegration.

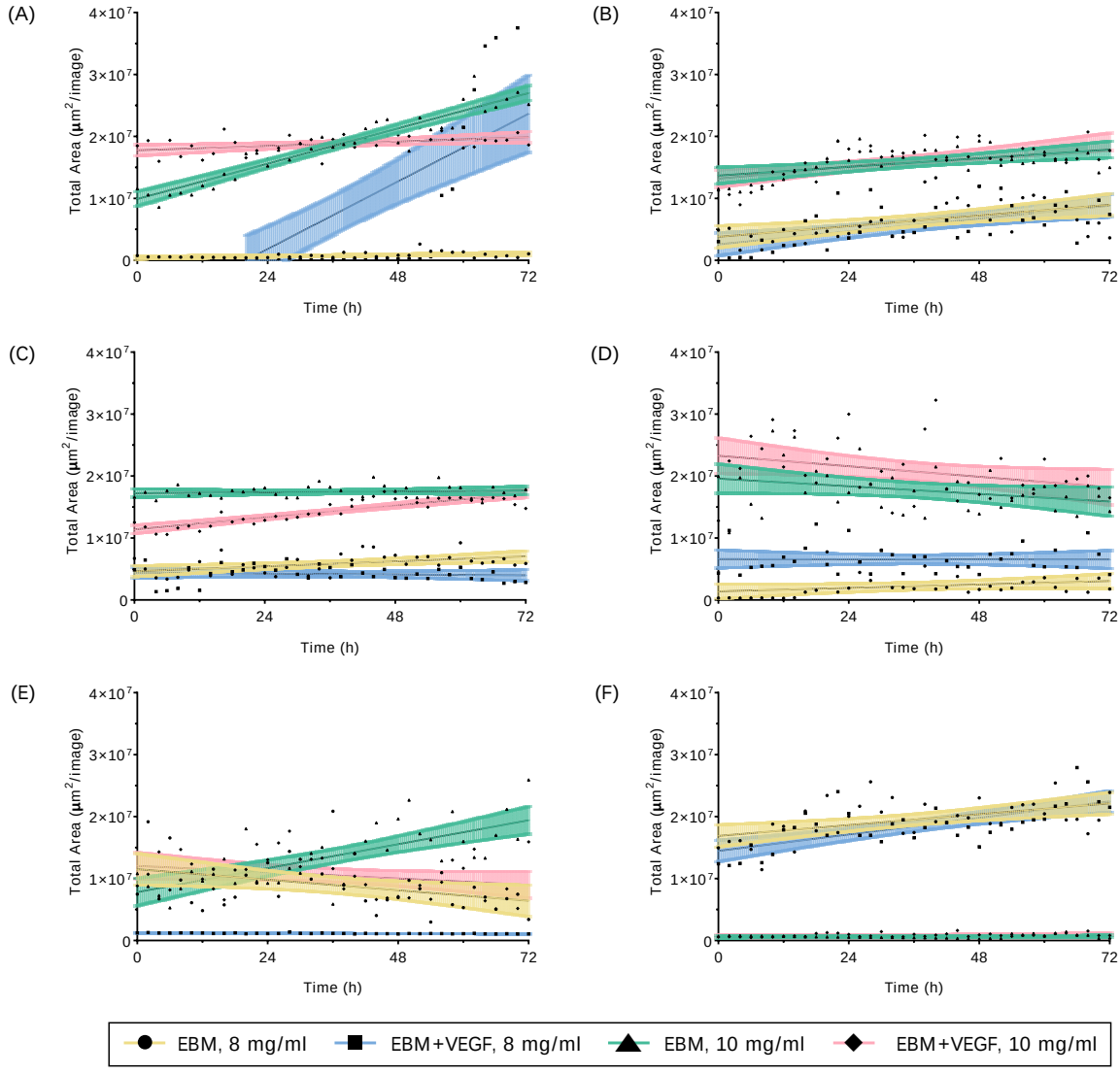


Figure 6.4: **Phase 1 live-imaging analysis of total occupied area in MVEC-containing hydrogels over 72 h.** Total area occupied by tube-like cells within each well (µm^2 per image) was quantified from whole-well scans acquired every 2 h over a 72 h period during **Phase 1** optimisation experiments. Six cell-seeding densities were evaluated: **(A)** 1.5 $\times$ 10^4, **(B)** 2.75 $\times$ 10^4, **(C)** 4 $\times$ 10^4, **(D)** 5.25 $\times$ 10^4, **(E)** 6.5 $\times$ 10^4 and **(F)** 7.75 $\times$ 10^4 cells per construct. MVECs were embedded in fibrin hydrogels formulated as EBM (yellow) or EBM + VEGF (blue) at 8 mg/mL fibrinogen, and EBM (green) or EBM + VEGF (pink) at 10 mg/mL fibrinogen. Hydrogel formulations were supplemented with 10% foetal bovine serum (FBS). For each condition, a simple linear regression was fitted to the time-series data, with shaded regions representing the 95% confidence bands (n = 3).

Across all conditions, linear regression analysis demonstrated significantly non-zero slopes, confirming a statistically significant association between time and occupied area; however, the magnitude and stability of these trends depended on hydrogel formulation (Figure 6.4). Hydrogels fabricated with 10 mg/mL fibrinogen more frequently supported sustained increases, reaching approximately 2 $\times$ 10^7 µm^2 by 72 h at intermediate seeding densities (4–6.5 $\times$ 10^4), whereas 8 mg/mL formulations were generally lower and more variable.

These findings indicate that higher fibrinogen concentration provides a more permissive microenvironment for early endothelial organisation.

Quantification of endothelial structures further reinforced the dominant role of fibrinogen concentration and revealed clear density-dependent behaviour (Figure F.16). Overall, 10 mg/mL hydrogels produced higher and more stable object counts (Figure F.16C & D) than 8 mg/mL formulations (Figure F.16A & B), with peak values approximately doubling at intermediate seeding densities (10 mg/mL: ~2–4 $\times$ 10^4; 8 mg/mL: ~1–1.5 $\times$ 10^4). These intermediate densities most consistently supported tube-like formation, whereas the highest density remained near the baseline, indicating that excessive cell crowding impaired tubular organisation. At 8 mg/mL, tube-like counts were more variable across densities, while at 10 mg/mL they were generally more sustained, albeit with reduced formation at the highest seeding level.

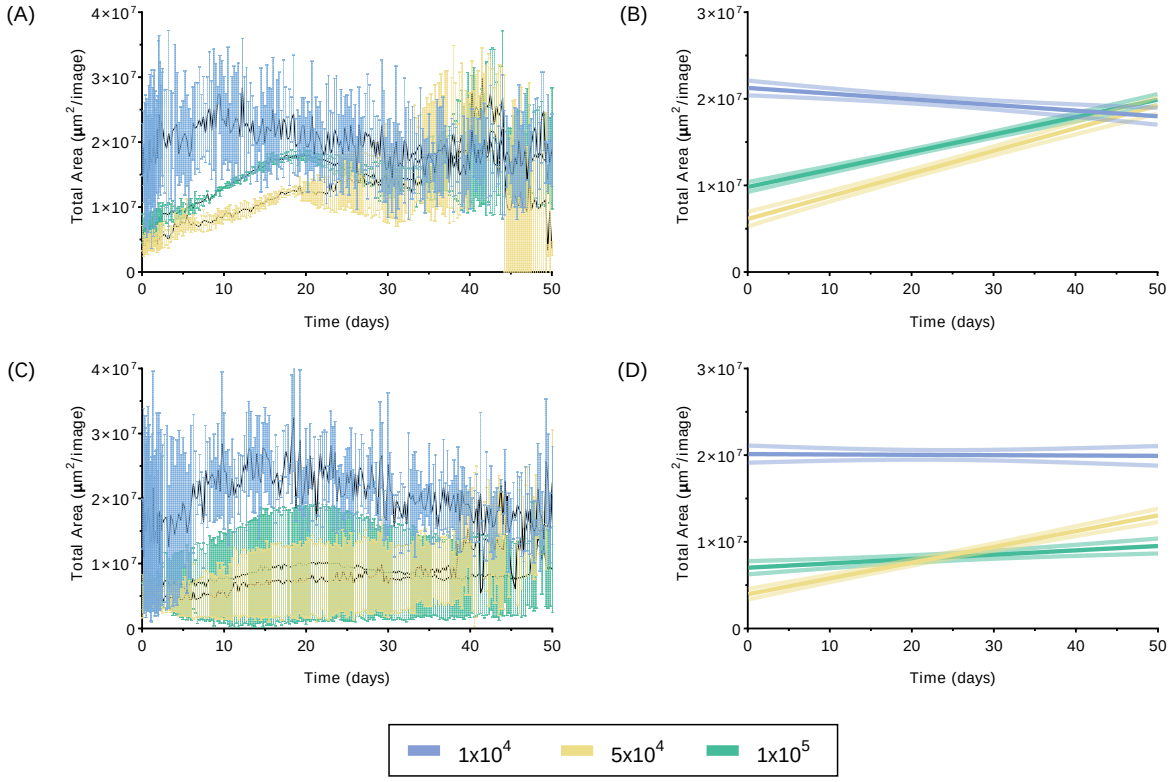


Figure 6.5: **Phase 2 live-imaging analysis of total occupied area in microvascular endothelial cell (MVEC)-containing hydrogels over 50 days.** Total area occupied by tube-like endothelial structures within each well (µm^2 per image) was quantified from whole-well scans acquired every 2 h for the first 2.5 days and subsequently every 6 h until day 5. MVECs were embedded in fibrin hydrogels fabricated with 10 mg/mL fibrinogen in **(A, B)** EBM or **(C, D)** EBM + VEGF. Hydrogel formulations were supplemented with 10% foetal bovine serum (FBS). Three cell-seeding densities were evaluated: 1 $\times$ 10^4 (blue), 5 $\times$ 10^4 (yellow) and 1 $\times$ 10^5 (green) cells per construct. Panels **(A)** and **(C)** show mean values $\pm$ standard deviation, whereas panels **(B)** and **(D)** display simple linear regressions fitted to the time-series data, with shaded regions representing the 95% confidence bands (n = 3).

VEGF supplementation did not provide a consistent advantage across seeding densities, indicating that matrix concentration was the primary driver of early tube-like structure formation. Although VEGF was associated with higher peak counts at 8 mg/mL and supported robust counts at 10 mg/mL, responses were not uniformly improved. Consequently, while 10 mg/mL fibrinogen formulations were broadly more favourable, neither EBM nor EBM + VEGF emerged as universally superior across seeding densities, highlighting the need for additional network-quality metrics.

Morphological analysis based on average object eccentricity provided further insight into network organisation (Figure F.17). Eccentricity values remained within a narrow range (0.45–0.80) and generally increased from approximately 14 h onwards, consistent with a transition from rounded to elongated, tube-like morphologies. Hydrogels fabricated with 10 mg/mL fibrinogen exhibited higher and earlier eccentricity across a wider range of seeding densities than 8 mg/mL formulations. Differences were most pronounced at either high or low cell densities, with the highest density frequently showing reduced or stable eccentricity in line with limited tube-like formation. Notably, VEGF supplementation did not consistently influence eccentricity. Together, these results identified 10 mg/mL fibrinogen and intermediate seeding densities as optimal conditions for long-term investigation.

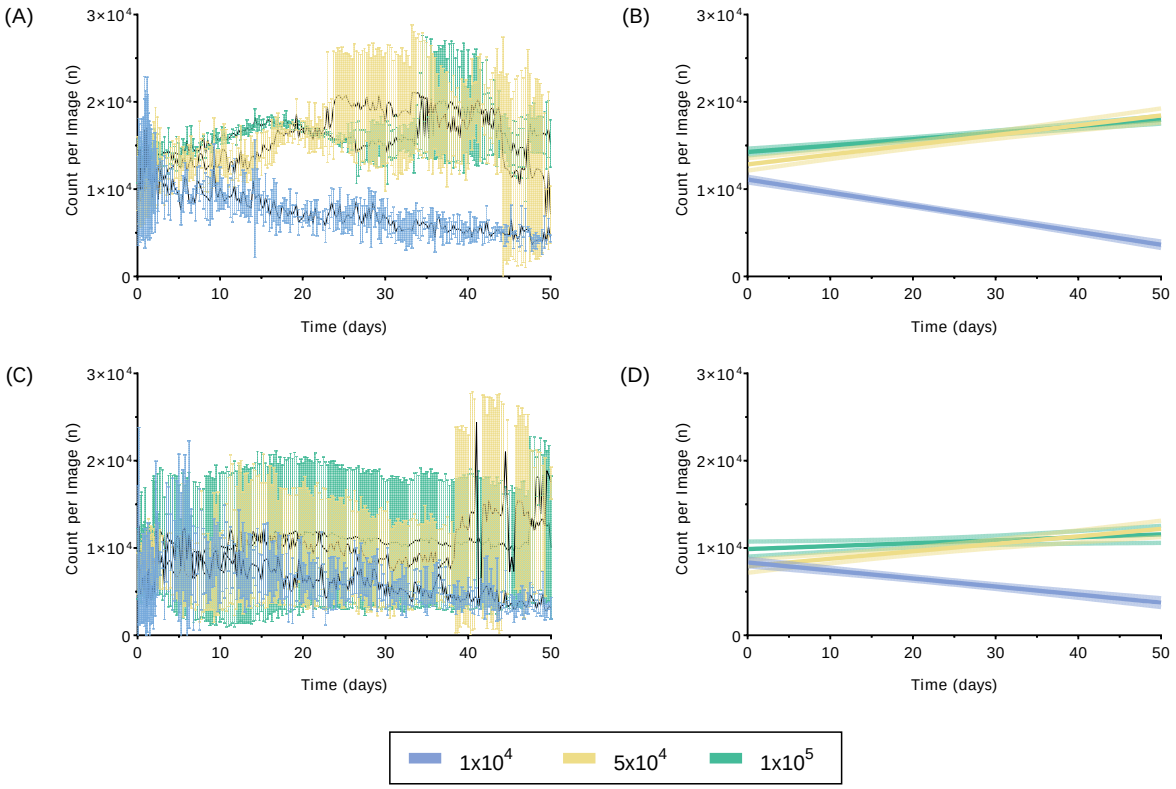


Figure 6.6: **Phase 2 live-imaging analysis of tube-like structure count in microvascular endothelial cell (MVEC)-containing hydrogels over 50 days.** The number of tube-like endothelial objects detected per image were quantified from whole-well scans acquired every 2 h for the first 2.5 days and subsequently every 6 h until day 5. MVECs were embedded in fibrin hydrogels fabricated with 10 mg/mL fibrinogen in **(A, B)** EBM or **(C, D)** EBM + VEGF. Hydrogel formulations were supplemented with 10% foetal bovine serum (FBS). Three cell-seeding densities were evaluated: 1×10^4 (blue), 5×10^4 (yellow) and 1×10^5 (green) cells per construct. Panels **(A)** and **(C)** show mean values $\pm$ standard deviation, whereas panels **(B)** and **(D)** display simple linear regressions fitted to the time-series data, with shaded regions representing the 95% confidence bands (n = 3).

Building on these results, **Phase 2** employed 10 mg/mL fibrinogen hydrogels and a reduced set of cell seeding densities to enable extended imaging of network maturation, stability and disintegration. Over the 50–day live-imaging period, both total occupied area (Figure 6.5) and endothelial structure counts (Figure 6.6) exhibited strong cell seeding density-dependent behaviour, with hydrogel formulation exerting a secondary influence. Constructs seeded with 1×10^4 cells initially occupied larger areas but declined steadily over time, whereas higher seeding densities increased from lower initial values. Tube-like counts followed similar trends: the lowest density declined substantially, losing approximately half of its initial objects by day 50, while intermediate and high densities showed sustained increases. Average eccentricity increased rapidly within the first week and then stabilised, indicating early establishment and long-term maintenance of elongated morphologies, with cell-seeding density exerting a stronger influence than VEGF supplementation (Figure 6.7). Collectively, these findings indicate that cell-seeding density was the principal determinant of long-term network stability in this Phase, with intermediate densities providing the most balanced support for sustained tubular organisation and morphological integrity over extended culture periods.

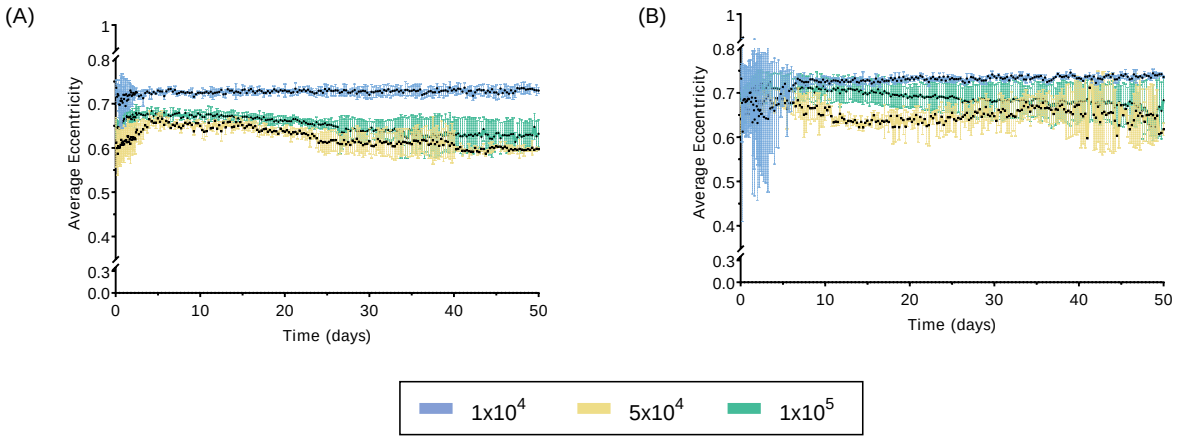


Figure 6.7: **Phase 2 live-imaging analysis of average object eccentricity in MVEC-containing hydrogels over 50 days.** Average eccentricity of detected objects was quantified from whole-well scans acquired every 2 h for the first 2.5 days and subsequently every 6 h until day 50 during **Phase 2** experiments. Eccentricity was used as a descriptor of object morphology, where values approaching 0 indicate circular objects and values approaching 1 indicate elongated, line-like structures. MVECs were embedded in fibrin hydrogels fabricated at 10 mg/mL fibrinogen as either **(A)** EBM or **(B)** EBM + VEGF formulations. Hydrogel formulations were supplemented with 10% foetal bovine serum (FBS). Three cell-seeding densities were evaluated: 1×10^4 (blue), 5×10^4 (yellow) and 1×10^5 (green) cells per construct. Data are presented as mean values $\pm$ standard deviation (n = 3).

6.3.3 Mechanical Characterisation: Compressive Loading of Acellular Hydrogels

Fibrin hydrogels were subjected to compressive loading using the MicroTester LT to characterise the mechanical response. Tip and base displacements, sample height and compressive force were recorded over time (Figure 6.8). Representative images of each phase of the test are presented in Figure F.2.

Tip displacement increased steadily from 0 µm to a maximum of 1,544.41 µm at 32.8 s, corresponding to peak compression. The programmed compression phase in the cycle was from 0–30 s, so a minor delay in reaching the maximum tip displacement was observed. After peak compression was reached, tip displacement exhibited minor oscillations around 1,500–1,545 µm during the hold phase, reflecting small adjustments.

Base displacement followed a similar trend but with a slight lag behind tip displacement, reaching its maximum of 2,239.69 µm at 31.4 s. This delay indicates that the sample deformed under the applied load,

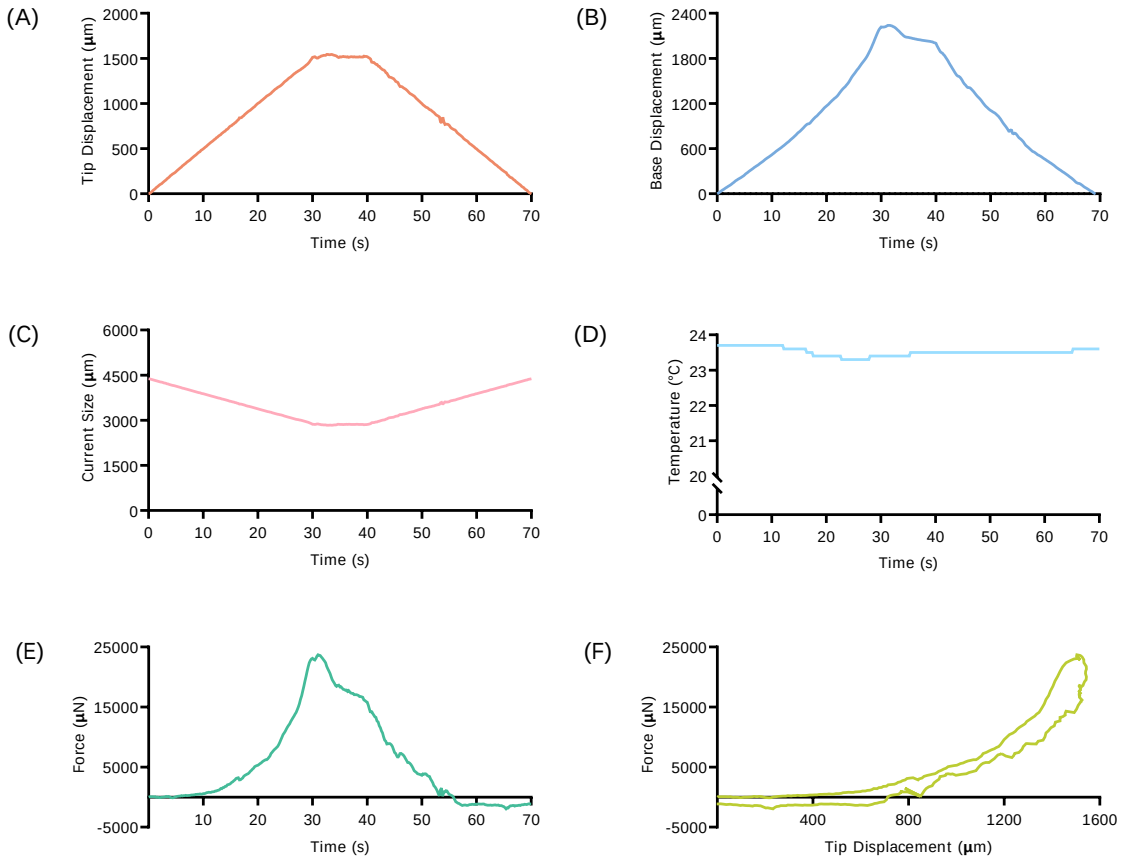


Figure 6.8: **Mechanical response of fibrin hydrogels under compressive loading.** Fibrin hydrogels were subjected to a single compression cycle on the MicroTester LT, consisting of loading to 35% strain over 30 s, a 10 s hold and a 30 s recovery phase. Data were recorded every 0.2 s, including displacement, force, size and temperature. The resulting plots show **(A)** tip displacement (µm), **(B)** base displacement (µm), **(C)** sample height (µm), **(D)** temperature (°C) and **(E)** force (µN) over time (s). Panel **(F)** shows force (µN) as a function of tip displacement (µm). Hydrogels were prepared with fibrinogen from human plasma (10 mg/mL) in endothelial cell basal medium (EBM) and crosslinked using thrombin (10 U/mL in MES/NaCl buffer) and $CaCl_2$ (1 M in distilled water) at a ratio of 200:10:1 (fibrinogen : thrombin : $CaCl_2$).

with the base moving minimally compared to the tip. During the hold phase, the base displacement remained relatively stable, showing only small fluctuations due to material relaxation.

The resulting sample height decreased from an initial 4,378.8 µm to a minimum 2,834.39 µm at peak compression (t = 32.8 s). At the end of the compression phase (t = 30 s), the height was 2,867.81 µm, which was slightly larger than the minimum sample height, indicating a small delay in reaching peak compression. This corresponds to a compressive strain of 34.09% at 30 s (end of compression phase) and 35.27% at 32.8 s (minimum sample height), which are consistent with the 35% compressive strain programmed in the experiment. The continued decrease in sample height after the compression phase stopped reflects the viscoelastic relaxation of the hydrogel before gradual recovery. Following peak compression, the sample height gradually increased, reflecting elastic recovery and viscoelastic relaxation. This is consistent with the viscoelastic properties of fibrin, where its elasticity is characterised by reversible mechanical deformation [629]. Hong *et al.* (2016) used dual-mode ultrasound elasticity technique using ultrasound pulses to show that fibrin hydrogels display characteristic creep and stress relaxation under compressive loading, with time-dependent recovery after load removal. These behaviours are consistent with the gradual recovery and minor oscillations you observed during the hold and recovery phases [630].

When tip displacement and sample height were plotted against time, their relationship highlighted the expected inverse correlation, albeit with a slight time lag between them: as the tip displacement increased, the sample height decreased, reflecting internal material deformation and relaxation dynamics. Kim *et al.* (2017) investigated fibrin-collagen hydrogels under unconfined compression, showing that increased compression led to a more dense network and reduced sample height. Simultaneously, displacement measurements reflected the internal deformation and viscoelastic relaxation dynamics of the hydrogels, revealing non-linear, time-dependent mechanical responses that produce a lag between applied displacement and resulting sample height changes [631].

Temperature was monitored throughout the period and remained stable between 23.3 and 23.7°C, ensuring negligible thermal impact on the measurements. Maintaining a controlled temperature range is particularly important for biomaterials to ensure the polymer can maintain its mechanical properties, ensuring reliable and reproducible results [306, 632].

The compressive force increased in a non-linear fashion with both tip displacement and time, starting from 0 µN and reaching 23,125.2 µN at 30 s, with a maximum of 23,693.5 µN at 31 s. The initial non-linear increase in force reflects the softening and subsequent stiffening behaviour of the fibrin hydrogel, which coincides with findings reported by other researchers [629, 633]. During the hold and relaxation phases after peak compression, the force decreased gradually, showing characteristic viscoelastic relaxation behaviour. Peak force coincided with maximum tip displacement and maximum sample compression, confirming a consistent mechanical response. Force–displacement curves showed a nonlinear profile characteristic of soft tissue–like materials. Several authors have reported that fibrin-based and composite scaffolds show non-linear force-displacement profiles and viscoelastic relaxation, mirroring the mechanics of native soft tissues [629, 633, 634].

Overall, these measurements demonstrate controlled compression of the fibrin hydrogel, with tip and base displacements, sample height reduction and force response all consistent with its viscoelastic properties. The negligible temperature variation ensures that these responses reflect the intrinsic material behaviour rather than being the result of variations in temperature, supporting the suitability of fibrin hydrogels for tissue engineering (TE) applications in soft tissue and microvascular scaffold development.

Mechanical testing with the MicroTester LT, a micro-scale tension–compression system commonly used for biological tissues, scaffolds and hydrogels [626], showed that the fibrin hydrogel displayed viscoelastic properties comparable to those of native tissues as well as of fibrin clots [633].

This system enabled precise measurement of displacement–time, force–time and force–displacement profiles under physiologically relevant compression. The hydrogel exhibited gradual force relaxation during the hold phase and partial recovery during the recovery phase, with a non-linear force–displacement profile consistent with native soft tissue behaviour [629, 633, 634]. These results highlight the fibrin hydrogel's suitability as a soft tissue model and provide preliminary insights into its compressive response, supporting its potential for soft tissue TE and *in vitro* microvascular model development.

6.3.4 Biocompatibility Evaluation of 3D-Printed Objects

6.3.4.1 MVEC Number-Fluorescence Standard Curve

A standard curve relating PrestoBlue fluorescence to MVEC number was generated by plotting background-corrected fluorescence intensity against MVEC seeding density. PrestoBlue florescence increased with increasing MVEC seeding density across all measured time points (15 min, 30 min, 1 h and 2 h), demonstrating a clear dependence of fluorescence signal on cell number. Although fluorescence readings were obtained at four time points (data not shown), the 30 min incubation period was selected for standard curve construction and

all subsequent experiments, as it provided a robust and reproducible signal with limited variability between replicates, indicating that longer incubation times were unnecessary.

A positive linear correlation between fluorescence intensity and cell seeding density was observed. As such, a linear regression analysis was performed to generate the standard curve (Figure 6.9) so that it can be used as a benchmark to extrapolate MVEC numbers from fluorescence measurements in further experimental work. The linear model was evaluated using regression analysis with ANOVA at a 99% confidence level. The resulting multiple correlation coefficient (R) was 0.9844, indicating a strong positive relationship between fluorescence intensity and MVEC number, while the coefficient of determination (R^2) value was 0.9692, demonstrating a good fit of the linear model. ANOVA analysis yielded a significance F value < 0.05, confirming the statistical validity of the regression model.

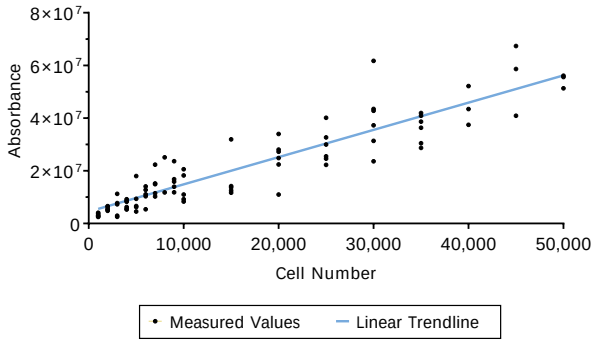


Figure 6.9: **Standard curve relating human dermal microvascular endothelial cell (MVEC) number to PrestoBlue absorbance.** MVECs were seeded in 96–well plates at varying seeding densities (0–50 $\times$ 10^3 cells per well). PrestoBlue floresence was measured after an incubation period (here, values measured at t = 30 min are shown), shown as black data points. The fitted linear regression model is shown in blue (Regression analysis with ANOVA; 99% confidence level; R^2 = 0.9692; significance F < 0.05; n = 6).

6.3.4.2 Biocompatibility Assessment of Conditioned Media

3D printing has become a widely used method for prototyping and fabricating devices for TE applications [635]. As cell-embedded constructs will be in direct contact with 3D-printed components in these models, it was necessary to assess potential cytotoxic effects arising from prolonged resin-medium interactions. Three commonly used 3D printing resins (black, clear and BioMed amber) were evaluated for biocompatibility to identify a suitable material for the fabrication of devices intended for contusion and crush injury models. Black resin is suitable for general-purpose prototyping and intricate models, offering improved print reliability and mechanical properties; clear resin offers optical transparency, high printing resolution and mechanical performance; and BioMed amber is a durable, rigid, biocompatible resin designed for extended skin contact (> 30 days) or brief contact (< 24 h) with bone, tissue, dentin, or mucous membranes [627, 635].

Conditioned media were generated by incubating EBM within 3D-printed containers for six weeks to allow accumulation of any resin-derived leachates, followed by supplementation to generate EGM prior to cell exposure. The 3D-printed containers used for conditioning media (Figure F.18) were designed to maximise resin-medium contact. The container design yielded a surface are of 15,246.72 mm^2 and a volume of 19,750.51 mm^3, resulting in a surface-to-area ratio of 0.77196. These values were calculated using SolidWorks by measuring the negative space of the tray, which fulfilled the design criterion of the ratio being greater than 0.75, ensuring sufficient exposure of the medium to the printed resin. Each container held 20 mL of medium when filled to the rim.

MVEC viability was assessed over a 14–day period using the PrestoBlue assay (Figures 6.10 & F.19), with fluorescence values normalised to fresh media (C1) and incubated media (C2), and converted to estimated cell numbers using a standard curve (Figure 6.9).

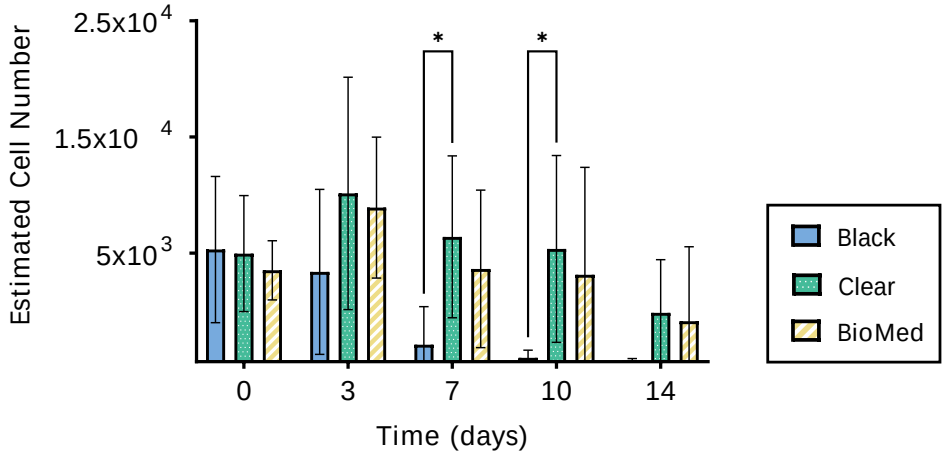


Figure 6.10: **Resin-conditioned media effects on Microvascular endothelial cells (MVECs) over 14 days, with estimated cell number.** MVECs were seeded at 5×10^3 cells per well and cultured in media conditioned by black, clear, or BioMed Amber resins. Estimated cell numbers were calculated by matching absorbance values to the standard curve (Figure 6.9). Values are plotted as mean $\pm$ standard deviation. (Two-way ANOVA/Tukey's HSD; $^*p \leq 0.05$; only statistically significant differences are shown; $n = 10$).

When normalised to either fresh media (C1; Figure F.19A) or incubated media (C2; Figure F.19B), relative absorbance exhibited similar overall trends across all resin conditions, with values decreasing from day 3 onwards. However, estimated cell numbers derived from the standard curve indicated that both clear and BioMed Amber resin-conditioned media supported an increase in cell number between day 0 and day 3. The observed reduction in relative absorbance during this period can therefore be attributed to a greater increase in cell number in the control conditions (C1 & C2) used for normalisation, rather than a decrease in cell viability.

Both relative absorbance against the controls (Figure F.19A & B) and estimated MVEC numbers (Figure 6.10) followed the same overall pattern. All resins supported comparable cell numbers at day 0, with clear and BioMed Amber resin-conditioned media promoting increased cell numbers by day 3, while the black resin condition remained lower. A marked divergence was observed at days 7 and 10: black resin-conditioned media supported substantially fewer cells than either clear or BioMed Amber resins; and clear resin yielded significantly higher values than black resin ($p < 0.05$). By day 14, no viable cells were detected in the black resin condition, whereas clear and BioMed Amber resin-conditioned media continued to support measurable cell numbers.

Although BioMed Amber consistently yielded slightly lower values than clear resin, these differences were not statistically significant. Based on these findings, clear resin was selected for further experimental work, as it demonstrated superior performance relative to black resin and comparable biocompatibility to BioMed Amber without the additional material cost.

6.3.5 Crush Injury

Hydrogels were subjected to a crush injury using Perspex cylinders (12–well plates) for 1 h and imaged at 5–min intervals or with 3D-printed cylinders for up to 120 h. Incremental strain measured by feature-tracking was small overall: mean incremental values for axial and radial strain clustered around −1 to 1% with interquartile ranges typically −2 to 2% (Figure 6.11). No significant differences were observed between 8 and 10 mg/mL

fibrinogen hydrogels in incremental strain (Figure 6.11) or in maximum extension to failure (Figure 6.12). Tensile loading of cell-embedded hydrogels resulted in a macroscopic elongation ranging from 10 mm to 25 mm (250% overall), but incremental strain per step decreased as the sample lengthened. This is consistent with geometric effects and viscoelastic relaxation properties of the hydrogel.

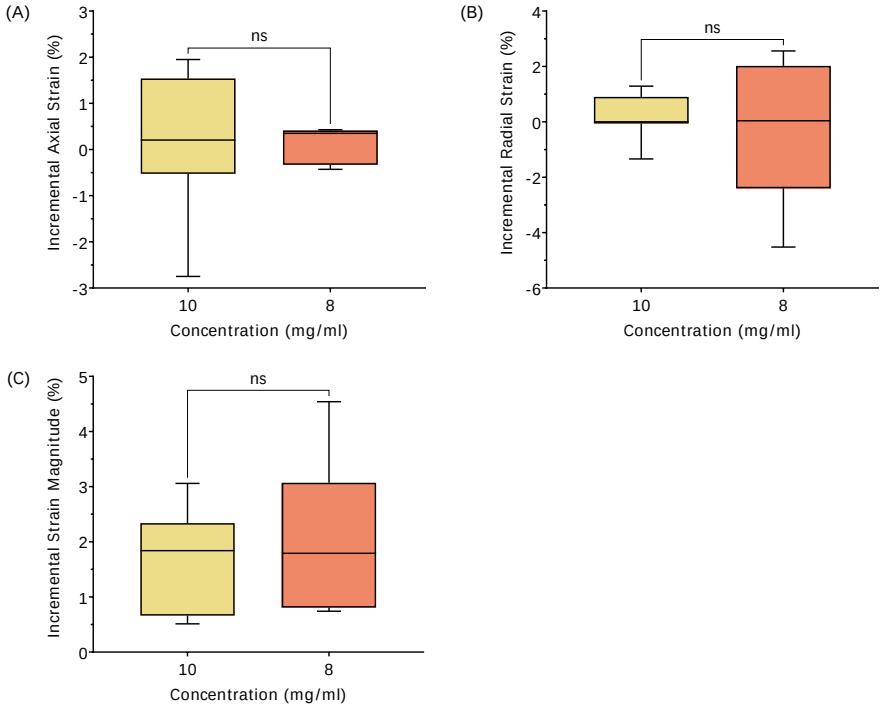


Figure 6.11: **Incremental strain following crush injury in MVEC-containing hydrogels.** Incremental strain (%) as a function of hydrogel concentration (8 or 10 mg/mL fibrinogen) following a 1 h crush injury. Microvascular endothelial cell (MVEC)–embedded fibrin hydrogels were subjected to compressive loading using Perspex cylinders in a 12–well plate format. No significant difference in incremental strain was observed between concentrations. Unpaired, two-tailed Welch's *t*-test assuming normal distribution (99% confidence level; $n = 10$).

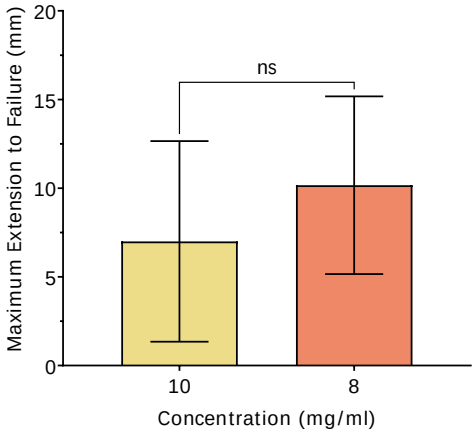


Figure 6.12: **Maximum extension to failure following crush injury in MVEC-containing hydrogels.** Maximum extension to failure (mm) for MVEC-embedded fibrin hydrogels with concentrations of 8 or 10 mg/mL fibrinogen following a 1 h crush injury using Perspex cylinders in a 12–well plate. No significant difference was observed between groups. Unpaired, two-tailed Welch's *t*-test assuming normal distribution (99% confidence level; $n = 10$ per group).

Conditioned-media assays following crush injury showed minimal effects on MVEC viability: live/dead indices for crush-conditioned media (cylinder heights: 15–18 mm) did not differ consistently from uninjured controls across EBM and EBM + VEGF formulations, and EthD-1 (dead-cell) signal remained near the baseline (Figure 6.17B). Taken together, these data suggest that for the crush injury model, bulk mechanical deformation and viscoelastic relaxation dominate the acute mechanical environment experienced by MVECs, while soluble factor release after crush produced only modest and inconsistent effects on MVEC viability in conditioned-media assays.

Mechanistically, the low incremental strain magnitudes to which the cell-embedded hydrogel constructs were subjected to and the lack of robust conditioned-media toxicity suggest that crush in this configuration causes limited immediate EC necrosis. However, further work to quantify and characterise responses at the molecular level are required.

6.3.6 Contusion Injury

Contusion injury was modelled by dropping a metallic mass from 5, 10 and 15 cm using a guide. After impact, the mass was left in place for 30 min before careful removal to avoid provoking a penetrating injury on the hydrogel construct (Figure F.4). Unlike crush injuries, contusion produced clear, severity-dependent biological signals in conditioned-media assays (Section 6.3.8).

For EBM hydrogels, only the 5 cm drop produced a significantly lower live/dead index when compared to the uninjured EBM hydrogel control. Interestingly, when dropping the mass from 10 and 15 cm heights, no statistically significant differences were observed against the uninjured hydrogel (Figure 6.17A). For EBM + VEGF hydrogels, significant differences were only observed at 15 cm. Direct comparisons between equal mass drop heights showed that EBM + VEGF hydrogel-conditioned media yielded higher live/dead indices than the corresponding EBM hydrogels at 5 and 10 cm but not at 15 cm. This potentially suggests that any VEGF-associated benefit, if any, is rather limited to lower-energy impacts.

Qualitative fluorescence images corroborated these trends: contusion-conditioned media often increased calcein AM signal (live cells) relative to fresh EBM, while EthD-1 (dead cells) remained modest, implying enhanced metabolic activity or survival rather than widespread cytotoxicity (Figures 6.16 & 6.18). This pattern suggests that contusion releases biologically active soluble factors (matrix fragments, growth factors, stress-associated mediators) in a non-linear manner with respect to impact energy, producing complex effects on endothelial behaviour.

Mechanistically, the contusion setup used in this research combines the weight-drop impact with a period of sustained compression, as the metallic mass was left in contact with the construct for 30 min. While this duration is not expected to induce extensive cell death, it could be sufficient to promote partial matrix disruption and the release of soluble factors, such as matrix fragments, growth factors and damage-associated molecules, which may exacerbate the initial impact-related injury. The results obtained when inducing contusion injuries on cell- and network-embedded constructs, together with the secondary effects observed following exposure to contusion-conditioned media, suggest that the combination of impact and short-duration sustained compression is sufficient to induce partial matrix disruption and release biologically active soluble factors without causing widespread acute cell death. This could potentially explain the modest EthD-1 signals observed in the live/dead cytotoxicity assay. The partial protection observed with a few EBM + VEGF hydrogels at lower mass-drop heights suggests that the hydrogel composition can modulate early endothelial responses and network resilience; however, this effect is not observed when higher heights are use.

6.3.7 Strain Injury

Hydrogel and dog-bone constructs were subjected to axial tensile loading in 0.5 mm increments using a custom loading device (Figure F.20). Images were captured before injury and after each increment, and were used to calculate incremental axial and radial strain from which incremental strain magnitude was derived (Figure 6.13). These strain measures were also plotted as a function of displacement to characterise total strain accumulation during loading (Figure 6.14).

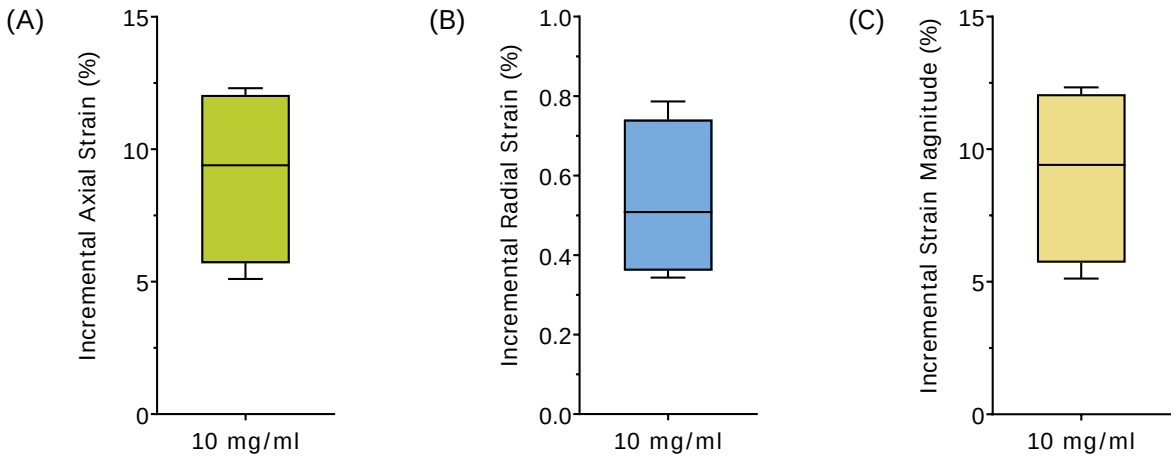


Figure 6.13: **Incremental strain components following strain injury in MVEC-containing hydrogels.** Incremental strain responses in MVEC-embedded fibrin hydrogels of differing concentrations (8 or 10 mg/mL fibrinogen) subjected to strain injury. Panels show **(A)** incremental axial strain (%), **(B)** incremental radial strain (%) and **(C)** incremental strain magnitude (%). Unpaired, two-tailed Welch's *t*-test assuming normal distribution (99% confidence level).

Incremental axial and radial strains exhibited a directional dependence, as expected. Importantly, the use of 0.5 mm displacement increments resulted in modest incremental strain magnitudes at each step, demonstrating that this injury protocol enables controlled induction of strain-based NPTIs. When plotting total strain as a function of displacement, total axial strain increased significantly at every displacement step, whereas total radial strain did not show statistically significant differences between steps. This underscores the need to use additional measures, such as the total strain magnitude, which integrates both axial and radial components. Therefore, when total strain magnitude is used for analysis, the effect of each variable as well as their relation with each other is translated into a more informative measure.

Network-level analysis revealed a biologically significant response that was not captured when using cell-tracking. Following strain injury, the percent change in confluence relative to the pre-injury baseline decreased noticeable, thus indicating a disruption of the endothelial network (Figure 6.15). This reduction was significantly greater in EBM hydrogels than in EBM + VEGF hydrogels (2.17–fold increase, $p < 0.05$), potentially suggesting that the absence of VEGF either made the EBM construct and its embedded microvasculature more susceptible to strain-induced disintegration or that VEGF supplementation acts as a mitigating factor preventing or reducing endothelial damage.

Together, these findings demonstrate that microvascular damage cannot be fully predicted from mechanical strain metrics on their own, it is necessary to incorporate more complex models that take into account physiological arrangements such as endothelial networks. Beyond this, the results highlight the importance of combining mechanical, cellular and network-level analyses when modelling strain-based NPTIs *in vitro*.

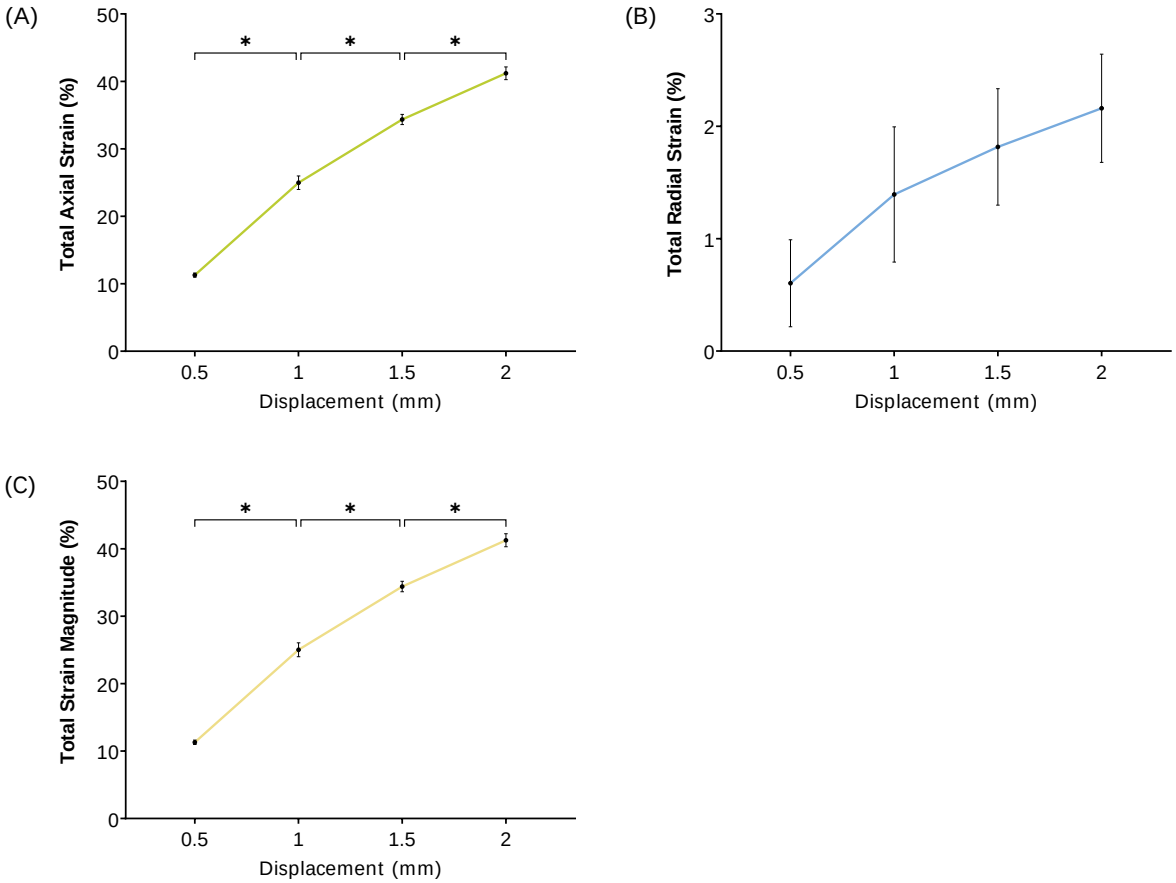


Figure 6.14: **Total strain as a function of displacement during strain injury.** Total strain responses plotted against applied displacement (mm) during strain injury of MVEC-embedded fibrin hydrogels. Panels show **(A)** total axial strain (%), **(B)** total radial strain (%) and **(C)** total strain magnitude (%). Unpaired, two-tailed Welch's *t*-test assuming normal distribution (99% confidence level).

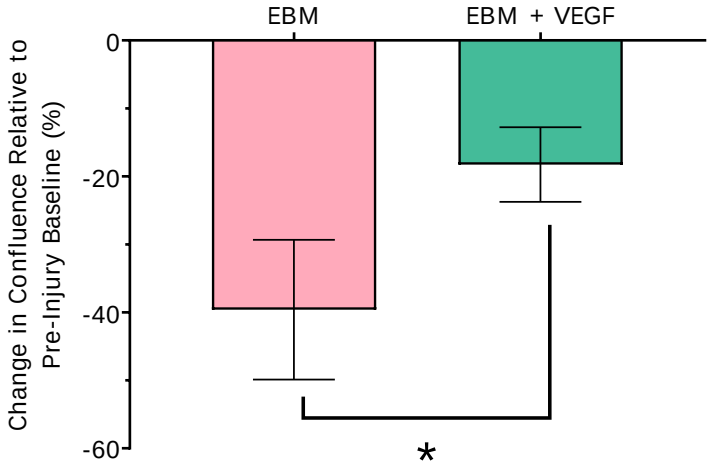


Figure 6.15: **Change in endothelial network confluence following strain injury.** Percent change in confluence (ΔC) relative to the pre-injury baseline for 3D microvascular endothelial network-embedded fibrin hydrogels (10 mg/mL) subjected to strain injury. Endothelial cell basal medium (EBM) hydrogels exhibited significantly greater network loss compared with EBM + VEGF hydrogels, indicating increased susceptibility to strain-induced network disruption in the absence of VEGF. Unpaired, two-tailed Welch's *t*-test assuming normal distribution.

6.3.8 Conditioned Media

MVEC viability following exposure to conditioned media derived from crush and contusion injury models was assessed using a live/dead cytotoxicity assay, with calcein AM (excitation/emission: 485/530 nm) indicating metabolically active cells and EthD-1 (530/645 nm) indicating membrane-compromised cells. After background subtraction, all fluorescence values were normalised to the corresponding fresh EBM control for the same seeding density (Figure 6.16), allowing direct comparison across conditions.

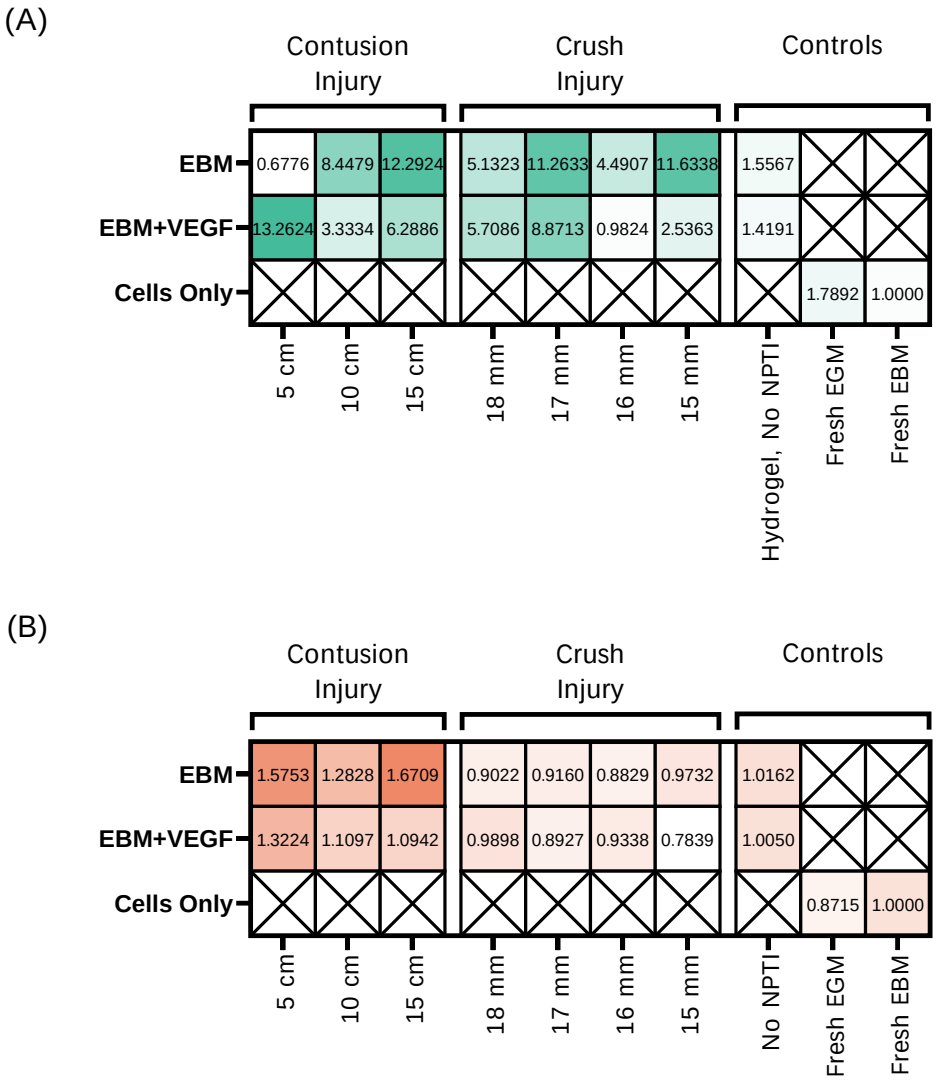


Figure 6.16: **Impact of exposure to conditioned media from crush and contusion injury models on MVEC viability.** Heatmaps display average fluorescence values normalised to the corresponding excitation/emission absorbance of microvascular endothelial cells (MVECs) cultured in fresh endothelial cell basal medium (EBM). Cells were initially cultured in endothelial cell growth medium (EGM) for 24 h, after which the medium was replaced with conditioned or control media and maintained for 72 h. Conditioned media were collected from MVEC-embedded EBM or EBM + VEGF hydrogels subjected to either contusion injury (drop heights: 5, 10 and 15 cm) or crush injury (cylinder heights: 15–18 mm). Control conditions included fresh EBM, fresh EGM and media from uninjured hydrogels. A live/dead cytotoxicity assay was then performed, with calcein AM and EthD-1 added and incubated for 2 h prior to fluorescence measurements. **(A)** Calcein AM fluorescence (excitation/emission 485/530 nm), representing metabolically active (live) cells. **(B)** EthD-1 fluorescence (excitation/emission 530/645 nm), representing membrane-compromised (dead) cells. Data corresponds to a seeding density of 5×10^3 cells per well and is presented as mean normalised fluorescence relative to fresh EBM ($n = 6$).

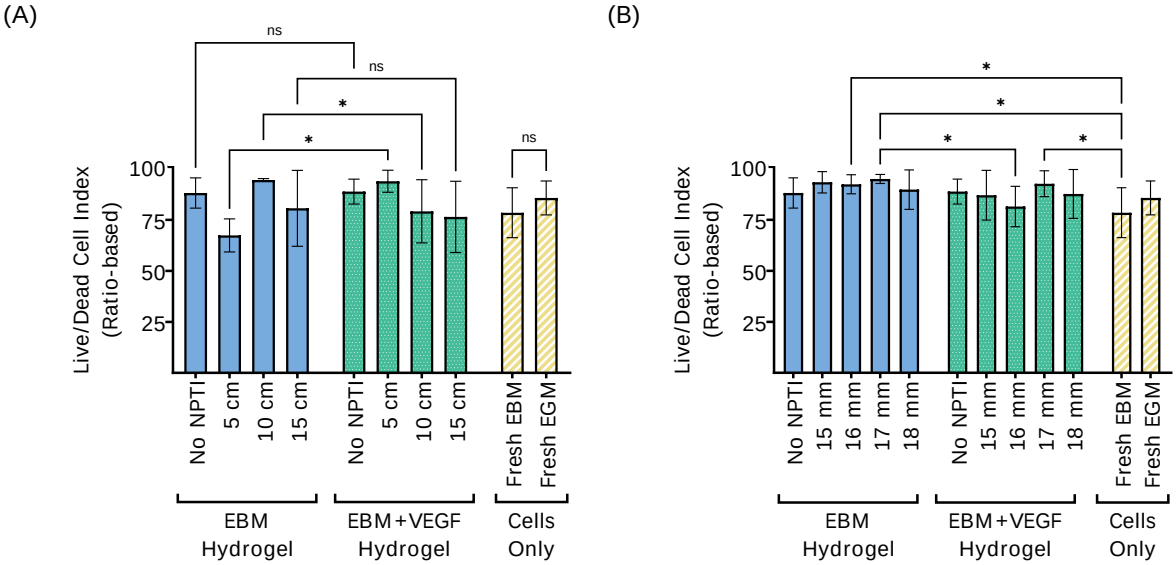


Figure 6.17: **Effects of trauma-conditioned media on Microvascular endothelial cell (MVEC) viability.** The live–dead cell index of MVECs cultured in conditioned media derived from **(A)** contusion injury and **(B)** crush injury applied to 3D microvascular hydrogels is shown. In both panels, four control conditions are included: conditioned media from uninjured EBM and EBM + VEGF hydrogels (no non-penetrating traumatic injury; No NPTI) and cells cultured in fresh media only (fresh EBM: endothelial cell basal medium; and fresh EGM: endothelial cell growth medium), without hydrogel exposure. Here, data corresponding to cell seeding density of 5×10^3 cells per well is shown. In panel **(A)**, contusion injury was induced by dropping a metallic mass from defined heights (5, 10 and 15 cm) onto the hydrogel. In panel **(B)**, crush injury was applied using cylindrical indenters of different heights (15, 16, 17 and 18 mm) over a 24 h period. Two hydrogel formulations were assessed independently: EBM and EBM supplemented with VEGF (EBM + VEGF). MVECs were expanded in EGM prior to embedding and, following embedding, all constructs were maintained exclusively in EBM. MVECs were exposed to trauma-conditioned media and imaged 2 h after live/dead staining (72 h post-exposure to conditioned media). Quantification was performed using Incucyte adherent cell-by-cell analysis. Data are presented as mean $\pm$ standard deviation. The live–dead index (y-axis) was calculated as the ratio of integrated calcein AM fluorescence intensity (live cells) to the sum of integrated calcein AM and EthD-1 fluorescence intensities (dead cells). In panel **(A)**, a representative subset of statistically significant differences is shown due to the large number of comparisons, whereas in panel **(B)** all statistically significant differences are indicated. (One-way ANOVA/Tukey's HSD; $^*p \leq 0.01$; $n = 6$ independent samples per group, 9 images per sample).

Within each hydrogel type, contusion-conditioned media produced injury-severity–dependent effects on MVEC viability (Figure 6.17A). For EBM hydrogels, only the 5 cm contusion resulted in a significantly lower live–dead index compared with the EBM no-NPTI control, whereas the 10 and 15 cm conditions were not significantly different from uninjured EBM. For EBM + VEGF hydrogels, a significant reduction relative to the EBM + VEGF no-NPTI control was observed only at 15 cm, while 5 cm and 10 cm did not differ from the uninjured EBM + VEGF hydrogel. The four control conditions (EBM hydrogel not subjected to a NPTI, EBM + VEGF hydrogel not subjected to a NPTI, Fresh EBM, and Fresh EGM) formed a consistent baseline with no significant differences between fresh media controls and either uninjured hydrogel. Direct comparisons at matched contusion severities demonstrated a clear EBM + VEGF-associated increase in the live–dead index at 5 and 10 cm, but not at 15 cm, indicating that the apparent VEGF-mediated benefit was limited to lower-impact contusion injuries.

Crush-conditioned media induced minimal changes in MVEC viability across hydrogel formulations and compression depths (Figure 6.17B). Within both EBM and EBM + VEGF hydrogels, none of the crush conditions (15–18 mm) differed significantly from their respective no-NPTI controls. For the crush injury conditions, the live–dead index demonstrated minimal sensitivity to hydrogel composition or compression depth, with no sta-

tistically significant differences observed between EBM and EBM + VEGF hydrogels at matched crush distances, indicating that VEGF supplementation did not measurably alter cell viability or conditioned media effects under equivalent compressive loading. Fresh EBM and Fresh EGM did not differ from either uninjured hydrogel condition, confirming a stable baseline. Only a small number of statistically significant differences were detected within the crush injury dataset, all of which were limited to specific intermediate compression depths rather than representing a systematic trend. These included differences between EBM 16 mm and Fresh EBM, EBM 17 mm and Fresh EBM, EBM 17 mm and EBM + VEGF 16 mm, and EBM + VEGF 17 mm and Fresh EBM. Collectively, these findings indicate that crush injury induced only isolated and non-monotonic changes in the live–dead index, with no consistent dependence on hydrogel composition or compressive severity.

In parallel, representative fluorescence images were acquired to qualitatively visualise live and dead cells exposed to conditioned media extracted from hydrogels subjected to contusion (Figure 6.18) or crush (Figures 6.19 & 6.20) injuries, as well as control media derived from uninjured hydrogels and cells only grown in either EBM or EGM (Figure 6.21).

At a seeding density of 5×10^3 cells per well, calcein AM fluorescence showed substantial variation across injury severities and hydrogel compositions. In general, media conditioned by mechanically injured EBM and EBM + VEGF hydrogels resulted in markedly higher live-cell fluorescence than fresh EBM, with only a small number of exceptions (EBM hydrogels subjected to 5 cm contusion and EBM + VEGF hydrogels subjected to 16 mm crush). These findings indicate that factors released following mechanical injury did not impair MVEC viability and, unexpectedly, appeared to enhance metabolic activity or survival. Media from uninjured hydrogels and cells exposed to fresh media alone produced values close to baseline, suggesting that the observed increases were primarily driven by injury-related processes rather than hydrogel formulation.

Comparison between EBM and EBM + VEGF hydrogels did not reveal a consistent trend across matched injury conditions. For contusion injuries, EBM + VEGF–conditioned media produced the largest live-cell signal at the lowest drop height (5 cm), whereas EBM hydrogels showed minimal response at this level but a pronounced increase at higher contusion heights. Similarly, crush injury generally produced higher signals in EBM than in EBM + VEGF hydrogels, although no clear relationship with increasing cylinder height was observed. These findings suggest a complex, non-linear interaction between injury severity and biochemical composition may exist, so further experimental work is required to investigate this.

EthD-1 fluorescence exhibited more moderate changes across conditions. Normalised dead-cell fluorescence generally remained close to fresh EBM levels, indicating no substantial increase in cytotoxicity. Contusion injury tended to produce slightly higher EthD-1 values than crush injury for both hydrogel types. Importantly, the pronounced increases in calcein AM fluorescence were not accompanied by proportional increases in EthD-1 signal, supporting the interpretation that injury-conditioned media primarily promoted viability rather than inducing cell death.

The observation that mechanically injured hydrogels generated conditioned media capable of enhancing MVEC metabolic activity was unexpected and warrants further investigation. Potential mechanisms may include the release of soluble factors, matrix-derived signals, or stress-associated mediators following hydrogel deformation and damage. Overall, these findings demonstrate that crush and contusion models can generate biologically active conditioned media that modulate EC behaviour *in vitro*, supporting their relevance for studying cellular responses to NPTIs and subsequent repair processes.

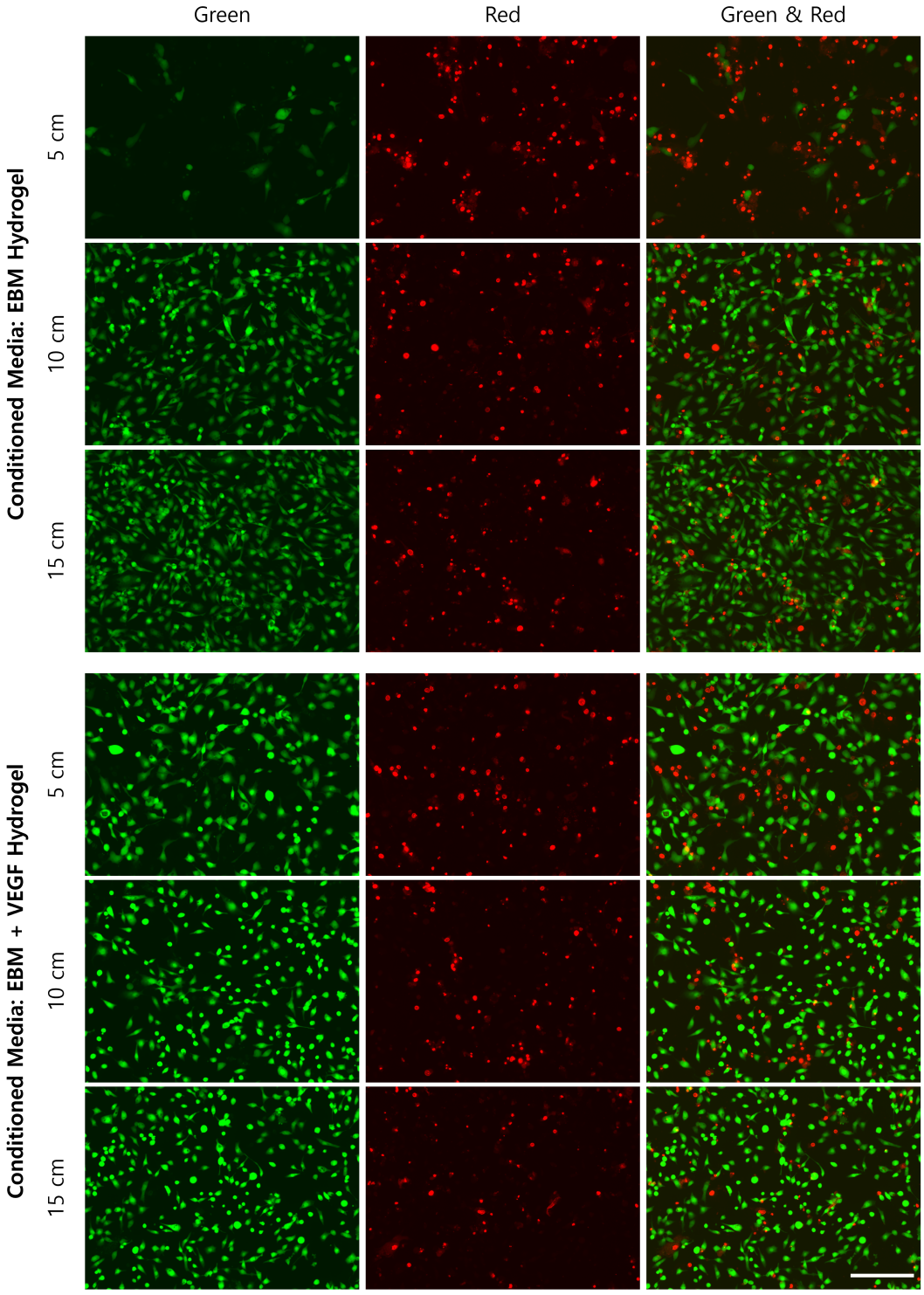


Figure 6.18: **Representative images of Microvascular endothelial cells (MVECs) exposed to contusion injury–conditioned media, captured 2 h after live/dead staining (72 h post-exposure to conditioned media).** Representative images of MVECs following 72 h exposure to conditioned media derived from MVEC-embedded EBM or EBM + VEGF hydrogels subjected to contusion injury. Injuries were induced by dropping a metallic mass from heights of 5, 10, or 15 cm. Cells were stained using a live/dead cytotoxicity assay, with calcein AM (green; live cells) and EthD-1 (red; dead cells) and incubated for 2 h before imaging. Shown are the green and red channels, as well as the merged green-red overlays. Brightfield images were acquired but are not shown. Here, images from cell seeding density of 5×10^3 cells per well are shown. Scale bar: 200 µm.

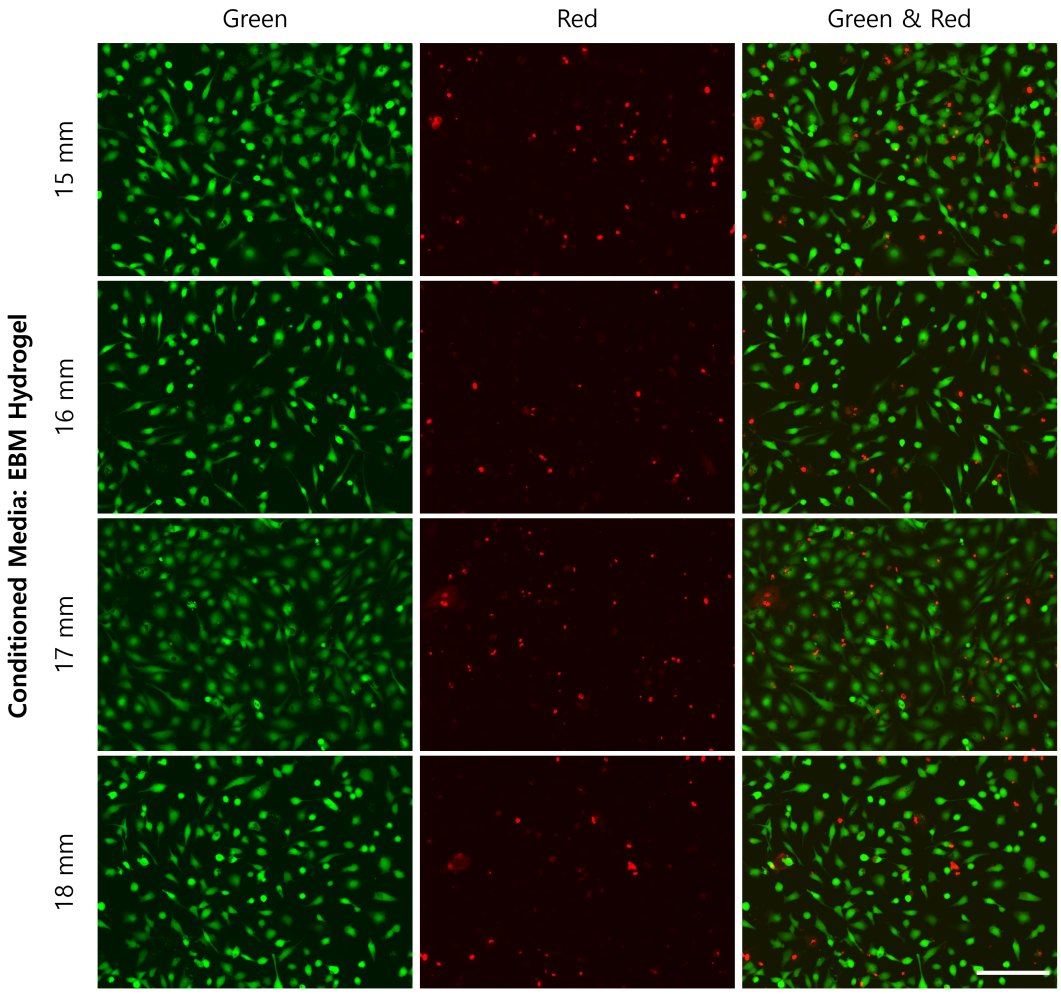


Figure 6.19: **Representative images of MVECs exposed to conditioned media from crush injury-EBM hydrogels.** Representative images of microvascular endothelial cells (MVECs) following 72 h exposure to conditioned media derived from MVEC-embedded EBM hydrogels subjected to crush injury. Injuries were induced by using a 3D-printed cylindrical press of 15–18 mm height. Cells were stained using a live/dead cytotoxicity assay, with calcein AM (green; live cells) and EthD-1 (red; dead cells), and incubated for 2 h before imaging. Shown are the green and red channels, as well as the merged green-red overlays. Brightfield images were acquired but are not shown. Here, images from cell seeding density of 5×10^3 cells per well are shown. Scale bar: 200 µm.

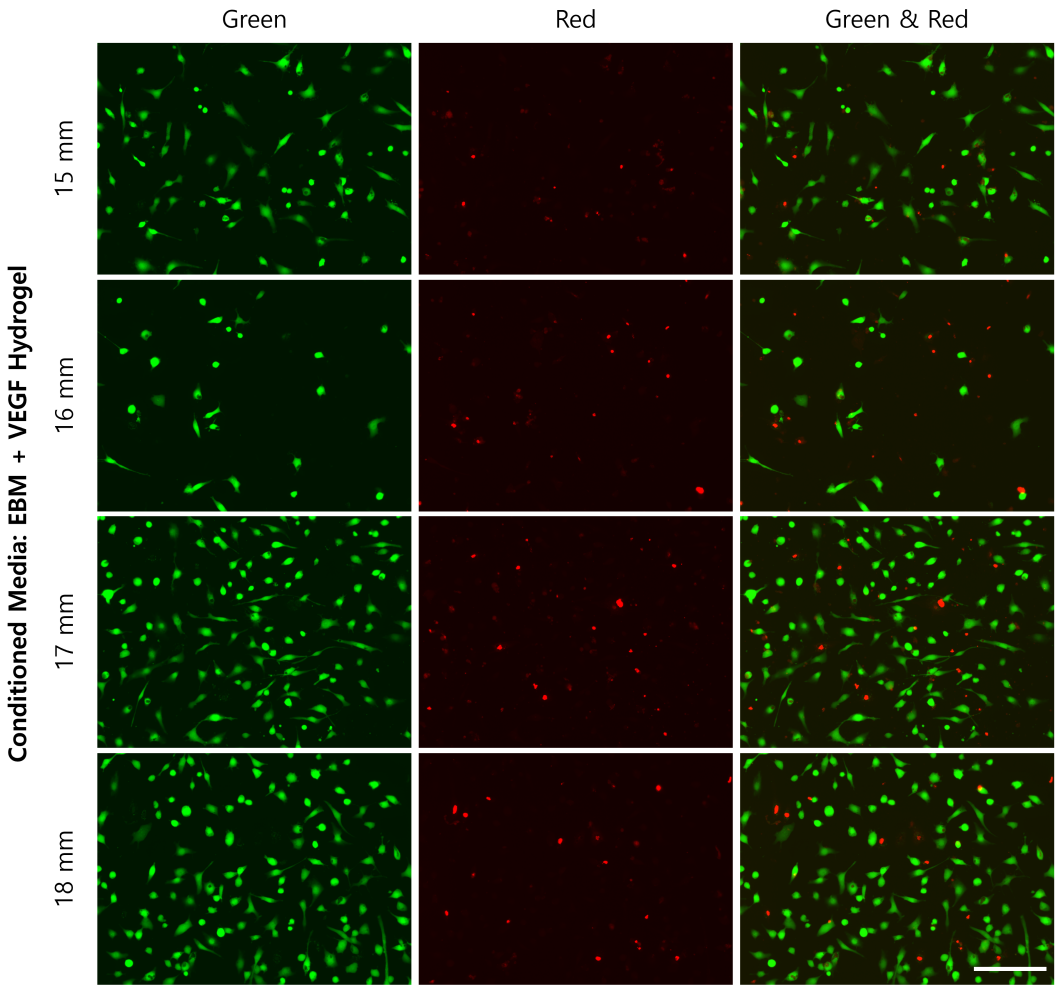


Figure 6.20: **Representative images of MVECs exposed to conditioned media from crush injury-EBM + VEGF hydrogels.** Representative images of microvascular endothelial cells (MVECs) following 72 h exposure to conditioned media derived from MVEC-embedded EBM + VEGF hydrogels subjected to crush injury. Injuries were induced by using a 3D-printed cylindrical press of 15–18 mm height. Cells were stained using a live/dead cytotoxicity assay, with calcein AM (green; live cells) and EthD-1 (red; dead cells), and incubated for 2 h before imaging. Shown are the green and red channels, as well as the merged green-red overlays. Brightfield images were acquired but are not shown. Here, images from cell seeding density of 5×10^3 cells per well are shown. Scale bar: 200 µm.

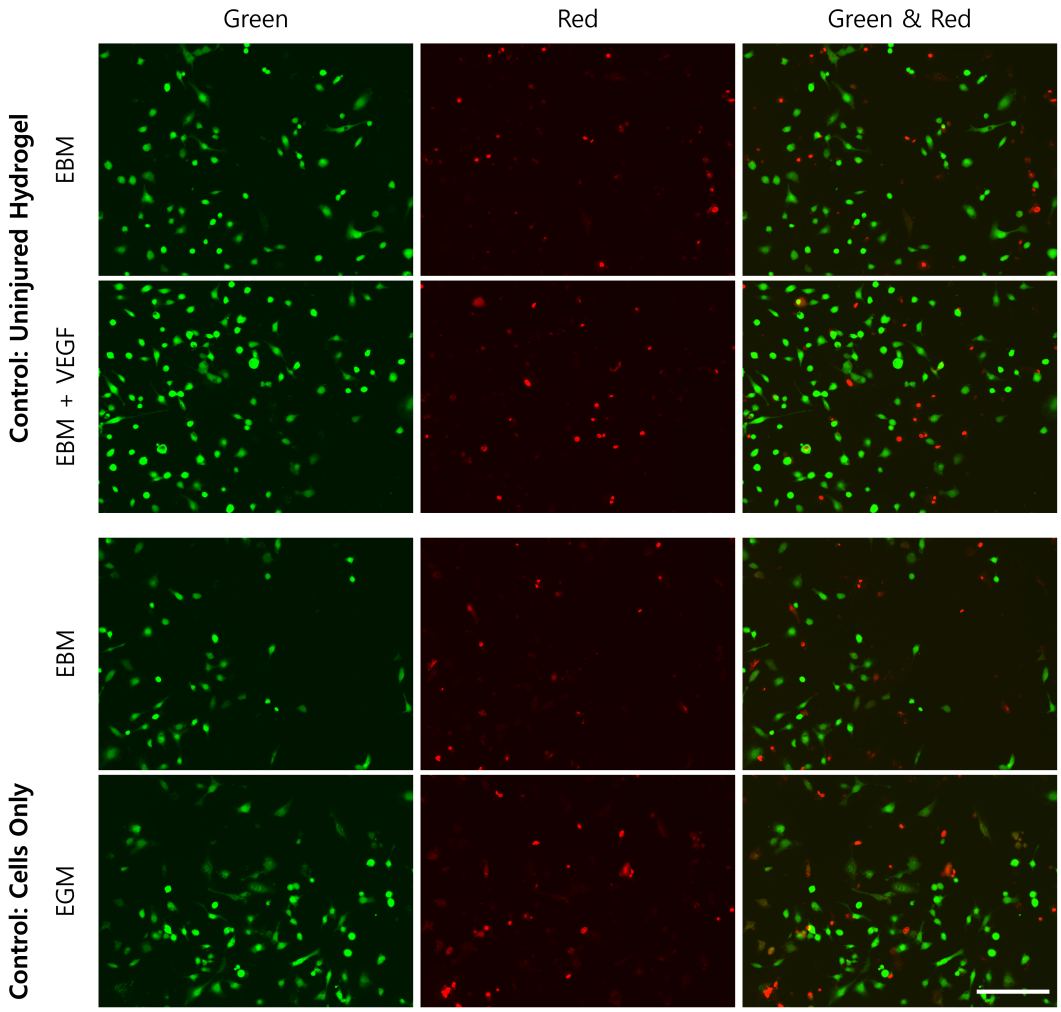


Figure 6.21: **Representative images of MVECs exposed to control media.** Representative images of microvascular endothelial cells (MVECs) following 72 h exposure to control media derived from either MVEC-embedded EBM or EBM + VEGF hydrogels not subjected to any injuries or cells only grown with either endothelial cell basal medium (EBM) or endothelial cell growth media (EGM). Cells were stained using a live/dead cytotoxicity assay, with calcein AM (green; live cells) and EthD-1 (red; dead cells), and incubated for 2 h before imaging. Shown are the green and red channels, as well as the merged green-red overlays. Brightfield images were acquired but are not shown. Here, images from cell seeding density of 5×10^3 cells per well are shown. Scale bar: 200 µm.

6.4 Conclusion

In conclusion, this work demonstrates the feasibility and relevance of an engineered 3D MVEC-embedded fibrin hydrogels as a controllable and physiologically relevant *in vitro* platform for modelling NPTIs. By applying well-defined crush, contusion and strain inputs, this study establishes links between mechanical loading conditions, matrix mechanics and microvascular responses at both the cellular and network levels. While mechanical behaviour was largely governed by the material properties of the fibrin hydrogel and construct geometry, biological outcomes (*e.g.* endothelial network disruption, cell death) were also impacted. The analyses of microvascular network architecture before and after trauma (not presented here in full), further informed the conditioned media experiments and support that mechanically injured constructs generate biologically active signals capable of modulating EC behaviour. Together, these findings constitute a proof of concept that showcases the 3D model as a valuable tool for early-stage trauma research, enabling network-level research while reducing reliance on animal models. Future work includes further refinements in NPTI protocols, incorporation of additional cell types into the model, and direct comparison with *in vivo*, injury metrics and clinical data. This would further enhance the translational relevance of the platform proposed here and broaden its application for not only basic research on NPTIs but also for testing potential therapeutics that mitigate damage and accelerate repair and regeneration.

Acknowledgements

Thanks to Jonathan Tollervey and Matt Brunsting (World Precision Instruments) for guidance with the use of the MicroTester LT and to James Fisk for the kind gift of the metallic spheres and tubing for the experimental work on crush and contusion injury modelling.

Chapter 7
Conclusions & Future Directions

Thesis Integration and Chapter Structure

This final chapter synthesises the findings of the preceding experimental and systematic work, highlighting both the novelty and limitations of the research. It reflects critically on the thesis objectives, demonstrating how Objectives Objective 1 through Objective 4 were addressed: from scaffold selection and optimisation, through systematic evidence synthesis, to the development of a robust long-lasting microvascular construct, and finally the controlled induction of traumatic injury. The contributions of the thesis lie in advancing a mechanobiologically relevant *in vitro* microvascular model, demonstrating its utility in studying the immediate and short-term consequences of NPTIs, and proposing a reporting framework to improve reproducibility in fibrin scaffold research. At the same time, this chapter acknowledges the boundaries of this research, including the absence of immune and systemic interactions and the need for further validation against *in vivo* models. Looking forward, the chapter outlines future directions to refine the model for translational applications, including therapeutic testing, patient-specific modelling, and integration with broader tissue and organ systems. In doing so, it situates the research as a foundation for reducing reliance on animal models and advancing precision medicine in the field of trauma mechanobiology.

Conclusions & Future Directions

7.1 Fulfilment of Thesis Aims and Objectives

The overarching aim of this thesis was to develop and optimise a three-dimensional (3D) *in vitro* microvascular model based on natural polymer scaffolds incorporating physiologically relevant cells. Then, to apply this model to investigate the microvascular consequences of non-penetrating traumatic injuries (NPTIs) under controlled mechanical loading conditions during the immediate and short-term post-injury period. This aim was achieved through four interlinked objectives, addressed across four core chapters: three experimental sections and a systematic review (SR).

Objective 1 aimed to develop and optimise a natural polymer–based scaffold capable of supporting endothelial cell (EC) adhesion, viability, migration, and the formation of microvascular networks *in vitro*. In Chapter 3, a microvascular model comprising a hydrogel embedded with ECs was developed. Here, the suitability of three natural polymer candidates (collagen, fibrin and gelatine) was investigated alongside key formulation parameters (*e.g.* polymer concentration, medium composition), to identify the most appropriate scaffold system for microvascular modelling.

This was achieved by embedding human umbilical vein endothelial cells (HUVECs) within the different hydrogel formulations and evaluating cell seeding density, adhesion, migration, viability, and tube formation, alongside qualitative assessments of hydrogel shape retention and consistency. Through this comparative optimisation process, Chapter 3 identified fibrin-based hydrogels as the most promising hydrogel composition for supporting EC organisation into interconnected microvascular structures, thereby establishing the foundation for further model development.

Objective 2 sought to systematically review and evaluate the existing literature on fibrin-based soft tissue scaffolds used in tissue engineering (TE), with a focus on identifying scaffold design parameters that lead to successful endothelial formation and migration processes (EFMPs) (*i.e.* tube formation, network formation, and cell migration). This objective was directly informed by the findings of Chapter 3, where fibrin emerged as the most suitable polymer.

Chapter 4 addressed this objective through a SR of fibrin-based scaffolds used in soft tissue TE applications, focusing on EFMPs. By synthesising the existing literature, this Chapter contextualised the experimental findings of Chapter 3 where fibrin scaffolds successfully enabled the formation of tube-like structures. Chapter 4 demonstrated that, while fibrin is widely used to support endothelial organisation, outcomes are highly sensitive to scaffold formulation and experimental design choices.

The SR identified scaffold formulation, fibrinogen origin, coagulant and crosslinker selection, cell type, and cell incorporation strategy as critical parameters influencing EFMPs. Importantly, EFMPs were frequently reported interchangeably despite representing distinct biological processes with different sensitivities to material and mechanical cues. Human-derived, commercially sourced fibrinogen combined with thrombin and cell pre-embedding reported the most consistent success in supporting tube and network formation. Also, the selection of cell lines emerged to be an important aspect in scaffold success. Based on this, further development of the 3D model incorporated these findings to pre-embed cells into the construct, carefully select an appropriate cell line, and integrate thrombin into the formulation.

Objective 3 focused on the development, optimisation, and characterisation of a robust 3D *in vitro* microvascular model incorporating an appropriate cell line, capable of maintaining microvascular network integrity beyond 24 h and extending observations beyond the early period after network formation. In Chapter

5, the fibrin-based scaffold developed in Chapter 3 and refined through the evidence synthesised in Chapter 4 was further developed into a stable 3D microvascular construct.

This objective was achieved by embedding microvascular endothelial cells (MVECs), specifically human dermal microvascular endothelial cells (HDMEC-1), within optimised fibrin hydrogels and validating their performance against a gold-standard endothelial cell line (HUVECs). In parallel, key material properties (*e.g.* degradation, gelation) were utilised to evaluate how scaffold composition influenced material properties and, subsequently, impact network formation, architecture, and integrity over time.

Variations in hydrogel composition such as the source and concentration of fibrinogen, the crosslinking ratio, and the medium were identified as key parameters that significantly impact the material properties of the scaffold, and its network architecture and long-term integrity. Hydrogels using human serum-derived fibrinogen at higher concentrations (6–10 mg/mL), crosslinked at a ratio of 200:10:1 (fibrinogen : thrombin: $CaCl_2$), and with endothelial cell basal medium (EBM) as the medium consistently supported more complex and stable networks. In the longer term, these compositions exhibited slower degradation rates, shorter gelation times, enabled more complex networks, maintaining their integrity for at least 13 days post-seeding, thereby overcoming a key temporal limitation of many existing *in vitro* microvascular models.

Objective 4 targetted a proof of concept for the application of the developed 3D microvascular model as an *in vitro* platform for NPTIs, enabling controlled investigations of mechanical inputs-microvascular damage relationships. To achieve this goal, the optimised and validated 3D microvascular construct developed in Chapter 5 was subjected to well-defined and reproducible mechanical loading regimes representative of NPTIs.

In Chapter 6, controlled contusion, crush, and strain injuries were induced onto both cell-embedded and network-embedded hydrogels. Injury responses were assessed through comparative EC tracking and microvascular network architecture before and after loading. By systematically varying biomechanical inputs (*e.g.* height for object drop; time for crush injury) relationships were established between defined mechanical insults and resulting patterns of microvascular disruption. This worked validated the use of the 3D microvascular model in the context of NPTI research, showcasing its use for investigating the immediate and short-term consequences of trauma at the microvascular scale under controlled and reproducible conditions.

The four objectives of this thesis are deliberately interdependent and together form a coherent pathway from material selection to biological application. Objective 1 established the biological and material foundation of the work by identifying a natural polymer scaffold capable of supporting EC viability and microvascular network formation. Building on this foundation, Objective 2 embedded scaffold optimisation within the existing body of TE knowledge. Objective 3 translated these material and design insights into a functional 3D microvascular construct with improved temporal stability, achieving network integrity beyond 24 h. Finally, Objective 4 delivered a proof of concept for the application of this 3D microvascular model to NPTI research, specifically under controlled conditions. Taken together, these interconnected objectives function as complementary components of a single framework, culminating in a mechanobiologically relevant and experimentally feasible *in vitro* model that can be used for controlled mechanical loading, delivering physiologically relevant microvascular injury outcomes.

7.2 Positioning of the Work Within the Field

By integrating the aforementioned aim and specific objectives, this thesis advanced the state of the art in *in vitro* microvascular and trauma modelling y directly addressing critical gaps in the current understanding of NPTIs. While hydrogel-based vascular constructs are well established, y directly addressing critical gaps in the current understanding of their application has largely focused on regenerative contexts or long-term vasculari-

sation outcomes, with limited attention to modelling injury-specific microvascular responses. In particular, the deliberate integration of human microvasculature into a platform explicitly designed to study the immediate and short-term effects of NPTIs has remained largely unexplored.

Current trauma research continues to rely predominantly on animal models or simplified 2D systems. Although these approaches have provided valuable insights, they obscure direct relationships between mechanical loading parameters and microvascular damage, and are constrained by limited experimental control, scalability, ethical concerns, and human relevance. In contrast, the work presented here enables systematic isolation and delivery of controlled biomechanical inputs while retaining essential features of human microvascular architecture.

A central contribution of this work lies in filling the gap between clinical descriptions of trauma and microscale vascular injury. Despite extensive investigation of contusion, crush, and strain injuries at the tissue and systemic level, there has been little mechanistic understanding of how such forces are transmitted to, and experienced by, microvascular networks, particularly in the context of soft tissues other than the brain. By developing a vascularised *in vitro* model tailored to NPTIs, this thesis provides a tool for quantifying microvascular responses to defined mechanical insults, enabling foundational mechanistic studies of trauma-induced (micro)vascular dysfunction.

Importantly, this thesis aligns with the shift in bioengineering that favours well-characterised, deliberately simple models over increasingly complex systems that are difficult to interpret or reproduce. In the context of trauma research, where variability and poor experimental control remain persistent challenges, this research prioritises transparency and reproducibility. The initial focus on skeletal muscle microvasculature is therefore both biologically and clinically motivated, given the prevalence of blunt trauma in musculoskeletal tissues and the extensibility of the platform to other soft tissue environments.

In parallel, this work addresses a further methodological gap in the study of (micro)vascularisation within trauma and TE: the limited systematic evaluation of fibrin-based scaffold formulations, their coupled mechanical and biological effects on microvascular network formation, and the reporting heterogeneity in the scientific literature. Although fibrin is widely used for soft tissue applications, its material properties are often treated independently from EC behaviour, and scaffold optimisation is rarely linked to quantitative assessments of angiogenic outcomes. By correlating defined fibrin compositions with endothelial network stability and architecture, this thesis establishes a rational basis for scaffold selection and design in vascular models.

Finally, this work makes a conceptual contribution by reframing angiogenesis not as a single outcome, but as a set of related yet distinct endothelial processes. The combined experimental and SR findings demonstrate that EFMPs are frequently interchanged in the literature, despite exhibiting distinct responses to scaffold composition and mechanical environment. By explicitly disentangling these EFMPs, this thesis challenges prevailing assumptions and provides a clearer interpretive framework for both microvascular model development and trauma-focused vascular research.

7.3 Novelty and Contributions of the Thesis

The principal novelty of this thesis lies in the coherent integration of multiple research strands: material optimisation, systematic evidence synthesis, long-term microvascular modelling, and controlled mechanical injury induction into a single experimental platform for microvascular trauma research. While individual components such as hydrogel scaffolds and microvascular assays are well represented in the literature, their deliberate, joint application to enable mechanistic interrogation of NPTIs (*in vitro*) remains underdeveloped. By bridging these elements, this work introduces a reproducible, robust human cell–compatible system capable of shedding light on the relationships between mechanical inputs and microvascular outcomes.

A significant conceptual contribution arises from the evidence-led approach to scaffold design. Rather than assuming that commonly used formulations are optimal, this thesis systematically compared collagen, fibrin, and gelatine hydrogels under controlled conditions, identifying fibrin as the most promising polymer for EFMPs. Complementing this experimental work, the SR of fibrin-based scaffolds for angiogenesis provided a robust synthesis of soft tissue models and revealed heterogeneity in experimental design and reporting. Derived from this SR, the '*Minimum Information for Fibrin Scaffold Experiments (MIFSE) Checklist*' was developed. Its aim was to address a critical barrier to reproducibility by establishing reporting requirements for scaffold parameters, manufacturing methods, and characterisation techniques. The MIFSE framework is intended to guide future scaffold studies across regenerative medicine, disease modelling, and preclinical testing by promoting consistent and transparent methodology, thereby enhancing the utility of fibrin scaffolds as reproducible TE platforms.

This thesis also makes methodological contributions through the development of a long-term microvascular construct that sustains capillary-like network integrity beyond 24 h, a limitation for many existing models. The identification of key formulation parameters that favour network stability addresses both biological and materials engineering challenges. Coupled with cross-validation against a gold-standard EC line, this work establishes a biologically relevant baseline platform.

In extending the platform to controlled injury modelling, the thesis demonstrates its capacity to apply distinct non-penetrating insults including contusion, compression, and strain to the engineered microvasculature. This multimodal injury induction platform and the associated quantitative analyses of microvascular architecture represent a step beyond traditional injury models, providing a foundation for mechanistic studies of trauma-induced microvascular dysfunction.

Beyond the scientific contributions presented in this thesis, this research has produced in multiple peer-reviewed publications. To date, three publications have been published, with two more currently in preparation, all of which directly arise from the research described in this thesis. In parallel, a further eight peer-reviewed scientific articles have been published during the course of the DPhil. In terms of innovation and translation, a priority patent application was filed in the previous year, with two additional applications currently under review, one of which directly stems from a tangential component of this thesis. These outputs have been complemented by presentations at international and UK-based conferences, symposia, and public engagement events, thereby extending the impact of this research and facilitating knowledge exchange with both the scientific community and the wider public.

7.4 Limitations

Despite its contributions, this work has several important limitations that must be acknowledged. Biologically, the model does not incorporate immune cells, pericytes, circulating blood components, or systemic inflammatory signalling, all of which are central to trauma pathophysiology *in vivo*. As a result, the findings are most directly applicable to the immediate and early post-injury period rather than long-term healing or remodelling phases.

The model is also static and lacks perfusion and associated shear stress, which are known regulators of endothelial function and vascular remodelling. While this was a deliberate design choice to facilitate the isolation of mechanical injury effects on the endothelial network at a cellular level, it necessarily limits physiological complexity. Similarly, the use of an immortalised EC line does not capture inter-donor or patient-specific variability.

From a design perspective, the focus on simplicity inherently limited the ability of the model to replicate whole-organ or systemic trauma responses. While this trade-off enhanced reproducibility, it highlighted the

need for careful positioning of the model as a mechanistic tool rather than a comprehensive physiological replica. Validation against complementary *in vivo* or *ex vivo* systems would therefore be essential to support broader translational claims.

7.5 Further Development & Future Work

There are a several promising avenues to further develop the 3D microvascular model. Firstly, incorporating perfusion and controlled mechanical stimulation would allow for the investigation of secondary injury mechanisms, endothelial adaptation, and early repair processes. In parallel, integrating high-resolution molecular readouts such as RNA sequencing of exposed versus non-exposed cells would enable detailed characterisation of injury-induced transcriptional responses and pathway activation. Complementary analysis of the biomarker content of conditioned media (*e.g.* inflammatory cytokines, chemokines, growth factors, angiogenic mediators) would further allow assessment of the secretory profile associated with injury and repair, providing insights into paracrine signalling and inflammatory modulation. Biological complexity could be increased through a modular approach by integrating additional cell types, such as pericytes, fibroblasts, or immune cells, enabling targeted study of specific microenvironmental interactions. Extending the platform to incorporate multiple endothelial and stromal cell sources, including patient-derived cells, would further enhance relevance for personalised and translational applications.

Architecturally, alternative construct configurations such as embedding a vascular tree at a higher hierarchical order than the endothelial network or developing macroscale 3D constructs in which ECs are patterned into hierarchical networks offer promising opportunities to investigate injury propagation and network resilience within more physiologically representative geometries. Importantly, such developments can be layered onto the existing framework rather than replacing it.

Looking forward, the injury paradigms developed in this thesis could be applied to *ex vivo* soft tissues to bridge the gap between *in vitro* and *in vivo* systems. Expansion of the platform to other tissues would further broaden its applicability to trauma, regenerative medicine, and disease modelling.

From a translational perspective, further down the line, the model is well suited for therapeutic screening, mechanopharmacology, and preclinical evaluation of interventions targeting microvascular dysfunction. Its reliance on human cells, combined with controlled mechanical loading and high reproducibility, could position it as a viable alternative to selected classes of animal experiments.

Finally, there is also clear scope for entrepreneurial pathways to support wider adoption, including licensing to pharmaceutical & biotechnology companies, medical device developers, and research organisations seeking human-relevant trauma models. Such routes would enhance the societal and economic impact of the work while supporting the broader objective of reducing reliance on animal models.

7.6 Concluding Remarks

In conclusion, this thesis establishes a robust and mechanobiologically relevant 3D *in vitro* platform for investigating microvascular injury under controlled mechanical loading. By systematically integrating scaffold optimisation, evidence synthesis, microvascular modelling, and reproducible injury induction, it delivers both methodological and conceptual advances to the fields of TE and trauma mechanobiology. While deliberately simple, the model captures essential features of microvascular networks and injury, and enables mechanistic investigations of cause–effect relationships that are difficult to resolve using existing approaches. As such, this work lays a strong foundation for future translational research and contributes meaningfully to the advancement of human-relevant, reproducible models in trauma and (micro)vascular biology.

Bibliography

[1] Sakran JV, Greer SE, Werlin E, *et al.* Care of the injured worldwide: Trauma still the neglected disease of modern society. Scandinavian Journal of Trauma, Resuscitation and Emergency Medicine. 2012;20:1-6. DOI: 10.1186/1757-7241-20-64.

[2] Relja B, Horstmann JP. Traumatic Injury. In: Cordero MD, Alcocer-Gómez E, editors. Inflammasomes: Clinical and Therapeutic Implications. vol. 108. Springer International Publishing; 2018. p. 85-110. DOI: 10.1007/978-3-319-89390-7_5.

[3] GBD 2021 Diseases and Injuries Collaborators. Global incidence, prevalence, years lived with disability (YLDs), disability-adjusted life-years (DALYs), and healthy life expectancy (HALE) for 371 diseases and injuries in 204 countries and territories and 811 subnational locations, 1990–2021: a systematic analysis for the Global Burden of Disease Study 2021. The Lancet. 2024;403:2133-61. DOI: 10.1016/S0140-6736(24)00757-8.

[4] Craig HA, Lowe DJ, Khan A, *et al.* Exploring the impact of traumatic injury on mortality: An analysis of the certified cause of death within one year of serious injury in the Scottish population. Injury. 2024;55:111470. DOI: 10.1016/j.injury.2024.111470.

[5] World Health Organization. Injuries and Violence [Fact sheet]. WHO; 2024. Available from: https://www.who.int/news-room/fact-sheets/detail/injuries-and-violence.

[6] Brinck T, Heinänen M, Handolin L, *et al.* Trauma-registry survival outcome follow up: 30 days is mandatory and appears sufficient. Injury. 2021;52:142-6. DOI: 10.1016/j.injury.2020.11.011.

[7] Sawe HR. Impact of trauma systems on injury morbidity: important considerations for low-income and middle-income countries. Emergency Medicine Journal : EMJ. 2024;41:415-6. DOI: 10.1136/emermed-2024-214005.

[8] Gosselin RA, Spiegel DA, Coughlin R, *et al.* Injuries: The neglected burden in developing countries. Bulletin of the World Health Organization. 2009;87(4):246-246a. DOI: 10.2471/blt.08.052290.

[9] Osuka A, Ogura H, Ueyama M, *et al.* Immune response to traumatic injury: harmony and discordance of immune system homeostasis. Acute Medicine & Surgery. 2014;1(2):63-9. DOI: 10.1002/ams2.17.

[10] Holtslag HR, Van Beeck EF, Lichtveld RA, *et al.* Individual and population burdens of major trauma in the Netherlands. Bulletin of the World Health Organization. 2008;86:111-7. DOI: 10.2471/blt.06.033803.

[11] Wafaisade A, Lefering R, Bouillon B, *et al.* Epidemiology and risk factors of sepsis after multiple trauma: An analysis of 29,829 patients from the Trauma Registry of the German Society for Trauma Surgery. Critical Care Medicine. 2011;39(4):621-8. DOI: 10.1097/CCM.0b013e318206d3df.

[12] Haagsma JA, Graetz N, Bolliger I, *et al.* The global burden of injury: incidence, mortality, disability-adjusted life years and time trends from the Global Burden of Disease study 2013. Injury Prevention. 2016;22(1):3-18. DOI: 10.1136/injuryprev-2015-041616.

[13] Evans JA, Van Wessem KJP, McDougall D, *et al.* Epidemiology of traumatic deaths: Comprehensive population-based assessment. World Journal of Surgery. 2010;34(1):158-63. DOI: 10.1007/s00268-009-0266-1.

[14] Weber B, Lackner I, Haffner-Luntzer M, *et al.* Modeling trauma in rats: Similarities to humans and potential pitfalls to consider. Journal of Translational Medicine. 2019;17(1):305. DOI: 10.1186/s12967-019-2052-7.

[15] McCullough AL, Haycock JC, Forward DP, *et al.* Early management of the severely injured major trauma patient. British Journal of Anaesthesia. 2014;113(2):234-41. DOI: 10.1093/bja/aeu235.

[16] Greer M, Wessman BT. Commonly Missed Traumatic Injuries. In: The Emergency Medicine Trauma Handbook. Cambridge University Press; 2019. p. 334-46. DOI: 10.1017/9781108647397.024.

[17] Tuma M, Canestrini S, Alwahab Z, *et al.* Trauma and Endothelial Glycocalyx: The Microcirculation Helmet? Shock. 2016;46(4):352-7. DOI: 10.1097/SHK.0000000000000635.

[18] Chappell D, Westphal M, Jacob M. The impact of the glycocalyx on microcirculatory oxygen distribution in critical illness. Current Opinion in Anaesthesiology. 2009;22(2):155-62. DOI: 10.1097/ACO.0b013e328328d1b6.

[19] Olfert IM, Baum O, Hellsten Y, *et al.* Advances and challenges in skeletal muscle angiogenesis. American journal of physiology Heart and circulatory physiology. 2016;310(3):H326-36. DOI: 10.1152/ajpheart.00635.2015.

[20] Fernando CA, Pangan AM, Cornelison DDW, *et al.* Recovery of blood flow regulation in microvascular resistance networks during regeneration of mouse gluteus maximus muscle. The Journal of Physiology. 2019;597:1401. DOI: 10.1113/JP277247.

[21] Holzapfel GA, Humphrey JD, Ogden RW. Biomechanics of soft biological tissues and organs, mechanobiology, homeostasis and modelling. Journal of the Royal Society Interface. 2025;22:20240361. DOI: 10.1098/RSIF.2024.0361.

[22] Zimmerman A, Fox S, Griffin R, *et al.* An analysis of emergency care delays experienced by traumatic brain injury patients presenting to a regional referral hospital in a low-income country. 2020. DOI: 10.1371/journal.pone.0240528.

[23] Badkur M, Kharkongor M, Sharma N, *et al.* Factors Influencing Treatment Delays in Trauma Patients: A Three-delay Model Approach. Journal of Emergencies, Trauma, and Shock. 2024;17:172. DOI: 10.4103/JETS.JETS$_{92}$4.

[24] Funk K, Scheerer N, Verhaegh R, *et al.* Severe blunt muscle trauma in rats: Only marginal hypoxia in the injured area. PLoS ONE. 2014;9(10). DOI: 10.1371/journal.pone.0111151.

[25] Horst K, Greven J, Lüken H, *et al.* Trauma Severity and Its Impact on Local Inflammation in Extremity Injury—Insights From a Combined Trauma Model in Pigs. Frontiers in Immunology. 2020;10. DOI: 10.3389/fimmu.2019.03028.

[26] Morgan CE, Prakash VS, Vercammen JM, *et al.* Development and validation of 4 different rat models of uncontrolled hemorrhage. JAMA Surgery. 2015;150(4):316-24. DOI: 10.1001/jamasurg.2014.1685.

[27] Villarreal CL, Price MA, Moreno AN, *et al.* Regulatory challenges in conducting human subjects research in emergency settings: the National Trauma Research Action Plan (NTRAP) scoping review. Trauma Surgery & Acute Care Open. 2023;8:1044. DOI: 10.1136/TSACO-2022-001044.

[28] Schneider BSP, Zhang L, Dombrowsky T, *et al.* A scoping review and evaluation of hyperbaric oxygen therapy for skeletal muscle injury in preclinical models. Medical Gas Research. 2025;16(2):125. DOI: 10.4103/MGR.MEDGASRES-D-24-00163.

[29] Li Y, Huard J. Differentiation of muscle-derived cells into myofibroblasts in injured skeletal muscle. American Journal of Pathology. 2002;161(3):895-907. DOI: 10.1016/S0002-9440(10)64250-2.

[30] Liaudanskaya V, Chung JY, Mizzoni C, *et al.* Modeling Controlled Cortical Impact Injury in 3D Brain-Like Tissue Cultures. Advanced Healthcare Materials. 2020;9(12):2000122. DOI: 10.1002/adhm.202000122.

[31] Howes DW, Stratford A, Stirling M, *et al.* Administration of recombinant factor VIIa decreases blood loss after blunt trauma in noncoagulopathic pigs. Journal of Trauma - Injury, Infection and Critical Care. 2007;62:311-5. DOI: 10.1097/01.ta.0000229704.06991.9d.

[32] Liu J, Li R, Huang Z, *et al.* A Cervical Spinal Cord Hemi-Contusion Injury Model Based on Displacement Control in Non-Human Primates (Macaca fascicularis). https://homeliebertpubcom/neu. 2020;37:1669-86. DOI: 10.1089/NEU.2019.6822.

[33] Salegio EA, Bresnahan JC, Sparrey CJ, *et al.* A Unilateral Cervical Spinal Cord Contusion Injury Model in Non-Human Primates (Macaca mulatta). Journal of Neurotrauma. 2016;33:439. DOI: 10.1089/NEU.2015.3956.

[34] Bentley C, Hazeldine J, Bravo L, *et al.* The ultra-acute steroid response to traumatic injury: a cohort study. European Journal of Endocrinology. 2023;188(3):290-9. DOI: 10.1093/EJENDO/LVAD024.

[35] Wang Nd, Stevens MH, Doty DB, *et al.* Blunt Chest Trauma: An Experimental Model for Heart and Lung Contusion. The Journal of Trauma: Injury, Infection, and Critical Care. 2003;54(4):744-9. DOI: 10.1097/01.TA.0000052362.40754.F2.

[36] Pilipović K, Harej Hrkać A, Kučić N, *et al.* Modeling Central Nervous System Injury In Vitro: Current Status and Promising Future Strategies. Biomedicines 2023, Vol 11, Page 94. 2022;11(1):94. DOI: 10.3390/BIOMEDICINES11010094.

[37] Valarmathi MT, Fuseler JW, Potts JD, *et al.* Functional Tissue Engineering: A Prevascularized Cardiac Muscle Construct for Validating Human Mesenchymal Stem Cells Engraftment Potential in Vitro. Tissue Engineering - Part A. 2018;24(1-2):157-85. DOI: 10.1089/ten.tea.2016.0539.

[38] Martinez-Seara Monne H, Danne R, Róg T, *et al.* Structure of Glycocalyx. Biophysical Journal. 2013;104(2):251a. DOI: 10.1016/j.bpj.2012.11.1412.

[39] Naumann DN, Hazeldine J, Midwinter MJ, *et al.* Poor microcirculatory flow dynamics are associated with endothelial cell damage and glycocalyx shedding after traumatic hemorrhagic shock. Journal of Trauma and Acute Care Surgery. 2018;84(1):81-8. DOI: 10.1097/TA.0000000000001695.

[40] Zimmermann WH, Fink C, Kralisch D, *et al.* Three-dimensional engineered heart tissue from neonatal rat cardiac myocytes. Biotechnol Bioeng. 2000;68(1):106-14.

[41] Gholobova D, Decroix L, Muylder VV, *et al.* Endothelial Network Formation Within Human Tissue-Engineered Skeletal Muscle. Tissue Engineering Part A. 2015;21:2548-58. DOI: 10.1089/ten.tea.2015.0093.

[42] Sutton P, Fagan T. Cardiovascular System. 3rd ed. New York: Mosby Inc.; 2008.

[43] Sherwood L. In: 10: The Blood Vessels and Blood Pressure. Cengage Learning,; 2016. p. 335-79.

[44] JR L. An introduction to cardiovascular physiology. London: Hodder Arnold; 2010.

[45] Yuan SY, Rigor RR. Structure and Function of Exchange Microvessels. In: Regulation of Endothelial Barrier Function. San Rafael (CA): Morgan & Claypool Life Sciences; 2010. .

[46] Standring S, Gray H, Anand N, *et al.* The anatomy of the vascular and lymphatic systems. In: Gray's Anatomy: The Anatomical Basis of Clinical Practice. 42nd ed. Elsevier; 2021. p. 1464.e56-1464.e129. DOI: 10.1016/B978-0-7020-7705-0.00081-1.

[47] Pawlina W. In: 13. Cardiovascular System. 9th ed. Lippincott Williams & Wilkins, a Wolters Kluwer business; 2024. p. 0.

[48] Betts JG, Young KA, Wise JA, *et al.* Open Histology - Cells and Tissues. OpenStax; 2013.

[49] Whitney Menefee, Julie Jenks, Chiara Mazzasette, *et al.* 18.2: Structure and Function of Blood Vessels . In: Lange J, Polos J, Aquino Y, *et al.*, editors. General Human Anatomy. LibreTexts; 2025. .

[50] Evans JDW. In: Horton-Szar D, editor. Anatomy, Histology and Development of the Cardiovascular System. updated 4th ed. ed. Mosby; 2015. .

[51] da Silva Meirelles L, Caplan AI, Nardi NB. Chapter 12 - Pericytes as the Source of Mesenchymal Stem Cells. In: dos Santos Goldenberg RC, Campos de Carvalho AC, editors. Resident Stem Cells and Regenerative Therapy. Academic Press; 2013. p. 233-50. DOI: https://doi.org/10.1016/B978-0-12-416012-5.00012-8.

[52] Bergers G, Song S. The role of pericytes in blood-vessel formation and maintenance. Neuro-Oncology. 2005 10;7(4):452. DOI: 10.1215/S1152851705000232.

[53] Hudlicka O. Microcirculation in skeletal muscle. CIC Edizioni Internazionali; 2011.

[54] Rubenstein DA, Yin W, Frame MD. Microvascular Beds. In: Biofluid Mechanics. Elsevier; 2012. p. 181-215. DOI: 10.1016/b978-0-12-381383-1.00006-0.

[55] Adams RH, Alitalo K. Molecular regulation of angiogenesis and lymphangiogenesis. Nature reviews Molecular cell biology. 2007;8:464-78. DOI: 10.1038/NRM2183.

[56] Patan S. Vasculogenesis and angiogenesis as mechanisms of vascular network formation, growth and remodeling. Journal of Neuro-Oncology. 2000;50(1-2):1-15. DOI: 10.1023/A:1006493130855.

[57] Li X, Kumar A, Carmeliet P. Metabolic Pathways Fueling the Endothelial Cell Drive. Annual review of physiology. 2019;81:483-503. DOI: 10.1146/ANNUREV-PHYSIOL-020518-114731.

[58] Bock KD, Georgiadou M, Schoors S, *et al.* XRole of PFKFB3-driven glycolysis in vessel sprouting. Cell. 2013;154. DOI: 10.1016/j.cell.2013.06.037.

[59] Eelen G, Zeeuw PD, Simons M, *et al.* Endothelial cell metabolism in normal and diseased vasculature. Circulation research. 2015;116:1231-44. DOI: 10.1161/CIRCRESAHA.116.302855.

[60] Rohlenova K, Veys K, Miranda-Santos I, *et al.* Endothelial Cell Metabolism in Health and Disease. Trends in Cell Biology. 2018;28:224-36. DOI: 10.1016/j.tcb.2017.10.010.

[61] Falkenberg KD, Rohlenova K, Luo Y, *et al.* The metabolic engine of endothelial cells. Nature metabolism. 2019;1:937-46. DOI: 10.1038/S42255-019-0117-9.

[62] Chien S. Mechanotransduction and endothelial cell homeostasis: the wisdom of the cell. American journal of physiology Heart and circulatory physiology. 2007;292. DOI: 10.1152/AJPHEART.01047.2006.

[63] Ades EW, Candal FJ, Swerlick RA, *et al.* HMEC-1: Establishment of an Immortalized Human Microvascular Endothelial Cel1 Line. J Invest Dermatol. 1992;99(6):683-90. DOI: 10.1111/1523-1747.ep12613748.

[64] Potente M, Gerhardt H, Carmeliet P. Basic and therapeutic aspects of angiogenesis. Cell. 2011;146:873-87. DOI: 10.1016/j.cell.2011.08.039.

[65] Weinbaum S, Tarbell JM, Damiano ER. The Structure and Function of the Endothelial Glycocalyx Layer EC: endothelial cell. 2007. DOI: 10.1146/annurev.bioeng.9.060906.151959.

[66] Squire JM, Chew M, Nneji G, *et al.* Quasi-periodic substructure in the microvessel endothelial glycocalyx: A possible explanation for molecular filtering? Journal of Structural Biology. 2001;136:239-55. DOI: 10.1006/jsbi.2002.4441.

[67] Weinbaum S, Zhang X, Han Y, *et al.* Mechanotransduction and flow across the endothelial glycocalyx. Proceedings of the National Academy of Sciences of the United States of America. 2003;100(13):7988-95. DOI: 10.1073/pnas.1332808100.

[68] Tarbell JM, Pahakis MY. Mechanotransduction and the glycocalyx. Journal of internal medicine. 2006;259:339-50. DOI: 10.1111/J.1365-2796.2006.01620.X.

[69] Liu HB, Zhang J, Xin SY, *et al.*. Mechanosensitive properties in the endothelium and their roles in the regulation of endothelial function. J Cardiovasc Pharmacol; 2013. DOI: 10.1097/FJC.0b013e31828c0933.

[70] Conway D, Schwartz MA. Lessons from the endothelial junctional mechanosensory complex; 2012. DOI: 10.3410/B4-1.

[71] Pahakis MY, Kosky JR, Dull RO, *et al.* The role of endothelial glycocalyx components in mechanotransduction of fluid shear stress. Biochemical and Biophysical Research Communications. 2007;355(1):228-33. DOI: 10.1016/j.bbrc.2007.01.137.

[72] Kvietys PR. 3: Regulation of Vascular Tone and Oxygenation. In: The Gastrointestinal Circulation. San Rafael, CA: Morgan & Claypool Life Sciences; 2010. .

[73] Masciantonio MG, Lee CKS, Arpino V, *et al.* The Balance Between Metalloproteinases and TIMPs: Critical Regulator of Microvascular Endothelial Cell Function in Health and Disease. In: Progress in Molecular Biology and Translational Science. vol. 147. Elsevier B.V.; 2017. p. 101-31. DOI: 10.1016/bs.pmbts.2017.01.001.

[74] Ma Y, Zhou R, Yang M, *et al.* Soft tissue scaffold fabrication based on electrospinning: Application and prospect. Advances in Colloid and Interface Science. 2025;346:103660. DOI: 10.1016/J.CIS.2025.103660.

[75] Patel S, Caldwell JM, Doty SB, *et al.* Integrating soft and hard tissues via interface tissue engineering. Journal of Orthopaedic Research. 2018;36:1069-77. DOI: 10.1002/JOR.23810.

[76] Louis DN, Perry A, Reifenberger G, *et al.* The 2016 World Health Organization Classification of Tumors of the Central Nervous System: a summary. Acta Neuropathologica. 2016;131:803-20. DOI: 10.1007/S00401-016-1545-1/TABLES/5.

[77] Graham BB. Necrotizing Soft Tissue Infections. Current Emergency and Hospital Medicine Reports 2019 7:1. 2019;7:19-25. DOI: 10.1007/S40138-019-00179-0.

[78] Davies CE, Davies AM, Kindblom LG, *et al.* Soft Tissue Tumors with Muscle Differentiation. Seminars in Musculoskeletal Radiology. 2020;2:245-56. DOI: 10.1055/s-0030-1253165.

[79] Cao S, Bo R, Zhang Y. Polymeric Scaffolds for Regeneration of Central/Peripheral Nerves and Soft Connective Tissues. Advanced NanoBiomed Research. 2023;3. DOI: 10.1002/ANBR.202200147.

[80] Fuenteslópez CV, Ye H. Electrospun Fibres with Hyaluronic Acid-Chitosan Nanoparticles Produced by a Portable Device. Nanomaterials. 2020;10. DOI: 10.3390/nano10102016.

[81] Pawlina W. In: Pawlina W, editor. 11: Muscle Tissue. 9th ed. Lippincott Williams & Wilkins, a Wolters Kluwer business; 2024. p. 0.

[82] Jelínková H. In: 1 - Introduction: the history of lasers in medicine. Woodhead Publishing; 2013. p. 1-13. DOI: 10.1533/9780857097545.1.

[83] Standring S. In: 5: Functional anatomy of the musculoskeletal system. 42nd ed.; 2021. p. 85-126.

[84] Dong R, Ma PX, Guo B. Conductive biomaterials for muscle tissue engineering. Biomaterials. 2020;229:119584. DOI: 10.1016/J.BIOMATERIALS.2019.119584.

[85] Arrigoni C, Petta D, Bersini S, *et al.* Engineering complex muscle-tissue interfaces through microfabrication Engineering complex muscle-tissue interfaces through microfabrication. Biofabrication. 2019;11:32004. DOI: 10.1088/1758-5090/ab1e7c.

[86] Kotani T, Saito T, Suzuka T, *et al.* Adipose-derived mesenchymal stem cell therapy for connective tissue diseases and complications. Inflammation and Regeneration. 2024;44:1-23. DOI: 10.1186/S41232-024-00348-Z/TABLES/4.

[87] Choe SS, Huh JY, Hwang IJ, *et al.* Adipose tissue remodeling: Its role in energy metabolism and metabolic disorders. Frontiers in Endocrinology. 2016;7:178543. DOI: 10.3389/FENDO.2016.00030/FULL.

[88] Luo L, Liu M. Adipose tissue in control of metabolism. Journal of Endocrinology. 2016;231:R77-99. DOI: 10.1530/JOE-16-0211.

[89] Pillai EK, Franze K. Mechanics in the nervous system: From development to disease. Neuron. 2024;112:342-61. DOI: 10.1016/J.NEURON.2023.10.005.

[90] Boni R, Ali A, Shavandi A, *et al.* Current and novel polymeric biomaterials for neural tissue engineering. Journal of Biomedical Science. 2018;25:1-21. DOI: 10.1186/S12929-018-0491-8/TABLES/4.

[91] Hasan A, Memic A, Annabi N, *et al.* Electrospun scaffolds for tissue engineering of vascular grafts. Acta Biomaterialia. 2014;10:11-25. DOI: 10.1016/J.ACTBIO.2013.08.022.

[92] Pashneh-Tala S, MacNeil S, Claeyssens F. The Tissue-Engineered Vascular Graft—Past, Present, and Future. https://homeliebertpubcom/teb. 2015;22:68-100. DOI: 10.1089/TEN.TEB.2015.0100.

[93] Kallen ME, Hornick JL. The 2020 WHO classification: What's new in soft tissue tumor pathology? American Journal of Surgical Pathology. 2021;45:1-23. DOI: 10.1097/PAS.0000000000001552.

[94] Anderson WJ, Doyle LA. Updates from the 2020 World Health Organization Classification of Soft Tissue and Bone Tumours. Histopathology. 2021;78:644-57. DOI: 10.1111/HIS.14265.

[95] Nordin M, Frankel VH, Meere PA, *et al.* Basic biomechanics of the musculoskeletal system. 5th ed. Wilke HJ, editor. Philadelphia: Wolters Kluwer; 2022.

[96] Duncan RL, Turner CH. Mechanotransduction and the functional response of bone to mechanical strain. Calcified tissue international. 1995;57(5):344-58. DOI: 10.1007/BF00302070.

[97] Shaker JL, Deftos L. Calcium and Phosphate Homeostasis. Endocrine and Reproductive Physiology. 2023:77-e1. DOI: 10.1016/b978-0-323-08704-9.00004-x.

[98] Mescher AL. 10: Muscle Tissue. In: Junqueira's basic histology : text and atlas. 16th ed. McGraw-Hill; 2021. p. 193-214.

[99] Abdalla A, Benissan-Messan D, Zhu H. 3 - Skeletal muscle tissue engineering. In: Chen Y, editor. Musculoskeletal Tissue Engineering. Elsevier; 2022. p. 67-80. DOI: 10.1016/B978-0-12-823893-6.00007-3.

[100] Carlson BM. The regeneration of skeletal muscle — a review. American Journal of Anatomy. 1973;137(2):119-49. DOI: 10.1002/AJA.1001370202.

[101] Gillies AR, Lieber RL. Structure and function of the skeletal muscle extracellular matrix. Muscle and Nerve. 2011;44(3):318-31. DOI: 10.1002/MUS.22094.

[102] Cormack GC. The arterial anatomy of skin flaps. 2nd ed. Lamberty BGH, editor. Edinburgh: Churchill Livingstone; 1994.

[103] Mathes SJ, Nahai F. Classification of the vascular anatomy of muscles: experimental and clinical correlation - PubMed. Plastic and Reconstructive Surgery. 1981;67(2):177-87.

[104] Schiaffino S, Reggiani C. Fiber types in mammalian skeletal muscles. Physiological reviews. 2011;91:1447-531. DOI: 10.1152/PHYSREV.00031.2010.

[105] Latroche C, Gitiaux C, Chrétien F, *et al.* Skeletal Muscle Microvasculature: A Highly Dynamic Lifeline. Physiology. 2015;30(6):417-27. DOI: 10.1152/physiol.00026.2015.

[106] Kusters YHAM, Barrett EJ. Muscle microvasculature's structural and functional specializations facilitate muscle metabolism. American Physiological Society; 2016. DOI: 10.1152/ajpendo.00443.2015.

[107] Trojian TH. Muscle Contusion (Thigh). Clinics in Sports Medicine. 2013;32(2):317-24. DOI: 10.1016/J.CSM.2012.12.009.

[108] Beyer R, Ingerslev J, Sørensen B. Muscle bleeds in professional athletes – diagnosis, classification, treatment and potential impact in patients with haemophilia. Haemophilia. 2010;16(6):858-65. DOI: 10.1111/J.1365-2516.2010.02278.X.

[109] Järvinen TAH, Järvinen TLN, Kääriäinen M, *et al.* Muscle injuries: optimising recovery. Best Practice & Research Clinical Rheumatology. 2007;21(2):317-31. DOI: 10.1016/J.BERH.2006.12.004.

[110] Schultz GS, Chin GA, Moldawer L, *et al.* 23: Principles of Wound Healing. In: Mechanisms of Vascular Disease: A Reference Book for Vascular Specialists. University of Adelaide Press; 2011. p. 395-402. DOI: 10.1142/9789812791535_0028.

[111] Everts PA, Lana JF, Onishi K, *et al.* Angiogenesis and Tissue Repair Depend on Platelet Dosing and Bioformulation Strategies Following Orthobiological Platelet-Rich Plasma Procedures: A Narrative Review. Biomedicines. 2023;11(7):1922. DOI: 10.3390/BIOMEDICINES11071922.

[112] Brey EM, McIntire LV. Vascular Assembly in Engineered and Natural Tissues. In: Principles of Regenerative Medicine. Academic Press; 2008. p. 1020-37. DOI: 10.1016/B978-012369410-2.50061-9.

[113] Lowry LE, Herzig MC, Christy BA, *et al.* Neglected No More: Emerging Cellular Therapies in Traumatic Injury. Stem Cell Reviews and Reports. 2021;17:1194. DOI: 10.1007/S12015-020-10086-7.

[114] Hooper N, Armstrong TJ. Hemorrhagic Shock. StatPearls. 2022.

[115] Dumovich J, Singh P. Physiology, Trauma. StatPearls. 2022.

[116] Jaramillo CA, Tapia RN, Eapen BC. 146 - Polytrauma Rehabilitation. In: Essentials of Physical Medicine and Rehabilitation: Musculoskeletal Disorders, Pain, and Rehabilitation. Elsevier; 2018. p. 828-33. DOI: 10.1016/B978-0-323-54947-9.00146-2.

[117] Leslie V Simon, Richard A Lopez, Kevin C King. Blunt Force Trauma. StatPearls [Internet]. 2023.

[118] Yang J, Tibbetts AS, Covassin T, *et al.* Epidemiology of Overuse and Acute Injuries Among Competitive Collegiate Athletes. Journal of Athletic Training. 2012;47(2):198. DOI: 10.4085/1062-6050-47.2.198.

[119] de Souza J, Gottfried C. Muscle injury: Review of experimental models. Elsevier; 2013. DOI: 10.1016/j.jelekin.2013.07.009.

[120] Reynolds TA, Stewart B, Drewett I, *et al.* The Impact of Trauma Care Systems in Low- and Middle-Income Countries. Annual review of public health. 2017;38:507-32. DOI: 10.1146/ANNUREV-PUBLHEALTH-032315-021412.

[121] Wesson HKH, Boikhutso N, Bachani AM, *et al.* The cost of injury and trauma care in low- and middle-income countries: a review of economic evidence. Health policy and planning. 2014;29(6):795-808. DOI: 10.1093/HEAPOL/CZT064.

[122] GBD 2019 Diseases and Injuries Colalborators. Global burden of 369 diseases and injuries in 204 countries and territories, 1990–2019: A systematic analysis for the Global Burden of Disease Study 2019. The Lancet. 2020;396:S182-3. DOI: https://doi.org/10.1016/S0140-6736(20)30925-9.

[123] Javali RH, Krishnamoorthy, Patil A, *et al.* Comparison of injury severity score, new injury severity score, revised trauma score and trauma and injury severity score for mortality prediction in elderly trauma patients. Indian Journal of Critical Care Medicine. 2019;23(2):73-7. DOI: 10.5005/jp-journals-10071-23120.

[124] Kehoe A, Smith JE, Edwards A, *et al.* The changing face of major trauma in the UK. Emergency Medicine Journal. 2015;32(12):911-5. DOI: 10.1136/emermed-2015-205265.

[125] Bruijns SR, Guly HR, Bouamra O, *et al.* The value of traditional vital signs, shock index, and age-based markers in predicting trauma mortality. Journal of Trauma and Acute Care Surgery. 2013;74(6):1432-7. DOI: 10.1097/TA.0b013e31829246c7.

[126] Grossman MD, Ofurum U, Stehly CD, *et al.* Long-term survival after major trauma in geriatric trauma patients: The glass is half full. Journal of Trauma and Acute Care Surgery. 2012;72(5):1181-5. DOI: 10.1097/TA.0b013e31824d0e6d.

[127] Kuske B, Hamilton DF, Pattle SB, *et al.* Patterns of Hamstring Muscle Tears in the General Population: A Systematic Review. PLoS ONE. 2016;11(5):e0152855. DOI: 10.1371/JOURNAL.PONE.0152855.

[128] Poudel B, Pandey S. Hamstring Injury. In: StatsPearls. StatPearls Publishing; 2023. p. 157-69. DOI: 10.1007/978-3-030-55870-3_18.

[129] Ahmad CS, Redler LH, Ciccotti MG, *et al.* Evaluation and Management of Hamstring Injuries. The American Journal of Sports Medicine. 2013;41(12):2933-47. DOI: 10.1177/0363546513487063.

[130] Pluetrattanabha N, Direksunthorn T. Recent Advances in Ultrasound of Soft Tissue Lesions. International Journal of General Medicine. 2023;16:1163-70. DOI: 10.2147/IJGM.S404682.

[131] Wu S, Tu R, Liu G, *et al.* Role of ultrasound in the diagnosis of common soft tissue lesions of the limbs. Ultrasound Quarterly. 2013;29:67-71. DOI: 10.1097/RUQ.0B013E3182823617.

[132] Nagira K, Yamamoto T, Akisue T, *et al.* Reliability of fine-needle aspiration biopsy in the initial diagnosis of soft-tissue lesions. Diagnostic Cytopathology. 2002;27:354-61. DOI: 10.1002/DC.10200.

[133] Philipone E, Yoon AJ. Mucosal Soft Tissue Lesions. Pediatric and Developmental Pathology. 2023;26:596-608. DOI: 10.1177/10935266231198724.

[134] Chargé SBP, Rudnicki MA. Cellular and Molecular Regulation of Muscle Regeneration. https://doiorg/101152/physrev000192003. 2004;84:209-38. DOI: 10.1152/PHYSREV.00019.2003.

[135] Seale P, Sabourin LA, Girgis-Gabardo A, *et al.* Pax7 Is Required for the Specification of Myogenic Satellite Cells. Cell. 2000;102(6):777-86. DOI: 10.1016/S0092-8674(00)00066-0.

[136] Hawke TJ, Garry DJ. Myogenic satellite cells: physiology to molecular biology. https://doiorg/101152/jappl2001912534. 2001;91(2):534-51. DOI: 10.1152/JAPPL.2001.91.2.534.

[137] Ron Walls, Robert Hockberger, Marianne Gausche-Hill, *et al.* Rosen's Emergency Medicine: Concepts and Clinical Practice. vol. 1. 9th ed. Elsevier Health Sciences; 2017.

[138] Dumovich J, Singh P. Physiology, Trauma. StatPearls Publishing; 2020.

[139] Gabay C, Kushner I. Acute-Phase Proteins and Other Systemic Responses to Inflammation. New England Journal of Medicine. 1999;340(6):448-54. DOI: 10.1056/nejm199902113400607.

[140] Beneat A, Lobo CM, Collier SA. Wound Imaging. StatPearls Publishing; 2025.

[141] Rama E, Jayawant S, Zhang J, *et al.* Crush injuries to the lower limbs at a major UK trauma centre: a retrospective observational study. European Journal of Orthopaedic Surgery & Traumatology. 2024;35(1):44. DOI: 10.1007/S00590-024-04164-6.

[142] Michaelson M. Crush injury and crush syndrome. World Journal of Surgery. 1992;16(5):899-903. DOI: 10.1007/BF02066989.

[143] Rajagopalan CS. Crush injuries and the crush syndrome. Medical Journal Armed Forces India. 2010;66(4):317-20. DOI: 10.1016/S0377-1237(10)80007-3.

[144] a Jagodzinski N, Weerasinghe C, Porter K. Crush injuries and crush syndrome — a review. Part 1: the systemic injury. Trauma. 2010;12:69-88. DOI: 10.1177/1460408610372440.

[145] Demirkiran O, Dikmen Y, Utku T, *et al.* Crush syndrome patients after the Marmara earthquake. Emergency medicine journal : EMJ. 2003;20:247-50. DOI: 10.1136/EMJ.20.3.247.

[146] Zhou C, Chen R, Huang F, *et al.* Characteristics of crush syndrome caused by prolonged limb compression longer than 24 h in the Sichuan earthquake. Emergency medicine journal : EMJ. 2010;27:627-30. DOI: 10.1136/EMJ.2008.070961.

[147] Ozturk I, Gungor O, Ozturk S, *et al.* Epidemiological analysis of the victims with crush syndrome in earthquakes of southeastern Turkey. Journal of nephrology. 2024;37(9):2589-99. DOI: 10.1007/S40620-024-02051-1.

[148] Gümüşoğlu E, Asfuroğlu ZM, Eskandari MM. Demographic and clinical features of extremity crush injuries resulting from entrapment under the rubble: an orthopedic perspective. Archives of Orthopaedic and Trauma Surgery 2025 145:1. 2025;145(1):1-8. DOI: 10.1007/S00402-025-06077-3.

[149] Ramaiola I, Lopez L, Moron M, *et al.* Characterization of the Components and Functional Properties of a Plasma-Derived Fibrin Sealant. Plasmatology. 2023;17. DOI: 10.1177/26348535231171332.

[150] Greaves I, Porter K, Smith JE. Consensus statement on the early management of crush injury and prevention of crush syndrome. Journal of the Royal Army Medical Corps. 2003;149:255-9. DOI: 10.1136/JRAMC-149-04-02.

[151] Sever MS, Vanholder R. Management of crush victims in mass disasters: highlights from recently published recommendations. Clinical journal of the American Society of Nephrology : CJASN. 2013;8(2):328-35. DOI: 10.2215/CJN.07340712.

[152] Gibney RTN, Sever MS, Vanholder RC. Disaster nephrology: Crush injury and beyond. Kidney International. 2014;85(5):1049-57. DOI: 10.1038/ki.2013.392.

[153] Huard J, Li Y, Fu FH. Muscle injuries and repair: Current trends in research. Journal of Bone and Joint Surgery. 2002;84(5):822-32. DOI: 10.2106/00004623-200205000-00022.

[154] Strauss MB. The role of hyperbaric oxygen for acute traumatic ischemias - PubMed. Undersea & hyperbaric medicine : journal of the Undersea and Hyperbaric Medical Society, Inc. 2022;49(2):233-48.

[155] Rubinstein I, Abassi Z, Coleman R, *et al.* Involvement of nitric oxide system in experimental muscle crush injury. Journal of Clinical Investigation. 1998;101(6):1325. DOI: 10.1172/JCI810.

[156] Bywaters EGL. 50 years on: the crush syndrome. BMJ : British Medical Journal. 1990;301(6766):1412. DOI: 10.1136/BMJ.301.6766.1412.

[157] Gunal AI, Celiker H, Dogukan A, *et al.* Early and vigorous fluid resuscitation prevents acute renal failure in the crush victims of catastrophic earthquakes. Journal of the American Society of Nephrology : JASN. 2004;15(7):1862-7. DOI: 10.1097/01.ASN.0000129336.09976.73.

[158] Oda J, Tanaka H, Yoshioka T, *et al.* Analysis of 372 patients with Crush syndrome caused by the Hanshin-Awaji earthquake. The Journal of trauma. 1997;42(3):470-6. DOI: 10.1097/00005373-199703000-00015.

[159] Yoshimura N, Nakayama S, Nakagiri K, *et al.* Profile of chest injuries arising from the 1995 southern hyogo prefecture earthquake. Chest. 1996;110(3):759-61. DOI: 10.1378/chest.110.3.759.

[160] Gonzalez Tortosa J, Poza Poza M. Crush injuries to the head. Neurosurgery. 1996;39(4):877-8. DOI: 10.1097/00006123-199610000-00055.

[161] Yeşil E, Tezol ?, Gokay N, *et al.* Analysis of wound infections among pediatric patients following the 2023 Türkiye-Syria earthquakes. Pediatric surgery international. 2024;40(1). DOI: 10.1007/S00383-024-05755-4.

[162] Eryilmaz-Eren E, Yalcin S, Ozan F, *et al.* An outbreak analysis of wound infection due to Acinetobacter baumannii in earthquake-trauma patients. American Journal of Infection Control. 2024;52(5):599-604. DOI: 10.1016/j.ajic.2023.12.005.

[163] Wang T, Li D, Xie Y, *et al.* The microbiological characteristics of patients with crush syndrome after the Wenchuan earthquake. Scandinavian journal of infectious diseases. 2010;42(6-7):479-83. DOI: 10.3109/00365541003671226.

[164] Fernandez WG, Yard EE, Comstock RD. Epidemiology of Lower Extremity Injuries among U.S. High School Athletes. Academic Emergency Medicine. 2007;14(7):641-5. DOI: 10.1197/j.aem.2007.03.1354.

[165] Rechel JA, Yard EE, Comstock RD. An Epidemiologic Comparison of High School Sports Injuries Sustained in Practice and Competition. Journal of Athletic Training. 2008;43(2):197-204. DOI: 10.4085/1062-6050-43.2.197.

[166] Ekstrand J, Hägglund M, Waldén M. Epidemiology of Muscle Injuries in Professional Football (Soccer). The American Journal of Sports Medicine. 2011;39(6):1226-32. DOI: 10.1177/0363546510395879.

[167] Lee JC, Mitchell AWM, Healy JC. Imaging of muscle injury in the elite athlete. British Journal of Radiology. 2012;85:1173-85. DOI: 10.1259/bjr/84622172.

[168] Megliola A, Eutropi F, Scorzelli A, *et al.* Ultrasound and magnetic resonance imaging in sports-related muscle injuries. Radiologia Medica. 2006;111:836-45. DOI: 10.1007/S11547-006-0077-5/METRICS.

[169] Hayashi D, Hamilton B, Guermazi A, *et al.* Traumatic injuries of thigh and calf muscles in athletes: Role and clinical relevance of MR imaging and ultrasound. Insights into Imaging. 2012;3:591-601. DOI: 10.1007/S13244-012-0190-Z/TABLES/1.

[170] Fornage BD. Soft tissue masses: The underutilization of sonography. Seminars in Musculoskeletal Radiology. 1999;3:115-33. DOI: 10.1055/S-2008-1080056/BIB.

[171] Blankenbaker DG, Tuite MJ. Temporal changes of muscle injury. Seminars in Musculoskeletal Radiology. 2010;14:176-93. DOI: 10.1055/S-0030-1253159/ID/33/BIB.

[172] Yeung LL, McDonald AA, Como JJ, *et al.* Management of blunt force bladder injuries: A practice management guideline from the Eastern Association for the Surgery of Trauma. The journal of trauma and acute care surgery. 2019;86(2):326-36. DOI: 10.1097/TA.0000000000002132.

[173] Fakhry SM, Trask AL, Waller MA, *et al.* Management of brain-injured patients by an evidence-based medicine protocol improves outcomes and decreases hospital charges. The Journal of trauma. 2004;56(3):492-500. DOI: 10.1097/01.TA.0000115650.07193.66.

[174] Stassen NA, Bhullar I, Cheng JD, *et al.* Nonoperative management of blunt hepatic injury: an Eastern Association for the Surgery of Trauma practice management guideline. The journal of trauma and acute care surgery. 2012;73(5 Suppl 4). DOI: 10.1097/TA.0B013E318270160D.

[175] Schoenfeld AJ, Lehman RA, Hsu JR. Evaluation and management of combat-related spinal injuries: A review based on recent experiences. Spine Journal. 2012;12(9):817-23. DOI: 10.1016/j.spinee.2011.04.028.

[176] Koolmees DS, Klott JD, Poppe TR, *et al.* Distal Hamstring Injuries and Disorders. JAAOS Global Research & Reviews. 2025;9:e25.00248. DOI: 10.5435/JAAOSGLOBAL-D-25-00248.

[177] Noonan TJ, Garrett WE. Muscle strain injury: diagnosis and treatment. The Journal of the American Academy of Orthopaedic Surgeons. 1999;7(4):262-9. DOI: 10.5435/00124635-199907000-00006.

[178] Choi SJ. Cellular mechanism of eccentric-induced muscle injury and its relationship with sarcomere heterogeneity. Journal of Exercise Rehabilitation. 2014;10(4):200. DOI: 10.12965/JER.140139.

[179] Garrett WE, Nikolaou PK, Ribbeck BM, *et al.* The effect of muscle architecture on the biomechanical failure properties of skeletal muscle under passive extension. The American journal of sports medicine. 1988;16(1):7-12. DOI: 10.1177/036354658801600102.

[180] Barroso GC, Thiele ES. MUSCLE INJURIES IN ATHLETES. Revista Brasileira de Ortopedia. 2015;46(4):354. DOI: 10.1016/S2255-4971(15)30245-7.

[181] Renström P, Johnson RJ. Overuse Injuries in Sports: A Review. Sports Medicine: An International Journal of Applied Medicine and Science in Sport and Exercise. 1985;2(5):316-33. DOI: 10.2165/00007256-198502050-00002/METRICS.

[182] Santanna JPC, Pedrinelli A, Hernandez AJ, *et al.* Muscle Injury: Pathophysiology, Diagnosis, and Treatment. Revista Brasileira de Ortopedia. 2022;57(1):1. DOI: 10.1055/S-0041-1731417.

[183] Lempainen L, Sarimo J, Mattila K, *et al.* Distal tears of the hamstring muscles: review of the literature and our results of surgical treatment. British journal of sports medicine. 2007;41(2):80-3. DOI: 10.1136/BJSM.2006.031211.

[184] Wood DG, Packham I, Trikha SP, *et al.* Avulsion of the proximal hamstring origin. The Journal of bone and joint surgery American volume. 2008;90(11):2365-74. DOI: 10.2106/JBJS.G.00685.

[185] Lazzaretti Fernandes T, Pedrinelli A, Hernandez AJ. MUSCLE INJURY – PHYSIOPATHOLOGY, DIAGNOSIS, TREATMENT AND CLINICAL PRESENTATION. Revista Brasileira de Ortopedia. 2015;46(3):247. DOI: 10.1016/S2255-4971(15)30190-7.

[186] Sandsmark DK, Bashir A, Wellington CL, *et al.* Cerebral Microvascular Injury: A Potentially Treatable Endophenotype of Traumatic Brain Injury-Induced Neurodegeneration. Neuron. 2019;103(3):367-79. DOI: 10.1016/j.neuron.2019.06.002.

[187] Wani ML, Ahangar AG, Ganie FA, *et al.* Vascular Injuries: Trends in Management. Trauma Monthly. 2012;17(2):266. DOI: 10.5812/TRAUMAMON.6238.

[188] Bouma GJ, Muizelaar JP. Cerebral blood flow, cerebral blood volume, and cerebrovascular reactivity after severe head injury; 1992.

[189] Torsello GB, Sandmann W, Lenz W, *et al.* Experimental studies with absorbable and nonabsorbable sutures in infected canine arterial anastomoses. Journal of vascular surgery. 1986;3(1):135-9. DOI: 10.1067/MVA.1986.AVS0030135.

[190] Dauber IM, Pluss WT, VanGrondelle A, *et al.* Specificity and sensitivity of noninvasive measurement of pulmonary vascular protein leak. Journal of Applied Physiology. 1985;59(2):564-74. DOI: 10.1152/jappl.1985.59.2.564.

[191] Dauber IM, VanBenthuysen KM, McMurtry IF, *et al.* Functional coronary microvascular injury evident as increased permeability due to brief ischemia and reperfusion. Circulation Research. 1990;66(4):986-98. DOI: 10.1161/01.RES.66.4.986.

[192] Rahbar E, Cardenas JC, Baimukanova G, *et al.* Endothelial glycocalyx shedding and vascular permeability in severely injured trauma patients. Journal of Translational Medicine. 2015;13(1):117. DOI: 10.1186/s12967-015-0481-5.

[193] Kumar P, Shen Q, Pivetti CD, *et al.*. Molecular mechanisms of endothelial hyperpermeability: Implications in inflammation. Expert Rev Mol Med; 2009. DOI: 10.1017/S1462399409001112.

[194] Becker BF, Jacob M, Leipert S, *et al.* Degradation of the endothelial glycocalyx in clinical settings: Searching for the sheddases. British Journal of Clinical Pharmacology. 2015;80(3):389-402. DOI: 10.1111/bcp.12629.

[195] Uchimido R, Schmidt EP, Shapiro NI. The glycocalyx: A novel diagnostic and therapeutic target in sepsis. BioMed Central Ltd.; 2019. DOI: 10.1186/s13054-018-2292-6.

[196] Mulivor AW, Lipowsky HH. Inhibition of glycan shedding and leukocyte-endothelial adhesion in postcapillary venules by suppression of matrixmetalloprotease activity with doxycycline. Microcirculation. 2009;16(8):657-66. DOI: 10.3109/10739680903133714.

[197] Lipowsky HH, Lescanic A. Shear-Dependent Adhesion of Leukocytes and Lectins to the Endothelium and Concurrent Changes in Thickness of the Glycocalyx of Post-Capillary Venules in the Low-Flow State. Microcirculation. 2013;20(2):149-57. DOI: 10.1111/micc.12013.

[198] Torres Filho I, Torres LN, Sondeen JL, *et al.* In vivo evaluation of venular glycocalyx during hemorrhagic shock in rats using intravital microscopy. Microvascular Research. 2013;85(1):128-33. DOI: 10.1016/j.mvr.2012.11.005.

[199] Ghaly A, Marsh DR. Ischaemia–reperfusion modulates inflammation and fibrosis of skeletal muscle after contusion injury. International Journal of Experimental Pathology. 2010;91(3):244-55. DOI: 10.1111/J.1365-2613.2010.00708.X.

[200] Abhilash KPP, Sivanandan A. Early management of trauma: The golden hour. Current Medical Issues. 2020;18(1):39. DOI: 10.4103/CMI.CMI_61_19.

[201] Rasiah PK, Hardenburger J, Dong H, *et al*. Subcellular and macrostructural immediate responders to airblast traumatic brain injury. Scientific Reports 2025 15:1. 2025;15(1):1-19. DOI: 10.1038/s41598-025-13288-6.

[202] Donat CK, Yanez Lopez M, Sastre M, *et al*. From biomechanics to pathology: predicting axonal injury from patterns of strain after traumatic brain injury. Brain. 2021;144(1):70-91. DOI: 10.1093/BRAIN/AWAA336.

[203] Hazeldine J, Naumann DN, Toman E, *et al*. Prehospital immune responses and development of multiple organ dysfunction syndrome following traumatic injury: A prospective cohort study. PLOS Medicine. 2017;14(7):e1002338. DOI: 10.1371/JOURNAL.PMED.1002338.

[204] Jarragh A, Shuaib A, Al-Khaledi G, *et al*. A custom-made weight-drop impactor to produce consistent spinal cord injury outcomes in a rat model. Translational Neuroscience. 2023;14(1). DOI: 10.1515/TNSCI-2022-0287/XML.

[205] Waheed N, Huma Z, Wazir NU, *et al*. Developing Sciatic nerve compression model in rats using aneurysm clip and validating it by histological and behavior studies. Journal of Population Therapeutics and Clinical Pharmacology. 2023;30(17):1579-85. DOI: 10.53555/JPTCP.V30I17.2767.

[206] Filippin LI, Cuevas MJ, Lima E, *et al*. Nitric oxide regulates the repair of injured skeletal muscle. Nitric Oxide - Biology and Chemistry. 2011;24(1):43-9. DOI: 10.1016/j.niox.2010.11.003.

[207] Fuenteslópez CV. Transfer of Status Report: Development of a Vascularised Bioartificial Muscle Model for Trauma Research. University of Oxford; 2021.

[208] Shi W, Dong P, Kuss MA, *et al*. Design and Evaluation of an In Vitro Mild Traumatic Brain Injury Modeling System Using 3D Printed Mini Impact Device on the 3D Cultured Human iPSC Derived Neural Progenitor Cells. Advanced Healthcare Materials. 2021;10(12):2100180. DOI: 10.1002/adhm.202100180.

[209] Pischiutta F, Cavaleiro H, Caruso E, *et al*. A novel organotypic cortical slice culture model for traumatic brain injury: molecular changes induced by injury and mesenchymal stromal cell secretome treatment. Frontiers in Cellular Neuroscience. 2023;17:1217987. DOI: 10.3389/FNCEL.2023.1217987/BIBTEX.

[210] Kemp SWP, Szynkaruk M, Stanoulis KN, *et al*. Pharmacologic rescue of motor and sensory function by the neuroprotective compound P7C3 following neonatal nerve injury. Neuroscience. 2015;284:202-16. DOI: 10.1016/J.NEUROSCIENCE.2014.10.005.

[211] Kitano D, Katana D, Madanat AR, *et al*. Crush nerve injury model in the rat sciatic nerve: A comprehensive review and validation of various methods. Journal of Neuroscience Methods. 2025;423:110556. DOI: 10.1016/J.JNEUMETH.2025.110556.

[212] Dias FJ, Cury DP, Dias PE, *et al*. Effects of Low-Level Laser Therapy and Purified Natural Latex (Hevea brasiliensis) Protein on Injured Sciatic Nerve in Rodents: Morpho-Functional Analysis. International Journal of Molecular Sciences 2023, Vol 24, Page 14031. 2023;24(18):14031. DOI: 10.3390/IJMS241814031.

[213] Qiao O, Wang X, Li Z, *et al*. Paving the way ahead: protocol optimization of mouse models in crush syndrome related acute kidney injury research. Frontiers in Pharmacology. 2024;15:1438127. DOI: 10.3389/FPHAR.2024.1438127/BIBTEX.

[214] Matsumoto H, Matsumoto N, Shimazaki J, *et al*. Therapeutic Effectiveness of Anti-RAGE Antibody Administration in a Rat Model of Crush Injury. Scientific Reports 2017 7:1. 2017;7(1):1-9. DOI: 10.1038/s41598-017-12065-4.

[215] Zimowska M, Duchesnay A, Dragun P, *et al*. Immunoneutralization of TGF-β1 Improves Skeletal Muscle Regeneration: Effects on Myoblast Differentiation and Glycosaminoglycan Content . International Journal of Cell Biology. 2009;2009:1-16. DOI: 10.1155/2009/659372.

[216] Greiner-Perth AK, Wilke HJ, Liebsch C. How do compression and flexion-compression injuries destabilize the spine? A novel in vitro protocol for analyzing three-dimensional biomechanical instability. Frontiers in Bioengineering and Biotechnology. 2025;13:1576720. DOI: 10.3389/FBIOE.2025.1576720/BIBTEX.

[217] Xu D, Zhang N, Wang S, *et al*. A Novel In Vitro Platform Development in the Lab for Modeling Blast Injury to Microglia. Frontiers in Bioengineering and Biotechnology. 2022;10:883545. DOI: 10.3389/FBIOE.2022.883545/BIBTEX.

[218] Yeh CF, Juang DS, Chen YW, *et al*. A Portable Controllable Compressive Stress Device to Monitor Human Breast Cancer Cell Protrusions at Single-Cell Resolution. Frontiers in Bioengineering and Biotechnology. 2022;10:852318. DOI: 10.3389/FBIOE.2022.852318/BIBTEX.

[219] Soluki M, Mahmoudi F, Abdolmaleki A, *et al*. Cerium oxide nanoparticles as a new neuroprotective agent to promote functional recovery in a rat model of sciatic nerve crush injury. British Journal of Neurosurgery. 2024;38(2):301-6. DOI: 10.1080/02688697.2020.1864292.

[220] Sempere L, Rodríguez-Rodríguez A, Boyero L, *et al*. Experimental models in traumatic brain injury: From animal models to in vitro assays. Medicina Intensiva (English Edition). 2019;43(6):362-72. DOI: 10.1016/j.medine.2019.05.003.

[221] Salvador E, Burek M, Forster CY. An In Vitro Model of Traumatic Brain Injury. In: Tharakan B, editor. Traumatic and Ischemic Injury. Temple, TX: Humana Press Inc.; 2018. p. 219-28. DOI: 10.1007/978-1-4939-7526-6$_1$7.

[222] Meaney DF, Morrison B, Bass CD. The mechanics of traumatic brain injury: A review of what we know and what we need to know for reducing its societal burden. American Society of Mechanical Engineers; 2014. DOI: 10.1115/1.4026364.

[223] Vajda J, Milojević M, Maver U, *et al.* Microvascular Tissue Engineering-A Review. Biomedicines. 2021;9. DOI: 10.3390/BIOMEDICINES9060589.

[224] Ho TC, Chang CC, Chan HP, *et al.* Hydrogels: Properties and Applications in Biomedicine. Molecules. 2022;27. DOI: 10.3390/molecules27092902.

[225] Abdul Sisak MA, Louis F, Matsusaki M. In vitro fabrication and application of engineered vascular hydrogels. Polymer Journal. 2020;52(8):871-81. DOI: 10.1038/S41428-020-0331-Z;TECHMETA.

[226] Parhi R. Cross-Linked Hydrogel for Pharmaceutical Applications: A Review. Advanced Pharmaceutical Bulletin. 2017;7(4):515. DOI: 10.15171/APB.2017.064.

[227] Kim JS, Kim TH, Kang DL, *et al.* Chondrogenic differentiation of human ASCs by stiffness control in 3D fibrin hydrogel. Biochemical and Biophysical Research Communications. 2020;522:213-9. DOI: 10.1016/J.BBRC.2019.11.049.

[228] Ahmed TAE, Dare EV, Hincke M. Fibrin: A versatile scaffold for tissue engineering applications. Mary Ann Liebert, Inc. 140 Huguenot Street, 3rd Floor New Rochelle, NY 10801 USA; 2008. DOI: 10.1089/ten.teb.2007.0435.

[229] Vacanti JP, Langer R. Tissue engineering: The design and fabrication of living replacement devices for surgical reconstruction and transplantation. Lancet. 1999;354(SUPPL.1):32-4. DOI: 10.1016/s0140-6736(99)90247-7.

[230] Campo H, Santamaria X, Cervelló I, *et al.* Scaffolds for bioengineered uterus. In: Handbook of Tissue Engineering Scaffolds: Volume Two. Elsevier; 2019. p. 283-316. DOI: 10.1016/B978-0-08-102561-1.00011-7.

[231] Guilak F, Butler DL, Goldstein SA, *et al.* Biomechanics and mechanobiology in functional tissue engineering. Journal of Biomechanics. 2014;47(9):1933-40. DOI: 10.1016/j.jbiomech.2014.04.019.

[232] Lanza R. Principles of Tissue Engineering. 5th ed. Lanza R, editor. Elsevier; 2020.

[233] Molina MIE, Malollari KG, Komvopoulos K. Design Challenges in Polymeric Scaffolds for Tissue Engineering. Frontiers in Bioengineering and Biotechnology. 2021;9:617141. DOI: 10.3389/fbioe.2021.617141.

[234] Ud-Din S, Volk SW, Bayat A. Regenerative healing, scar-free healing and scar formation across the species: current concepts and future perspectives. Experimental Dermatology. 2014;23(9):615-9. DOI: 10.1111/EXD.12457.

[235] Baudequin T, Tabrizian M. Multilineage Constructs for Scaffold-Based Tissue Engineering: A Review of Tissue-Specific Challenges. Advanced Healthcare Materials. 2018;7(3):1700734. DOI: 10.1002/ADHM.201700734.

[236] Sekar MP, Budharaju H, Zennifer A, *et al.* Current standards and ethical landscape of engineered tissues—3D bioprinting perspective. Journal of Tissue Engineering. 2021;12. DOI: 10.1177/20417314211027677.

[237] Bhargava A, Srivastava S. Biotechnology: Recent Trends and Emerging Dimensions. 1st ed. Bhargava A, Srivastava S, editors. CRC Press; 2017.

[238] Grosberg A, Alford PW, McCain ML, *et al.* Ensembles of engineered cardiac tissues for physiological and pharmacological study: Heart on a chip. Lab on a Chip. 2011;11(24):4165-73. DOI: 10.1039/C1LC20557A.

[239] Tzatzalos E, Abilez OJ, Shukla P, *et al.* Engineered heart tissues and induced pluripotent stem cells: Macro- and microstructures for disease modeling, drug screening, and translational studies. Advanced Drug Delivery Reviews. 2016;96:234-44. DOI: 10.1016/J.ADDR.2015.09.010.

[240] Coulombe KLK, Bajpai VK, Andreadis ST, *et al.* Heart regeneration with engineered myocardial tissue. Annual Review of Biomedical Engineering. 2014;16(Volume 16, 2014):1-28. DOI: 10.1146/ANNUREV-BIOENG-071812-152344/CITE/REFWORKS.

[241] Chen M, Jiang R, Deng N, *et al.* Natural Polymer-based Scaffolds for Soft Tissue Repair. Frontiers in Bioengineering and Biotechnology. 2022;10. DOI: 10.3389/fbioe.2022.954699.

[242] Sadidi H, Hooshmand S, Ahmadabadi A, *et al.* Cerium Oxide Nanoparticles (Nanoceria): Hopes in Soft Tissue Engineering. Molecules 2020, Vol 25, Page 4559. 2020;25:4559. DOI: 10.3390/MOLECULES25194559.

[243] Fu JN, Wang X, Yang M, *et al.* Scaffold-Based Tissue Engineering Strategies for Osteochondral Repair. Frontiers in Bioengineering and Biotechnology. 2022;9:812383. DOI: 10.3389/FBIOE.2021.812383/FULL.

[244] O'Brien FJ. Biomaterials & scaffolds for tissue engineering. Materials Today. 2011;14(3):88-95. DOI: 10.1016/S1369-7021(11)70058-X.

[245] Murphy CM, O'Brien FJ, Little DG, *et al.* Cell-scaffold interactions in the bone tissue engineering triad. European cells & materials. 2013;26:120-32. DOI: 10.22203/ECM.V026A09.

[246] García-Gareta E, Abduldaiem Y, Sawadkar P, *et al.* Decellularised scaffolds: just a framework? Current knowledge and future directions. Journal of Tissue Engineering. 2020;11. DOI: 10.1177/2041731420942903.

[247] Varner VD, Nelson CM. Toward the directed self-Assembly of engineered tissues. Annual Review of Chemical and Biomolecular Engineering. 2014;5(Volume 5, 2014):507-26. DOI: 10.1146/ANNUREV-CHEMBIOENG-060713-040016/CITE/REFWORKS.

[248] Ortuño-Costela MdC, García-López M, Cerrada V, *et al.* iPSCs: A powerful tool for skeletal muscle tissue engineering. Journal of Cellular and Molecular Medicine. 2019;23(6):3784-94. DOI: 10.1111/JCMM.14292.

[249] Chan BP, Leong KW. Scaffolding in tissue engineering: General approaches and tissue-specific considerations. European Spine Journal. 2008;17(SUPPL. 4):467-79. DOI: 10.1007/S00586-008-0745-3/TABLES/3.

[250] Athanasiou KA, Eswaramoorthy R, Hadidi P, *et al.* Self-organization and the self-assembling process in Tissue engineering. Annual Review of Biomedical Engineering. 2013;15(Volume 15, 2013):115-36. DOI: 10.1146/ANNUREV-BIOENG-071812-152423/CITE/REFWORKS.

[251] Ratner BD, Bryant SJ. Biomaterials: Where we have been and where we are going. Annual Review of Biomedical Engineering. 2004;6(Volume 6, 2004):41-75. DOI: 10.1146/ANNUREV.BIOENG.6.040803.140027/CITE/REFWORKS.

[252] Ku SH, Lee SH, Park CB. Synergic effects of nanofiber alignment and electroactivity on myoblast differentiation. Biomaterials. 2012;33:6098-104. DOI: 10.1016/J.BIOMATERIALS.2012.05.018.

[253] Mateu-Sanz M, Fuenteslópez CV, Uribe-Gomez J, *et al.* Redefining biomaterial biocompatibility: challenges for artificial intelligence and text mining. Trends in Biotechnology. 2023. DOI: 10.1016/j.tibtech.2023.09.015.

[254] Alavi SH, Kheradvar A. Metal Mesh Scaffold for Tissue Engineering of Membranes. https://homeliebertpubcom/tec. 2011;18(4):293-301. DOI: 10.1089/TEN.TEC.2011.0531.

[255] Ikada Y. Challenges in tissue engineering. Journal of The Royal Society Interface. 2006;3(10):589-601. DOI: 10.1098/RSIF.2006.0124.

[256] Dhandayuthapani B, Yoshida Y, Maekawa T, *et al.* Polymeric Scaffolds in Tissue Engineering Application: A Review. International Journal of Polymer Science. 2011;2011:290602. DOI: 10.1155/2011/290602.

[257] Grasman JM, Zayas MJ, Page RL, *et al.* Biomimetic scaffolds for regeneration of volumetric muscle loss in skeletal muscle injuries. Acta Biomaterialia. 2015;25:2-15. DOI: 10.1016/J.ACTBIO.2015.07.038.

[258] Nakayama KH, Shayan M, Huang NF. Engineering Biomimetic Materials for Skeletal Muscle Repair and Regeneration. Advanced Healthcare Materials. 2019;8(5):1801168. DOI: 10.1002/ADHM.201801168.

[259] Karg M, Hellweg T. New "smart" poly(NIPAM) microgels and nanoparticle microgel hybrids: Properties and advances in characterisation. Current Opinion in Colloid & Interface Science. 2009 12;14(6):438-50. DOI: 10.1016/J.COCIS.2009.08.002.

[260] Bahram M. An Introduction to Hydrogels and Some Recent Applications. IntechOpen; 2016. DOI: 10.5772/64301.

[261] Hou C, Duan Y, Zhang Q, *et al.* Bio-applicable and electroactive near-infrared laser-triggered self-healing hydrogels based on graphene networks. Journal of Materials Chemistry. 2012;22(30):14991-6. DOI: 10.1039/C2JM32255B.

[262] Wei Z, Yang JH, Zhou J, *et al.* Self-healing gels based on constitutional dynamic chemistry and their potential applications. Chemical Society Reviews. 2014;43(23):8114-31. DOI: 10.1039/C4CS00219A.

[263] Huebsch N, Kearney CJ, Zhao X, *et al.* Ultrasound-triggered disruption and self-healing of reversibly cross-linked hydrogels for drug delivery and enhanced chemotherapy. Proceedings of the National Academy of Sciences. 2014;111(27):9762-7. DOI: 10.1073/PNAS.1405469111.

[264] Schneider-Barthold C, Baganz S, Wilhelmi M, *et al.* Hydrogels based on collagen and fibrin - Frontiers and applications. BioNanoMaterials. 2016;17(1-2):3-12. DOI: 10.1515/BNM-2015-0025/MACHINEREADABLECITATION/RIS.

[265] Janmey PA, Winer JP, Weisel JW. Fibrin gels and their clinical and bioengineering applications. Journal of The Royal Society Interface. 2008;6(30):1-10. DOI: 10.1098/RSIF.2008.0327.

[266] Ramshaw JAM, Peng YY, Glattauer V, *et al.* Collagens as biomaterials. Journal of Materials Science: Materials in Medicine. 2009;20(SUPPL. 1):3-8. DOI: 10.1007/S10856-008-3415-4/METRICS.

[267] Lai VK, Lake SP, Frey CR, *et al.* Mechanical behavior of collagen-fibrin co-gels reflects transition from series to parallel interactions with increasing collagen content. Journal of biomechanical engineering. 2012;134(1). DOI: 10.1115/1.4005544.

[268] Laurens N, Koolwijk P, de Maat MP. Fibrin Structure and Wound Healing. Journal of Thrombosis and Haemostasis. 2006;4:932-9. DOI: 10.1111/j.1538-7836.2006.01861.x.

[269] Krishnan L, Chang CC, Nunes SS, *et al.* Manipulating the Microvasculature and Its Microenvironment. Critical reviews in biomedical engineering. 2013;41(2):91. DOI: 10.1615/CRITREVBIOMEDENG.2013008077.

[270] Tiruvannamalai Annamalai R, Rioja AY, Putnam AJ, *et al.* Vascular Network Formation by Human Microvascular Endothelial Cells in Modular Fibrin Microtissues. ACS Biomaterials Science and Engineering. 2016;2(11):1914-25. DOI: 10.1021/acsbiomaterials.6b00274.

[271] Eltom A, Zhong G, Muhammad A. Scaffold Techniques and Designs in Tissue Engineering Functions and Purposes: A Review. Advances in Materials Science and Engineering. 2019;2019(1):3429527. DOI: 10.1155/2019/3429527.

[272] Sharma P, Kumar P, Sharma R, *et al.* Tissue Engineering; Current Status & Futuristic Scope. Journal of Medicine and Life. 2019;2019:225-9. DOI: 10.25122/jml-2019-0032.

[273] Olson JL, Atala A, Yoo JJ. Tissue engineering: current strategies and future directions. Chonnam medical journal. 2011;47(1):1. DOI: 10.4068/CMJ.2011.47.1.1.

[274] Huang CP, Yang CY, Shyr CR. Utilizing Xenogeneic Cells As a Therapeutic Agent for Treating Diseases. Cell Transplantation. 2021;30:09636897211011995. DOI: 10.1177/09636897211011995.

[275] Kimsa MC, Strzalka-Mrozik B, Kimsa MW, *et al.* Porcine endogenous retroviruses in xenotransplantation–molecular aspects. Viruses. 2014;6(5):2062-83. DOI: 10.3390/V6052062.

[276] Cassell OCS, Morrison WA, Messina A, *et al.* The Influence of Extracellular Matrix on the Generation of Vascularized, Engineered, Transplantable Tissue. Annals of the New York Academy of Sciences. 2001;944(1):429-42. DOI: 10.1111/J.1749-6632.2001.TB03853.X.

[277] Hall MN, Hall JK, Cadwallader AB, *et al.* Transplantation of Skeletal Muscle Stem Cells. Methods in Molecular Biology. 2017;1556:237-44. DOI: 10.1007/978-1-4939-6771-1_12.

[278] Fishman JM, Tyraskis A, Maghsoudlou P, *et al.* Skeletal Muscle Tissue Engineering: Which Cell to Use? https://homeliebertpubcom/teb. 2013;19(6):503-15. DOI: 10.1089/TEN.TEB.2013.0120.

[279] Rao L, Qian Y, Khodabukus A, *et al.* Engineering human pluripotent stem cells into a functional skeletal muscle tissue. Nature Communications. 2018;9(1):1-12. DOI: 10.1038/S41467-017-02636-4;TECHMETA.

[280] Takahashi K, Yamanaka S. Induction of Pluripotent Stem Cells from Mouse Embryonic and Adult Fibroblast Cultures by Defined Factors. Cell. 2006;126(4):663-76. DOI: 10.1016/J.CELL.2006.07.024.

[281] Humphrey JD. Vascular adaptation and mechanical homeostasis at tissue, cellular, and sub-cellular levels. Cell Biochemistry and Biophysics. 2008;50(2):53-78. DOI: 10.1007/s12013-007-9002-3.

[282] Ceccarelli J, Putnam AJ. Sculpting the blank slate: How fibrin's support of vascularization can inspire biomaterial design. Elsevier BV; 2014. DOI: 10.1016/j.actbio.2013.07.043.

[283] Butler DL, Goldstein SA, Guilak F. Functional tissue engineering: The role of biomechanics. Journal of Biomechanical Engineering. 2000;122(6):570-5. DOI: 10.1115/1.1318906.

[284] Bogorad MI, DeStefano J, Karlsson J, *et al.* Review: In Vitro Microvessel Models. Lab on a Chip. 2015;15:4242-55. DOI: 10.1039/c5lc00832h.

[285] Cao Y, Gong Y, Liu L, *et al.* The use of human umbilical vein endothelial cells (HUVECs) as an in vitro model to assess the toxicity of nanoparticles to endothelium: A review. Journal of Applied Toxicology. 2017;37:1359-69. DOI: 10.1002/JAT.3470.

[286] Kocherova I, Bryja A, Mozdziak P, *et al.* Human Umbilical Vein Endothelial Cells (HUVECs) Co-Culture with Osteogenic Cells: From Molecular Communication to Engineering Prevascularised Bone Grafts. Journal of Clinical Medicine. 2019;8. DOI: 10.3390/jcm8101602.

[287] Bogorad MI, DeStefano J, Wong AD, *et al.* Tissue-engineered 3D microvessel and capillary network models for the study of vascular phenomena. 2017;24(5). DOI: 10.1111/micc.12360.

[288] Ganapathy A, Narayanan K, Chen Y, *et al.* Dentin matrix protein 1 and HUVEC-ECM scaffold promote the differentiation of human dental pulp stem cells into endothelial lineage: implications in regenerative medicine. Frontiers in Physiology. 2024;15:1429247. DOI: 10.3389/FPHYS.2024.1429247.

[289] Medina-Leyte DJ, Domínguez-Pérez M, Mercado I, *et al.* Use of Human Umbilical Vein Endothelial Cells (HUVEC) as a Model to Study Cardiovascular Disease: A Review. Applied Sciences 2020, Vol 10, Page 938. 2020;10:938. DOI: 10.3390/APP10030938.

[290] Moya ML, Hsu YH, Lee AP, *et al.* In vitro perfused human capillary networks. Tissue Engineering - Part C: Methods. 2013;19(9):730-7. DOI: 10.1089/ten.tec.2012.0430.

[291] Traore MA, George SC. Tissue Engineering the Vascular Tree. Tissue Engineering: Part B. 2017;23(6):505-14. DOI: 10.1089/ten.teb.2017.0010.

[292] Bagley RG, Walter-Yohrling J, Cao X, *et al.* Endothelial Precursor Cells As a Model of Tumor Endothelium: Characterization and Comparison with Mature Endothelial Cells. Cancer Research. 2003;63:5866-73.

[293] Abhinand CS, Galipon J, Mori M, *et al.* Temporal phosphoproteomic analysis of VEGF-A signaling in HUVECs: An insight into early signaling events associated with angiogenesis. Journal of Cell Communication and Signaling. 2023;17:1067. DOI: 10.1007/S12079-023-00736-Z.

[294] Li X, Wang C, Zhang H, *et al.* circFNDC3B Accelerates Vasculature Formation and Metastasis in Oral Squamous Cell Carcinoma. Cancer Research. 2023;83:1459. DOI: 10.1158/0008-5472.CAN-22-2585.

[295] Liu YX, Xu BW, Niu XD, *et al.* Inhibition of Src/-STAT3 signaling-mediated angiogenesis is involved in the anti-melanoma effects of dioscin. Pharmacological Research. 2022;175:1043-6618. DOI: 10.1016/j.phrs.2021.105983.

[296] Teichert-Kuliszewska K, Maisonpierre PC, Jones N, *et al.* Biological action of angiopoietin-2 in a fibrin matrix model of angiogenesis is associated with activation of Tie2. Cardiovascular Research. 2001;49:659-70.

[297] Narayan R, Agarwal T, Mishra D, *et al.* Goat Tendon Collagen-Human Fibrin Hydrogel for Comprehensive Parametric Evaluation of HUVEC Microtissue-Based Angiogenesis. Colloids and Surfaces B: Biointerfaces. 2018;163:291-300. DOI: 10.1016/j.colsurfb.2017.12.056.

[298] DeCicco-Skinner KL, Henry GH, Cataisson C, *et al.* Endothelial Cell Tube Formation Assay for the In Vitro Study of Angiogenesis. Journal of Visualized Experiments : JoVE. 2014:51312. DOI: 10.3791/51312.

[299] Xu L, Zhou J, Liu J, *et al.* Different Angiogenic Potentials of Mesenchymal Stem Cells Derived from Umbilical Artery, Umbilical Vein, and Wharton's Jelly. Stem Cells International. 2017;2017:3175748. DOI: 10.1155/2017/3175748.

[300] Bonnefoy A, Harsfalvi J, Pfliegler G, *et al.* The subendothelium of the HMEC-1 cell line supports thrombus formation in the absence of von Willebrand factor and collagen types I, III and VI. Thromb Haemost. 2001;85(3):552-9.

[301] Kluger MS, Clark PR, Tellides G, *et al.* Claudin-5 Controls Intercellular Barriers of Human Dermal Microvascular but not Human Umbilical Vein Endothelial Cells. Arteriosclerosis, thrombosis, and vascular biology. 2013;33:489. DOI: 10.1161/ATVBAHA.112.300893.

[302] Gariboldi MI, Butler R, Best SM, *et al.* Engineering vasculature: Architectural effects on microcapillary-like structure self-assembly. PLoS ONE. 2019;14(1):e0210390. DOI: 10.1371/JOURNAL.PONE.0210390.

[303] Bakhshandeh B, Ranjbar N, Abbasi A, *et al.* Recent progress in the manipulation of biochemical and biophysical cues for engineering functional tissues. Bioengineering & Translational Medicine. 2022;8(2):e10383. DOI: 10.1002/BTM2.10383.

[304] Lee K, Silva EA, Mooney DJ. Growth factor delivery-based tissue engineering: general approaches and a review of recent developments. Journal of The Royal Society Interface. 2011;8(55):153-70. DOI: 10.1098/RSIF.2010.0223.

[305] Wang Z, Wang Z, Lu WW, *et al.* Novel biomaterial strategies for controlled growth factor delivery for biomedical applications. NPG Asia Materials. 2017;9(10):e435-5. DOI: 10.1038/AM.2017.171;TECHMETA.

[306] Król-Morkisz K, Pielichowska K. Thermal Decomposition of Polymer Nanocomposites With Functionalized Nanoparticles. Polymer Composites with Functionalized Nanoparticles: Synthesis, Properties, and Applications. 2019:405-35. DOI: 10.1016/B978-0-12-814064-2.00013-5.

[307] Liebschner M, Bucklen B, Wettergreen M. Mechanical Aspects of Tissue Engineering. Seminars in Plastic Surgery. 2005;19(3):217. DOI: 10.1055/S-2005-919717.

[308] Dutta RC, Dey M, Dutta AK, *et al.* Competent processing techniques for scaffolds in tissue engineering. Biotechnology Advances. 2017;35(2):240-50. DOI: 10.1016/J.BIOTECHADV.2017.01.001.

[309] Bajaj P, Schweller RM, Khademhosseini A, *et al.* 3D biofabrication strategies for tissue engineering and regenerative medicine. Annual Review of Biomedical Engineering. 2014;16(Volume 16, 2014):247-76. DOI: 10.1146/ANNUREV-BIOENG-071813-105155/CITE/REFWORKS.

[310] Auger FA, Gibot L, Lacroix D. The pivotal role of vascularization in tissue engineering. Annual Review of Biomedical Engineering. 2013;15(Volume 15, 2013):177-200. DOI: 10.1146/annurev-bioeng-071812-152428.

[311] Zadpoor AA. Bone tissue regeneration: the role of scaffold geometry. Biomaterials Science. 2015 1;3(2):231-45. DOI: 10.1039/C4BM00291A.

[312] Choi SW, Zhang Y, Xia Y. Three-Dimensional Scaffolds for Tissue Engineering: The Importance of Uniformity in Pore Size and Structure. Langmuir. 2010 12;26(24):19001-6. DOI: 10.1021/LA104206H.

[313] Mouthuy PA, Groszkowski L, Ye H. Performances of a portable electrospinning apparatus. Biotechnology Letters. 2015;37(5):1107-16. DOI: 10.1007/s10529-014-1760-6.

[314] Gsib O, Deneufchatel M, Goczkowski M, *et al.* FibriDerm: Interpenetrated Fibrin Scaffolds for the Construction of Human Skin Equivalents for Full Thickness Burns. IRBM. 2018;39(2):103-8. DOI: 10.1016/J.IRBM.2017.10.006.

[315] Chen A, Wang W, Mao Z, *et al.* Multimaterial 3D and 4D Bioprinting of Heterogenous Constructs for Tissue Engineering. Advanced Materials. 2024;36(34):2307686. DOI: 10.1002/ADMA.202307686.

[316] Raeisdasteh Hokmabad V, Davaran S, Ramazani A, *et al.* Design and fabrication of porous biodegradable scaffolds: a strategy for tissue engineering. Journal of biomaterials science Polymer edition. 2017;28(16):1797-825. DOI: 10.1080/09205063.2017.1354674.

[317] Rustad KC, Sorkin M, Levi B, *et al.* Strategies for organ level tissue engineering. Organogenesis. 2010;6(3):151. DOI: 10.4161/ORG.6.3.12139.

[318] Ouyang L, Armstrong JPK, Salmeron-Sanchez M, *et al.* Void-free 3D Bioprinting for In-situ Endothelialization and Microfluidic Perfusion. Advanced functional materials. 2020;30(26). DOI: 10.1002/ADFM.201909009.

[319] Leong MF, Toh JKC, Du C, *et al.* Patterned prevascularised tissue constructs by assembly of polyelectrolyte hydrogel fibres. Nature communications. 2013;4. DOI: 10.1038/NCOMMS3353.

[320] Takahashi H, Shimizu T, Nakayama M, *et al.* The use of anisotropic cell sheets to control orientation during the self-organization of 3D muscle tissue. Biomaterials. 2013;34(30):7372-80. DOI: 10.1016/j.biomaterials.2013.06.033.

[321] Ahmad T, Byun H, Lee J, *et al.* Stem cell spheroids incorporating fibers coated with adenosine and polydopamine as a modular building blocks for bone tissue engineering. Biomaterials. 2020;230. DOI: 10.1016/j.biomaterials.2019.119652.

[322] Lawlor KT, Vanslambrouck JM, Higgins JW, *et al.* Cellular extrusion bioprinting improves kidney organoid reproducibility and conformation. Nature materials. 2021;20(2):260-71. DOI: 10.1038/S41563-020-00853-9.

[323] Tasoglu S, Yu CH, Gungordu HI, *et al.* Guided and magnetic self-assembly of tunable magnetoceptive gels. Nature communications. 2014;5. DOI: 10.1038/NCOMMS5702.

[324] Wolf KJ, Weiss JD, Uzel SGM, *et al.* Biomanufacturing human tissues via organ building blocks. Cell Stem Cell. 2022;29(5):667-77. DOI: 10.1016/j.stem.2022.04.012.

[325] Duval K, Grover H, Han LH, *et al.* Modeling Physiological Events in 2D vs. 3D Cell Culture. Physiology (Bethesda, Md). 2017;32(4):266-77. DOI: 10.1152/physiol.00036.2016.

[326] Jedrzejczak-Silicka M. History of Cell Culture. IntechOpen; 2017. DOI: 10.5772/66905.

[327] Houkin K, Abe K, Kuroda S. Cell therapy against cerebral stroke : comprehensive reviews for translational researches and clinical trials. 1st ed. Abe K, Kuroda S, Houkin K, editors. Tokyo: Springer; 2017. DOI: 10.1007/978-4-431-56059-3.

[328] Tiruvannamalai-Annamalai R, Armant DR, Matthew HWT. A Glycosaminoglycan Based, Modular Tissue Scaffold System for Rapid Assembly of Perfusable, High Cell Density, Engineered Tissues. PloS one. 2014;9(1):e84287. DOI: 10.1371/journal.pone.0084287.

[329] Murphy SV, Atala A. 3D bioprinting of tissues and organs. Nature Biotechnology. 2014;32:773-85. DOI: 10.1038/nbt.2958.

[330] Park H, Baek S, Kang H, *et al.* Biomaterials to Prevent Post-Operative Adhesion. Materials 2020, Vol 13, Page 3056. 2020;13(14):3056. DOI: 10.3390/MA13143056.

[331] Sola A, Bertacchini J, D'Avella D, *et al.* Development of solvent-casting particulate leaching (SCPL) polymer scaffolds as improved three-dimensional supports to mimic the bone marrow niche. Materials Science and Engineering C. 2019;96:153-65. DOI: 10.1016/j.msec.2018.10.086.

[332] Hossainpour H, Zare S, Alvandi H, *et al.* Gelatin-sodium alginate hydrogel infused with Onosma dichroanthum Boiss. root extract: Preparation, characterization, and application in wound dressing. Biochemistry and Biophysics Reports. 2025;44:102236. DOI: 10.1016/J.BBREP.2025.102236.

[333] Song P, Zhou C, Fan H, *et al.* Novel 3D porous biocomposite scaffolds fabricated by fused deposition modeling and gas foaming combined technology. Composites Part B: Engineering. 2018;152:151-9. DOI: 10.1016/J.COMPOSITESB.2018.06.029.

[334] Guo S, Kang G, Phan DT, *et al.* Polymerization-Induced Phase Separation Formation of Structured Hydrogel Particles via Microfluidics for Scar Therapeutics. Scientific Reports. 2018;8(1):1-10. DOI: 10.1038/S41598-018-20516-9;TECHMETA.

[335] Mao D, Li Q, Li D, *et al.* 3D porous poly(ε-caprolactone)/58S bioactive glass–sodium alginate/gelatin hybrid scaffolds prepared by a modified melt molding method for bone tissue engineering. Materials & Design. 2018;160:1-8. DOI: 10.1016/J.MATDES.2018.08.062.

[336] Luo Q, Huang X, Gao F, *et al.* Preparation and Characterization of High Amylose Corn Starch–Microcrystalline Cellulose Aerogel with High Absorption. Materials 2019, Vol 12, Page 1420. 2019;12(9):1420. DOI: 10.3390/MA12091420.

[337] Rowley JA, Madlambayan G, Mooney DJ. Alginate hydrogels as synthetic extracellular matrix materials. Biomaterials. 1999;20(1):45-53. DOI: 10.1016/S0142-9612(98)00107-0.

[338] Mansour FR, Waheed S, Paull B, *et al.* Porogens and porogen selection in the preparation of porous polymer monoliths. Journal of Separation Science. 2020;43(1):56-69. DOI: 10.1002/JSSC.201900876.

[339] Hennink WE, Van Nostrum CF. Novel crosslinking methods to design hydrogels. Advanced Drug Delivery Reviews. 2002;54(1):13-36. DOI: 10.1016/S0169-409X(01)00240-X.

[340] Mastrullo V, Cathery W, Velliou E, *et al.* Angiogenesis in Tissue Engineering: As Nature Intended? Frontiers in Bioengineering and Biotechnology. 2020;8. DOI: 10.3389/fbioe.2020.00188.

[341] Chaudhuri O, Gu L, Klumpers D, *et al.* Hydrogels with tunable stress relaxation regulate stem cell fate and activity. Nature Materials. 2016;15(3):326-34. DOI: 10.1038/NMAT4489;TECHMETA.

[342] Highley CB, Prestwich GD, Burdick JA. Recent advances in hyaluronic acid hydrogels for biomedical applications. Current Opinion in Biotechnology. 2016;40:35-40. DOI: 10.1016/J.COPBIO.2016.02.008.

[343] Passipieri JA, Baker HB, Siriwardane M, *et al.* Keratin Hydrogel Enhances In Vivo Skeletal Muscle Function in a Rat Model of Volumetric Muscle Loss. https://homeliebertpubcom/tea. 2017;23(11-12):556-71. DOI: 10.1089/TEN.TEA.2016.0458.

[344] Sukmana I. Bioactive Polymer Scaffold for Fabrication of Vascularized Engineering Tissue. Journal of Artificial Organs. 2012;15:215-24. DOI: 10.1007/s10047-012-0644-6.

[345] Morin KT, Tranquillo RT. In Vitro Models of Angiogenesis and Vasculogenesis in Fibrin Gel. Experimental cell research. 2013;319(16):2409. DOI: 10.1016/J.YEXCR.2013.06.006.

[346] Geckil H, Xu F, Zhang X, *et al.* Engineering hydrogels as extracellular matrix mimics. Nanomedicine (Lond). 2010;5:469-84. DOI: 10.2217/nnm.10.12.

[347] Nelson DW, Gilbert RJ. Extracellular Matrix-Mimetic Hydrogels for Treating Neural Tissue Injury: A Focus on Fibrin, Hyaluronic Acid, and Elastin-Like Polypeptide Hydrogels. Advanced Healthcare Materials. 2021;10:2101329. DOI: 10.1002/adhm.202101329.

[348] Eyrich D, Brandl F, Appel B, *et al.* Long-term stable fibrin gels for cartilage engineering. Biomaterials. 2007;28:55-65. DOI: 10.1016/J.BIOMATERIALS.2006.08.027.

[349] Jarrell DK, Vanderslice EJ, Lennon ML, *et al.* Increasing salinity of fibrinogen solvent generates stable fibrin hydrogels for cell delivery or tissue engineering. PLoS ONE. 2021;16. DOI: 10.1371/journal.pone.0239242.

[350] Ren Y, Zhang H, Wang Y, *et al.* Hyaluronic Acid Hydrogel with Adjustable Stiffness for Mesenchymal Stem Cell 3D Culture via Related Molecular Mechanisms to Maintain Stemness and Induce Cartilage Differentiation. ACS Applied Bio Materials. 2021;4:2601-13. DOI: 10.1021/acsabm.0c01591.

[351] Wang Q, Wang X, Feng Y. Chitosan Hydrogel as Tissue Engineering Scaffolds for Vascular Regeneration Applications. Gels (Basel, Switzerland). 2023;9. DOI: 10.3390/GELS9050373.

[352] Gillette BM, Jensen JA, Tang B, *et al.* In situ collagen assembly for integrating microfabricated three-dimensional cell-seeded matrices. Nature materials. 2008;7:636-40. DOI: 10.1038/NMAT2203.

[353] Kilmer CE, Battistoni CM, Cox A, *et al.* Collagen Type I and II Blend Hydrogel with Autologous Mesenchymal Stem Cells as a Scaffold for Articular Cartilage Defect Repair. ACS biomaterials science engineering. 2020;6:3464. DOI: 10.1021/ACSBIOMATERIALS.9B01939.

[354] Moxon SR, Corbett NJ, Fisher K, *et al.* Blended alginate/collagen hydrogels promote neurogenesis and neuronal maturation. 2019. DOI: 10.1016/j.msec.2019.109904.

[355] Smidsrød O, Skjåk-Braek G. Alginate as immobilization matrix for cells. Ind Eng Chem Process Des Dev. 1990;8:76-80.

[356] Zhang W, Jiang Y, Wang H, *et al.* In situ forming hydrogel recombination with tissue adhesion and antibacterial property for tissue adhesive. Journal of Biomaterials Applications. 2022;37:12-22. DOI: 10.1177/08853282221078159.

[357] Cosola A, Chiappone A, Martinengo C, *et al.* Gelatin Type A from Porcine Skin Used as Co-Initiator in a Radical Photo-Initiating System. Polymers. 2019;11. DOI: 10.3390/POLYM11111901.

[358] Peppas NA, Hilt JZ, Khademhosseini A, *et al.* Hydrogels in biology and medicine: From molecular principles to bionanotechnology. Advanced Materials. 2006;18:1345-60. DOI: 10.1002/ADMA.200501612.

[359] Rivest C, Morrison DWG, Ni B, *et al.* Microscale hydrogels for medicine and biology: Synthesis characteristics and applications. Journal of Mechanics of Materials and Structures. 2007;2:1103-19. DOI: 10.2140/JOMMS.2007.2.1103.

[360] Shoulders MD, Raines RT. Collagen structure and stability. Annual Review of Biochemistry. 2009 7;78(Volume 78, 2009):929-58. DOI: 10.1146/ANNUREV.BIOCHEM.77.032207.120833/CITE/REFWORKS.

[361] Broderick EP, O'Halloran DM, Rochev YA, *et al.* Enzymatic stabilization of gelatin-based scaffolds. Journal of Biomedical Materials Research - Part B Applied Biomaterials. 2005 1;72(1):37-42. DOI: 10.1002/JBM.B.30119;ISSUE:ISSUE:DOI.

[362] Mikhailov OV. Molecular nanotechnologies of gelatin-immobilization using macrocyclic metal chelates. Nano Reviews. 2014 1;5(1):10.3402/nano.v5.21485. DOI: 10.3402/NANO.V5.21485.

[363] Roth CC, Kropp BP, Cheng EY. 12 - Natural biomaterials for urological tissue engineering. In: John Denstedt, Anthony Atala, editors. Biomaterials and Tissue Engineering in Urology. Woodhead Publishing; 2009. p. 255-80. DOI: 10.1533/9781845696375.3.255.

[364] Salvatore L, Gallo N, Natali ML, *et al.* Mimicking the Hierarchical Organization of Natural Collagen: Toward the Development of Ideal Scaffolding Material for Tissue Regeneration. Frontiers in Bioengineering and Biotechnology. 2021 4;9:644595. DOI: 10.3389/FBIOE.2021.644595/FULL.

[365] Klangjorhor J, Nimkingratana P, Settakorn J, *et al.* Hyaluronan production and chondrogenic properties of primary human chondrocyte on gelatin based hematostatic spongostan scaffold. Journal of Orthopaedic Surgery and Research 2012 7:1. 2012 12;7(1):40. DOI: 10.1186/1749-799X-7-40.

[366] Li X, Zhang Q, Yu SM, *et al.* The Chemistry and Biology of Collagen Hybridization. Journal of the American Chemical Society. 2023;145:10901-16. DOI: 10.1021/jacs.3c00713.

[367] Zitnay JL, Li Y, Qin Z, *et al.* Molecular level detection and localization of mechanical damage in collagen enabled by collagen hybridizing peptides. Nature Communications 2017 8:1. 2017 3;8(1):14913. DOI: 10.1038/ncomms14913.

[368] Bella J, Eaton M, Brodsky B, *et al.* Crystal and molecular structure of a collagen-like peptide at 1.9 Å resolution. Science. 1994 10;266(5182):75-81. DOI: 10.1126/science.7695699.

[369] Bonnans C, Chou J, Werb Z. Basement membrane Remodelling the extracellular matrix in development and disease. Nature Reviews Molecular Cell Biology. 2014;15. DOI: 10.1038/nrm3904.

[370] Fields GB. Interstitial Collagen Catabolism. Journal of Biological Chemistry. 2013 3;288(13):8785-93. DOI: 10.1074/JBC.R113.451211.

[371] Zhu Y, Chen S, Zhang C, *et al.* Novel microsphere-packing synthesis, microstructure, formation mechanism and in vitro biocompatibility of porous gelatin/hydroxyapatite microsphere scaffolds. Ceramics International. 2021 11;47(22):32187-94. DOI: 10.1016/J.CERAMINT.2021.08.111.

[372] Yue K, Trujillo-de Santiago G, Alvarez MM, *et al.* Synthesis, properties, and biomedical applications of gelatin methacryloyl (GelMA) hydrogels. Biomaterials. 2015 12;73:254. DOI: 10.1016/J.BIOMATERIALS.2015.08.045.

[373] Mikhailov OV. Gelatin as It Is: History and Modernity. International Journal of Molecular Sciences. 2023 2;24(4):3583. DOI: 10.3390/IJMS24043583.

[374] Pieters M, Wolberg AS, Wolberg CSA. Fibrinogen and fibrin: An illustrated review. Res Pract Thromb Haemost. 2019;3:161-72. DOI: 10.1002/rth2.12191.

[375] Weisel JW, Litvinov RI. In: Parry DAD, Squire JM, editors. Fibrin Formation, Structure and Properties. vol. 82. Springer International Publishing; 2017. p. 405-56. DOI: 10.1007/978-3-319-49674-0$_1$3.

[376] Weisel JW. Fibrinogen and Fibrin. Advances in Protein Chemistry. 2005 1;70:247-99. DOI: 10.1016/S0065-3233(05)70008-5.

[377] Belcher HA, Litwa K, Guthold M, *et al.* The Applicability of Current Turbidimetric Approaches for Analyzing Fibrin Fibers and Other Filamentous Networks. Biomolecules. 2022 6;12(6):807. DOI: 10.3390/BIOM12060807/S1.

[378] Jansen KA, Zhmurov A, Vos BE, *et al.* Molecular packing structure of fibrin fibers resolved by X-ray scattering and molecular modeling. Soft Matter. 2020 9;16(35):8272-83. DOI: 10.1039/D0SM00916D.

[379] Lampejo AO, Hu NW, Lucas D, *et al.* A Challenge for Engineering Biomimetic Microvascular Models: How do we Incorporate the Physiology? Frontiers in Bioengineering and Biotechnology. 2022;10. DOI: 10.3389/FBIOE.2022.912073.

[380] Kaunas R, Kang H, Bayless KJ. Synergistic Regulation of Angiogenic Sprouting by Biochemical Factors and Wall Shear Stress. Cellular and molecular bioengineering. 2011;4:547-59. DOI: 10.1007/S12195-011-0208-5.

[381] Campisi M, Shin Y, Osaki T, *et al.* 3D self-organized microvascular model of the human blood-brain barrier with endothelial cells, pericytes and astrocytes. Biomaterials. 2018;180:117-29. DOI: 10.1016/J.BIOMATERIALS.2018.07.014.

[382] Chen H, Cheng Y, Wang X, *et al.* 3D printed in vitro tumor tissue model of colorectal cancer. Theranostics. 2020;10:12127-43. DOI: 10.7150/THNO.52450.

[383] Diebel LN, Diebel ME, Martin JV, *et al.* Acute hyperglycemia exacerbates trauma-induced endothelial and glycocalyx injury: An in vitro model. Journal of Trauma and Acute Care Surgery. 2018;85(5):960-7. DOI: 10.1097/TA.0000000000001993.

[384] Young EWK, Watson MWL, Srigunapalan S, *et al.* Technique for real-time measurements of endothelial permeability in a microfluidic membrane chip using laser-induced fluorescence detection. Analytical Chemistry. 2010;82(3):808-16. DOI: 10.1021/ac901560w.

[385] Booth R, Kim H. Characterization of a microfluidic in vitro model of the blood-brain barrier (μBBB). Lab on a Chip. 2012;12(10):1784-92. DOI: 10.1039/c2lc40094d.

[386] Wong AD, Ye M, Levy AF, *et al.*. The blood-brain barrier: An engineering perspective. Front Neuroeng; 2013. DOI: 10.3389/fneng.2013.00007.

[387] Bersini S, Jeon JS, Dubini G, *et al.* A microfluidic 3D invitro model for specificity of breast cancer metastasis to bone. Biomaterials. 2014;35(8):2454-61. DOI: 10.1016/j.biomaterials.2013.11.050.

[388] Zervantonakis IK, Hughes-Alford SK, Charest JL, *et al.* Three-dimensional microfluidic model for tumor cell intravasation and endothelial barrier function. Proceedings of the National Academy of Sciences of the United States of America. 2012;109(34):13515-20. DOI: 10.1073/pnas.1210182109.

[389] Ren B, Song K, Sanikommu AR, *et al.* Study of sacrificial ink-assisted embedded printing for 3D perfusable channel creation for biomedical applications. Applied physics reviews. 2022;9. DOI: 10.1063/5.0068329.

[390] Zheng Y, Chen J, Craven M, *et al.* In vitro microvessels for the study of angiogenesis and thrombosis. Proceedings of the National Academy of Sciences of the United States of America. 2012;109(24):9342-7. DOI: 10.1073/pnas.1201240109.

[391] Buchanan CF, Voigt EE, Szot CS, *et al.* Three-dimensional microfluidic collagen hydrogels for investigating flow-mediated tumor-endothelial signaling and vascular organization. Tissue engineering Part C, Methods. 2014;20(1):64-75. DOI: 10.1089/TEN.TEC.2012.0731.

[392] Golden AP, Tien J. Fabrication of microfluidic hydrogels using molded gelatin as a sacrificial element. Lab on a Chip. 2007;7(6):720-5. DOI: 10.1039/b618409j.

[393] Sarker MD, Naghieh S, Sharma NK, *et al.* Bioprinting of Vascularized Tissue Scaffolds: Influence of Biopolymer, Cells, Growth Factors, and Gene Delivery. Journal of Healthcare Engineering. 2019;2019:9156921. DOI: 10.1155/2019/9156921.

[394] Benning L, Gutzweiler L, Tröndle K, *et al.* Assessment of hydrogels for bioprinting of endothelial cells. Journal of Biomedical Materials Research - Part A. 2018;106:935-47. DOI: 10.1002/JBM.A.36291.

[395] de Melo BAG, Jodat YA, Cruz EM, *et al.* Strategies to use fibrinogen as bioink for 3D bioprinting fibrin-based soft and hard tissues. Acta Biomaterialia. 2020;117:60-76. DOI: 10.1016/J.ACTBIO.2020.09.024.

[396] Nishiyama Y, Nakamura M, Henmi C, *et al.* Development of a three-dimensional bioprinter: construction of cell supporting structures using hydrogel and state-of-the-art inkjet technology. Journal of biomechanical engineering. 2009;131(3). DOI: 10.1115/1.3002759.

[397] Fuenteslópez CV, Thompson MS, Ye H. Development and Optimisation of Hydrogel Scaffolds for Microvascular Network Formation. Bioengineering. 2023;10:964. DOI: 10.3390/bioengineering10080964.

[398] Kaur S, Kaur I, Rawal P, *et al.* Non-matrigel scaffolds for organoid cultures. Cancer Letters. 2021;504:58-66. DOI: 10.1016/j.canlet.2021.01.025.

[399] Habanjar O, Diab-Assaf M, Caldefie-Chezet F, *et al.* 3D cell culture systems: Tumor application, advantages, and disadvantages. International Journal of Molecular Sciences. 2021;22. DOI: 10.3390/ijms222212200.

[400] Kozlowski MT, Crook CJ, Ku HT. Towards organoid culture without Matrigel. Communications Biology. 2021;4:1387. DOI: 10.1038/s42003-021-02910-8.

[401] Lim X, Potter M, Cui Z, *et al.* Manufacture and characterisation of EmDerm—novel hierarchically structured bio-active scaffolds for tissue regeneration. Journal of Materials Science: Materials in Medicine. 2018;29(6). DOI: 10.1007/s10856-018-6060-6.

[402] Sharma V, Patel N, Dye JF, *et al.* Albumin removal from human fibrinogen preparations for manufacturing human fibrin-based biomaterials. Biochimie Open. 2015;1:6-10. DOI: 10.1016/j.biopen.2015.05.002.

[403] Jonkman JEN, Cathcart JA, Xu F, *et al.* An introduction to the wound healing assay using live-cell microscopy. Cell Adhesion and Migration. 2014;8(5):440-51. DOI: 10.4161/cam.36224.

[404] Schindelin J, Arganda-Carreras I, Frise E, *et al.* Fiji: An open-source platform for biological-image analysis. Nature Methods 2012 9:7. 2012;9:676-82. DOI: 10.1038/nmeth.2019.

[405] Hasenberg T, Mühleder S, Dotzler A, *et al.* Emulating Human Microcapillaries in a Multi-Organ-Chip Platform. Journal of Biotechnology. 2015;216:1-10. DOI: 10.1016/j.jbiotec.2015.09.038.

[406] Anderson SM, Siegman SN, Segura T. The effect of vascular endothelial growth factor (VEGF) presentation within fibrin matrices on endothelial cell branching. Biomaterials. 2011;32:7432-43. DOI: 10.1016/j.biomaterials.2011.06.027.

[407] Benwood C, Chrenek J, Kirsch RL, *et al.* Natural biomaterials and their use as bioinks for printing tissues. Bioengineering. 2021;8:1-19. DOI: 10.3390/bioengineering8020027.

[408] Rosińska K, Bartniak M, Wierzbicka A, *et al.* Solvent types used for the preparation of hydrogels determine their mechanical properties and influence cell viability through gelatine and calcium ions release. Journal of Biomedical Materials Research - Part B Applied Biomaterials. 2023;111:314-30. DOI: 10.1002/jbm.b.35152.

[409] Zhuang J, Gao P, Chen H, *et al.* Extracellular vesicles from human urine-derived stem cells merged in hyaluronic acid ameliorate erectile dysfunction in type 2 diabetic rats by glans administration. Andrology. 2022;10:1673-86. DOI: 10.1111/andr.13293.

[410] Zuo L, Zhu S, Gu S, *et al.* Anti-scarring effects of conbercept on human Tenon's fibroblasts: comparisons with bevacizumab. BMC Ophthalmology. 2023;23:183. DOI: 10.1186/s12886-023-02914-4.

[411] Karamysheva AF. Mechanisms of angiogenesis. Biochemistry (Moscow). 2008;73(7):751-62. DOI: 10.1134/S0006297908070031.

[412] Kutcher ME, Herman IM. The pericyte: Cellular regulator of microvascular blood flow. Microvascular Research. 2009;77(3):235-46. DOI: 10.1016/j.mvr.2009.01.007.

[413] Fuenteslópez CV, Bahcevanci S, Patrulea V, *et al.* Fibrin scaffolds for angiogenesis in soft tissue models: a systematic review. Bioactive Materials. 2026;56:703-25. DOI: 10.1016/j.bioactmat.2025.10.019.

[414] Kumar A, Sood A, Han SS. Technological and Structural Aspects of Scaffold Manufacturing for Cultured Meat: Recent Advances, Challenges, and Opportunities. Critical Reviews in Food Science and Nutrition. 2023;63:585-612. DOI: 10.1080/10408398.2022.2132206.

[415] Patrulea V, Fuenteslópez CV, Ye H. [P06-050] Biomimetic 3D-Bioprinted Skin Scaffolds for Wound Healing and Regeneration. In: Tissue Engineering and Regenerative Medicine International Society Asia-Pacific Chapter Conference 2022. vol. 28. Tissue Engineering Part A; 2022. p. 561. DOI: 10.1089/ten.tea.2022.29036.abstracts.

[416] Straeten CVD. In: De Smet K, Campbell P, Van Der Straeten C, editors. 24 - The Use of Magnetic Resonance Imaging (MRI) to Evaluate Hip Resurfacing. Woodhead Publishing Series in Biomaterials. Woodhead Publishing; 2013. p. 242-52. DOI: 10.1533/9780857096203.2.242.

[417] Raia NR, McGill M, Marcet T, *et al.* In: Wagner WR, Sakiyama-Elbert SE, Zhang G, *et al.*, editors. 2.6.8 - Soft Tissue Engineering. fourth edition ed. Academic Press; 2020. p. 1399-414. DOI: 10.1016/B978-0-12-816137-1.00087-8.

[418] Klimek K, Ginalska G. Proteins and Peptides as Important Modifiers of the Polymer Scaffolds for Tissue Engineering Applications—A Review. Polymers. 2020;12. DOI: 10.3390/polym12040844.

[419] Davari N, Bakhtiary N, Khajehmohammadi M, *et al.* Protein-Based Hydrogels: Promising Materials for Tissue Engineering. Polymers (Basel). 2022. DOI: 10.3390/polym14050986.

[420] Agocsova SV, Culenova M, Birova I, *et al.* Resorbable Biomaterials Used for 3D Scaffolds in Tissue Engineering: A Review. Materials. 2023;16. DOI: 10.3390/ma16124267.

[421] Abdollahiyan P, Oroojalian F, Mokhtarzadeh A, *et al.* Hydrogel-Based 3D Bioprinting for Bone and Cartilage Tissue Engineering. Biotechnology Journal. 2020;15. DOI: 10.1002/biot.202000095.

[422] Nulty J, Freeman FE, Browe DC, *et al.* 3D Bioprinting of Prevascularised Implants for the Repair of Critically-sized Bone Defects. Acta Biomaterialia. 2021;126:154-69. DOI: 10.1016/j.actbio.2021.03.003.

[423] Han X, Saiding Q, Cai X, *et al.* Intelligent Vascularized 3D/4D/5D/6D-Printed Tissue Scaffolds. Nano-Micro Letters. 2023;15. DOI: 10.1007/s40820-023-01187-2.

[424] Kant RJ, Coulombe KLK. Integrated Approaches to Spatiotemporally Directing Angiogenesis in Host and Engineered Tissues. Acta Biomaterialia. 2018;69:42-62. DOI: 10.1016/j.actbio.2018.01.017.

[425] Shafiee A, Atala A. Tissue Engineering: Toward a New Era of Medicine. Annual Review of Medicine. 2017;68:29-40. DOI: 10.1146/annurev-med-102715-092331.

[426] Masson-Meyers DS, Tayebi L. Vascularization Strategies in Tissue Engineering Approaches for Soft Tissue Repair. Journal of Tissue Engineering and Regenerative Medicine. 2021;15:747-62. DOI: 10.1002/term.3225.

[427] Larsen JB, Hvas AM. Thrombin: A Pivotal Player in Hemostasis and Beyond. Seminars in Thrombosis and Hemostasis. 2021;47:759-74. DOI: 10.1055/s-0041-1727116.

[428] Fernandez PM, Patierno SR, Rickles FR. Tissue Factor and Fibrin in Tumor Angiogenesis. Seminars in Thrombosis and Hemostasis. 2004;30:31-44. DOI: 10.1055/s-2004-822969.

[429] Zhang Y, Heher P, Hilborn J, *et al.* Hyaluronic Acid-Fibrin Interpenetrating Double Network Hydrogel Prepared *In Situ* by Orthogonal Disulfide Cross-linking Reaction for Biomedical Applications. Acta Biomaterialia. 2016;38:23-32. DOI: 10.1016/j.actbio.2016.04.041.

[430] Zhou G, Zhu J, Inverarity C, *et al.* Fabrication of Fibrin/Polyvinyl Alcohol Scaffolds for Skin Tissue Engineering *via* Emulsion Templating. Polymers. 2023;15:1151. DOI: 10.3390/polym15051151.

[431] de Melo BAG, França CG, Dávila JL, *et al.* Hyaluronic Acid and Fibrin from L-PRP Form Semi-IPNs with Tunable Properties Suitable for Use in Regenerative Medicine. Materials Science and Engineering C. 2020;109. DOI: 10.1016/j.msec.2019.110547.

[432] Man W, Yang S, Cao Z, *et al.* A Multi-Modal Delivery Strategy for Spinal Cord Regeneration Using a Composite Hydrogel Presenting Biophysical and Biochemical Cues Synergistically. Biomaterials. 2021;276. DOI: 10.1016/j.biomaterials.2021.120971.

[433] Kohli N, Sharma V, Orera A, *et al.* Pro-angiogenic and osteogenic composite scaffolds of fibrin, alginate and calcium phosphate for bone tissue engineering. Journal of Tissue Engineering. 2021;12. DOI: 10.1177/20417314211005610.

[434] Chung E, Rytlewski JA, Merchant AG, *et al.* Fibrin-based 3D Matrices Induce Angiogenic Behavior of Adipose-derived Stem Cells. Acta Biomaterialia. 2015;17:78-88. DOI: 10.1016/j.actbio.2015.01.012.

[435] Feng X, Tonnesen MG, Mousa SA, *et al.* Fibrin and Collagen Differentially but Synergistically Regulate Sprout Angiogenesis of Human Dermal Microvascular Endothelial Cells in 3-Dimensional Matrix. International Journal of Cell Biology. 2013;2013:231279. DOI: 10.1155/2013/231279.

[436] Lukin I, Erezuma I, Maeso L, *et al.* Progress in Gelatin as Biomaterial for Tissue Engineering. Pharmaceutics 2022, Vol 14, Page 1177. 2022;14:1177. DOI: 10.3390/PHARMACEUTICS14061177.

[437] Shpichka A, Osipova D, Efremov Y, *et al.* Fibrin-based Bioinks: New Tricks from an Old Dog. International Journal of Bioprinting. 2020;6:1-14. DOI: 10.18063/ijb.v6i3.269.

[438] Tomasch J, Maleiner B, Heher P, *et al.* Changes in Elastic Moduli of Fibrin Hydrogels Within the Myogenic Range Alter Behavior of Murine C2C12 and Human C25 Myoblasts Differently. Frontiers in Bioengineering and Biotechnology. 2022 5;10:836520. Available from: https://pmc.ncbi.nlm.nih.gov/articles/PMC9164127/. DOI: 10.3389/FBIOE.2022.836520/FULL.

[439] Feller T, McPherson HR, Connell SD, *et al.* Fibrinogen αC-region acts as a functional safety latch: Implications for a fibrin biomechanical behaviour model. Acta Biomaterialia. 2024;189:179-91. DOI: 10.1016/J.ACTBIO.2024.10.005.

[440] Liu W, Jawerth LM, Sparks EA, *et al.* Fibrin Fibers Have Extraordinary Extensibility and Elasticity. Science (New York, NY). 2006;313:634. DOI: 10.1126/SCIENCE.1127317.

[441] Glaser DE, Curtis MB, Sariano PA, *et al.* Organ-on-a-chip model of vascularized human bone marrow niches. Biomaterials. 2022;280:121245. DOI: 10.1016/J.BIOMATERIALS.2021.121245.

[442] Spotnitz WD, Bianchi CF, Foster KN, *et al.* Fibrin Sealant: The Only Approved Hemostat, Sealant, and Adhesive—a Laboratory and Clinical Perspective. ISRN Surgery. 2014. DOI: 10.1155/2014/203943.

[443] Sanz-Horta R, Matesanz A, Gallardo A, *et al.* Technological Advances in Fibrin for Tissue Engineering. Journal of Tissue Engineering. 2023;14. DOI: 10.1177/20417314231190288.

[444] Li S, Dan X, Chen H, *et al.* Developing Fibrin-based Biomaterials/Scaffolds in Tissue Engineering. Bioactive Materials. 2024;40:597-623. DOI: 10.1016/j.bioactmat.2024.08.006.

[445] Liu H, Chen H, Han Q, *et al.* Recent Advancement in Vascularized Tissue-Engineered Bone Based on Materials Design and Modification. Materials Today Bio. 2023;23:100858. DOI: 10.1016/j.mtbio.2023.100858.

[446] DeMars MM, Perruso C. MeSH and Text-Word Search Strategies: Precision, Recall, and Their Implications for Library Instruction. Journal of the Medical Library Association. 2022;110:23-3323–33. DOI: 10.5195/jmla.2022.1283.

[447] Hooijmans CR, Rovers MM, Vries RBMD, *et al.* SYRCLE's Risk of Bias Tool for Animal Studies. BMC Medical Research Methodology. 2014;14. DOI: 10.1186/1471-2288-14-43.

[448] Norecopa. Systematic Review Centre for Laboratory Animal Experimentation (SYRCLE); 2024.

[449] Latitudes Network. SYRCLE RoB Tool; 2025.

[450] Ahmadzadeh K, Dizaji SR, Yousefifard M. Lack of Concordance Between Reporting Guidelines and Risk of Bias Assessments of Preclinical Studies: A Call for Integrated Recommendations. International Journal of Surgery. 2023;109:2557. DOI: 10.1097/JS9.0000000000000475.

[451] QUEST-BIH Charité. Preclinical Systematic Reviews & Meta-Analysis, CAMARADES Berlin; 2025.

[452] Romantsik O, Bank M, Menon JML, *et al.* Value of Preclinical Systematic Reviews and Meta-Analyses in Pediatric Research. Pediatric Research. 2024;96:643. DOI: 10.1038/s41390-024-03197-1.

[453] Li ZX, Li Y, Yang WT, *et al.* The Reporting Quality of Acupuncture for Neurogenesis in Experimental Ischemic Stroke Study. Annals of Translational Medicine. 2019;7:123-3. DOI: 10.21037/atm.2019.02.16.

[454] Horn J, Haan RJD, Vermeulen M, *et al.* Nimodipine in Animal Model Experiments of Focal Cerebral Ischemia: A Systematic Review. Stroke. 2001;32:2433-8. DOI: 10.1161/hs1001.096009.

[455] Ouzzani M, Hammady H, Fedorowicz Z, *et al.* Rayyan — A Web and Mobile App for Systematic Reviews. Systematic Reviews. 2016;5:1-10. DOI: 10.1186/s13643-016-0384-4.

[456] Mauri M, Elli T, Caviglia G, *et al.* RAWGraphs: A Visualisation Platform to Create Open Outputs. In: Proceedings of the 12th Biannual Conference on Italian SIGCHI Chapter. Association for Computing Machinery; 2017. p. 1-5. DOI: 10.1145/3125571.3125585.

[457] Yang P, Xie F, Zhu L, *et al.* Fabrication of Chitin-Fibrin Hydrogels to Construct the 3D Artificial Extracellular Matrix Scaffold for Vascular Regeneration and Cardiac Tissue Engineering. Journal of Biomedical Materials Research Part A. 2024;112:2257-72. DOI: 10.1002/jbm.a.37774.

[458] Vanderslice EJ, Golding SGH, Jacot JG. Vascularization of PEGylated Fibrin Hydrogels Increases the Proliferation of Human iPSC-Cardiomyocytes. Journal of Biomedical Materials Research - Part A. 2024;112:625-34. DOI: 10.1002/jbm.a.37662.

[459] Yang CY, Meng Z, Yang K, *et al.* External Magnetic Field Non-invasively Stimulates Spinal Cord Regeneration in Rat *via* a Magnetic-responsive Aligned Fibrin Hydrogel. Biofabrication. 2023;15:035022. DOI: 10.1088/1758-5090/acdbec.

[460] Dasgupta S, Gope A, Mukhopadhyay A, *et al.* Chitosan-Collagen-Fibrinogen Uncrosslinked Scaffolds Possessing Skin Regeneration and Vascularization Potential. Journal of Biomedical Materials Research Part A. 2023;111:725-39. DOI: 10.1002/jbm.a.37488.

[461] Chang T, Liu C, Yang H, *et al.* Fibrin-based Cardiac Patch Containing Neuregulin-1 for Heart Repair After Myocardial Infarction. Colloids and Surfaces B: Biointerfaces. 2022;220. DOI: 10.1016/j.colsurfb.2022.112936.

[462] Helms F, Zippusch S, Theilen J, *et al.* An Encapsulated Fibrin-based Bioartificial Tissue Construct with Integrated Macrovessels, Microchannels, and Capillary Tubes. Biotechnology and Bioengineering. 2022;119:2239-49. DOI: 10.1002/bit.28111.

[463] Sezgin B, Tatar S, Karahuseyinoglu S, *et al.* The Effects of Oral Mucosa-derived Heterotopic Fibroblasts on Cutaneous Wound Healing. Journal of Plastic, Reconstructive & Aesthetic Surgery. 2021;74:2751-8. DOI: 10.1016/j.bjps.2021.02.011.

[464] Heene S, Thoms S, Kalies S, *et al.* Vascular Network Formation on Macroporous Polydioxanone Scaffolds. Tissue Engineering Part A. 2021;27:1239-49. DOI: 10.1089/ten.tea.2020.0232.

[465] Melly L, Grosso A, Pop CS, *et al.* Fibrin Hydrogels Promote Scar Formation and Prevent Therapeutic Angiogenesis in the Heart. Journal of Tissue Engineering and Regenerative Medicine. 2020;14:1513-23. DOI: 10.1002/term.3118.

[466] Nilforoushzadeh MA, Sisakht MM, Amirkhani MA, *et al.* Engineered Skin Graft with Stromal Vascular Fraction Cells Encapsulated in Fibrin–Collagen Hydrogel: A Clinical Study for Diabetic Wound Healing. Journal of Tissue Engineering and Regenerative Medicine. 2020;14:424-40. DOI: 10.1002/term.3003.

[467] Elliott MB, Ginn B, Fukunishi T, *et al.* Regenerative and Durable Small-diameter Graft as an Arterial Conduit. Proceedings of the National Academy of Sciences of the United States of America. 2019;116:12710-9. DOI: 10.1073/pnas.1905966116.

[468] Koo MA, Hong SH, Lee MH, *et al.* Effective Stacking and Transplantation of Stem Cell Sheets Using Exogenous ROS-Producing Film for Accelerated Wound Healing. Acta Biomaterialia. 2019;95:418-26. DOI: 10.1016/j.actbio.2019.01.019.

[469] Mirzaei-Parsa MJ, Ghanbari H, Alipoor B, *et al.* Nanofiber-Acellular Dermal Matrix as a Bilayer Scaffold Containing Mesenchymal Stem Cell for Healing of Full-Thickness Skin Wounds. Cell and Tissue Research. 2019;375:709-21. DOI: 10.1007/s00441-018-2927-6.

[470] Yao S, Yu S, Cao Z, *et al.* Hierarchically Aligned Fibrin Nanofiber Hydrogel Accelerated Axonal Regrowth and Locomotor Function Recovery in Rat Spinal Cord Injury. International Journal of Nanomedicine. 2018;13:2883. DOI: 10.2147/ijn.s159356.

[471] Gorkun AA, Shpichka AI, Zurina IM, *et al.* Angiogenic Potential of Spheroids from Umbilical Cord and Adipose-derived Multipotent Mesenchymal Stromal Cells within Fibrin Gel. Biomedical Materials. 2018;13. DOI: 10.1088/1748-605X/aac22d.

[472] Burmeister DM, Stone R, Wrice N, *et al.* Delivery of Allogeneic Adipose Stem Cells in Polyethylene Glycol-Fibrin Hydrogels as an Adjunct to Meshed Autografts After Sharp Debridement of Deep Partial Thickness Burns. Stem Cells Translational Medicine. 2018;7:360-72. DOI: 10.1002/sctm.17-0160.

[473] Manavella DD, Cacciottola L, Desmet CM, *et al.* Adipose Tissue-derived Stem Cells in a Fibrin Implant Enhance Neovascularization in a Peritoneal Grafting Site: A Potential Way to Improve Ovarian Tissue Transplantation. Human Reproduction. 2018;33:270-9. DOI: 10.1093/humrep/dex374.

[474] Ja KPMM, Lim KP, Chen A, *et al.* Construction of a Vascularized Hydrogel for Cardiac Tissue Formation in a Porcine Model. Journal of Tissue Engineering and Regenerative Medicine. 2018;12:e2029-38. DOI: 10.1002/term.2634.

[475] Solovieva EV, Fedotov AY, Mamonov VE, *et al.* Fibrinogen-modified Sodium Alginate as a Scaffold Material for Skin Tissue Engineering. Biomedical Materials. 2018;13. DOI: 10.1088/1748-605X/aa9089.

[476] Zeng RX, He JY, Zhang YL, *et al.* Experimental Study on Repairing Skin Defect by Tissue-Engineered Skin Substitute Compositely Constructed by Adipose-derived Stem Cells and Fibrin Gel. European Review for Medical and Pharmacological Sciences. 2017:1.

[477] Grasman JM, Do DM, Page RL, *et al.* Rapid Release of Growth Factors Regenerates Force Output in Volumetric Muscle Loss Injuries. Biomaterials. 2015;72:49. DOI: 10.1016/j.biomaterials.2015.08.047.

[478] Barreto-Ortiz SF, Fradkin J, Eoh J, *et al.* Fabrication of 3-dimensional Multicellular Microvascular Structures. The FASEB Journal. 2015;29:3302-14. DOI: 10.1096/fj.14-263343.

[479] Awada HK, Johnson NR, Wang Y. Sequential Delivery of Angiogenic Growth Factors Improves Revascularization and Heart Function After Myocardial Infarction. Journal of Controlled Release. 2015;207:7-17. DOI: 10.1016/j.jconrel.2015.03.034.

[480] Bellamy V, Vanneaux V, Bel A, *et al.* Long-term Functional Benefits of Human Embryonic Stem Cell-derived Cardiac Progenitors Embedded into a Fibrin Scaffold. The Journal of Heart and Lung Transplantation. 2015;34:1198-207. DOI: 10.1016/j.healun.2014.10.008.

[481] Mendez JJ, Ghaedi M, Sivarapatna A, *et al.* Mesenchymal Stromal Cells Form Vascular Tubes when Placed in Fibrin Sealant and Accelerate Wound Healing *In Vivo*. Biomaterials. 2015;40:61-71. DOI: 10.1016/j.biomaterials.2014.11.011.

[482] La WG, Yang HS. Heparin-Conjugated Poly(Lactic-Co-Glycolic Acid) Nanospheres Enhance Large-Wound Healing by Delivering Growth Factors in Platelet-Rich Plasma. Artificial Organs. 2015;39:388-94. DOI: 10.1111/aor.12389.

[483] Atluri P, Miller JS, Emery RJ, *et al.* Tissue-engineered, Hydrogel-based Endothelial Progenitor Cell Therapy Robustly Revascularizes Ischemic Myocardium and Preserves Ventricular Function. The Journal of Thoracic and Cardiovascular Surgery. 2014;148:1090-8. DOI: 10.1016/j.jtcvs.2014.06.038.

[484] Rohringer S, Hofbauer P, Schneider KH, *et al.* Mechanisms of Vasculogenesis in 3D Fibrin Matrices Mediated by the Interaction of Adipose-derived Stem Cells and Endothelial Cells. Angiogenesis. 2014;17:921-33. DOI: 10.1007/s10456-014-9439-0.

[485] Cheung EYL, Weijers EM, Tuk B, *et al.* Specific Effects of Fibrinogen and the γA and γ'-Chain Fibrinogen Variants on Angiogenesis and Wound Healing. Tissue Engineering Part A. 2015;21:106-14. DOI: 10.1089/ten.tea.2014.0020.

[486] Sacchi V, Mittermayr R, Hartinger J, *et al.* Long-lasting Fibrin Matrices Ensure Stable and Functional Angiogenesis by Highly Tunable, Sustained Delivery of Recombinant $VEGF_{164}$. Proceedings of the National Academy of Sciences of the United States of America. 2014;111:6952-7. DOI: 10.1073/pnas.1404605111.

[487] Bearzi C, Gargioli C, Baci D, *et al.* PlGF–MMP9-Engineered iPS Cells Supported on a PEG–fibrinogen Hydrogel Scaffold Possess an Enhanced Capacity to Repair Damaged Myocardium. Cell Death & Disease. 2014;5:e1053. DOI: 10.1038/cddis.2014.12.

[488] Marino D, Luginbühl J, Scola S, *et al.* Bioengineering Dermo-Epidermal Skin Grafts with Blood and Lymphatic Capillaries. Science Translational Medicine. 2014;6. DOI: 10.1126/scitranslmed.3006894.

[489] Ruangsawasdi N, Zehnder M, Weber FE. Fibrin Gel Improves Tissue Ingrowth and Cell Differentiation in Human Immature Premolars Implanted in Rats. Journal of Endodontics. 2014;40:246-50. DOI: 10.1016/j.joen.2013.09.022.

[490] Zhao X, Liu L, Wang J, *et al.* *In Vitro* Vascularization of a Combined System Based on a 3D Printing Technique. Journal of Tissue Engineering and Regenerative Medicine. 2016;10:833-42. DOI: 10.1002/term.1863.

[491] Barreto-Ortiz SF, Zhang S, Davenport M, *et al.* A Novel *In Vitro* Model for Microvasculature Reveals Regulation of Circumferential ECM Organization by Curvature. PLoS One. 2013;8. DOI: 10.1371/journal.pone.0081061.

[492] Ucuzian AA, Bufalino DV, Pang Y, *et al.* Angiogenic Endothelial Cell Invasion into Fibrin is Stimulated by Proliferating Smooth Muscle Cells. Microvascular Research. 2013;90:40-7. DOI: 10.1016/j.mvr.2013.06.012.

[493] Bhang SH, Jung MJ, Shin JY, *et al.* Mutual Effect of Subcutaneously Transplanted Human Adipose-derived Stem Cells and Pancreatic Islets Within Fibrin Gel. Biomaterials. 2013;34:7247-56. DOI: 10.1016/j.biomaterials.2013.06.018.

[494] Zamora DO, Natesan S, Becerra S, *et al.* Enhanced Wound Vascularization Using a dsASCs Seeded FPEG Scaffold. Angiogenesis. 2013;16:745-57. DOI: 10.1007/s10456-013-9352-y.

[495] Centola M, Abbruzzese F, Scotti C, *et al.* Scaffold-Based Delivery of a Clinically Relevant Anti-Angiogenic Drug Promotes the Formation of *In Vivo* Stable Cartilage. Tissue Engineering Part A. 2013;19:1960-71. DOI: 10.1089/ten.tea.2012.0455.

[496] Horimizu M, Kawase T, Nakajima Y, *et al.* An Improved Freeze-Dried PRP-Coated Biodegradable Material Suitable for Connective Tissue Regenerative Therapy. Cryobiology. 2013;66:223-32. DOI: 10.1016/j.cryobiol.2013.01.006.

[497] Skardal A, Mack D, Kapetanovic E, *et al.* Bioprinted Amniotic Fluid-derived Stem Cells Accelerate Healing of Large Skin Wounds. Stem Cells Translational Medicine. 2012;1:792-802. DOI: 10.5966/sctm.2012-0088.

[498] Holnthoner W, Hohenegger K, Husa AM, *et al.* Adipose-derived Stem Cells Induce Vascular Tube Formation of Outgrowth Endothelial Cells in a Fibrin Matrix. Journal of Tissue Engineering and Regenerative Medicine. 2015;9:127-36. DOI: 10.1002/term.1620.

[499] Verseijden F, van Sluijs SJP, van Neck JW, *et al.* Comparing Scaffold-free and Fibrin-based Adipose-derived Stromal Cell Constructs for Adipose Tissue Engineering: An *In Vitro* and *In Vivo* Study. Cell Transplantation. 2012;21:2283-97. DOI: 10.3727/096368912x653129.

[500] Xiong Q, Ye L, Zhang P, *et al.* Bioenergetic and Functional Consequences of Cellular Therapy: Activation of Endogenous Cardiovascular Progenitor Cells. Circulation Research. 2012;111:455-68. DOI: 10.1161/circresaha.112.269894.

[501] Lisi A, Briganti E, Ledda M, *et al.* A Combined Synthetic-Fibrin Scaffold Supports Growth and Cardiomyogenic Commitment of Human Placental Derived Stem Cells. PLoS One. 2012;7. DOI: 10.1371/journal.pone.0034284.

[502] Reichenberger MA, Mueller W, Schäfer A, *et al.* Fibrin-Embedded Adipose Derived Stem Cells Enhance Skin Flap Survival. Stem Cell Reviews and Reports. 2012;8:844-53. DOI: 10.1007/s12015-011-9341-8.

[503] Verseijden F, van Sluijs SJP, van Neck JW, *et al.* Vascularization of Prevascularized and Non-Prevascularized Fibrin-based Human Adipose Tissue Constructs After Implantation in Nude Mice. Journal of Tissue Engineering and Regenerative Medicine. 2012;6:169-78. DOI: 10.1002/term.410.

[504] Anilkumar TV, Muhamed J, Jose A, *et al.* Advantages of Hyaluronic Acid as a Component of Fibrin Sheet for Care of Acute Wound. Biologicals. 2011;39:81-8. DOI: 10.1016/j.biologicals.2011.01.003.

[505] Bleiziffer O, Hammon M, Naschberger E, *et al.* Endothelial Progenitor Cells are Integrated in Newly Formed Capillaries and Alter Adjacent Fibrovascular Tissue After Subcutaneous Implantation in a Fibrin Matrix. Journal of Cellular and Molecular Medicine. 2011;15:2452-61. DOI: 10.1111/j.1582-4934.2010.01247.x.

[506] Barsotti MC, Magera A, Armani C, *et al.* Fibrin Acts as Biomimetic Niche Inducing Both Differentiation and Stem Cell Marker Expression of Early Human Endothelial Progenitor Cells. Cell Proliferation. 2011;44:33-48. DOI: 10.1111/j.1365-2184.2010.00715.x.

[507] Lugo LM, Lei P, Andreadis ST. Vascularization of the Dermal Support Enhances Wound Re-

Epithelialization by *In Situ* Delivery of Epidermal Keratinocytes. Tissue Engineering Part A. 2011;17:665-75. DOI: 10.1089/ten.tea.2010.0125.

[508] Shen X, Tanaka K, Takamori A. Coronary Arteries Angiogenesis in Ischemic Myocardium: Biocompatibility and Biodegradability of Various Hydrogels. Artificial Organs. 2009;33:781-7. DOI: 10.1111/J.1525-1594.2009.00815.x.

[509] Verseijden F, Sluijs SJPV, Pavljasevic P, *et al.* Adult Human Bone Marrow- and Adipose Tissue-derived Stromal Cells Support the Formation of Prevascular-like Structures from Endothelial Cells *In Vitro*. Tissue Engineering Part A. 2010;16:101-14. DOI: 10.1089/ten.tea.2009.0106.

[510] Inoue S, Kijima H, Kidokoro M, *et al.* The Effectiveness of Basic Fibroblast Growth Factor in Fibrin-based Cultured Skin Substitute *In Vivo*. Journal of Burn Care & Research. 2009;30:514-9. DOI: 10.1097/BCR.0b013e3181a28e4b.

[511] Cho SW, Song KW, Rhie JW, *et al.* Engineered Adipose Tissue Formation Enhanced by Basic Fibroblast Growth Factor and a Mechanically Stable Environment. Cell Transplantation. 2007;16:421-34. DOI: 10.3727/000000007783464795.

[512] Torio-Padron N, Borges J, Momeni A, *et al.* Implantation of VEGF Transfected Preadipocytes Improves Vascularization of Fibrin Implants on the Cylinder Chorioallantoic Membrane (CAM) Model. Minimally Invasive Therapy & Allied Technologies. 2007;16:155-62. DOI: 10.1080/13645700701384116.

[513] Borges J, Müller MC, Momeni A, *et al.* *In Vitro* Analysis of the Interactions Between Preadipocytes and Endothelial Cells in a 3D Fibrin Matrix. Minimally Invasive Therapy & Allied Technologies. 2007;16:141-8. DOI: 10.1080/13645700600935398.

[514] Alsberg E, Feinstein E, Joy MP, *et al.* Magnetically-guided Self-assembly of Fibrin Matrices with Ordered Nano-scale Structure for Tissue Engineering. Tissue Engineering. 2006;12:3247-56. DOI: 10.1089/ten.2006.12.3247.

[515] Wilcke I, Lohmeyer JA, Liu S, *et al.* $VEGF^{165}$ and bFGF Protein-based Therapy in a Slow Release System to Improve Angiogenesis in a Bioartificial Dermal Substitute *In Vitro* and *In Vivo*. Langenbeck's Archives of Surgery. 2007;392:305-14. DOI: 10.1007/s00423-007-0194-1.

[516] Kellouche S, Mourah S, Bonnefoy A, *et al.* Platelets, Thrombospondin-1 and Human Dermal Fibroblasts Cooperate for Stimulation of Endothelial Cell Tubulogenesis through VEGF and PAI-1 Regulation. Experimental Cell Research. 2007;313:486-99. DOI: 10.1016/j.yexcr.2006.10.023.

[517] Borges J, Torío-Padrón N, Momeni A, *et al.* Adipose Precursor Cells (Preadipocytes) Induce Formation of New Vessels in Fibrin Glue on the Newly Developed Cylinder Chorioallantoic Membrane Model (CAM). Minimally Invasive Therapy & Allied Technologies. 2006;15:246-52. DOI: 10.1080/14017450600761620.

[518] Trentin D, Hall H, Wechsler S, *et al.* Peptide-Matrix-mediated Gene Transfer of an Oxygen-insensitive Hypoxia-inducible Factor-1α Variant for Local Induction of Angiogenesis. Proceedings of the National Academy of Sciences of the United States of America. 2006;103:2506-11. DOI: 10.1073/pnas.0505964102.

[519] Jeon O, Soo HR, Ji HC, *et al.* Control of Basic Fibroblast Growth Factor Release from Fibrin Gel with Heparin and Concentrations of Fibrinogen and Thrombin. Journal of Controlled Release. 2005;105:249-59. DOI: 10.1016/j.jconrel.2005.03.023.

[520] Griffith CK, Miller C, Sainson RCA, *et al.* Diffusion Limits of an *In Vitro* Thick Prevascularized Tissue. Tissue Engineering. 2005;11:257-66. DOI: 10.1089/ten.2005.11.257.

[521] Liu J, Hu Q, Wang Z, *et al.* Autologous Stem Cell Transplantation for Myocardial Repair. American Journal of Physiology - Heart and Circulatory Physiology. 2004;287:501-11. DOI: 10.1152/ajpheart.00019.2004.

[522] Haroon ZA, Amin K, Jiang X, *et al.* A Novel Role for Erythropoietin During Fibrin-Induced Wound-Healing Response . The American Journal of Pathology. 2003;163:993-1000. DOI: 10.1016/S0002-9440(10)63459-1.

[523] Nakatsu MN, Sainson RCA, Aoto JN, *et al.* Angiogenic Sprouting and Capillary Lumen Formation Modeled by Human Umbilical Vein Endothelial Cells (HUVEC) in Fibrin Gels: The Role of Fibroblasts and Angiopoietin-1. Microvascular Research. 2003;66:102-12. DOI: 10.1016/s0026-2862(03)00045-1.

[524] Chekanov V, Akhtar M, Tchekanov G, *et al.* Transplantation of Autologous Endothelial Cells Induces Angiogenesis. Pacing and Clinical Electrophysiology. 2003;26:496-9. DOI: 10.1046/j.1460-9592.2003.00080.x.

[525] Jozkowicz A, Fügl A, Nanobashvili J, *et al.* Delivery of High Dose VEGF Plasmid Using Fibrin Carrier does not Influence its Angiogenic Potency. International Journal of Artificial Organs. 2003;26:161-9. DOI: 10.1177/039139880302600211.

[526] Brey EM, King TW, Johnston C, *et al.* A Technique for Quantitative Three-dimensional Analysis of Microvascular Structure. Microvascular Research. 2002;63:279-94. DOI: 10.1006/mvre.2002.2395.

[527] Dallabrida SM, Sousa MAD, Farrell DH. Expression of Antisense to Integrin Subunit β_3 Inhibits Microvascular Endothelial Cell Capillary Tube Formation in Fibrin. Journal of Biological Chemistry. 2000;275:32281-8. DOI: 10.1074/jbc.M001446200.

[528] Feng X, Clark RAF, Galanakis D, *et al.* Fibrin and Collagen Differentially Regulate Human Dermal Microvascular Endothelial Cell Integrins: Stabilization of αv/β3 mRNA by Fibrin. Journal of Investigative Dermatology. 1999;113:913-9. DOI: 10.1046/j.1523-1747.1999.00786.x.

[529] Nehls V, Herrmann R, Hühnken M, *et al.* Contact-dependent Inhibition of Angiogenesis by Cardiac Fibroblasts in Three-dimensional Fibrin Gels *In Vitro*: Implications for Microvascular Network Remodeling and Coronary Collateral Formation. Cell and Tissue Research. 1998;293:479-88. DOI: 10.1007/s004410051140.

[530] Fournier N, Doillon CJ. Biological Molecule-impregnated Polyester: An *In Vivo* Angiogenesis Study. Biomaterials. 1996;17:1659-65. DOI: 10.1016/0142-9612(96)87645-9.

[531] Nehls V, Drenckhahn D. A Microcarrier-based Cocultivation System for the Investigation of Factors and Cells Involved in Angiogenesis in Three-dimensional Fibrin Matrices *In Vitro*. Histochemistry and Cell Biology. 1995;104:459-66. DOI: 10.1007/BF01464336.

[532] Nehls V, Schuchardt E, Drenckhahn D. The Effect of Fibroblasts, Vascular Smooth Muscle Cells, and Pericytes on Sprout Formation of Endothelial Cells in a Fibrin Gel Angiogenesis System. Microvascular Research. 1994;48:349-63. DOI: 10.1006/mvre.1994.1061.

[533] Dvorak HF, Dvorak AM, EJ M, *et al.* Fibrin Gel Investment Associated with Line 1 And Line 10 Solid Tumor Growth, Angiogenesis, and Fibroplasia in Guinea Pigs. Role Of Cellular Immunity, Myofibroblasts, Microvascular Damage, and Infarction in Line 1 Tumor Regression. Journal of the National Cancer Institute. 1979;62:1459-72.

[534] Du Y, Xu XX, Yu SX, *et al.* Dynamics of endothelial cells migration in nature-mimicking blood vessels. Talanta. 2024;277:126415. DOI: 10.1016/J.TALANTA.2024.126415.

[535] Michaelis UR. Mechanisms of endothelial cell migration. Cellular and Molecular Life Sciences: CMLS. 2014;71:4131. DOI: 10.1007/S00018-014-1678-0.

[536] Álvaro Sierra-Sánchez, de la Torre RS, Ubago-Rodríguez A, *et al.* Blood Plasma, Fibrinogen or Fibrin Biomaterial for the Manufacturing of Skin Tissue-Engineered Products and Other Dermatological Treatments: A Systematic Review. Journal of Functional Biomaterials. 2025;16:79. DOI: 10.3390/JFB16030079/S1.

[537] Li Y, Hirayasu K, Hasegawa G, *et al.* Fibrinogen induces inflammatory responses via the immune activating receptor LILRA2. Frontiers in Immunology. 2024;15:1435236. DOI: 10.3389/FIMMU.2024.1435236/FULL.

[538] Boucard E, Vidal L, Coulon F, *et al.* The degradation of gelatin/alginate/fibrin hydrogels is cell type dependent and can be modulated by targeting fibrinolysis. Frontiers in Bioengineering and Biotechnology. 2022;10:920929. DOI: 10.3389/FBIOE.2022.920929/BIBTEX.

[539] Shokrani H, Shokrani A, Sajadi SM, *et al.* Cell-Seeded Biomaterial Scaffolds: The Urgent Need for Unanswered Accelerated Angiogenesis. International Journal of Nanomedicine. 2022;17:1035. DOI: 10.2147/IJN.S353062.

[540] Domingues MM, Macrae FL, Duval C, *et al.* Thrombin and Fibrinogen γ' Impact Clot Structure by Marked Effects on Intrafibrillar Structure and Protofibril Packing. Blood. 2016;127:487-95. DOI: 10.1182/blood-2015-06-652214.

[541] Lee HW, Shin JH, Simons M. Flow Goes Forward and Cells Step Backward: Endothelial Migration. Experimental and Molecular Medicine. 2022;54:711-9. DOI: 10.1038/s12276-022-00785-1.

[542] Libby JR, Royce H, Walker SR, *et al.* The Role of Extracellular Matrix in Angiogenesis: Beyond Adhesion and Structure. Biomaterials and Biosystems. 2024;15. DOI: 10.1016/j.bbiosy.2024.100097.

[543] Guvendiren M, Molde J, Soares RMD, *et al.* Designing Biomaterials for 3D Printing. ACS Biomaterials Science & Engineering. 2016;2:1679-93. DOI: 10.1021/acsbiomaterials.6b00121.

[544] Fuenteslópez CV, Papapavlou M, Thompson MS, *et al.* Engineering a Long-lasting Microvasculature *In Vitro* Model for Traumatic Injury Research. Biomaterials Advances. 2025;174:214310. DOI: 10.1016/j.bioadv.2025.214310.

[545] Sahni A, Sahni SK, Francis CW. Endothelial Cell Activation by IL-1β in the Presence of Fibrinogen Requires $\alpha_v\beta_3$. Arteriosclerosis, Thrombosis, and Vascular Biology. 2005;25:2222-7. DOI: 10.1161/01.atv.0000183605.27125.6f.

[546] Risman RA, Paynter B, Percoco V, *et al.* Internal Fibrinolysis of Fibrin Clots is Driven by Pore Expansion. Scientific Reports 2024 14:1. 2024;14:1-16. DOI: 10.1038/s41598-024-52844-4.

[547] Dupuy E, Habib A, Lebret M, *et al.* Thrombin Induces Angiogenesis and Vascular Endothelial Growth Factor Expression in Human Endothelial Cells: Possible Relevance to HIF-1α. Journal of Thrombosis and Haemostasis. 2003;1:1096-102. DOI: 10.1046/j.1538-7836.2003.00208.x.

[548] Dong C, Lv Y. Application of Collagen Scaffold in Tissue Engineering: Recent Advances and New Perspectives. Polymers. 2016;8:42. DOI: 10.3390/polym8020042.

[549] Dadashzadeh A, Moghassemi S, Amorim CA. Evaluation of PEGylated Fibrin as a Three-dimensional Biodegradable Scaffold for Ovarian Tissue Engineering. Materials Today Chemistry. 2021;22:100626. DOI: 10.1016/j.mtchem.2021.100626.

[550] Salehi S, Ghomi H, Hassanzadeh-Tabrizi SA, *et al.* The Effect of Polyethylene Glycol on Printability, Physical and Mechanical Properties and Osteogenic Potential of 3D-Printed Poly (L-Lactic Acid)/Polyethylene Glycol Scaffold for Bone Tissue Engineering. International Journal of Biological Macromolecules. 2022;221:1325-34. DOI: 10.1016/j.ijbiomac.2022.09.027.

[551] Ge Z, Zhang Q, Lin W, *et al.* The Role of Angiogenic Growth Factors in the Immune Microenvironment of Glioma. Frontiers in Oncology. 2023;13:1254694. DOI: 10.3389/fonc.2023.1254694.

[552] Rautiainen S, Laaksonen T, Koivuniemi R. Angiogenic Effects and Crosstalk of Adipose-derived Mesenchymal Stem/Stromal Cells and their Extracellular Vesicles with Endothelial Cells. International Journal of Molecular Sciences. 2021;22. DOI: 10.3390/ijms221910890.

[553] Hove LV, Hoste E. Activation of Fibroblasts in Skin Cancer. Journal of Investigative Dermatology. 2022;142:1026-31. DOI: 10.1016/j.jid.2021.09.010.

[554] Nowak-Sliwinska P, Alitalo K, Allen E, *et al.* Consensus Guidelines for the Use and Interpretation of Angiogenesis Assays. Angiogenesis. 2018;21:425-532. DOI: 10.1007/s10456-018-9613-x.

[555] Stryker ZI, Rajabi M, Davis PJ, *et al.* Evaluation of Angiogenesis Assays. Biomedicines. 2019;7. DOI: 10.3390/biomedicines7020037.

[556] AlMalki W, Shahid I, Mehdi A, *et al.* Assessment Methods for Angiogenesis and Current Approaches for its Quantification. Indian Journal of Pharmacology. 2014;46:251. DOI: 10.4103/0253-7613.132152.

[557] Rapp J, Ness J, Wolf J, *et al.* 2D and 3D *In Vitro* Angiogenesis Assays Highlight Different Aspects of Angiogenesis. Biochimica et Biophysica Acta - Molecular Basis of Disease. 2024;1870. DOI: 10.1016/j.bbadis.2024.167028.

[558] Volpi M, Paradiso A, Costantini M, *et al.* Hydrogel-based Fiber Biofabrication Techniques for Skeletal Muscle Tissue Engineering. ACS Biomaterials Science and Engineering. 2022;8:379-405. DOI: 10.1021/acsbiomaterials.1c01145.

[559] Gholobova D, Terrie L, Gerard M, *et al.* Vascularization of Tissue-Engineered Skeletal Muscle Constructs. Biomaterials. 2020;235. DOI: 10.1016/j.biomaterials.2019.119708.

[560] Fuenteslópez CV, Bahcevanci S, Patrulea V, *et al.*. Fibrin-based Scaffolds for Soft Tissue Microvasculature: A Systematic Review [ID CRD42025612994]; 2024. PROSPERO International Prospective Register of Systematic Reviews.

[561] Fuenteslópez CV, Bahcevanci S, Patrulea V, *et al.*. Fibrin-based Scaffolds for Soft Tissue Microvasculature: A Systematic Review [ID: nvfdj]. OSF; 2024.

[562] Fuenteslópez CV, Bahcevanci S, Patrulea V, *et al.*. Project: "Fibrin-based Scaffolds for Soft Tissue Microvasculature: a Systematic Review". OSF; 2024.

[563] Fuenteslópez CV, Bahcevanci S, Patrulea V, *et al.*. Dataset of "Fibrin Scaffolds for Angiogenesis in Soft Tissue Models: a Systematic Review"; 2025. DOI: 10.5281/ZENODO.16921023.

[564] Fuenteslópez CV. Minimum Information for Fibrin Scaffold Experiments (MIFSE) Checklist; 2025. DOI: 10.5281/ZENODO.16921390.

[565] Schaser KD, Vollmar B, Menger MD, *et al.* In vivo analysis of microcirculation following closed soft-tissue injury. Journal of Orthopaedic Research. 1999;17:678-85. DOI: 10.1002/JOR.1100170509.

[566] Senarathna J, Pathak AP. Visualizing the Microcirculation. Microcirculation. 2022;29:e12785. DOI: 10.1111/MICC.12785.

[567] Roberts KA, Colley L, Agbaedeng TA, *et al.* Vascular Manifestations of COVID-19 - Thromboembolism and Microvascular Dysfunction. Frontiers in cardiovascular medicine. 2020;7. DOI: 10.3389/FCVM.2020.598400.

[568] Hanahan D. Hallmarks of Cancer: New Dimensions. Cancer discovery. 2022;12:31-46. DOI: 10.1158/2159-8290.CD-21-1059.

[569] Xia P, Luo Y. Vascularization in tissue engineering: The architecture cues of pores in scaffolds. Journal of biomedical materials research Part B, Applied biomaterials. 2022;110:1206-14. DOI: 10.1002/JBM.B.34979.

[570] Mazloomnejad R, Babajani A, Kasravi M, *et al.* Angiogenesis and Re-endothelialization in decellularized scaffolds: Recent advances and current challenges in tissue engineering. Frontiers in Bioengineering and Biotechnology. 2023;11. DOI: 10.3389/FBIOE.2023.1103727.

[571] Whisler JA, Chen MB, Kamm RD. Control of Perfusable Microvascular Network Morphology Using a Multiculture Microfluidic System. Tissue Engineering: Part C. 2014;20:543-52. DOI: 10.1089/ten.tec.2013.0370.

[572] Shakeel A, Corridon PR. Mitigating challenges and expanding the future of vascular tissue engineering—are we there yet? Frontiers in Physiology. 2022;13. DOI: 10.3389/FPHYS.2022.1079421.

[573] Calafel MI, Criado-Gonzalez M, Aguirresarobe R, *et al.* From rheological concepts to additive manufacturing assessment of hydrogel-based materials for advanced bioprinting applications. Materials Advances. 2025 7;6(14):4566-97. Available from: https://dx.doi.org/10.1039/d5ma00019j. DOI: 10.1039/D5MA00019J.

[574] Eguchi R, Naitou H, Kunimasa K, *et al.* Proteomic analysis of hypoxia-induced tube breakdown of an in vitro

capillary model composed of HUVECs: Potential role of p38-regulated reduction of HSP27. Proteomics. 2008;8:2897-906. DOI: 10.1002/PMIC.200800055.

[575] Kelley M, Fierstein S, Purkey L, *et al.* Endothelial Cell Tube Formation Assay: An In Vitro Model for Angiogenesis. Methods in Molecular Biology. 2022;2475:187-96. DOI: 10.1007/978-1-0716-2217-9_12/FIGURES/3.

[576] Suarez-Arnedo A, Figueroa FT, Clavijo C, *et al.* An image J plugin for the high throughput image analysis of in vitro scratch wound healing assays. PLoS ONE. 2020;15. DOI: 10.1371/JOURNAL.PONE.0232565.

[577] Carpentier G, Berndt S, Ferratge S, *et al.* Angiogenesis Analyzer for ImageJ — A comparative morphometric analysis of "Endothelial Tube Formation Assay" and "Fibrin Bead Assay". Scientific Reports 2020 10:1. 2020;10:1-13. DOI: 10.1038/s41598-020-67289-8.

[578] Lu M, Zhang ZG, Chopp M. Analysis of cerebral microvascular architecture—application to cortical and subcortical vessels in rat brain. Journal of Neuroscience Methods. 2004;138:81-7. DOI: 10.1016/J.JNEUMETH.2004.03.011.

[579] Konerding M, Fait E, Gaumann A. 3D microvascular architecture of pre-cancerous lesions and invasive carcinomas of the colon. British Journal of Cancer. 2001;84:1354-62. DOI: 10.1054/bjoc.2001.1809.

[580] Yu PK, Balaratnasingam C, Cringle SJ, *et al.* Microstructure and Network Organization of the Microvasculature in the Human Macula. Investigative Ophthalmology & Visual Science. 2010;51:6735-43. DOI: 10.1167/IOVS.10-5415.

[581] Evrard J, Siriez R, Morimont L, *et al.* Optimal wavelength for the clot waveform analysis: Determination of the best resolution with minimal interference of the reagents. International Journal of Laboratory Hematology. 2019;41:316-24. DOI: 10.1111/IJLH.12975.

[582] Sproul E, Nandi S, Brown A. In: Fibrin biomaterials for tissue regeneration and repair. Woodhead Publishing; 2018. p. 151-73. DOI: 10.1016/B978-0-08-100803-4.00006-1.

[583] Allan P. Microrheology of Fibrin Clots. The University of Leeds; 2012.

[584] Montero A, Quílez C, Valencia L, *et al.* Effect of fibrin concentration on the in vitro production of dermo-epidermal equivalents. International Journal of Molecular Sciences. 2021;22:6746. DOI: 10.3390/IJMS22136746/S1.

[585] Mangione PP, Verona G, Corazza A, *et al.* Plasminogen activation triggers transthyretin amyloidogenesis in vitro. The Journal of Biological Chemistry. 2018;293:14192. DOI: 10.1074/JBC.RA118.003990.

[586] Gonçalves S, Santos NC, Martins-Silva J, *et al.* Fluorescence spectroscopy evaluation of fibrinogen–β-estradiol binding. Journal of Photochemistry and Photobiology B: Biology. 2007;86:170-6. DOI: 10.1016/J.JPHOTOBIOL.2006.09.001.

[587] Weigandt KM, White N, Chung D, *et al.* Fibrin clot structure and mechanics associated with specific oxidation of methionine residues in fibrinogen. Biophysical Journal. 2012;103:2399-407. DOI: 10.1016/j.bpj.2012.10.036.

[588] Huang E, Skoufis A, Denning T, *et al.* OpenDrop: Open-source software for pendant drop tensiometry contact angle measurements. Journal of Open Source Software. 2021;6:2604. DOI: 10.21105/JOSS.02604.

[589] Chen T. Quantifying Polymer Crosslinking Density Using Rheology and DMA; 2020.

[590] Tinevez JY. Directionality plugin for Fiji/ImageJ; 2018.

[591] Peng M, Yang M, Ding Y, *et al.* Mechanism of endogenous digitalis-like factor-induced vascular endothelial cell damage in patients with severe preeclampsia. International Journal of Molecular Medicine. 2018;41:985-94. DOI: 10.3892/IJMM.2017.3316.

[592] Lin JY, Lo KY, Sun YS. Effects of Substrate-Coating Materials on the Wound-Healing Process. Materials. 2019;12:2775. DOI: 10.3390/MA12172775.

[593] Zhang X, Kang X, Jin L, *et al.* Stimulation of wound healing using bioinspired hydrogels with basic fibroblast growth factor (bFGF). International Journal of Nanomedicine. 2018;13:3897. DOI: 10.2147/IJN.S168998.

[594] Sayyar Z, Mahdavinia GR, Khataee A. Dual-drug (Curcumin/Ciprofloxacin) loading and release from chitosan-based hydrogels embedded with magnetic Montmorillonite/Hyaluronic acid for enhancing wound healing. Journal of Biological Engineering. 2023;17:66. DOI: 10.1186/S13036-023-00385-1.

[595] Jeong DP, Hall E, Neu E, *et al.* Podoplanin is Responsible for the Distinct Blood and Lymphatic Capillaries. Cellular and Molecular Bioengineering. 2022;15:467. DOI: 10.1007/S12195-022-00730-2.

[596] Ammann KR, DeCook KJ, Tran PL, *et al.* Collective cell migration of smooth muscle and endothelial cells: Impact of injury versus non-injury stimuli. Journal of Biological Engineering. 2015;9:1-15. DOI: 10.1186/S13036-015-0015-Y/FIGURES/13.

[597] Doyle AD, Carvajal N, Jin A, *et al.* Local 3D matrix microenvironment regulates cell migration through spatiotemporal dynamics of contractility-dependent adhesions. Nature Communications 2015 6:1. 2015;6:1-15. DOI: 10.1038/ncomms9720.

[598] Solbu AA, Caballero D, Damigos S, *et al.* Assessing cell migration in hydrogels: An overview of relevant materials and methods. Materials Today Bio. 2023;18:100537. DOI: 10.1016/J.MTBIO.2022.100537.

[599] Abdullah Z, Bayraktutan U. NADPH oxidase mediates TNF-α-evoked in vitro brain barrier dysfunction: roles of apoptosis and time. Molecular and Cellular Neuroscience. 2014;61:72-84. DOI: 10.1016/J.MCN.2014.06.002.

[600] Colgin LM, Reddel RR. Telomere maintenance mechanisms and cellular immortalization. Current Opinion in Genetics & Development. 1999;9:97-103. DOI: 10.1016/S0959-437X(99)80014-8.

[601] Akther F, Little P, Li Z, *et al.* Hydrogels as artificial matrices for cell seeding in microfluidic devices. RSC Advances. 2020;10:43682. DOI: 10.1039/D0RA08566A.

[602] Ballester-Beltrán J, Lebourg M, Salmerón-Sánchez M. Dorsal and ventral stimuli in sandwich-like microenvironments. Effect on cell differentiation. Biotechnology and Bioengineering. 2013;110:3048-58. DOI: 10.1002/BIT.24972.

[603] Song J, Gerecht S. Hydrogels to Recapture Extracellular Matrix Cues That Regulate Vascularization. Arteriosclerosis, Thrombosis, and Vascular Biology. 2023;43:E291-302. DOI: 10.1161/ATVBAHA.122.318235.

[604] Pahapale GJ, Tao J, Nikolic M, *et al.* Directing Multicellular Organization by Varying the Aspect Ratio of Soft Hydrogel Microwells. Advanced Science. 2022;9:2104649. DOI: 10.1002/ADVS.202104649.

[605] Wang W, Lollis EM, Bordeleau F, *et al.* Matrix stiffness regulates vascular integrity through focal adhesion kinase activity. FASEB journal : official publication of the Federation of American Societies for Experimental Biology. 2019;33:1199-208. DOI: 10.1096/FJ.201800841R.

[606] Bordeleau F, Mason BN, Lollis EM, *et al.* Matrix stiffening promotes a tumor vasculature phenotype. Proceedings of the National Academy of Sciences of the United States of America. 2017;114:492-7. DOI: 10.1073/PNAS.1613855114/-/DCSUPPLEMENTAL.

[607] Kang HW, Lee SJ, Ko IK, *et al.* A 3D bioprinting system to produce human-scale tissue constructs with structural integrity. Nature Biotechnology 2016 34:3. 2016;34:312-9. DOI: 10.1038/nbt.3413.

[608] Das S, Pati F, Choi YJ, *et al.* Bioprintable, cell-laden silk fibroin–gelatin hydrogel supporting multilineage differentiation of stem cells for fabrication of three-dimensional tissue constructs. Acta Biomaterialia. 2015;11:233-46. DOI: 10.1016/J.ACTBIO.2014.09.023.

[609] Kuo KC, Lin RZ, Tien HW, *et al.* Bioengineering vascularized tissue constructs using an injectable cell-laden enzymatically crosslinked collagen hydrogel derived from dermal extracellular matrix. Acta Biomaterialia. 2015;27:151-66. DOI: 10.1016/J.ACTBIO.2015.09.002.

[610] Bjørnøy SH, Mandaric S, Bassett DC, *et al.* Gelling kinetics and in situ mineralization of alginate hydrogels: A correlative spatiotemporal characterization toolbox. Acta Biomaterialia. 2016;44:243-53. DOI: 10.1016/J.ACTBIO.2016.07.046.

[611] Dunmire EN, Plenys AM, Katz DF. Spectrophotometric analysis of molecular transport in gels. Journal of Controlled Release. 1999;57:127-40. DOI: 10.1016/S0168-3659(98)00111-4.

[612] Carr ME, Gabriel DA. The effect of dextran 70 on the structure of plasma-derived fibrin gels. The Journal of Laboratory and Clinical Medicine. 1980;96:985-93.

[613] Ferri F, Calegari GR, Molteni M, *et al.* Size and Density of Fibers in Fibrin and Other Filamentous Networks from Turbidimetry: Beyond a Revisited Carr-Hermans Method, Accounting for Fractality and Porosity. Macromolecules. 2015;48:5423-32. DOI: 10.1021/acs.macromol.5b00893.

[614] Winkler T. Pendant Drop Measurements Method: Determining the surface tension of liquids by measurements on pendant drops; 2010.

[615] Miller C, Bolden J, Corder Z, *et al.*. Determining Surface Tension Using The Pendant Drop Method;.

[616] Yeromonahos C, Polack B, Caton F. Nanostructure of the fibrin clot. Biophysical Journal. 2010;99:2018-27. DOI: 10.1016/j.bpj.2010.04.059.

[617] Fantl P, Ward HA. Molecular Weight of Human Fibrinogen Derived from Phosphorus Determinations. Biochem J. 1965;96:886-9. DOI: 10.1042/bj0960886.

[618] Gersh KC, Edmondson KE, Weisel JW. Flow rate and fibrin fiber alignment. Journal of Thrombosis and Haemostasis. 2010;8:2826-8. DOI: 10.1111/J.1538-7836.2010.04118.X.

[619] Gessmann J, Seybold D, Peter E, *et al.* Alignment of the Fibrin Network Within an Autologous Plasma Clot. Tissue Engineering Part C, Methods. 2016;22:30. DOI: 10.1089/TEN.TEC.2015.0207.

[620] Kotlarchyk MA, Shreim SG, Alvarez-Elizondo MB, *et al.* Concentration independent modulation of local micromechanics in a fibrin gel. PloS one. 2011;6. DOI: 10.1371/JOURNAL.PONE.0020201.

[621] Francis CW, Marder VJ. A Molecular Model of Plasmic Degradation of Crosslinked Fibrin. SEMINARS IN THROMBOSIS AND HEMOSTASIS. 1982;8:25-35. DOI: 10.1055/s-2007-1005040.

[622] Tran N, Garcia T, Aniqa M, *et al.* Endothelial Nitric Oxide Synthase (eNOS) and the Cardiovascular System: in Physiology and in Disease States. Am J Biomed Sci Res. 2022;15:153-77.

[623] Campbell B, Chuhran C, Lefer AM. Vascular endothelial growth factor attenuates trauma-induced injury in rats. British Journal of Pharmacology. 2000;129(1):71-6. DOI: 10.1038/sj.bjp.0703010.

[624] Lu P, Ruan D, Huang M, *et al.* Harnessing the potential of hydrogels for advanced therapeutic applications: current achievements and future directions. Signal Transduction and Targeted Therapy 2024 9:1. 2024;9:1-66. DOI: 10.1038/s41392-024-01852-x.

[625] Scientific T. Useful Numbers for Cell Culture; 2025.

[626] CellScale. MicroTester LT Micro-scale Tension-Compression Test System User Manual version 4.5; 2019.

[627] FormLabs. Form Cure time and temperature settings; 2024.

[628] Taylor L. Design of an in vitro microvasculature model for trauma research. University of Oxford; 2022.

[629] Litvinov RI, Weisel JW. Fibrin mechanical properties and their structural origins. Matrix biology : journal of the International Society for Matrix Biology. 2016;60-61:110. DOI: 10.1016/J.MATBIO.2016.08.003.

[630] Hong X, Stegemann JP, Deng CX. Microscale Characterization of the Viscoelastic Properties of Hydrogel Biomaterials using Dual-Mode Ultrasound Elastography. Biomaterials. 2016;88:12. DOI: 10.1016/J.BIOMATERIALS.2016.02.019.

[631] Kim OV, Litvinov RI, Chen J, *et al.* Compression-induced structural and mechanical changes of fibrin-collagen composites. Matrix biology : journal of the International Society for Matrix Biology. 2016;60-61:141. DOI: 10.1016/J.MATBIO.2016.10.007.

[632] Torgbo S, Sukyai P. Biodegradation and thermal stability of bacterial cellulose as biomaterial: The relevance in biomedical applications. Polymer Degradation and Stability. 2020;179:109232. DOI: 10.1016/J.POLYMDEGRADSTAB.2020.109232.

[633] Kim OV, Litvinov RI, Weisel JW, *et al.* Structural basis for the nonlinear mechanics of fibrin networks under compression. Biomaterials. 2014;35(25):6739-49. DOI: 10.1016/J.BIOMATERIALS.2014.04.056.

[634] Liu S, Bahmani A, Ghezelbash F, *et al.* Fibrin clot fracture under cyclic fatigue and variable rate loading. Acta Biomaterialia. 2024;177:265-77. DOI: 10.1016/J.ACTBIO.2024.01.046.

[635] Kreß S, Schaller-Ammann R, Feiel J, *et al.* 3D Printing of Cell Culture Devices: Assessment and Prevention of the Cytotoxicity of Photopolymers for Stereolithography. Materials. 2020;13(13). DOI: 10.3390/MA13133011.

[636] Pan D, Schofield JB, Schellhardt L, *et al.* A Feasibility Study Transplanting Macrophages to a Segmental Nerve Injury. Muscle & Nerve. 2023;68:894-900. DOI: 10.1002/mus.27977.

[637] Reichenberger MA, Mueller W, Hartmann J, *et al.* ADSCs in a Fibrin Matrix Enhance Nerve Regeneration After Epineural Suturing in a Rat Model. Microsurgery. 2016;36:491-500. DOI: 10.1002/micr.30018.

[638] Allan IU, Tolhurst BA, Shevchenko RV, *et al.* An *In Vitro* Evaluation of Fibrinogen and Gelatin Containing Cryogels as Dermal Regeneration Scaffolds. Biomaterials Science. 2016;4:1007-14. DOI: 10.1039/c6bm00133e.

[639] Cronin KJ, Messina A, Thompson EW, *et al.* The Role of Biological Extracellular Matrix Scaffolds in Vascularized Three-Dimensional Tissue Growth *In Vivo*. Journal of Biomedical Materials Research - Part B Applied Biomaterials. 2007;82:122-8. DOI: 10.1002/jbm.b.30713.

[640] Nikolaychik VV, Chekanov VS, Hernandez I, *et al.* Biodesign of a Skeletal Muscle Flap as a Model for Cardiac Assistance. Artificial Organs. 2000;24:137-47. DOI: 10.1046/j.1525-1594.2000.024002137.x.

[641] Godier-Furnémont AFG, Martens TP, Koeckert MS, *et al.* Composite Scaffold Provides a Cell Delivery Platform for Cardiovascular Repair. Proceedings of the National Academy of Sciences of the United States of America. 2011;108:7974-9. DOI: 10.1073/pnas.1104619108.

[642] Hadad I, Johnstone BH, Brabham JG, *et al.* Development of a Porcine Delayed Wound-Healing Model and Its Use in Testing a Novel Cell-Based Therapy. International Journal of Radiation Oncology Biology Physics. 2010;78:888-96. DOI: 10.1016/j.ijrobp.2010.05.002.

[643] Sun CK, Zhen YY, Leu S, *et al.* Direct Implantation Versus Platelet-Rich Fibrin-embedded Adipose-derived Mesenchymal Stem Cells in Treating Rat Acute Myocardial Infarction. International Journal of Cardiology. 2014;173:410-23. DOI: 10.1016/j.ijcard.2014.03.015.

[644] Shen D, Tang J, Hensley MT, *et al.* Effects of Matrix Metalloproteinases on the Performance of Platelet Fibrin Gel Spiked with Cardiac Stem Cells in Heart Repair. Stem Cells Translational Medicine. 2016;5:793-803. DOI: 10.5966/sctm.2015-0194.

[645] Chung E, Nam SY, Ricles LM, *et al.* Evaluation of Gold Nanotracers to Track Adipose-derived Stem Cells in a PEGylated Fibrin Gel for Dermal Tissue Engineering Applications. International Journal of Nanomedicine. 2013;8:325-36. DOI: 10.2147/IJN.S36711.

[646] Dvorak HF, Harvey VS, Estrella P, *et al.* Fibrin Containing Gels Induce Angiogenesis. Implications for Tumor Stroma Generation and Wound Healing. Laboratory Investigation. 1987;57:673-86.

[647] Nam K, dos Santos HT, Maslow F, *et al.* Fibrin Hydrogels Fortified with FGF-7/10 and Laminin-1 Peptides Promote Regeneration of Irradiated Salivary Glands. Acta Biomaterialia. 2023;172:147-58. DOI: 10.1016/j.actbio.2023.10.013.

[648] Humar R, de Miguel LS, Kiefer FN, *et al.* Formation of New Blood Vessels in the Heart can be Studied in Cell Cultures. ALTEX. 2007;24:35-8.

[649] Woods I, Black A, Jockenhoevel S, *et al.* Harnessing Topographical & Biochemical Cues to Enhance Elastogenesis by Paediatric Cells for Cardiovascular Tissue Engineering Applications. Biochemical and Biophysical Research Communications. 2019;512:156-62. DOI: 10.1016/j.bbrc.2019.03.026.

[650] Hojo M, Inokuchi S, Kidokoro M, *et al.* Induction of Vascular Endothelial Growth Factor by Fibrin as a Dermal Substrate for Cultured Skin Substitute. Plastic and Reconstructive Surgery. 2003;111:1638-45. DOI: 10.1097/01.PRS.0000053842.90564.26.

[651] McLuckie M, Robotti F, Sanchez-Macedo N, *et al.* Lipoconstruct Surface Topography Grating Size Influences Vascularization Onset in the Dorsal Skinfold Chamber Model. Acta Biomaterialia. 2020;106:136-44. DOI: 10.1016/j.actbio.2020.01.050.

[652] Bookholt FD, Monsuur HN, Gibbs S, *et al.* Mathematical Modelling of Angiogenesis Using Continuous Cell-based Models. Biomechanics and Modeling in Mechanobiology. 2016;15:1577-600. DOI: 10.1007/s10237-016-0784-3.

[653] Hiraoka N, Allen E, Apel IJ, *et al.* Matrix Metalloproteinases Regulate Neovascularization by Acting as Pericellular Fibrinolysins. Cell. 1998;95:365-77. DOI: 10.1016/s0092-8674(00)81768-7.

[654] Jung SH, Jang BH, Kwon S, *et al.* Nematic Fibrin Fibers Enabling Vascularized Thrombus Implants Facilitate Scarless Cutaneous Wound Healing. Advanced Materials. 2023;35:2211149. DOI: 10.1002/adma.202211149.

[655] Rohr S, Toti F, Brisson C, *et al.* Quantitative Image Analysis of Angiogenesis in Rats Implanted with a Fibrin Gel Chamber. Nouvelle Revue Francaise d'Hematologie. 1992;34:287-94.

[656] Montesano R, Mouron P, Orci L. Vascular Outgrowths from Tissue Explants Embedded in Fibrin or Collagen Gels: A Simple *In Vitro* Model of Angiogenesis. Cell Biology International Reports. 1985;9:869-75.

[657] Paulhe F, Bogyo A, Chap H, *et al.* Vascular Smooth Muscle Cell Spreading onto Fibrinogen Is Regulated by Calpains and Phospholipase C. Biochemical and Biophysical Research Communications. 2001;288:875-81. DOI: 10.1006/bbrc.2001.5859.

[658] Gigante A, Torto MD, Manzotti S, *et al.* Platelet Rich Fibrin Matrix Effects on Skeletal Muscle Lesions: An Experimental Study. Journal of Biological Regulators & Homeostatic Agents. 2012;26:475-84.

[659] Thomson KS, Korte FS, Giachelli CM, *et al.* Prevascularized Microtemplated Fibrin Scaffolds for Cardiac Tissue Engineering Applications. Tissue Engineering Part A. 2013;19:967-77. DOI: 10.1089/ten.tea.2012.0286.

[660] Müller M, Becher J, Schnabelrauch M, *et al.* Printing Thermoresponsive Reverse Molds for the Creation of Patterned Two-component Hydrogels for 3D Cell Culture. Journal of Visualized Experiments. 2013:e50632. DOI: 10.3791/50632.

[661] Sánchez-Muñoz I, Granados R, Holgado PH, *et al.* The Use of Adipose Mesenchymal Stem Cells and Human Umbilical Vascular Endothelial Cells on a Fibrin Matrix for Endothelialized Skin Substitute. Tissue Engineering Part A. 2015;21:214-23. DOI: 10.1089/ten.tea.2013.0626.

[662] Nan W, Liu R, Chen H, *et al.* Umbilical Cord Mesenchymal Stem Cells Combined with a Collagenfibrin Double-layered Membrane Accelerates Wound Healing. Wounds. 2015;27:134-40.

Appendix A

Supplementary Materials for Chapter 3

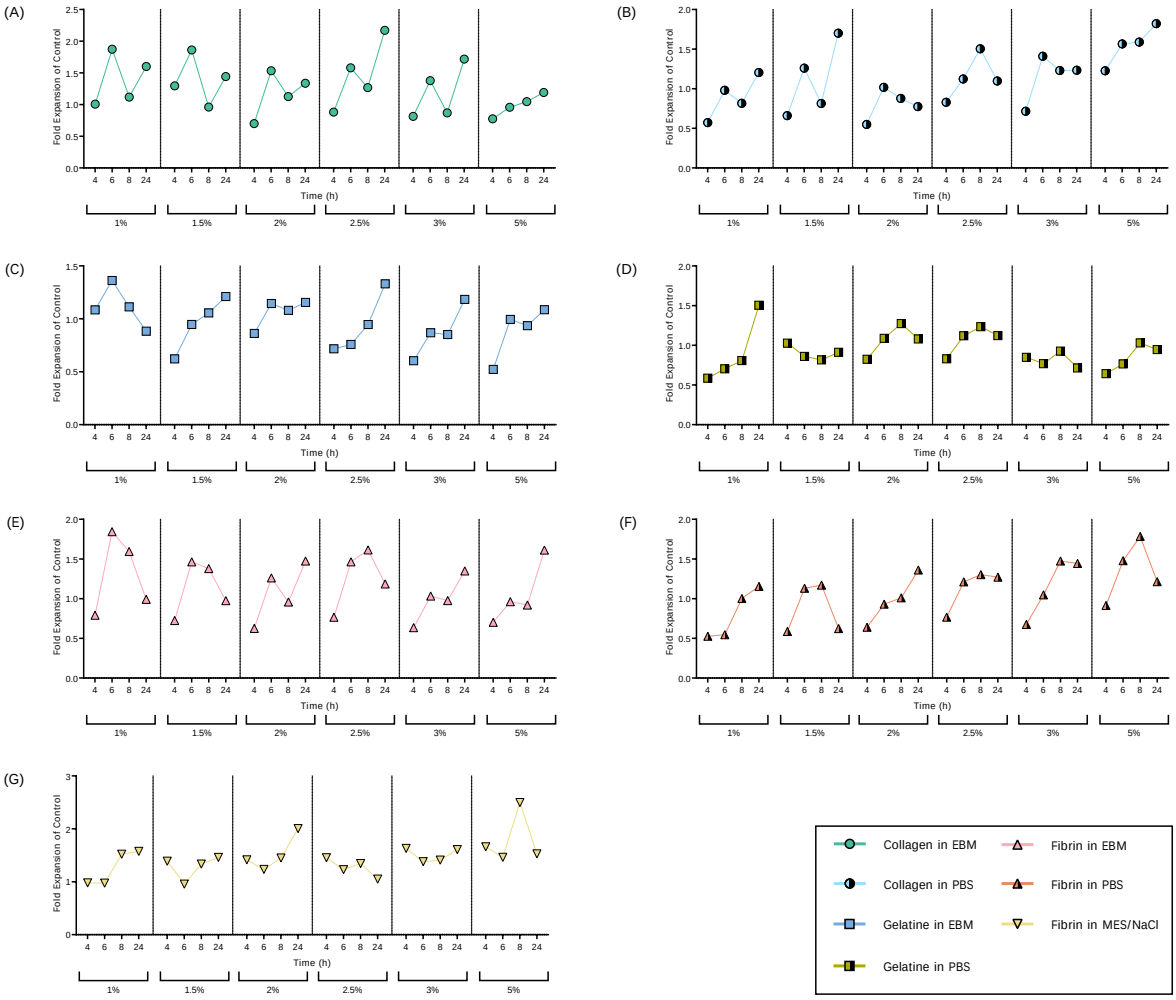


Figure A.1: **Cell adhesion as a fold expansion of the cells-only control, by coating and concentration. (A, B)** Collagen, **(C, D)** gelatine and **(E–G)** fibrin in **(A, C, E)** endothelial cell basal medium (EBM), **(B, D, F)** phosphate-buffered saline (PBS), or **(G)** MES/NaCl. Human umbilical vein endothelial cells (HUVECs) were cultured in endothelial cell growth medium (EGM) and seeded at a density of 2×10^4 cells/well (96-well plate). A total of 14 hydrogel compositions had statistically significant differences compared to the control. (ANOVA/Tukey's HSD, $p \leq 0.05$; $n = 4$).

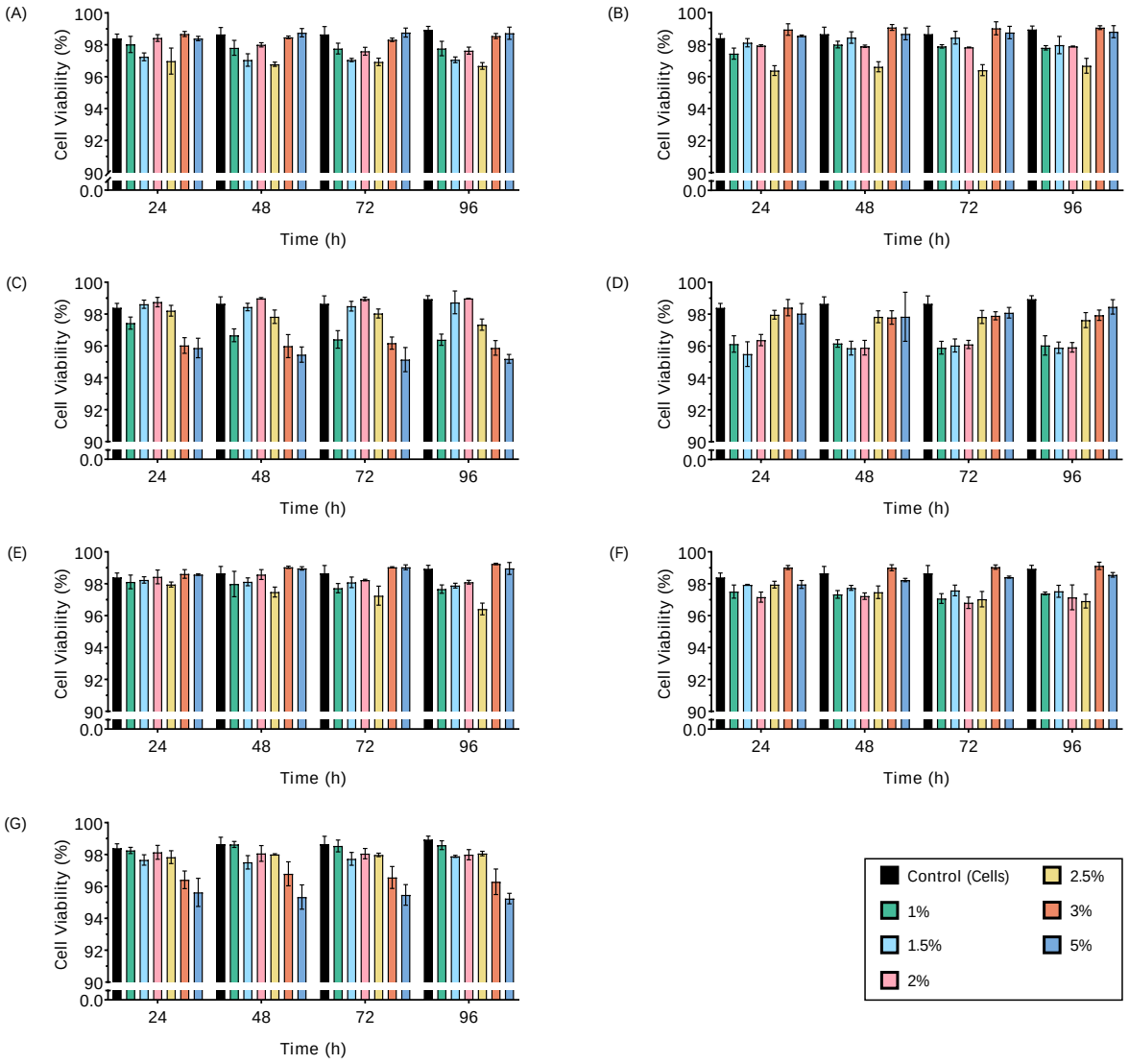


Figure A.2: **Cell viability (%) by hydrogel composition. (A, B)** Collagen, **(C, D)** fibrin-collagen (1:1 ratio) and **(E–G)** fibrin in **(A, C, E)** endothelial cell basal medium (EBM), **(B, D, F)** phosphate-buffered saline (PBS), or **(G)** MES/NaCl were prepared at a range of concentrations (1, 1.5, 2, 2.5, 3, or 5% *w*/*v*). Human umbilical vein endothelial cells (HUVECs) (seeding density: 2×10^4 cells/well) were cultured with endothelial cell growth medium (EGM) in 96-well plates on top of the hydrogel. Readings were taken at 24, 48, 72, and 96 h. A cells-only control (repeated in every graph for comparison purposes) was used. (ANOVA/Tukey's HSD, $p \leq 0.05$; $n = 3$).

Appendix B

Supplementary Materials for Chapter 4

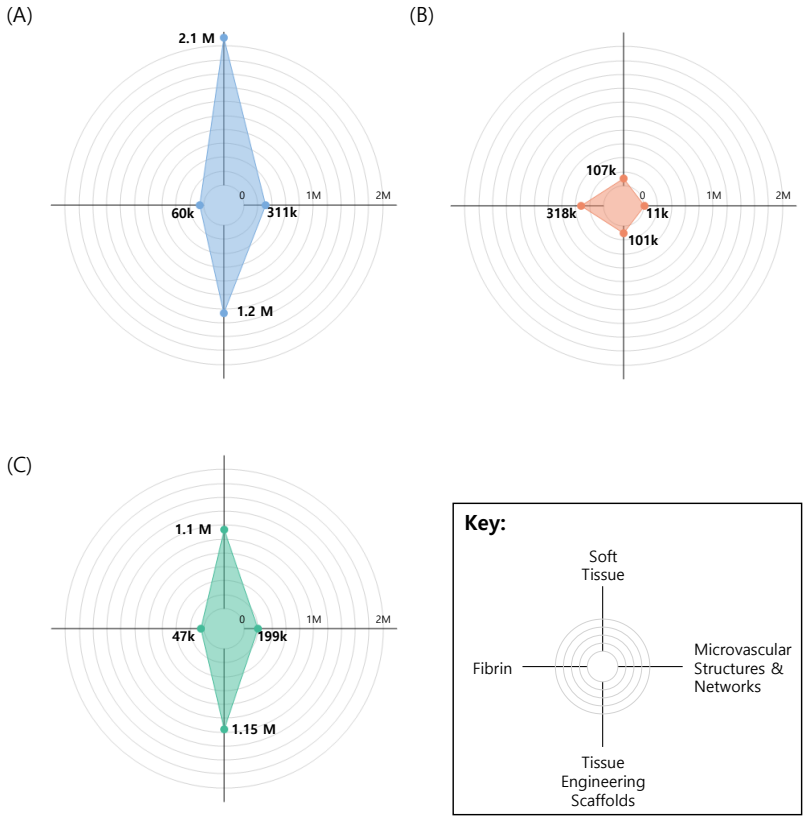


Figure B.1: **Visual representation of the number of records found in each database when independently searching for each of the four search query components: 'Soft Tissue', 'Microvascular Structures and/or Network', 'Tissue Engineering Scaffolds', and 'Fibrin'. (A)** PubMed, **(B)** Scopus and **(C)** OVID. The full search query used for each database can be found in Appendix C. Each ring represents 200,000 records.

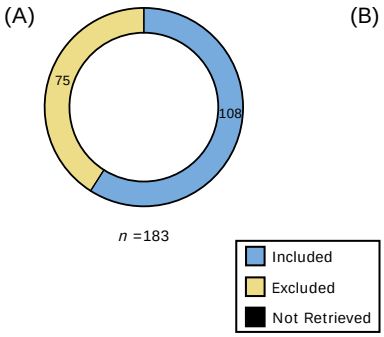


Figure B.2: **Systematic review (SR) screening decisions**, as agreed by the three reviewers after independent binary classification of the study based on the inclusion and exclusion criteria. Two rounds of screening were conducted to evaluate the relevance of each record based on **(A)** title and abstract, and **(B)** full-text review. Two full-text articles could not be retrieved and were thus excluded.

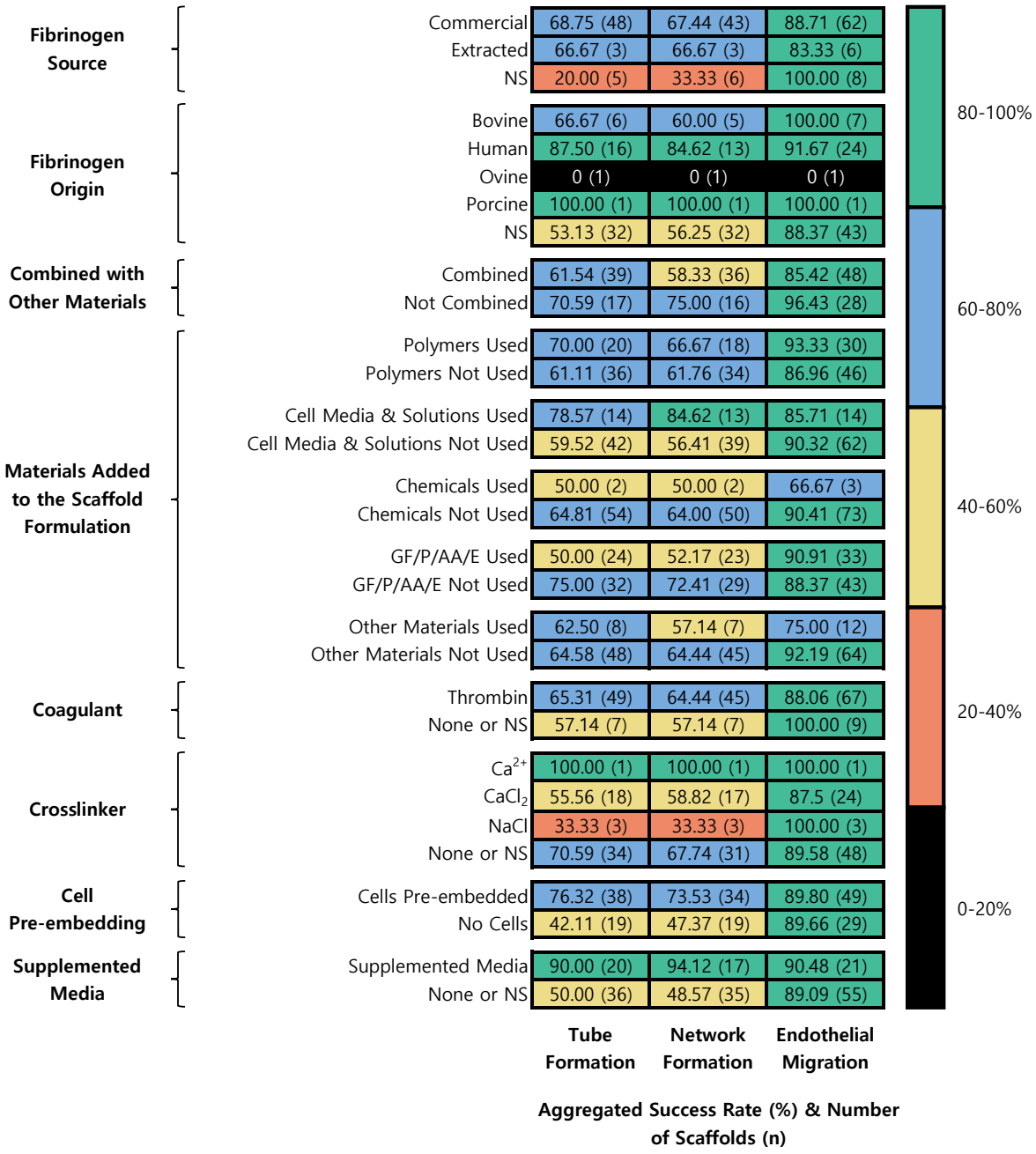


Figure B.3: **Aggregated success rates (%) and number of scaffolds used for success rate calculations (n) of fibrin scaffold design parameters.** Each cell presents the percentage of successful scaffolds (aggregated success rate) followed by the number of scaffolds contributing to the calculation. Success rates were calculated as the proportion of successful scaffolds relative to the total number of successful and unsuccessful scaffolds. Only scaffolds for which study authors reported an outcome and included the specified formulation element were considered; scaffolds with no reported outcome or without the relevant element were excluded. The heatmap is colour-coded in five tiers based on the aggregated success rate: green (80–100% success), blue (60–80%), yellow (40–60%), orange (20–40%), and black (0–20%). Reported outcomes include tube and network formation, and endothelial cell (EC) migration. Scaffold parameters analysed were: fibrinogen source and origin, combination with other materials (and material type), use and type of coagulant and crosslinker, cell pre-embedding, and use of supplemented media. GF/P/AA/E: Growth Factors, Peptides, Amino Acids & Enzymes. NS: Not specified.

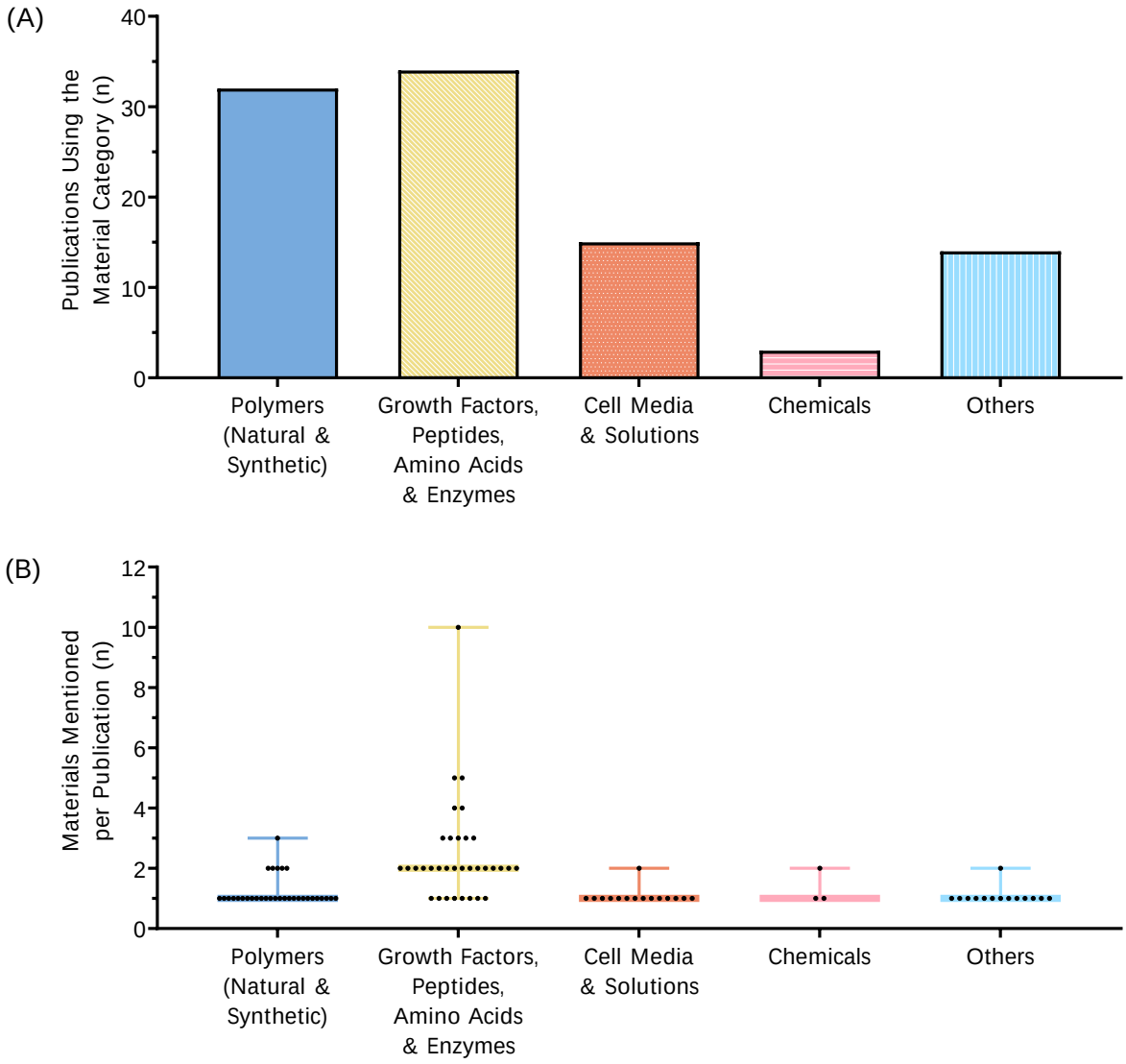


Figure B.4: **Materials used in combination with fibrin, coagulants and crosslinkers. (A)** Number of publications using each category of material. **(B)** Median number of different materials used per scaffold within each category. Error bars indicate the range.

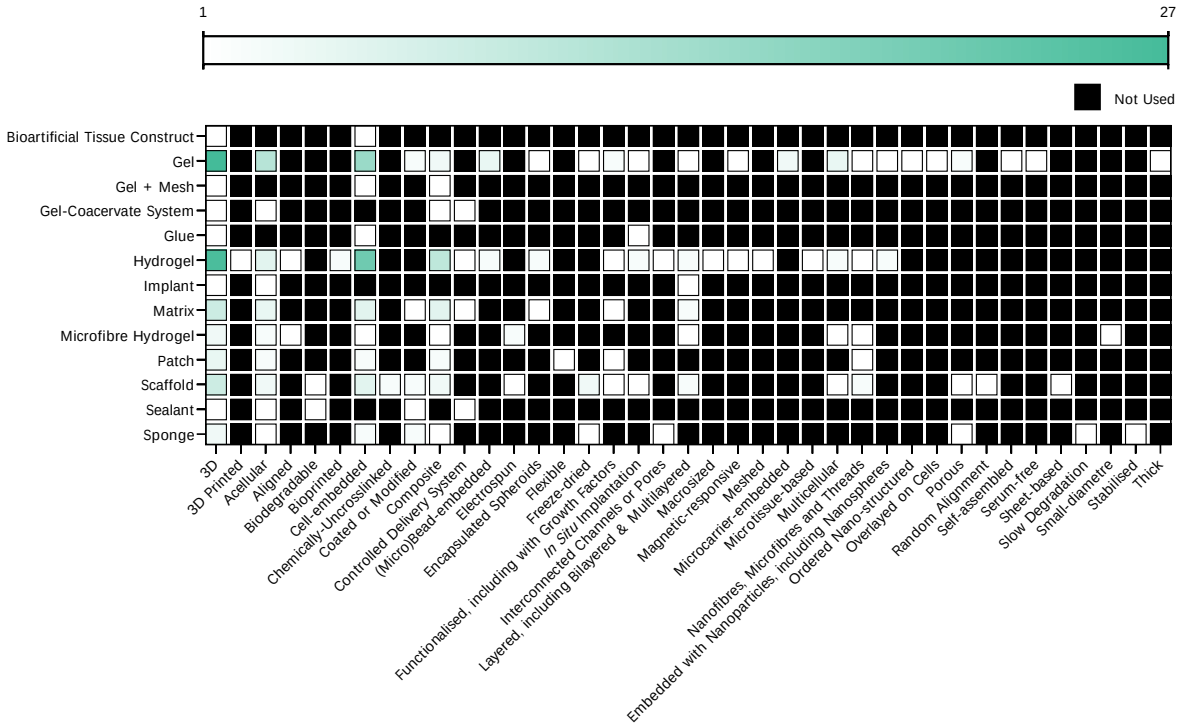


Figure B.5: **Features associated with the manufactured objects used in the corpus**, as described in the studies.

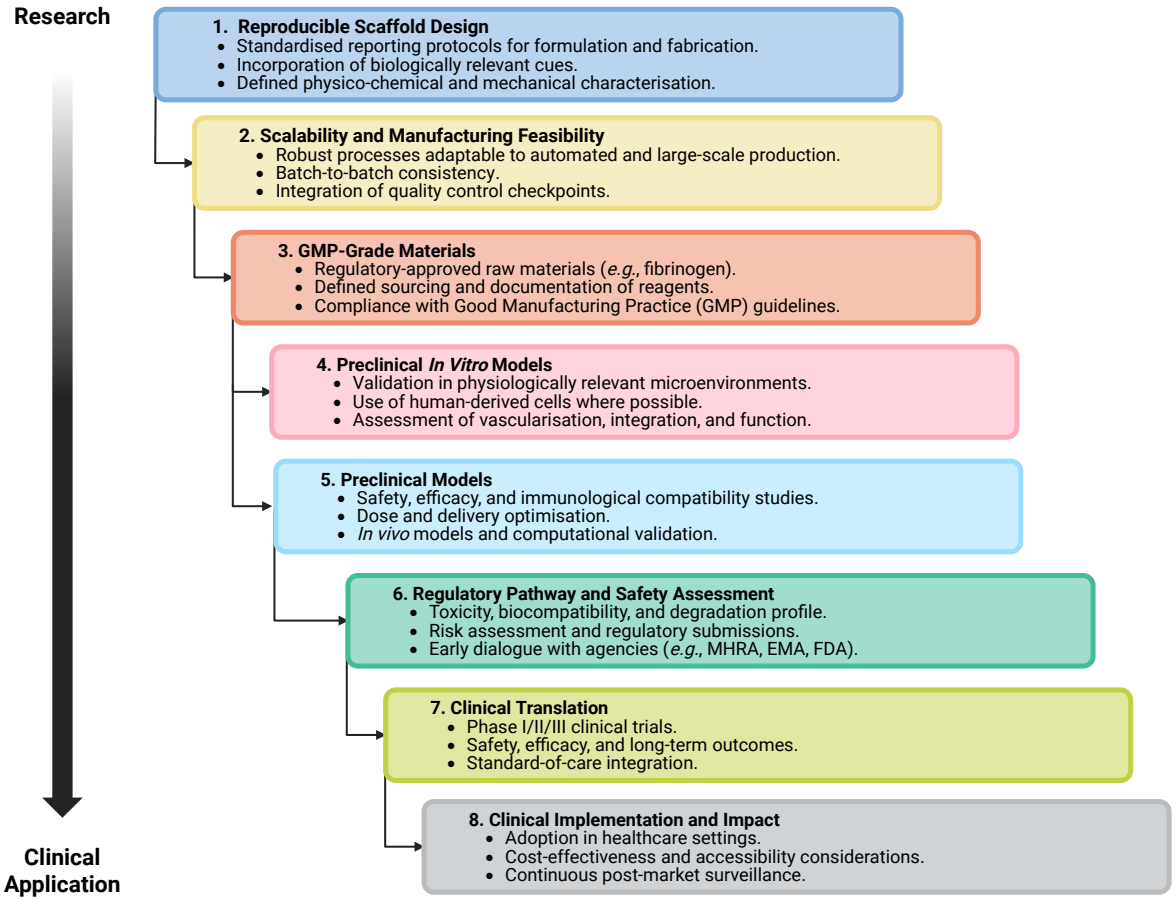


Figure B.6: **Roadmap for fibrin scaffolds from reproducible scaffold design to clinical application**, depicting eight key stages to improve reproducibility, allow for meaningful comparisons across studies and advance clinical translation.

Table B.1: **Articles excluded during the 2nd screening round (full-text screening)**, by reason for exclusion. [636–662]

Studies Not Retrieved	n
Full-text not available.	2

Reason for Exclusion	n
Retracted publications.	1
Non-peer-reviewed publications.	0
Non-original research articles.	2
Articles not published in English.	0
Studies do not include data and/or outcomes of endothelial formation and migration processes.	10
Studies do not contain fibrin-based scaffolds.	0
Studies do not focus on soft tissue applications.	1
Studies with exclusive use of autologous or allogenic grafts or materials.	11

Table B.2: **Studies included in the corpus (*n* = 81)**, with their corresponding bibliographical data. [41, 297, 405, 434, 457–533]

	Title	Reference	DOI	PMID
1	Fabrication of chitin-fibrin hydrogels to construct the 3D artificial extracellular matrix scaffold for vascular regeneration and cardiac tissue engineering.	Pengcheng Yang *et al.*, 2024	10.1002/jbm.a.37774	39007419
2	Vascularization of PEGylated fibrin hydrogels increases the proliferation of human iPSC-cardiomyocytes.	Ethan J Vanderslice *et al.*, 2024	10.1002/jbm.a.37662	38155509
3	External magnetic field non-invasively stimulates spinal cord regeneration in rat *via* a magnetic-responsive aligned fibrin hydrogel.	Chun-Yi Yang *et al.*, 2023	10.1088/1758-5090/acdbec	37279745
4	Chitosan-collagen-fibrinogen uncrosslinked scaffolds possessing skin regeneration and vascularization potential.	Shalini Dasgupta *et al.*, 2023	10.1002/jbm.a.37488	36573698
5	Fibrin-based cardiac patch containing neuregulin-1 for heart repair after myocardial infarction.	Tianqi Chang *et al.*, 2022	10.1016/j.colsurfb.2022.112936	36265312
6	An encapsulated fibrin-based bioartificial tissue construct with integrated macrovessels, microchannels, and capillary tubes.	Florian Helms *et al.*, 2022	10.1002/bit.28111	35485750
7	The effects of oral mucosa-derived heterotopic fibroblasts on cutaneous wound healing.	Billur Sezgin *et al.*, 2021	10.1016/j.bjps.2021.02.011	33935009
8	Vascular Network Formation on Macroporous Polydioxanone Scaffolds.	Sebastian Heene *et al.*, 2021	10.1089/ten.TEA.2020.0232	33397206
9	Fibrin hydrogels promote scar formation and prevent therapeutic angiogenesis in the heart.	Ludovic Melly *et al.*, 2020	10.1002/term.3118	32841501
10	Engineered skin graft with stromal vascular fraction cells encapsulated in fibrin-collagen hydrogel: A clinical study for diabetic wound healing.	Mohammad Ali Nilforoushzadeh *et al.*, 2020	10.1002/term.3003	31826321
11	Regenerative and durable small-diameter graft as an arterial conduit.	Morgan B Elliotti *et al.*, 2019	10.1073/pnas.1905966116	31182572
12	Effective stacking and transplantation of stem cell sheets using exogenous ROS-producing film for accelerated wound healing.	Min-Ah Koo *et al.*, 2019	10.1016/j.actbio.2019.01.019	30660002
13	Nanofiber-acellular dermal matrix as a bilayer scaffold containing mesenchymal stem cell for healing of full-thickness skin wounds.	Mohamad Javad Mirzaei-Parsa *et al.*, 2019	10.1007/s00441-018-2927-6	30338376
14	Hierarchically aligned fibrin nanofiber hydrogel accelerated axonal regrowth and locomotor function recovery in rat spinal cord injury.	Shenglian Yao *et al.*, 2018	10.2147/IJN.S159356	29844671
15	Angiogenic potential of spheroids from umbilical cord and adipose-derived multipotent mesenchymal stromal cells within fibrin gel.	Anastasiya A Gorkun *et al.* , 2018	10.1088/1748-605X/aac22d	29722292
16	Delivery of Allogeneic Adipose Stem Cells in Polyethylene Glycol-Fibrin Hydrogels as an Adjunct to Meshed Autografts After Sharp Debridement of Deep Partial Thickness Burns.	David M Burmeister *et al.*, 2018	10.1002/sctm.17-0160	29457376
17	Goat tendon collagen-human fibrin hydrogel for comprehensive parametric evaluation of HUVEC microtissue-based angiogenesis.	Rajan Narayan *et al.*, 2018	10.1016/j.colsurfb.2017.12.056	29329074
18	Adipose tissue-derived stem cells in a fibrin implant enhance neovascularization in a peritoneal grafting site: a potential way to improve ovarian tissue transplantation.	Diego D Manavella *et al.*, 2018	10.1093/humrep/dex374	29304240
19	Construction of a vascularized hydrogel for cardiac tissue formation in a porcine model.	Kp Myu Mai Ja *et al.*, 2018	10.1002/term.2634	29266858
20	Fibrinogen-modified sodium alginate as a scaffold material for skin tissue engineering.	Elena V Solovieva *et al.*, 2018	10.1088/1748-605X/aa9089	28972200
21	Experimental study on repairing skin defect by tissue-engineered skin substitute compositely constructed by adipose-derived stem cells and fibrin gel.	Rui-Xi Zeng *et al.*, 2017	No DOI Registered.	28745800
22	Emulating human microcapillaries in a multi-organ-chip platform.	Tobias Hasenberg *et al.*, 2015	10.1016/j.jbiotec.2015.09.038	26435219
23	Rapid release of growth factors regenerates force output in volumetric muscle loss injuries.	Jonathan M Grasman *et al.*, 2015	10.1016/j.biomaterials.2015.08.047	26344363
24	Endothelial Network Formation Within Human Tissue-Engineered Skeletal Muscle.	Dacha Gholobova *et al.*, 2015	10.1089/ten.TEA.2015.0093	26177063
25	Fabrication of 3-dimensional multicellular microvascular structures.	Sebastian F Barreto-Ortiz *et al.*, 2015	10.1096/fj.14-263343	25900808
26	Sequential delivery of angiogenic growth factors improves revascularization and heart function after myocardial infarction.	Hassan K Awada *et al.*, 2015	10.1016/j.jconrel.2015.03.034	25836592
27	Fibrin-based 3D matrices induce angiogenic behavior of adipose-derived stem cells.	Eunna Chung *et al.*, 2015	10.1016/j.actbio.2015.01.012	25600400
28	Long-term functional benefits of human embryonic stem cell-derived cardiac progenitors embedded into a fibrin scaffold.	Valérie Bellamy *et al.*, 2015	10.1016/j.healun.2014.10.008	25534019
29	Mesenchymal stromal cells form vascular tubes when placed in fibrin sealant and accelerate wound healing *in vivo*.	Julio J Mendez *et al.*, 2015	10.1016/j.biomaterials.2014.11.011	25433608
30	Heparin-conjugated poly(lactic-co-glycolic acid) nanospheres enhance large-wound healing by delivering growth factors in platelet-rich plasma.	Wan-Geun La *et al.*, 2015	10.1111/aor.12389	25284020
31	Tissue-engineered, hydrogel-based endothelial progenitor cell therapy robustly revascularizes ischemic myocardium and preserves ventricular function.	Pavan Atluri *et al.*, 2014	10.1016/j.jtcvs.2014.06.038	25129603
32	Mechanisms of vasculogenesis in 3D fibrin matrices mediated by the interaction of adipose-derived stem cells and endothelial cells.	Sabrina Rohringer *et al.*, 2014	10.1007/s10456-014-9439-0	25086616
33	Specific effects of fibrinogen and the γA and γ'-chain fibrinogen variants on angiogenesis and wound healing.	Elim Y L Cheung *et al.*, 2015	10.1089/ten.TEA.2014.0020	24974891
34	Long-lasting fibrin matrices ensure stable and functional angiogenesis by highly tunable, sustained delivery of recombinant $VEGF_{164}$.	Veronica Sacchi *et al.*, 2014	10.1073/pnas.1404605111	24778233
35	PlGF-MMP9-engineered iPS cells supported on a PEG-fibrinogen hydrogel scaffold possess an enhanced capacity to repair damaged myocardium.	Claudia Bearzi *et al.*, 2014	10.1038/cddis.2014.12	24525729
36	Bioengineering dermo-epidermal skin grafts with blood and lymphatic capillaries.	Daniela Marino *et al.*, 2014	10.1126/scitranslmed.3006894	24477001
37	Fibrin gel improves tissue ingrowth and cell differentiation in human immature premolars implanted in rats.	Nisarat Ruangsawasdi *et al.*, 2014	10.1016/j.joen.2013.09.022	24461412
38	*In vitro* vascularization of a combined system based on a 3D printing technique.	Xinru Zhao *et al.*, 2016	10.1002/term.1863	24399638
39	A novel *in vitro* model for microvasculature reveals regulation of circumferential ECM organization by curvature.	Sebastian F Barreto-Ortiz *et al.*, 2013	10.1371/journal.pone.0081061	24278378
40	Angiogenic endothelial cell invasion into fibrin is stimulated by proliferating smooth muscle cells.	Areck A Ucuzian *et al.*, 2013	10.1016/j.mvr.2013.06.012	23886898
41	Mutual effect of subcutaneously transplanted human adipose-derived stem cells and pancreatic islets within fibrin gel.	Suk Ho Bhang *et al.*, 2013	10.1016/j.biomaterials.2013.06.018	23827190
42	Enhanced wound vascularization using a dsASCs seeded FPEG scaffold.	David O Zamora *et al.*, 2013	10.1007/s10456-013-9352-y	23709171
43	Scaffold-based delivery of a clinically relevant anti-angiogenic drug promotes the formation of *in vivo* stable cartilage.	Matteo Centola *et al.*, 2013	10.1089/ten.TEA.2012.0455	23611597
44	An improved freeze-dried PRP-coated biodegradable material suitable for connective tissue regenerative therapy.	Makoto Horimizu *et al.*, 2013	10.1016/j.cryobiol.2013.01.006	23422785
45	Bioprinted amniotic fluid-derived stem cells accelerate healing of large skin wounds.	Aleksander Skardal *et al.*, 2012	10.5966/sctm.2012-0088	23197691
46	Adipose-derived stem cells induce vascular tube formation of outgrowth endothelial cells in a fibrin matrix.	Wolfgang Holnthoner *et al.*, 2015	10.1002/term.1620	23038666
47	Comparing scaffold-free and fibrin-based adipose-derived stromal cell constructs for adipose tissue engineering: an *in vitro* and *in vivo* study.	Femke Verseijden *et al.*, 2012	10.3727/096368912X653129	22840523
48	Bioenergetic and functional consequences of cellular therapy: activation of endogenous cardiovascular progenitor cells.	Qiang Xiong *et al.*, 2012	10.1161/CIRCRESAHA.112.269894	22723295
49	A combined synthetic-fibrin scaffold supports growth and cardiomyogenic commitment of human placental derived stem cells.	Antonella Lisi *et al.*, 2012	10.1371/journal.pone.0034284	22509287
50	Fibrin-embedded adipose derived stem cells enhance skin flap survival.	Matthias A Reichenberger *et al.*, 2012	10.1007/s12015-011-9341-8	22215322
51	Vascularization of prevascularized and non-prevascularized fibrin-based human adipose tissue constructs after implantation in nude mice.	Femke Verseijden *et al.*, 2012	10.1002/term.410	21360688
52	Advantages of hyaluronic acid as a component of fibrin sheet for care of acute wound.	Thapasimuthu V Anilkumar *et al.*, 2011	10.1016/j.biologicals.2011.01.003	21334921
53	Endothelial progenitor cells are integrated in newly formed capillaries and alter adjacent fibrovascular tissue after subcutaneous implantation in a fibrin matrix.	Oliver Bleiziffer *et al.*, 2011	10.1111/j.1582-4934.2010.01247.x	21199325
54	Fibrin acts as biomimetic niche inducing both differentiation and stem cell marker expression of early human endothelial progenitor cells.	Maria Chiara Barsotti *et al.*, 2011	10.1111/j.1365-2184.2010.00715.x	21199008

	Title (cont.)	Reference (cont.)	DOI (cont.)	PMID (cont.)
55	Vascularization of the dermal support enhances wound re-epithelialization by in situ delivery of epidermal keratinocytes.	Liana M Lugo *et al.*, 2011	10.1089/ten.tea.2010.0125	20929281
56	Coronary arteries angiogenesis in ischemic myocardium: biocompatibility and biodegradability of various hydrogels.	Xiaodong Shen *et al.*, 2009	10.1111/j.1525-1594.2009.00815.x	19681839
57	Adult human bone marrow- and adipose tissue-derived stromal cells support the formation of prevascular-like structures from endothelial cells *in vitro*.	Femke Verseijden *et al.*, 2010	10.1089/ten.TEA.2009.0106	19642855
58	The effectiveness of basic fibroblast growth factor in fibrin-based cultured skin substitute *in vivo*.	Shigeaki Inoue *et al.*, 2009	10.1097/BCR.0b013e3181a28e4b	19349876
59	Engineered adipose tissue formation enhanced by basic fibroblast growth factor and a mechanically stable environment.	Seung-Woo Cho *et al.*, 2007	10.3727/000000007783464795	17658132
60	Implantation of VEGF transfected preadipocytes improves vascularization of fibrin implants on the cylinder chorioallantoic membrane (CAM) model.	Nestor Torio-Padron *et al.*, 2007	10.1080/13645700701384116	17573620
61	*In vitro* analysis of the interactions between preadipocytes and endothelial cells in a 3D fibrin matrix.	Jörg Borges *et al.*, 2007	10.1080/13645700600935398	17573618
62	Magnetically-guided self-assembly of fibrin matrices with ordered nano-scale structure for tissue engineering.	Eben Alsberg *et al.*, 2006	10.1089/ten.2006.12.3247	17518638
63	VEGF(165) and bFGF protein-based therapy in a slow release system to improve angiogenesis in a bioartificial dermal substitute *in vitro* and *in vivo*.	I Wilcke *et al.*, 2007	10.1007/s00423-007-0194-1	17404752
64	Platelets, thrombospondin-1 and human dermal fibroblasts cooperate for stimulation of endothelial cell tubulogenesis through VEGF and PAI-1 regulation.	Sabrina Kellouche *et al.*, 2007	10.1016/j.yexcr.2006.10.023	17126831
65	Adipose precursor cells (preadipocytes) induce formation of new vessels in fibrin glue on the newly developed cylinder chorioallantoic membrane model (CAM).	Joerg Borges *et al.*, 2006	10.1080/14017450600761620	16966139
66	Peptide-matrix-mediated gene transfer of an oxygen-insensitive hypoxia-inducible factor-1alpha variant for local induction of angiogenesis.	Diana Trentin *et al.*, 2006	10.1073/pnas.0505964102	16477043
67	Control of basic fibroblast growth factor release from fibrin gel with heparin and concentrations of fibrinogen and thrombin.	Oju Jeon *et al.*, 2005	10.1016/j.jconrel.2005.03.023	16088988
68	Diffusion limits of an *in vitro* thick prevascularized tissue.	Craig K Griffith *et al.*, 2005	10.1089/ten.2005.11.257	15738680
69	Autologous stem cell transplantation for myocardial repair.	Jingbo Liu *et al.*, 2004	10.1152/ajpheart.00019.2004	15277194
70	A novel role for erythropoietin during fibrin-induced wound-healing response.	Zishan A Haroon *et al.*, 2003	10.1016/S0002-9440(10)63459-1	12937140
71	Angiogenic sprouting and capillary lumen formation modeled by human umbilical vein endothelial cells (HUVEC) in fibrin gels: the role of fibroblasts and Angiopoietin-1.	Martin N Nakatsu *et al.*, 2003	10.1016/s0026-2862(03)00045-1	12935768
72	Transplantation of autologous endothelial cells induces angiogenesis.	Valeri Chekanov *et al.*, 2003	10.1046/j.1460-9592.2003.00080.x	12687876
73	Delivery of high dose VEGF plasmid using fibrin carrier does not influence its angiogenic potency.	Alicia Jozkowicz *et al.*, 2003	10.1177/039139880302600211	12653351
74	A technique for quantitative three-dimensional analysis of microvascular structure.	Eric M Brey *et al.*, 2002	10.1006/mvre.2002.2395	11969305
75	Expression of antisense to integrin subunit beta 3 inhibits microvascular endothelial cell capillary tube formation in fibrin.	Susan M Dallabrida *et al.*, 2000	10.1074/jbc.M001446200	10922359
76	Fibrin and collagen differentially regulate human dermal microvascular endothelial cell integrins: stabilization of alphav/beta3 mRNA by fibrin1.	Xiaodong Feng *et al.*, 1999	10.1046/j.1523-1747.1999.00786.x	10594730
77	Contact-dependent inhibition of angiogenesis by cardiac fibroblasts in three-dimensional fibrin gels *in vitro* : implications for microvascular network remodeling and coronary collateral formation.	Volker Nehls *et al.*, 1998	10.1007/s004410051140	9716738
78	Biological molecule-impregnated polyester: an *in vivo* angiogenesis study.	Nancy Fournier *et al.*, 1996	10.1016/0142-9612(96)87645-9	8866027
79	A microcarrier-based cocultivation system for the investigation of factors and cells involved in angiogenesis in three-dimensional fibrin matrices *in vitro*.	Volker Nehls *et al.*, 1995	10.1007/BF01464336	8777732
80	The effect of fibroblasts, vascular smooth muscle cells, and pericytes on sprout formation of endothelial cells in a fibrin gel angiogenesis system.	Volker Nehls *et al.*, 1994	10.1006/mvre.1994.1061	7537351
81	Fibrin gel investment associated with line 1 and line 10 solid tumor growth, angiogenesis, and fibroplasia in guinea pigs. Role of cellular immunity, myofibroblasts, microvascular damage, and infarction in line 1 tumor regression.	Harold F Dvorak *et al.*, 1979	10.1093/jnci/62.6.1459	286118

Table B.3: **Overview of key study details highlighting the heterogeneity of the corpus.** For each article, information is provided on the: soft tissue type; study type (*in vitro*, *in vivo*, *ex vivo*, or clinical); endothelial cell (EC), non-endothelial cell (non-EC) lines and *in vivo* models used; assays employed; and the type of data reported (quantitative, qualitative, or both) for assessing endothelial formation and migration processes (EFMPs).

Study Code	Soft Tissue Type	Includes *in vitro* work	Includes *in vivo* work	Includes *ex vivo* work	Includes clinical work	Endothelial Cell Lines Used	Non-Endothelial Cell Lines Used	*In Vivo* Models Used	Assays for Evaluation of Endothelial Formation & Migration Processes	Type of Data on Endothelial Formation and Migration Processes
SR01	Cardiac Muscle	Yes	Yes	No	No	N/A	Human Amniotic Mesenchymal Stromal Cells (hAMSCs)	N/A	mRNA Expression	Quantitative
SR02	Cardiac Muscle	Yes	No	No	No	Calf Pulmonary Artery Endothelial Cells (PAECs)	Bovine (Corneal) Fibroblasts; Bovine (Retinal) Pericytes; Bovine (Pulmonary Artery) Vascular Smooth Muscle Cells (VSMCs)	N/A	Imaging	Quantitative & Qualitative
SR03	Nervous Tissue	Yes	Yes	No	No	Human Endothelial Colony Forming Cells (ECFCs)	Human Vascular Smooth Muscle Cells (vSMCs)	N/A	Confocal Imaging; Immunostaining & Immunofluorescence Staining	Quantitative & Qualitative
SR04	Skin	Yes	Yes	No	No	N/A	N/A	Lewis Rat	Brightfield Imaging; Immunohistochemistry	Quantitative & Qualitative
SR05	Cardiac Muscle	Yes	Yes	No	No	N/A	Human (Subcutaneous) Preadipocytes	White-Leghorn (Eggs) Domestic Chicken	Histology; Histomorphometric Analysis	Quantitative & Qualitative
SR06	Vascular Tissue	Yes	No	No	No	Outgrowth endothelial cells (OECs) from human peripheral blood	Human Adipose Tissue-derived Stem Cells (ASCs); Mouse C2C12 Cells	N/A	ELISA; Image Analysis; Immunoblotting; Immunostaining & Immunofluorescence Staining; Tube Formation	Quantitative & Qualitative
SR07	Skin	Yes	Yes	No	No	Human Umbilical Vein Endothelial Cells (HUVECs)	Human Adipose Tissue-derived Stromal Cells (ASCs); Human Bone Marrow-derived Stromal Cells (BMSCs)	N/A	ELISA; Histomorphometric Analysis; Imaging; Immunocytochemistry	Quantitative & Qualitative
SR08	Microvasculature	Yes	No	No	No	Red Fluorescent Protein-expressing Human Umbilical Vein Endothelial Cells (RFP-HUVECs)	Human Adipose Tissue-derived Stem Cells (ASCs)	N/A	Fluorescent Imaging; Image Analysis	Quantitative & Qualitative
SR09	Cardiac Muscle	No	Yes	No	No	N/A	Human Alveolar Periosteal Cells (hAPCs)	BALB/c-nu/nu Mouse	Cytology; Histology; Immunohistochemistry	Qualitative
SR10	Skin	Yes	No	No	Yes	Canine (External Jugular Vein) Endothelial Cells (ECs)	Canine (Carotid Artery) Smooth Muscle Cells (SMCs)	N/A	Angiogenesis Assay; Co-culture Agregate Assay; Histology; Immunostaining & Immunofluorescence Staining	Quantitative & Qualitative
SR11	Vascular Tissue	Yes	Yes	No	No	N/A	Human Adipose-derived Stromal Cells (hADSCs); Human Umbilical Cord Multipotent Mesenchymal Stromal Cells (hUC MMSCs)	N/A	3D Angiogenesis Assay; Imaging; Immunocytochemical Staining; Morphometeric Analysis; RT-PCR	Quantitative & Qualitative
SR12	Skin	Yes	Yes	No	No	Bovine Aortic Endothelial Cells (BAECs)	Skin Fibroblasts (SF)	N/A	Angiogenesis Assay; Histology; Imaging; RT-PCR	Quantitative & Qualitative
SR13	Skin	Yes	Yes	No	No	Human Embryonic Stem Cell-derived Endothelial Cells (hESC-ECs)	Human Embryonic Stem Cell-derived Smooth Muscle Cells (hESC-SMCs)	Yorkshire Pig Swine; NOD/SCIDγc$^{-/-}$ Mouse	Histology; Imaging; Immunostaining & Immunofluorescence Staining; Tube Formation	Quantitative & Qualitative
SR14	Spinal Cord Tissue	No	Yes	No	No	Human Lymphatic Endothelial Cells (hLECs); Human Dermal Microvascular Endothelial Cells (HDMECs)	Human (Foreskin) Dermal Fibroblasts (DFs)	nu/nu Rat	Image Analysis; Imaging; Immunostaining & Immunofluorescence Staining	Qualitative
SR15	Vascular Tissue	Yes	No	No	No	N/A	N/A	CD-1 Mouse	Histology	Quantitative & Qualitative
SR16	Skin	Yes	Yes	No	No	Human Umbilical Vein Endothelial Cells (HUVECs)	Human Amniotic Fluid-derived Stem Cells (AFSs); Human Bone Marrow-derived Mesenchymal Stem Cells (MSCs)	nu/nu Mouse	Histology; Immunohistochemistry; Migration Assay	Quantitative & Qualitative
SR17	Skin	Yes	Yes	No	No	N/A	Human Adult Dermal Fibroblasts (HDFa)	Swiss Albino Mouse	Histology; Immunohistochemistry	Quantitative & Qualitative
SR18	Ovarian	No	Yes	No	No	N/A	Human Adipose-derived Stromal Cells (ASCs)	Athymic Nude Mouse	ELISA; Histology; Image Analysis; Imaging	Quantitative & Qualitative
SR19	Cardiac Muscle	No	Yes	No	No	N/A	Human Embryonic Stem Cell-derived Cardiomyocytes (hESC-CMs); Human Induced Pluripotent Stem Cell-derived Cardiomyocytes (hiPSC-CMs); Human Dermal Fibroflasts (HDF)	Yorkshire Pig Swine	Histology; Image Analysis; Imaging; Immunostaining & Immunofluorescence Staining; RT-PCR	Quantitative & Qualitative
SR20	Skin	Yes	Yes	No	No	Porcine Aortic Endothelial Cells (PAOECs)	Mouse NIH/3T3 Fibroblasts; Porcine Epicardial Adipose Tissue-derived Fibroblasts; Porcine Myocardial Fibroblasts	N/A	Angiogenesis Assay	Quantitative & Qualitative
SR21	Skin	No	Yes	No	No	N/A	Human Fibroblasts	C57BL/6 Mouse	Immunohistochemistry	Quantitative & Qualitative
SR22	Vascular Tissue	Yes	No	No	No	N/A	Rat Aortic Vascular Smooth Muscle Cells (VSMCs)	Sprague-Dawley Rat	Immunohistochemistry	Quantitative & Qualitative
SR23	Skeletal Muscle	Yes	Yes	No	No	N/A	Porcine Subcutaneous Adipose-derived Stem Cells (ASCs)	Yorkshire Pig Swine	Immunohistochemistry; Western Blot	Quantitative & Qualitative
SR24	Skeletal Muscle	Yes	No	No	No	Human Umbilical Vein Endothelial Cells (HUVECs)	Human Dermal Fibroblasts	N/A	Image Analysis	Quantitative & Qualitative
SR25	Microvasculature	Yes	No	No	No	N/A	Human Bone Marrow-derived Mesenchymal Stem Cells (hMSCs)	BALB/c Nude Mouse	Immunohistochemistry	Qualitative
SR26	Cardiac Muscle	Yes	Yes	Yes	No	Green Fluorescent Protein-expressing Human Umbilical Vein Endothelial Cells (GFP-HUVECs)	Human Adipose-derived Stromal Cells (ASCs)	N/A	Fluorescent Imaging; Imaging; Quantitative Real-Time RT-PCR	Quantitative & Qualitative
SR27	Vascular Tissue	Yes	No	No	No	Green Fluorescent Protein-expressing Human Umbilical Vein Endothelial Cells (GFP-HUVECs)	Human Muscle Cells	N/A	Angiogenesis Assay	Quantitative & Qualitative
SR28	Cardiac Muscle	Yes	No	No	No	N/A	Mouse T17b Embryonal Endothelial Progenitor Cells (eEPCs)	Lewis Rat	Immunohistochemistry	Quantitative & Qualitative
SR29	Skin	Yes	Yes	No	No	N/A	Human Adipose Stromal Vascular Fraction (SVF)-derived Preadipocytes	Athymic Mouse	Immunohistochemistry	Quantitative & Qualitative
SR30	Skin	Yes	Yes	No	No	Human Adipose Stromal Vascular Fraction (SVF)-derived Endothelial Cells	Human Dermal Fibroblasts	N/A	Immunostaining & Immunofluorescence Staining	Quantitative & Qualitative
SR31	Cardiac Muscle	Yes	Yes	No	No	N/A	Human Discarded Burn Skin Adipose-derived Stem Cells (dsASCs)	Rowett Nude Rat	Histology; Immunochemistry	Quantitative & Qualitative
SR32	Vascular Tissue	Yes	No	No	No	N/A	Mouse Green Fluorescent Protein-labelled Adipose-derived Stem Cells (GFP-ADSCs)	GFP Transgenic Mouse; Sprague-Dawley Rat	Immunostaining & Immunofluorescence Staining	Quantitative
SR33	Skin	Yes	Yes	No	No	Human Dermal Microvascular Endothelial Cells (HMEC-1)	N/A	N/A	Fluorescent Imaging	Quantitative & Qualitative
SR34	Soft Tissue (Unspecified)	Yes	Yes	No	No	Human Endothelial Colony-Forming Cells (ECFCs)	Human Vascular Smooth Muscle Cells (vSMCs); Human Placental Pericytes	N/A	Imaging; Immunostaining & Immunofluorescence Staining	Qualitative
SR35	Cardiac Muscle	Yes	Yes	No	No	Human Umbilical Vein Endothelial Cells (HUVECs)	Human Endothelial Progenitor Cells (EPCs) from Peripheral Blood Mononuclear Cell-derived (PBMC)	N/A	Tube Formation	Quantitative & Qualitative
SR36	Skin	Yes	Yes	No	No	Human Dermal Microvascular Endothelial Cells (HDMECs)	N/A	White Yorkshire Pig Swine	Northern Blot Hybridisation; RNA Isolation	Quantitative
SR37	Dental Pulp	No	Yes	No	No	N/A	N/A	Sewall Wright Inbred Strain 2 Guinea Pig	Imaging; Immunostaining & Immunofluorescence Staining	Qualitative
SR38	Vascular Tissue	Yes	No	No	No	N/A	N/A	Sprague-Dawley Nude Crl: NIH-Foxn1^{rnu} Rat; Sprague-Dawley RjHan:SD Rat	Immunochemistry	Quantitative & Qualitative
SR39	Vascular Tissue	Yes	No	No	No	N/A	Human Adipose-derived Stem Cells (ASCs)	N/A	Calcein AM Staining; Imaging	Quantitative & Qualitative
SR40	Vascular Tissue	Yes	No	No	No	N/A	Rat H9c2 Cells	C57BL/6 Mouse	Immunohistochemistry	Quantitative & Qualitative
SR41	Skin	Yes	Yes	No	No	N/A	Rat DiI-labelled Fluorescent Adipose-derived Stem Cells (ADSCs)	Lewis Rat	Immunochemistry	Qualitative
SR42	Skin	Yes	Yes	No	No	Human Umbilical Vein Endothelial Cells (HUVECs)	Human Skin Dermal Fibroblasts (sFb); Human Immortalised N-TERT Epidermal Keratinocytes; Human Mesenchymal Stem Cells (MSCs); Human Subcutaneous Adipose-derived Stromal Cells (sadSC)	Unspecified Mouse	Immunostaining & Immunofluorescence Staining	Quantitative & Qualitative
SR43	Skin	Yes	Yes	Yes	No	Human Umbilical Vein Endothelial Cells (HUVECs)	N/A	Swiss Albino Mouse	3D Angiogenesis Assay; Semi qRT-PCR	Quantitative & Qualitative
SR44	Connective Tissue	Yes	Yes	No	No	N/A	N/A	Athymic Mouse	ELISA; Histology; Immunostaining & Immunofluorescence Staining; RT-PCR	Quantitative & Qualitative
SR45	Skin	Yes	Yes	No	No	Human Dermal Microvascular Endothelial Cells (HDMVECs)	Human Preadipocytes	N/A	Immunostaining & Immunofluorescence Staining;	Quantitative & Qualitative
SR46	Vascular Tissue	Yes	No	No	No	Human Umbilical Vein Endothelial Cells (HUVECs)	N/A	Crl:CD1 Foxn1^{rnu} Nude Mouse; Sprague-Dawley Rat; BALB/c nu/nu Nude Mouse; CB.17 SCID Mouse	ELISA; Histology; Imaging; Immunostaining & Immunofluorescence Staining	Quantitative & Qualitative
SR47	Adipose Tissue	Yes	Yes	No	No	N/A	Human I6 Embryonic Stem Cell (ESC)-derived Cardiac Progenitors	N/A	Histology; Immunohistochemistry	Qualitative
SR48	Cardiac Muscle	Yes	Yes	No	No	Human Microvascular Endothelial Cells (HMECs)	N/A	N/A	Confocal Imaging	Qualitative
SR49	Cardiac Muscle	Yes	No	No	No	Human Umbilical Vein Endothelial Cells (HUVECs); Green Fluorescent Protein-expressing Human Umbilical Vein Endothelial Cells (GFP-HUVECs)	Human Endothelial Progenitor Cells (EPCs) from Peripheral Blood Mononuclear Cell-derived (PBMC); Human Adipose-derived Stem Cells (ASCs)	N/A	Angiogenesis Protein Array; Immunostaining & Immunofluorescence Staining	Quantitative & Qualitative
SR50	Skin	No	Yes	No	No	N/A	Human Adipose-derived Mesenchymal Stromal Cells (ADSCs)	C57/B6 Mouse	ELISA; Fluorescence-Activated Cell Sorting; Histology; Immunohistochemistry; Quantitative Real-Time RT-PCR	Qualitative
SR51	Adipose Tissue	Yes	Yes	No	No	N/A	Human Adipose-derived Stem Cells (hADSCs); Rat Islets	Athymic Mouse	Immunohistochemistry; Proteome Profiler Human Angiogenesis Antibody Array	Quantitative & Qualitative
SR52	Skin	No	Yes	No	No	N/A	Rat Adipose-derived Mesenchymal Stem Cells (ADSCs); Normal Human Epidermal Keratinocytes (NHEK)	Wistar Rat	Histomorphometric Analysis; Immunohistochemistry	Quantitative & Qualitative
SR53	Fibrovascular Tissue	Yes	Yes	No	No	Human Umbilical Vein Endothelial Cells (HUVECs)	Human Embryonic Kidney 293 Cells (293T3)	BALB/c Mouse	Histology; Immunostaining & Immunofluorescence Staining; Immunohistochemistry	Quantitative & Qualitative

Study Code (cont.)	Soft Tissue Type (cont.)	Includes *in vitro* work (cont.)	Includes *in vivo* work (cont.)	Includes *ex vivo* work (cont.)	Includes clinical work (cont.)	Endothelial Cell Lines Used (cont.)	Non-Endothelial Cell Lines Used (cont.)	*In Vivo* Models Used (cont.)	Assays for Evaluation of Endothelial Formation & Migration Processes (cont.)	Type of Data on Endothelial Formation and Migration Processes (cont.)
SR54	Vascular Tissue	Yes	No	No	No	Human Endothelial Colony-Forming Cells (ECFCs)	N/A	Fox Chase SCID Beige Mouse	Histology; Imaging; Immunostaining & Immunofluorescence Staining	Quantitative & Qualitative
SR55	Skin	No	Yes	No	No	Human Umbilical Vein Endothelial Cells (HUVECs)	Human Monocytes derived from Peripheral Blood Mononuclear Cell-derived (PBMC)	CD1 nu/nu Mouse	Immunostaining & Immunofluorescence Staining	Quantitative & Qualitative
SR56	Cardiac Muscle	No	Yes	No	No	Human Umbilical Vein Endothelial Cells (HUVECs)	Baboon Smooth Muscle Cells (SMCs)	Sprague-Dawley Rat	Confocal Imaging; ELISA	Quantitative & Qualitative
SR57	Vascular Tissue	Yes	No	No	No	Human Umbilical Vein Endothelial Cells (HUVECs)	N/A	WAG/Rij|Hsd Rat	Angiogenesis Assay; Tube Formation	Quantitative & Qualitative
SR58	Skin	No	Yes	No	No	Calf Calf Pulmonary Artery-derived Endothelial Cells; Bovine Brain Capillary Endothelial Cells (BBE); Bovine Adrenocortical Microvascular Endothelial Cells (ACE)	Bovine Vascular Smooth Muscle Cells (vSMCs); Bovine Corneal Fibroblasts; Bovine Retinal Pericytes	N/A	Angiogenesis *In Situ*	Qualitative
SR59	Adipose Tissue	No	Yes	No	No	N/A	Human Dermal Fibroblasts; Human Epidermal Keratinocytes	Athymic Mouse	Imaging; Immunohistochemistry	Qualitative
SR60	Soft Tissue (Unspecified)	No	Yes	No	No	N/A	Rat Endothelial Progenitor Cells (EPCs) from Bone Marrow Mononuclear Cells; Rat Green Fluorescent Protein-expressing Endothelial Progenitor Cells (GFP-EPCs) from Bone Marrow Mononuclear Cells	Wistar Rat	Histochemistry; Histology; Immunostaining & Immunofluorescence Staining	Quantitative & Qualitative
SR61	Skin	Yes	No	No	No	Sheep Jugular Vein-derived Endothelial Cells	N/A	Unspecified Sheep	Immunostaining & Immunofluorescence Staining; Transmission Electron Microscopy	Quantitative & Qualitative
SR62	Soft Tissue (Unspecified)	Yes	No	No	No	Green Fluorescent Protein-expressing Human Umbilical Vein Endothelial Cells (GFP-HUVECs)	Human Adipose Tissue-derived Mesenchymal Stem Cells (AD-hMSCs)	N/A	Dextran Assay; Fluorescent Imaging; Confocal Imaging; Image Analysis	Quantitative & Qualitative
SR63	Skin	No	Yes	No	No	N/A	N/A	nu/nu Mouse	Histology; Immunohistochemistry; Morphometeric Analysis	Quantitative & Qualitative
SR64	Skin	Yes	No	No	No	N/A	N/A	Fischer 344 Rat	Immunohistochemistry	Quantitative
SR65	Adipose Tissue	No	Yes	No	No	N/A	Human Adipose Tissue-derived Stem Cells (ASCs)	SCID Mouse	Immunohistochemistry	Quantitative & Qualitative
SR66	Skin	Yes	Yes	No	No	N/A	N/A	New Zealand White European Rabbit	Histopathology	Quantitative
SR67	Skeletal Muscle	Yes	Yes	No	No	N/A	Porcine Bone Marrow-derived Mesenchymal Stem Cells (MSCs)	Yorkshire Pig Swine	Histology; Quantitative Real-Time RT-PCR	Quantitative & Qualitative
SR68	Vascular Tissue	Yes	No	No	No	N/A	N/A	New Zealand White European Rabbit	Alkaline Phosphatase Assay	Quantitative & Qualitative
SR69	Cardiac Muscle	Yes	Yes	No	No	Human Umbilical Vein Endothelial Cells (HUVECs)	Rat PC12 Cells	Sprague-Dawley Rat	Immunohistochemistry	Quantitative & Qualitative
SR70	Skin	No	Yes	No	No	Green Fluorescent Protein-expressing Human Umbilical Vein Endothelial Cells (GFP-HUVECs)	N/A	BALB/c-nu Mouse	Immunostaining & Immunofluorescence Staining	Qualitative
SR71	Vascular Tissue	Yes	No	No	No	N/A	N/A	Sprague-Dawley Crl:CD Rat	Histology	Qualitative
SR72	Cardiac Muscle	No	Yes	No	No	N/A	N/A	Sprague-Dawley Rat	Immunocytochemistry; Immunostaining & Immunofluorescence Staining; Confocal Imaging	Quantitative & Qualitative
SR73	Soft Tissue (Unspecified)	Yes	Yes	No	No	N/A	Green Fluorescent Protein-expressing Human Preadipocytes	White-Leghorn (Eggs) Domestic Chicken	Histomorphometric Analysis	Quantitative & Qualitative
SR74	Skeletal Muscle	No	Yes	No	No	N/A	Rat Adipose-derived Stem Cells (ADSCs)	N/A	Histology; Immunostaining & Immunofluorescence Staining	Qualitative
SR75	Vascular Tissue	Yes	No	No	No	Human Dermal Microvascular Endothelial Cells (HMEC-1)	Human Dermal Fibroblasts	N/A	Tube Formation	Quantitative & Qualitative
SR76	Skin	Yes	Yes	No	No	Human Umbilical Vein Endothelial Cells (HUVECs)	Neonatal Mouse Cardiomyocyte-derived iPS Cells (iPS); Mouse MMP9-secreting iPS Cells (MiPS); Mouse PlGF-secreting iPS Cells (PiPS)	NOD-SCID Mouse	Angiogenesis Assay; Fluorescence-Activated Cell Sorting; Histology; Immunostaining & Immunofluorescence Staining; Quantitative Real-Time RT-PCR	Quantitative & Qualitative
SR77	Cardiac Muscle	Yes	No	No	No	N/A	Mouse C2C12 Cells	SCID Nude Hairless Outbred Mouse	Angiogenesis Assay; Histology; Immunohistochemistry	Quantitative & Qualitative
SR78	Vascular Tissue	No	Yes	No	No	N/A	Human Dermis-derived Fibroblasts; Human Oral Mucosa-derived Fibroblasts	Nude Mouse	Histology; Migration Assay	Qualitative
SR79	Vascular Tissue	Yes	No	No	No	Human Umbilical Vein Endothelial Cells (HUVECs); Green Fluorescent Protein-expressing Human Umbilical Vein Endothelial Cells (GFP-HUVECs)	Cardiomyocytes from Human Induced Pluripotent Stem Cells (CM-iPSCs)	N/A	Fluorescent Imaging	Quantitative & Qualitative
SR80	Vascular Tissue	Yes	No	No	No	Human Umbilical Vein Endothelial Cells (HUVECs)	Human Adipose Tissue-derived Stem Cells (ASCs)	Athymic Nude Mouse	Histology; Immunohistochemistry; Immunostaining & Immunofluorescence Staining	Qualitative
SR81	Vascular Tissue	No	Yes	No	No	N/A	Human Neonatal Foreskin Keratinocytes; Human Immortalised HaCaT Keratinocytes; Mouse 3T3-J2 Fibroblasts	Athymic nu/nu Mouse	Histology; Immunohistochemistry	Quantitative & Qualitative

Table B.4: **Overview of the key scaffold formulation details, highlighting the heterogeneity of the corpus.** For each article, details are provided on the fibrinogen, coagulant and crosslinker used (including concentration and formulation stage at which it was incorporated). The inclusion of additional materials beyond fibrinogen, coagulants and crosslinkers is categorised by type: Polymers; Growth Factors, Peptides, Amino Acids & Enzymes (GF/P/AA/E), Cell Media & Solutions, Chemicals, and Other Materials. For each category, the number of distinct materials incorporated into the formulation is reported. The table also summarises the type of manufactured object used and its associated features, whether cells were pre-embedded within the scaffold, and the factors (with concentrations) added to the standard cell medium.

Study Code	Fibrin Concentration and Formulation Stage	Coagulant, with Concentration and Formulation Stage	Crosslinker, with Concentration and Formulation Stage	Were Additional Materials Used in the Formulation?	Number of Different Polymers (Natural & Synthetic) Used	Number of Different Growth Factors, Peptides, Amino Acids & Enzymes Used	Number of Different Cell Media & Solutions Used	Number of Different Chemicals Used	Number of Different Materials Used (Others)	Manufactured Object	Manufactured Object Features	Were Cells Pre-embedded into the Scaffold?	Factors Added to the Standard Cell Medium with Concentrations
SR01	Not Specified	Not Used or Non Specified	Not Used or Non Specified	Yes	1	3	N/A	N/A	N/A	Scaffold	3D; Bilayered; Biodegradable; Randomly Oriented Nanofibres; Cell-embedded	Yes	N/A
SR02	10 mg/ml (Final)	Thrombin (11 µl at 100 U/ml; Stock)	*NaCl* (NS; Not Specified)	Yes	N/A	3	N/A	N/A	1	Gel	3D; Coated; Microcarrier-embedded; Cell-embedded	Yes	N/A
SR03	Not Specified	Thrombin (NS; Not Specified)	Not Used or Non Specified	Yes	1	N/A	N/A	N/A	N/A	Hydrogel	3D; Microfibre-embedded; Cell-embedded	Yes	VEGF (50 ng/ml)
SR04	2 wt% (Stock)	Thrombin (10 U/ml; Stock)	$CaCl_2$ (50 mM; Stock)	No	N/A	N/A	N/A	N/A	N/A	Implant	3D; Bilayered; Acellular	No	N/A
SR05	Not Specified	Thrombin (500 U/ml; Stock)	Not Used or Non Specified	Yes	N/A	4	N/A	N/A	N/A	Matrix	3D; Composite; Cell-embedded	Yes	Aprotinin (200 U/ml); Aprotinin (200 U/ml) + hr-bFGF (50 ng/ml) + hr-VEGF (40 ng/ml)
SR06	Not Specified	Thrombin (NS; Not Specified)	Not Used or Non Specified	Yes	N/A	N/A	1	N/A	1	Hydrogel	3D; Cytodex Bead-embedded; Cell-embedded	Yes	Aprotinin (100 KIU/ml)
SR07	20 mg/ml (Stock)	Thrombin (4 U/ml; Stock)	Not Used or Non Specified	No	N/A	N/A	N/A	N/A	N/A	Hydrogel	Spheroid-embedded; 3D; Cell-embedded	Yes	VEGF (50 ng/ml)
SR08	10 mg/ml (Not Specified)	Thrombin (50 U/ml; Stock)	$CaCl_2$ (150 mM; Stock)	Yes	N/A	2	1	N/A	N/A	Bioartificial Tissue Construct	3D; Cell-embedded	Yes	Aprotinin (100 U/ml) + L-Ascorbic Acid-2-Phosphate (50 µg/ml) + FGF (40 ng/ml) + VEGF (40 ng/ml)
SR09	36.59 or 23.59 mg/ml (Stock)	Thrombin (223 kIU/ml or 144.6 kIU/ml; Stock)	Not Used or Non Specified	Yes	1	N/A	N/A	N/A	N/A	Sponge	3D; Coated; and either Acellular or Cell-embedded	Both	N/A
SR10	2.5 mg/ml (Stock)	Thrombin (2.5 U/ml; Final)	Not Used or Non Specified	Yes	1	N/A	1	N/A	N/A	Hydrogel	3D; Bilayered; Cell-embedded; Cell Aggregate-embedded	Yes	Amphotericin (0.25 µg/ml) + Aprotinin (100 kIU/ml) + Heparan Sulfate (5 U/ml); Amphotericin (0.25 µg/ml) + Aprotinin (100 kIU/ml) + Heparan Sulfate (5 U/ml) + Methocel Solution (20%)
SR11	3 mg/ml (Final)	Thrombin (30 U/ml; Stock)	$CaCl_2$ (100 M; Stock)	Yes	1	N/A	N/A	N/A	N/A	Hydrogel	3D; Encapsulated Spheroids; Cell-embedded	Yes	N/A
SR12	10 mg/ml (Final)	Thrombin (50 U/ml; Final)	Not Used or Non Specified	Yes	N/A	1	N/A	N/A	1	Hydrogel	3D; Embedded Beads; Cell-embedded	Yes	Angiopoietin-1 (1-125 ng/ml) + bFGF (25 ng/ml) + TGF-β (0.5-2 ng/ml) + VEGF (25 ng/ml)
SR13	8 mg/ml (Final)	Thrombin (2 U/ml; Final)	Ca^{2+} (2.5 mmol/L; Final)	Yes	N/A	N/A	N/A	1	N/A	Patch	3D; Cell-embedded	Yes	N/A
SR14	0.02 (Stock)	Thrombin (100 IU/ml; Final)	Not Used or Non Specified	No	N/A	N/A	N/A	N/A	N/A	Hydrogel	3D; Cell-embedded	Yes	N/A
SR15	0.2 mg/ml (Stock)	Thrombin (0.2 ml; Stock)	*NaCl* (0.009; Stock)	Yes	3	2	2	N/A	N/A	Matrix	3D; Composite; Acellular	No	N/A
SR16	Not Specified	Thrombin (20 µl; Stock)	Not Used or Non Specified	Yes	1	N/A	N/A	N/A	N/A	Hydrogel	3D; Bioprinted; Cell-embedded	Yes	N/A
SR17	20 mg/ml (Final)	Thrombin (1250 U/ml; Not Specified)	$CaCl_2$ (275 mM; Not Specified)	Yes	2	N/A	N/A	N/A	N/A	Scaffold	3D; Chemically-Uncrosslinked; Freeze-dried; Composite; and either Acellular or Cell-embedded	Both	N/A
SR18	Not Specified	Not Used or Non Specified	Not Used or Non Specified	No	N/A	N/A	N/A	N/A	N/A	Gel	3D; Spheroid-embedded; Acellular	No	Dexamethasone (1 µM) + Foetal Calf Serum (10%) + Gentamycin (0.5%) + Indomethacin (0.2 mM) + Insulin (0.01 mg/ml) + 3-isobutyl- l-methyl-xanthine (0.5 mM)
SR19	1 mg/ml (Not Specified)	Thrombin (0.3 U/ml; Not Specified)	Not Used or Non Specified	Yes	1	2	N/A	N/A	N/A	Hydrogel	3D; Macrosized; Composite; Cell-embedded	Yes	N/A
SR20	Not Specified	Thrombin (NS; Not Specified)	Not Used or Non Specified	Yes	N/A	10	1	N/A	N/A	Gel	3D; Serum-free; Microcarrier-embedded; Cell-embedded	Yes	Insulin (1 µg/ml) + Penicillin (100 U/ml) + Selenium (1 ng/ml) + Streptomycin (100 g/ml) + Transferrin (1 µg/ml)
SR21	20 mg/ml (Not Specified)	Thrombin (50 IU/ml; Not Specified)	Not Used or Non Specified	Yes	1	2	N/A	N/A	N/A	Gel	3D; Composite; Acellular	No	N/A
SR22	1.5 mg/ml (Final)	Thrombin (0.6 U/ml; Stock)	Not Used or Non Specified	No	N/A	N/A	N/A	N/A	N/A	Hydrogel	3D; Acellular	No	N/A
SR23	2 wt% (Stock)	Thrombin (5 U/ml; Stock)	*CaCl2* (50 mM; Stock)	Yes	1	N/A	N/A	N/A	N/A	Hydrogel	3D; Composite; Cell-embedded; Meshed	Yes	N/A
SR24	Not Specified	Not Used or Non Specified	Not Used or Non Specified	Yes	N/A	N/A	1	N/A	N/A	Gel	3D; Thick; Cytodex Bead-embedded; Cell-embedded	Yes	Aprotinin (0.15 U/mL)
SR25	70 - 110 mg/ml (Stock)	Thrombin (37 U/ml; Not Specified)	$CaCl_2$ (40 mmol; Stock)	No	N/A	N/A	N/A	N/A	N/A	Gel	3D; Layered; Cell Sheet-stacked; Cell-embedded	Yes	N/A
SR26	2.5 mg/ml (Final)	Thrombin (0.2 U/ml; Final)	Not Used or Non Specified	No	N/A	N/A	N/A	N/A	N/A	Hydrogel	3D; Cell-embedded; Co-culture	Yes	Aprotinin (100 KIU/ml)
SR27	6 mg/ml (Stock)	Thrombin (0.32 U/ml; Stock)	Not Used or Non Specified	Yes	N/A	N/A	N/A	N/A	1	Hydrogel	3D; Co-culture; Cell-embedded	Yes	Aprotinin (92.5 µg/ml) + Tranexamic acid (400 µM)
SR28	5 mg/ml (core matrix with cells) surrounded by 25 mg/ml (acellular capsule) (Final)	Thrombin (2.5 U/ml; Stock)	$CaCl_2$ (40 mM ; Stock)	No	N/A	N/A	N/A	N/A	N/A	Gel	3D; Cell-embedded	Yes	N/A
SR29	2.5 mg/ml (Stock)	Thrombin (0.32 U/ml; Stock)	Not Used or Non Specified	Yes	1	2	N/A	N/A	1	Gel	3D; Cell-embedded	Yes	N/A
SR30	1 mg (Not Specified)	Thrombin (0.2 U; Not Specified)	Not Used or Non Specified	Yes	1	N/A	N/A	N/A	N/A	Hydrogel	3D; Multilayered; Cell-embedded; Composite	Yes	N/A
SR31	2.5 mg/ml (Stock)	Thrombin (0.625 U/well; Stock)	Not Used or Non Specified	Yes	1	N/A	N/A	N/A	N/A	Hydrogel	3D; Composite; Cell-embedded	Yes	N/A
SR32	25 mg/ml (Stock)	Thrombin (75 NIH U/ml; Stock)	$CaCl_2$ (4 ml; Stock)	No	N/A	N/A	N/A	N/A	N/A	Gel	3D; Composite; Cell-embedded	Yes	N/A
SR33	3 mg/ml (Stock)	Thrombin (50 U/ml; Stock)	Not Used or Non Specified	Yes	N/A	2	N/A	N/A	N/A	Gel	3D; Microcarrier Bead-embedded; Cell-embedded	Yes	N/A
SR34	50 mg/ml (Stock)	Thrombin (20 IU/ml; Stock)	Not Used or Non Specified	Yes	2	N/A	N/A	N/A	N/A	Microfibre Hydrogel	3D; Multicellular; Multilayered; Cell-embedded	Yes	Aminocaproic Acid (30 mM) + VEGF (50 ng/ml)
SR35	0.01 v/v% (Final)	Not Used or Non Specified	Not Used or Non Specified	No	N/A	N/A	N/A	N/A	N/A	Gel	3D; Cell-embedded	Yes	N/A
SR36	Not Specified	Thrombin (NS; Not Specified)	Not Used or Non Specified	Yes	N/A	2	1	N/A	N/A	Gel	3D; Overlay on Cells	Yes	bFGF (50 ng/ml) + VEGF (100 ng/ml)
SR37	24 mg/ml (Stock)	Thrombin (5 IU/ml; Stock)	Not Used or Non Specified	No	N/A	N/A	N/A	N/A	N/A	Gel	3D; Acellular	No	N/A
SR38	1 mg/ml (Stock)	Thrombin (0.625 U/ml; Stock)	Not Used or Non Specified	Yes	N/A	5	N/A	N/A	N/A	Hydrogel	3D; Factor-decorated; *In Situ*; Acellular	No	N/A
SR39	9.4, 94.3 or 188.6 mg/ml (Stock)	Thrombin (3.3, 33.3 or 66.66 mg/ml; Stock)	$CaCl_2$ (5.9 mg/ml; Not Specified)	Yes	1	N/A	N/A	N/A	N/A	Hydrogel	3D; Composite; Cell-embedded	Yes	N/A
SR40	Not Specified	Thrombin (NS; Not Specified)	Not Used or Non Specified	Yes	N/A	1	1	N/A	N/A	Patch	3D; NRG-1-loaded; Composite; Nanometric Fibrous Structure; Acellular	No	N/A
SR41	11/mg/ml (Stock)	Thrombin (1 kU/ml; Stock)	$CaCl_2$ (40 mM ; Stock)	No	N/A	N/A	N/A	N/A	N/A	Glue	3D; *In Situ*; Cell-embedded	Yes	N/A
SR42	2.5 mg/ml (Stock)	Thrombin (50 U/ml; Stock)	Not Used or Non Specified	Yes	1	N/A	N/A	N/A	N/A	Sponge	3D; Composite; Interconnected Porous Structure; Slow Degradation; Stabilised; Freeze-dried; Cell-embedded	Yes	N/A
SR43	2.5, 5, 10 or 20 mg/ml (Not Specified)	Thrombin (0.2 IU/ml; Not Specified)	Not Used or Non Specified	Yes	1	N/A	N/A	N/A	N/A	Hydrogel	3D; Composite; Microtissue-based; Cell-embedded	Yes	N/A
SR44	2 mg/ml (Not Specified)	Thrombin (4 U/ml; Not Specified)	Not Used or Non Specified	Yes	N/A	N/A	N/A	N/A	1	Hydrogel	3D; Nanosphere-embedded; Acellular	No	N/A
SR45	10 mg/ml (Not Specified)	Thrombin (2 IU/ml; Not Specified)	Not Used or Non Specified	Yes	N/A	5	1	N/A	N/A	Matrix	3D; Bilayered; Cell-embedded; Spheroid-embedded	Yes	N/A
SR46	100 mg/ml (Stock)	Thrombin (500 IU/ml; Stock)	$CaCl_2$ (5.9 mg/ml; Stock)	Yes	N/A	3	N/A	N/A	N/A	Hydrogel	3D; VEGF Controlled Delivery; *In Situ*; Acellular	No	N/A
SR47	10 mg/ml (Final)	Thrombin (100 U/ml; Stock)	Not Used or Non Specified	No	N/A	N/A	N/A	N/A	N/A	Patch	3D; Cell-embedded	Yes	N/A
SR48	40 mg/ml (Stock)	Thrombin (10 U/ml; Final)	$CaCl_2$ (40 mM; Not Specified)	Yes	N/A	N/A	N/A	1	2	Gel	3D; Ordered Nano-structured; Microbead-embedded; Magnetically guided; Self-assembled; Acellular	No	N/A
SR49	1.5 mg/ml (Not Specified)	Thrombin (0.625 NIH U/ml; Not Specified)	Not Used or Non Specified	No	N/A	N/A	N/A	N/A	N/A	Gel	3D; Co-culture; Cell-embedded; (group 3 & 4)Cytodex Bead-embedded	Yes	Aprotinin (100 KIU/ml)
SR50	60 mg/ml (Stock)	Thrombin (1250 U/ml; Stock)	$CaCl_2$ (275 mM; Stock)	Yes	N/A	2	N/A	N/A	N/A	Gel	3D; Cell-embedded	Yes	N/A
SR51	2.5 - 25 mg/ml (Not Specified)	Thrombin (2 U/ml; Not Specified)	$CaCl_2$ (2.5 nM; Not Specified)	Yes	N/A	1	N/A	N/A	N/A	Gel	3D; Cell-embedded; Co-culture	Yes	N/A
SR52	32 mg/ml (Stock)	Thrombin (25 U/ml; Stock)	$CaCl_2$ (40 mM ; Stock)	Yes	1	N/A	N/A	N/A	N/A	Scaffold	3D; Nanofibrous; Bilayered; Electrospun; Acellular	No	N/A
SR53	10 or 20 mg/ml (Stock)	Thrombin (10 U/ml; Stock)	$CaCl_2$ (0.063 M; Stock)	Yes	N/A	2	N/A	N/A	1	Gel	3D; Peptide-DNA Nanoparticle-embedded; Acellular	No	N/A
SR54	0.1 (Stock)	Thrombin (50 U/ml; Stock)	$CaCl_2$ (7%) or $MgCl_6$ (3%) (0.07; Stock)	Yes	1	N/A	N/A	N/A	N/A	Microfibre Hydrogel	3D; Electrospun; Acellular; Small-diametre; Composite	No	N/A
SR55	4 mg/ml (Stock)	Thrombin (0.5 U/ml; Stock)	Not Used or Non Specified	Yes	1	2	N/A	N/A	1	Gel	3D; Functionalised; Composite; Porous; Freeze-dried; Acellular	No	N/A
SR56	Not Specified	Not Used or Non Specified	Not Used or Non Specified	Yes	N/A	3	N/A	N/A	N/A	Gel-Coacervate System	3D; Composite; Controlled Delivery System; Acellular	No	N/A

Study Code (cont.)	Fibrin Concentration and Formulation Stage (cont.)	Coagulant, with Concentration and Formulation Stage (cont.)	Crosslinker, with Concentration and Formulation Stage (cont.)	Were Additional Materials Used in the Formulation? (cont.)	Number of Different Polymers (Natural & Synthetic) Used (cont.)	Number of Different Growth Factors, Peptides, Amino Acids & Enzymes Used (cont.)	Number of Different Cell Media & Solutions Used (cont.)	Number of Different Chemicals Used (cont.)	Number of Different Materials Used (Others) (cont.)	Manufactured Object (cont.)	Manufactured Object Features (cont.)	Were Cells Pre-embedded into the Scaffold? (cont.)	Factors Added to the Standard Cell Medium with Concentrations (cont.)
SR57	70 - 110 mg/ml (Stock)	Thrombin (NS; Not Specified)	$CaCl_2$ (40 mM; Stock)	Yes	N/A	1	N/A	N/A	N/A	Matrix	3D; Cell-embedded	Yes	FGF-2 (10 ng/ml) + TNFa (10 ng/ml) + VEGF (25 ng/ml)
SR58	10 mg/ml (Stock)	Thrombin (2 U/ml; Stock)	$CaCl_2$ (2.5 or 5 mM; Stock)	Yes	N/A	3	1	N/A	N/A	Gel	3D; Co-culture; Cell-embedded	Yes	Aprotinin (200 U/ml) + bFGF (30 ng/ml) + VEGF (100 ng/ml)
SR59	2.5 mg/ml (Final)	Thrombin (4 U/ml; Stock)	$CaCl_2$ (NS; Not Specified)	Yes	N/A	2	1	N/A	N/A	Gel	3D; bFGF-treated; Acellular	No	N/A
SR60	Not Specified	Not Used or Non Specified	Not Used or Non Specified	No	N/A	N/A	N/A	N/A	N/A	Gel + Mesh	3D; Cell-embedded; Composite	Yes	N/A
SR61	10 wt% (Final)	Not Used or Non Specified	Not Used or Non Specified	No	N/A	N/A	N/A	N/A	N/A	Matrix	3D; Cell-embedded; *In Situ* Delivery	Yes	N/A
SR62	10 mg/ml (Not Specified)	Not Used or Non Specified	Not Used or Non Specified	Yes	1	N/A	1	N/A	N/A	Scaffold	3D; Macroporous; Freeze-dried; Coated; Cell-embedded; Co-culture	Yes	bFGF (10 or 20 ng/ml) + Human Serum (2%) + Hydrocortisone (20 ng/ml) + VEGF (10 or 20 ng/ml)
SR63	10 mg/ml (Stock)	Thrombin (20 U/ml; Stock)	$CaCl_2$ (50 mM; Stock)	Yes	1	1	N/A	N/A	N/A	Matrix	(1) 3D; Bilayered; Composite (2) 3D; Bilayered; Composite; Sealant Solution-Impregnated (3) 3D; Bilayered; Composite; VEGF and bFGF Growth Factor-embedded; Acellular	No	N/A
SR64	20 mg/ml (Stock)	Thrombin (100 IU/ml; Stock)	Not Used or Non Specified	Yes	N/A	2	N/A	N/A	N/A	Gel	3D; Porous; Acellular	No	N/A
SR65	20 mg/ml (Stock)	Thrombin (1 mg/ml; Stock)	$NaCl$ (0.009; Stock)	Yes	N/A	N/A	N/A	N/A	1	Scaffold	3D; Cell-embedded	Yes	N/A
SR66	2 mg/ml (Final)	Thrombin (0.5 U/ml; Final)	$CaCl_2$ (2.5 mM; Final)	Yes	1	N/A	N/A	N/A	N/A	Scaffold	3D; HA-modified; Composite; Sheet-based; Acellular	No	N/A
SR67	10 or 20 mg/ml (Final)	Thrombin (0.8 U/ml; Stock)	Not Used or Non Specified	Yes	N/A	2	N/A	2	N/A	Patch	3D; Composite; Flexible; Acellular	No	N/A
SR68	20 mg/ml (Not Specified)	Thrombin (3 U/ml; Final)	Not Used or Non Specified	Yes	1	2	N/A	N/A	1	Sealant	3D; Degradable; DNA-Delivery; VEGF-encoding; Acellular	No	N/A
SR69	5 mg/ml (Stock)	Thrombin (0.2 ml; Stock)	Not Used or Non Specified	Yes	1	N/A	N/A	N/A	1	Hydrogel	3D; Magnetic-responsive; Aligned; Nanoparticle-embedded; Acellular	No	N/A
SR70	12 µl (Stock)	Thrombin (NS; Not Specified)	Not Used or Non Specified	Yes	2	N/A	N/A	N/A	1	Hydrogel	3D; Composite; Bioprinted; Cell-embedded	Yes	6-Aminocaproic Acid (2mg/ml)
SR71	50 mg/ml (Stock)	Thrombin (50 U/ml; Stock)	Not Used or Non Specified	Yes	N/A	N/A	1	N/A	N/A	Gel	3D; *In Situ;* Acellular	No	N/A
SR72	100 mg/ml (Not Specified)	Thrombin (400 IU/ml; Not Specified)	Not Used or Non Specified	Yes	2	N/A	N/A	N/A	N/A	Microfibre Hydrogel	3D; Hierarchically Aligned; Nanofibre-based; Electrospun; Acellular	No	N/A
SR73	70 - 110 mg/ml (Stock)	Thrombin (500 IU/ml; Not Specified)	Not Used or Non Specified	Yes	N/A	2	1	N/A	N/A	Matrix	3D; Composite; and either Acellular or Cell-embedded	Both	Aprotinin (200 U/ml)
SR74	4 wt% (Stock)	Thrombin (15 U/ml; Stock)	$CaCl_2$ (50 mM; Stock)	Yes	2	N/A	1	N/A	N/A	Hydrogel	3D; Interconnected Channels; 3D Printed; Cell-embedded	Yes	N/A
SR75	0.01 (Stock)	Thrombin (20 U/ml; Stock)	$CaCl_2$ (50 mM; Not Specified)	Yes	N/A	4	N/A	N/A	N/A	Gel	3D; Cell-embedded	Yes	N/A
SR76	2 - 9 mg/ml (Stock)	Thrombin (37.5 U/ml; Final)	$CaCl_2$ (40 mmol; Stock)	Yes	1	N/A	N/A	N/A	N/A	Hydrogel	3D; PlGF-secreting; MMP9-secreting; Composite; Cell-embedded	Yes	N/A
SR77	6 mg/ml (Final)	Thrombin (1 U/ml; Stock)	Not Used or Non Specified	Yes	N/A	1	N/A	N/A	N/A	Gel	3D; HGF-loaded; Extruded Microthread-embedded; Acellular	No	N/A
SR78	Not Specified	Not Used or Non Specified	Not Used or Non Specified	Yes	N/A	1	N/A	N/A	N/A	Gel	3D; Acellular	No	N/A
SR79	70 mg/ml (Stock)	Thrombin (6 U/ml; Final)	$CaCl_2$ (40 mM; Stock)	Yes	1	N/A	N/A	N/A	N/A	Hydrogel	3D; Cell-embedded; Composite	Yes	EGM-2 Supplements, which are: Ascorbic Acid (0.1%) + hEGF (0.1%) + Foetal Bovine Serum (2%) + hFGF-b (0.4%) + GA-1000 (0.1%) + Heparin (0.1%) + Hydrocortisone (0.04%) + R3-IGF-1 (0.1%) + VEGF (0.1%)
SR80	Not Specified	Thrombin (20 U/ml; Stock)	$CaCl_2$ (11.1 mM; Stock)	Yes	N/A	2	N/A	N/A	N/A	Gel	3D; Cell-embedded; Co-culture	Yes	Dexamethasone (1 µM) + Gentamycin (0.5%) + Indomethacin (0.2 mM) + Insulin (0.01 mg/ml) + 3-isobutyl-l-methyl-xanthine (0.5 mM)
SR81	8 mg/ml (Stock)	Thrombin (2.5 mU/ml; Stock)	Not Used or Non Specified	Yes	1	1	N/A	N/A	N/A	Scaffold	3D; *In Situ;* Angiogenic Factor-infiltrated; Cell-embedded	Yes	N/A

Table B.5: **Fibrinogen, coagulant and crosslinker formulations used in the corpus**, by article, outlining the concentration used at the reported formulation step as reported by the authors of the study, as well as the type of coagulant or crosslinker chosen. NS: Not Specified; N: Not Reported; N/A: Non-Applicable.

	Fibrin		Coagulant			Crosslinker		
	Concentration	Stage	Coagulant	Concentration	Stage	Crosslinker	Concentration	Stage
1	20 mg/ml	Final	Thrombin	1250 U/ml	NS	$CaCl_2$	275 mM	NS
2	1.5 mg/ml	Final	Thrombin	0.6 U/ml	Stock	N	N/A	N/A
3	2 wt%	Stock	Thrombin	5 U/ml	Stock	$CaCl_2$	50 mM	Stock
4	NS	NS	N	N/A	N/A	N	N/A	N/A
5	70 - 110 mg/ml	Stock	Thrombin	37 U/ml	NS	$CaCl_2$	40 mmol	Stock
6	2.5 mg/ml	Final	Thrombin	0.2 U/ml	Final	N	N/A	N/A
7	6 mg/ml	Stock	Thrombin	0.32 U/ml	Stock	N	N/A	N/A
8	5 mg/ml (core matrix with cells) surrounded by 25 mg/ml (acellular capsule)	Final	Thrombin	2.5 U/ml	Stock	$CaCl_2$	40 mM	Stock
9	NS	NS	N	N/A	N/A	N	N/A	N/A
10	2.5 mg/ml	Stock	Thrombin	0.32 U/ml	Stock	N	N/A	N/A
11	1 mg	NS	Thrombin	0.2 U	NS	N	N/A	N/A
12	2.5 mg/ml	Stock	Thrombin	0.625 U/well	Stock	N	N/A	N/A
13	25 mg/ml	Stock	Thrombin	75 NIH U/ml	Stock	$CaCl_2$	4 ml	Stock
14	10 mg/ml	Final	Thrombin	11 µl at 100 U/ml	Stock	*NaCl*	NS	NS
15	3 mg/ml	Stock	Thrombin	50 U/ml	Stock	N	N/A	N/A
16	50 mg/ml	Stock	Thrombin	20 IU/ml	Stock	N	N/A	N/A
17	0.01 v/v%	Final	N	N/A	N/A	N	N/A	N/A
18	NS	NS	Thrombin	NS	NS	N	N/A	N/A
19	24 mg/ml	Stock	Thrombin	5 IU/ml	Stock	N	N/A	N/A
20	1 mg/ml	Stock	Thrombin	0.625 U/ml	Stock	N	N/A	N/A
21	9.4, 94.3 or 188.6 mg/ml	Stock	Thrombin	3.3, 33.3 or 66.66 mg/ml	Stock	$CaCl_2$	5.9 mg/ml	NS
22	NS	NS	Thrombin	NS	NS	N	N/A	N/A
23	11/mg/ml	Stock	Thrombin	1 kU/ml	Stock	$CaCl_2$	40 mM	Stock
24	2.5 mg/ml	Stock	Thrombin	50 U/ml	Stock	N	N/A	N/A
25	NS	NS	Thrombin	NS	NS	N	N/A	N/A
26	2.5, 5, 10 or 20 mg/ml	NS	Thrombin	0.2 IU/ml	NS	N	N/A	N/A
27	2 mg/ml	NS	Thrombin	4 U/ml	NS	N	N/A	N/A
28	10 mg/ml	NS	Thrombin	2 IU/ml	NS	N	N/A	N/A
29	100 mg/ml	Stock	Thrombin	500 IU/ml	Stock	$CaCl_2$	5.9 mg/ml	Stock
30	10 mg/ml	Final	Thrombin	100 U/ml	Stock	N	N/A	N/A
31	40 mg/ml	Stock	Thrombin	10 U/ml	Final	$CaCl_2$	40 mM	NS
32	NS	NS	N	N/A	N/A	N	N/A	N/A
33	1.5 mg/ml	NS	Thrombin	0.625 NIH U/ml	NS	N	N/A	N/A
34	2 wt%	Stock	Thrombin	10 U/ml	Stock	$CaCl_2$	50 mM	Stock
35	60 mg/ml	Stock	Thrombin	1250 U/ml	Stock	$CaCl_2$	275 mM	Stock
36	1 mg/ml	NS	Thrombin	0.3 U/ml	NS	N	N/A	N/A
37	NS	NS	Thrombin	500 U/ml	Stock	N	N/A	N/A
38	2.5 - 25 mg/ml	NS	Thrombin	2 U/ml	NS	$CaCl_2$	2.5 nM	NS
39	32 mg/ml	Stock	Thrombin	25 U/ml	Stock	$CaCl_2$	40 mM	Stock
40	10 or 20 mg/ml	Stock	Thrombin	10 U/ml	Stock	$CaCl_2$	0.063 M	Stock
41	NS	NS	Thrombin	NS	NS	N	N/A	N/A
42	10%	Stock	Thrombin	50 U/ml	Stock	$CaCl_2$	7%	Stock
						$MgCl_2$	3%	Stock
43	4 mg/ml	Stock	Thrombin	0.5 U/ml	Stock	N	N/A	N/A
44	NS	NS	N	N/A	N/A	N	N/A	N/A
45	70 - 110 mg/ml	Stock	Thrombin	NS	NS	$CaCl_2$	40 mM	Stock
46	10 mg/ml	Stock	Thrombin	2 U/ml	Stock	$CaCl_2$	2.5 or 5 mM	Stock
47	20 mg/ml	Stock	Thrombin	4 U/ml	Stock	N	N/A	N/A

	Fibrin (cont.)		Coagulant (cont.)			Crosslinker (cont.)		
	Concentration	Stage	Coagulant	Concentration	Stage	Crosslinker	Concentration	Stage
48	10 mg/ml	NS	Thrombin	50 U/ml	Stock	$CaCl_2$	150 mM	Stock
49	2.5 mg/ml	Final	Thrombin	4 U/ml	Stock	$CaCl_2$	NS	NS
50	36.59 or 23.59 mg/ml	Stock	Thrombin	223 kIU/ml or 144.6 kIU/ml	Stock	N	N/A	N/A
51	NS	NS	N	N/A	N/A	N	N/A	N/A
52	10 wt%	Final	N	N/A	N/A	N	N/A	N/A
53	10 mg/ml	NS	N	N/A	N/A	N	N/A	N/A
54	10 mg/ml	Stock	Thrombin	20 U/ml	Stock	$CaCl_2$	50 mM	Stock
55	20 mg/ml	Stock	Thrombin	100 IU/ml	Stock	N	N/A	N/A
56	20 mg/ml	Stock	Thrombin	1 mg/ml	Stock	*NaCl*	0.90%	Stock
57	2 mg/ml	Final	Thrombin	0.5 U/ml	Final	$CaCl_2$	2.5 mM	Final
58	2.5 mg/ml	Stock	Thrombin	2.5 U/ml	Final	N	N/A	N/A
59	3 mg/ml	Final	Thrombin	30 U/ml	Stock	$CaCl_2$	100 M	Stock
60	10 or 20 mg/ml	Final	Thrombin	0.8 U/ml	Stock	N	N/A	N/A
61	20 mg/ml	NS	Thrombin	3 U/ml	Final	N	N/A	N/A
62	5 mg/ml	Stock	Thrombin	0.2 ml	Stock	N	N/A	N/A
63	12 µl	Stock	Thrombin	NS	NS	N	N/A	N/A
64	NS	NS	Thrombin	NS	NS	N	N/A	N/A
65	50 mg/ml	Stock	Thrombin	50 U/ml	Stock	N	N/A	N/A
66	20 mg/ml	NS	Thrombin	50 IU/ml	NS	N	N/A	N/A
67	100 mg/ml	NS	Thrombin	400 IU/ml	NS	N	N/A	N/A
68	70 - 110 mg/ml	Stock	Thrombin	500 IU/ml	NS	N	N/A	N/A
69	4 wt%	Stock	Thrombin	15 U/ml	Stock	$CaCl_2$	50 mM	Stock
70	10 mg/ml	Final	Thrombin	50 U/ml	Final	N	N/A	N/A
71	8 mg/ml	Final	Thrombin	2 U/ml	Final	Ca^{2+}	2.5 mmol/L	Final
72	1%	Stock	Thrombin	20 U/ml	Stock	$CaCl_2$	50 mM	NS
73	2 - 9 mg/ml	Stock	Thrombin	37.5 U/ml	Final	$CaCl_2$	40 mmol	Stock
74	2%	Stock	Thrombin	100 IU/ml	Final	N	N/A	N/A
75	6 mg/ml	Final	Thrombin	1 U/ml	Stock	N	N/A	N/A
76	NS	NS	N	N/A	N/A	N	N/A	N/A
77	70 mg/ml	Stock	Thrombin	6 U/ml	Final	$CaCl_2$	40 mM	Stock
78	0.2 mg/ml	Stock	Thrombin	0.2 ml	Stock	*NaCl*	0.90%	Stock
79	NS	NS	Thrombin	20 U/ml	Stock	$CaCl_2$	11.1 mM	Stock
80	NS	NS	Thrombin	20 µl	Stock	N	N/A	N/A
81	8 mg/ml	Stock	Thrombin	2.5 mU/ml	Stock	N	N/A	N/A

Table B.6: **Polymers, both natural and synthetic, used in fibrin scaffolds** by frequency of use in the studies included in the corpus.

Polymers (Natural & Synthetic)	n
Collagen	7
Polyethylene Oxide (PEO)	4
Alginate	3
Fibronectin	3
Heparin	3
Polyethylene Glycol (PEG)	3
Succinimidyl Glutarate-modified Polyethylene Glycol	3
Hyaluronic Acid	2
Alginate (Chemically Modified)	1
Chitosan	1
Dacron	1
Hyaluronic Acid	1
Oxidised Dextran	1
Poly Lactic - *co* - Glycolic Acid (PLGA)	1
Polycaprolactone (PCL)	1
Polydimethylsiloxane (PDMS)	1
Polydioxanone (PDO)	1
Quaternized β-Chitin Derivative	1
s-IPN PEtU-PDMS	1

Table B.7: **Growth factors, peptides, amino acids and enzymes (GF/P/AA/E) used in fibrin scaffolds** by frequency of use in the studies included in the corpus.

Growth Factors, Peptides, Amino Acids & Enzymes	n
Aprotinin	19
Basic Fibroblast Growth Factor (bFGF)	11
Vascular Endothelial Growth Factor (VEGF)	8
Factor XIII	6
Fibroblast growth factor 2 (FGF-2)	3
Factor XIIIa	2
Glycine	2
Human Recombinant Basic Fibroblast Growth Factor (hr-bFGF)	2
Plasminogen	2
Platelet-derived Growth Factor-BB (PDGF-BB)	2
Transforming Growth Factor β1 (TGF-β1)	2
α-Interferon	1
Bovine Serum Albumin (BSA)	1
Epidermal Growth Factor (EGF)	1
Fibroblast Growth Factor 1 (FGF-1)	1
Hematopoietic Cytokine Erythropoietin	1
Hepatocyte Growth Factor (HGF)	1
(Human) Factor XIIIa	1
Human Recombinant Vascular Endothelial Growth Factor (hr-VEGF)	1
Human Serum Albumin (HSA)	1
Insulin	1
Keratinocyte Growth Factor (KGF)	1
L- Arginine	1
L- Lysine	1
Neuregulin-1 (NRG-1)	1
Penicillin	1
Platelet Lysate	1
Platelet-derived Growth Factor (PDGF)	1
Selenium	1
Streptomycin	1
Thrombospondin-1 (TSP-1)	1
Transferrin	1
Transglutaminase	1
Vascular Endothelial Growth Factor Isoform 164 ($VEGF_{164}$)	1
Vascular Endothelial Growth Factor Isoform 165 ($VEGF_{165}$)	1

Table B.8: **Cell media & solutions used in fibrin scaffolds** by frequency of use in the studies included in the corpus.

Cell Media & Solutions	n
Dulbecco's Modified Eagle Medium (DMEM)	2
Foetal Bovine Serum (FBS)	2
M199	2
NaCl	2
Endothelial Basal Medium (EBM)	1
Endothelial Cell Growth Medium 2 (EGM-2)	1
Endothelial Cell Growth Supplement	1
Foetal Calf Serum (FCS)	1
Hank's Balanced Salt Solution (HBSS)	1
HEPES	1
Serum	1
Tris-Buffered Saline (TBS) Solution	1

Table B.9: **Chemicals used in fibrin scaffolds** by frequency of use in the studies included in the corpus.

Chemicals	n
ε-Aminocaproic Acid	1
Tranexamic Acid	1
Trisodium Citrate	1
Triton-X	1

Table B.10: **Other materials used in fibrin scaffolds** by frequency of use in the studies included in the corpus.

Others	n
Cytodex-3 Microcarriers	2
Matrigel	2
Bevacizumab	1
Cytodex Beads	1
Deoxyribonucleic acid (DNA)	1
Fe_3O_4 Magnetic Nanoparticles	1
Heparin-Conjugated PLGA Nanospheres	1
Lithium Phthalocyanine Crystals	1
Plasmids	1
Plasmin Inhibitor Aprotinin Solution	1
Thrombin Coated Tosyl-Activated Superparamagnetic Beads	1
Tosyl-Activated Superparamagnetic Beads	1

Table B.11: **Composition of modified cell media used for fibrin scaffolds**, by the number of scaffolds in which a given combination was used.

Factors Used to Supplement the Cell Medium	n
Aprotinin (100 kIU/ml)	3
Aprotinin (200 U/ml)**	2
VEGF (50 ng/ml)	2
6-Aminocaproic Acid (2mg/ml)	1
Aminocaproic Acid (30 mM) + VEGF (50 ng/ml)	1
Amphotericin (0.25 µg/ml) + Aprotinin (100 kIU/ml) + Heparan Sulfate (5 U/ml)*	1
Amphotericin (0.25 µg/ml) + Aprotinin (100 kIU/ml) + Heparan Sulfate (5 U/ml) + Methocel Solution (20%)*	1
Angiopoietin-1 (1-125 ng/ml) + bFGF (25 ng/ml) + TGF-β (0.5-2 ng/ml) + VEGF (25 ng/ml)	1
Aprotinin (0.15 U/ml)	1
Aprotinin (100 U/ml) + L-Ascorbic Acid-2-Phosphate (50 µg/ml) + FGF (40 ng/ml) + VEGF (40 ng/ml)	1
Aprotinin (200 U/ml) + bFGF (30 ng/ml) + VEGF (100 ng/ml)	1
Aprotinin (200 U/ml) + hr-bFGF (50 ng/ml) + hr-VEGF (40 ng/ml)**	1
Aprotinin (92.5 µg/ml) + Tranexamic acid (400 µM)	1
Ascorbic Acid (0.1%) + hEGF (0.1%) + Foetal Bovine Serum (2%) + hFGF-b (0.4%) + GA-1000 (0.1%) + Heparin (0.1%) + Hydrocortisone (0.04%) + R3-IGF-1 (0.1%) + VEGF (0.1%)	1
Dexamethasone (1 µM) + Foetal Calf Serum (10%) + Gentamycin (0.5%) + Indomethacin (0.2 mM) + Insulin (0.01 mg/ml) + 3-isobutyl- I-methyl-xanthine (0.5 mM)	1
Dexamethasone (1 µM) + Gentamycin (0.5%) + Indomethacin (0.2 mM) + Insulin (0.01 mg/ml) + 3-isobutyl-I-methyl-xanthine (0.5 mM)	1
bFGF (10 or 20 ng/ml) + Human Serum (2%) + Hydrocortisone (20 ng/ml) + VEGF (10 or 20 ng/ml)	1
bFGF (50 ng/ml) + VEGF (100 ng/ml)	1
FGF-2 (10 ng/ml) + TNFa (10 ng/ml) + VEGF (25 ng/ml)	1
Insulin (1 µg/ml) + Penicillin (100 U/ml) + Selenium (1 ng/ml) + Streptomycin (100 g/ml) + Transferrin (1 µg/ml)	1

** Used in the same publication.*

*** Used in the same publication.*

Appendix C

Detailed Search Strategies Used per Database, displaying the number of records found on 28 October 2024 in PubMed, Scopus and OVID

(A) PubMed

Database Name	PubMed PubMed includes MEDLINE, PubMed Central (PMC) and the NCBI Bookshelf.
Limits and Restrictions	Search terms included Medical Subject Headings (MeSH) terms.
Search Filters Used	No filters were applied in the initial search.
Search Query	(vascular network OR vascular network formation[MeSH Terms] OR microvascular network[MeSH Terms] OR microvascular network formation[MeSH Terms] OR neovascularization[MeSH Terms] OR angiogenesis OR vasculogenesis OR endothelial network OR endothelial network formation[MeSH Terms] OR microvessel[MeSH Terms] OR microcirculation[MeSH Terms] OR endothelial tube OR tube formation[MeSH Terms] OR tube-like) AND (soft tissue[MeSH Terms] OR muscle[MeSH Terms] OR nerve OR ligament[MeSH Terms] OR tendon[MeSH Terms] OR fascia[MeSH Terms] OR skin[MeSH Terms] OR fibrous tissue[MeSH Terms] OR connective tissue[MeSH Terms] OR synovial membrane[MeSH Terms]) AND (scaffold OR construct[MeSH Terms] OR mesh[MeSH Terms] OR matrix OR matrices OR gel OR hydrogel[MeSH Terms] OR tissue engineered product) AND (fibrin[MeSH Terms] OR fibrinogen[MeSH Terms])

(B) SCOPUS

Database Name	Scopus
Limits and Restrictions	No limits or restrictions were imposed.
Search Filters Used	The following three document types were excluded: Review, Book Chapter, and Book.
Search Query	vascular AND network OR vascular AND network AND formation OR microvascular AND network OR microvascular AND network AND formation OR neovascularization OR angiogenesis OR vasculogenesis OR endothelial AND network OR endothelial AND network AND formation OR microvessel OR microcirculation OR endothelial AND tube OR tube AND formation OR tube-like AND soft AND tissue OR muscle OR nerve OR ligament OR tendon OR fascia OR skin OR fibrous AND tissue OR connective AND tissue OR synovial AND membrane AND scaffold OR construct OR mesh OR matrix OR matrices OR gel OR hydrogel OR tissue AND engineered AND product AND fibrin OR fibrinogen

(C) OVID

Database Name	OVID
Limits and Restrictions	No limits or restrictions were imposed.
Search Filters Used	No filters were applied in the initial search.
Search Query	vascular network.mp. or vascular network formation/ or microvascular network/ or microvascular network formation/ or neovascularization/ or angiogenesis.mp. or vasculogenesis.mp. or endothelial network.mp. or endothelial network formation/ or microvessel/ or microcirculation/ or endothelial tube.mp. or tube formation/ or tube-like.mp. AND soft tissue/ or muscle/ or nerve.mp. or ligament/ or tendon/ or fascia/ or skin/ or fibrous tissue/ or connective tissue/ or synovial membrane/ AND scaffold.mp. or construct/ or mesh/ or matrix.mp. or matrices.mp. or gel.mp. or hydrogel/ or tissue engineered product.mp. AND fibrin/ or fibrinogen/ [mp=title, book title, abstract, original title, name of substance word, subject heading word, floating sub-heading word, keyword heading word, organism supplementary concept word, protocol supplementary concept word, rare disease supplementary concept word, unique identifier, synonyms, population supplementary concept word, anatomy supplementary concept word]

Appendix D

Minimum Information for Fibrin Scaffold Experiments (MIFSE) Checklist

Minimum Information for Fibrin Scaffold Experiments (MIFSE) Checklist

Version: 1.0 (August 2025)

This checklist provides key reporting points for fibrin- or fibrinogen-based scaffold studies, including scaffold composition & fabrication, scaffold properties, cell pre-embedding, experimental context, functional & biological assessments, and general reporting standards.

Items in standard typeface are recommended as mandatory, when applicable, while items in *italics* are suggested.

While designed for fibrin scaffolds, the checklist can be applied to other tissue engineering scaffolds, and we encourage its use to improve reproducibility, transparency, and comparability across studies.

1. Scaffold Composition & Fabrication

Fibrinogen

- ☐ Source (*e.g.,* commercial, extracted).
- ☐ If commercially sourced, manufacturer and country of origin.
- ☐ Species of origin (*e.g.,* human, bovine).
- ☐ *Purity.*
- ☐ *Clottability.*
- ☐ Concentration with units (*e.g.,* mg/ml) and stage of the formulation at which this is used (*e.g.,* initial stock, final concentration).
- ☐ Media/buffer/solvent used.
- ☐ *Storage conditions.*

Coagulant(s)

- ☐ Type (*e.g.,* thrombin).
- ☐ Source (*e.g.,* commercial, extracted).
- ☐ If commercially sourced, manufacturer and country of origin.
- ☐ Species of Origin (*e.g.,* human, bovine).
- ☐ Concentration with units (*e.g.,* mg/ml) and stage of the formulation at which this is used (*e.g.,* initial stock, final concentration).
- ☐ Media/buffer/solvent used.
- ☐ *Storage conditions.*

Crosslinker(s)

- ☐ Type (*e.g.,* $CaCl_2$).
- ☐ Source (*e.g.,* commercial, extracted).
- ☐ If commercially sourced, manufacturer and country of origin.
- ☐ Species of Origin (*e.g.,* human, bovine).
- ☐ Concentration with units (*e.g.,* mg/ml) and stage of the formulation at which this is used (*e.g.,* initial stock, final concentration).
- ☐ Media/buffer/solvent used.
- ☐ *Storage conditions.*

Other Materials Used - the following details should be provided for each additional material and if applicable.

- ☐ Type (*e.g.,* Collagen I).
- ☐ Source (*e.g.,* commercial, extracted).
- ☐ If commercially sourced, manufacturer and country of origin.
- ☐ Species of Origin (*e.g.,* human, bovine).
- ☐ Concentration with units (*e.g.,* mg/ml) and stage of the formulation at which this is used (*e.g.,* initial stock, final concentration).
- ☐ Media/buffer/solvent used.
- ☐ *Storage conditions.*

Formulation & Fabrication

- ☐ Ratio of fibrinogen : coagulant : crosslinker : other materials.
- ☐ Method of mixing and polymerisation conditions (*e.g.,* temperature, time, order of addition).
- ☐ *Sterilisation method(s).*
- ☐ *Storage conditions.*

2. Scaffold Design & Properties

- ☐ Manufactured Object Type (*e.g.,* hydrogel, sheet, fibre, composite).
- ☐ *Dimensions and geometry (e.g., thickness, volume, pore size).*
- ☐ *Mechanical properties (e.g., stiffness, tensile strength, rheology).*
- ☐ *Degradation profile (e.g., enzymatic stability, in vitro degradation rate).*
- ☐ *Swelling ratio or water content.*

3. Cell Pre-embedding

- ☐ Specify whether cells were pre-embedded into the scaffold or not.

If cells were pre-embedded:

- ☐ Cell line(s) used, including type (*e.g.,* primary, immortalised), species (*e.g.,* human, rat), tissue source (*e.g.,* umbilical vein), and name (*e.g.,* HUVEC).
- ☐ Cell density or seeding concentration.
- ☐ Passage number.
- ☐ Encapsulation or embedding method.
- ☐ *Preconditioning of cells (e.g., differentiation state, growth factor treatment).*

4. Experimental Context

- ☐ Study type (*e.g., in vitro, in vivo*).
- ☐ Cell culture media conditions, including culture media (*e.g.,* DMEM) , media supplements (*e.g.,* FBS, VEGF), antibiotics (*e.g.,* penicillin, streptomycin).
- ☐ Cell culture conditions (*e.g.,* CO_2, temperature, time between media changes).
- ☐ Duration of culture or observation.
- ☐ *In vivo* model used (*e.g.,* species, strain, age, sex).
- ☐ Experimental groups conditions and number of replicates.
- ☐ Controls used and number of replicates.
- ☐ Randomisation or blinding procedures.

5. Functional & Biological Assessments

- ☐ Assays performed (*e.g.,* angiogenesis, cell viability, contractility, histology, perfusion).
- ☐ Quantitative outcomes measured, including units, mean ± SD/SEM, sample size.
- ☐ Time points of measurement.
- ☐ Imaging modalities (*e.g.,* brighfield microscopy, SEM).
- ☐ Image analysis software (*e.g.,* Fiji/ImageJ) and plugins (*e.g.,* Angiogenesis Analyzer) used.
- ☐ Criteria for success or endpoint definition.
- ☐ Statistical methods used (*e.g.,* t-test, 2-way ANOVA).

6. Reporting Standards

- ☐ Ethical approval, including organisation granting approval and registration number/ID.
- ☐ Limitations acknowledged.
- ☐ Conflict of Interests statement.
- ☐ Funding sources.
- ☐ Data and materials availability.

Appendix E

Supplementary Materials for Chapter 5

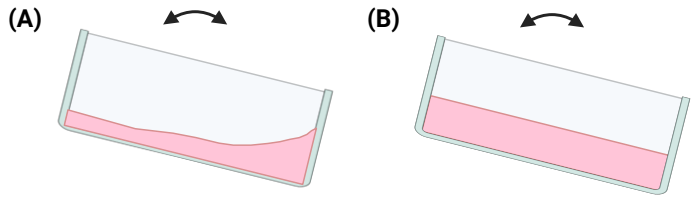


Figure E.1: **Schematic illustration of gelation determination**, achieved by tilting the plate to identify the time point at which the hydrogel first holds its shape, depicting hydrogels that **(A)** have not yet or **(B)** have gelled. Created with *BioRender.com*

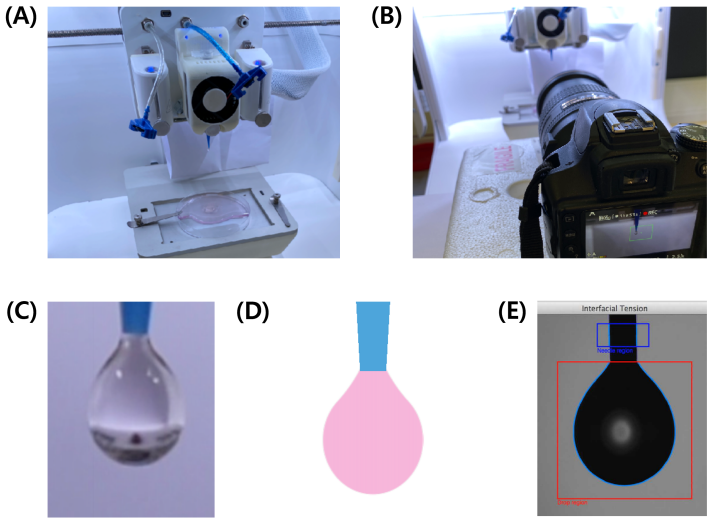


Figure E.2: **Overview of the process to measure pendant drop tensiometry**, including **(A)** 3D bioprinter setup; **(B)** video acquisition setup; **(C)** droplet still image and **(D)** profile; and **(E)** a screenshot of the *OpenSource* [588] software interface.

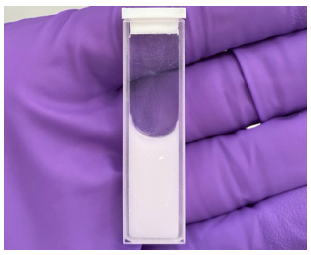


Figure E.3: **Photograph of gelled sample with tracer solution.** Here shown is the hydrogel crafted with human fibrinogen in EBM (10 mg/mL).

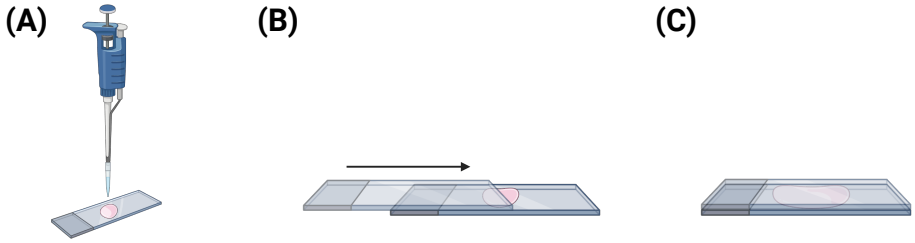


Figure E.4: **Schematic illustration of the shearing process**, depicting **(A)** depositing the hydrogel solution onto a microscope slide, **(B)** carefully placing a second slide on top of the hydrogel and shearing it until **(C)** the slides are aligned. Created using *BioRender.com*

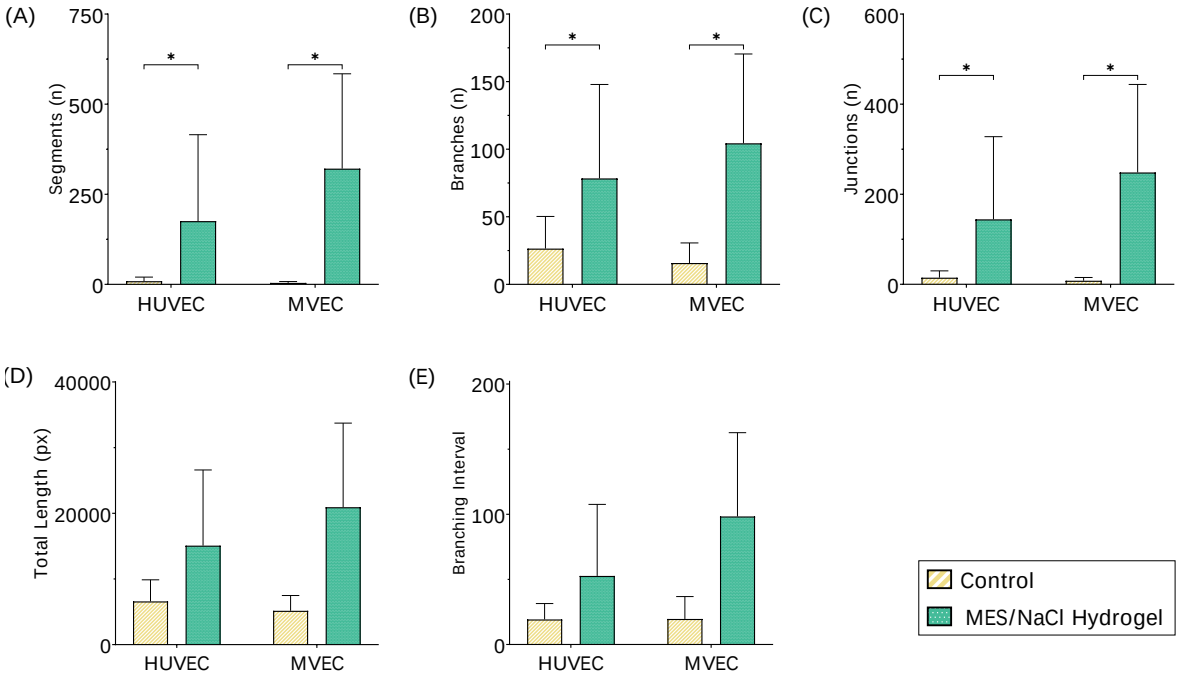


Figure E.5: **Endothelial network characterisation of HUVECs and MVECs in MES/NaCl hydrogels** using bovine fibrinogen (4 mg/mL), 12 h post-seeding. The number of **(A)** segments, **(B)** branches and **(C)** junctions, as well as the **(D)** total network length and **(E)** branching interval were obtained. Cell-embedded hydrogels (seeding density: 5×10^4 cells/well) were cultured with EGM in 24-well plates. Cells-only controls were used. (2-way ANOVA/Fisher's LSD; $^*p \leq 0.05$; only statistically significant differences are shown; $n = 12$).

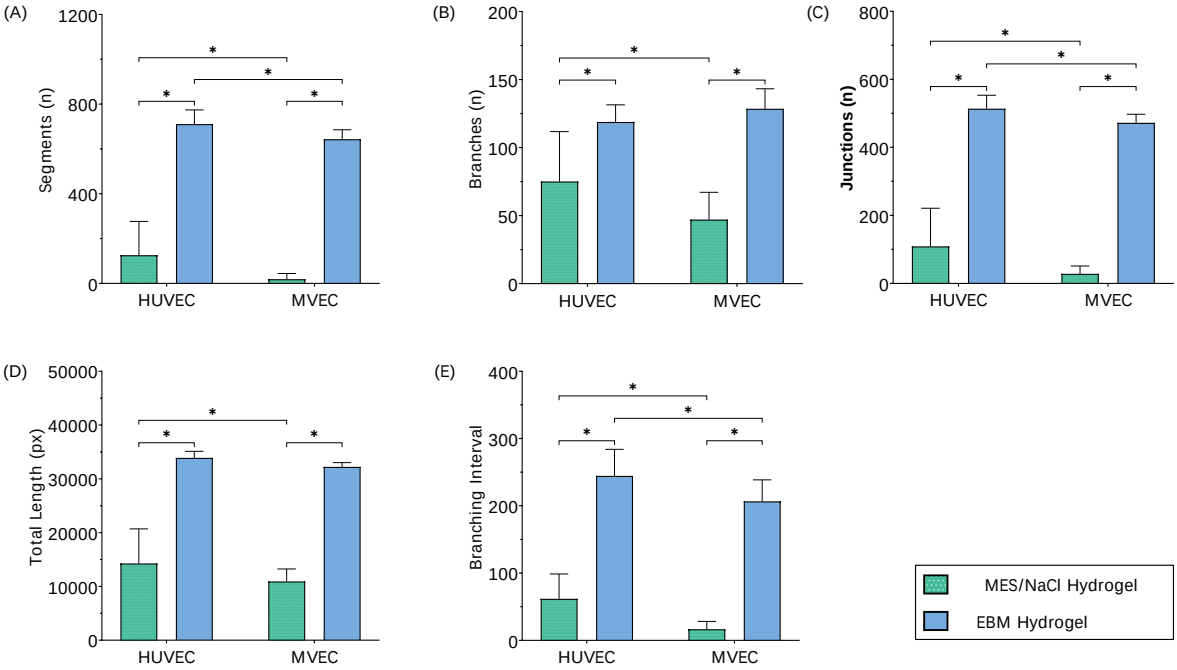


Figure E.6: **Endothelial network characterisation of HUVECs and MVECs in MES/NaCl or EBM hydrogels** using bovine fibrinogen (4 mg/mL), 10 h post-seeding. The number of **(A)** segments, **(B)** branches and **(C)** junctions, as well as the **(D)** total network length and **(E)** branching interval were obtained. Cell-embedded hydrogels (seeding density: 5×10^4 cells/well) were cultured with EGM in 24-well plates. (2-way ANOVA/Fisher's LSD; $^*p \leq 0.05$; only statistically significant differences are shown; $n = 30$).

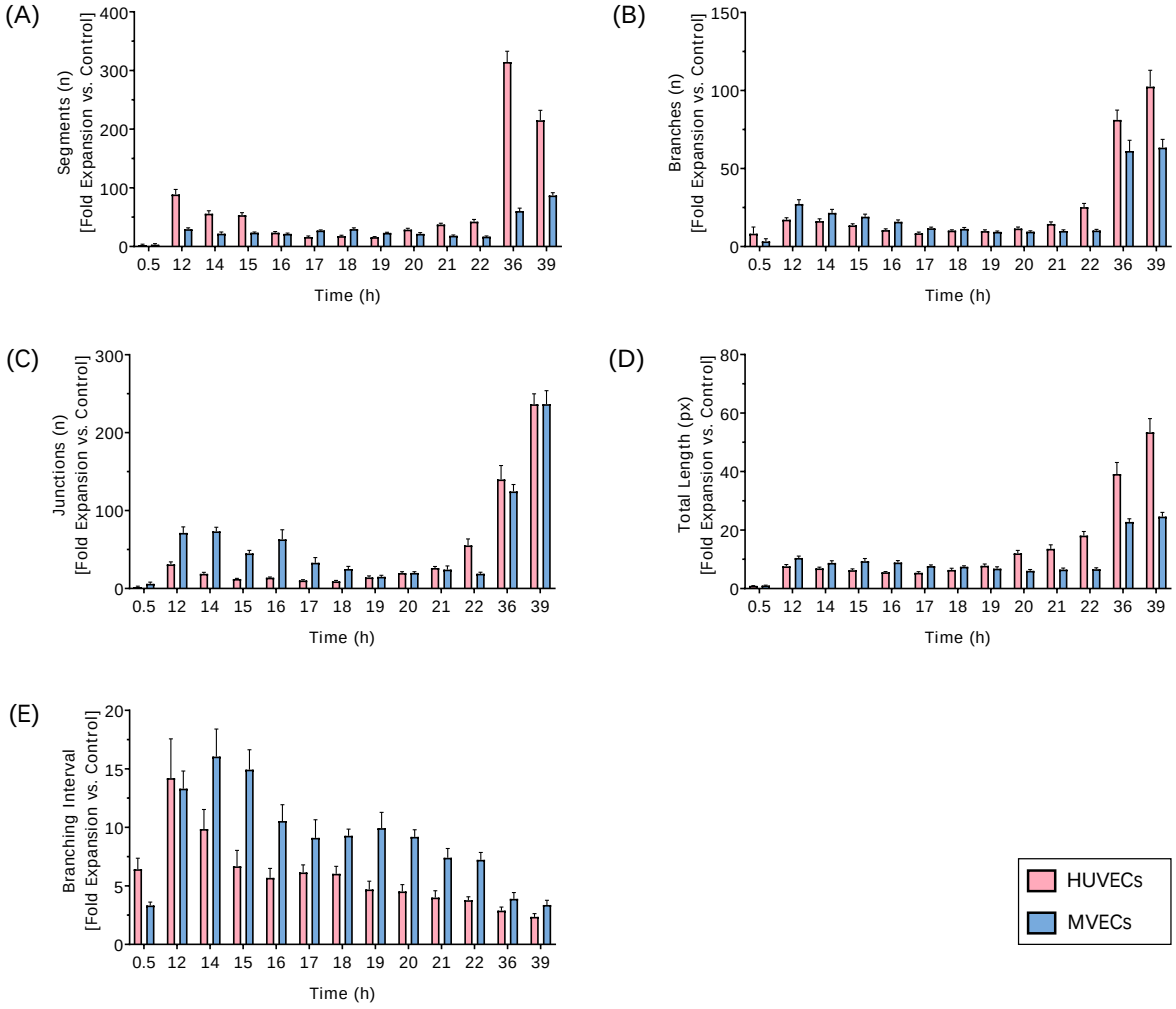


Figure E.7: **Endothelial network characterisation of HUVECs and MVECs in EBM hydrogels** using bovine fibrinogen (4 mg/mL), for up to 39 h. The number of **(A)** segments, **(B)** branches and **(C)** junctions, as well as the **(D)** total network length and **(E)** branching interval were obtained for each sample. Values are presented as a fold expansion against the respective control (HUVEC or MVEC cells-only samples). Cell-embedded hydrogels (seeding density: 5×10^4 cells/well) were cultured with EGM in 24-well plates. (2-way ANOVA/Fisher's LSD; $p \leq 0.05$; $n = 9$).

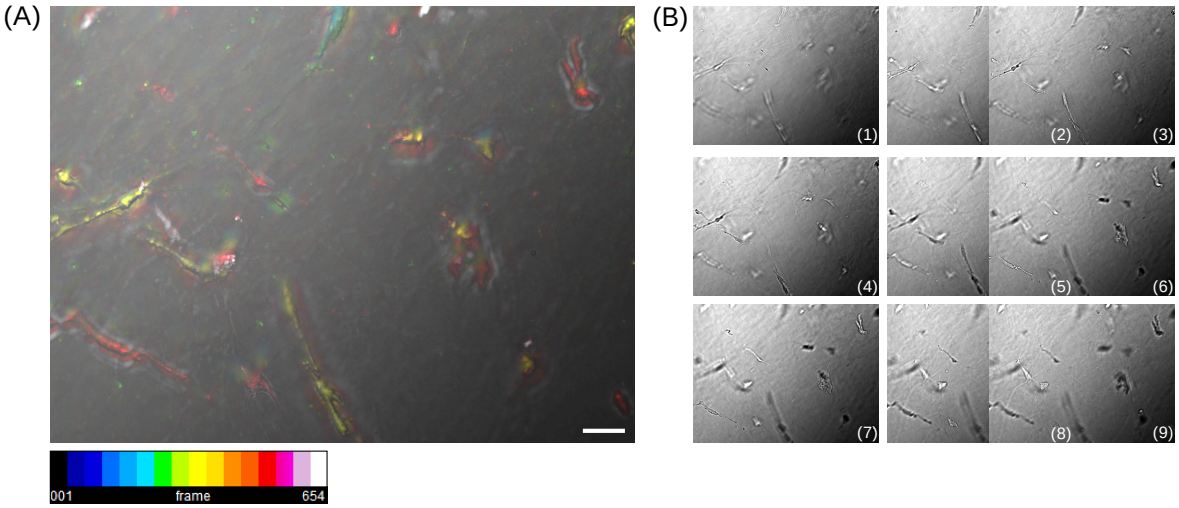


Figure E.8: **Depth visualisation of MVEC-embedded hydrogels at 24 h post-seeding.** Here, a bovine fibrinogen hydrogel (2 mg/mL) in EGM is shown (hydrogel thickness: 2 mm). MVECs were cultured with EGM and seeded at a density of 5×10^4 cells/well (24-well plate). **(A)** A depth-coded image was generated using *ImageJ/Fiji*'s *Temporal-Color Code* plugin (16-colour scale) to visualise the 3D structure of the hydrogel. Scale bar: 100 px. **(B)** Selected slices from the z-stack (1 µm steps; the distance between the images shown here is 30–50 µm) demonstrate cell distribution and structural variation throughout the hydrogel.

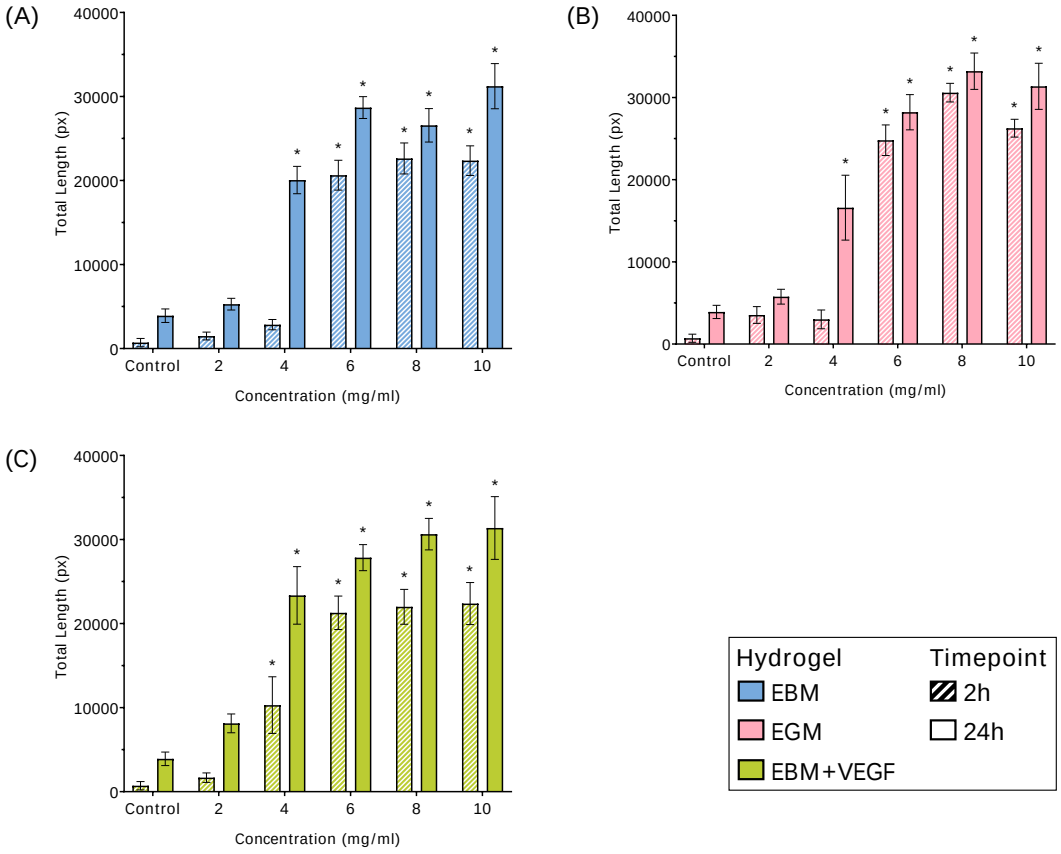


Figure E.9: **Total network length by fibrinogen concentration, at 2 and 24 h.** Bovine fibrinogen hydrogels of different concentrations using **(A)** EBM, **(B)** EBM + VEGF, or **(C)** EGM as a medium were compared. MVECs were cultured with EGM and seeded at a density of 5×10^4 cells/well (24-well plate). Cells-only controls were used. (2-way ANOVA/Dunnett; $^*p \leq 0.05$; only statistically significant differences are shown; $n = 3$).

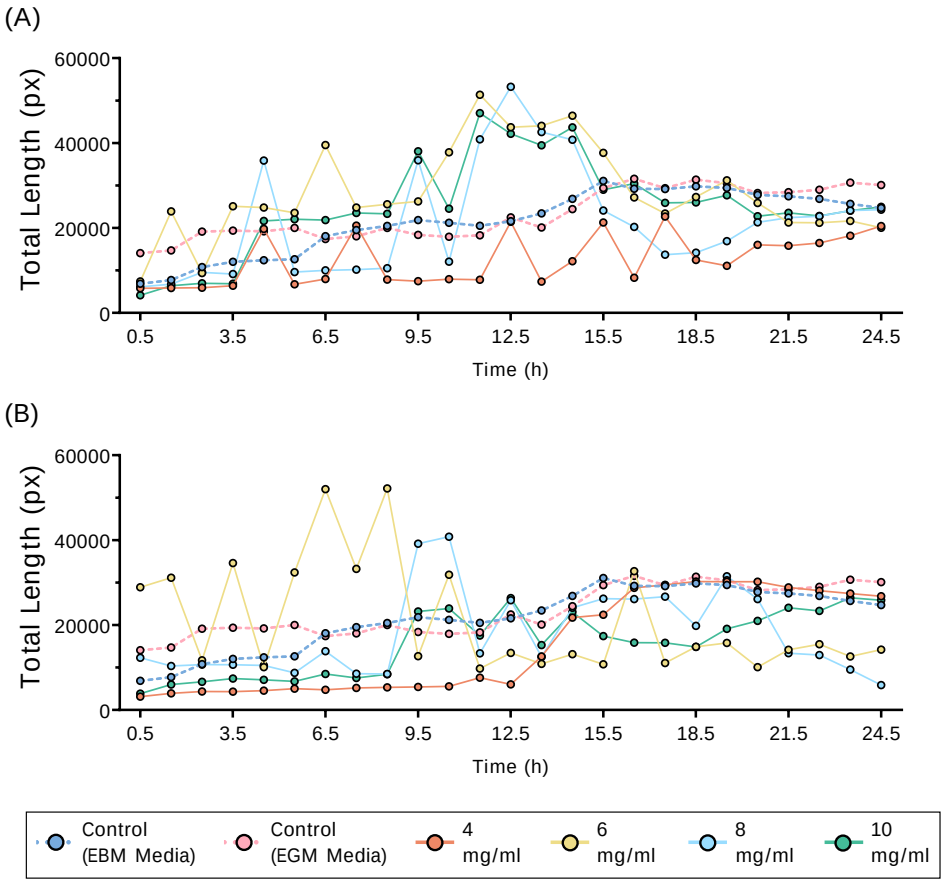


Figure E.10: **Total network length by fibrinogen : thrombin : $CaCl_2$ crosslinking ratio for MVECs, quantified every hour during a 24 h period (t_1 = 0.5 h).** Two crosslinking ratios were explored: **(A)** 200:10:1 and **(B)** 100:10:1. Hydrogels were created using fibrinogen from human serum at different concentrations, paired with EBM as medium. MVECs were cultured with EGM and seeded at a density of 2×10^4 cells/well (96-well plate). Two cells-only controls, in either EBM or EGM, were used. (ANOVA/Tukey's HSD; $p \leq 0.05$; $n = 6$).

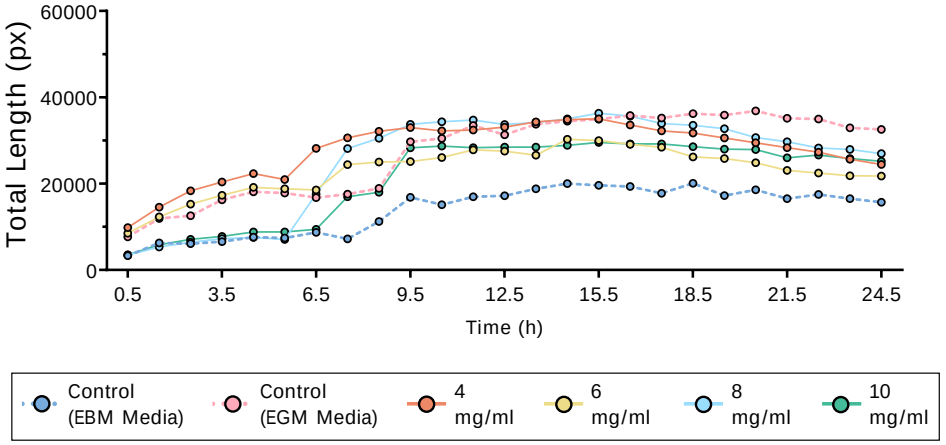


Figure E.11: **Total HUVEC network length quantified every hour during a 24 h period (t_1 = 0.5 h).** Hydrogels were created using fibrinogen from human serum at different concentrations, paired with EBM as medium and using a fibrinogen : thrombin : $CaCl_2$ crosslinking ratio of 200:10:1. HUVECs were cultured with EGM and seeded at a density of 2×10^4 cells/well (96-well plate). Two cells-only controls, in either EBM or EGM, were used. (ANOVA/Tukey's HSD; $p \leq 0.05$; $n = 6$).

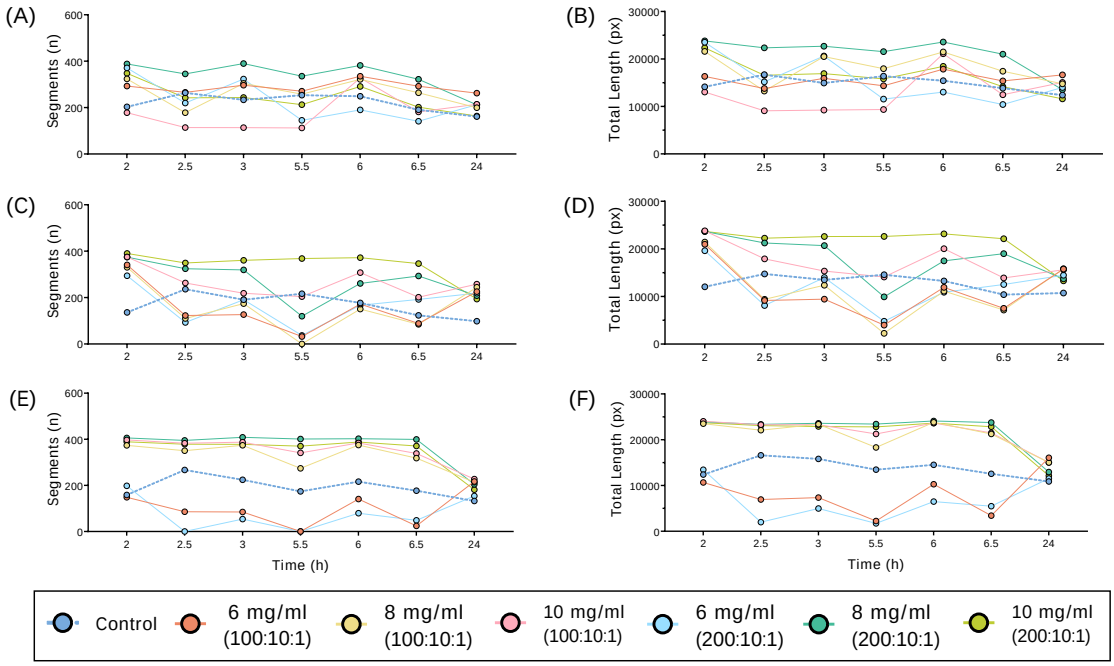


Figure E.12: **Impact of variations in medium and crosslinking ratio on microvascular endothelial network architecture. (A, C, E)** Number of segments and **(B, D, F)** total MVEC network length by medium, fibrinogen concentration and crosslinking ratio (fibrinogen : thrombin : $CaCl_2$), during a 24 h period. Here, three media were explored: **(A, B)** EBM, **(C, D)** EBM + VEGF and **(E, F)** PBS. Hydrogels were created using fibrinogen from human serum at different concentrations and a crosslinking ratio of either 200:10:1 or 100:10:1. MVECs were cultured with EGM and seeded at a density of 2×10^4 cells/well (96-well plate). Cells-only controls were used. (ANOVA/Tukey's HSD; $p \leq 0.05$; $n = 12$).

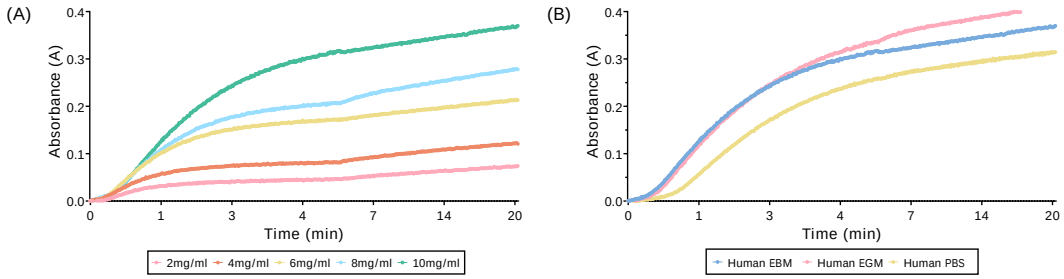


Figure E.13: **Spectrophotometry absorbance plots showing the normalised change in 340 nm light absorbance for 20 min. (A)** EBM hydrogels created with human fibrinogen at different concentrations. **(B)** Human fibrinogen hydrogels (10 mg/mL) created with EBM, EGM or PBS. ($n = 9$).

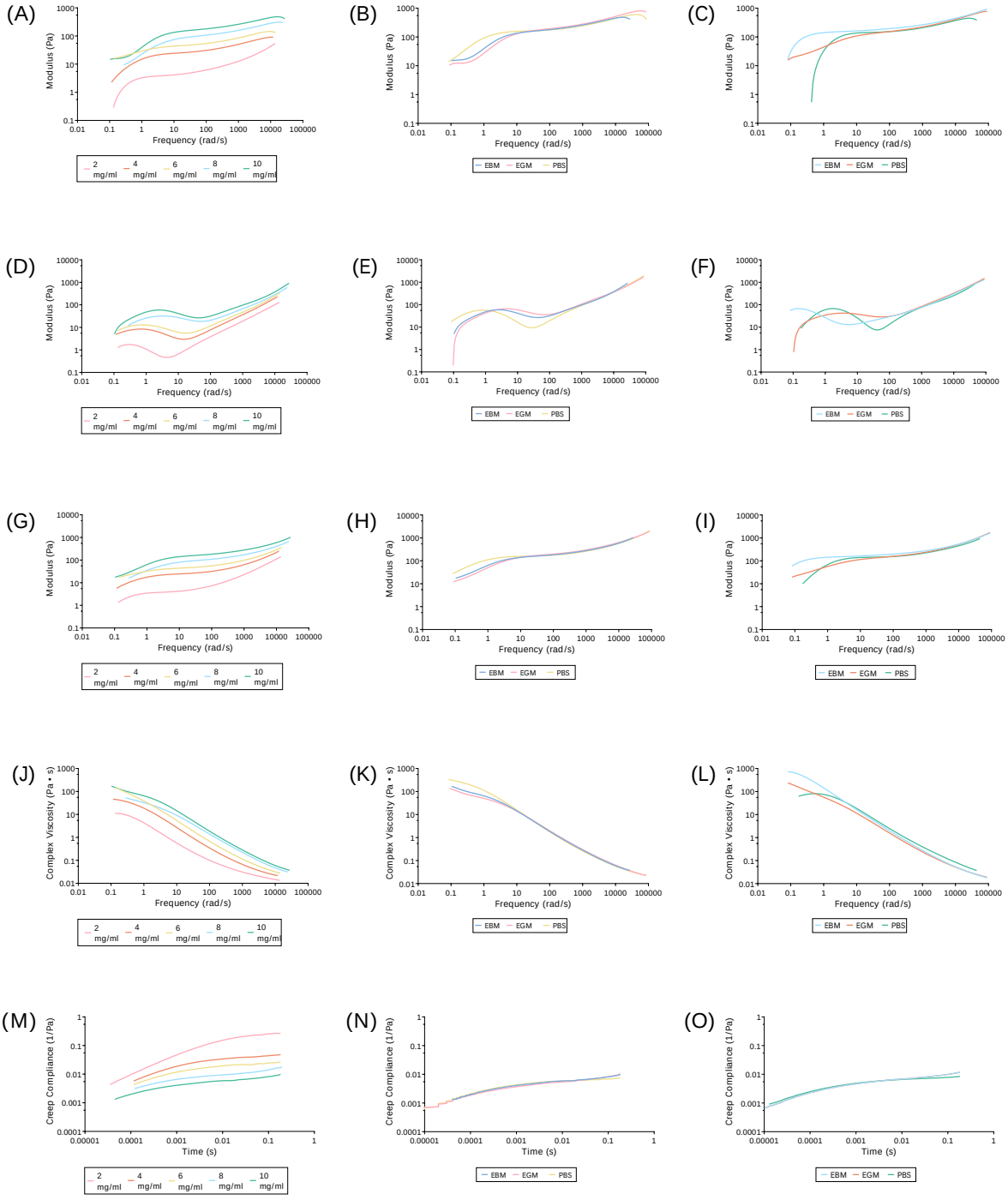
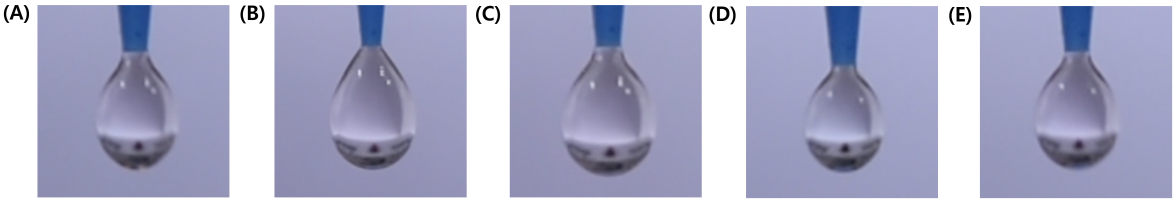


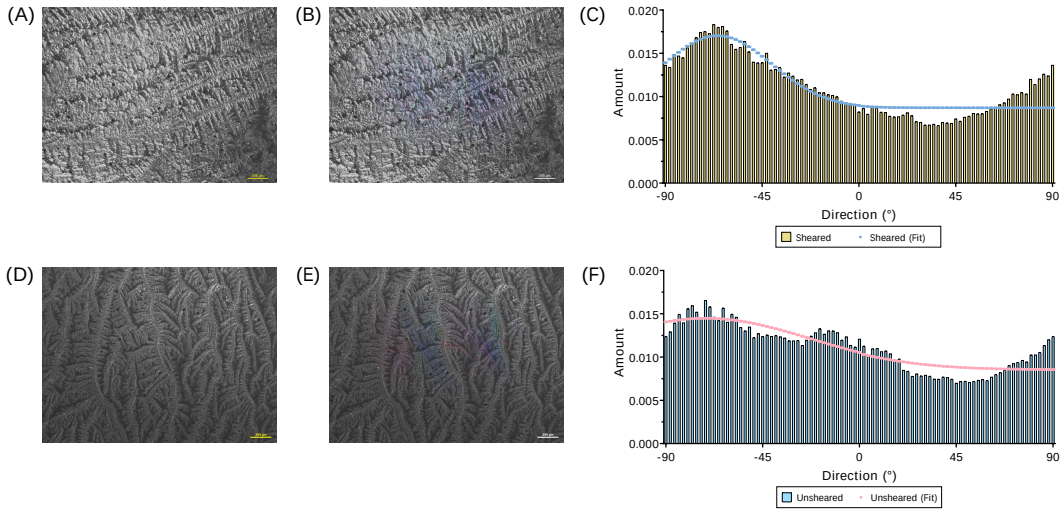
Figure E.14: **Microrheology characterisation**, showing the **(A–C)** storage modulus (G'), **(D–F)** loss modulus (G"), **(G–I)** complex shear modulus (G*) and **(J–L)** complex viscosity (η*) as a function of frequency, as well as **(M–O)** creep compliance as a function of time 1 h after gelation of **(A, D, G, J, M)** human fibrinogen EBM hydrogels with different fibrinogen concentrations (2–10 mg/mL), and hydrogels with a 10 mg/mL fibrinogen concentration of **(B, E, H, K, N)** bovine or **(C, F, I, L, O)** human origin.



(F)

	Human Fibrinogen (10 mg/ml)			Deionised H_2O	EBM
	Pre-gelation	Gelation: 0-5 min	Gelation: 6-15 min		
Interfacial Tension [mN/m]	13.690 ± 0.297	18.176 ± 1.955	29.605 ± 2.510	14.763 ± 2.223	14.615 ± 1.435

Figure E.15: **Interfacial tension values from pendant drop tensiometry. (A–E)** Using still images extracted from a recording of pendant drops from a 3D bioprinter nozzle, **(F)** interfacial tension values were obtained using *OpenDrop* [588]. **(A–C)** Fibrinogen at different stages of gelation: **(A)** pre-gelation, and **(B)** 0–5 min and **(C)** 6-15 min after gelation. Controls of **(D)** deionised water and **(E)** EBM were used. (n = 9).



(H)

Type	Direction (°)	Dispersion (°)	Amount	Goodness
Sheared	-65.910	24.870	0.53	0.84
Unsheared	-71.587	47.823	0.72	0.75

Figure E.16: **Dendrite alignment** of **(A, B, C)** sheared and **(D, E, F)** unsheared hydrogels. **(A, D)** Samples were imaged at 4× and processed using *ImageJ/Fiji* and the *Directionality* plugin [590] to quantify alignment. **(B, E)** Dendrite orientation was colour mapped, as indicated by **(G)** the angle colour wheel. **(C, F)** The highest peak was fitted by a Gaussian function considering the periodic nature of the histogram. From this data, **(H)** direction, dispersion, amount and goodness were calculated to quantify the alignment. Direction and dispersion (°) indicate the centre and the standard deviation, respectively, of the Gaussian. The amount was obtained through sum of the histogram from the centre point ± standard deviation divided by the total sum of the histogram. The goodness value reports the how well the fit of the model was in a range of 0 (worst) to 1 (best). (n = 3). Scale bar: 200 µm

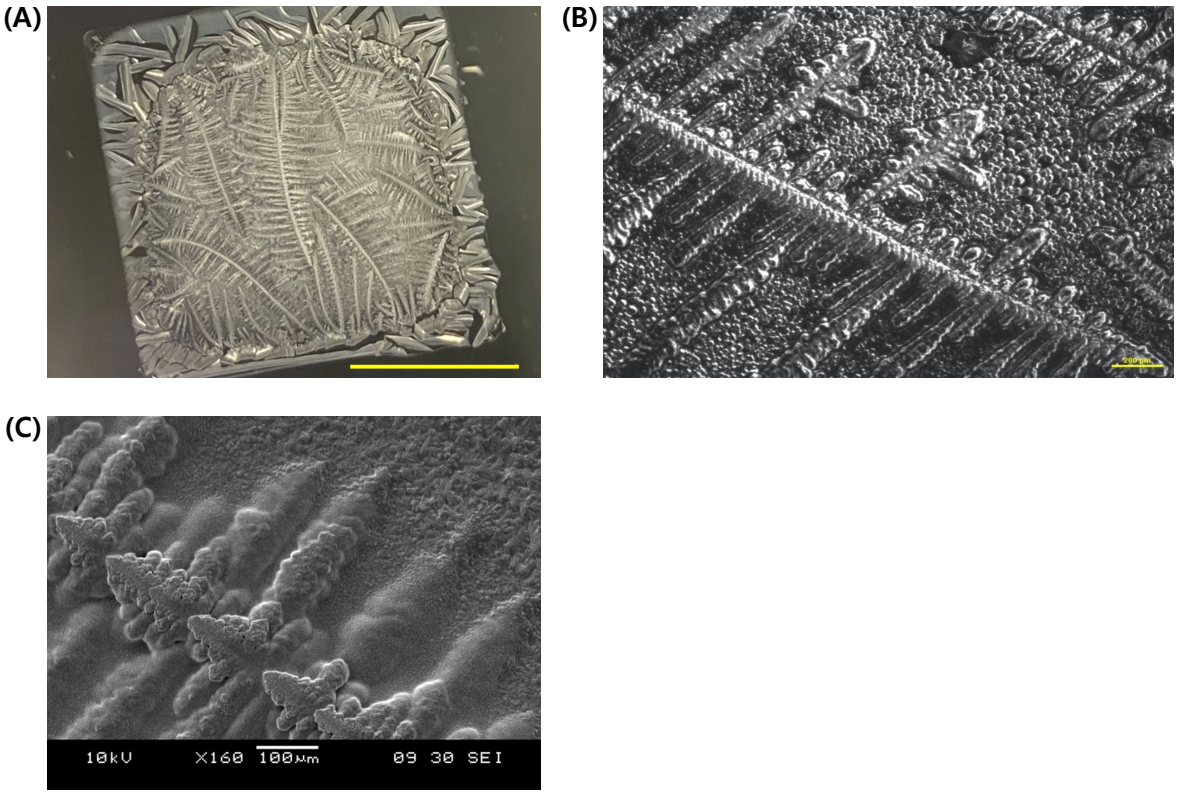


Figure E.17: **Microscopy images of hydrogel samples** captured using a widefield microscope at **(A)** 1× and **(B)** 4×, as well as **(C)** SEM at 160×. Here, a 10 mg/mL human fibrinogen in EBM hydrogel is shown. Scale bars: **(A)** 1 cm, **(B)** 200 µm, **(C)** 100 µm.

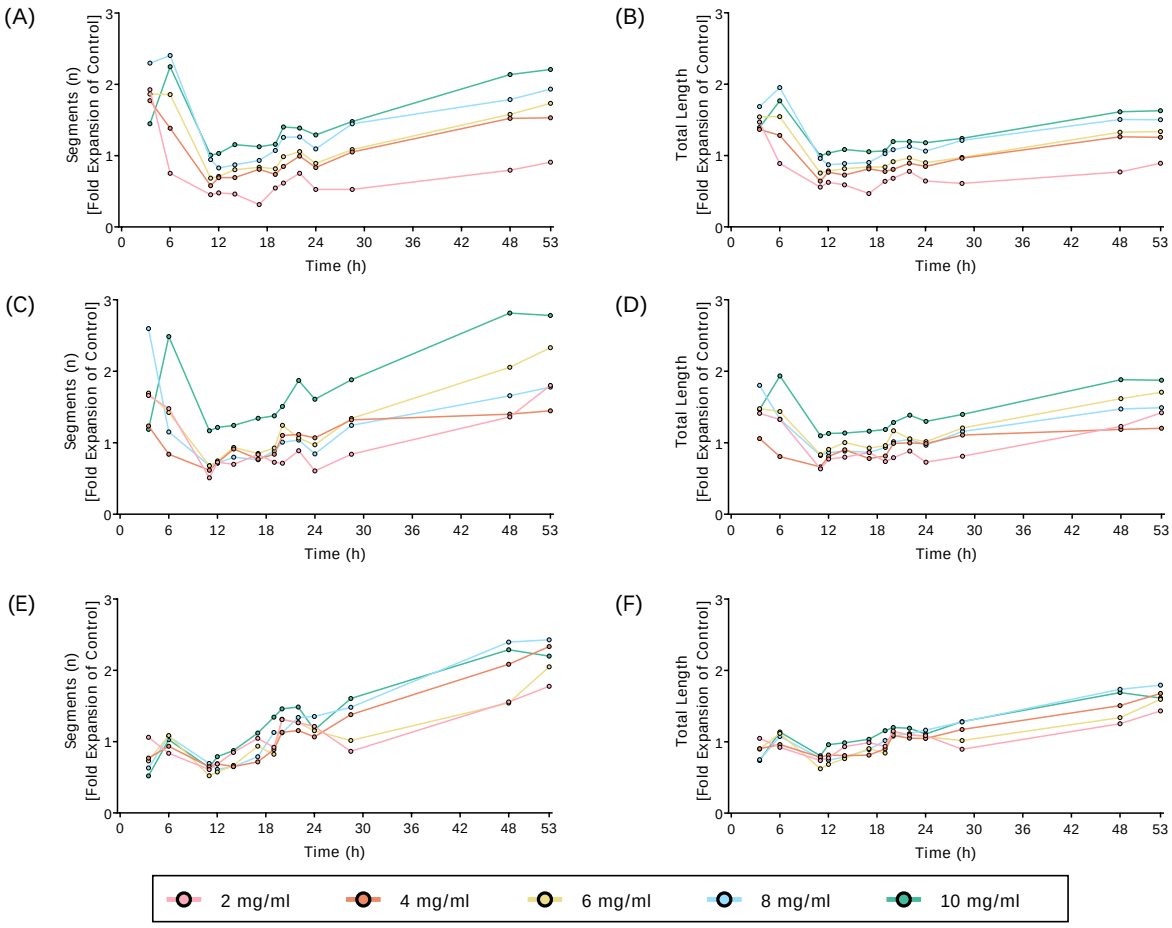


Figure E.18: **Characterisation of MVEC networks by medium and fibrinogen concentration, quantified throughout a period of 53 h**, depicting **(A, C, E)** number of segments and **(B, D, F)** total network length as a fold expansion of the control. Here, three media were explored: **(A, B)** EBM, **(C, D)** EBM + VEGF and **(E, F)** EGM. Hydrogels were created using fibrinogen from human serum at different concentrations (2, 4, 6, 8 & 10 mg/mL). MVECs were cultured with EGM until hydrogel casting, after which they were cultured with EBM. Cells were seeded at a density of 1.5×10^4 cells/well (48-well plate). Cells-only controls were used. (ANOVA/-Tukey's HSD; $p \leq 0.05$; $n = 30$).

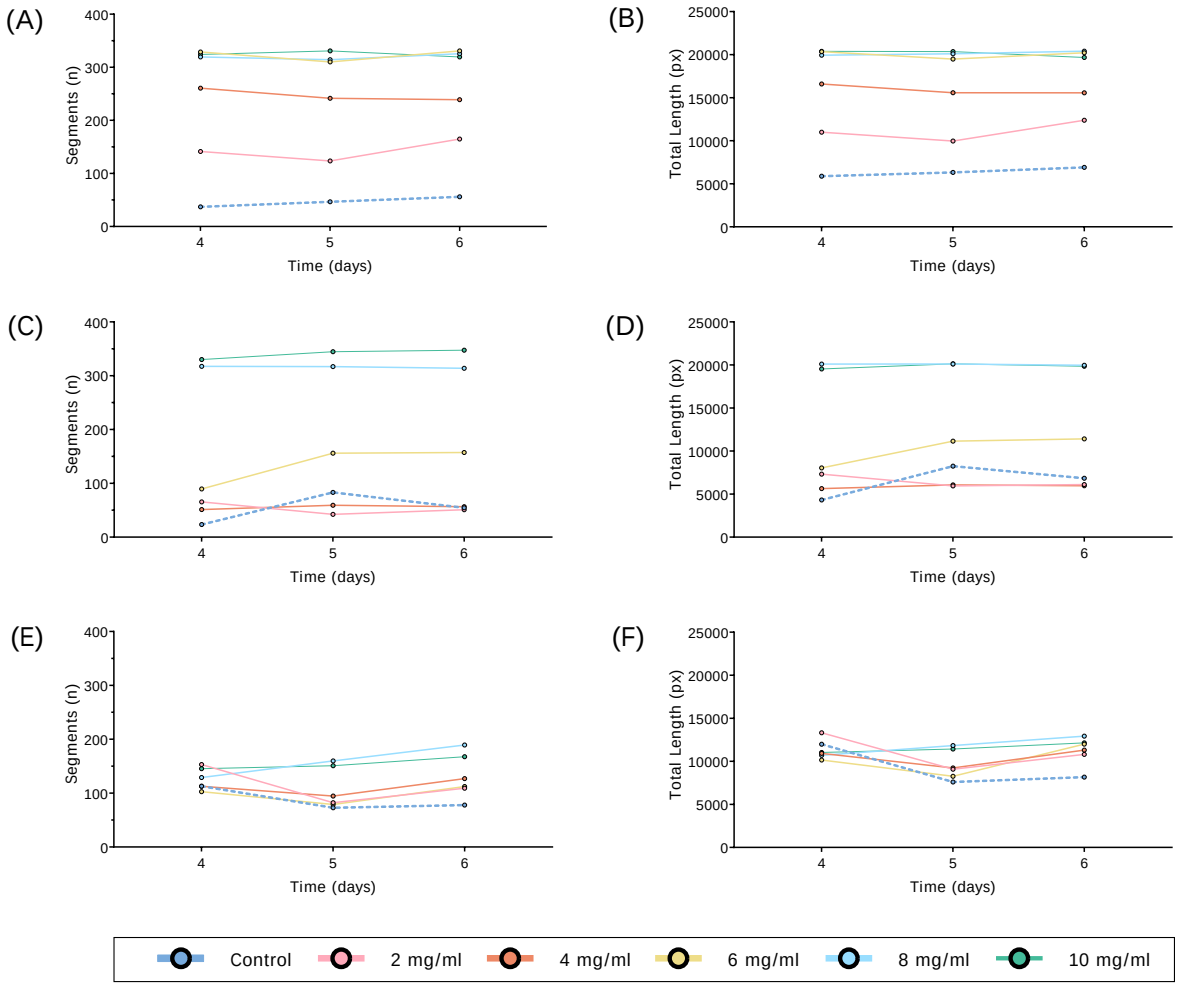


Figure E.19: **MVEC network characterisation at 4-, 5- and 6-days post-seeding by fibrinogen concentration and medium.** Networks were characterised in terms of **(A, C, E)** segment number and **(B, D, F)** total length. Hydrogels were created using fibrinogen from human serum at different concentrations and using **(A, B)** EBM, **(C, D)** EBM + VEGF, or **(E, F)** EGM as a medium. MVECs were cultured with EGM and seeded at a density of 5.25×10^4 cells/well (24-well plate). Cells-only controls were used. (ANOVA/Tukey's HSD; $p \leq 0.05$; seven random images per sample, $n = 15$).

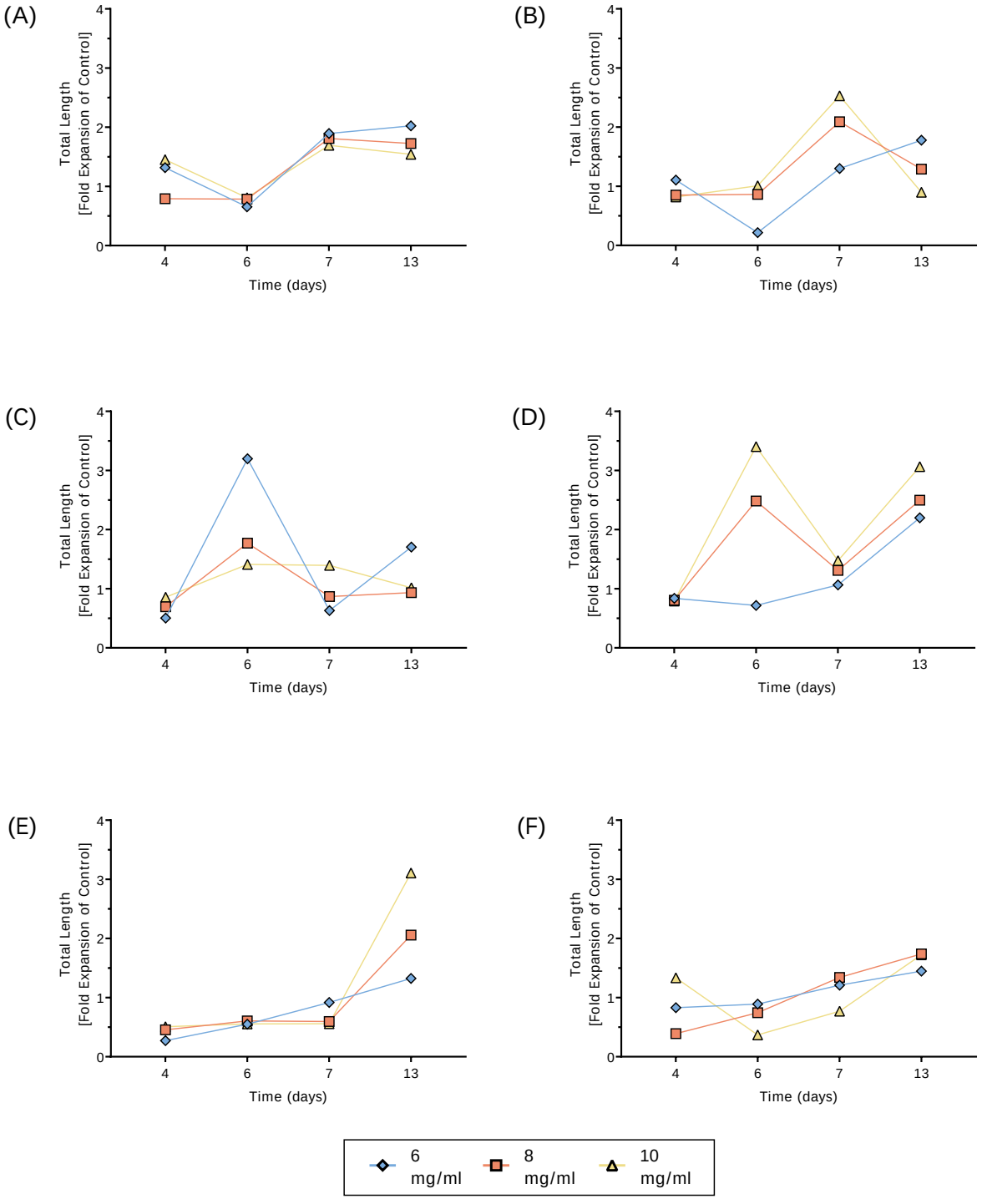


Figure E.20: **Total network length by medium, fibrinogen concentration and crosslinking ratio (fibrinogen : thrombin : $CaCl_2$) as fold expansion of the control, quantified throughout 13 days.** MVEC networks were monitored and quantified at 4–, 6–, 7– and 13–days post-seeding. Hydrogels were created using fibrinogen from human serum at different concentrations (6, 8 and 10 mg/mL), a crosslinking ratio of either **(A, C, E)** 200:10:1 or **(B, D, F)** 100:10:1, and **(A, B)** EBM, **(C, D)** EBM + VEGF or **(E, F)** PBS as the medium. MVECs were cultured with EGM and seeded at a density of 2×10^4 cells/well (96-well plate). Cells-only controls were used. (ANOVA/Dunnett; $p \leq 0.05$; $n = 6$).

E.1 Effect of Crosslinking Ratios on Hydrogel Consistency

E.1.1 Materials & Methods

Hydrogels of fibrinogen in endothelial cell basal medium (EBM; Lonza, Walkersville, MD, USA) or in Phosphate Buffered Saline (PBS; Gibco, United Kingdom) were prepared in a range of fibrinogen : thrombin : $CaCl_2$ crosslinking ratios. Briefly, fibrinogen from human plasma (Sigma-Life Science; St Louis, MO, USA) was dissolved in either EBM or PBS at a concentration of 5 or 10 mg/mL, and stored at 37 ℃ for 30 min until fully dissolved. Then, the solution was filtered twice using 0.22 µm filters and irradiated with UV light for 20 min.

Hydrogel solutions for each ratio were prepared and gently mixed to ensure a homogeneous mixture. 100 µL of the hydrogel solution was carefully deposited into each well (96-well plate) carefully to avoid bubble formation. Following gel casting, plates were incubated at 37 ℃ and 5% CO_2 for 12 days. Then, hydrogel scaffolds were carefully removed from their moulds. The samples were visually inspected 1 h after demoulding and classified as 'good', 'acceptable' or 'poor' based on scaffold 3D shape retention.

E.1.2 Key Results

The consistency of the hydrogel scaffolds 1 h after demoulding was visually inspected (Figure E.21) and classified based on the shape retention achieved after 12 days of incubation as 'good', 'acceptable' or 'poor' (Figure E.22), simulating the conditions to which cell-embedded constructs would be exposed to.

Hydrogels created using PBS as a medium were transparent, while those fabricated with EBM were pink. Upon observation, higher fibrinogen concentrations result in more opaque hydrogels; however, this was not quantified, so additional experimental work is required on this aspect.

The fibrinogen to thrombin to calcium chloride ratios explored revealed interesting insights. First, these ratios play a more significant role on hydrogel consistency and shape retention than the selection of fibrinogen concentration (5 or 10 mg/mL) or medium (EBM or PBS). Also, a ratio between fibrinogen and thrombin of 10:1 or 20:1 is associated with better shape retention. This is illustrated by the 200:10:1, 100:10:1 and 20:1:1 ratios explored, which result in a 'good' consistency in both EBM and PBS hydrogels (except for 20:1:1 PBS). This effect seems to be diminished when the corresponding ratio of thrombin to calcium chloride is low, as illustrated by 40:2:1 and 20:2:1 in both EBM and PBS. Nevertheless, these result in acceptable hydrogel shape retention.

Focusing on EBM hydrogels, it is also possible to identify a trend when looking into the ratio between fibrinogen and $CaCl_2$. As this ratio increases, shape retention improves. Bearing this in mind, two fibrinogen to thrombin to calcium chloride ratios were selected for further experimental work: 200:10:1 and 100:10:1. Moreover, higher fibrinogen concentrations result in better shape retention. However, it is difficult to quantify this based on a visual inspection solely. As such, it is necessary to complement these findings with material characterisation. In particular, coagulation time, spectrophotometry and microrheology would be particularly useful to provide further insights into hydrogel consistency.

Fibrin : Thrombin : $CaCl_2$ Ratio	EBM Hydrogel		PBS Hydrogel	
	5 mg/ml	10 mg/ml	5 mg/ml	10 mg/ml
200:10:1				
100:10:1				
40:10:1				
40:2:1				
20:10:1				
20:2:1				
20:1:1				
10:10:1				
10:1:1				
8:2:1				
4:1:1				
2:1:1				
1:1:1				

Figure E.21: **Representative photographs of hydrogel scaffolds 12 days after casting and 1 h after demoulding**, by crosslinking ratio (fibrinogen : thrombin : $CaCl_2$) and medium (EBM or PBS). Hydrogels were prepared using fibrinogen from human serum at a concentration of 5 or 10 mg/mL in either EBM or PBS, and then 100 µL of this hydrogel solution were cast into each well (96-well plate). Six hydrogel compositions, indicated by crossed out cells, fully degraded by 12 days.

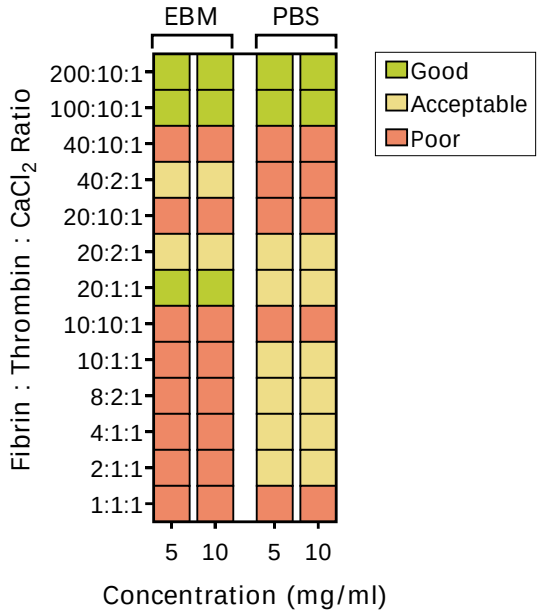


Figure E.22: **Classification based on the visual inspection of hydrogel consistency and shape retention 12 days after hydrogel casting**, by crosslinking ratio (fibrinogen : thrombin : $CaCl_2$) and medium (EBM or PBS). Shape retention was evaluated 1 h after demoulding and classified as 'good', 'acceptable' or 'poor'. Hydrogels were prepared using fibrinogen from human serum at a concentration of 5 or 10 mg/mL in either EBM or PBS. Hydrogel scaffolds were created by casting 100 µL per well (96-well plate; n = 3).

Appendix F

Supplementary Materials for Chapter 6

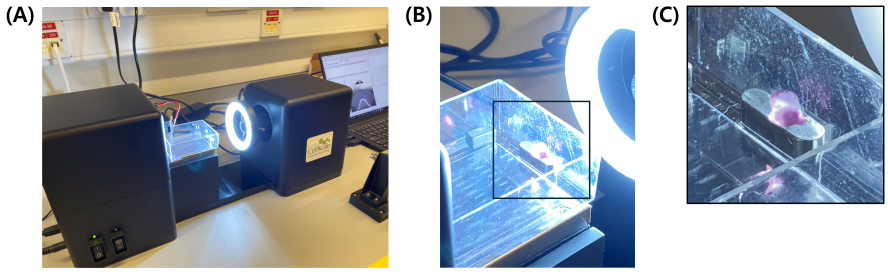


Figure F.1: **Experimental setup for compressive testing of fibrin hydrogels. (A)** Photograph of the MicroTester LT system during testing, with the laptop in the background displaying the live image capture from the device. **(B, C)** Close-up view of the hydrogel sample (pink) positioned on a metallic bar within the testing chamber, illustrating the precise location where compressive loading was applied and visualised.

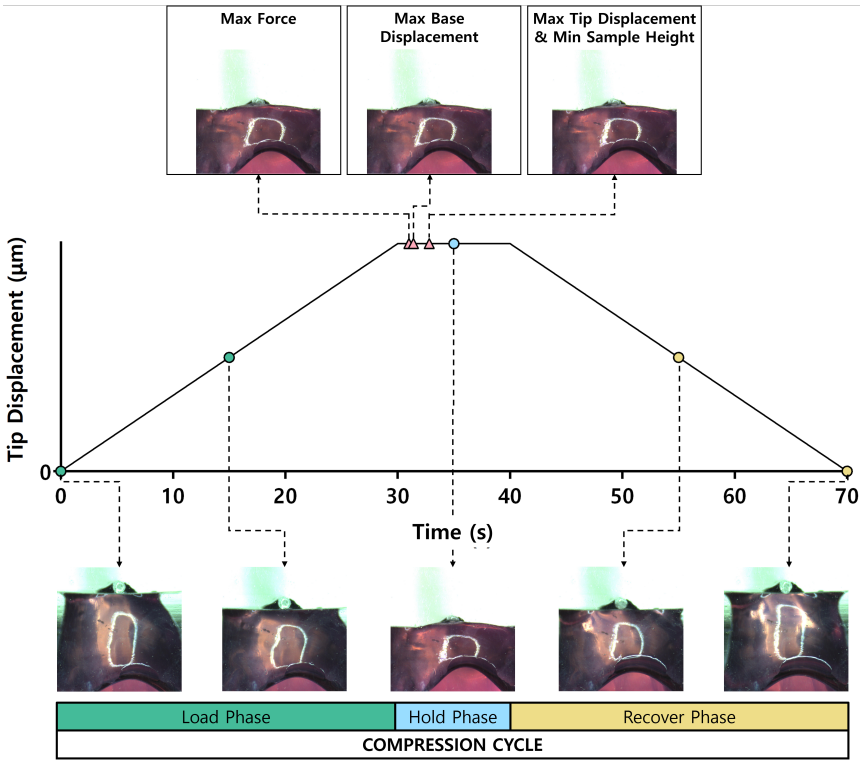


Figure F.2: **Compressive loading profile of fibrin hydrogel over a single cycle.** The plot illustrates the three phases of the compression cycle: load, during which 35% compression was applied (0–30 s); hold, where the deformation is maintained (30–40 s); and recovery, during which the applied force is removed (40–70 s). Representative photographs corresponding to five points throughout the compression cycle (t = 0, 15, 35, 55 and 70 s) illustrate the three separate phases: load (*teal circles*), hold (*blue circle*) and recovery (*yellow circles*). Three additional points (*teal triangles*) indicate key mechanical events: maximum force (µN) at 31 s, maximum base displacement (µm) at 31.4 s, and both maximum tip displacement (µm) and minimum hydrogel sample height (µm) at 32.8 s, with images captured at these time points also shown.

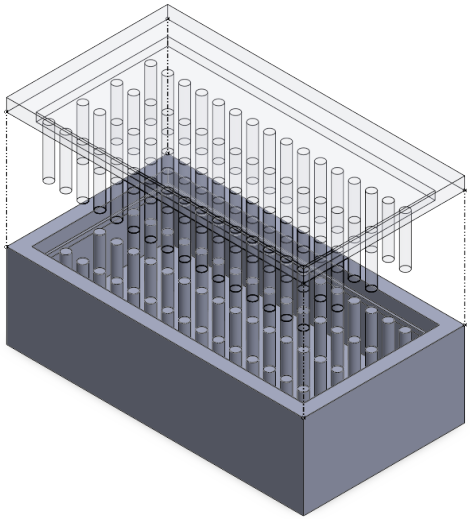


Figure F.3: **3D-printed container and lid design for resin biocompatibility assessment.** The custom container and lid feature internal column structures to maximise internal surface area, increasing the exposure of the medium to the 3D-printed surfaces and thereby enhancing compound leaching for assessment. The lid is drawn in transparent line view to show the internal geometry and its alignment with the container. The container was design to hold 20 mL of medium and provide a surface area-to-volume ratio of at least 7.5.

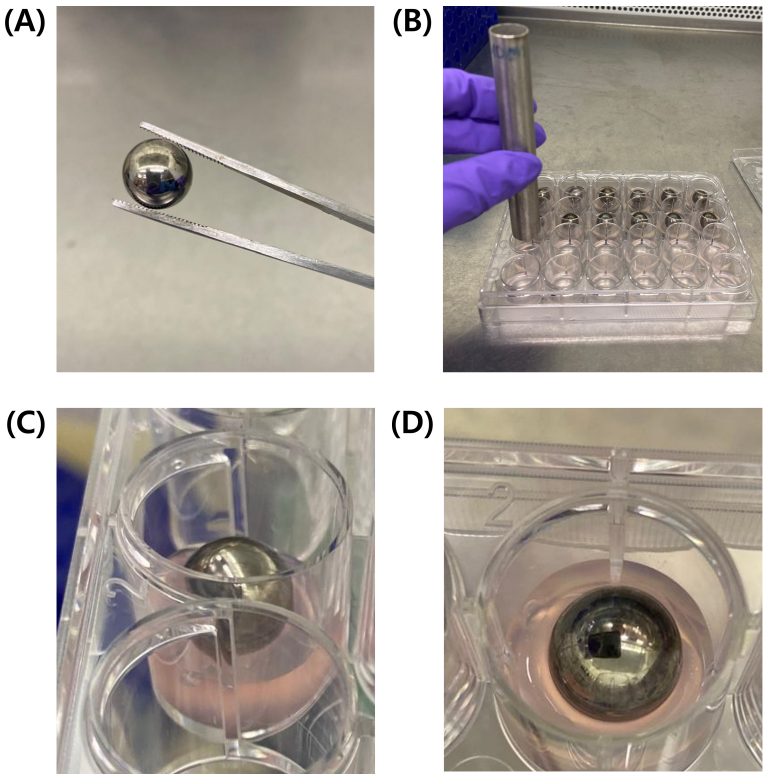


Figure F.4: **Contusion injury model for three-dimensional (3D) microvascular constructs. (A)** Metallic mass used to induce contusion injury. **(B)** Vertical guiding tube used to control drop height and alignment during impact, with the 10 cm configuration shown. **(C, D)** The metallic mass positioned on top of the hydrogel construct immediately following impact, where it was left in place to maintain compressive loading during the contusion injury period.

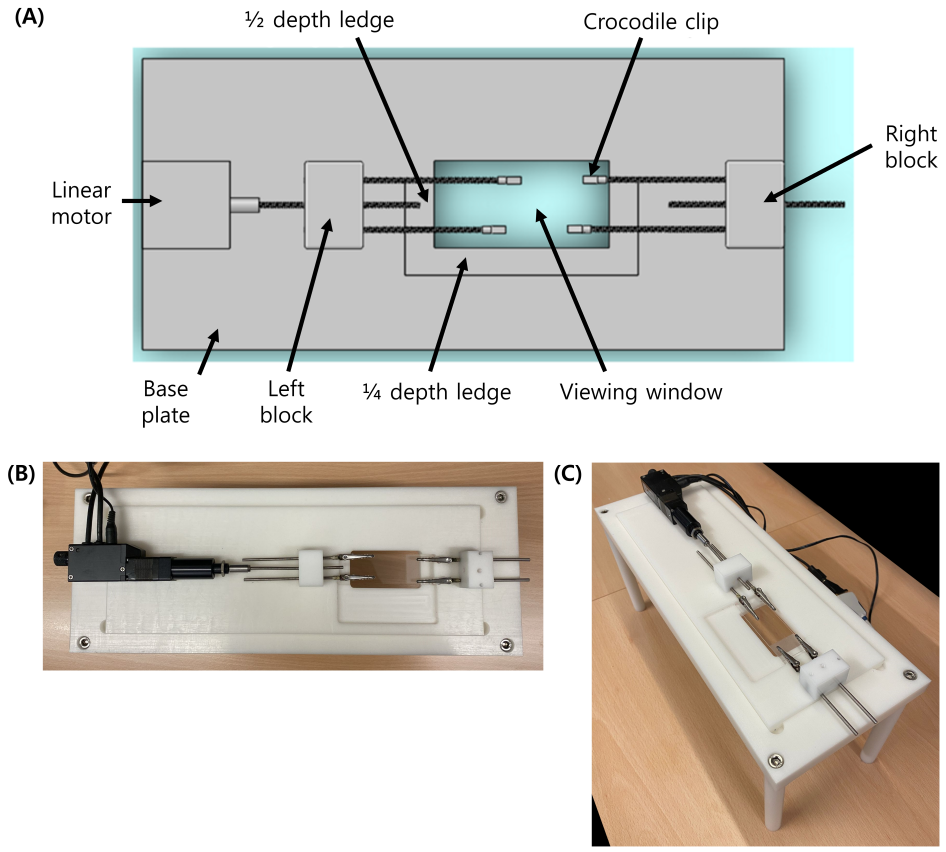


Figure F.5: **Custom tensile loading device used to apply a strain injury**, shown as **(A)** a top-view diagram illustrating the major components and **(B, C)** photographs of the device from **(B)** top and **(C)** isometric views. The sample is secured by four crocodile clips, each mounted on a threaded pole attached to a stabilising block. The right-hand block is fixed to the base plate, while the left-hand block is connected to a linear motor, allowing controlled displacement. A viewing window beneath the sample accommodates a microscope slide for imaging during tensile loading. A quarter-depth ledge machined into the base plate enables the slide to be inserted beneath the clips, while the half-length ledge provides stable support during imaging. The entire system is elevated by a 15 cm-tall base frame. The linear motor is controlled using Zaber Console software.

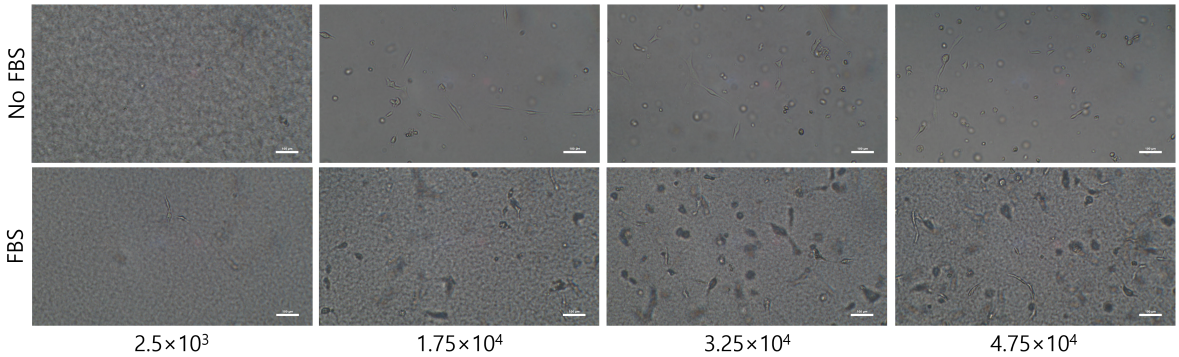


Figure F.6: **Effect of FBS on early endothelial cell morphology in hydrogels.** Representative 10× microscopy images of human dermal microvascular endothelial cells (MVECs) embedded at different cell seeding densities (cells/cm^2, reported based on well surface area) in fibrin scaffolds with (*bottom row*) or without (*top row*) foetal bovine serum (FBS). Hydrogels were cast in 12-well plates (500 µL per well) and imaged three days post-seeding. Hydrogels were fabricated using fibrinogen from human plasma (10 mg/mL) in endothelial cell basal medium (EBM) and crosslinked using thrombin (10 U/mL in MES/NaCl buffer) and $CaCl_2$ (1 M in distilled water) at a ratio of 200:10:1 (fibrinogen : thrombin : $CaCl_2$). Scale bar: 100 µm.

Table F.1: **Well size and hydrogel volume (µL) used for construct fabrication, with resulting hydrogel height (mm).** Well surface areas were obtained from Thermo Fisher Scientific [625] and hydrogel heights were calculated based on the corresponding volumes.

Well Size	Well Surface Area (cm^2)	Hydrogel Volume (µL)	Hydrogel Height (mm)
24-well	1.9	100	0.5263
		200	1.0526
		300	1.5789
		400	2.1052
		500	2.6315
		1,000	5.2629
12-well	3.5	300	0.8571
		400	1.1429
		500	1.4286
		600	1.7143
		700	2.0000
		800	2.2857
		900	2.5714
		1,000	2.8572
		1,500	4.2857
		2,000	5.7143
		2,500	7.1429
		3,000	8.5715
6-well	9.6	1,000	1.0418
		2,000	2.0835
		3,000	3.1253
		4,000	4.1670
		5,000	5.2088
		6,000	6.2506

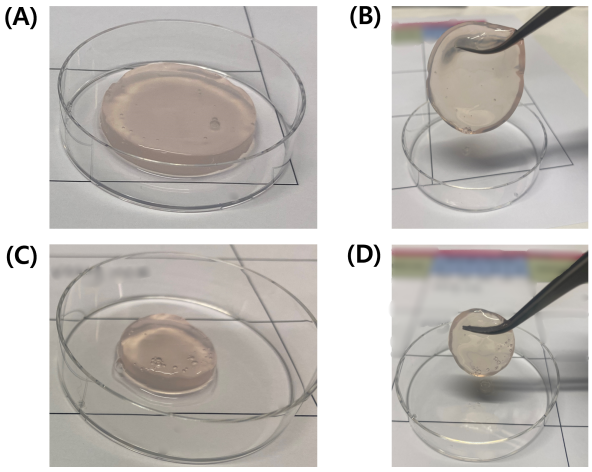


Figure F.7: **Representative photographs of fibrin hydrogel constructs**, taken two days after casting and after removal from their moulds. Here, hydrogels cast in **(A, B)** 6-well (6 mL per well) and **(C, D)** 12-well plates (2.5 mL per well) are shown. Hydrogels were fabricated using fibrinogen from human plasma (10 mg/mL in endothelial cell basal medium; EBM) and crosslinked with thrombin (10 U/mL) and $CaCl_2$ (1 M) at a ratio of 200:10:1 (fibrinogen : thrombin : $CaCl_2$). Foetal bovine serum (FBS) was also added to the hydrogel formulation.

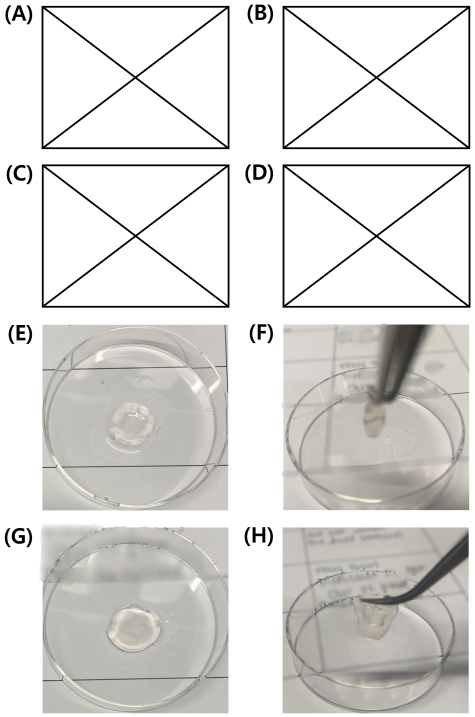


Figure F.8: **Representative photographs of fibrin hydrogel constructs cast in 24-well plates.** Photographs were taken two days after casting, following removal of the hydrogels from their moulds. Different hydrogel volumes were tested: **(A, B)** 100, **(C, D)** 200, **(E, F)** 300 and **(G, H)** 400 µL per well. **(A, C, E, G)** Top-down photographs of the hydrogels and **(B, D, F, H)** of the hydrogels held with curved-tip forceps are shown. Crossed-out cells indicate hydrogels that fractured or disintegrated during demoulding. Hydrogels were fabricated using fibrinogen from human plasma (10 mg/mL in endothelial cell basal medium; EBM) and crosslinked with thrombin (10 U/mL) and $CaCl_2$ (1 M) at a ratio of 200:10:1 (fibrinogen : thrombin : $CaCl_2$). Foetal bovine serum (FBS) was also added to the hydrogel formulation.

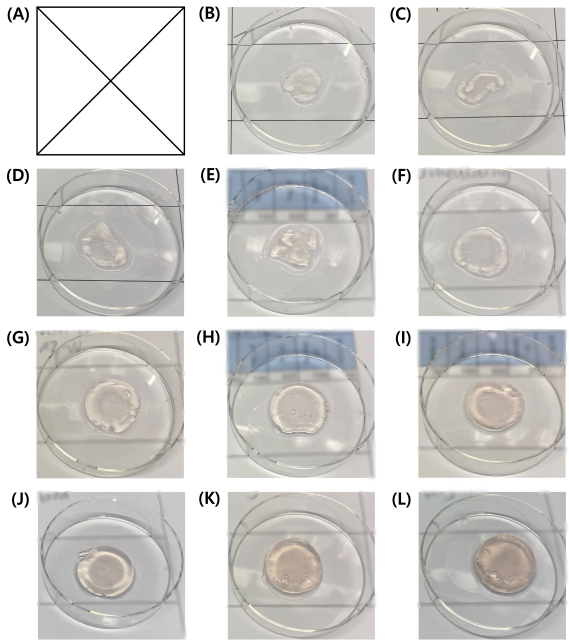


Figure F.9: **Representative photographs of fibrin hydrogel constructs cast in 12-well plates.** Photographs were taken two days after casting, following removal of the hydrogels from their moulds. Different hydrogel volumes were tested: **(A)** 300, **(B)** 400, **(C)** 500, **(D)** 600, **(E)** 700, **(F)** 800, **(G)** 900, **(H)** 1,000, **(I)** 1,500, **(J)** 2,000, **(K)** 2,500 and **(L)** 3,000 µL per well. Crossed-out cells indicate hydrogels that fractured or disintegrated during demoulding. Hydrogels were fabricated using fibrinogen from human plasma (10 mg/mL in endothelial cell basal medium; EBM) and crosslinked with thrombin (10 U/mL) and $CaCl_2$ (1 M) at a ratio of 200:10:1 (fibrinogen : thrombin : $CaCl_2$). Foetal bovine serum (FBS) was also added to the hydrogel formulation.

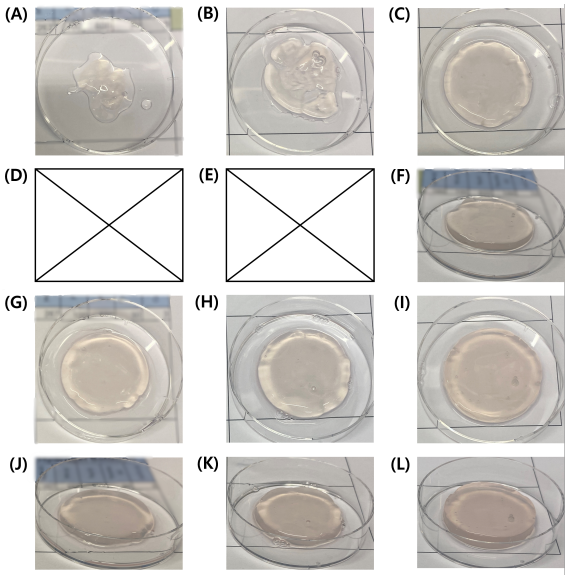


Figure F.10: **Representative photographs of fibrin hydrogel constructs cast in 6-well plates.** Photographs were taken two days after casting, following removal of the hydrogels from their moulds. Two hydrogel views are shown: **(A, B, C, G, H, I)** top-down photographs of the hydrogels and **(D, E, F, J, K, L)** angled photographs showcasing hydrogel thickness. Different hydrogel volumes were tested: **(A, D)** 1 mL, **(B, E)** 2 mL, **(C, F)** 3 mL, **(G, J)** 4 mL, **(H, K)** 5 mL and **(I, L)** 6 mL per well. Crossed-out cells indicate hydrogels that fractured or disintegrated during demoulding. Hydrogels were fabricated using fibrinogen from human plasma (10 mg/mL in endothelial cell basal medium; EBM) and crosslinked with thrombin (10 U/mL) and $CaCl_2$ (1 M) at a ratio of 200:10:1 (fibrinogen : thrombin : $CaCl_2$). Foetal bovine serum (FBS) was also added to the hydrogel formulation.

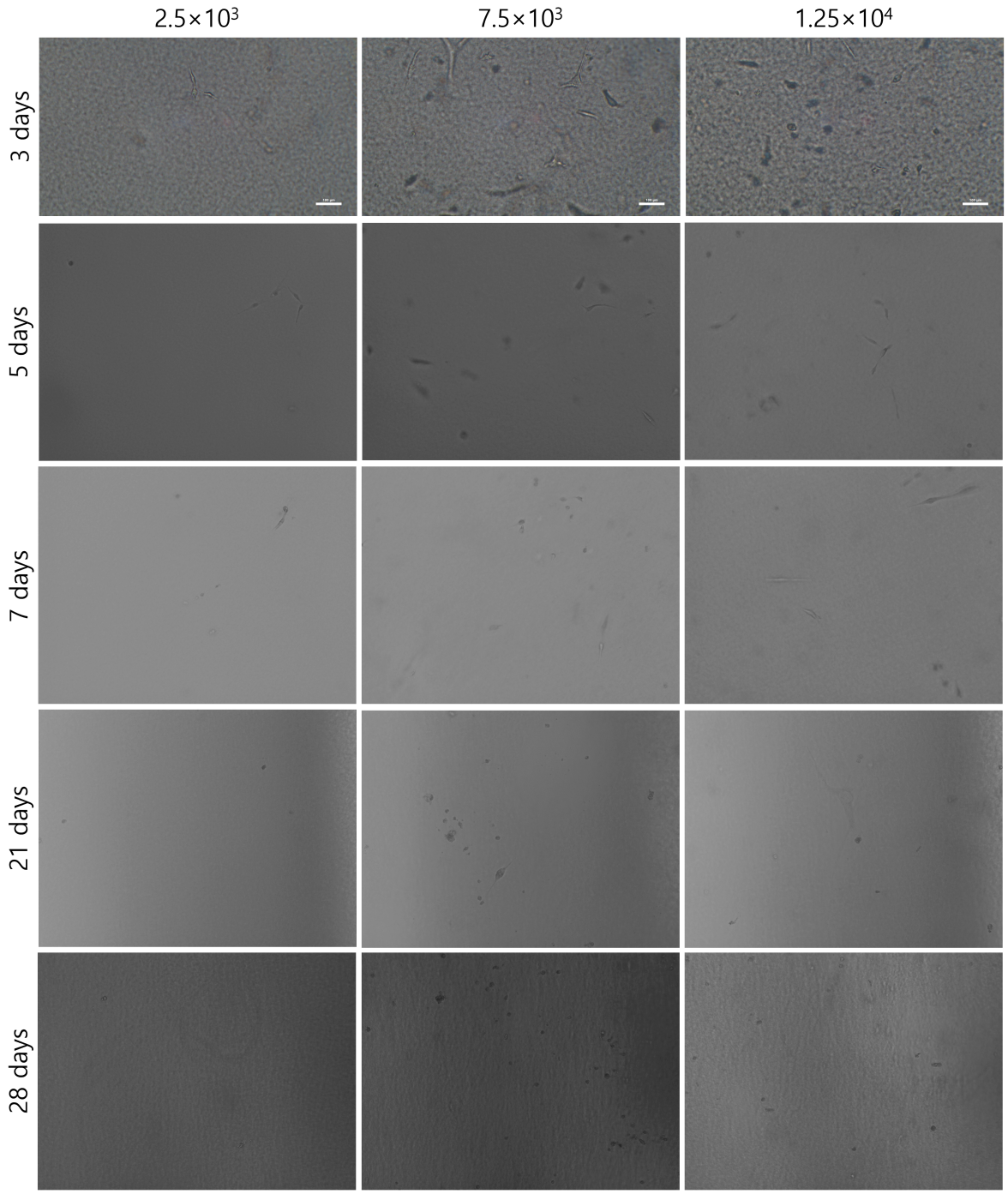


Figure F.11: **Impact of cell seeding density on fibrin hydrogel constructs.** Representative 10× microscopy images of human dermal microvascular endothelial cells (MVECs) embedded at different seeding densities (cells/cm^2, reported based on well surface area) in fibrin hydrogels. Here, 2.5×10^3, 7.5×10^3 and 1.25×10^4 seeding densities are shown. Hydrogels were prepared with fibrinogen from human plasma (10 mg/mL) in endothelial cell basal medium (EBM) and crosslinked using thrombin (10 U/mL in MES/NaCl buffer) and $CaCl_2$ (1 M in distilled water) at a ratio of 200:10:1 (fibrinogen : thrombin : $CaCl_2$). Hydrogels were cast in 12-well plates (1,000 µL per well). Scale bar: 100 µm.

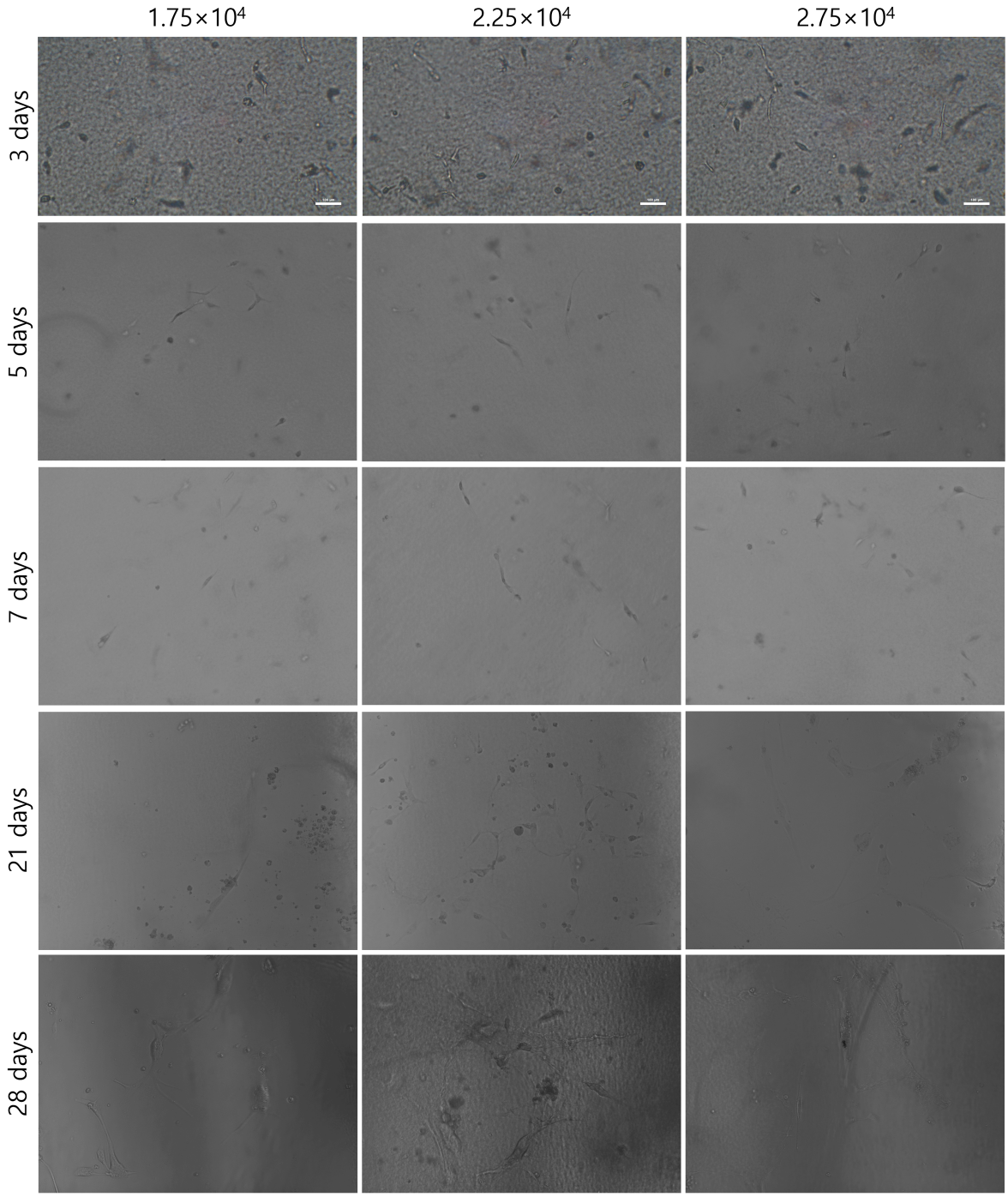


Figure F.12: **Impact of cell seeding density on fibrin hydrogel constructs.** Representative 10× microscopy images of human dermal microvascular endothelial cells (MVECs) embedded at different seeding densities (cells/cm^2, reported based on well surface area) in fibrin hydrogels. Here, 1.75×10^4, 2.25×10^4 and 2.75×10^4 seeding densities are shown. Hydrogels were prepared with fibrinogen from human plasma (10 mg/mL) in endothelial cell basal medium (EBM) and crosslinked using thrombin (10 U/mL in MES/NaCl buffer) and $CaCl_2$ (1 M in distilled water) at a ratio of 200:10:1 (fibrinogen : thrombin : $CaCl_2$). Hydrogels were cast in 12-well plates (1,000 µL per well). Scale bar: 100 µm.

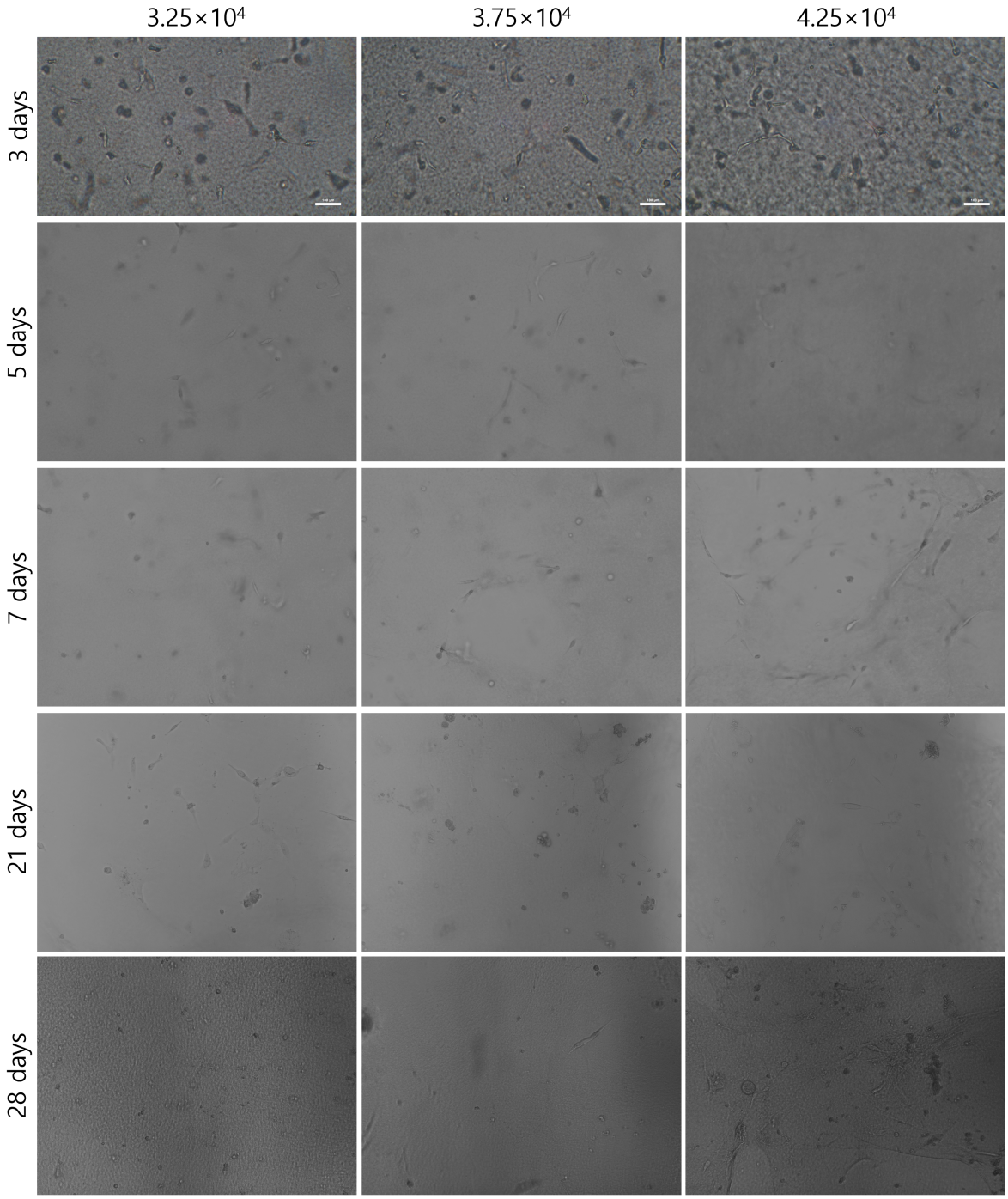


Figure F.13: **Impact of cell seeding density on fibrin hydrogel constructs.** Representative 10× microscopy images of human dermal microvascular endothelial cells (MVECs) embedded at different seeding densities (cells/cm^2, reported based on well surface area) in fibrin hydrogels. Here, 3.25×10^4, 3.75×10^4 and 4.25×10^4 seeding densities are shown. Hydrogels were prepared with fibrinogen from human plasma (10 mg/mL) in endothelial cell basal medium (EBM) and crosslinked using thrombin (10 U/mL in MES/NaCl buffer) and $CaCl_2$ (1 M in distilled water) at a ratio of 200:10:1 (fibrinogen : thrombin : $CaCl_2$). Hydrogels were cast in 12-well plates (1,000 µL per well). Scale bar: 100 µm.

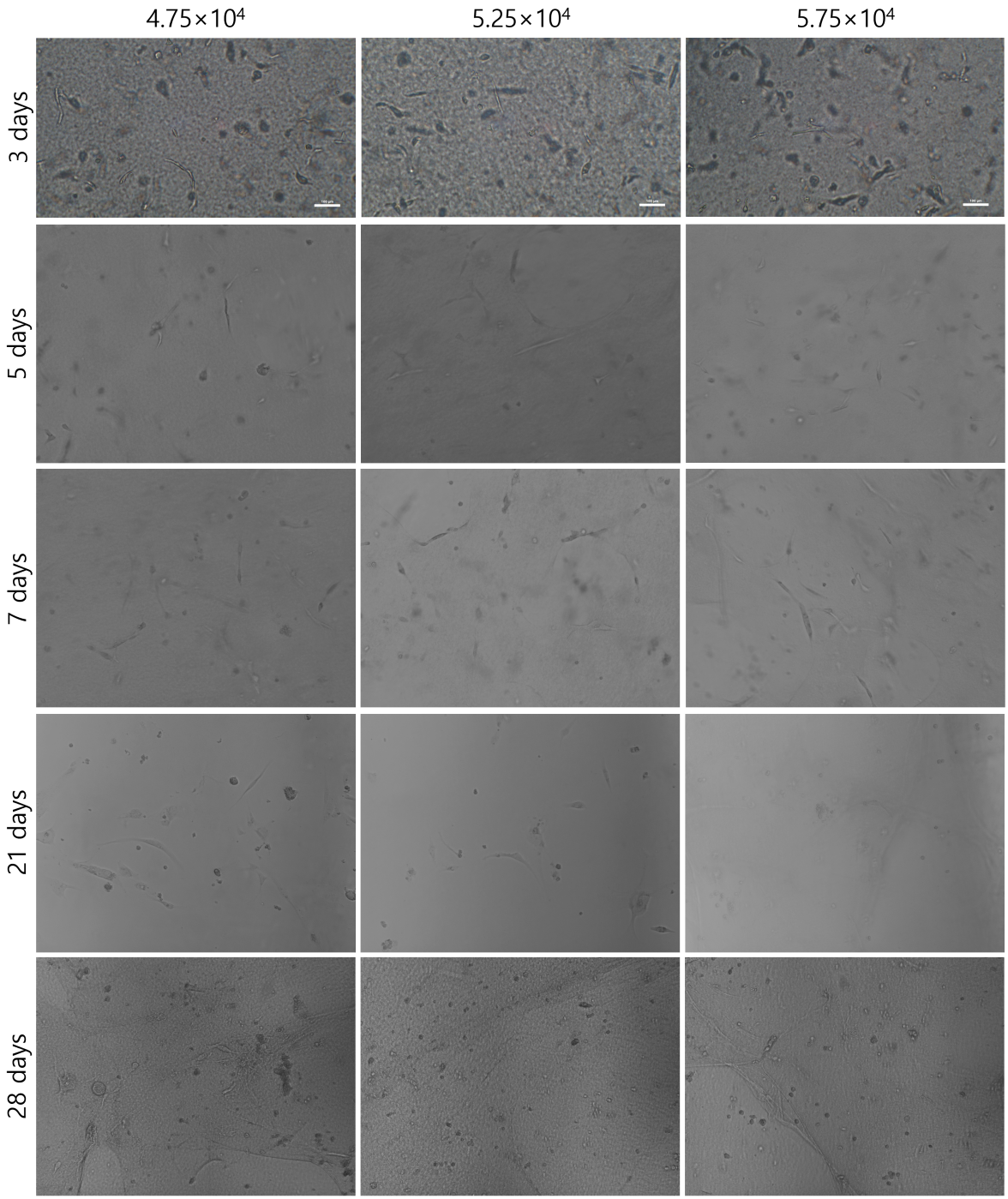


Figure F.14: **Impact of cell seeding density on fibrin hydrogel constructs.** Representative 10× microscopy images of human dermal microvascular endothelial cells (MVECs) embedded at different seeding densities (cells/cm^2, reported based on well surface area) in fibrin hydrogels. Here, 4.75×10^4, 5.25×10^4 and 5.75×10^4 seeding densities are shown. Hydrogels were prepared with fibrinogen from human plasma (10 mg/mL) in endothelial cell basal medium (EBM) and crosslinked using thrombin (10 U/mL in MES/NaCl buffer) and $CaCl_2$ (1 M in distilled water) at a ratio of 200:10:1 (fibrinogen : thrombin : $CaCl_2$). Hydrogels were cast in 12-well plates (1,000 µL per well). Scale bar: 100 µm.

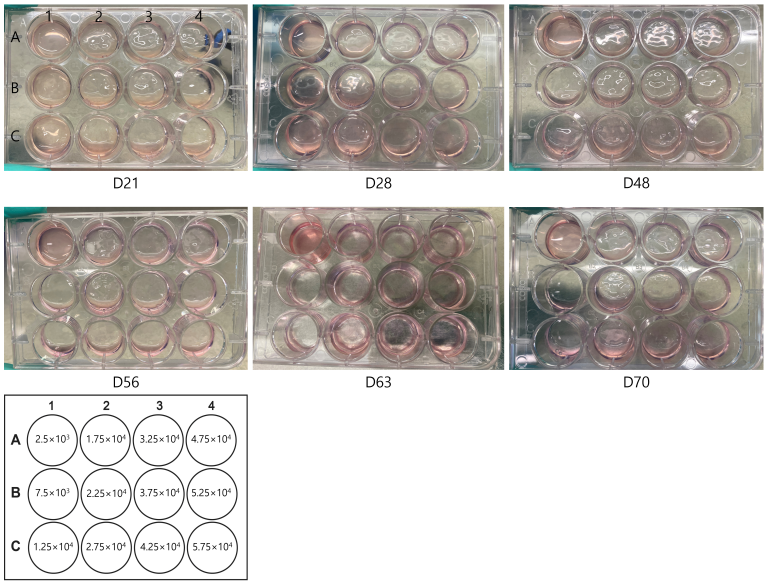


Figure F.15: **Photographs of plate containing hydrogel constructs embedded with human dermal microvascular endothelial cells (MVECs), captured at 21, 28, 48, 56, 63 and 70 days post-seeding.** Hydrogels were fabricated using fibrinogen from human plasma (10 mg/mL in endothelial cell basal medium; EBM) and crosslinked with thrombin (10 U/mL) and $CaCl_2$ (1 M) at a ratio of 200:10:1 (fibrinogen : thrombin : $CaCl_2$). Hydrogels were embedded with MVECs at varying seeding densities and were prepared with foetal bovine serum (FBS). The different cell seeding densities (cells/cm^2, reported based on well surface area) used are specified in the legend. Here, photographs of hydrogels cast in 12-well plates (1,000 µL per well) are shown.

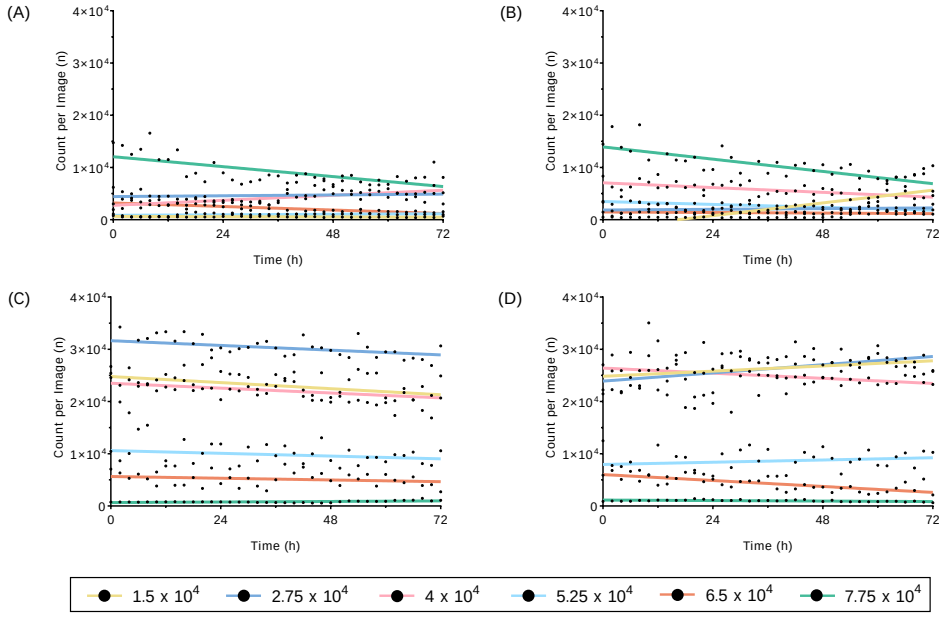


Figure F.16: **Phase 1 live-imaging analysis of endothelial cells and tube-like structures count in MVEC-containing hydrogels over 72 h.** The number of tube-like objects detected per image was quantified from whole-well scans acquired every 2 h over a 72 h period during **Phase 1** optimisation experiments. Tube-like objects were identified as endothelial cell-derived tubular structures using automated image analysis. Four hydrogel formulations were evaluated: **(A)** EBM at 8 mg/mL fibrinogen; **(B)** EBM + VEGF at 8 mg/mL fibrinogen; **(C)** EBM at 10 mg/mL fibrinogen; and **(D)** EBM + VEGF at 10 mg/mL fibrinogen. Within each panel, six MVEC seeding densities were assessed: 1.5, 2.75, 4.0, 5.25, 6.5 and 7.75 $\times$ 10^4 cells per construct. For each condition, a simple linear regression was fitted to the time-series data, with shaded regions representing the 95% confidence bands (n = 3).

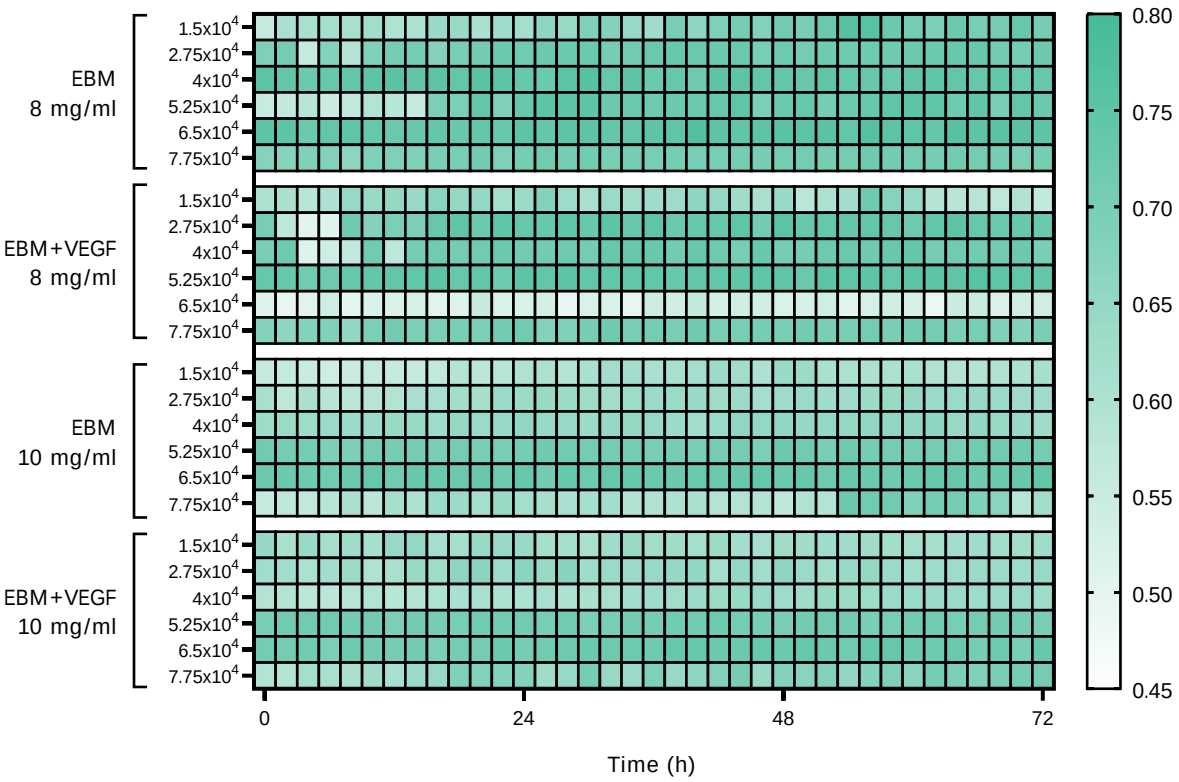


Figure F.17: **Phase 1 heatmap of average object eccentricity in MVEC-containing hydrogels over 72 h.** Average eccentricity of detected objects (mean per image, $n = 3$) was quantified from whole-well scans acquired every 2 h over a 72 h period during **Phase 1** optimisation experiments. Data are presented as a heatmap with the x-axis representing time (0–72 h, 2-h intervals) and the y-axis listing hydrogel compositions in the format: *cell seeding number — hydrogel formulation (EBM or EBM + VEGF) — fibrinogen concentration (mg/mL)*. Colour intensity (green scale) encodes average eccentricity: darker green indicates higher eccentricity values (closer to 1, *i.e.* more elongated/line-like structures) and lighter green indicates lower eccentricity values (closer to 0, *i.e.* more circular morphology). All observed values ranged between 0.45 and 0.80 and are shown on the accompanying colour bar.

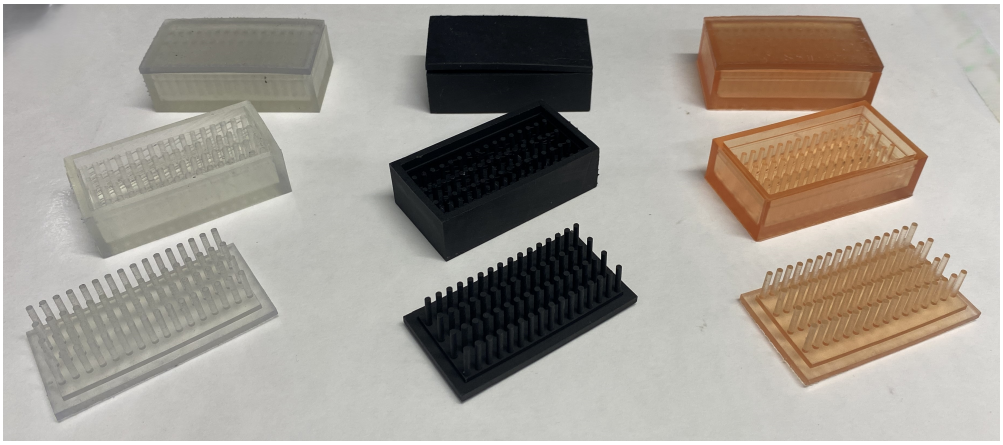


Figure F.18: **3D-printed containers and lids fabricated with three resin materials.** Photograph of the assembled containers with lids (top row), containers (middle) and lids (bottom) printed in clear, black and BioMed Amber resin (left to right). The internal column structures incorporated into the design are visible in this view and serve to maximise internal surface area for compound retention during the biocompatibility assessment. Each container can hold 20 mL of medium and has a surface area-to-volume ratio of 0.77196.

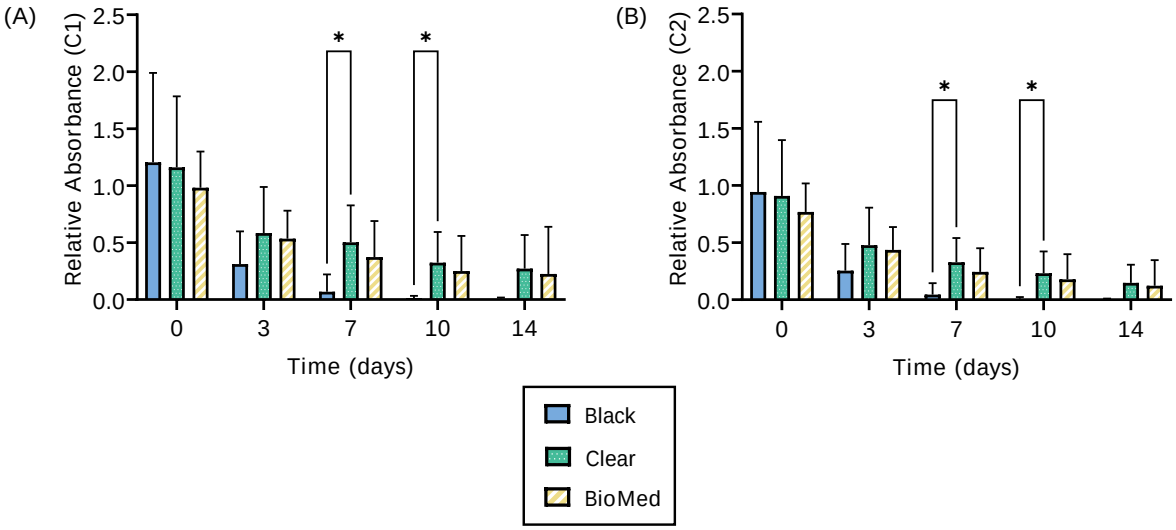


Figure F.19: **Resin-conditioned media effects on microvascular endothelial cells (MVECs) over 14 days, relative to controls.** MVECs were seeded at 5×10^3 cells per well and cultured in media conditioned by black, clear, or BioMed Amber resins. Relative absorbance was measured and normalised to **(A)** fresh media (C1) and **(B)** incubated media (C2). Values are plotted as mean $\pm$ standard deviation. (Two-way ANOVA/Tukey's HSD; $^*p \leq 0.05$; only statistically significant differences are shown; $n = 10$).

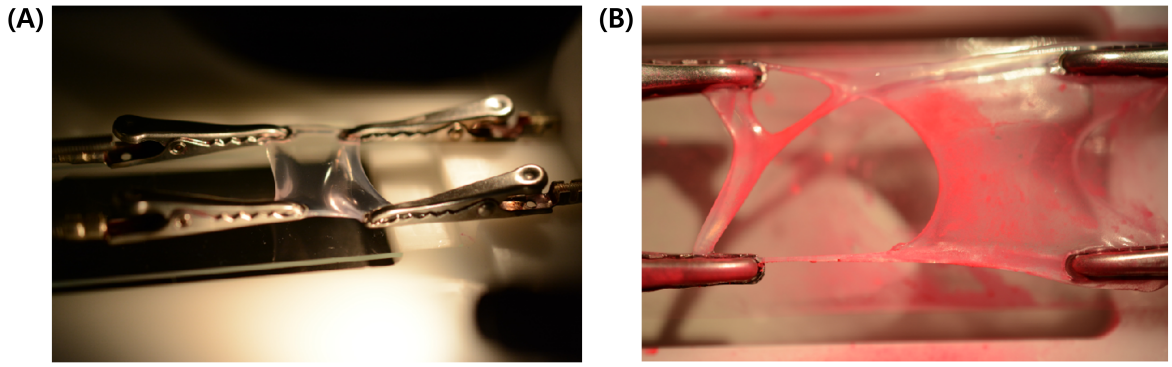


Figure F.20: **Photograph of a 3D hydrogel construct undergoing strain injury. (A)** Fibrin hydrogel mounted on the loading device before and **(B)** after tensile loading. A 10 mg/mL EBM hydrogel is shown. In **(B)**, powder was applied to the construct surface to enable particle tracking for strain quantification (data not shown).